Expanding the Catalytic Repertoire of Hemeproteins as Carbene Transferases to Access Diverse Molecular Structures

Thesis by

Kai Chen

In Partial Fulfillment of the Requirements for the Degree of
Doctor of Philosophy in Chemistry

CALIFORNIA INSTITUTE OF TECHNOLOGY
Pasadena, California

2020
Defended May 5th, 2020

Kai Chen
ORCID: 0000-0002-3325-3536

ACKNOWLEDGEMENT

To my advisor, and also my heroine and role model, Prof. Frances Arnold, who has inspired and will be continuously inspiring me with her comprehension, discernment, and fearlessness in science. Her attitude to science, with a strong sense of responsibility and faith as a scientist, keeps reminding me to have deep, broad, and long-term vision for the science I am and will be doing. Her approach to science, with emphasis on novelty, accuracy and practicality, has set up a standard for my future scientific career. Frances is, undoubtedly, the person who has influenced me the most and who I want to express my greatest gratitude to on my way to science.

I would like to thank my committee members, Prof. Harry Gray, Prof. Bob Grubbs and Prof. Greg Fu, for sharing their expertise, giving me suggestions and also being extremely supportive throughout my graduate period. In particular, Harry, with his impressive knowledge of chemistry, has provided me with thought-provoking comments on the bioinorganic part of my research, which has driven me to dig deeply on the theoretical side. Bob has offered numerous beneficial suggestions on how to develop functional materials with the molecules I can uniquely make, which has prompted me to think broadly on the application side. Greg has called attention to critical details in my research (or proposals) and also laid a lot of emphasis on scientific novelty, which is so important to me especially for my future independent career. I feel so fortunate and grateful that I have these three committee members, from whom I have learned the three most important factors of doing science: theoretical basis, practical application, and scientific details. Looking back, I should have visited my committee members more frequently so that I would learn more valuable knowledge and experience from them.

I have been privileged to work with and learn from many outstanding scientists at Caltech, especially Dr. Sabine Brinkmann-Chen, Dr. Xiongyi Huang, Dr. Kelly Zhang, Dr. Olli Brandenberg, Dr. Jenny Kan, Dr. David Romney, Dr. Stephan Hammer, Dr. Yang Yang, Dr. Noah Dunham, Dr. Zhijun Jia, Dr. Hans Renata, Dr. Chris Prier, Dan Wackelin, Andrew Zhou, and a lot more. The Arnold lab is a cheerful and positive community comprised of talented people from different directions, and with full energy in science – people are always happy to have scientific discussions, share valuable experiences and help each other in research. The time I spent in Spalding will definitely be my treasured memory for the whole life. I also had wonderful experiences collaborating with excellent computational scientists outside of Caltech, particularly Dr. Shuo-Qing Zhang and Dr. Marc Garcia-Borràs. Dr. Scott Virgil and Larry Henling have been generous and patient in sharing their expertise, which has been so helpful to my graduate research. All these great people together – mentors, friends and colleagues – have made the me today as a scientist.

To my ZJU friends at Caltech, particularly Ke Ding, Jiaming Li and Danni Ma, who have made my life outside the lab with many unforgettable moments. And finally, to my family in China, Meifeng Chen, Shaoyu Chen, and Mingyi Chen, for their endless love and support over the ocean.

ABSTRACT

The efficiency, selectivity, and sustainability benefits offered by enzymes are enticing chemists to consider biocatalytic transformations to complement or even supplant more traditional synthetic routes. Increasing demands for efficient and versatile synthetic methods combined with powerful new discovery and engineering tools have prompted innovations in biocatalysis, especially the development of new enzymes for precise transformations. The past decade has witnessed impressive expansion of the catalytic repertoire of enzymes to include new and useful transformations not known (or relevant) in the biological world. The continuing discovery and improvement of these new enzyme activities is opening a floodgate that connects the chemistry of the biological world to that invented by humans over the last 100 years.

This thesis describes a new set of enzymes, derived from a cytochrome P450 monooxygenase and a cytochrome *c* electron-transfer protein, which are able to function as carbene transferases to construct diverse molecular structures, including strained carbocycles and lactone derivatives. Chapter 1 illustrates different approaches researchers have utilized to explore and develop new catalytic machineries of diverse enzymes. These efforts have identified new genetically-encoded biocatalysts that can be tuned and diversified through directed evolution. Chapter 2 presents the discovery of P450 variants that catalyze the formation of highly strained carbocycles, bicyclobutanes and cyclopropenes, via carbene addition to carbon–carbon triple bonds. The intrinsic strain energies of these small rigid carbocycles allow them to have broad applications in different fields, but also create challenges for their construction. Using a diazo substrate as the carbene precursor, the enzyme variants optimized by directed evolution could act on structurally diverse alkynes (aromatic or aliphatic, terminal or internal) with high efficiency and selectivity, providing an effective route to an array of chiral strained structures. The carbene transferase activity is then extended to the assembly of various lactone structures, a fundamental class of organic moieties with applications in fields varying from synthetic chemistry, to materials science, to medicinal chemistry. Chapter 3 details a strategy using lactone-based carbenes, for the transfer to different functionalities, enabling rapid access to a broad range of α-substituted and *spiro*-lactones with unprecedented efficiencies and selectivities. A different approach based on intramolecular carbene C–H insertion is outlined in Chapter 4, which allows for the synthesis of lactones in a higher order of structural diversity. Directed evolution of a P450 variant identified a lineage of potent variants, capable of assembling lactones in different sizes (5- to 7-membered) and also with sophisticated three-dimensional structures based on fused, spiro and bridged rings. Computational tools were employed to understand the reaction mechanisms and to explain some mutational effect. In sum, the thesis work lays out how protein engineering integrated with chemical rationalization enables the expansion of the chemical space accessible to native hemeproteins, especially in building diverse molecular structures.

PUBLICATIONS AND CONTRIBUTIONS

([*] corresponding author; [†] equal contribution)

(1) **Chen, K.**; Huang, X.; Kan, S. B. J.; Zhang, R. K.; Arnold, F. H.[*], Enzymatic construction of highly strained carbocycles. *Science* **360**, 71–75 (2018). **DOI**: 10.1126/science.aar4239.

K. C. participated in the design and execution of the research. K. C. prepared the manuscript.

(2) **Chen, K.**[†]; Zhang, S.-Q.[†]; Brandenberg, O. F.; Hong, X.[*]; Arnold, F. H.[*], Alternate heme ligation steers activity and selectivity in engineered cytochrome P450-catalyzed carbene transfer reactions. *J. Am. Chem. Soc.* **140**, 16402–16407 (2018). **DOI**: 10.1021/acscatal.6b02550.

K. C. participated in the design and execution of the research. K. C. prepared the manuscript.

(3) **Chen, K.**; Arnold, F. H.[*], Engineering cytochrome P450s for enantioselective cyclopropenation of internal alkynes. *J. Am. Chem. Soc.* **142**, 6891–6895 (2020). **DOI**: 10.1021/jacs.0c01313.

K. C. participated in the design and execution of the research. K. C. prepared the manuscript.

(4) **Chen, K.**; Arnold, F. H.[*], Engineering new catalytic activities in enzymes. *Nat. Catal.* **3**, 103–113 (2020). **DOI**: 10.1038/s41929-019-0385-5.

K. C. prepared the review article.

(5) **Chen, K.**; Huang, X.; Zhang, S.-Q.; Kan, S. B. J.; Zhou, A. Z.; Hong, X.[*]; Arnold, F. H.[*], Engineered cytochrome *c*-catalyzed lactone-carbene B–H insertion. *Synlett* **30**, *Pearl Anniversary Issue of the 30 Years SYNLETT*, 378–382 (2019). **DOI**: 10.1055/s-0037-1611662.

K. C. participated in the design and execution of the research. K. C. prepared the manuscript.

(6) Zhou, A. Z.; **Chen, K.**[*]; Arnold, F. H.[*], Enzymatic lactone-carbene C–H insertion to build contiguous chiral centers. *ACS Catal.* **10**, 5393–5398 (2020). **DOI**: 10.1021/acscatal.0c01349.

K. C. participated in the design and execution of the research. K. C. prepared the manuscript.

(7) Zhang, R. K.; **Chen, K.**; Huang, X.; Wohlschlager, L.; Renata, H.; Arnold, F. H.[*], Enzymatic assembly of carbon–carbon bonds *via* iron-catalysed sp^3 C–H functionalization. *Nature* **565**, 67–72 (2019). **DOI**: 10.1038/s41586-018-0808-5.

K. C. participated in the execution of the research, including enzymatic reactions, substrate scope study and synthetic applications. K. C. participated in reviewing and editing the manuscript.

(8) Brandenberg, O. F.; **Chen, K.**; Arnold, F. H.[*], Directed evolution of a cytochrome P450 carbene transferase for selective functionalization of cyclic compounds. *J. Am. Chem. Soc.* **141**, 8989–8995 (2019). **DOI**: 10.1021/jacs.9b02931.

K. C. participated in the preparation and analysis of chemical substances, and reviewing and editing the manuscript.

(9) Kan, S. B. J.; Lewis, R. D.; **Chen, K.**; Arnold, F. H.[*], Directed evolution of cytochrome c for carbon–silicon bond formation: Bringing silicon to life. *Science* **354**, 1048–1051 (2016). **DOI**:

10.1126/science.aah6219.

K. C. participated in the execution of the research, including enzymatic reactions, chemical synthesis and mechanistic studies. K. C. participated in reviewing and editing the manuscript.

(10) Brandenberg, O. F.; Prier, C. K.; **Chen, K.**; Knight, A. M.; Wu, Z.; Arnold, F. H.*, Stereoselective enzymatic synthesis of heteroatom-substituted cyclopropanes. *ACS Catal.* **8**, 2629–2634 (2018). **DOI**: 10.1021/acscatal.7b04423.

K. C. participated in the preparation and analysis of chemical substances, and reviewing and editing the manuscript.

(11) Kan, S. B. J.; Huang, X.; Gumulya, Y.; **Chen, K.**; Arnold, F. H.*, Genetically programmed chiral organoborane synthesis. *Nature* **552**, 132–136 (2017). **DOI**: 10.1038/nature24996.

K. C. participated in the preparation and analysis of chemical substances, and reviewing and editing the manuscript.

(12) Knight, A. M.; Kan, S. B. J.; Lewis, R. D.; Brandenberg, O. F.; **Chen, K.**; Arnold, F. H.*, Diverse engineered heme proteins enable stereodivergent cyclopropanation of unactivated alkenes. *ACS Cent. Sci.* **4**, 372–377 (2018). **DOI**: 10.1021/acscentsci.7b00548.

K. C. participated in the preparation and analysis of chemical substances, and reviewing and editing the manuscript.

TABLE OF CONTENTS

LIST OF TABLES

LIST OF FIGURES

ABBREVIATIONS

$[\alpha]_D$	angle of optical rotation of plane-polarized light
Å	angstrom(s)
Amp	ampicillin (in sodium salt form)
Ar	aryl group
BM3	cytochrome P450 from Bacillus megaterium (CYP102A1)
BSA	bovine serum albumin
c	concentration of sample for measurement of optical rotation
Chlor	chloramphenicol
CYP	cytochrome P450 monooxygenase identifier
de	diastereomeric excess
DFT	density functional theory
d.r.	diastereomeric ratio
E. coli	*Escherichia coli*
ee	enantiomeric excess
e.r.	enantiomeric ratio
Et	ethyl
EtOH	ethanol
GC	gas chromatography
GC-MS	gas chromatography with mass spectrometry
h	hour(s)
HB_{Amp}	Hyperbroth medium with 0.1 mg/mL ampicillin
HPLC	high performance liquid chromatography
HRMS	high resolution mass spectrometry
k	rate constant
KPi	potassium phosphate
LB_{Amp}	Luria-Bertani medium with 0.1 mg/mL ampicillin
LC-MS	liquid chromatography with mass spectrometry
M9-N	M9 minimal media with no nitrogen source added
Me	methyl
min	minute(s)
NADPH	reduced nicotine adenine dinucleotide phosphate
P450	cysteine-ligated cytochrome P450 monooxygenase
P411	serine-ligated cytochrome P450 enzyme
PDB	Protein Data Bank
Ph	phenyl
PMP	*para*-methoxyphenyl
r.r.	regiomeric ratio
RT	room temperature
TON	turnover number
t_R	retention time
TTN	total turnover number

Chapter 1

ENZYME ENGINEERING FOR NEW CATALYTIC ACTIVITIES: AN INTRODUCTION

Material for this chapter appears in: **Chen, K.**; Arnold, F. H.*, Engineering new catalytic activities in enzymes. *Nat. Catal.* **3**, 103–113 (2020).

1.1 Opening remarks

Nature has evolved an astonishing array of enzymes to catalyze the chemical transformations that enable biological systems to eke out a living in diverse environments. Enzymes synthesize biological building blocks from available elemental resources, from which more enzymes go on to assemble new life, including essential biomolecules, complex natural products and macromolecular materials. Enzymes also break down these compounds into reusable fragments. While executing their biologically-relevant functions, enzymes can, when needed, exert precise control over reaction outcomes. The unique ability of enzymes to do such 'molecular editing' has prompted addition of some of nature's catalysts to the organic synthesis toolbox[1–3].

Nature's repertoire of enzyme functions is striking – from photosynthesis to nitrogen fixation, water splitting to aliphatic carbon assembly, there are still no human-made catalysts that can match these fundamental processes of life. On the other hand, the biological world has not followed the same path as human-invented chemistry, and many valuable transformations invented by synthetic chemists have no known enzyme-catalyzed counterparts. Among other reasons, nature does not use many of our favorite transformations because the products are not useful to living systems, the required reagents do not (stably) exist in nature, or because conditions to effect the reactions are not available.

To bridge nature's catalytic repertoire and the demands of synthetic chemistry, chemists and biologists have started to import human-invented chemistry into enzymes. One approach researchers have tried is computational *de novo* enzyme design based on knowledge of the reaction transition-state structure[4,5]. Given our limited understanding of how enzymes function at an atomic level and how sequence encodes catalytic function in macromolecular design, however, an alternative avenue of engineering existing proteins has proven more successful, at least for now. Researchers are quickly unlocking new catalytic activities of existing enzymes simply by challenging and/or engineering them to work with non-natural reagents and in new environments. New activities can be released with relatively small modifications, such as introducing a different metal center or changing a few amino acids in an active site. (Perhaps this is not surprising, since it is also nature's innovation strategy.) Powerful molecular biology tools like directed evolution can then tune and diversify these new functions to provide catalysts that bring the benefits of nature's

biosynthetic machinery to chemical synthesis. This review will cover these latter efforts to engineer new enzymes by starting from nature's designs (**Fig. 1.1**).

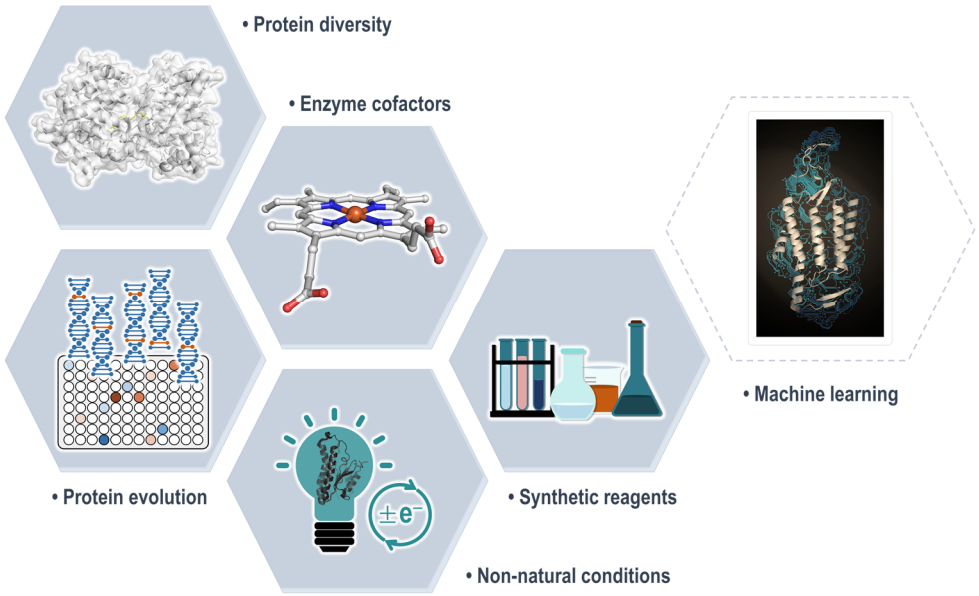

Figure 1.1. Strategies in discovery of new enzyme functions. Discovery of new enzymes, engineering and diversification of proteins by directed evolution, exploitation of cofactors for new reactivities, and use of synthetic reagents and non-natural conditions have accelerated new enzyme activity development; other advances such as machine learning will expand biocatalysts' capabilities by learning from growing gene/function databases.

A pivotal feature of enzymes, their promiscuity with respect to the substrates they accept and even the reactions they catalyze, has played a central role in the discovery and development of new biocatalytic functions. Enzymes can often accept various substrates in addition to their native one(s); they can even catalyze different transformations when offered the right reagents and environments[6]. These promiscuous activities may be left over from ancestral enzyme functions, or they may be activities that were never explored in the natural world and come simply as a result of having catalytic machinery that exhibits its hidden capabilities when the environment changes[7]. There is immense potential in nature's vast repertoire of contemporary enzymes for us to discover and use, just as nature has done for more than three billion years. Early examples with hydrolytic enzymes showed, for instance, that enzymes whose native functions are amide or ester hydrolysis can also utilize their finely tuned networks of active-site residues for hydrolysis of other bonds or even formation of new bonds[8]. More recently, chemo-mimetic approaches developed by transferring human-invented chemistries to cofactor-dependent enzymes have significantly expanded the chemical space accessible to biocatalysis. Protein engineering, using non-physiological reaction conditions, and combination of chemo- and biocatalysis have further unveiled the potential for chemical innovation in existing enzymes.

Increasing demands for efficient, selective and versatile synthetic methods call for new

enzymatic functions that may not be relevant in the biological world[9]. The challenges are daunting, requiring not only that enzymes take on new functions, but also that the newly developed biocatalysts exhibit activity and selectivity comparable to or better than current chemo-catalytic methods or that they fill gaps in synthetic chemistry. In this chapter, we summarize the current status of non-natural biocatalysis and describe how protein engineering integrated with chemical rationalization enables innovations that expand the chemical space accessible to enzymes. Creating abiological enzymatic functions represents a rising area of research that requires knowledge from different fields, including protein engineering, enzymology and synthetic chemistry. We hope this introduction will help chemists and biologists recognize, explore and use enzymes for new chemistry.

1.2 Utilizing established active sites for new enzymatic functions

Early studies of enzyme promiscuity illustrated how enzyme active sites can catalyze physiologically irrelevant chemical transformations[10]. Although different in mechanism or path of bond formation and breakage, these non-native enzyme functions are typically enabled by the superior capacity of enzyme active sites to stabilize similar transition states and precisely control key intermediates, as exemplified by a large set of hydrolytic enzymes. Many hydrolases feature an oxyanion hole, consisting of backbone amides or positively charged residues that stabilize the negative charge on a deprotonated oxygen or alkoxide in the transition state. Such structural properties allow the same hydrolases to catalyze diverse chemical reactions proceeding through oxyanionic intermediates, including aldol reactions, Michael additions, Mannich reactions, and even peroxide-involved oxidative reactions[8]. For example, in 2003, Berglund and co-workers reported that *Candida antarctica* lipase B (CAL-B) catalyzes aldol reactions between aliphatic aldehydes; they used quantum molecular modeling to illustrate the importance of the oxyanion hole in stabilizing the enolate intermediate (**Fig. 1.2.a**)[11]. Another class of hydrolase, glycosidase, was intensively investigated and engineered for promiscuous activities of glycoside synthesis: by mutating key residues such as catalytic acid/base pairs, Withers and co-workers converted a glycosidase into a glycosynthase[12] or a thioglycoligase[13] employing different α-glycosyl substrates and acceptor sugars.

The promiscuous functions of enzymes have been used for industrial production of valuable compounds. One representative example is halohydrin dehalogenase (HHDH), which in nature catalyzes epoxide formation from corresponding substituted chloro- or bromohydrins[14]. Structural studies on various HHDHs revealed several highly conserved catalytic residues in the active sites that specifically bind epoxide and halide anion. A key tyrosine residue can act as a catalytic base for hydroxyl group deprotonation or a catalytic acid for epoxide protonation, which raised the possibility that it could catalyze the reverse reaction, epoxide ring opening. Acceptance of various

nucleophiles, including azide, cyanide, nitrite, cyanate, thiocyanate and formate, and high enantioselectivity in the epoxide opening process, render HHDHs desirable catalysts for synthetic purposes, especially for preparation of enantio-enriched β-substituted alcohol and epoxide products. Among the biocatalytic applications of HHDH is the asymmetric synthesis of ethyl (*R*)-4-cyano-3-hydroxybutyrate, a precursor of atorvastatin, as reported by scientists at Codexis (**Fig. 1.2.b**)[15]. Directed evolution was used to enhance the activity of *Agrobacterium radiobacter* HHDH, enabling production of the precursor with >99.9% *ee* based on a substrate loading of 130 g·L^{-1}.

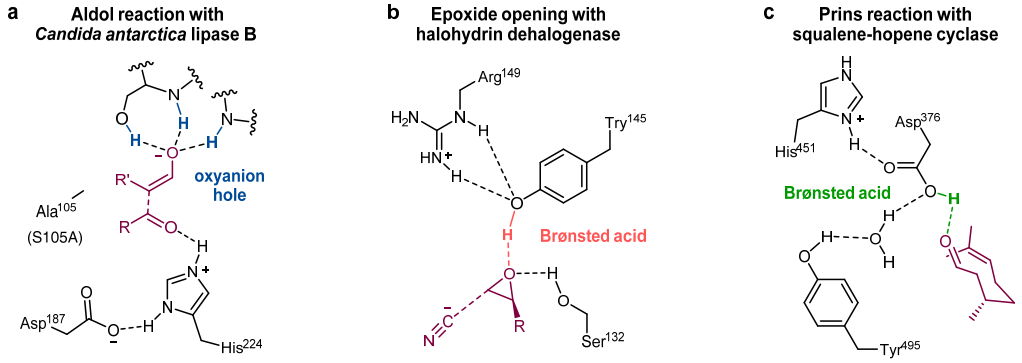

Figure 1.2. Promiscuous functions enabled by versatile active sites. a, Aldol reaction with *Candida antarctica* lipase B. **b**, Epoxide opening with halohydrin dehalogenase. **c**, Prins reaction with squalene-hopene cyclase.

The promiscuity of terpene cyclases has also attracted attention for abiological chemistry[16]. Terpene cyclases typically use acid/base catalytic residues for cationic cyclization of polyenes. Squalene-hopene cyclase (SHC), natively responsible for polycyclization of squalene to pentacyclic hopene and hopanol, has been explored as a promiscuous Brønsted-acid biocatalyst to harness a plethora of non-natural reactions driven by protonation processes. Hauer and co-workers employed SHC to construct abiological carbocyclic skeletons by using different internal nucleophilic terminators in the cyclization process[17]. Reshaping the active-site structure of SHC also allowed non-native acidic isomerizations of β-pinene, monocyclization of geraniol and Prins reaction of citronellal (**Fig. 1.2.c**)[18]. For instance, a single amino acid mutation I261A in SHC from *A. acidocaldarius* (*Aac*SHC) improved activity 11-fold for a Prins reaction of (*S*)-citronellal to an (–)-iso-isopulegol isomer product (>99% *ee* and >99% *de*). The literature offers more examples of native enzymes displaying promiscuous activities. But this scenario for searching new enzymatic activities has the obvious limitation that the new reactivity must be quite closely related to the naturally-established function.

1.3 Exploiting the catalytic potentials of organo-cofactors

Cofactor-dependent enzymes are of particular interest, as many cofactors possess expansive catalytic potential for chemical transformations. This potential has been exploited in natural

evolution to create families of enzymes whose functions cover two-electron and single-electron redox/non-redox chemistries. The protein scaffold can distinguish and direct the pathway through which a given reaction will proceed from among two or more possibilities. In this section, we will outline recent advances in realizing new chemistries with enzymes having organo-cofactors, including nicotinamide adenine dinucleotide (NADH or NADPH), flavin nucleotides (FMN or FAD), thiamine diphosphate (TDP) and pyridoxal phosphate (PLP) (**Fig. 1.3**). Reaction design and protein engineering have both promoted the discovery of new functions for these enzymes.

Nicotinamide adenine dinucleotides in their reduced form (NADH or NADPH) act as biological reducing cofactors/co-substrates of numerous oxidoreductases. For example, keto-reductases (KREDs) reduce endogenous carbonyl compounds to alcohols. NADPH-dependent imine reductases (IREDs)[19] are also physiologically capable of reducing carbon–nitrogen double bonds. Recently, Turner and co-workers identified a subclass of IREDs which catalyze imine formation from ketones and amines prior to imine reduction and named them reductive aminases (RedAms)[20]. A RedAm from *Aspergillus oryzae* (*Asp*RedAm), an IRED homologue from a eukaryotic source, was discovered to accept a broad range of structurally diverse amines and ketones, which provides an attractive biocatalytic route to secondary and tertiary amines[21].

NAD(P)H is generally recognized as a hydride donor in catalysis. But NAD(P)H was recently found to be able to implement single-electron-transfer chemistry as well. Hyster and co-workers reported an abiological asymmetric radical dehalogenation of α-bromo-α-aryl/alkyl lactones with KREDs enabled by a photo-induced electron-transfer strategy[22]. The NAD(P)H cofactor can be excited by blue light to a triplet state, which serves as a potent single-electron reductant. A single electron transfer forms a substrate radical anion, which undergoes heterolytic cleavage of a C–Br bond to generate an alkyl radical. Then $NAD(P)H^{+\bullet}$ serves as a hydrogen atom donor to afford the dehalogenated lactone product. Several KREDs were found to catalyze dehalogenation of α-bromo γ/δ-lactones in good yields and enantioselectivities. Another system based on the combination of a NADPH-dependent double bond reductase (DBR) and the photocatalyst Rose Bengal (RB) enables enantioselective radical deacetoxylation of α-acetoxyl ketones, where the enzyme plays a role in activating the substrate for electron transfer followed by deacetoxylation and hydrogen atom transfer from NADPH[23].

Flavin cofactor natively appears in the form of flavin mononucleotide (FMN) or flavin adenine dinucleotide (FAD) and is exceptionally versatile in enzymes, mediating a plethora of oxidative and reductive activities[24]. Flavin can exist in multiple redox states, including flavin-N_5-oxide (FMN or FAD oxide), oxidized flavin (quinone, FMN or FAD), flavin semiquinone ($FMNH^{\bullet}$ or $FADH^{\bullet}$), reduced flavin (hydroquinone, $FMNH_2$ or $FADH_2$), as well as flavin-C_4-peroxide (FMNOOH or FADOOH) when engaging with molecular oxygen. The protein scaffold and reaction conditions determine which states of the cofactor are accessible, leading to the diverse redox chemistry of

natural flavoenzymes.

Compared to two-electron processes catalyzed by flavoenzymes, biological reactions with a single-electron mechanism involving the semiquinone state are rare. The Hyster lab discovered a promiscuous radical dehalogenation of α-bromo esters with flavin-dependent ene-reductases (EREDs) by making use of the semiquinone state[25]. Interestingly, mutation Y177F in ERED from *G. oxydans* abolishes the native ene-reduction function in the absence of a proton donor, but significantly improves this non-native function, which further supports the radical mechanism for dehalogenation. Coupled with photoredox catalysis, EREDs could also perform ketone reduction via a radical-mediated pathway[26]. Recently, Hyster and his team further expanded the capacity of EREDs to perform photo-induced radical cyclization to make various lactams (**Fig. 1.3.a**)[27]. They reasoned that hydroquinone in the excited state can act as a single-electron reductant strong enough to activate α-chloro acetamide and generate the α-acetamide radical, which would cyclize to an *endo*-double bond and then abstract a hydrogen atom from semiquinone to form the desired lactam product. Lactam products with ring sizes ranging from 5 to 8 members were accessible via *endo*- or *exo*-cyclization processes in this system. A naturally-occurring flavin-dependent photodecarboxylase from *Chlorella variabilis* NC64A (*Cv*FAP) was discovered recently by Beisson and his team to employ a semiquinone state for a light-induced radical decarboxylation of fatty acids to alkanes or alkenes[28,29]. These newly demonstrated photoenzymatic platforms have revealed previously unknown catalytic potentials of the flavin cofactor.

The thiamine-dependent enzymes offer another good example of how promiscuous catalytic functions can be exploited, in nature and by chemists. The TDP cofactor comprises a thiazolium core, an aminopyrimidine group and a diphosphate moiety. The aminopyrimidine group acts as a key base for deprotonation of the C_2 position in the thiazolium ring, which leads to the formation of a nucleophilic thiazolium carbene and initiates all types of thiamine catalysis in nature[30]. The thiazolium carbene is a superior nucleophile for addition to carbonyl groups, resulting in an enaminol species, known as the Breslow intermediate, for a variety of nucleophilic reactions[31]. In such a way, thiamine enzymes can take electrophilic aldehydes or other carbonyl substrates, turn them into a nucleophilic form and further enable desired bond constructions.

Thiamine-dependent enzymes have been explored for abiological asymmetric C–C bond-forming reactions that take advantage of the nucleophilic feature of the Breslow intermediate. A cross-benzoin condensation between acetaldehyde (after decarboxylation of pyruvate) and benzaldehyde was achieved by Müller and co-workers using the cyclohexane-1,2-dione hydrolase (CDH) from *Azoarcus sp.* to produce chiral α-hydroxy ketone products in high enantioselectivity[32]. CDH was also engineered to accept ketones as electrophiles[33,34]. The cross-benzoin reaction between two aromatic aldehydes is particularly challenging due to the chemo-selectivity problem arising from homo-couplings and mixed cross-couplings[35]. However, benzaldehyde lyase (BAL)

from *Pseudomonas fluorescens* and a variant of benzoylformate decarboxylase (BFD) from *Pseudomonas putida* were found to catalyze this reaction, where the steric control from the *ortho*-substituted aldehyde as the electrophile substrate is key to high chemoselectivity[36]. Instead of aldehydes or ketones, α,β-unsaturated carbonyl substrates have also been investigated for this nucleophilic addition of the Breslow intermediate in a 1,4-conjugate manner (the Stetter reaction). A thiamine enzyme, PigD from *Serratia marcescens*, catalyzes acetaldehyde addition to α,β-unsaturated ketones with high enantioselectivity[37].

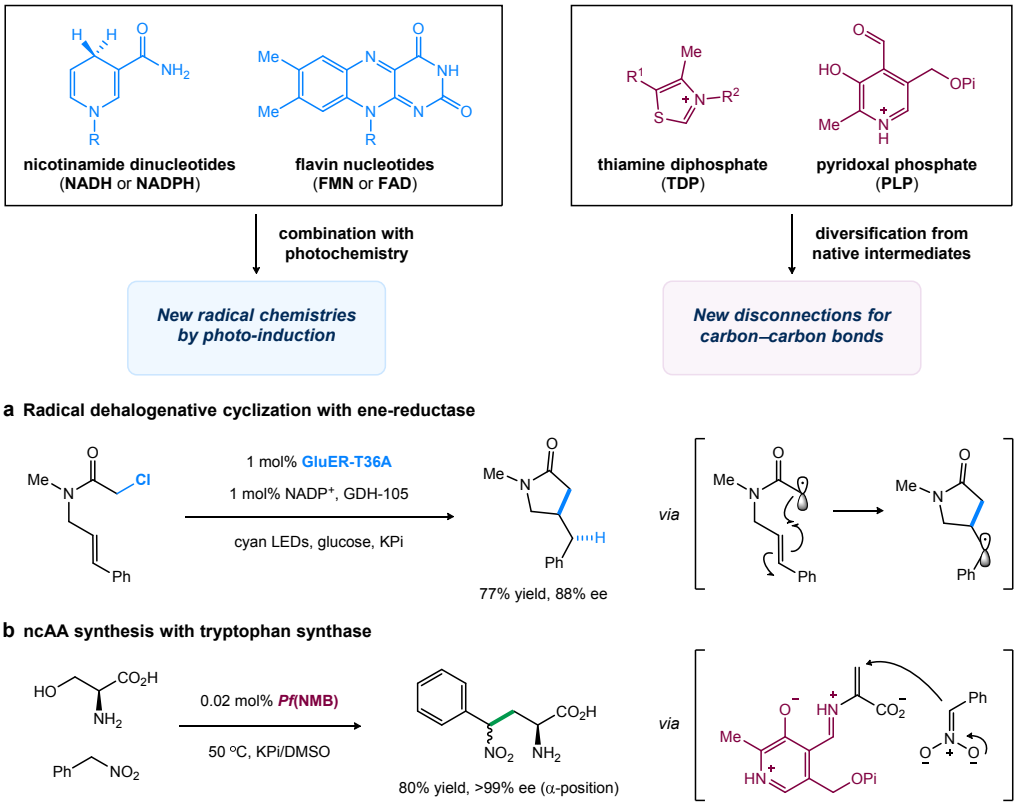

Figure 1.3. New chemistries with cofactor-dependent enzymes. a, Radical dehalogenative cyclization with ene-reductase. **b**, Non-canonical amino acid synthesis with engineered tryptophan synthase.

Pyridoxal phosphate (PLP) is another highly versatile enzyme cofactor. Taking advantage of the aldimine intermediate formed through the condensation between the aldehyde group of PLP and amino group from a substrate, PLP-dependent enzymes catalyze transamination, amino acid decarboxylation, deamination, racemization, and more. *O*-Acetylserine sulfhydrylase (OASS) is a PLP-dependent enzyme used for cysteine biosynthesis. It forms a key aminoacrylate intermediate through the loss of an acetate from the aldimine between *O*-acetylserine and PLP, and nucleophilic addition of H_2S to the aminoacrylate gives *L*-cysteine[38]. Early work reported that a variety of heteroatom-based nucleophiles could also be used by OASS to synthesize non-canonical β-substituted alanine derivatives[39].

Similar to OASS in mechanism, tryptophan synthase (TrpS) catalyzes the formation of tryptophan through addition of indole to the aminoacrylate electrophile formed with serine and

PLP in its β-subunit (TrpB). Early work demonstrated that TrpS could accept some indole derivatives or other heterocyclic nucleophiles for the synthesis of tryptophan analogues[40]. Buller and co-workers engineered the β-subunit of tryptophan synthase from *Pyrococcus furiosus* (*Pf*TrpB) to serve as a stand-alone enzyme for non-canonical amino acid (ncAA) synthesis with different nucleophiles[41,42]. Further engineering of *Pf*TrpB expanded the scope of the serine electrophile to include threonine and other β-alkyl serine derivatives for production of β-substituted tryptophan analogues[43,44]. Recently, Romney and co-workers reported that an evolved *Pf*TrpB can accommodate nitroalkane nucleophiles structurally distinct from the indole analogues, amines and thiols that were demonstrated previously (**Fig. 1.3.b**)[45]. Because the nitro group can serve as a handle for further modification, this biocatalytic strategy provides a convenient route to diverse ncAAs with aryl and alkyl side-chains.

Compared to the diversity of small-molecule catalyst scaffolds invented by chemists, nature uses a more limited set of organo-cofactors for catalysis. However, the catalytic potential of these cofactors is still far from fully discovered or explored. Different protein structures or reaction conditions may completely alter the properties of the cofactors, a feature that natural evolution has exploited to create functionally diverse enzyme families. This chemical flexibility provides opportunities to use the diverse electronic and photo-chemical properties of cofactors to develop new reaction pathways that have not been explored by nature. Taking inspiration from the studies described here, we imagine that future efforts to the cofactors described here and others such as tetrahydrobiopterin (THB)[46], 4-methylideneimidazole-5-one (MIO)[47] and prenylated flavin (prFMN)[48], will lead to the discovery of yet more functionally diverse enzymes.

1.4 Taming metalloenzymes for non-native reactions

Natural enzymes also use metal ions or metal-based cofactors to implement diverse, challenging transformations, as exemplified by nitrogenase for nitrogen fixation. The versatility of transition metal electronic states and coordination modes lays the foundation for transition metal catalysis in chemistry. This versatility also provides opportunities to develop new chemistries starting from nature's vast collection of metalloproteins.

A given metalloenzyme family can encompass diverse functions, but usually their reactions proceed via a specific type of metallo-intermediate. For instance, iron(II)- and α-ketoglutarate-dependent (Fe/αKG) enzymes employ a high-valent iron-oxo (Fe^{IV}) intermediate for C–H hydroxylation, desaturation of aliphatic hydrocarbons, epoxidation of olefins, epimerization of sp^3-hybridized carbon centers and others. SyrB2, an Fe/αKG enzyme from the syringomycin biosynthetic pathway of *Pseudomonas syringae* B301D, is responsible for C–H halogenation of the side-chain methyl group of a threonine moiety tethered with its carrier protein SyrB1[49,50].

Mechanistically, a homolytic coupling between a halogen ligand of iron and a carbon-centered radical formed through a hydrogen-atom abstraction process results in the carboN–Halogen bond formation. This halogenation activity is thought to originate from the hydroxylation activity of Fe/αKG enzyme homologues. Based on further mechanistic study, Bollinger and co-workers discovered that incorporation of a non-oxygen ligand at the iron center could lead to new enzymatic functions. Azide or nitrite anions can bind to the iron center of SyrB2, thus proceeding through radical azidation and nitration with different amino acid-based substrates[51]. These reactions still require carrier protein-appended substrates and can only occur in modest yields under single-turnover conditions, but such activity provides an unprecedented enzymatic route to C–N bond formation with aliphatic C–H bonds. Future work to identify other homologues and enzyme engineering may further expand the C–H functionalization chemistries of Fe/αKG enzymes and also allow these enzymes to accept diverse substrates for synthetic purposes[52].

Iron-oxo-mediated alkene epoxidation via oxo transfer to C–C double bonds is a well-established transformation with iron-based oxygenases, such as Fe/αKG or cytochrome P450 enzymes. Epoxidation typically follows a concerted [2+1] cycloaddition pathway with a low energy barrier. With a particular cytochrome P450, however, aldehydes were observed as side-products of this epoxidation reaction[53]. Hammer *et al.* hypothesized that this promiscuous activity resulted from a step-wise pathway of radical addition of iron-oxo to the alkene substrate, single electron transfer and a subsequent 1,2-hydride migration to deliver the *anti*-Markovnikov oxidation product[54]. Hammer then engineered this P450 from the rhodobacterium *Labrenzia aggregata* ($P450_{LA1}$) to divert the iron-oxo intermediate into this *anti*-Markovnikov oxidation over the kinetically favored epoxidation. Accumulation of mutations in the heme domain of $P450_{LA1}$ through directed evolution led to a variant, aMOx, that catalyzes the *anti*-Markovnikov oxidation of styrene to phenylacetaldehyde with 3800 TTN and 81% selectivity. By providing a chiral environment in the enzyme's active site for this step-wise oxo-transfer pathway, the first example of *enantioselective anti*-Markovnikov oxidation was demonstrated with a prochiral α-methylstyrene substrate, giving 82% ee.

The above examples demonstrate the feasibility of hijacking key intermediates in the catalytic cycles of metalloenzymes into different reaction pathways in order to access new enzymatic activities. Alternatively, one could also enable new chemistries by introducing new reactive intermediates that mimic the native intermediates, structurally and functionally[55]. Metalloporphyrin complexes have been investigated for more than half a century as structural analogues to heme cofactors in proteins. Many metalloporphyrins were developed in an effort to mimic the oxo-transfer activities of cytochrome P450s through the formation of high-valent metal-oxo intermediates[56]. Meanwhile, intermediates analogous to metal-oxo species, typically metallo-carbenes and metallo-nitrenes, could also be formed by the metalloporphyrins and used for carbene

and nitrene transfer reactions[57,58]. For instance, a precursor such as a diazo compound can react with the transition metal center (*e.g.*, iron, cobalt, rhodium, ruthenium, iridium, osmium, *etc.*) in metalloporphyrin complexes to generate a metal-carbenoid intermediate, which can undergo transfer to organic molecules[59,60]. Reasoning that translating the non-natural activities of metalloporphyrin catalysts to the corresponding heme-dependent enzymes would be a promising way to access new enzymatic activities, Coelho and co-workers described the first 'carbene transferase' enzyme in 2013 (**Fig. 1.4**)[61].

Cytochrome P450 from *Bacillus megaterium* ($P450_{BM3}$) catalyzes alkene cyclopropanation via an abiological iron-carbenoid intermediate[61]. A diazo reagent, ethyl diazoacetate (EDA), reacts with the cytochrome P450 in the Fe^{II} state and yields an iron-carbenoid intermediate; subsequent carbene transfer to styrene substrates led to the corresponding cyclopropane products. A cysteine-to-serine mutation at the heme-ligating residue furnished a new set of enzymes, designated P411s; this mutation increased the reduction potential of the ferric state of the iron center, allowing *endo*-cellular reductant NADPH to reduce the ferric state and thus conferred carbene transfer activity *in vivo* (**Fig. 1.4.a**)[62,63]. Histidine ligation was also structurally tolerated by the P450, where it accelerated cyclopropanation of acrylamide substrates[64]. Nature offers a diversity of hemeproteins, and our group and the Fasan group have demonstrated that various small hemeproteins, including protoglobin, nitric oxide dioxygenase[65] and myoglobin[66], could also be engineered to catalyze cyclopropanation reactions in high efficiency and stereoselectivity, even with electron-deficient and electron-neutral alkenes.

Aziridination via nitrene transfer to alkenes can also be achieved with P411 hemeproteins. Our group initially demonstrated aziridination of styrene-type substrates with engineered P411 variants using tosyl azide as the reactive nitrene precursor (**Fig. 1.4.a**)[67]. After this work, Ohnishi and co-workers disclosed that BezE, a cytochrome P450 in the biosynthetic pathway of benzastatin from *Streptomyces* sp. RI18, is responsible for an aziridination process via formation of an iron-nitrenoid intermediate with an *N*-acetoxy substrate and a subsequent nitrene transfer to a proximal double bond[68]. This is an excellent example of how non-natural biocatalysis can illuminate underexplored paths and lead to new discoveries in biological chemistry. In turn, the Ohnishi study inspired the Arnold group to look at hydroxylamine-type nitrene precursors, which can be more accessible and have fewer stability issues compared to the azide compounds. Recently, cytochrome *c*, an electron-transfer protein, was shown to be capable of styrene aziridination, using *O*-pivaloyl hydroxylammonia triflate as the reagent to generate a putative unprotected nitrene species[69]. Under aqueous conditions, these aziridines are labile and undergo hydrolysis to afford unprotected chiral 1,2-amino alcohols.

In carbene- and nitrene-transfer chemistries, alkene cyclopropanation and aziridination are analogous to P450s' native epoxidation activities; the abiological counterparts to C–H hydroxylation

are C–H alkylation and C–H amination. Early in the 1980s, Dawson and co-workers reported that a rabbit-liver cytochrome P450 catalyzed a nitrene C–H insertion reaction using an abiological iminoiodinane substrate as nitrene precursor with very limited turnovers[70]. Inspired by this work, McIntosh *et al.* achieved intramolecular nitrene insertion into a proximal C(sp^3)–H bond using a P411 as a whole-cell catalyst, affording sultam products in decent yield and good enantioselectivity[71]. Fasan also showed that $P450_{BM3}$[72] or myoglobin[73] variants are capable of such intramolecular C–H amination reactions. In addition, the evolved P450 variants can also function with azidoformates for intramolecular C–N bond formation, providing oxazolidinones as the amination products[74].

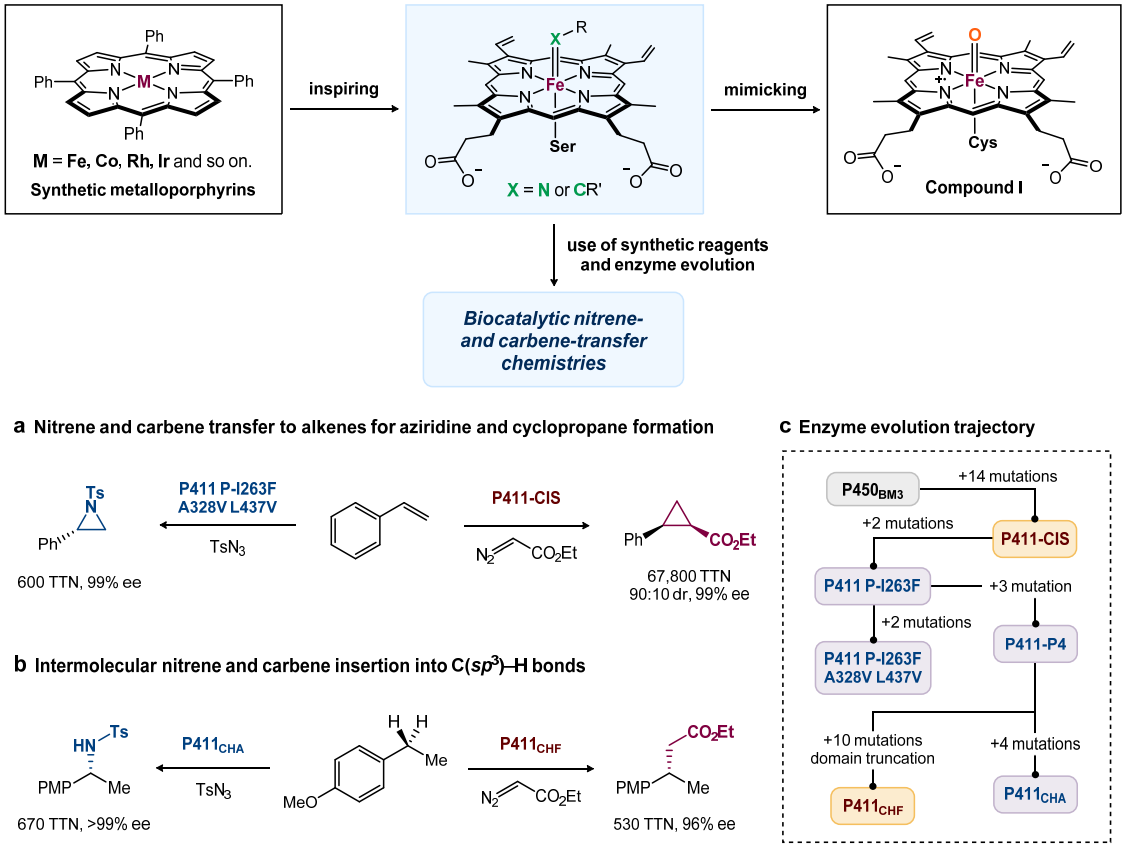

Figure 1.4. Chemo-mimetic carbene- and nitrene-transfer chemistries with engineered hemeproteins. **a**, Nitrene and carbene transfer to alkenes for aziridine and cyclopropane formation. **b**, Intermolecular nitrene and carbene insertion into C(sp^3)–H bonds. **c**, Enzyme evolution trajectory.

Engineering site-selective C–H amination is of great interest, since regioselectivity with small-molecule catalysis is usually dominated by the inherent properties of the C–H bonds. Hyster and co-workers demonstrated that the active site of P450 can be reshaped to facilitate C–H amination in a regio-divergent manner[75]. With a sulfonylazide bearing two types of C(sp^3)–H bonds geometrically accessible to amination, different P411 variants were evolved to direct intramolecular nitrene insertion to benzylic and homo-benzylic C(sp^3)–H bonds, forming 5- and 6-membered sultam products selectively. Given the differences in bond dissociation energies of the C–H bonds, the distinct product outcomes show that properly engineering the active-site environment for

catalysis can override the inherent reactivity of the C–H bonds and guide product formation along desired reaction pathways. P411s were also engineered to catalyze intermolecular nitrene C–H insertion enantioselectively[76], a problem with only limited examples of solutions with small-molecule catalysts. Accumulation of active-site mutations in a P411 enzyme helped to precisely orient the substrate in the distal pocket and accelerate the desired C–H insertion. Using tosyl azide as the nitrene precursor, evolved $P411_{CHA}$ enantioselectively aminated benzylic C–H bonds of alkyl benzene substrates (**Fig. 1.4.b** and **1.4.c**).

Carbene C–H insertion to install alkyl groups onto organic molecules is also feasible with cytochrome P411 variants[77,78]. A variant obtained in the evolutionary lineage of $P411_{CHA}$ displayed promiscuous activity for carbene insertion into C–H bonds and thus served as a parent for evolution of a powerful alkyl-transferase, $P411_{CHF}$, which can target benzylic, allylic, propargylic and α-amino C–H bonds for carbene insertion (**Fig. 1.4.b** and **1.4.c**). Interestingly, $P411_{CHF}$ alkylates a benzylic C–H bond in a substrate bearing a terminal alkene moiety, while an early P411 variant, **P**-I263F only cyclopropanates the double bond in the same molecule. This demonstration of catalyst-controlled chemoselectivity once again speaks to the high tunability of enzyme catalysis, which provides a promising solution to long-standing selectivity challenges.

Analogous to heteroatom oxidation by cytochrome P450s, electrophilic nitrene or carbene intermediates formed with hemeproteins, such as P411 or myoglobin variants, can be intercepted by sulfides to furnish sulfimides[79] and sulfonium ylides. Moreover, with prochiral allylic sulfides, the corresponding allylic sulfimide or sulfonium ylide products can further undergo [2,3]-sigmatropic rearrangement to yield chiral allylic amines[80] or chiral sulfides[81].

Another useful class of carbene-transfer reactions is X–H (X = heteroatom, including N, S, Si, B, P and others) bond insertion. Our group showed that $P450_{BM3}$ variants can catalyze *N*-alkylation of aniline substrates via a formal carbene N–H insertion process[82]; the Fasan lab also described N–H insertion[83] and S–H insertion[84] reactions with engineered myoglobins. Carbene Si–H or B–H insertion reactions provide efficient routes for building C–Si and C–B bonds, which are not found in biological systems but are useful and important in human-made products. Hemeproteins are capable of forming these bonds with much higher activities than reported for transition metal catalysts. Wild-type cytochrome *c* from *Rhodothermus marinus* (*Rma* cyt *c*) was discovered to catalyze carbene Si–H insertion using ethyl 2-diazopropanoate (Me-EDA) and phenyldimethylsilane as substrates with a modest turnover (44 TTN) but good enantioselectivity (97% ee)[85]. Introduction of three active-site mutations improved catalytic efficiency by over 30-fold. Evaluation of silane scope established that the evolved *Rma* cyt *c* is particularly selective for the desired silylation even with substrates bearing other functionalities that can participate in carbene-transfer chemistry. *Rma* cyt *c* was also engineered for enantioselective carbene B–H insertion reactions using *N*-heterocyclic carbene-stabilized boranes[86,87]. By modifying the active-site

structure of *Rma* cyt *c*, a variety of structurally different carbenes can be accommodated for this B–H insertion reaction.

With the established carbene chemistries of hemeproteins, Lewis was able to capture a carbene intermediate bound to the iron center of an *Rma* cyt *c* mutant in a crystal structure[88]. The physical chemistry study of this iron-carbenoid species together with computational investigation provided insight into how protein structure enables the desired chemistries. The Hilvert lab also characterized a different type of carbene adduct with an N_δ-methylhistidine-ligated myoglobin variant, a bridged Fe(III)–C–N(pyrrole) carbenoid, which could equilibrate with an end-on carbenoid isomer and thus participate in carbene-transfer reactions[89].

These newly-discovered carbene- and nitrene-transfer activities of hemeproteins expand nature's catalytic repertoire to include many transformations which are not biologically relevant but are highly useful for chemical synthesis. For most of the reactions described here, the free heme cofactor catalyzes the reaction not at all or only with very poor efficiency, highlighting the contribution of the protein to enabling and facilitating these transformations. Although small-molecule catalysts have been developed for many of these chemistries, hemeproteins stand out as competent catalysts with high catalytic efficiency and readily tunable stereo-/regio-/chemoselectivities. With the help of strategies to discover and improve new carbene and nitrene transferases, we foresee that hemeprotein biocatalysts will address more challenging problems in synthetic chemistry and will move to wider use at scale.

1.5 Developing new enzymes with artificial cofactors

The above examples show how small-molecule catalysis can inspire discovery of new enzyme functions. However, there are still many synthetically important reactions carried out with human-invented catalysts for which enzyme candidates have not yet been identified. Chemists have been trying to fill some of this large gap between classical catalysis and biocatalysis by incorporating catalytically competent artificial cofactors into proteins. Artificial metalloenzymes (ArMs), for example, can be traced back to the late 1970s when Wilson and Whitesides assembled an artificial metallo-hydrogenase for hydrogenation of α-acetamidoacrylic acid by introducing a biotin-tethered diphosphine-rhodium(I) complex to avidin[90]. Most early studies focused on proving that new enzymes with human-invented metallocatalysts could be made, and many functions performed by these ArMs, such as ester/amide hydrolysis, alcohol/olefin oxidation and ketone/imine/acrylate reduction, were already well-known for enzymes, despite mechanistic differences. More recently, the development of ArMs has been greatly accelerated by advances in organometallic chemistry and protein engineering. A broad range of ArMs have been created for important transformations in synthetic chemistry. A recent review from the Ward and Lewis groups comprehensively summarizes

work in the field of ArMs[91]. Here we will focus only on representative ArMs with abiological functions.

Non-covalent binding of metallo-cofactors using specific protein ligands is a strategy used widely to construct ArMs. The biotin-(strept)avidin system is a typical example, as avidin and streptavidin (Sav) feature deep binding pockets for biotin and provide a chiral environment for the catalytic center. Ward and co-workers applied this to the creation of palladium-ArMs for Suzuki-cross coupling[92] and allylic alkylation[93] and rhodium-ArMs for C–H activation/annulation reactions[94]. Based on their early work on ruthenium-ArMs for olefin metathesis[95], the team developed a system for selective assembly of artificial 'metathases' within the periplasm of *E. coli* cells through the fusion of Sav with the signal peptide OmpA[96]. This *in vivo* construction strategy substantially expedited application of directed evolution, leading to an evolved metathase with higher activity than the free 2nd-generation Grubbs catalyst towards a ring-closing metathesis reaction. Recently, the Rovis lab also reported a monomeric streptavidin (mSav) Rh(III)-ArM for enantioselective C–H activation/annulation with acrylamide hydroxamate esters and styrenes for the synthesis of a variety of substituted δ-lactams (**Fig. 1.5.a**) [97]. Artificial transfer hydrogenases (ATHases) based on iridium cofactors have been constructed with the biotin-Sav framework, and engineering the protein has enabled enantioselective reduction of ketone, imine and quinoline substrates with high efficiency[98,99]. A similar non-covalent anchoring strategy based on the high binding affinity of an iron(III)-containing azotochelin complex with protein CeuE was also employed by Duhme-Klair for the assembly of an Ir-based ATHase; interestingly, the (dis)association of the cofactor could be tuned through the different oxidation states of the iron center[100]. A recent study of an ArM created with an albumin binding protein demonstrated prodrug activation of an anticancer agent through ring-closing metathesis[101].

ArMs can also be assembled through covalent linkages of metallo-cofactors to the protein. The thiol group on cysteine is typically used as a handle for covalent assembly via nucleophilic substitution or conjugate addition, as demonstrated for the Ru-based olefin metathases reported by Hilvert[102] and Rh(I)-based olefin hydroformylase reported by Jarvis and Kamer[103]. However, selective ArM assembly with this thiol-linkage strategy is difficult when the protein has multiple accessible cysteine residues. Lewis and co-workers thus used a genetically-encoded azidophenylalanine (*p*N_3Phe) for specific coupling with strained alkyne-modified metallocofactors through click chemistry[104]. They selected a prolyl oligopeptidase (POP) featuring a large internal cavity as the protein scaffold and constructed diRh(II)-ArMs through the cycloaddition between a strained alkyne pre-installed on a dirhodium catalyst and a *p*N_3Phe residue in the active site of POP[105]. This rapid and selective assembly system allowed them to develop a practical platform to evolve diRh(II)-ArMs for stereo-selective cyclopropanation of styrenes with donor-acceptor diazos using random mutagenesis and screening (**Fig. 1.5.b**)[106].

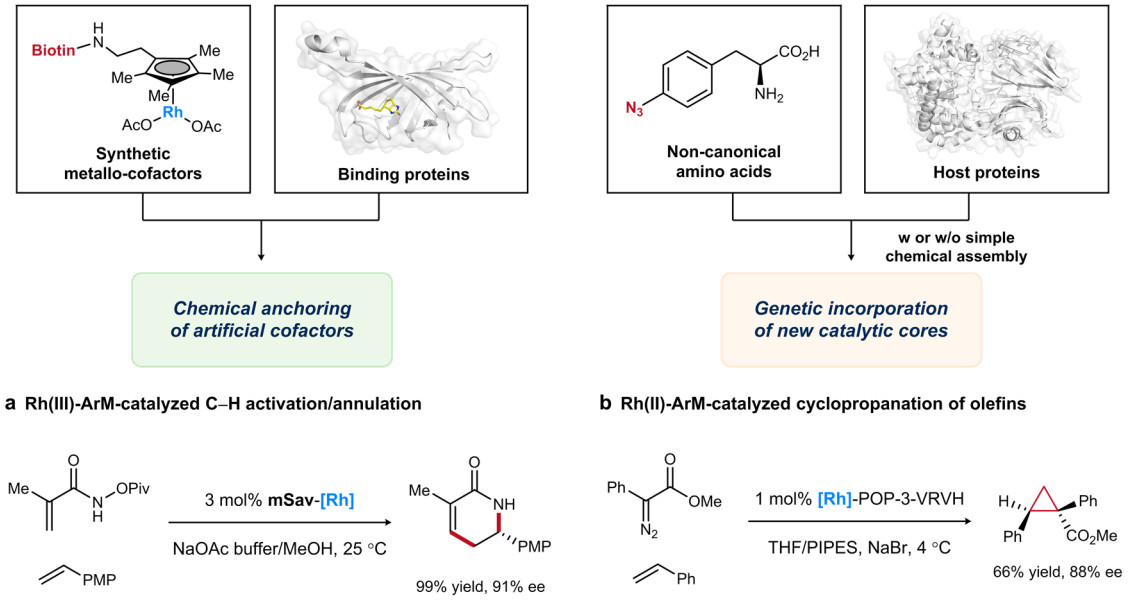

Figure 1.5. Different strategies for artificial enzyme assembly. a, Artificial Rh(III)-enzyme-catalyzed C–H activation/annulation. **b**, Artificial diRh(II)-enzyme-catalyzed olefin cyclopropanation.

Binding of metals or metal complexes with coordinating residues represents an alternative strategy for constructing ArMs. Ueno, Watanabe and co-workers reported a 'Suzukiase' enabled by ligation of a $[Pd(allyl)Cl]_2$ complex in apo-ferritin[107]. Metalation of native carbonic anhydrase (hCA) with a $[Rh(acac)(CO)_2]$ complex generated a hydroformylase, and further protein engineering helped to improve the overall enzyme activity and selectivity for the linear aldehyde product over the branched one[108]. The Roelfes group also utilized coordinating ncAAs to bind metal ions for new catalytic functions, as exemplified by the Cu(II)-ArMs for Friedel–Crafts alkylation of indoles[109] and hydration with α,β-unsaturated ketones[110]. A cofactor switch strategy has also been realized to generate ArMs. Hartwig, Clark and co-workers explored a set of iridium-substituted ArMs generated from myoglobin [111] and cytochrome P450 [112] for carbene C–H insertion reactions. Engineered Ir-ArMs are also able to carry out cyclopropanation of unactivated or internal alkenes[113] and intramolecular nitrene C–H insertion[114]. It is interesting to note that most of these functions have been demonstrated with engineered iron-hemeproteins that are fully genetically encoded.

Artificial enzymes with non-natural catalytic centers can be constituted in a fully genetically-encoded scenario using non-canonical amino acid (ncAA) incorporation. A wide range of ncAAs can now be genetically encoded and incorporated into protein scaffolds, which allows introduction of unnatural cofactors for new catalytic functions. A recent review by Budisa summarizes the development of biocatalysts using this genetic strategy[115]. Most examples only employ ncAAs to tune the properties of enzyme active sites or natural cofactors and to enhance the native catalytic functions. Until now, there are only a few examples of using catalytically functional ncAAs for new enzymatic activity, among which is the use of *p*-aminophenylalanine (*p*AF) for catalytic condensation of carbonyls with hydrazines and hydroxylamines by the Roelfes' group[116,117]. And,

recently, the Green lab designed and evolved an artificial hydrolytic enzyme using an unconventional mechanism based on a non-canonical N_δ-methylhistidine (Me-His) as the catalytically functional residue[118].

Reaction design based on the selection of suitable catalytic scaffolds together with protein engineering has produced artificial enzymes for synthetically important chemical transformations. However, compared to natural enzymes, most artificial enzymes still exhibit low catalytic efficiency with limited turnovers and are usually not as versatile as the best small-molecule catalysts for the same type of reactions. Preparation of most ArMs still requires tedious processes, including chemical synthesis of specific metal cofactors, purification of the apo-proteins followed by assembly steps, and sometimes removal of excess cofactor from the system, which render tuning by directed evolution difficult. Developing versatile, amenable, readily evolvable systems is an important challenge for future research.

1.6 Conclusion and outlook

The third wave of biocatalysis, starting in the early 1990s and empowered by directed evolution and other methods, saw solutions to many practical problems in enzyme catalysis, including enzyme stability issues, limitations in substrate breadth, efficiency, selectivity, and others[119]. These developments laid a solid foundation for widespread adoption of biocatalysis in pharmaceuticals, fine chemicals, agriculture, materials and more[120]. In a recent perspective, Bornscheuer describes a fourth wave of biocatalysis[121] with discovery of new enzyme classes and development of non-natural activities as major new directions. These efforts lead not only to a broader appreciation of enzymes' capabilities but also fulfill the demand for new, sustainable methods in organic synthesis[122].

We predict that enzymes invented in the laboratory will become powerful complements and alternatives to synthetic catalysts. For example, engineered hemeprotein carbene and nitrene transferases, unknown less than ten years ago, are capable of catalyzing diverse transformations which are also accessible with synthetic catalysts based on rhodium, iridium and other transition metals. However, directed evolution has enabled the enzymes to display orders of magnitude higher turnovers, using an earth-abundant iron center; the enzymes also have selectivities that none of the small-molecule catalysts can offer. Perhaps most exciting, the enzymes can make molecules that are inaccessible to small-molecule catalysts. It is thrilling to realize that the ability of enzymes to control reaction intermediates and specifically accelerate a desired reaction can now be used to control chemistry invented by us!

On the other hand, many of the new enzymes described here still exhibit low catalytic efficiencies, limited substrate ranges and moderate selectivities. It is reasonable to think that a

natural enzyme co-opted for new chemistry or an artificial enzyme assembled from a protein scaffold and a synthetic cofactor does not have an active site that is optimal for the entire mechanistic pathway of a new reaction. Directed evolution can step in to reorganize enzyme structures for non-natural catalysis, but this requires systems for mutagenesis and screening to identify beneficial changes in the protein sequence. We can anticipate that improved rational protein design as well as new protein engineering methods based on machine learning will help navigate the landscape of enzyme activities and protein sequence to guide further engineering with reduced experimental effort[123].

The field still has to grapple with the fact that the catalytic repertoire of enzymes is still quite restricted compared to synthetic methods. For example, organofluorine moieties are particularly important in medicinal chemistry, but until now only one class of enzyme, fluorinase, is known to catalyze a C–F bond-forming reaction with high substrate specificity[124]. Bimolecular cycloadditions, developed by synthetic chemists to build various ring structures in a modular way, are barely utilized by natural enzymes[125]. Furthermore, most newly identified enzymes are not robust enough for synthetic or industrial application. Compared to transaminases, for example, which natively catalyze C–N bond formation and are also used widely in the pharmaceutical industry[126], the recent enzymatic C–H amination strategy using nitrene transfer to a C–H bond provides a straightforward way to get to the same targets without needing a pre-installed carbonyl functionality. However, utility for synthetic purposes necessitates further improvements in the enzyme and reaction engineering; the enzymes also have to be made broadly available to users. In principle, genetically encoded catalysts are available to anyone with access to the sequence. In practice, however, few synthetic laboratories have the expertise and equipment to exploit them.

Overall, we see a bright future for enzymes in a world that needs clean, efficient catalysts. New activities will be discovered at an ever faster pace as chemists look at enzymes with their goals in mind. The current challenges are feasible and worthy targets for creative problem solvers.

Chapter 2

ENZYMATIC CONSTRUCTION OF HIGHLY STRAINED CARBOCYLES, BICYCLOBUTANES AND CYCLOPROPENES

Material for this chapter appears in: (1) **Chen, K.**; Huang, X.; Kan, S. B. J.; Zhang, R. K.; Arnold, F. H.*, Enzymatic construction of highly strained carbocycles. *Science* **360**, 71–75 (2018). (2) **Chen, K.**; Arnold, F. H.*, Engineering cytochrome P450s for enantioselective cyclopropenation of internal alkynes. *J. Am. Chem. Soc.* **142**, 6891–6895 (2020).

2.1 Abstract

Small carbocycles are structurally rigid and possess high intrinsic energy due to their significant ring strain. These unique features lead to broad applications of these structures in different fields, but also create challenges for their construction. We report the discovery and engineering of hemeproteins that catalyze the formation of chiral bicyclobutanes, one of the most strained four-membered carbocycles, *via* successive carbene addition to unsaturated carbon–carbon bonds. Enzymes that produce cyclopropenes, putative intermediates to the bicyclobutanes, were also identified. These genetically-encoded proteins are readily optimized by directed evolution, function in *Escherichia coli*, and act on structurally diverse substrates with high efficiency and selectivity (up to 5760 TTN and >99.9% ee), providing an effective route to an array of chiral strained structures. This biotransformation is easily performed on preparative scale and the resulting strained carbocycles can be derivatized, opening myriad potential applications.

2.2 Introduction

In cyclic organic molecules, ring strain arises from distortions of bond angle and bond length, steric clashes of non-bonded substituents, and other effects [127]. The simplest carbocycles, cyclopropanes and cyclobutanes, possess ring strains of 26–28 kcal/mol[128]. Introducing carbon–carbon multiple bonds or bridges to these small ring systems induces additional strain as well as structural rigidity. For example, cyclopropenes with an *endo*-cyclic double bond bear a strain of 54 kcal/mol, whereas bicyclo[1.1.0]butanes, folded into puckered structures, distinguish themselves as one of the most strained four-membered carbocycles with around 66 kcal/mol strain (**Fig. 2.1.a**). These carbocycles are particularly attractive intermediates in chemical and materials synthesis, since they can undergo strain-release transformations to furnish a myriad of useful scaffolds[129-132]. The structural rigidity imparted by strained rings in supramolecular materials can lead to interesting physical properties, such as mechanical stability [133] and high glass-transition temperature[134]. The intrinsic energy of these strained structures can also be relieved in response to exogenous force, which leads to radical changes in physical properties (*e.g.* conductivity), a feature

highly desirable for stimulus-responsive materials[135,136].

High ring strain, however, greatly increases the difficulty of synthesis. A commonly used method for preparing bicyclobutanes starts from dibromo-2-(bromomethyl)cyclopropane substructures and utilizes organolithium reagents for lithium-halogen exchange followed by nucleophilic substitution under rigorously anhydrous and cryogenic conditions. An alternative route relies on the double transfer of a carbene to alkynes, but the few examples in the literature are mostly limited to methylene carbene[137-139]. Asymmetric bicyclobutane construction is particularly challenging, with multiple chiral centers generated at the same time[140,141] (**Fig. 2.1.b**). Cyclopropene synthesis through enantioselective single carbene addition to alkynes also requires chiral transition metal catalysts based on rhodium[142,143], iridium[144] and cobalt[145]. Development of a sustainable catalytic system that performs with high efficiency and selectivity under ambient conditions would be a significant advance for construction of these useful, highly strained carbocycles.

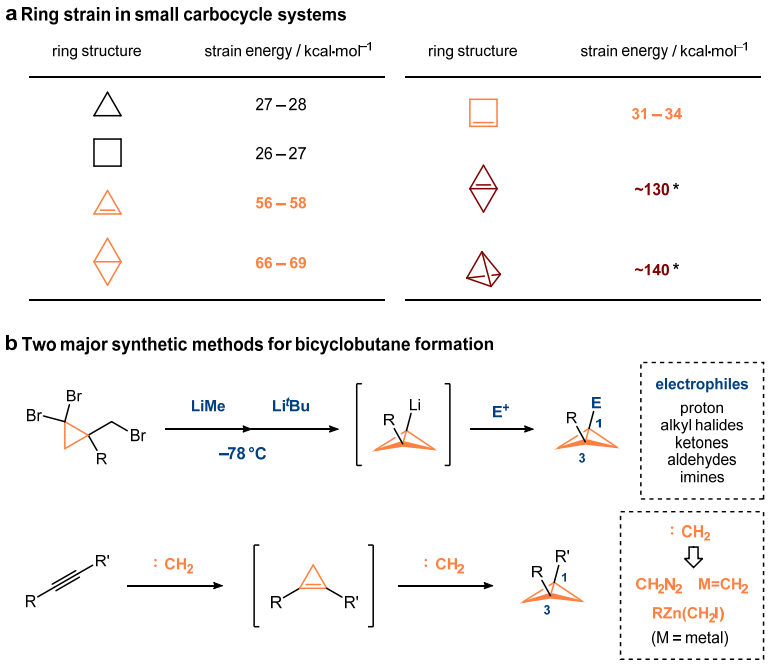

Figure 2.1. Strained carbocycles. a, Ring strain in small carbocycle systems. **b**, Two major synthetic methods for bicyclobutane formation. *Calculated strain energy values for hypothetical bicyclo[1.1.0]but-1(3)-ene and tricyclo[1.1.0.02,4]butane (tetrahedrane) structures.

Enzymes, the catalytic workhorses of biology, are capable of accelerating chemical transformations by orders of magnitude while exhibiting exquisite control over selectivity[146]. Although nature synthesizes various cyclopropane-containing products[147], cyclopropene or bicyclobutane fragments are extremely rare (**Fig. 2.2**)[148,149]. This may be attributed to the lack of biological machinery for synthesizing these motifs and/or the instability of these structures under biological or natural product isolation/purification conditions. Nevertheless, we envisioned that existing enzymes could be repurposed to forge strained carbocycles by taking advantage of their

catalytic promiscuity[6,7,10,150, 151] in the presence of non-natural substrates and by using directed evolution to increase the newly-discovered activity and selectivity[152].

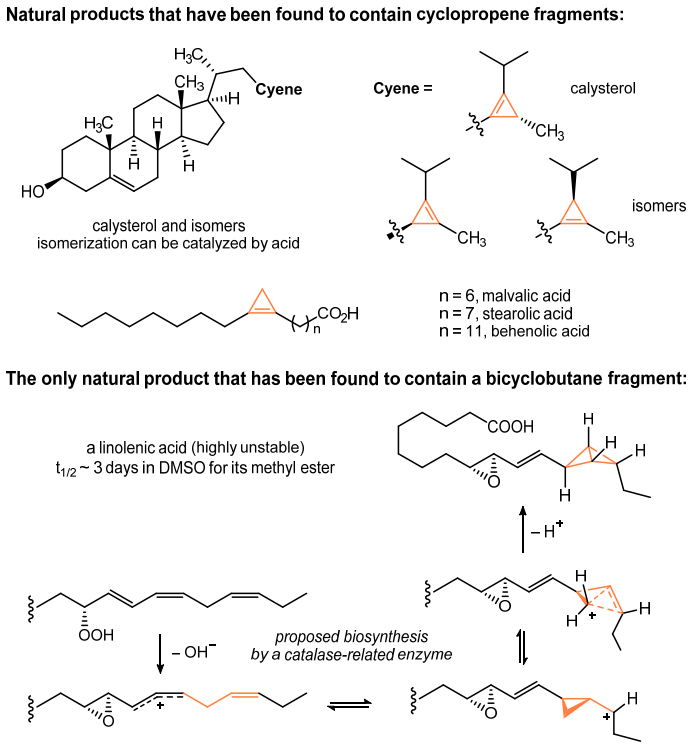

Figure 2.2. Cyclopropenes and bicyclobutanes in natural products. The proposed biosynthesis of the bicyclobutane fragment in a linolenic acid is outlined.

In the past several years, we and others have engineered natural hemeproteins to catalyze reactions not known in nature[61,62,67,71,75,76,85,86]. We hypothesized that carbene transfer to triple bonds with a heme-dependent enzyme might afford highly strained cyclopropene and bicyclobutane structures and do so enantioselectively. We anticipated several challenges at the outset, especially in bicyclobutane formation, as it involves two sequential carbene additions to the alkyne substrate: (1) the enzyme would need to bind the alkyne in a specific conformation in order to transfer the carbene enantioselectively; (2) the high-energy cyclopropene intermediate generated by the first carbene addition would need to be accepted and stabilized by the protein; (3) compared to methylene carbene used previously, a substituted carbene (*e.g.* with an ester group) might hinder access of the cyclopropene to the iron-carbenoid; and (4) the protein would also be expected to possess precise stereocontrol over the second carbene transfer step regardless of structural differences between the initial alkyne and the cyclopropene intermediate. Despite these challenges, we decided to investigate whether a starting enzyme with this unusual and non-natural activity could be identified, and whether its active site could be engineered to create a suitable environment for substrate binding, intermediate stabilization, and selective product formation.

2.3 Bicyclobutane formation from terminal aromatic alkynes

2.3.1 Identification of P411 enzymes capable of carbene transfer to alkynes

We first tested whether free heme (± bovine serum albumin), which is known to catalyze styrene cyclopropanation, could transfer carbene to an alkyne substrate. Reactions using ethyl diazoacetate (EDA) and phenylacetylene (**1a**) as substrates in neutral buffer (M9-N minimal medium, pH 7.4) at room temperature, however, gave no cyclopropene or bicyclobutane product. Next, a panel of hemeproteins including variants of cytochromes P450 and P411, cytochrome *c* and globins in the form of *E. coli* whole-cell catalysts were tested for the desired transformation under anaerobic conditions. Most of the hemeproteins tested were ineffective, except for several highly engineered P411 variants (**Table 1**). Interestingly, these P411 variants are closely related, with only a few mutations away from each other, but gave very different product outcomes (**Fig. 2.3**). Variant P411-**P** I263W, synthesized an unexpected furan product (**3b**) with a total turnover of 210. However, a related variant, P411-**P** I263F with only one mutation away, provided a product mixture of **3b** and the desired bicyclobutane product **2a**. However, several further variants, P411-**P4** and P411-**E10**, which were initially evolved for different nitrene-transfer reactions, sulfimidation[80] and C–H amination reactions[76], afforded the bicyclobutane products almost exclusively.

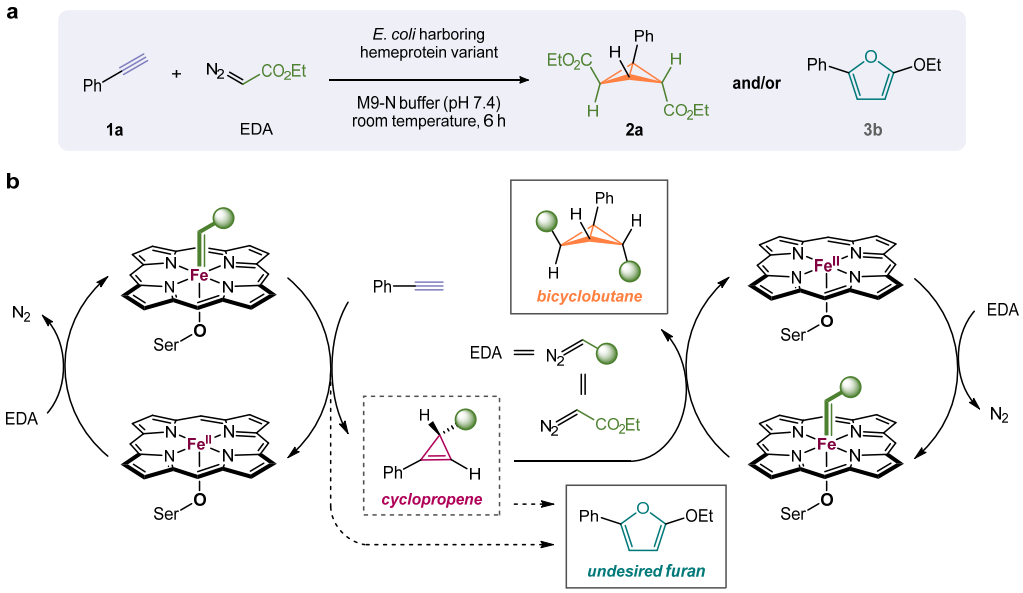

Figure 2.3. Enzymatic carbene transfer to alkynes for bicyclobutane synthesis. a, Overall reaction of carbene transfer to an alkyne catalyzed by an engineered hemeprotein. **b**, Proposed catalytic cycle of carbene transfer to phenylacetylene to form cyclopropene and bicyclobutane structures. *Simplified heme cofactor is presented here.

Since other furan analogs have been identified as adducts of carbenes and alkynes[153], we were curious as to how furan **3b** was generated and how different enzyme variants exerted different chemo-selectivity. Preliminary kinetic study of the enzymatic reaction with variant P411-**P** I263W revealed that a cyclopropene product was formed at the beginning of the reaction and then gradually disappeared as the furan adduct was slowly formed (**Fig. A-2** in **Appendix A**). This

observation suggests that the formation of the furan adduct might result from the rearrangement of the unstable cyclopropene intermediate (**3a**). Alternatively, another possible route to the furan **3b** could be via a formal [3+2] cycloaddition[154] between the carbene intermediate and the alkyne substrate, as elucidated in other metallo-carbene systems.

Table 2.1. Screening of different hemeproteins for bicyclobutane formation. *n.d. = not detected.

Hemin and negative controls		***Cytochrome c variants***	
none	n.d.	*Rma* cyt *c* wild type	n.d.
hemin	n.d.	*Rma* cyt *c* M100G	n.d.
hemin + BSA	n.d.	*Rma* cyt *c* V75T M100D M103E	n.d.
E. coli cell background	n.d.	*Hth* cyt *c* wild type	n.d.
Globin variants		*Rgl* cyt *c* wild type	n.d.
Sperm whale myoglobin	n.d.	***$P450_{BM3}$ variants***	
myoglobin H64V V68A	n.d.	P450-**CIS**	n.d.
Hell's gate globin Y29V Q50A H91N	n.d.	P411-**CIS** T268A	n.d.
Hell's gate globin K11Q Y29V Q50A	n.d.	P411-**CIS** I263W C400H	n.d.
thermoglobin	n.d.	P411-"H2-5-F10"	n.d.
neuroglobin	n.d.	P411-"H2A10"	n.d.
Bs truncated hemoglobin T45A	n.d.	P411-"H2A10" I263F A328V	n.d.
Rma nitric oxide dioxygenase (NOD)	n.d.	P450-"Hstar" H100N H92N	n.d.
Rma NOD Q52V	n.d.	P411-**CIS** T438S I263W	**3b** only
Rma NOD Y32G	n.d.	P411-**CIS** T438S I263F (**P1**)	**3b** + **2a**
Ape protoglobin	n.d.	P411-**P1** V87A A328V A268G (**P4**)	**2a** : **3b** (>50:1)
Ape protoglobin Y60G	n.d.	P411-**P4** A82L A78V F263L (**E10**)	**2a** : **3b** (>50:1)
Ape protoglobin W59A Y60G F145W	n.d.		

To gain more insight into the reaction details, we applied DFT calculations to study the reaction mechanism first with a truncated heme model. The computational study revealed a step-wise radical-addition pathway for carbene transfer to alkyne, where the resulting intermediate can easily rotate around the newly formed C–C bond, giving two conformations at similar energy levels, one eclipsed and another staggered (**Fig. A-4** in **Appendix A**). The two conformations undergo different cyclization processes, forming the cyclopropene and the furan products, respectively. Further molecular dynamic simulation in the active sites of different enzyme variants suggested that the active-site mutations, especially the residue at position 263, play a significant role in controlling the intermediate conformation, thus leading to different product outcomes (**Fig. A-5** in **Appendix A**). Further mechanistic study is still ongoing to obtain more information on reaction mechanism and selectivity.

2.3.2 Directed evolution of P411-E10 for bicyclobutane synthesis

According to the screening results, variant P411-**E10** (= **P4** A78V A82L F263L), which was engineered from **P4** for nitrene-transfer reactions, catalyzed the desired transformation with 530 TTN. NMR analysis revealed an *exo*, *endo*-configuration of the enzymatically-produced

bicyclobutane **2a**, which is distinct from the only reported achiral *endo*, *endo*-isomer, made using an osmium-porphyrin complex[155,156]. To further improve the catalytic efficiency for bicyclobutane formation, we then chose this P411-**E10** variant as the starting template for directed evolution of a more efficient bicyclobutane-constructing enzyme.

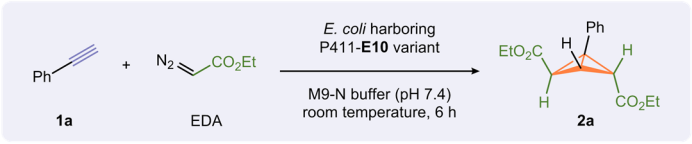

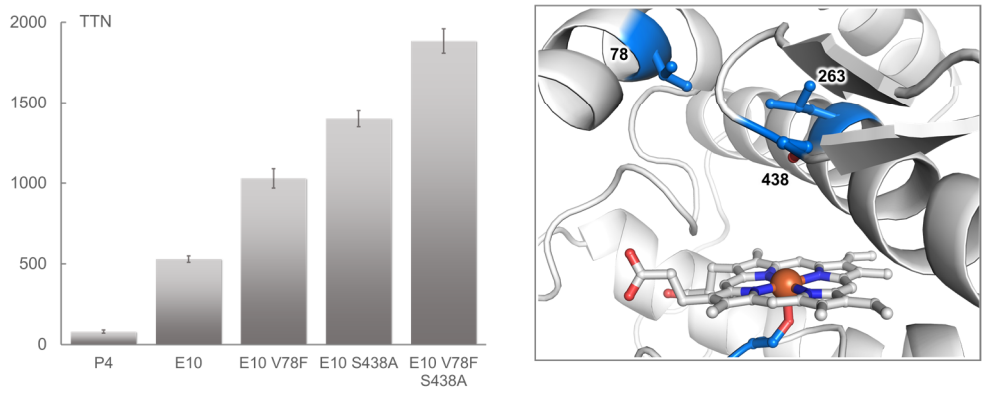

Figure 2.4. Directed evolution of P411-E10 for bicyclobutane synthesis. Active-site structure of P411-**E10** (PDB ID: 5UCW) is shown here, and amino acid residues V78, L263, S438 and S400 (heme axial ligand) are highlighted. Reactions in quadruplicate were performed on analytical scale using suspensions of *E. coli* expressing P411-**E10** variants (OD_{600} = 10–30), 10 mM phenylacetylene (**1a**), 10 mM EDA, 5 vol% EtOH, M9-N buffer (pH 7.4) at room temperature under anaerobic conditions for 6 h. TTN refers to the total desired product, as quantified by GC, divided by total hemeprotein.

As the active-site residues have been found to be important to enzyme activity and selectivity, we then performed site-saturation mutagenesis (SSM) of variant **E10** at various active-site positions and screened whole *E. coli* cells expressing the mutated proteins for improved production of bicyclobutane **2a** (**Fig. 2.4**). Specifically, as the side chain of residue 263, located right above the heme cofactor, has been found to influence the formation of the bicyclobutane product, site 263 was investigated first. However, the parent enzyme having leucine at this position (263L) turned out the most active, and other amino acid residues either lowered the reactivity towards bicyclobutane formation or delivered the furan product. In parallel, two additional residues in **E10**, V78 and S438, were also targeted by SSM. Aromatic residues were found to be activating at 78, with a phenylalanine (F) or tyrosine (Y) mutation giving 1.5 to 2-fold improvement over **E10**. This beneficial mutational effect may stem from some π-π stacking interaction between the side chain and the alkyne substrate or the cyclopropene intermediate. A single S438A mutation on a loop residing above the heme also significantly improves the catalytic efficiency, giving >2.5-fold increase in total turnover, presumably by releasing space for substrate accommodation. Finally, recombination of V78F/Y and S438A mutations led to the discovery of even more powerful biocatalysts for bicyclobutane formation; and variant **E10** V78F S438A was the most active with 1880

TTN to bicyclobutane product **2a**.

2.3.3 Evaluation of bicyclobutane scope with the evolved P411 enzyme

With the evolved **E10** V78F S438A variant in hand, we next assayed the bacterial catalyst (*E. coli* harboring **E10** double mutant) against a panel of aromatic alkyne coupling partners. Biotransformations with 10 different substrates were performed on 0.1 to 0.2 mmol scale. These preparative-scale reactions proceeded smoothly to furnish the corresponding bicyclobutanes with up to 1760 TTN and 80% yield (**Fig. 2.5.a**). Additionally, three alkynes, **1k**, **1l** and **1m**, were transformed in mmol scale, and bicyclobutanes were isolated in hundred-milligram quantities, demonstrating that the biocatalytic transformation is readily scalable. Among the 13 different substrates, the engineered P411 hemeprotein did not exhibit strong preference toward specific electronic or steric features by the substitutions on the aromatic groups. Electron-deficient halides (**2b**–**2d**), which can be used as pre-functionalities for further transformations as well as electron-rich alkyl or alkoxyl groups (**2e**–**2h** and **2k**) at *meta*- or *para*-position of the phenyl group were also accepted by this enzymatic platform. Even heterocyclic substrates such as thiophene (**2j**) served as suitable alkyne partners, albeit with lower reactivity.

Free functionalities, including alcohols (**2i** and **2m**) and a second terminal alkyne (**2l**), are well-preserved, providing an additional opportunity for derivatization of these products (**Fig. 2.5.b**). A terminal alkyne allows copper-catalyzed click chemistry, through which bicyclobutane **2l** can be modified with a simple sulfonyl azide (**4a**) or even decorated with biologically relevant fragments, such as a phenylalanine derivative (**4b**). An unprotected hydroxyl group could also offer the possibility of linkage to useful structures. In order to probe the enantiopurity of bicyclobutane products, we derivatized **2l** and **2m** with chiral molecules, *L*-azido-phenylalanine derivative and (*R*)-Mosher's acid, respectively, as the diastereomeric excess of these derivatized products would inform us the enantiomeric ratio of the bicyclobutanes. In fact, we observed only one diastereomer of derivatized bicyclobutanes **4b** and **4c** by NMR, based on further comparison to the bicyclobutane products derivatized with *D*-azido-phenylalanine derivative and (*S*)-Mosher's acid to guarantee the diastereomers can be resolved by NMR. These results suggest the specific stereocontrol by the enzyme scaffold in the two carbene-transfer steps, leading to only one stereoisomer out of four potential ones. In addition, the dicarboxylic esters on the bicyclobutane structure can be reduced easily with a mild reducing reagent, $LiBH_4$, to give a diol product **4d** with the strained ring preserved, while stronger reductants, such as $LiAlH_4$ or DIBAL, destroyed bicyclobutane structure and resulted in a cyclobutene product. The diol product **4d** allowed for the unequivocal confirmation of the bicyclobutane structure and determination of the absolute configuration through X-ray crystallography.

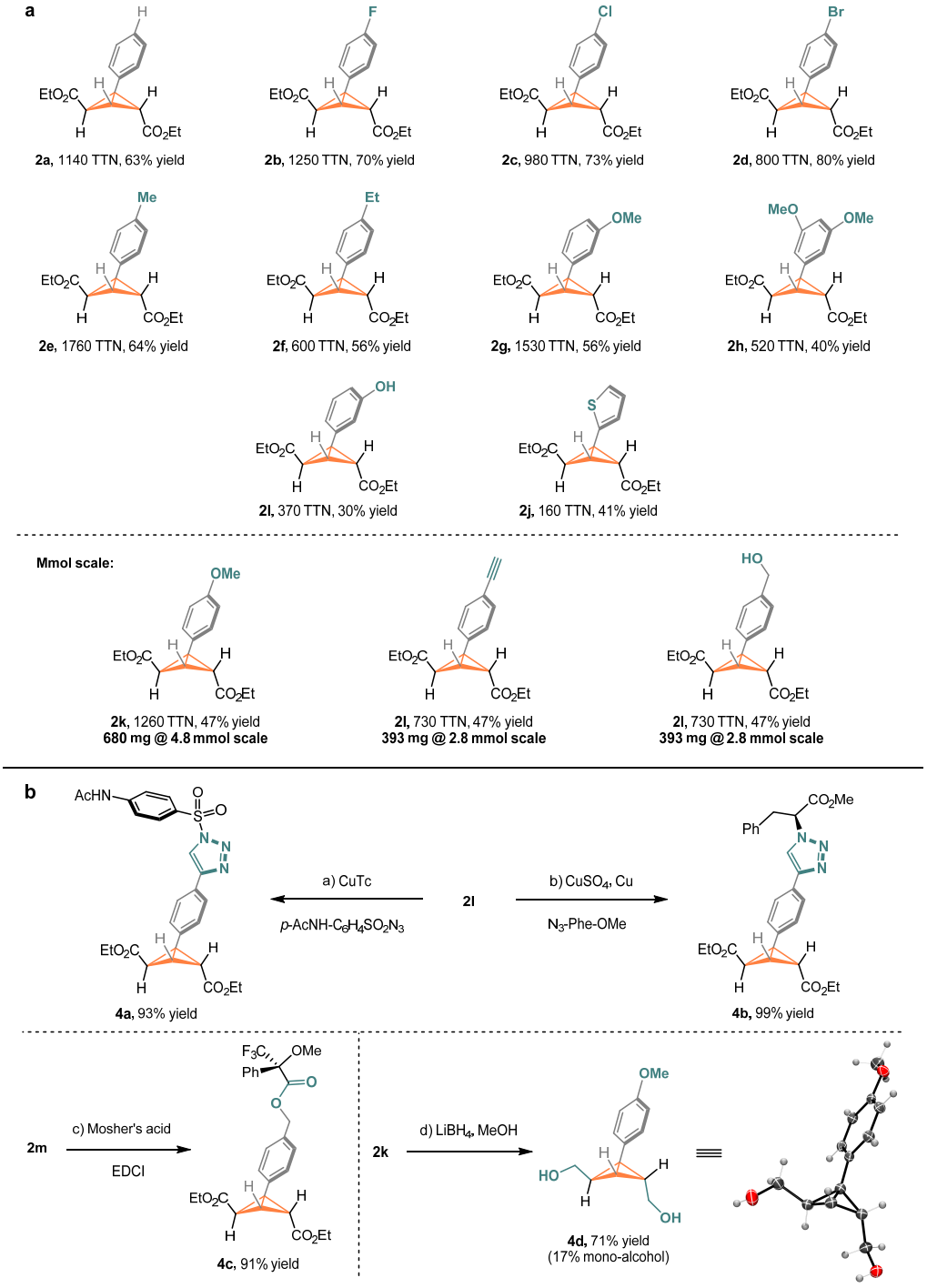

Figure 2.5. Scope of bicyclobutane formation and further derivatization of bicyclobutanes. a, Scope of P411-**E10** V78F S438A-catalyzed bicyclobutane formation. Standard conditions of preparative-scale reactions (0.1–0.2 mmol scale, unless otherwise indicated): suspension of *E. coli* (OD_{600}=15–20) expressing P411 **E10**-V78F S438A, 1.0 equiv. aromatic alkyne, 2.0–4.0 equiv. EDA, 10–15 mM *D*-glucose, 1–5 vol% EtOH, M9-N buffer (pH 7.4) at room temperature under anaerobic conditions for 12 hours. Isolated yields. TTN determined based on isolated yields. **b**, Derivatization of bicyclobutane products. a) and b) copper-catalyzed click cyclization of **2l** with azide substrates; c) esterification of **2m** with Mosher's acid; d) ester reduction of **2k** to diol with $LiBH_4$.

2.4 Cyclopropene formation from terminal aliphatic alkynes

2.4.1 Identification and evolution of P411 enzymes for cyclopropenation

Having established a biocatalytic platform for bicyclobutane construction, we next asked whether the enzyme could stop at the cyclopropene product if less reactive aliphatic alkynes are used. To this end, we examined enzyme variants from the P411-**P** lineage for cyclopropene formation, using 4-phenylbutyne (**5a**) and EDA as starting reagents. Encouragingly, **P4** catalyzed the desired cyclopropenation with 260 TTN and 91% ee. We then performed further evolution using **P4** as the engineering parent to improve its catalytic efficiency for cyclopropene synthesis.

We first targeted position 87 for site-saturation mutagenesis, as this site is known for its importance to substrate recognition in P450-catalyzed oxidation chemistries[157]. Interestingly, three mutations were observed with similar activity but very different enantioselectivities during library screening (**Fig. 2.6**). Tryptophan mutation (A87W) improved enantioselectivity to 94% ee. However, a phenylalanine mutation (A87F) completely flipped the stereo-selectivity, giving –94% ee, while only a small enantioselectivity (–24% ee) was obtained with an isoleucine mutation (A87I). It is pretty striking to us that tryptophan and phenylalanine mutations gave the opposite enantioselectivities, as they are both aromatic residues featuring similar structural and electronic properties. One possibility is that the two residues may have different orientations in the active site, therefore blocking one side for substrate approaching. However, the branched isoleucine residue does not give a clear preference on which side the substrate can approach from. Alternatively, mutations at site 87 may lead to a major effect on the orientation of the carbene intermediate, thus exerting distinct stereo-preference for cyclopropenation. No matter which scenario it is, this result has suggested that residue 87 can also exert precise stereocontrol for non-native carbene chemistry.

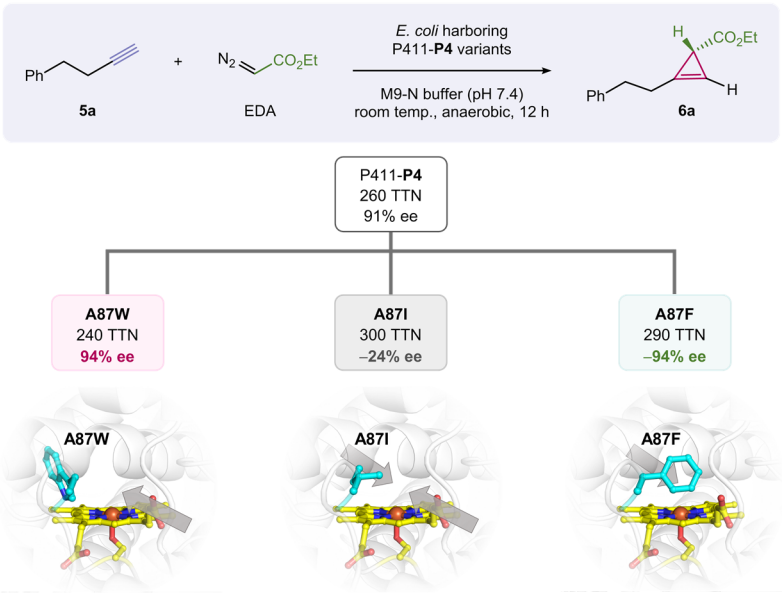

Figure 2.6. Mutational effect at site 87 on enantioselectivity of cyclopropenation. One possible scenario

is shown here to elucidate the origin of stereocontrol by residue 87.

Using **P4**-A87F and **P4**-A87W as parents, single- and double-site-saturation mutagenesis and screening were conducted sequentially to improve both reactivity and selectivity (**Fig. 2.7**). The final **K10** and **C6** variants performed with >10-fold higher reactivity compared to the initial **P4** variant and with excellent stereocontrol (99.1% ee and 99.9% ee, respectively). During the evolution, we also noticed that distinct mutations were obtained at the same sites for cyclopropenation with the opposite enantioselectivities, such as glycine (G) and phenylalanine (F) at site 437, valine (V) and proline (P) at site 327, and methionine (M) and glycine (G) at site 261. These results indicate that different orientations of substrate binding were imposed by the original mutation at site 87, and evolution helped to further reorganize the active site to improve the specificity of substrate binding and also facilitate the desired cyclopropene formation.

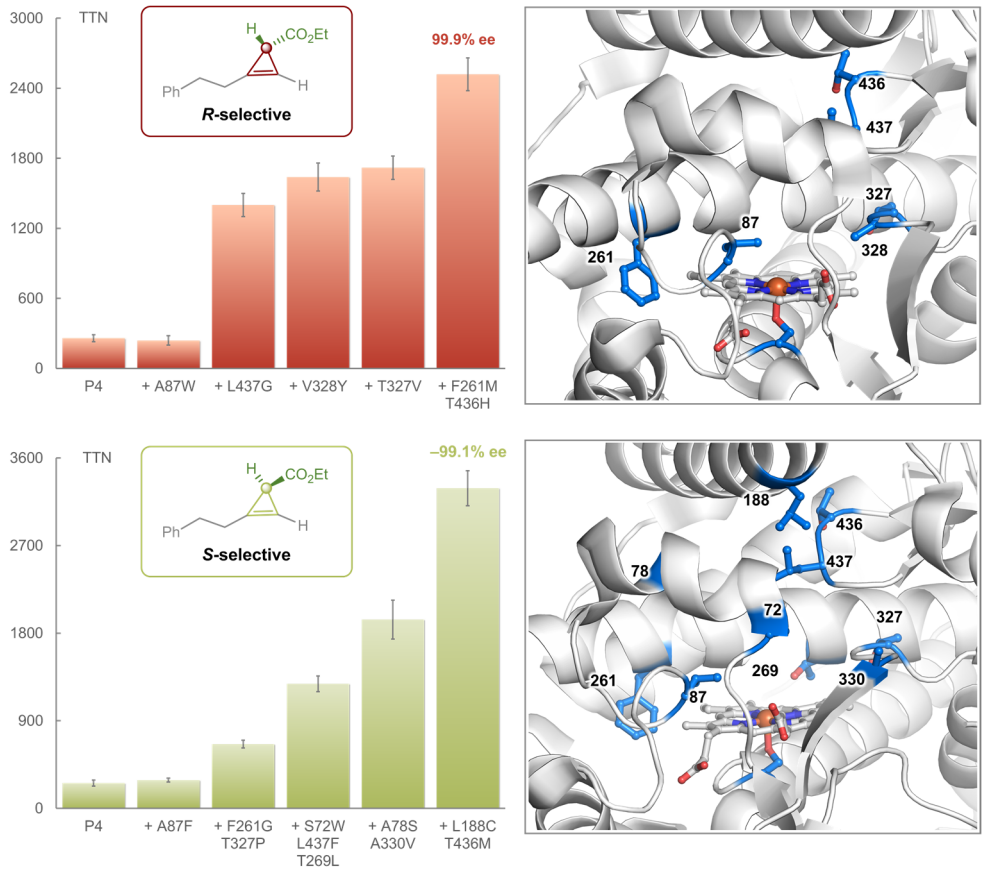

Figure 2.7. Directed evolution of P411-P4 for enantio-divergent synthesis of cyclopropenes. Active-site structure of P411-**E10** (PDB ID: 5UCW) was used to guide directed evolution, and amino acid residues targeted for mutagenesis are highlighted. Reactions in quadruplicate were performed on analytical scale using suspensions of *E. coli* expressing P411-**P4** variants (OD_{600} = 10–30), 10 mM 4-phenylbutyne (**5a**), 10 mM EDA, 5 vol% EtOH, M9-N buffer (pH 7.4) at room temperature under anaerobic conditions for 12 h. TTN refers to the total desired product, as quantified by GC, divided by total hemeprotein.

2.4.2 Scope evaluation of enzymatic cyclopropenation

With the evolved P411 enzymes for cyclopropene synthesis, we next set to evaluate the substrate range of this enzymatic platform. We focused on P411-**C6** and examined structurally diverse aliphatic alkynes. Enzymatic reactions with 12 alkynes in preparative scale (up to 5.0 mmol scale) afforded the desired cyclopropenes with TTNs ranging from hundreds to thousands and good to excellent stereoselectivities (**Fig. 2.8.a**). Alkynes with a linear carbon chain (**5b**) or cyclic fragments (**5g**, **5h** and **5j**) all served as good substrates. Different functional groups, including ether (**5f**, **5h**, **5i** and **5l**), ester (**5d**), acetal (**5e**), and chloride (**5k**), were well-tolerated. In fact, other functionalities, which can oftentimes inhibit general transition metal catalysts, such as free alcohols (**5m**), tertiary amines and heterocycles, were found to be compatible with our enzymatic system (**Fig. 2.8.a** and **Table A-7** in **Appendix A**). Further optimization of reaction conditions with slow addition of EDA, for example, would likely improve the isolated yields, as demonstrated for cyclopropene **6h** (from 66% yield to 94% yield).

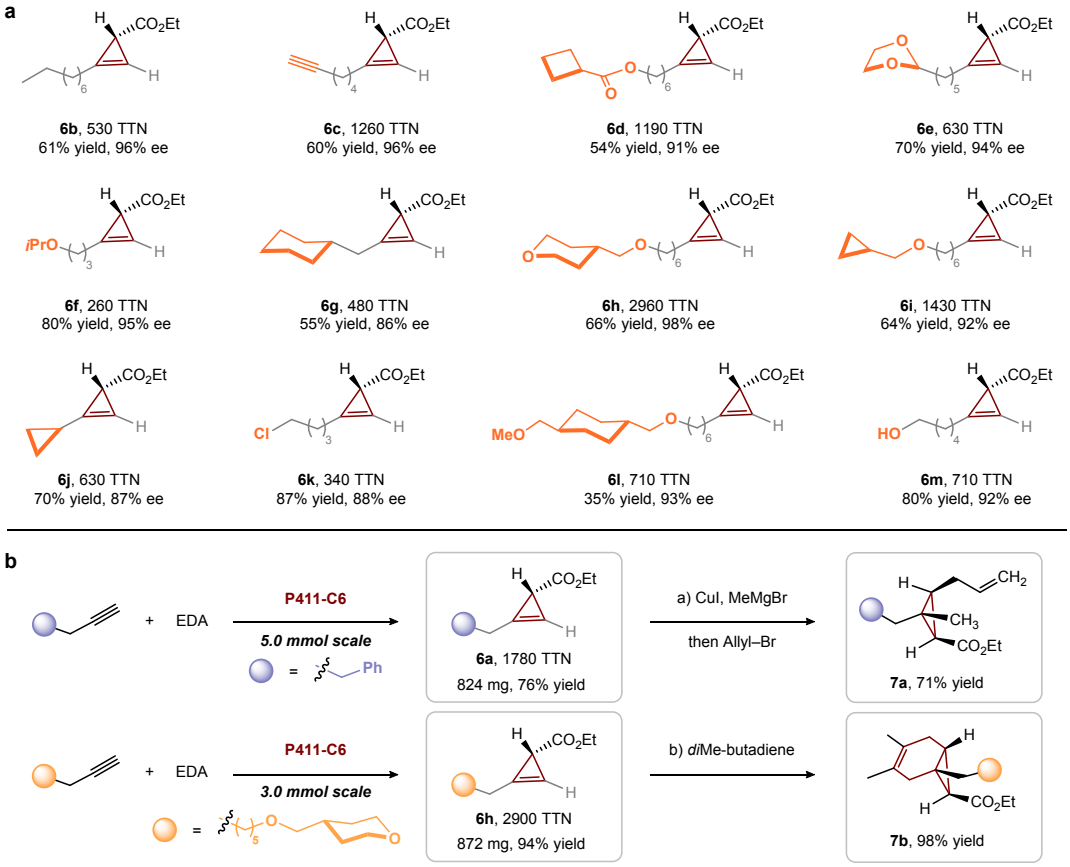

Figure 2.8. Scope of cyclopropene formation and further derivatization of cyclopropenes. a, Scope of P411-**C6**-catalyzed cyclopropene formation. Standard conditions of preparative-scale reactions (0.08–0.4 mmol scale): suspension of *E. coli* expressing P411-**C6** (OD_{600} = 10–32), 10–150 mM alkyne, 1.0–4.0 equiv EDA (6.0 equiv for **5m**), 10–15 mM *D*-glucose, 1–5 vol% EtOH, M9-N buffer (pH 7.4) at room temperature under anaerobic conditions for 12 hours. Isolated yields. TTN determined based on isolated yields and enantiomeric excess (ee) determined by chiral HPLC. **b**, Enzymatic cyclopropenation at mmol scale and derivatization of corresponding products. a) copper-catalyzed addition to cyclopropene **6a** for synthesizing a multi-substituted cyclopropane; b) Diels-Alder reaction of cyclopropene **6h** with 2,3-*di*Me-butadiene to form a fused ring system.

Cyclopropenes are used as synthetic building blocks[158], bio-orthogonal imaging precursors[159], and monomers in polymer synthesis[160]. Our ability to construct these motifs using bacteria at scale allows us to further explore their potential utility in diverse fields. Here we also present two simple transformations of cyclopropenes to build a multi-substituted cyclopropane **7a** and a fused ring system, bicyclo[4.1.0]heptene **7b** (**Fig. 2.8.b**), both of which are substructures common in pharmaceutical candidates and bioactive natural products.

2.5 Cyclopropene formation from internal alkynes

2.5.1 Background on cyclopropenation of internal alkynes

Until now, our P411 enzymes as well as small-molecule transition metal catalysts based on rhodium[141,142,161-165], iridium[144] and cobalt[145] have been shown to catalyze carbene transfer to terminal alkynes to yield enantio-enriched cyclopropenes. However, enantioselective carbene transfer to internal alkynes still remains largely unexplored. Only two systems with chiral gold/silver[166] or rhodium[167] (co-)catalysts have been reported to take internal aromatic alkynes for asymmetric cyclopropene synthesis with good stereoselectivities (**Fig. 2.9.a**). These systems require precious metal catalysts in relatively high loading together with complicated ligands and have not been shown to work with internal aliphatic alkynes. We wanted to develop an efficient biocatalytic platform that uses earth-abundant iron to access internal cyclopropenes.

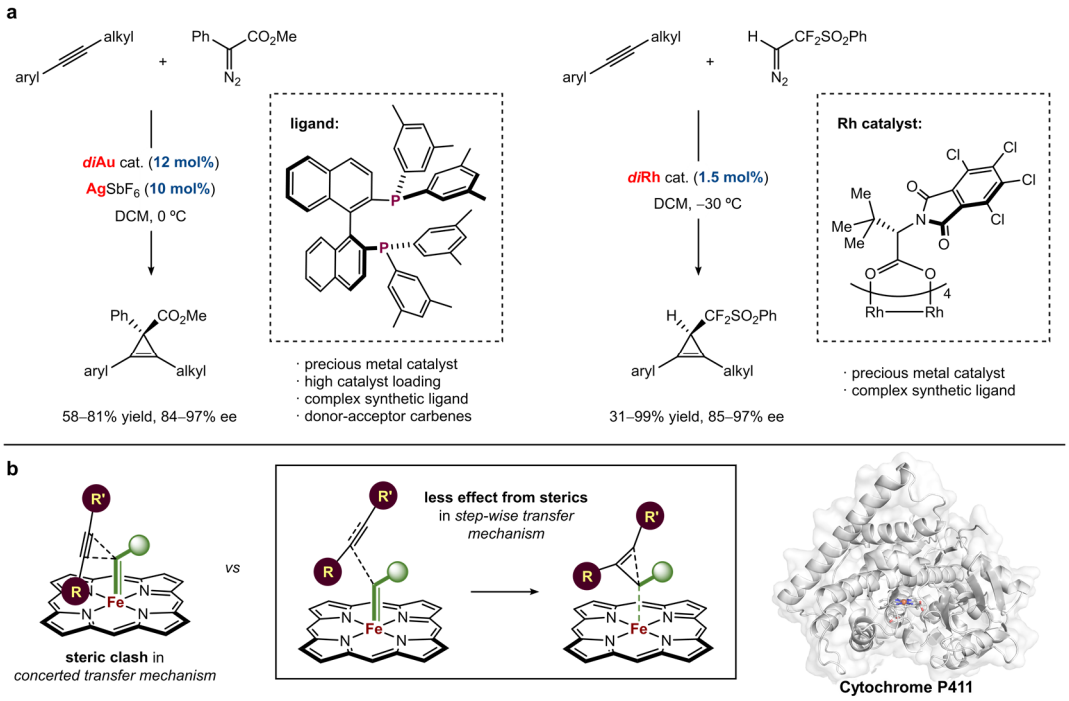

Figure 2.9. Catalytic cyclopropenation of internal alkynes. a, The only examples in literature on enantioselective cyclopropenation of internal alkynes. **b**, Rationalization of steric effect in different mechanisms of cyclopropenation with hemeprotein system.

With more and more challenging non-native reactions (based on carbene and nitrene transfers) achieved with our P450-based enzymatic platform, we hypothesized that P450 enzymes may have the potential to accomplish the difficult task, carbene transfer to internal alkynes for cyclopropene construction. The major difficulty for internal alkyne cyclopropenation lies in the severe steric clash between the linear π-system and the planar heme cofactor, especially if the reaction involves a concerted carbene-transfer mechanism[168] (**Fig. 2.9.b**). However, our previous computational study has revealed a step-wise carbene-transfer process for hemeprotein-catalyzed cyclopropenation with terminal alkynes. We thus reasoned that proper engineering of the enzyme active site may help to accommodate internal alkyne substrates and meanwhile facilitate the desired carbene transfer through a step-wise pathway to afford cyclopropene products.

2.5.2 Identification and evolution of P411 enzymes for internal cyclopropenation

We initiated investigation of internal aromatic alkyne cyclopropenation using ethyl diazoacetate (EDA) as the carbene precursor and 1-phenylbutyne (**8a**) as the model alkyne substrate. Screening various hemeprotein variants based on cytochromes P450 and P411, cytochromes *c* and globins in the form of whole *E. coli* cell catalysts identified a P411 variant, P411-**C10**, that formed the desired internal cyclopropene. P411-**C10** belongs to the family of **P411$_{CHF}$** (five amino acid substitutions away), which was evolved for a carbene C–H insertion reaction[77]. Surprisingly, the cyclopropene product **9a** synthesized by P411-**C10** was determined to be a single enantiomer, which suggests the enzyme scaffold binds the alkyne and directs carbene transfer in a well-defined orientation.

Having identified a promising enzyme, P411-**C10**, capable of cyclopropenation of an internal alkyne **8a** with modest activity (55 TTN) but excellent enantioselectivity (>99% ee), we next performed directed evolution targeting active-site residues for site-saturation mutagenesis to enhance the overall catalytic efficiency (**Fig. 2.10**). Residue 263, located right above the heme cofactor (in the heme domain), was previously found to play an important role in controlling carbene transfer to phenylacetylene using other P411 variants. To our delight, screening the enzyme library made by site-saturation mutagenesis at residue 263 yielded a tryptophan mutation at this site that improved TTN over 11 fold. Sequential mutagenesis targeting sites in the loop regions led to beneficial mutations Q437I, S72F and L436R and afforded the highly efficient variant WIRF, with 2680 TTN towards the desired cyclopropene formation.

With the evolved P411 variant, **C10**-WIRF, we evaluated the scope of internal alkynes bearing different aromatic rings or carbon chains. Unfortunately, a lot of internal alkynes with substitutions on the aromatic ring showed poor to moderate reactivities compared to the model substrate **8a**. Thinking that the evolved WIRF variant may have acquired some specificity for the non-substituted

aromatic ring or for electron-neutral/rich alkynes, we decided to use a less reactive alkyne substrate (compared to **8a**), **8b**, with an electron-deficient *para*-chloro substitution, to further evolve the enzyme (**Fig. 2.10**). A site-saturation library targeting residue 332 afforded mutation S332G, which boosted the total turnover by almost 5 fold. We reasoned that the glycine substitution might help make space in the active site to accommodate substrates with substitutions on the aromatic ring. Mutagenesis of residues spatially close to 332 was investigated, and two additional beneficial mutations, G74A and E70K, yielded the final WIRF_GAK variant with 2320 TTN for substrate **8b**.

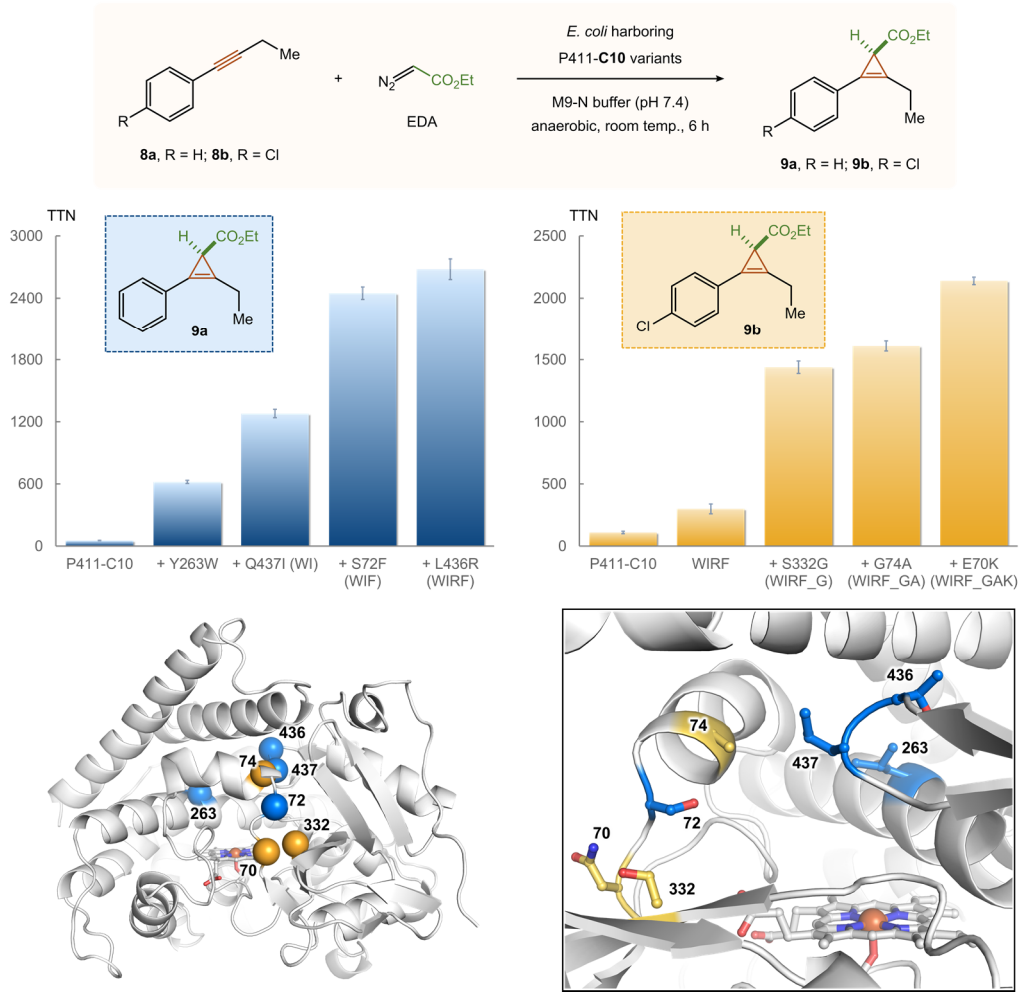

Figure 2.10. Directed evolution of P411-C10 for internal cyclopropene synthesis. Reaction conditions: 10 mM alkyne, 10 mM EDA, *E. coli* harboring P411-**C10** variants (OD_{600} = 15 to 60), D-glucose (25 mM), M9-N buffer/EtOH (19:1), anaerobic, 6 h. Product formation was quantified by GC and TTNs were determined based on protein concentration. The heme-domain structure of P411-**E10** variant (pdb: 5UCW) was used to guide site-saturation mutagenesis; mutation sites are highlighted.

To interrogate how evolution improved enzyme activity, we performed whole-cell kinetic studies using the two alkyne substrates, **8a** and **8b**, with respect to different enzyme variants (**Fig. A-3** in **Appendix A**). Comparison of the initial reaction rates established that evolution enhanced the reaction rate. Relative to parent P411-**C10**, the evolved variant WIRF catalyzed the cyclopropenation reaction of alkyne **8a** seventeen times faster; and WIRF_GAK exhibited 4.5-fold

improvement in initial rate of cyclopropenation with substrate **8b**, compared to WIRF. Evolution might have also improved the lifetime of the enzyme variants: WIRF_GAK remained fully active towards cyclopropenation of **8b** after 2 h, while the formation of product **9b** with variant WIRF slowed down after 100 min.

2.5.3 Scope study of enzymatic cyclopropenation of internal alkynes

We then revisited the substrate scope of this biocatalytic platform using the whole lineage of cyclopropene-forming enzyme variants (from **C10** to WIRF and then to WIRF_GAK) (**Fig. 2.11.a**). The WIRF variant turned out to be efficient for non-substituted or *ortho*-substituted aromatic alkynes (**8a**, **8c** and **8d**), catalyzing the desired cyclopropene synthesis with 1200 to 2670 total turnovers, while variants from later in the evolution showed impaired activity with these substrates. Although we did not specifically evolve the enzyme for activity on *meta*-substituted aromatic alkynes, variant WIRF_G exhibited improved efficiency for a *meta*-methoxyl alkyne substrate (**8f**), compared to WIRF. For aromatic alkynes bearing *para*-substitutions or *di*-substitutions (**8b** and **8g** to **8l**), the final variant WIRF_GAK catalyzes the desired transformations with unprecedentedly high efficiency compared to all previously reported systems for cyclopropene formation. For instance, an electronically-withdrawing trifluoromethyl-substituted alkyne (**8g**) was well-accepted by the enzymatic system. It is worth noting that all of the internal cyclopropenes produced enzymatically were determined to be single enantiomers (>99.9% ee for all), which further supports our hypothesis that the engineered enzymes impose a specific binding orientation of the alkyne substrate in the protein active site, allowing for efficient carbene addition to triple bonds with perfect stereocontrol.

To further demonstrate the utility of this highly stereoselective enzymatic platform, we carried out large-scale preparation of internal cyclopropenes at mmol scale (**Fig. 2.11.b**). With a simple modification of the reaction conditions using the diazo reagent in excess (2.4 equivalents added in three portions), we obtained high isolated yields of the desired cyclopropene products (90% for **9d** with variant WIRF, and 87% for **9g** with variant WIRF_GAK). Interestingly, the enzyme turnovers of the large-scale reactions are typically higher than those obtained with analytical-scale ones, indicating that the evolved enzymes in whole cells might still retain (partial) activity after the reactions and the turnovers were limited by consumption of the diazo substrate. Based on this, we also further derivatized the enzymatically-synthesized cyclopropene **9d** by sequential hydrogenation and ester reduction reactions to afford an all-*cis* cyclopropane product, which is otherwise difficult to prepare due to the *cis*-stereochemistry of the three substituents on the cyclopropane ring. As cyclopropenes are versatile building blocking, allowing for numerous transformations to furnish diverse molecular structures via strain-release processes, we anticipate that these enantio-pure cyclopropenes readily available through carbene transfer to internal alkynes

with our evolved enzymes will find applications in different fields, such as pharmaceutical development.

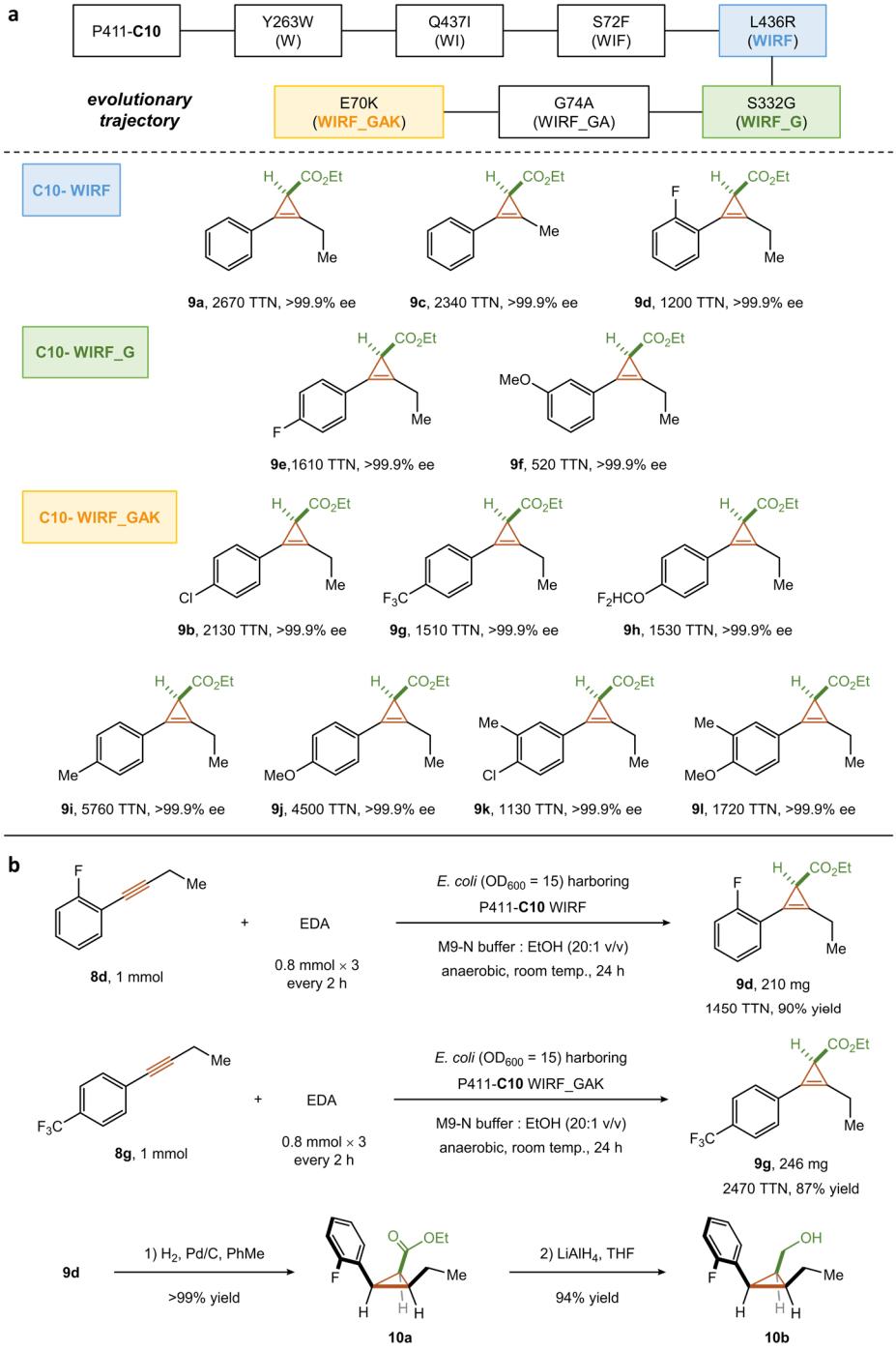

Figure 2.11. Scope of internal cyclopropene formation and further derivatization. a, Scope of P411-**C10** variants-catalyzed internal cyclopropene formation. Reactions were performed in quadruplicate under the following conditions: 10 mM alkyne, 10 mM EDA, *E. coli* harboring P411-**C10** variants (OD_{600} = 10–20), D-glucose (25 mM), M9-N buffer/EtOH (19:1), anaerobic, 16 h. Product formation was quantified by GC and TTNs were determined based on protein concentration. **b**, Preparative-scale synthesis of internal cyclopropenes and further derivatization.

2.5.4 Enzymatic cyclopropenation of internal aliphatic alkynes

Compared to internal aromatic alkynes described above, internal aliphatic alkynes are typically more challenging substrates for enantioselective cyclopropene formation in terms of reactivity and selectivity. As the aryl groups on aromatic alkynes can provide a stabilizing effect through the conjugated system in the carbene transfer process, purely aliphatic alkynes without additional intramolecular effects may suffer from a higher energy barrier for carbene transfer. Additionally, alkyl groups at the two ends of the triple bond are less easy to distinguish than the alkyl and aryl groups on aromatic alkynes. Until now, no catalytic systems have been reported for enantioselective cyclopropene synthesis with internal aliphatic alkynes. However, we believed that enzymes can accomplish this, as their active sites can provide a unique chiral environment that can recognize minor steric differences for chiral induction[169].

Testing the evolved enzymes for a cyclopropenation reaction with internal aliphatic alkyne **8m** was not fruitful, as only trace activity was detected. With the parent enzyme P411-**C10** we observed the desired cyclopropene product **9m** (**Fig. 2.12**) with only modest activity (43 TTN). This might be because the whole enzyme lineage was evolved for a set of structurally different aromatic alkynes. Further screening of variants in the **C10** family identified a triple mutant of **C10**, **C10**_VLC, which catalyzed the formation of internal cyclopropene **9m** with improved activity (64 TTN) and perfect stereocontrol (>99% ee). We anticipate that further evolution will lead to more efficient enzymes for internal aliphatic cyclopropene construction, as we have demonstrated for aromatic alkynes.

As the parent P411-**C10** enzyme was initially engineered for a carbene C–H insertion reaction, we took a deeper look at the chemoselectivity between cyclopropenation and C–H insertion[77] (**Fig. 2.12**). Internal alkyne substrate **8n**, bearing a propargylic ether group, was found to mainly undergo a carbene insertion reaction into the propargylic C–H bond with high enantioselectivity with catalyst **P411$_{CHF}$**, while a cyclopropene compound **9n** was also detected as a minor product. However, P411-**C10** reversed the chemoselectivity to favor the cyclopropene **9n** as the major product. And a third product observed in low proportion in this latter reaction was confirmed to be a furan derivative, **9n-2**, which may be generated through a [3+2]-cycloaddition[154]. After intensive screening of variants in the families of **P411$_{CHF}$** and P411-**C10**, we discovered two related variants, P411-**C11** and P411-**L8**, which could catalyze the C–H insertion reaction and the cyclopropenation reaction with even higher activity and selectivity (compared to **P411$_{CHF}$** and P411-**C10**, respectively). A **C10** triple mutant, **C10**_PVV, was found to flip the chemoselectivity to favor formation of the furan product. These variants are closely related, differing by only a few amino acid substitutions, but gave very different chemoselectivities without any specific enzyme evolution. We believe that further evolution can improve both catalytic efficiency and selectivity. These results, together with our previous demonstration of enzyme-controlled reaction selectivity between C–H insertion and cyclopropanation[77], highlight how enzyme catalysis can solve chemoselectivity problems in

synthetic methodology.

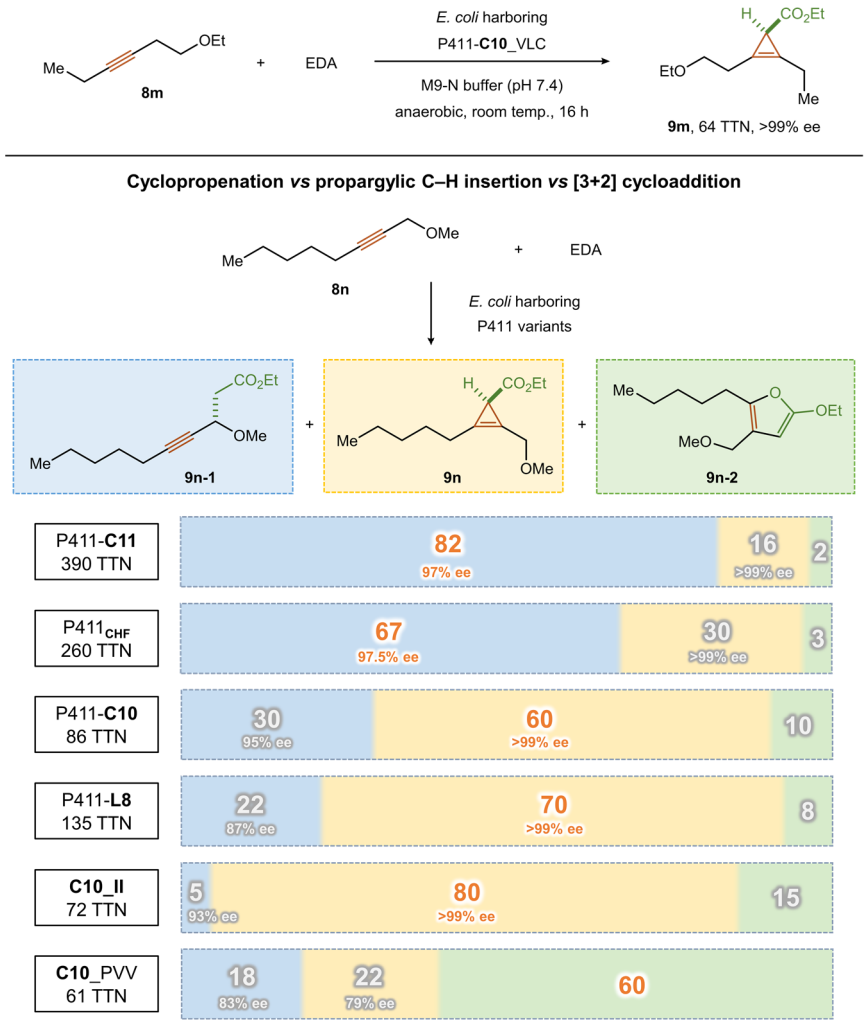

Figure 2.12. Cyclopropenation of internal aliphatic alkynes and chemoselectivity study. Reactions were performed in quadruplicate under the following conditions: 10 mM alkyne, 10 mM EDA, *E. coli* harboring P411 variants (OD_{600} = 15 to 20), D-glucose (25 mM), M9-N buffer/EtOH (19:1), anaerobic, 16 h. Product formation was quantified by GC and TTNs were determined based on protein concentration.

2.6 Conclusion

From terminal alkynes to internal alkynes, we have witnessed and explored the potential of cytochrome P450 enzymes in carbene-transfer chemistries. Engineering a set of serine-ligated P450 (P411) enzymes allowed these hemeproteins to be quickly adapted (in 2–6 mutational steps) to produce these highly strained structures, including cyclopropenes and bicyclobutanes, highlighting the superior evolvability of the P411 scaffolds and their potential to direct the construction of complex molecular architectures. Directed evolution helped to reorganize the protein structures and thus enabled these desired biotransformations through activation of iron-carbenoid for carbene addition to alkynes, stabilization of the reactive cyclopropene intermediate (in bicyclobutane formation), and precise stereocontrol of the carbene transfer processes.

With terminal alkynes, the engineered enzymatic platform carried out the transformations with a surprisingly broad substrate scope with high activity and selectivity, providing a rapid route to more than 25 strained carbocycles in preparative scale. The enzymes were also engineered to perform the desired cyclopropenation in an enantio-divergent manner through specific stereocontrol by key active-site residues. With internal alkynes, the versatile biocatalytic system also offers rapid access to an array of structurally diverse internal cyclopropenes with unprecedentedly high stereoselectivities (>99.9% ee for all) and efficiencies (up to 5670 TTN). This enzymatic platform is also readily scalable for the production of the internal cyclopropenes in preparative quantities, with even higher efficiencies compared to the analytical-scale reactions. In addition, enantioselective cyclopropenation of internal aliphatic alkynes was shown to be possible. The versatility and tunability of these hemeprotein biocatalysts was demonstrated once again with chemoselectivity that can be switched among cyclopropenation, carbene C–H insertion and [3+2] cycloaddition.

Not only has the biocatalytic platform developed here expanded the catalytic repertoire of these hemeproteins to access highly strained carbocycles, through directed evolution, but also has provided synthetic chemists a new, efficient, selective and amenable biocatalytic strategy to construct these synthetically challenging structures. We anticipate that further engineering of this enzymatic platform would likely allow us to access even broader ranges of strained carbocycles for applications in different fields, not limited to synthetic purposes but also including chemical biology, material science and others.

2.7 Experimental methods

See **Appendix A** for supporting tables and figures, synthesis and characterization of compounds, assignment of absolute stereochemistry, and determination of enantioselectivity. NMR spectra and calibration curves are in the Supporting Information of the published paper, but not included here.

2.7.1 General information

Unless otherwise noted, all chemicals and reagents were obtained from commercial suppliers (Sigma-Aldrich, VWR, Alfa Aesar, Acros, Combi-Blocks, TCI and Ark Pharm) and used without further purification. Silica gel chromatography was carried out using AMD Silica Gel 60, 230-400 mesh. ^{1}H and ^{13}C NMR spectra were taken using a Bruker Prodigy 400 MHz instrument and are internally referenced to the residual solvent peak (chloroform). Data for ^{1}H NMR are reported as follows: chemical shift (δ ppm), multiplicity (s = singlet, d = doublet, t = triplet, q = quartet, p = pentet, m = multiplet, dd = doublet of doublets, dt = doublet of triplets, ddd = doublet of doublet

of doublets), coupling constant (Hz), integration. Sonication was performed using a Qsonica Q500 sonicator. High-resolution mass spectra were obtained at the California Institute of Technology Mass Spectral Facility. Synthetic reactions were monitored using thin layer chromatography (Merck 60 gel plates) using a UV-lamp for visualization.

2.7.2 Chromatography

Analytical reversed-phase high-performance liquid chromatography (HPLC) was carried out using an Agilent 1200 series instrument and a Kromasil 100 C18 column (4.6 × 50 mm, 5 μm) with water and acetonitrile as the mobile phase and visualization at 210 nm for library screening. Analytical normal-phase HPLC was carried out using an Agilent 1200 series instrument and chiral columns Chiralpak IC (4.6 mm × 25 cm), IA (4.6 mm × 25 cm), AS-H (4.6 mm × 25 cm) and OJ-H (4.6 mm × 25 cm) with *n*-hexane and isopropanol as the mobile phase and visualization at 210 nm for chiral separation. Gas chromatography (GC) analyses were carried out using an Agilent 7820A or Shimadzu GC-17A gas chromatograph, FID detector, a J&W HP-5 column (30 m × 0.32 mm, 0.25 μm film) and CycloSil-B column (30 m × 0.25 mm, 0.25 μm film). Gas chromatography-mass spectrometry (GC-MS) analyses were carried out using a Shimadzu GCMS-QP2010SE system and J&W HP-5m column. Semi-preparative HPLC was performed using an Agilent XDB-C18 column (9.4 × 250 mm, 5 μm) with water and acetonitrile as the mobile phase.

2.7.3 Cloning and site-saturation mutagenesis

pET22b(+) containing a C-terminal 6x-His tag was used as a cloning and expression vector for all enzymes described in this study. Site-saturation mutagenesis was performed using a modified QuikChange™ mutagenesis protocol[170]. Primer sequences are available upon request. The PCR products were digested with DpnI, gel purified, and fragments were assembled using Gibson Mix[171]. The ligation mixture was used to directly transform *E. coli* strain BL21 *E. cloni*® (Lucigen). Cells were grown using Luria-Bertani medium (LB) or Hyperbroth (AthenaES) (HB) with 0.1 mg/mL ampicillin (LB_{amp} or HB_{amp}). Electrocompetent *E. coli* cells were prepared following the protocol of Sambrook *et al*[172]. T5 exonuclease, Phusion polymerase, and Taq ligase were purchased from New England Biolabs (NEB, Ipswich, MA). M9-N minimal medium (abbreviated as M9-N buffer; pH 7.4) was used as a buffering system for whole cells, lysates, and purified proteins, unless otherwise specified. M9-N buffer was used without a carbon source; it contains 47.7 mM Na_2HPO_4, 22.0 mM KH_2PO_4, 8.6 mM NaCl, 2.0 mM $MgSO_4$, and 0.1 mM $CaCl_2$.

2.7.4 Determination of hemeprotein concentration

1. **Preparation of cell lysate**: Aliquots of ~3 mL OD_{600} = 60 cells were prepared in 15 mL conical tubes, which were then placed on wet ice. Cells were lysed by sonication following the program below: sonication for 4 min, 1 second on - 1 second off, 35% amplitude. The sonicated samples were then transferred to two Eppendorf tubes, and then centrifuged down (14,000 rpm, 15 min, 4 °C). The supernatants (~2.5 mL) were then collected to a 5-mL glass vial for analysis.

2. **Hemechrome assay for protein concentration measurement**:

Method 1 (used for **2.3** and **2.4**): A solution of sodium dithionite (10 mg/mL) was prepared in M9-N buffer. Separately, a solution of 1 M NaOH (0.4 mL) was mixed with pyridine (1 mL), followed by centrifugation (10,000 × g, 30 s) to separate the excess aqueous layer to give a pyridine-NaOH solution. To a cuvette containing 700 µL protein solution (purified protein or lysate) in M9-N buffer, 50 µL of dithionite solution (0.1 M in M9-N) and 250 µL pyridine-NaOH solution were added. The cuvette was sealed with Parafilm, and the UV-Vis spectrum of the reduced Fe^{II} state was recorded immediately. To another cuvette containing 700 µL protein solution (purified protein or lysate) in M9-N buffer, 50 µL of potassium ferricyanide (0.1 M in M9-N) and 250 µL pyridine-NaOH solution were added. The cuvette was sealed with Parafilm, and the UV-Vis spectrum of the oxidized Fe^{III} state was recorded immediately. The protein concentration was determined using $\varepsilon\_[557_{reduced} - 540_{oxidized}] = 23.98\ mM^{-1}cm^{-1}$ (ref 173).

Method 2 (used for **2.5**): A solution of NaOH/pyridine was prepared by mixing 1 mL of NaOH aqueous solution (1 M), 2 mL of water and 2 mL of pyridine. To 4.5 mL of NaOH/pyridine solution, 22.5 µL of $K_3Fe(CN)_6$ aqueous solution (0.1 M) was added to make **solution 1**. A **background solution** was prepared by mixing 500 µL M9-N and 500 µL of the NaOH/pyridine solution, which was used for UV background subtraction. When measuring samples with a UV spectrometer, a spectrum of a mixed solution (oxidized spectrum) with 500 µL cell lysate + 500 µL **solution 1** was taken at the wavelength range 380 nm to 650 nm. Subsequently, 5 µL of dithionite solution (0.5 M in 0.1 M NaOH solution) was added to the same sample and mixed by pipetting; a spectrum of this solution (reduced spectrum) was taken at 380 nm to 650 nm. The protein concentration was calculated using the extinction coefficient and dilution factor (2× dilution in volume): $\varepsilon\_[557_{reduced} - 540_{oxidized}] = 23.98\ mM^{-1}cm^{-1}$.

2.7.5 Expression of P450 and P411 proteins

E. coli BL21 *E. cloni*® cells carrying a plasmid encoding a P450 or P411 variant were grown overnight in 5 mL LB_{amp} (37 °C, 250 rpm). The pre-culture was used to inoculate 45 mL of HB_{amp} in a 125 mL Erlenmeyer flask; this culture was incubated at 37 °C, 220 rpm for 2 h and 15 min. Cultures were then cooled on ice (20–40 min), and expression was induced with isopropyl β-D-1-thiogalactopyranoside (IPTG) and 5-aminolevulinic acid (ALA) with final concentrations of 0.5 mM

and 1.0 mM, respectively. Expression was conducted: (1) at 23 °C, at 130 rpm, for 18–22 h (for **2.3** and **2.4**); (2) at 24 °C, at 140 rpm, for 20 h (± 20 min) (for **2.5**). Cultures were then centrifuged (4,500 × g, 5 min, 4 °C), and the pellets were resuspended to an OD_{600} of 60 or 30 in M9-N minimal medium (no nitrogen). Aliquots of the cell suspension (3–4 mL) were used to determine the P450 and P411 expression level after lysis by sonication. The expression level in OD_{600} = 60 lysates is typically in the range of 4–14 μM for P411-**P4** or **E10** variants and 6–13 μM for P411-**C10** variants.

2.7.6 Biotransformations

The cell suspension in M9-N (with a certain OD_{600}) was degassed by sparging with argon in sealed vials or flasks for 30 min (no degassing process for **2.5**). Separately, a glucose solution (250 mM in M9-N) was degassed by sparging with argon for 30 minutes. All solutions were uncapped and transferred into an anaerobic chamber (oxygen level: < 40 ppm). Resuspended cells (340 μL) were added to 2 mL vials, followed by D-glucose (40 μL, 250 mM in M9-N), alkyne (10 μL of an EtOH stock), and EDA (10 μL of an EtOH stock). Final concentrations were typically 10.0–20.0 mM alkyne, 10.0–20.0 mM EDA (alkyne:EDA = 1:1), and 25 mM glucose; final reaction volume was 400 μL. The vials were sealed, removed from the anaerobic chamber, and shaken at room temperature and 560 or 600 rpm for a set time. After the reaction was completed and the vials removed from the anaerobic chamber, internal standard 1,3,5-trimethoxybenzene, 1,2,3-trimethoxybenzene or ethyl 2-phenylacetate (20 μL of 20 mM stock solution in toluene) was added followed by mixed solvent (hexane/ethyl acetate = 1:1, 1.0 mL). The mixture was transferred to a 1.7 mL Eppendorf tube, and then subjected to vortexing (15 s × 3) and centrifugation (14,000 rpm, 5 min) to completely separate the organic and aqueous layers. A sample of the organic layer (0.8 mL) was transferred to a vial for GC analysis. The procedures for preparative-scale enzymatic reactions are outlined in detail (See **Appendix A**).

2.7.7 Reaction screening in 96-well plate format

Libraries (single/double-site-saturation libraries generated employing the "22c-trick" method or collections of heme protein variants) were screened in 96-well plates. *E. coli* libraries for P411 variants were cultured in LB_{amp} (300 μL/well) at 37 °C, 250 rpm and 80% relative humidity overnight. HB_{amp} (950 μL/well) was inoculated with the pre-culture (50 μL/well) and incubated at 37 °C, 230 rpm, 80% humidity for 2 h and 45 min. The plates were cooled on ice for 30 minutes, and expression was induced with 0.5 mM IPTG and 1.0 mM ALA (final concentrations). Expression was conducted: (1) at 20 °C and 200 rpm for 18–22 h (for **2.3** and **2.4**); (2) at 22 °C and 220 rpm for 20 h (for **2.5**). The cells were pelleted (4,500 × g, 5 min, 4 °C) and resuspended with M9-N buffer (340 μL/well) and D-glucose solution (40 μL/well, in M9-N). The 96-well plate was then transferred to an anaerobic

chamber. In the anaerobic chamber, alkyne (10 μL/well, 400 mM in EtOH) and EDA (10 μL/well, 400 mM in EtOH) were added to the plate. The plate was sealed with an aluminum foil and shaken inside the anaerobic chamber at 560 or 600 rpm.

Bicyclobutane formation screening with terminal alkynes. After 16 h, the plate was taken out of the anaerobic chamber. The seal was removed and mixed solvent (cyclohexane/ethyl acetate = 1:1, 600 μL/well) and internal standard 1,3,5-trimethoxybenzene (20 μL/well of a toluene stock) were added. The plate was tightly sealed with a reusable silicone mat, vortexed (15 s × 3) and centrifuged (4,500 × g, 5 min) to completely separate the organic and aqueous layers. The organic layers (200 μL/well) were transferred to 300 μL vial inserts, which were then placed in 2 mL vials labeled with corresponding wells in the plate for GC or GC-MS analysis (HP-5 column, gradient from 130 °C to 280 °C, 60 °C/min, 2.5 min).

Cyclopropene formation screening with terminal alkynes. After 16 h, the plate was taken out of the anaerobic chamber. The seal was removed and acetonitrile (580 μL/well) and internal standard ethyl phenylacetate (PhEA, 20 mM in acetonitrile, 20 μL/well) were added. The plate was tightly sealed with a reusable silicone mat, vortexed (15 s × 3) and centrifuged (4,500 × g, 5 min). The supernatant (200 μL/well) was filtered through an AcroPrep 96-well filter plate (0.2 μm) into a shallow-well plate for reversed-phase HPLC analysis (Poroshell C18 column, MeCN:H_2O = 70:30, 1.2 mL/min flow, 1.7 min, 210 nm).

Cyclopropene formation screening with internal alkynes. After 6 h, the plate was taken out of the anaerobic chamber. The seal was removed and acetonitrile (580 μL/well) and internal standard *p*-methylanisole (20 mM in acetonitrile, 20 μL/well) were added. The plate was tightly sealed with a reusable silicone mat, vortexed (15 s × 3) and centrifuged (4,500 × g, 5 min). The supernatant (200 μL/well) was filtered through an AcroPrep 96-well filter plate (0.2 μm) into a shallow-well plate for reversed-phase HPLC analysis (Kromasil C18 column, MeCN:H_2O = 60:40 or 70:30, 1.2 mL/min flow, 3.2 min, 210 nm).

2.7.8 Protein purification

E. coli BL21 *E. cloni*® cells carrying a plasmid encoding a P411 variant were grown overnight in 105 mL LB_{amp} (37 °C, 250 rpm). HB_{amp} (1 L) in a 2.8 L flask was inoculated with 100 mL of the pre-culture and incubated at 37 °C and 240 rpm for 2 h and 15 min. Cultures were then cooled on ice (30 min) and induced with 0.5 mM IPTG and 1.0 mM ALA (final concentrations). Expression was conducted at 20 °C, 130 rpm, for 20 h. Cultures were then centrifuged (4,500 × g, 8 min, 4 °C) and the cell pellets frozen at –20 °C. For purification, frozen cells from two such cultures were resuspended in buffer A (25 mM Tris-HCl buffer, 20 mM imidazole, 100 mM NaCl, pH 7.5, 4 mL/g of cell wet weight), loaded with hemin (1 mg/gram wet cell weight) and powdered DNaseI, and lysed

by sonication. To pellet cell debris, lysates were centrifuged (20,000 × g, 20 min, 4 °C). Proteins were expressed in a construct containing a 6x-His tag and purified using a nickel NTA column (1 mL HisTrap HP, GE Healthcare, Piscataway, NJ) using an AKTA or AKTAxpress purifier FPLC system (GE healthcare). P411 enzymes were eluted with a linear gradient from 100% buffer A to 100% buffer B (25 mM tris, 300 mM imidazole, 100 mM NaCl, pH 7.5) over 10 column volumes. Proteins were then pooled, concentrated, and subjected to three exchanges of phosphate buffer (0.1 M KPi, pH 8.0) using centrifugal filters (10 kDa molecular weight cut-off, Amicon Ultra, Merck Millipore) to remove excess salt and imidazole. Concentrated proteins were aliquoted, flash frozen on powdered dry ice, and stored at –80 or –20 °C.

Appendix A

SUPPLEMENTARY INFORMATION FOR CHAPTER 2

Material for this chapter appears in: (1) **Chen, K.**; Huang, X.; Kan, S. B. J.; Zhang, R. K.; Arnold, F. H.*, Enzymatic construction of highly strained carbocycles. *Science* **360**, 71–75 (2018). (2) **Chen, K.**; Arnold, F. H.*, Engineering cytochrome P450s for enantioselective cyclopropenation of internal alkynes. *J. Am. Chem. Soc.* **142**, 6891–6895 (2020).

A.1 Supporting Tables A-1 to A-7

Table A-1. Detailed information of P450 variants in **2.3.1**.

variant	mutations
P450-WT (CYP102A1)[174]	-
P450-**CIS**[61]	V78A F87V P142S T175I A184V S226R H236Q E252G T268A A290V L353V I366V E442K (relative to P450-WT)
P411-**CIS**[62]	C400S (relative to P450-**CIS**)
P411-"**H2-5-F10**"	L75A I263A L437A (relative to P411-**CIS**)
P411-"**H2A10**"	L75A L181A (relative to P411-**CIS**)
P411-"**H2A10**" I263F A328V	L75A L181A I263F A328V (relative to P411-**CIS**)
P450-**Hstar** H100N H92N[175]	V78M H92N H100N L181V T268A C400H L437W (relative to P450-WT)
P411-**CIS** T438S (**P**)[67]	T438S (relative to P411-**CIS**)
P411-**CIS** T438S I263W	I263W T438S (relative to P411-**CIS**)
P411-**P1**[75]	I263F T438S (relative to P411-**CIS**)
P411-**P2**[80]	I263F A328V T438S (relative to P411-**CIS**)
P411-**P3**	V87A I263F A328V T438S (relative to P411-**CIS**)
P411-**P4**	V87A I263F A268G A328V T438S (relative to P411-**CIS**)
P411-"A82L"	A82L V87A I263F A268G A328V T438S (relative to P411-**CIS**)
P411-**E10**[76]	A78V A82L V87A I263L A268G A328V T438S (relative to P411-**CIS**)

Table A-2. P411 variants with activities of carbene transfer to alkyne in **2.3.1**.

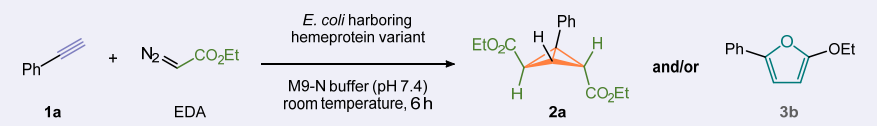

variant	activities
P411-**P**	-
P411-**P** I263W	210 ± 20 TTN, **3b** only
P411-**P1**	low activity (<20 TTN), **3b**:**2a** ~ 2:1
P411-**P2**	23 ± 8 TTN, **2a**:**3b** ~ 10:1
P411-**P3**	60 ± 10 TTN, **2a**:**3b** > 20:1
P411-**P4**	80 ± 10 TTN, **2a**:**3b** > 50:1

P411-"A82L"	280 ± 30 TTN, **2a**:**3b** > 50:1
P411-**E10**	530 ± 20 TTN, **2a**:**3b** > 50:1

Note: TTNs reported are the average of biological replicates from enzymatic reactions using whole-cell catalysts (at OD_{600}=30). The errors in all tables are standard deviations.

Table A-3. Directed evolution of P411-**E10** in **2.3.2**.

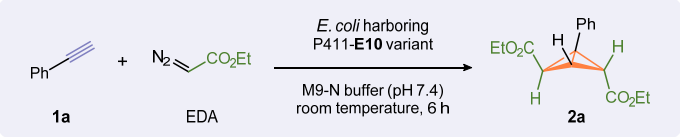

P411 variants	TTN
P411-**P4**	80 ± 10
P411-"A82L"	280 ± 20
E10	530 ± 20
E10-V78Y	800 ± 30
E10-V78F	1030 ± 60
E10-S438A	1400 ± 50
E10-V78Y S438A	1560 ± 70
E10-V78F S438A	1880 ± 80

Note: The TTNs were obtained for OD_{600}=30 for P411-**P4**, P411-"A82L" and P411-**E10** variants, OD_{600}=15 for **E10**-V78Y and **E10**-V78F variants, and OD_{600}=10 for **E10**-S438A, **E10**-V78Y S438A and **E10**-V78F S438A variants. TTNs reported are the average of biological duplicates. Each biological set contains four experiments. The errors in all tables are standard deviations.

Table A-4. Directed evolution of P411-**P4** in **2.4.1**.

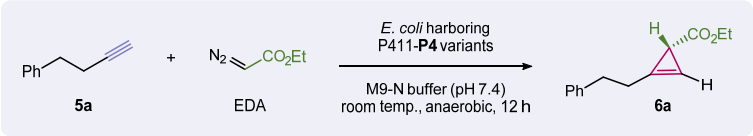

P411-**P4** variants	TTN	ee
P4	260 ± 30	+91.0%
P4-A87F (**K1**)	290 ± 20	–94.0%
K1-F261G T327P (**K3**)	660 ± 40	–94.8%
K3-S72W L437F (**K5**)	1100 ± 120	–95.8%
K5-T269L (**K6**)	1280 ± 80	–96.2%
K6-A78S A330V (**K8**)	1900 ± 200	–98.9%
K8-L188C T436M (**K10**)	3300 ± 180	–99.1%
P4-A87W (**C1**)	240 ± 40	+94.2%
C1-L437G (**C2**)	1400 ± 100	+98.7%
C2-V328Y (**C3**)	1600 ± 120	+99.6%

C3-T327V (**C4**)	1700 ± 100	+99.8%
C4-F261M T436H (**C6**)	2500 ± 140	+99.9%

Note: The TTNs were obtained for OD_{600}=60 for P411-**P4**, **C1** and **K1** variants, OD_{600}=30 for **K3**, **K5**, **K6**, **C2**, **C3** and **C4** variants, and OD_{600}=15 for **K8**, **K10** and **C6** variants. TTNs reported are the average of biological duplicates. Each biological set contains four experiments. The errors in all tables are standard deviations.

Table A-5. Directed evolution of P411-**C10** in **2.5.2**.

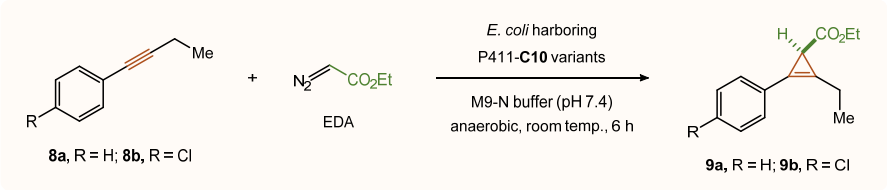

8a, R = H; **8b**, R = Cl

9a, R = H; **9b**, R = Cl

P411-C10 variant (with substrate **8a**)	**TTN**	**ee**
C10	55 ± 2	>99%
C10-Y263W (**W**)	620 ± 15	>99.9%
C10-A87V	110 ± 10	>99.9%
C10-Y263W Q437I (**WI**)	1280 ± 40	>99.9%
C10-Y263W Q437I S72F (**WIF**)	2450 ± 60	>99.9%
C10-Y263W Q437I L436R S72F (**WIRF**)	2680 ± 100	>99.9%

Note: The TTNs were obtained for OD_{600}=60 for P411-**C10**, OD_{600}=30 for **C10-W**, and OD_{600}=15 for the rest. TTNs reported are the average of four experiments. The errors in all tables are standard deviations.

P411-C10 variant (with substrate **8b**)	**TTN**	**ee**
C10	110 ± 10	>99%
WIRF	300 ± 10	>99%
WIRF-S332G (**WIRF_G**)	1440 ± 40	>99.9%
WIRF-S332G G74A (**WIRF_GA**)	1610 ± 50	>99.9%
WIRF-S332G G74A E70K (**WIRF_GAK**)	2140 ± 40	>99.9%

Note: The TTNs were obtained for OD_{600}=30 for P411-**C10** and **WIRF**, OD_{600}=20 for the rest. TTNs reported are the average of four experiments. The errors in all tables are standard deviations.

Table A-6. List of mutations in P411 variants involved in Chapter 2.

P411 variant	**Mutations relative to wild-type $P450_{BM3}$**
P4	V78A F87A P142S T175I A184V S226R H236Q E252G I263F T268G A290V A328V L353V I366V C400S T438S E442K
"A82L"	V78A **A82L** F87A P142S T175I A184V S226R H236Q E252G I263F T268G A290V A328V L353V I366V C400S T438S E442K
E10	A82L F87A P142S T175I A184V S226R H236Q E252G I263L T268G A290V A328V L353V I366V C400S T438S E442K

E10-V78Y	**V78Y** A82L F87A P142S T175I A184V S226R H236Q E252G I263L T268G A290V A328V L353V I366V C400S T438S E442K
E10-V78F	**V78F** A82L F87A P142S T175I A184V S226R H236Q E252G I263L T268G A290V A328V L353V I366V C400S T438S E442K
E10-S438A	A82L F87A P142S T175I A184V S226R H236Q E252G I263L T268G A290V A328V L353V I366V C400S **T438A** E442K
E10-V78Y S438A	**V78Y** A82L F87A P142S T175I A184V S226R H236Q E252G I263L T268G A290V A328V L353V I366V C400S **T438A** E442K
E10-V78F S438A	**V78F** A82L F87A P142S T175I A184V S226R H236Q E252G I263L T268G A290V A328V L353V I366V C400S **T438A** E442K
K1	V78A P142S T175I A184V S226R H236Q E252G I263F T268G A290V A328V L353V I366V C400S T438S E442K
K3	V78A P142S T175I A184V S226R H236Q E252G **F261G** I263F T268G A290V **T327P** A328V L353V I366V C400S T438S E442K
K5	**S72W** V78A P142S T175I A184V S226R H236Q E252G **F261G** I263F T268G A290V **T327P** A328V L353V I366V C400S **L437F** T438S E442K
K6	**S72W** V78A P142S T175I A184V S226R H236Q E252G **F261G** I263F T268G **T269L** A290V **T327P** A328V L353V I366V C400S **L437F** T438S E442K
K8	**S72W V78S** P142S T175I A184V S226R H236Q E252G **F261G** I263F T268G **T269L** A290V **T327P** A328V **A330V** L353V I366V C400S **L437F** T438S E442K
K10	**S72W V78S** P142S T175I A184V **L188C** S226R H236Q E252G **F261G** I263F T268G **T269L** A290V **T327P** A328V **A330V** L353V I366V C400S **T436M L437F** T438S E442K
C1	V78A **F87W** P142S T175I A184V S226R H236Q E252G I263F T268G A290V A328V L353V I366V C400S T438S E442K
C2	V78A **F87W** P142S T175I A184V S226R H236Q E252G I263F T268G A290V A328V L353V I366V C400S **L437G** T438S E442K
C3	V78A **F87W** P142S T175I A184V S226R H236Q E252G I263F T268G A290V **A328Y** L353V I366V C400S **L437G** T438S E442K
C4	V78A **F87W** P142S T175I A184V S226R H236Q E252G I263F T268G A290V **T327V A328Y** L353V I366V C400S **L437G** T438S E442K
C6	V78A **F87W** P142S T175I A184V S226R H236Q E252G **F261M** I263F T268G A290V **T327V A328Y** L353V I366V C400S **T436H L437G** T438S E442K
P411-**C10**	N70E A74G V78L A82L F87A M118S P142S F162L T175I M177L A184V S226R H236Q E252G I263Y H266V T268G A290V A328V A330Y L353V I366V C400S I401L T436L L437Q E442K ΔFAD
P411$_{CHF}$	N70E A74P V78L A82L F87A P142S T175I M177L A184V S226R H236Q E252G I263Y H266V T268G A290V A328V A330Y L353V I366V C400S T436L E442K ΔFAD
C10-W	N70E A74G V78L A82L F87A M118S P142S F162L T175I M177L A184V S226R H236Q E252G **I263W** H266V T268G A290V A328V A330Y L353V I366V C400S I401L T436L L437Q E442K ΔFAD
C10-WI	N70E A74G V78L A82L F87A M118S P142S F162L T175I M177L A184V S226R H236Q E252G **I263W** H266V T268G A290V A328V A330Y L353V I366V C400S I401L T436L **L437I** E442K ΔFAD
C10-WIF	N70E **S72F** A74G V78L A82L F87A M118S P142S F162L T175I M177L A184V S226R H236Q

	E252G **I263W** H266V T268G A290V A328V A330Y L353V I366V C400S I401L T436L **L437I** E442K ΔFAD
C10-WIRF	N70E **S72F** A74G V78L A82L F87A M118S P142S F162L T175I M177L A184V S226R H236Q E252G **I263W** H266V T268G A290V A328V A330Y L353V I366V C400S I401L **T436R L437I** E442K ΔFAD
C10-WIRF_G	N70E **S72F** A74G V78L A82L F87A M118S P142S F162L T175I M177L A184V S226R H236Q E252G **I263W** H266V T268G A290V A328V A330Y **S332G** L353V I366V C400S I401L **T436R L437I** E442K ΔFAD
C10-WIRF_GA	N70E **S72F** V78L A82L F87A M118S P142S F162L T175I M177L A184V S226R H236Q E252G **I263W** H266V T268G A290V A328V A330Y **S332G** L353V I366V C400S I401L **T436R L437I** E442K ΔFAD
C10-WIRF_GAK	**N70K S72F** V78L A82L F87A M118S P142S F162L T175I M177L A184V S226R H236Q E252G **I263W** H266V T268G A290V A328V A330Y **S332G** L353V I366V C400S I401L **T436R L437I** E442K ΔFAD
C10-VLC	N70E A74G V78L A82L F87A M118S P142S F162L T175I M177L A184V S226R H236Q E252G I263Y H266V T268G A290V **T327V** A328V A330Y **S332C** L353V I366V C400S I401L T436L E442K ΔFAD
P411-**C11**	N70E A74T V78L A82L F87A P142S T175I M177L A184V S226R H236Q E252G I263Y H266V T268G A290V A328V A330Y L353V I366V C400S T436L E442K ΔFAD
P411-**L8**	N70E A74G V78L A82L **F87P** M118S P142S F162L T175I M177L A184V S226R H236Q E252G I263Y **A264S** H266V **E267D** T268G A290V **T327P** A328V A330Y **S332A** L353V I366V C400S I401L T436L E442K ΔFAD
C10-II	N70E A74G V78L A82L F87A M118S P142S F162L T175I M177L A184V S226R H236Q E252G I263Y H266V T268G A290V **A328I** A330Y L353V I366V C400S I401L T436L **L437I** E442K ΔFAD
C10-PVV	N70E A74G V78L A82L **F87V** M118S P142S F162L T175I M177L A184V S226R H236Q E252G I263Y H266V T268G A290V **T327V** A328V A330Y L353V I366V C400S I401L T436L **L437P** E442K ΔFAD

Note: ΔFAD means FAD domain truncation. See the publications for the nucleotide and amino acid sequences of the P411 variants.

Table A-7. Additional alkyne substrates tested with promising reactivity in **2.3.3** and **2.4.2**.

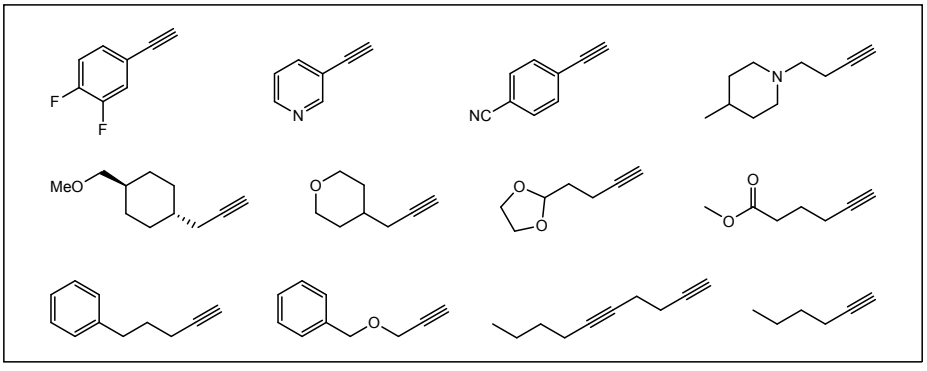

A.2 Supporting Figures A-1 to A-5

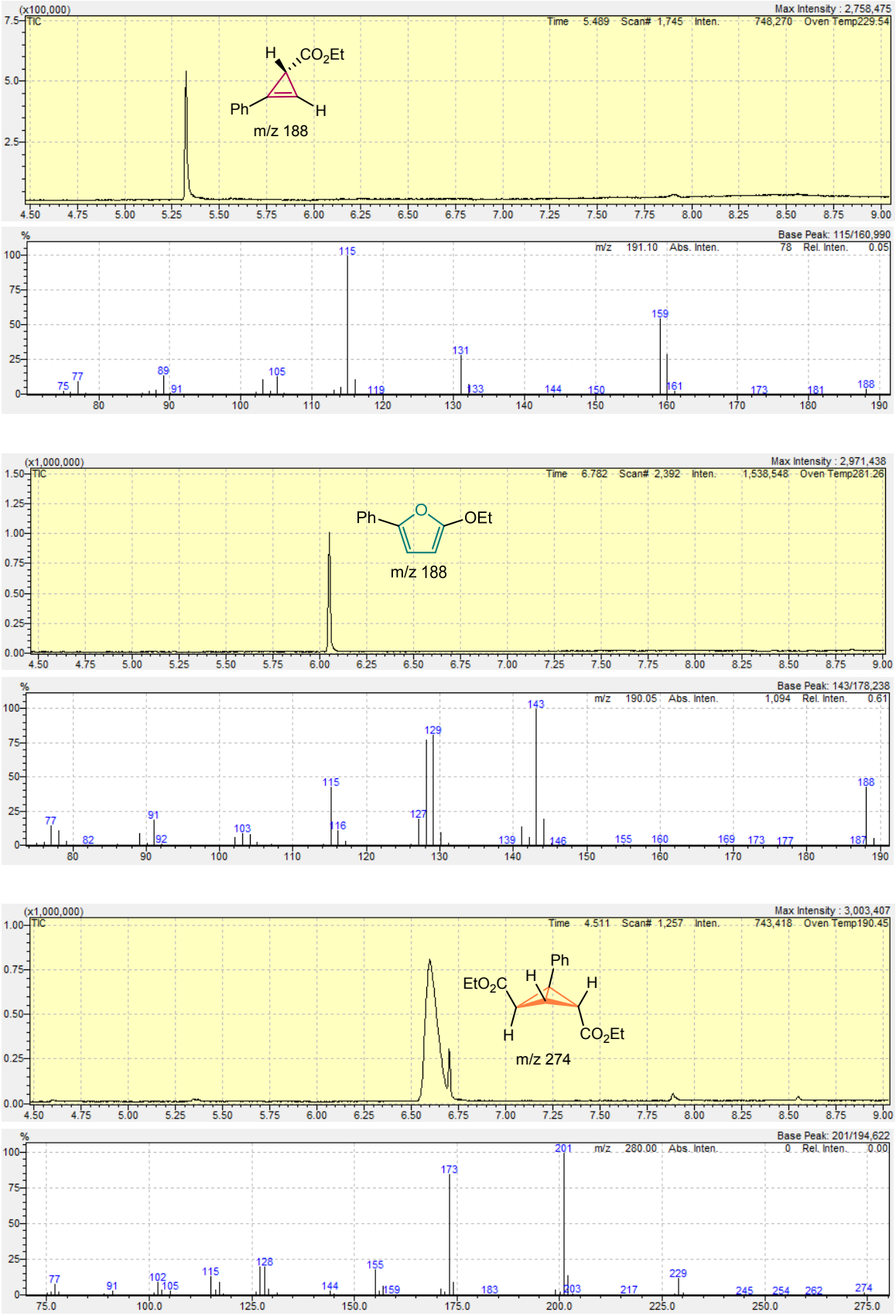

Figure A-1. GC-MS traces of cyclopropene **3a**, furan **3b** and bicyclobutane **2a**. *High temperature (> 250 °C) of the GC might degrade the bicyclobutane to some extent, resulting in a broad peak and another small peak (the

whole signal is from pure bicyclobutane 2a). The signal is nonetheless suitable for quantitative analysis.

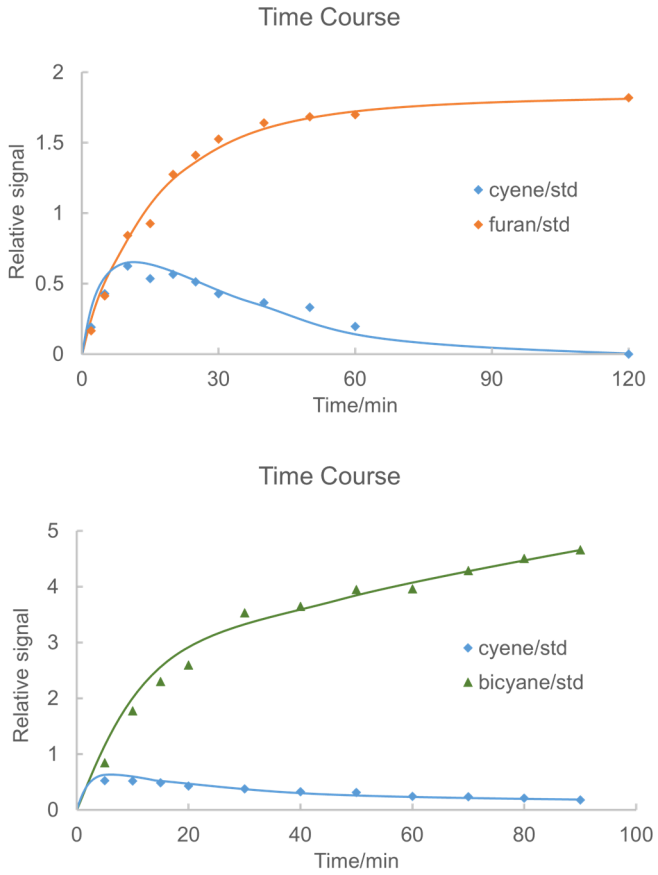

Figure A-2. Time courses of furan formation with P411-**P** I263W variant (top) and bicyclobutane formation with P411-**E10** variant (bottom). *Reactions were set up in parallel according to the standard procedure using whole-cell catalyst (OD_{600} = 30). The reactions were quenched at certain time points and analyzed by GC-MS. Every data point (average of two reaction) is the peak area of cyclopropene **3a,** furan **3b** or bicyclobutane **2a** divided by that of internal standard on GC-MS. Cyene = cyclopropene; bicyane = bicyclobutane.

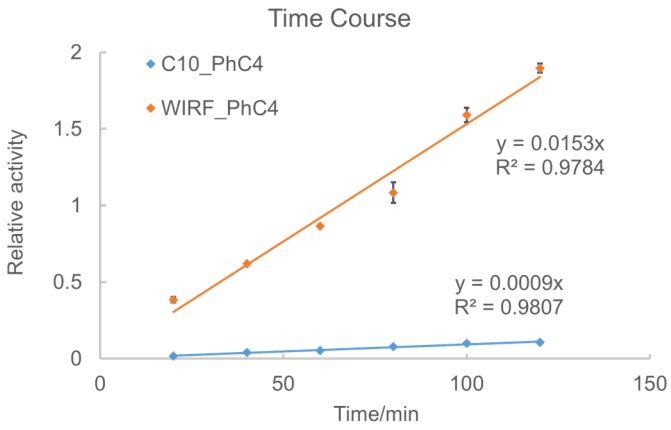

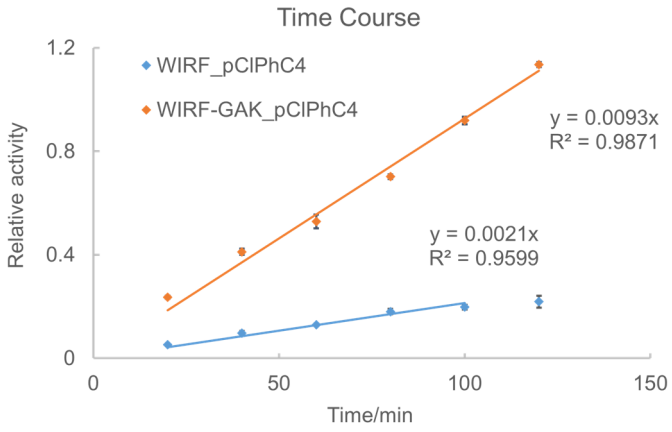

Figure A-3. Time courses of whole-cell cyclopropenation with different substrates (top: 1-phenylbutyne, bottom: 1-(4-chlorophenyl)butyne) and enzyme variants. *Reactions were set up in parallel according to the standard procedure using whole-cell catalyst (OD_{600} = 15 for **C10**, **WIRF** and **WIRF_GAK**). The reactions were quenched at certain time points and analyzed by GC-MS. Every data point (average of two reactions) is the peak area of cyclopropenes **9a** or **9b** divided by that of internal standard on GC. Relative activity was normalized by protein concentration.

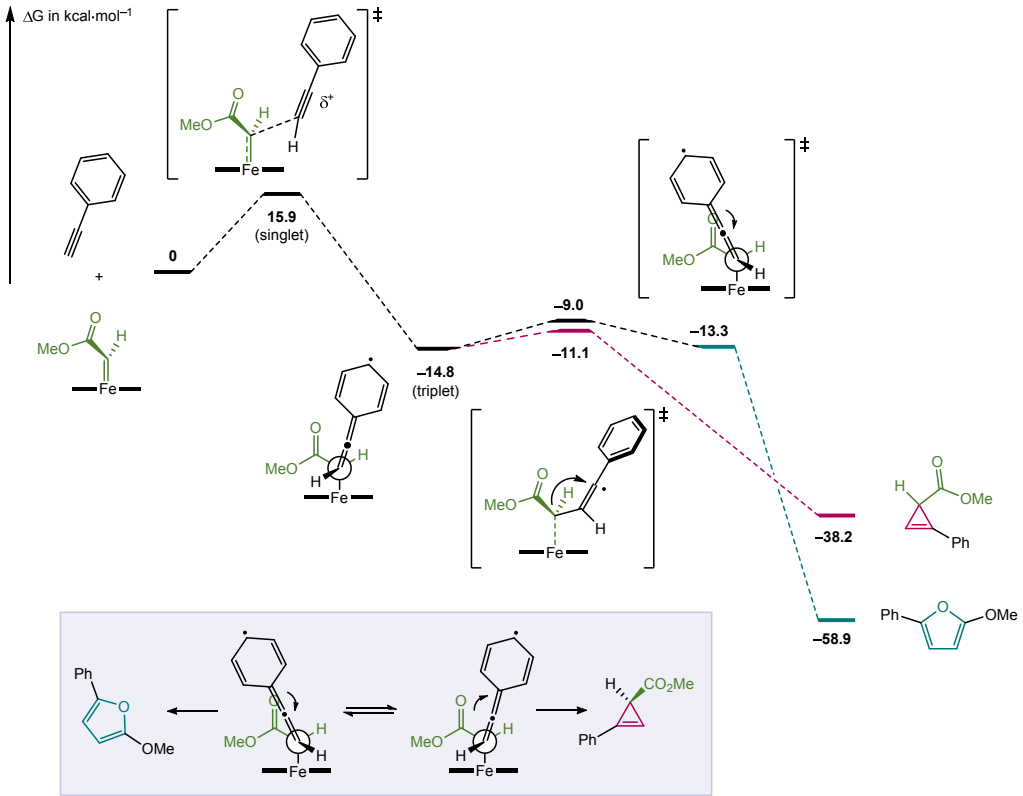

Figure A-4. Mechanism of carbene transfer to alkyne by computational calculation using a simplified iron-porphyrin model system with an oxygen axial ligand. Gibbs free energy was obtained at the (U)B3LYP-D3(BJ)/Def2TZVP/PCM(ε = 4)//(U)B3LYP/6-31G(d)+SDD(Fe)/PCM(ε = 4) level.

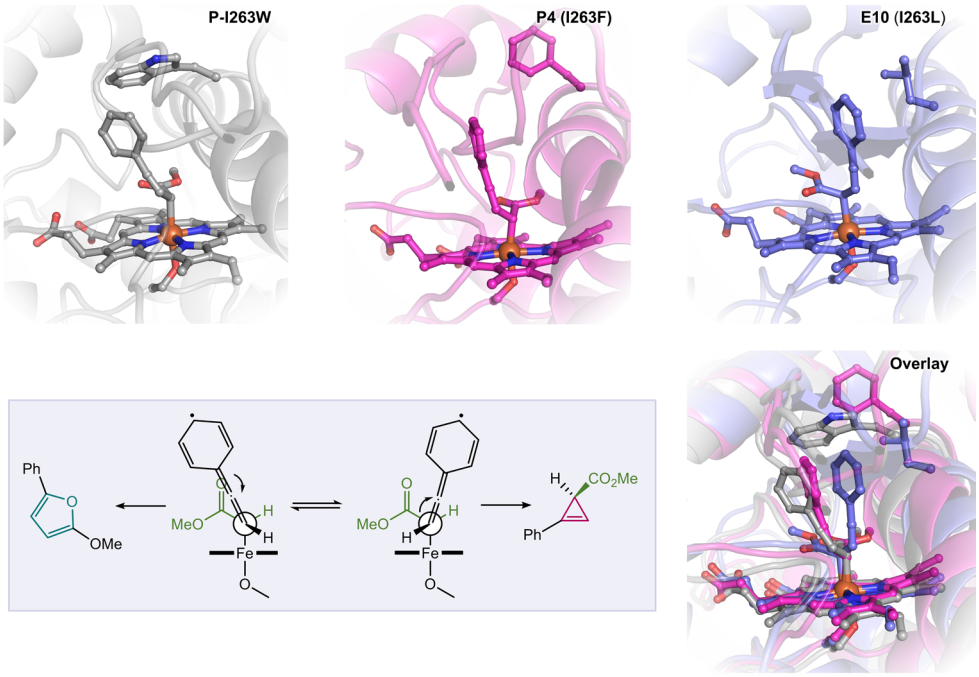

Figure A-5. Molecular dynamic (MD) simulation of reaction intermediates in the active sites of different P411 variants. Residue 263 may lead to a major influence on the conformation of the intermediate, leading to cyclopropene or furan formation.

A.3 Preparation of alkyne substrates

Oct-7-yn-1-yl cyclobutanecarboxylate (5d)

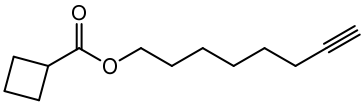

In a 100 mL round-bottom flask, oct-7-yn-1-ol (0.631 g, 5.0 mmol), triethylamine (0.9 mL, 1.3 equiv.) and *N*,*N*-dimethylpyridin-4-amine (DMAP, 61 mg, 10 mol%) in dry DCM (20 mL) was cooled to 0 °C. A solution of cyclobutanecarbonyl chloride (0.711 g, 6.0 mmol) in dry DCM (5 mL) was added dropwise slowly over 5 min. The reaction was allowed to warm to room temperature and stirred for 8 hours. The reaction mixture was diluted with DCM (20 mL) and washed with water (20 mL) and brine (20 mL), dried over $MgSO_4$, and then concentrated under reduced pressure. The crude product was purified by silica column chromatography with hexane/ethyl acetate (20:1) to afford **5d** (1.02 g, 98%). ^{1}H NMR (400 MHz, $CDCl_3$) δ 4.06 (t, *J* = 6.7 Hz, 2H), 3.12 (pd, *J* = 8.5, 1.0 Hz, 1H), 2.34–2.13 (m, 6H), 2.04–1.83 (m, 3H), 1.69–1.59 (m, 2H), 1.57–1.48 (m, 2H), 1.47–1.32 (m, 4H). ^{13}C NMR (101 MHz, $CDCl_3$) δ 175.62, 84.51, 68.25, 64.28, 38.17, 28.54, 28.34, 28.32, 25.45, 25.28, 18.43, 18.33. HRMS (FAB) m/z: 209.1548 ($M+H^+$); calc. for $C_{13}H_{21}O_2$: 209.1542.

2-(Hept-6-yn-1-yl)-1,3-dioxolane (5e)

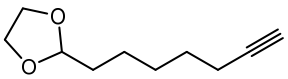

In a 250 mL round-bottom flask, DMSO (1.95 g, 25.0 mmol) was dissolved in dry DCM (40 mL) and then cooled to –78 °C under argon. A solution of oxalyl dichloride (2.6 mL, 30.0 mmol) in dry DCM (10 mL) was added dropwise slowly over 10 min. After the mixture was stirred at –78 °C for 1 h, a solution of oct-7-yn-1-ol (0.631 g, 5.0

mmol) in dry DCM (10 mL) was added dropwise slowly over 10 min. The resulting mixture was maintained at –78 °C for another 2 h before the dropwise addition of triethylamine (7.0 mL, 50.0 mmol) in dry DCM (10 mL). The reaction was then allowed to warm to room temperature over 1 h and stirred for another 2 h. The reaction mixture was diluted with DCM (30 mL) and washed with HCl (10%, 50 mL), $NaHCO_3$ (50 mL, sat. aq.), and brine (50 mL), dried over $MgSO_4$, and then concentrated under reduced pressure (100 torr). The crude product mixture was used for the next step without further purification. The crude product was dissolved in benzene (50 mL) in a 100 mL round-bottom flask. Ethylene glycol (0.465 g, 7.5 mmol) and TsOH (130 mg, 0.075 mmol) were added. The solution was heated up to a refluxing temperature, 90 °C, and maintained for 2 h. After removal of benzene under reduced pressure, the crude product was purified by silica column chromatography with hexane/ether (20:1 to 15:1) to afford **5e** (0.675 g, 80%). ^{1}H NMR (400 MHz, $CDCl_3$) δ 4.85 (t, *J* = 4.8 Hz, 1H), 4.01–3.91 (m, 2H), 3.90–3.79 (m, 2H), 2.19 (td, *J* = 7.0, 2.6 Hz, 2H), 1.93 (t, *J* = 2.7 Hz, 1H), 1.70–1.61 (m, 2H), 1.59–1.51 (m, 2H), 1.49–1.39 (m, 4H). ^{13}C NMR (101 MHz, $CDCl_3$) δ 104.66, 84.73, 68.32, 64.99, 33.89, 28.78, 28.53, 23.69, 18.45. HRMS (FAB) m/z: 167.1067 ($(M+H^+)–H_2$); calc. for $C_{10}H_{15}O_2$: 167.1072.

5-Isopropoxypent-1-yne (5f)

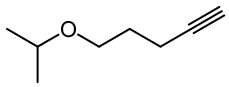

In a 100 mL round-bottom flask, pent-4-yn-1-ol (0.841 g, 10.0 mmol), triethylamine (1.8 mL, 1.3 equiv.) and DMAP (122 mg, 10 mol%) in dry DCM (50 mL) was cooled to 0 °C. 4-Methylbenzenesulfonyl chloride (TsCl, 2.10 g, 11.0 mmol) was added portion-wise. The reaction was allowed to warm to room temperature and stirred for 6 hours. The reaction mixture was diluted with DCM (30 mL) and washed with water (20 mL) and brine (20 mL), dried over $MgSO_4$, and then concentrated under reduced pressure. The crude product was purified by silica column chromatography with hexane/ethyl acetate (4:1) to afford pent-4-yn-1-yl 4-methylbenzenesulfonate (2.35 g, 99%).

Isopropanol (0.361 g, 6.0 mmol) and tetrabutylammonium bromide (161 mg, 0.5 mmol) were dissolved in anhydrous DMF (50 mL) and then cooled to 0 °C. NaH (60%, 240 mg, 6.0 mmol) was added portion-wise to the solution. The resulting mixture was stirred at 0 °C for 1 h before the dropwise addition of pent-4-yn-1-yl 4-methylbenzenesulfonate (1.19 g, 5.0 mmol) in anhydrous DMF (10 mL). The reaction was allowed to warm to room temperature and stirred for 4 hours. The reaction mixture was quenched with NH_4Cl (20 mL, sat. aq.) and the product was extracted with Et_2O (30 mL × 3). The combined organic layer was washed with water (20 mL), brine (20 mL), dried over $MgSO_4$, and then concentrated under reduced pressure (200 torr). The crude product was purified by silica column chromatography with pentane/ether (10:1) to afford **5f** (0.597 g, 95%).

4-((Oct-7-yn-1-yloxy)methyl)tetrahydro-2*H*-pyran (5h)

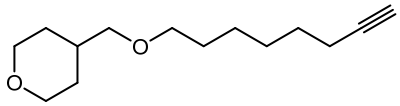

In a 500 mL round-bottom flask, oct-7-yn-1-ol (6.31 g, 50.0 mmol), triethylamine (9.1 mL, 1.3 equiv.) and DMAP (609 mg, 10 mol%) in dry DCM (200 mL) was cooled to 0 °C. TsCl (10.50 g, 55.0 mmol) was added portion-wise. The reaction was allowed to warm to room temperature and stirred for 6 hours. The reaction mixture was diluted with DCM (100 mL) and washed with water (200 mL) and brine (200 mL), dried over $MgSO_4$, and then concentrated under reduced pressure. The crude product was purified by

silica column chromatography with hexane/ethyl acetate (10:1) to afford oct-7-yn-1-yl 4-methylbenzenesulfonate (13.29 g, 95%).

In a 100 mL round-bottom flask, (tetrahydro-2*H*-pyran-4-yl)methanol (0.697 g, 6.0 mmol) and tetrabutylammonium bromide (161 mg, 0.5 mmol) were dissolved in anhydrous DMF (50 mL) and then cooled to 0 °C. NaH (60%, 240 mg, 6.0 mmol) was added portion-wise to the solution. The resulting mixture was stirred at 0 °C for 1 h before the dropwise addition of oct-7-yn-1-yl 4-methylbenzenesulfonate (1.40 g, 5.0 mmol) in anhydrous DMF (10 mL). Then reaction was allowed to warm to room temperature and stirred for 4 hours. The reaction mixture was quenched with NH_4Cl (20 mL, sat. aq.) and the product was extracted with Et_2O (50 mL × 3). The combined organic layer was washed with water (20 mL), brine (20 mL), dried over $MgSO_4$, and then concentrated under reduced pressure. The crude product was purified by silica column chromatography with hexane/ethyl acetate (10: 1) to afford **5h** (1.10 g, 98%). ^{1}H NMR (400 MHz, $CDCl_3$) δ 3.96 (ddt, *J* = 11.5, 4.6, 1.1 Hz, 2H), 3.43–3.34 (m, 4H), 3.24 (d, *J* = 6.6 Hz, 2H), 2.18 (td, *J* = 7.0, 2.7 Hz, 2H), 1.93 (t, *J* = 2.7 Hz, 1H), 1.89–1.77 (m, 1H), 1.68–1.61 (m, 2H), 1.60–1.49 (m, 4H), 1.46–1.34 (m, 4H), 1.33–1.25 (m, 2H). ^{13}C NMR (101 MHz, $CDCl_3$) δ 84.80, 76.11, 71.24, 68.28, 67.90, 35.60, 30.19, 29.70, 28.70, 28.56, 25.83, 18.49. HRMS (FAB) m/z: 225.1855 ($M+H^+$); calc. for $C_{14}H_{25}O_2$: 225.1855.

((Oct-7-yn-1-yloxy)methyl)cyclopropane (5i)

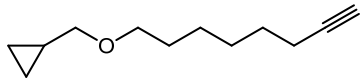

In a 100 mL round-bottom flask, cyclopropylmethanol (0.433 g, 6.0 mmol) and tetrabutylammonium bromide (161 mg, 0.5 mmol) were dissolved in anhydrous DMF (50 mL) and then cooled to 0 °C. NaH (60%, 240 mg, 6.0 mmol) was added portion-wise to the solution. The resulting mixture was stirred at 0 °C for 1 h before the dropwise addition of oct-7-yn-1-yl 4-methylbenzenesulfonate (1.40 g, 5.0 mmol) in anhydrous DMF (10 mL). The reaction was allowed to warm to room temperature and stirred for 4 hours. The reaction mixture was quenched with NH_4Cl (20 mL, sat. aq.) and the product was extracted with Et_2O (50 mL × 3). The combined organic layer was washed with water (20 mL), brine (20 mL), dried over $MgSO_4$, and then concentrated under reduced pressure. The crude product was purified by silica column chromatography with hexane/ether (50: 1) to afford **5i** (840 mg, 93%). ^{1}H NMR (400 MHz, $CDCl_3$) δ 3.42 (t, *J* = 6.7 Hz, 2H), 3.24 (d, *J* = 6.9 Hz, 2H), 2.18 (td, *J* = 7.0, 2.6 Hz, 2H), 1.93 (t, *J* = 2.6 Hz, 1H), 1.64–1.57 (m, 2H), 1.56–1.49 (m, 2H), 1.47–1.30 (m, 4H), 1.12–0.97 (m, 1H), 0.58–0.45 (m, 2H), 0.19 (dt, *J* = 6.0, 4.5 Hz, 2H). ^{13}C NMR (101 MHz, $CDCl_3$) δ 84.82, 75.73, 70.77, 68.26, 29.78, 28.72, 28.57, 25.85, 18.49, 10.82, 3.13. HRMS (FAB) m/z: 181.1590 ($M+H^+$); calc. for $C_{12}H_{21}O$: 181.1592.

***Trans*-1-(methoxymethyl)-4-((oct-7-yn-1-yloxy)methyl)cyclohexane (5l)**

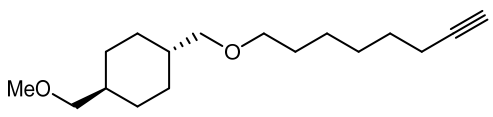

In a 100 mL round-bottom flask, (*tran*-cyclohexane-1,4-diyl) dimethanol (2.88 g, 20.0 mmol) and tetrabutylammonium bromide (32 mg, 0.1 mmol) were dissolved in anhydrous DMF (50 mL) and then cooled to 0 °C. NaH (60%, 960 mg, 24.0 mmol) was added portion-wise to the solution. The resulting mixture was stirred at 0 °C for 1 h before the dropwise addition of methyl iodide (MeI, 1.5 mL, 24.0 mmol) in anhydrous DMF (10 mL). The reaction was allowed to warm to room temperature and stirred for 4 hours. The reaction mixture was quenched with NH_4Cl (20 mL, sat. aq.) and the product was extracted with Et_2O (50 mL × 4).

The combined organic layer was washed with water (50 mL), brine (50 mL), dried over $MgSO_4$, and then concentrated under reduced pressure. The crude product was purified by silica column chromatography with hexane/ethyl acetate (1:1) to afford (*trans*-4-(methoxymethyl)cyclohexyl)methanol (2.02 g, 64%).

In a 100 mL round-bottom flask, (*trans*-4-(methoxymethyl)cyclohexyl)methanol (0.949 g, 6.0 mmol) and tetrabutylammonium bromide (161 mg, 0.5 mmol) were dissolved in anhydrous DMF (50 mL) and then cooled to 0 °C. NaH (60%, 240 mg, 6.0 mmol) was added portion-wise to the solution. The resulting mixture was stirred at 0 °C for 1 h before the dropwise addition of oct-7-yn-1-yl 4-methylbenzenesulfonate (1.40 g, 5.0 mmol) in anhydrous DMF (10 mL). Then reaction was allowed to warm to room temperature and stirred for 4 hours. The reaction mixture was quenched with NH_4Cl (20 mL, sat. aq.) and the product was extracted with Et_2O (50 mL × 3). The combined organic layer was washed with water (20 mL), brine (20 mL), dried over $MgSO_4$, and then concentrated under reduced pressure. The crude product was purified by silica column chromatography with hexane/ethyl acetate (10:1) to afford **5l** (743 mg, 56%). ^{1}H NMR (400 MHz, $CDCl_3$) δ 3.38 (t, *J* = 6.6 Hz, 2H), 3.32 (s, 3H), 3.20 (d, *J* = 6.5 Hz, 2H), 3.18 (d, *J* = 6.4 Hz, 2H), 2.18 (td, *J* = 7.0, 2.7 Hz, 2H), 1.93 (t, *J* = 2.7 Hz, 1H), 1.86–1.74 (m, 4H), 1.58–1.49 (m, 6H), 1.46–1.30 (m, 4H), 1.01–0.86 (m, 4H). ^{13}C NMR (101 MHz, $CDCl_3$) δ 84.84, 78.93, 76.90, 71.17, 68.26, 58.98, 38.37 (2 carbons), 29.73, 29.65, 29.55, 28.73, 28.58, 25.85, 18.50. HRMS (FAB) m/z: 267.2325 ($M+H^+$); calc. for $C_{17}H_{31}O_2$: 267.2324.

General procedure for internal aromatic alkyne synthesis (8b and 8d to 8l):

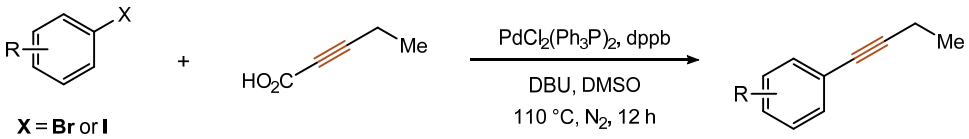

To a 100-mL flask were added aryl bromide or iodide (10.0 mmol, 1.0 equiv.), 2-pentynoic acid (1.18 g, 12.0 mmol, 1.2 equiv.), $PdCl_2(Ph_3P)_2$ (70 mg, 0.1 mol, 1 mol%), 1,4-bis(diphenylphosphino) butane (dppb, 86 mg, 0.2 mmol, 2 mol%) and anhydrous DMSO (30 mL). The mixture was stirred at room temperature for 3 minutes, and then the flask was capped, degassed and charged with N_2. 1,8-Diazabicyclo[5.4.0]undec-7-ene (DBU, 4.4 mL, 30 mmol, 3.0 equiv.) was added to the reaction under N_2. The reaction was stirred at 110 °C for 12 hours before being cooled to room temperature, quenched by NH_4Cl (sat. aq., 20 mL) and diluted with water (30 mL). The product was extracted by ether (25 mL × 3). The combined organic layer was then washed with water (30 mL) and brine (30 mL), and dried over magnesium sulfate. The organic layer was filtered and concentrated under reduced pressure. Distillation of the crude mixture under high vacuum (<100 Pa, 80-125 °C) gave the desired product in 60% to 90% yield and with NMR purity of 98% to >99%.

1-(But-1-yn-1-yl)-4-chlorobenzene (8b)

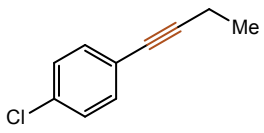

Compound **8b** was prepared following the general procedure using the corresponding aryl bromide. The reaction was set up in 80-mmol scale and distillation afforded the alkyne **8b** as a colorless liquid (11.4 g, 86%). ^{1}H NMR (400 MHz, $CDCl_3$) δ 7.32 (d, *J* = 8.7 Hz, 2H), 7.25 (d, *J* = 8.7 Hz, 2H), 2.41 (q, *J* = 7.5 Hz, 2H), 1.23 (t, *J* = 7.5 Hz, 3H). ^{13}C NMR (101 MHz, $CDCl_3$) δ 133.53, 132.88, 128.61, 122.64, 92.86, 78.97, 13.95,

13.24.

1-(But-1-yn-1-yl)-2-fluorobenzene (8d)

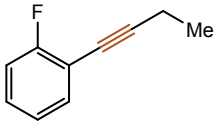

Compound **8d** was prepared following the general procedure using the corresponding aryl bromide. ^{1}H NMR (400 MHz, $CDCl_3$) δ 7.39 (td, *J* = 7.6, 1.8 Hz, 1H), 7.24 (dddd, *J* = 8.2, 7.2, 5.2, 1.8 Hz, 1H), 7.10–7.00 (m, 2H), 2.47 (q, *J* = 7.5 Hz, 2H), 1.26 (t, *J* = 7.5 Hz, 3H). ^{13}C NMR (101 MHz, $CDCl_3$) δ 164.14, 161.66 (d, *J* = 250.9 Hz), 133.70, 133.69 (d, *J* = 1.6 Hz), 129.28, 129.20 (d, *J* = 8.0 Hz), 123.93, 123.90 (d, *J* = 3.7 Hz), 115.57, 115.36 (d, *J* = 21.3 Hz), 112.65, 112.49 (d, *J* = 15.8 Hz), 97.28, 97.24 (d, *J* = 3.3 Hz), 73.31, 13.92, 13.45.

1-(But-1-yn-1-yl)-4-fluorobenzene (8e)

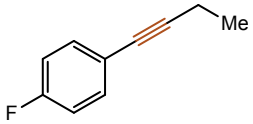

Compound **8e** was prepared following the general procedure using the corresponding aryl iodide. ^{1}H NMR (400 MHz, $CDCl_3$) δ 7.36 (dd, *J* = 8.8, 5.4 Hz, 2H), 6.97 (t, *J* = 8.8 Hz, 2H), 2.40 (q, *J* = 7.5 Hz, 2H), 1.23 (t, *J* = 7.5 Hz, 3H). ^{13}C NMR (101 MHz, $CDCl_3$) δ 163.39, 160.93 (d, *J* = 249.2 Hz), 133.46, 133.38 (d, *J* = 8.2 Hz), 120.20, 120.17 (d, *J* = 3.6 Hz), 115.62, 115.40 (d, *J* = 22.0 Hz), 91.41, 91.40 (d, *J* = 1.6 Hz), 78.94, 14.03, 13.18.

1-(But-1-yn-1-yl)-3-methoxybenzene (8f)

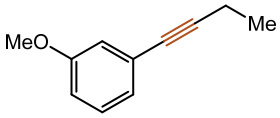

Compound **8f** was prepared following the general procedure using corresponding aryl iodide. ^{1}H NMR (400 MHz, $CDCl_3$) δ 7.21 (dd, *J* = 8.3, 7.6 Hz, 1H), 7.02 (dt, *J* = 7.6, 1.2 Hz, 1H), 6.96 (dd, *J* = 2.6, 1.4 Hz, 1H), 6.85 (ddd, *J* = 8.3, 2.6, 1.0 Hz, 1H), 3.82 (s, 3H), 2.44 (q, *J* = 7.5 Hz, 2H), 1.26 (t, *J* = 7.5 Hz, 3H). ^{13}C NMR (101 MHz, $CDCl_3$) δ 159.38, 129.36, 125.13, 124.22, 116.46, 114.30, 91.69, 79.92, 55.36, 14.04, 13.24.

1-(But-1-yn-1-yl)-4-trifluoromethylbenzene (8g)

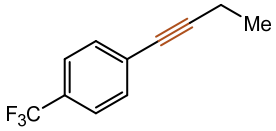

Compound **8g** was prepared following the general procedure using corresponding aryl iodide. ^{1}H NMR (400 MHz, $CDCl_3$) δ 7.53 (d, *J* = 8.2 Hz, 2H), 7.48 (d, *J* = 8.2 Hz, 2H), 2.44 (q, *J* = 7.5 Hz, 2H), 1.25 (t, *J* = 7.5 Hz, 3H). ^{13}C NMR (101 MHz, $CDCl_3$) δ 131.89, 129.38 (q, *J* = 32.7 Hz), 128.04 (q, *J* = 3.8 Hz), 125.24 (q, *J* = 38.7 Hz), 124.17 (q, *J* = 273.0 Hz), 94.62, 78.97, 13.84, 13.28.

1-(But-1-yn-1-yl)-4-difluoromethoxybenzene (8h)

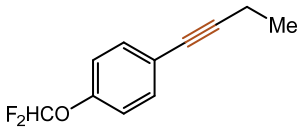

Compound **8h** was prepared following the general procedure using corresponding aryl bromide. ^{1}H NMR (400 MHz, $CDCl_3$) δ 7.41 (d, *J* = 8.7 Hz, 2H), 7.05 (d, *J* = 8.8 Hz, 2H), 6.52 (t, *J* = 73.7 Hz, 1H), 2.43 (q, *J* = 7.5 Hz, 2H), 1.26 (t, *J* = 7.5 Hz, 3H). ^{13}C NMR (101 MHz, $CDCl_3$) δ 150.48, 133.17, 121.47, 119.41, 118.48, 115.90, 113.31 (t, *J* = 260.8 Hz), 92.15, 78.90, 13.99, 13.21.

1-(But-1-yn-1-yl)-4-toluene (8i)

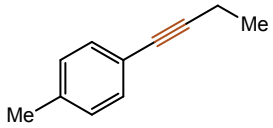

Compound **8i** was prepared following the general procedure using corresponding aryl iodide. ^{1}H NMR (400 MHz, $CDCl_3$) δ 7.29 (d, *J* = 8.2 Hz, 2H), 7.09 (d, *J* = 7.7 Hz, 2H), 2.41 (q, *J* = 7.5 Hz, 2H), 2.33 (s, 3H), 1.24 (t, *J* = 7.5 Hz, 3H). ^{13}C NMR (101 MHz, $CDCl_3$) δ 137.57, 131.52, 129.07, 121.02, 90.97, 80.00, 21.54, 14.13, 13.26.

1-(But-1-yn-1-yl)-4-anisole (8j)

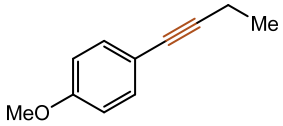

Compound **8j** was prepared following the general procedure using corresponding aryl iodide. ^{1}H NMR (400 MHz, $CDCl_3$) δ 7.33 (d, *J* = 8.9 Hz, 2H), 6.81 (d, *J* = 8.9 Hz, 2H), 3.80 (s, 3H), 2.40 (q, *J* = 7.5 Hz, 2H), 1.23 (t, *J* = 7.5 Hz, 3H). ^{13}C NMR (101 MHz, $CDCl_3$) δ 159.11, 132.97, 116.28, 113.92, 90.17, 79.68, 55.38, 14.19, 13.24.

4-(But-1-yn-1-yl)-2-methyl-1-chlorobenzene (8k)

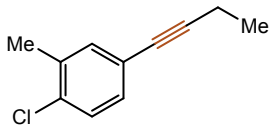

Compound **8k** was prepared following the general procedure using corresponding aryl bromide. ^{1}H NMR (400 MHz, $CDCl_3$) δ 7.26 (d, *J* = 1.9 Hz, 1H), 7.24 (d, *J* = 8.2 Hz, 1H), 7.14 (dd, *J* = 8.2, 1.9 Hz, 1H), 2.40 (q, *J* = 7.5 Hz, 2H), 2.33 (s, 3H), 1.23 (t, *J* = 7.5 Hz, 3H). ^{13}C NMR (101 MHz, $CDCl_3$) δ 136.09, 134.02, 133.82, 130.24, 129.04, 122.57, 92.35, 79.13, 20.01, 14.00, 13.24.

4-(But-1-yn-1-yl)-2-methyl-1-methoxybenzene (8l)

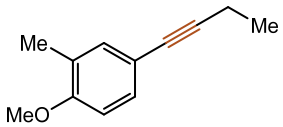

Compound **1l** was prepared following the general procedure using corresponding aryl bromide. ^{1}H NMR (400 MHz, $CDCl_3$) δ 7.24 (dd, *J* = 8.3, 2.0 Hz, 1H), 7.21 (d, *J* = 2.0 Hz, 1H), 6.75 (d, *J* = 8.3 Hz, 1H), 3.84 (s, 3H), 2.42 (q, *J* = 7.5 Hz, 2H), 2.20 (s, 3H), 1.25 (t, *J* = 7.5 Hz, 3H). ^{13}C NMR (101 MHz, $CDCl_3$) δ 157.43, 133.90, 130.37, 126.69, 115.69, 109.78, 89.78, 79.90, 55.43, 16.16, 14.23, 13.25.

1-Ethoxyhex-3-yne (8m)

Hex-3-yn-1-ol (2.94 g, 30 mmol, 1.0 equiv.) was dissolved in anhydrous DMF (60 mL) in a 250-mL flask. NaH (1.44 g, 60% in mineral oil, 36 mmol, 1.2 equiv.) was slowly added to the solution in portions over 20 min at 0 °C. The resulting mixture was stirred at 0 °C for 1.5 h before slow addition of ethyl iodide (3.6 mL, 45 mmol, 1.5 equiv.). The reaction was slowly warmed to room temperature over 30 min and then stirred for additional 2 h before being quenched by NH_4Cl (sat. aq., 20 mL) and diluted with water (30 mL). The product was extracted by ether (40 mL × 3). The combined organic layer was then washed with water (50 mL × 2) and brine (50 mL), and dried over sodium sulfate. The organic layer was filtered and concentrated under reduced pressure. The crude product was purified through a silica column using hexane/ethyl acetate (100:0 to 20:1) as eluents to afford the alkyne **8m** as a clear liquid (3.72 g, 98% yield). ^{1}H NMR

(400 MHz, $CDCl_3$) δ 3.51 (td, *J* = 7.1, 5.3 Hz, 4H), 2.42 (tt, *J* = 7.2, 2.4 Hz, 2H), 2.16 (qt, *J* = 7.5, 2.4 Hz, 2H), 1.20 (t, *J* = 7.0 Hz, 3H), 1.11 (t, *J* = 7.5 Hz, 3H). ^{13}C NMR (101 MHz, $CDCl_3$) δ 82.88, 76.15, 69.42, 66.36, 20.28, 15.29, 14.33, 12.58.

1-Methoxyoct-2-yne (8n)

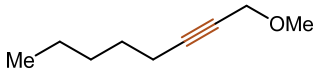

Oct-2-yn-1-ol (3.79 g, 30 mmol, 1.0 equiv.) was dissolved in anhydrous DMF (60 mL) in a 250-mL flask. NaH (1.44 g, 60% in mineral oil, 36 mmol, 1.2 equiv.) was slowly added to the solution in portions over 20 min at 0 °C. The resulting mixture was stirred at 0 °C for 1.5 h before slow addition of iodomethane (2.8 mL, 45 mmol, 1.5 equiv.). The reaction was slowly warmed to room temperature over 30 min and then stirred for additional 2 h before being quenched by NH_4Cl (sat. aq., 20 mL) and diluted with water (30 mL). The product was extracted by ether (40 mL × 3). The combined organic layer was then washed with water (50 mL × 2) and brine (50 mL), and dried over sodium sulfate. The organic layer was filtered and concentrated under reduced pressure. The crude product was purified through a silica column using hexane/ethyl acetate (100:0 to 20:1) as eluents to afford the alkyne **8n** as a clear liquid (4.04 g, 96% yield). ^1H NMR (400 MHz, $CDCl_3$) δ 4.07 (t, *J* = 2.2 Hz, 2H), 3.36 (s, 3H), 2.21 (tt, *J* = 7.2, 2.2 Hz, 2H), 1.56–1.48 (m, 2H), 1.41–1.26 (m, 4H), 0.89 (t, *J* = 7.1 Hz, 3H). ^{13}C NMR (101 MHz, $CDCl_3$) δ 87.39, 75.80, 60.38, 57.53, 31.19, 28.47, 22.34, 18.85, 14.11.

A.4 Preparation of racemic standard products

General procedure for rhodium-catalyzed cyclopropenation of terminal alkynes:

To a 20 mL vial was added alkyne (1.0 mmol, 1.0 equiv.), $Rh_2(OAc)_4$ (4.4 mg, 1 mol%) and DCM (10 mL). The mixture was cooled to −78 °C, after which EDA (2.0 mmol, 2.0 equiv.) was added dropwise to the solution. The reaction was allowed to slowly warm up to room temperature over 8 hours and stirred at room temperature for another 8 hours. Evaporation of the organic solvent and purification by silica column chromatography using hexane and ethyl acetate as eluents afforded racemic cyclopropene products **5a**–**5i**, **5k** and **5l** in 10–30% yields. (Note: this protocol did not work for cyclopropyl-substituted alkyne **5j**.)

Ethyl 2-phenethylcycloprop-2-ene-1-carboxylate (6a)

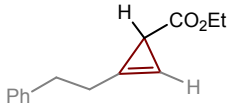

^1H NMR (400 MHz, $CDCl_3$) δ 7.33–7.27 (m, 2H), 7.24–7.18 (m, 3H), 6.36 (dt, *J* = 1.4 Hz, 1H), 4.21–4.05 (m, 2H), 2.96–2.79 (m, 4H), 2.14 (d, *J* = 1.5 Hz, 1H), 1.25 (t, *J* = 7.1 Hz, 3H). ^{13}C NMR (101 MHz, $CDCl_3$) δ 176.61, 140.81, 128.58, 128.45, 126.36, 115.01, 95.03, 60.39, 33.00, 26.90, 20.00, 14.52. HRMS (FAB) m/z: 217.1221 ($M+H^+$); calc. for $C_{14}H_{17}O_2$: 217.1229.

Ethyl 2-octylcycloprop-2-ene-1-carboxylate (6b)

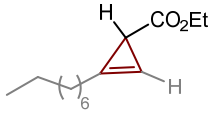

^1H NMR (400 MHz, $CDCl_3$) δ 6.31 (dt, *J* = 1.4 Hz, 1H), 4.12 (qd, *J* = 7.1, 5.0 Hz, 2H), 2.48 (td, *J* = 7.3, 1.4 Hz, 2H), 2.12 (d, *J* = 1.6 Hz, 1H), 1.61–1.52 (m, 2H), 1.35–1.22 (m, 13H), 0.91–0.83 (m, 3H). ^{13}C NMR (101 MHz, $CDCl_3$) δ 176.80, 115.77,

94.01, 60.28, 31.97, 29.39, 29.32, 29.27, 26.80, 25.10, 22.79, 19.86, 14.52, 14.24. HRMS (FAB) m/z: 225.1862 ($M+H^+$); calc. for $C_{14}H_{25}O_2$: 225.1855.

Ethyl 2-(hex-5-yn-1-yl)cycloprop-2-ene-1-carboxylate (6c)

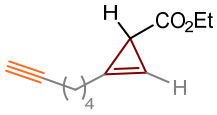

^{1}H NMR (400 MHz, $CDCl_3$) δ 6.35 (dt, *J* = 1.5 Hz, 1H), 4.20–4.04 (m, 2H), 2.52 (td, *J* = 7.2, 1.4 Hz, 2H), 2.21 (td, *J* = 6.9, 2.6 Hz, 2H), 2.13 (d, *J* = 1.6 Hz, 1H), 1.94 (t, *J* = 2.6 Hz, 1H), 1.71 (dtd, *J* = 8.7, 7.1, 5.4 Hz, 2H), 1.60 (dtd, *J* = 9.1, 6.9, 4.9 Hz, 2H), 1.24 (t, *J* = 7.1 Hz, 3H). ^{13}C NMR (101 MHz, $CDCl_3$) δ 176.63, 115.25, 94.60, 84.14, 68.69, 60.33, 27.89, 25.84, 24.63, 19.85, 18.23, 14.51. HRMS (FAB) m/z: 193.1220 ($M+H^+$); calc. for $C_{12}H_{17}O_2$: 193.1229.

6-(3-(Ethoxycarbonyl)cycloprop-1-en-1-yl)hexyl cyclobutanecarboxylate (6d)

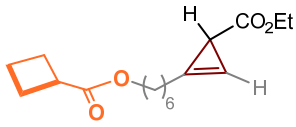

^{1}H NMR (400 MHz, $CDCl_3$) δ 6.33 (dt, *J* = 1.5 Hz, 1H), 4.17–4.08 (m, 2H), 4.05 (t, *J* = 6.7 Hz, 2H), 3.12 (p, *J* = 8.5 Hz, 1H), 2.49 (td, *J* = 7.3, 1.1 Hz, 2H), 2.33–2.13 (m, 4H), 2.12 (d, *J* = 1.6 Hz, 1H), 2.05–1.82 (m, 2H), 1.66–1.55 (m, 4H), 1.43–1.32 (m, 4H), 1.25 (t, *J* = 7.1 Hz, 3H). ^{13}C NMR (101 MHz, $CDCl_3$) δ 176.74, 175.74, 115.55, 94.26, 64.38, 60.33, 38.29, 28.87, 28.68, 26.68, 25.74, 25.42, 25.03, 19.85, 18.56, 14.54. HRMS (FAB) m/z: 295.1910 ($M+H^+$); calc. for $C_{17}H_{27}O_4$: 295.1909.

Ethyl 2-(5-(1,3-dioxolan-2-yl)pentyl)cycloprop-2-ene-1-carboxylate (6e)

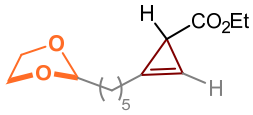

^{1}H NMR (400 MHz, Acetone-d_6) δ 6.61 (dt, *J* = 1.5 Hz, 1H), 4.81 (t, *J* = 4.8 Hz, 1H), 4.09 (qd, *J* = 7.1, 2.3 Hz, 2H), 3.98–3.88 (m, 2H), 3.87–3.76 (m, 2H), 2.54 (tdd, *J* = 7.1, 2.2, 1.4 Hz, 2H), 2.07 (d, *J* = 1.6 Hz, 1H), 1.67–1.57 (m, 4H), 1.52–1.41 (m, 4H), 1.23 (t, *J* = 7.1 Hz, 3H). ^{13}C NMR (101 MHz, Acetone-d_6) δ 175.78, 115.81, 104.67, 94.74, 65.05, 59.93, 34.29, 27.09, 25.03, 24.19, 19.69, 14.44 (one carbon peak may be overlapping with the solvent peaks). HRMS (FAB) m/z: 255.1593 ($M+H^+$); calc. for $C_{14}H_{23}O_4$: 255.1596.

Ethyl 2-(3-isopropoxypropyl)cycloprop-2-ene-1-carboxylate (6f)

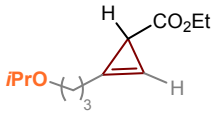

^{1}H NMR (400 MHz, $CDCl_3$) δ 6.34 (dt, *J* = 1.4 Hz, 1H), 4.12 (qd, *J* = 7.1, 4.2 Hz, 2H), 3.53 (hept, *J* = 6.2 Hz, 1H), 3.45 (td, *J* = 6.3, 1.9 Hz, 2H), 2.58 (td, *J* = 7.3, 1.4 Hz, 2H), 2.13 (d, *J* = 1.5 Hz, 1H), 1.88–1.78 (m, 2H), 1.24 (t, *J* = 7.1 Hz, 3H), 1.13 (d, *J* = 6.1 Hz, 6H). ^{13}C NMR (101 MHz, $CDCl_3$) δ 176.69, 115.36, 94.47, 71.61, 66.92, 60.31, 27.43, 22.24, 22.02, 19.89, 14.51. HRMS (FAB) m/z: 213.1485 ($M+H^+$); calc. for $C_{12}H_{21}O_3$: 213.1491.

Ethyl 2-(cyclohexylmethyl)cycloprop-2-ene-1-carboxylate (6g)

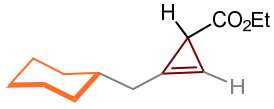

^{1}H NMR (400 MHz, $CDCl_3$) δ 6.33 (d, *J* = 1.4 Hz, 1H), 4.12 (qd, *J* = 7.1, 3.3 Hz, 2H), 2.38 (d, *J* = 7.2 Hz, 2H), 2.10 (d, *J* = 1.6 Hz, 1H), 1.82–1.52 (m, 6H), 1.27–1.07 (m, 6H), 0.98 (qt, *J* = 13.6, 3.7 Hz, 2H). ^{13}C NMR (101 MHz, $CDCl_3$) δ 176.76, 114.74, 94.58, 60.28, 36.22, 33.18, 33.17, 32.68, 26.41, 26.27, 26.25, 19.93, 14.53. HRMS (FAB) m/z: 209.1537 ($M+H^+$); calc. for $C_{13}H_{21}O_2$: 209.1542.

Ethyl 2-(6-((tetrahydro-2*H*-pyran-4-yl)methoxy)hexyl)cycloprop-2-ene-1-carboxylate (6h)

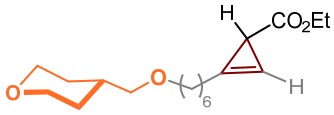

^{1}H NMR (400 MHz, $CDCl_3$) δ 6.32 (dt, *J* = 1.4 Hz, 1H), 4.13 (qd, *J* = 7.1, 5.5 Hz, 2H), 4.00–3.91 (m, 2H), 3.44–3.34 (m, 4H), 3.24 (d, *J* = 6.6 Hz, 2H), 2.49 (td, *J* = 7.3, 1.4 Hz, 2H), 2.12 (d, *J* = 1.5 Hz, 1H), 1.83 (ttt, *J* = 10.5, 6.7, 3.8 Hz, 1H), 1.67–1.62 (m, 2H), 1.60–1.52 (m, 4H), 1.43–1.34 (m, 4H), 1.34–1.28 (m, 2H), 1.25 (t, *J* = 7.1 Hz, 3H). ^{13}C NMR (101 MHz, $CDCl_3$) δ 176.78, 115.66, 94.15, 76.12, 71.25, 67.90, 60.32, 35.61, 30.19, 29.73, 29.11, 26.77, 26.02, 25.06, 19.86, 14.54. HRMS (FAB) m/z: 311.2210 ($M+H^+$); calc. for $C_{18}H_{31}O_4$: 311.2222.

Ethyl 2-(6-(cyclopropylmethoxy)hexyl)cycloprop-2-ene-1-carboxylate (6i)

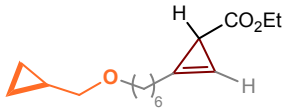

^{1}H NMR (400 MHz, $CDCl_3$) δ 6.32 (dt, *J* = 1.5 Hz, 1H), 4.12 (qd, *J* = 7.1, 5.2 Hz, 2H), 3.42 (t, *J* = 6.7 Hz, 2H), 3.24 (d, *J* = 6.9 Hz, 2H), 2.49 (td, *J* = 7.3, 1.4 Hz, 2H), 2.12 (d, *J* = 1.6 Hz, 1H), 1.62–1.54 (m, 4H), 1.41–1.34 (m, 4H), 1.25 (t, *J* = 7.2 Hz, 3H), 1.12–0.97 (m, 1H), 0.59–0.42 (m, 2H), 0.28–0.09 (m, 2H). ^{13}C NMR (101 MHz, $CDCl_3$) δ 176.78, 115.68, 94.13, 75.74, 70.78, 60.31, 29.79, 29.11, 26.76, 26.04, 25.05, 19.86, 14.54, 10.82, 3.13. HRMS (FAB) m/z: 267.1955 ($M+H^+$); calc. for $C_{16}H_{27}O_3$: 267.1960.

Ethyl 2-(4-chlorobutyl)cycloprop-2-ene-1-carboxylate (6k)

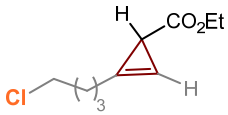

^{1}H NMR (400 MHz, $CDCl_3$) δ 6.37 (s, 1H), 4.12 (dd, *J* = 7.1, 4.2 Hz, 2H), 3.54 (t, *J* = 6.5 Hz, 2H), 2.54 (t, *J* = 7.0 Hz, 2H), 2.13 (s, 1H), 1.91–1.80 (m, 2H), 1.80–1.70 (m, 2H), 1.24 (t, *J* = 7.1 Hz, 3H). ^{13}C NMR (101 MHz, $CDCl_3$) δ 176.54, 114.98, 94.94, 60.37, 44.67, 31.89, 24.39, 24.12, 19.83, 14.49. HRMS (FAB) m/z: 203.0846 ($M+H^+$); calc. for $C_{10}H_{16}ClO_2$: 203.0839.

Ethyl 2-(6-((*trans*-4-(methoxymethyl)cyclohexyl)methoxy)hexyl)cycloprop-2-ene-1-carboxylate (6l)

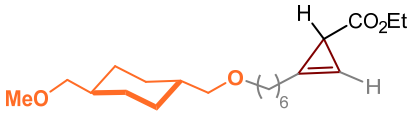

^{1}H NMR (400 MHz, $CDCl_3$) δ 6.32 (dt, *J* = 1.4 Hz, 1H), 4.12 (qd, *J* = 7.1, 5.4 Hz, 2H), 3.37 (t, *J* = 6.6 Hz, 2H), 3.32 (s, 3H), 3.21–3.17 (m, 4H), 2.49 (td, *J* = 7.3, 1.4 Hz, 2H), 2.12 (d, *J* = 1.6 Hz, 1H), 1.87–1.74 (m, 4H), 1.63–1.52 (m, 6H), 1.37 (tt, *J* = 6.3, 3.3 Hz, 4H), 1.25 (t, *J* = 7.1 Hz, 3H), 0.99–0.86 (m, 4H). ^{13}C NMR (101 MHz, $CDCl_3$) δ 176.79, 115.69, 94.12, 78.93, 76.90, 71.17, 60.31, 58.98, 38.37 (two carbons), 29.74, 29.65, 29.55, 29.11, 26.77, 26.03, 25.06, 19.86, 14.54. HRMS (FAB) m/z: 353.2699 ($M+H^+$); calc. for $C_{21}H_{37}O_4$: 353.2692.

Ethyl 2-(6-hydroxyhexyl)cycloprop-2-ene-1-carboxylate (6m)

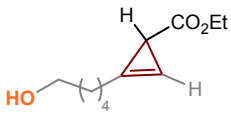

To a 100 mL flask, hept-6-yn-1-ol (1.12 g, 10.0 mmol) and imidazole (885 mg, 13.0 mmol) were dissolved in anhydrous DMF (50 mL). *Tert*-butylchlorodiphenylsilane (TBDPS–Cl, 3.30 g, 12.0 mmol) was added to the solution. The resulting mixture was stirred for 6 hours. The reaction mixture was quenched with water (40 mL) and the

product was extracted with Et_2O (50 mL × 3). The combined organic layer was washed with water (20 mL), brine (20 mL), dried over $MgSO_4$, and then concentrated under reduced pressure. The crude product was purified by silica column chromatography with hexane/ether (50:1) to afford *tert*-butyl(hept-6-yn-1-yloxy)diphenylsilane (3.44 g, 98%).

To a 20 mL vial was added *tert*-butyl(hept-6-yn-1-yloxy)diphenylsilane (1.0 mmol, 1.0 equiv.), $Rh_2(OAc)_4$ (4.4 mg, 1 mol%) and DCM (10 mL). The mixture was cooled to –78 °C, after which EDA (2.0 mmol in 2 mL DCM, 2.0 equiv.) was added dropwise to the solution. The reaction was allowed to slowly warm up to room temperature in 8 hours and stirred at room temperature for another 8 hours. Evaporation of the organic solvent and purification by silica column chromatography with hexane/ethyl acetate (20:1) as eluent afforded the crude cyclopropene product in ~30% yield.

To a 10 mL flask, the protected cyclopropene product was dissolved in THF (8 mL). Tetrabutylammonium fluoride (TBAF, 1M in THF, 0.9 mL) was added to the solution. The resulting mixture was stirred at room temperature for 5 h. Evaporation of the organic solvent and purification by silica column chromatography with hexane/ethyl acetate (1.5:1) as eluent afforded the racemic cyclopropene **6m** (48 mg, ~80% yield). ^{1}H NMR (400 MHz, Acetone-d_6) δ 6.56 (dt, J = 1.5 Hz, 1H), 4.05 (qd, J = 7.1, 2.5 Hz, 2H), 3.52 (t, J = 6.2 Hz, 2H), 2.50 (tt, J = 7.1, 1.6 Hz, 2H), 2.03 (d, J = 1.6 Hz, 1H), 1.63–1.56 (m, 2H), 1.55–1.49 (m, 2H), 1.48–1.40 (m, 2H), 1.19 (t, J = 7.1 Hz, 3H) (O–H proton is not resolved). ^{13}C NMR (101 MHz, Acetone-d_6) δ 176.12, 116.11, 94.99, 62.12, 60.23, 33.34, 27.33, 26.16, 25.47, 19.98, 14.72. HRMS (FAB) m/z: 199.1342 ($M+H^+$); calc. for $C_{11}H_{19}O_3$: 199.1334.

General procedure for rhodium-catalyzed cyclopropenation of internal alkynes:

To a 20 mL vial was added alkyne (1.5 mmol, 1.0 equiv.), $Rh_2(OAc)_4$ (6.6 mg, 2 mol%) and DCM (3 mL). A solution of EDA (3.0 mmol, 2.0 equiv.) in DCM (3 mL) was added dropwise to the reaction mixture over 10 hours through a syringe pump. The reaction was stirred at room temperature for another 6 hours. Evaporation of the organic solvent and purification by silica column chromatography using hexane and ethyl acetate as eluents afforded cyclopropene products (or products in mixture form with carbene dimers, diethyl maleate and diethyl fumarate). For most cyclopropene products, further purification by C18 column reverse-phase chromatography using acetonitrile and water as eluents was required to separate the cyclopropene products from the carbene dimers. The cyclopropene products were obtained mostly in 1% to 10% yields.

Ethyl 2-ethyl-3-phenylcycloprop-2-ene-1-carboxylate (9a)

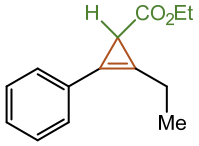

^{1}H NMR (400 MHz, $CDCl_3$) δ 7.44–7.37 (m, 2H), 7.35–7.29 (m, 2H), 7.27–7.22 (m, 1H), 4.15–4.02 (m, 2H), 2.62 (q, J = 7.5 Hz, 2H), 2.38 (s, 1H), 1.26 (t, J = 7.5 Hz, 3H), 1.18 (t, J = 7.1 Hz, 3H). ^{13}C NMR (101 MHz, $CDCl_3$) δ 176.05, 129.48, 128.75, 128.70, 127.19, 111.64, 104.65, 60.25, 22.34, 19.30, 14.57, 12.21. HRMS (TOF) m/z: 217.1194 ($M+H^+$); calc. for [$C_{14}H_{16}O_2+H^+$]: 217.1223.

Ethyl 2-ethyl-3-(4-chorophenyl)cycloprop-2-ene-1-carboxylate (9b)

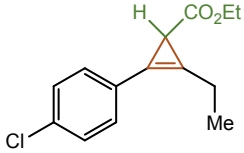

^{1}H NMR (400 MHz, $CDCl_3$) δ 7.45–7.31 (m, 4H), 4.22–4.07 (m, 2H), 2.69 (q, J = 7.5 Hz, 2H), 2.44 (s, 1H), 1.32 (t, J = 7.5 Hz, 3H), 1.24 (t, J = 7.1 Hz, 3H). ^{13}C NMR (101 MHz, $CDCl_3$) δ 175.71, 134.62, 130.63, 129.08, 125.79, 112.55,

103.78, 60.36, 22.34, 19.30, 14.55, 12.16. HRMS (TOF) m/z: 251.0847 ($M+H^+$); calc. for [$C_{14}H_{15}ClO_2+H^+$]: 251.0833.

Ethyl 2-methyl-3-phenylcycloprop-2-ene-1-carboxylate (9c)

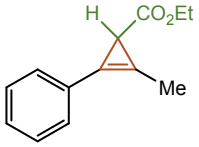

^{1}H NMR (400 MHz, $CDCl_3$) δ 7.49–7.44 (m, 2H), 7.42–7.36 (m, 2H), 7.35–7.28 (m, 1H), 4.16 (qd, *J* = 7.1, 3.7 Hz, 2H), 2.43 (s, 1H), 2.33 (s, 3H), 1.25 (t, *J* = 7.1 Hz, 3H). ^{13}C NMR (101 MHz, $CDCl_3$) δ 175.92, 129.42, 128.76, 128.71, 127.29, 106.51, 105.40, 60.30, 22.72, 14.59, 10.89. HRMS (TOF) m/z: 203.1054 ($M+H^+$); calc. for [$C_{13}H_{14}O_2+H^+$]: 203.1067.

Ethyl 2-ethyl-3-(2-fluorophenyl)cycloprop-2-ene-1-carboxylate (9d)

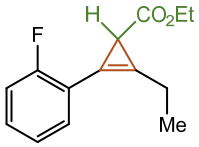

^{1}H NMR (400 MHz, $CDCl_3$) δ 7.38–7.27 (m, 2H), 7.16 (td, *J* = 7.5, 1.1 Hz, 1H), 7.10 (ddd, *J* = 9.3, 8.2, 1.0 Hz, 1H), 4.23–4.09 (m, 2H), 2.74 (qdd, *J* = 7.5, 2.4, 0.8 Hz, 2H), 2.43 (s, 1H), 1.30–1.22 (m, 6H). ^{13}C NMR (101 MHz, $CDCl_3$) δ 175.84, 161.02 (d, *J* = 253.5 Hz), 130.71 (d, *J* = 2.8 Hz), 130.49 (d, *J* = 8.0 Hz), 124.35 (d, *J* = 3.7 Hz), 115.80 (d, *J* = 15.4 Hz), 115.57 (d, *J* = 20.5 Hz), 114.08 (d, *J* = 3.8 Hz), 98.73 (d, *J* = 1.8 Hz), 60.34, 21.23, 19.26, 14.54, 11.45 (d, *J* = 2.0 Hz). HRMS (TOF) m/z: 235.1145 ($M+H^+$); calc. for [$C_{14}H_{15}FO_2+H^+$]: 235.1129.

Ethyl 2-ethyl-3-(4-fluorophenyl)cycloprop-2-ene-1-carboxylate (9e)

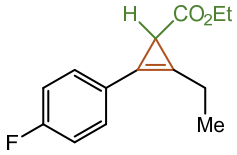

^{1}H NMR (400 MHz, $CDCl_3$) δ 7.51–7.38 (m, 2H), 7.13–7.04 (m, 2H), 4.23–4.07 (m, 2H), 2.68 (q, *J* = 7.5 Hz, 2H), 2.43 (s, 1H), 1.32 (t, *J* = 7.5 Hz, 3H), 1.25 (t, *J* = 7.1 Hz, 3H). ^{13}C NMR (101 MHz, $CDCl_3$) δ 175.89, 162.92 (d, *J* = 250.2 Hz), 131.25 (d, *J* = 8.5 Hz), 123.53 (d, *J* = 3.4 Hz), 115.97 (d, *J* = 22.1 Hz), 111.17, 103.71, 60.32, 22.37, 19.19, 14.56, 12.20. HRMS (TOF) m/z: 235.1134 ($M+H^+$); calc. for [$C_{14}H_{15}FO_2+H^+$]: 235.1129.

Ethyl 2-ethyl-3-(3-methoxyphenyl)cycloprop-2-ene-1-carboxylate (9f)

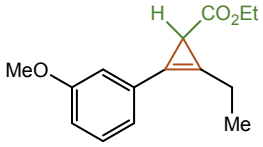

^{1}H NMR (400 MHz, $CDCl_3$) δ 7.34–7.27 (m, 1H), 7.08 (dt, *J* = 7.6, 1.2 Hz, 1H), 6.99 (dd, *J* = 2.7, 1.5 Hz, 1H), 6.87 (ddd, *J* = 8.3, 2.6, 1.0 Hz, 1H), 4.22–4.08 (m, 2H), 3.83 (s, 3H), 2.69 (q, *J* = 7.5 Hz, 2H), 2.44 (s, 1H), 1.33 (t, *J* = 7.5 Hz, 3H), 1.24 (t, *J* = 7.1 Hz, 3H). ^{13}C NMR (101 MHz, $CDCl_3$) δ 175.96, 159.84, 129.81, 128.46, 122.06, 114.69, 114.52, 112.03, 104.69, 60.26, 55.47, 22.48, 19.30, 14.57, 12.18. HRMS (TOF) m/z: 247.1331 ($M+H^+$); calc. for [$C_{15}H_{18}O_3+H^+$]: 247.1329.

Ethyl 2-ethyl-3-(4-trifluoromethylphenyl)cycloprop-2-ene-1-carboxylate (9g)

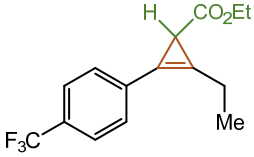

^{1}H NMR (400 MHz, $CDCl_3$) δ 7.64 (d, *J* = 8.1 Hz, 2H), 7.57 (d, *J* = 8.1 Hz, 2H), 4.16 (qd, *J* = 7.1, 5.3 Hz, 2H), 2.73 (q, *J* = 7.5 Hz, 2H), 2.49 (s, 1H), 1.34 (t, *J* = 7.5 Hz, 3H), 1.25 (t, *J* = 7.1 Hz, 3H). ^{13}C NMR (101 MHz, $CDCl_3$) δ 175.40, 130.72 (q, J = 2.2 Hz), 130.07 (q, J = 32.8 Hz), 129.57, 125.76 (q, J = 3.9 Hz), 124.11 (q, *J* = 272.0 Hz), 115.19, 103.88, 60.47, 22.41, 19.44, 14.53, 12.10. HRMS (TOF) m/z: 285.1118

(M+H⁺); calc. for [$C_{15}H_{15}F_3O_2$+H⁺]: 285.1097.

Ethyl 2-ethyl-3-(4-(difluoromethoxy)phenyl)cycloprop-2-ene-1-carboxylate (9h)

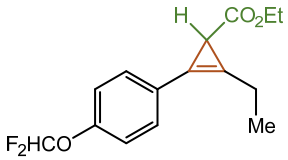

¹H NMR (400 MHz, $CDCl_3$) δ 7.47 (d, *J* = 8.7 Hz, 2H), 7.14 (d, *J* = 8.8 Hz, 2H), 6.52 (t, *J* = 73.6 Hz, 1H), 4.21–4.09 (m, 2H), 2.69 (q, *J* = 7.5 Hz, 2H), 2.44 (s, 1H), 1.32 (t, *J* = 7.5 Hz, 3H), 1.25 (t, *J* = 7.1 Hz, 3H). ¹³C NMR (101 MHz, $CDCl_3$) δ 175.80, 151.30 (t, *J* = 2.7 Hz), 130.95, 124.64, 119.87, 115.85 (t, *J* = 261.4 Hz), 111.95, 103.70, 60.35, 22.36, 19.25, 14.56, 12.20. HRMS (TOF) m/z: 283.1139 (M+H⁺); calc. for [$C_{15}H_{16}F_2O_3$+H⁺]: 283.1140.

Ethyl 2-ethyl-3-(*p*-tolyl)cycloprop-2-ene-1-carboxylate (9i)

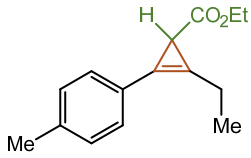

¹H NMR (400 MHz, $CDCl_3$) δ 7.37 (d, *J* = 8.1 Hz, 2H), 7.19 (d, *J* = 7.8 Hz, 2H), 4.21–4.06 (m, 2H), 2.67 (q, *J* = 7.5 Hz, 2H), 2.42 (s, 1H), 2.37 (s, 3H), 1.32 (t, *J* = 7.5 Hz, 3H), 1.24 (t, *J* = 7.1 Hz, 3H). ¹³C NMR (101 MHz, $CDCl_3$) δ 176.20, 138.79, 129.49, 129.42, 124.38, 110.28, 104.50, 60.19, 22.30, 21.60, 19.25, 14.57, 12.24. HRMS (TOF) m/z: 231.1378 (M+H⁺); calc. for [$C_{15}H_{18}O_2$+H⁺]: 231.1380.

Ethyl 2-ethyl-3-(4-methoxyphenyl)cycloprop-2-ene-1-carboxylate (9j)

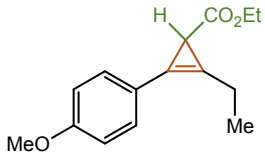

¹H NMR (400 MHz, $CDCl_3$) δ 7.41 (d, *J* = 8.8 Hz, 2H), 6.92 (d, *J* = 8.9 Hz, 2H), 4.20–4.09 (m, 2H), 3.83 (s, 3H), 2.66 (q, *J* = 7.4 Hz, 2H), 2.40 (s, 1H), 1.31 (t, *J* = 7.5 Hz, 3H), 1.24 (t, *J* = 7.1 Hz, 3H). ¹³C NMR (101 MHz, $CDCl_3$) δ 176.31, 160.04, 130.93, 128.47, 119.91, 114.32, 108.80, 104.05, 60.18, 55.50, 22.33, 19.17, 14.58, 12.29. HRMS (TOF) m/z: 247.1338 (M+H⁺); calc. for [$C_{15}H_{18}O_3$+H⁺]: 247.1329.

Ethyl 2-ethyl-3-(4-chloro-3-methylphenyl)cycloprop-2-ene-1-carboxylate (9k)

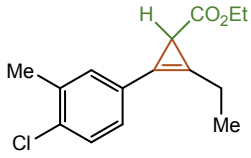

¹H NMR (400 MHz, $CDCl_3$) δ 7.35 (d, *J* = 8.2 Hz, 1H), 7.31 (d, *J* = 1.4 Hz, 1H), 7.24 (dd, *J* = 8.2, 1.9 Hz, 1H), 4.21–4.08 (m, 2H), 2.68 (q, *J* = 7.5 Hz, 2H), 2.42 (s, 1H), 2.38 (s, 3H), 1.32 (t, *J* = 7.5 Hz, 3H), 1.24 (t, *J* = 7.1 Hz, 3H). ¹³C NMR (101 MHz, $CDCl_3$) δ 175.84, 136.59, 134.87, 131.70, 129.51, 128.06, 125.74, 112.13, 103.86, 60.32, 22.34, 20.15, 19.28, 14.55, 12.16. HRMS (TOF) m/z: 265.1002 (M+H⁺); calc. for [$C_{15}H_{17}ClO_2$+H⁺]: 265.0990.

Ethyl 2-ethyl-3-(4-methoxy-3-methylphenyl)cycloprop-2-ene-1-carboxylate (9l)

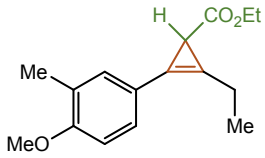

¹H NMR (400 MHz, $CDCl_3$) δ 7.30 – 7.24 (m, 2H), 6.83 (d, *J* = 8.2 Hz, 1H), 4.14 (dddd, *J* = 17.9, 10.8, 7.1, 3.7 Hz, 2H), 3.84 (s, 3H), 2.66 (q, *J* = 7.5 Hz, 2H), 2.39 (s, 1H), 2.22 (s, 3H), 1.31 (t, *J* = 7.5 Hz, 3H), 1.24 (t, *J* = 7.1 Hz, 3H). ¹³C NMR (101 MHz, $CDCl_3$) δ 176.43, 158.32, 131.76, 128.42, 127.19, 119.32, 110.08, 108.38, 104.17, 60.14, 55.55, 22.32, 19.15, 16.30, 14.59, 12.29. HRMS (TOF) m/z: 261.1463 (M+H⁺); calc. for [$C_{16}H_{20}O_2$+H⁺]: 261.1485.

Ethyl 2-(2-ethoxyethyl)-3-ethylcycloprop-2-ene-1-carboxylate (9m)

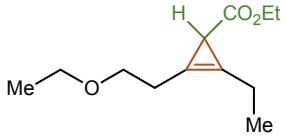

^{1}H NMR (400 MHz, $CDCl_3$) δ 4.11 (q, *J* = 7.1 Hz, 2H), 3.66 – 3.55 (m, 2H), 3.49 (qd, *J* = 7.0, 0.7 Hz, 2H), 2.69 (tq, *J* = 6.9, 1.5 Hz, 2H), 2.43 (qt, *J* = 7.5, 1.5 Hz, 2H), 2.07 (s, 1H), 1.24 (t, *J* = 7.1 Hz, 3H), 1.19 (t, *J* = 7.0 Hz, 3H), 1.14 (t, *J* = 7.5 Hz, 3H). ^{13}C NMR (101 MHz, $CDCl_3$) δ 177.01, 108.55, 102.81, 67.90, 66.38, 59.98, 25.58, 22.19, 18.35, 15.32, 14.56, 11.64. HRMS (TOF) m/z: 213.1481 ($M+H^+$); calc. for [$C_{12}H_{20}O_3+H^+$]: 213.1485.

Ethyl 2-(methoxymethyl)-3-pentylcycloprop-2-ene-1-carboxylate (9n)

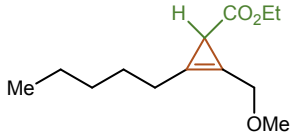

^{1}H NMR (400 MHz, $CDCl_3$) δ 4.37 (t, *J* = 1.5 Hz, 2H), 4.12 (q, *J* = 7.1 Hz, 2H), 3.39 (s, 3H), 2.47 (tt, *J* = 7.5, 1.5 Hz, 2H), 2.20 (s, 1H), 1.63–1.52 (m, 2H), 1.32 (tt, *J* = 6.7, 3.5 Hz, 4H), 1.24 (t, *J* = 7.1 Hz, 3H), 0.93–0.85 (m, 3H). ^{13}C NMR (101 MHz, $CDCl_3$) δ 176.17, 110.25, 102.48, 65.78, 60.19, 58.58, 31.54, 26.65, 24.68, 22.71, 22.48, 14.53, 14.13. HRMS (TOF) m/z: 227.1626 ($M+H^+$); calc. for [$C_{13}H_{22}O_3+H^+$]: 227.1642.

Ethyl 3-methoxydec-4-ynoate (9n-1)

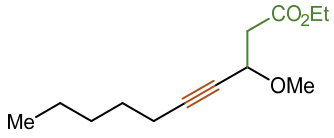

In a dry 100-mL round bottom flask, under argon, a solution of diisopropylamine (6 mmol, 1.2 equiv.) in THF (30 mL) was cooled to –78 °C. *n*-Butyllithium (6 mmol, 1.2 equiv., 1.6 M in hexanes) was added dropwise and the resulting mixture was stirred at the appropriate temperature for 30 min. The mixture was cooled to –78 °C before ethyl acetate (5 mmol, 1.0 equiv.) was added dropwise and the mixture was stirred for an additional 30 min. Then, a solution of oct-2-ynal (5.5 mmol, 1.1 equiv.) in THF (15 mL) was added slowly and the solution was stirred for a further 2 h. The reaction was allowed to room temperature and then quenched by NH_4Cl (sat. aq., 30 mL). Phases were separated and the aqueous phase was extracted with diethyl ether (30 mL × 3). The combined organics were washed with NH_4Cl (sat. aq., 2 × 10–15 mL), brine (10 mL), dried over Na_2SO_4, and concentrated under reduced pressure. Purification by silica column chromatography with hexanes/ethyl acetate afforded ethyl 3-hydroxydec-4-ynoate (1.02 g, 95% yield).

In a 50-mL round bottom flask, ethyl 3-hydroxydec-4-ynoate (3 mmol, 1.0 equiv.), Ag_2O (9 mmol, 3.0 equiv.), and dry ether (20 mL) were combined, followed by iodomethane (9 mmol, 3.0 equiv.). The reaction in aluminum foil to protect its contents from light was then stirred at the room temperature for 24 h. The crude mixture was filtered through a pad of Celite and concentrated under reduced pressure. Purification by silica column chromatography with hexanes/ethyl acetate afforded compound **9n-1** (302.6 mg, 45% yield). ^{1}H NMR (400 MHz, $CDCl_3$) δ 4.39 (ddt, *J* = 8.2, 5.4, 2.0 Hz, 1H), 4.16 (qd, *J* = 7.2, 1.0 Hz, 2H), 3.39 (s, 3H), 2.73 (dd, *J* = 15.5, 8.4 Hz, 1H), 2.63 (dd, *J* = 15.5, 5.4 Hz, 1H), 2.20 (td, *J* = 7.1, 2.0 Hz, 2H), 1.50 (p, *J* = 7.4 Hz, 2H), 1.40–1.28 (m, 4H), 1.26 (t, *J* = 7.1 Hz, 3H), 0.89 (t, *J* = 7.1 Hz, 3H). ^{13}C NMR (101 MHz, $CDCl_3$) δ 170.35, 87.30, 77.48, 67.75, 60.79, 56.57, 41.70, 31.11, 28.39, 22.30, 18.75, 14.32, 14.12. HRMS (TOF) m/z: 227.1634 ($M+H^+$); calc. for [$C_{13}H_{22}O_3+H^+$]: 227.1642.

A.5 Analysis of biotransformations for strained carbocycle construction

A.5.1 Enzymatic synthesis of bicyclobutanes

All enzymatic reactions for bicyclobutane formation in preparative scale were conducted following the general procedure described below and the corresponding bicyclobutane products were isolated. Detailed conditions for the preparative-scale reactions of different substrates are indicated separately.

General procedure for preparative-scale reactions:

To a 40 mL vial or 250 mL flask were added degassed suspension of *E. coli* expressing P411 **E10**-V78F S438A variant (OD_{600} = 10–20), alkyne (0.1–0.2 mmol, larger scales for **1k**–**1m**), EDA (2.0–4.0 equiv.), *D*-glucose (10–15 mM, 250 mM stock in M9-N), 1–5 vol% EtOH, M9-N buffer (pH 7.4) under anaerobic conditions. The vial or flask was capped and shaken (420 rpm for vials and 220 rpm for flasks) at room temperature for 12 h.

After the reaction was completed, every 30 mL portion of preparative-scale reaction mixture was transferred to a 50 mL Falcon centrifuge tube. The reaction container was washed with water (2 mL × 2) followed by mixed organic solvent (cyclohexane/ethyl acetate = 1:1, 2 mL × 3). The washing solution was combined with the reaction mixture in the centrifuge tubes. Additional 12 mL of cyclohexane/ethyl acetate solvent was added to every tube. After the tube (with ~45 mL mixture in total) was capped, it was vortexed (1 min × 3), shaken vigorously, and centrifuged (14,000 × g, 5 min). The organic layer was separated and the aqueous layer was subjected to three more rounds of extraction. Then organic layers were combined, dried over Na_2SO_4, and concentrated under reduced pressure. Purification by silica column chromatography with hexane/ethyl acetate as eluent afforded the desired bicyclobutanes. TTNs were calculated based on measured protein concentration and the isolated yield of the product.

Diethyl (2*R*,4*R*)-1-phenylbicyclo[1.1.0]butane-2,4-dicarboxylate (2a)

***E. coli* suspension in M9-N**				***D*-glucose in M9-N**	
OD_{600}	volume/mL	[PC]/μM	n_pro/μmol	volume/mL	[Glu]/mM
20	24.0	4.17	0.100	1.0	~10
alkyne (1a) stock in EtOH			**EDA stock in EtOH**		
stock/M	volume/μL	n_1/mmol	stock/M	volume/μL	n_2/mmol
1.00	180	0.18	2.00	180	0.36
purification eluent	**Product**				
Ethyl acetate in hexanes (0% to 10% gradient)	m[Pdt]/mg	n[Pdt]/mmol	yield	TTN	
	31.3	0.114	63%	1140	

Note: [PC] = protein concentration in original cell suspension, n_pro = amount of protein in the reaction, [Glu] = *D*-glucose concentration in reaction mixture, n_1 = amount of alkyne in the reaction, n_2 = amount of EDA in the reaction, m[Pdt] = mass of product isolated, n[Pdt] = amount of product. The same for the following tables.

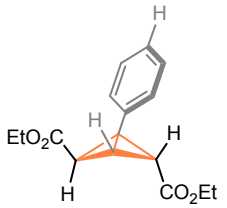

^{1}H NMR (400 MHz, $CDCl_3$) δ 7.34–7.22 (m, 5H), 4.14 (qd, *J* = 7.2, 2.4 Hz, 2H), 4.07 (qd, *J* = 7.2, 3.7 Hz, 2H), 3.26 (s, 1H), 3.13 (d, *J* = 3.0 Hz, 1H), 3.10 (d, *J* = 3.0 Hz, 1H), 1.27 (t, *J* = 7.1 Hz, 3H), 1.13 (t, *J* = 7.1 Hz, 3H). ^{13}C NMR (101 MHz, $CDCl_3$) δ 170.36, 167.91, 132.68, 128.50, 128.45, 127.56, 60.99, 60.91, 44.64, 42.55, 28.18, 20.47, 14.37, 14.16. HRMS (FAB) m/z: 275.1271 ($M+H^+$); calc. for $C_{16}H_{19}O_4$: 275.1283. $[\alpha]^{23}_D$ = –124.8 ± 1.1° (*c* 0.1, ethyl acetate).

Diethyl (2*R*,4*R*)-1-(4-fluorophenyl)bicyclo[1.1.0]butane-2,4-dicarboxylate (2b)

***E. coli* suspension in M9-N**				***D*-glucose in M9-N**	
OD_{600}	volume/mL	[PC]/μM	n_pro/μmol	volume/mL	[Glu]/mM
20	24.0	4.17	0.100	1.0	~10
alkyne (1b) stock in EtOH			**EDA stock in EtOH**		
stock/M	volume/μL	n_1/mmol	stock/M	volume/μL	n_2/mmol
1.0	180	0.18	2.0	180	0.36
purification eluent	**Product**				
Ethyl acetate in hexanes (0% to 10% gradient)	m[Pdt]/mg	n[Pdt]/mmol	yield	TTN	
	36.6	0.125	70%	1250	

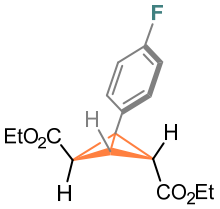

^{1}H NMR (400 MHz, $CDCl_3$) δ 7.32–7.26 (m, 2H), 7.05–6.94 (m, 2H), 4.21–4.11 (m, 2H), 4.11–4.00 (m, 2H), 3.23 (d, *J* = 0.5 Hz, 1H), 3.09 (d, *J* = 3.0 Hz, 1H), 3.04 (dd, *J* = 3.0, 0.6 Hz, 1H), 1.27 (t, *J* = 7.1 Hz, 3H), 1.14 (t, *J* = 7.1 Hz, 3H). ^{13}C NMR (101 MHz, $CDCl_3$) δ 170.20, 167.80, 163.59 (d, $J_{C\text{-}F}$ = 246.4 Hz), 130.55 (d, $J_{C\text{-}F}$ = 8.2 Hz), 128.31, (d, $J_{C\text{-}F}$ = 3.3 Hz), 115.63, (d, $J_{C\text{-}F}$ = 21.8 Hz), 61.06, 60.98, 44.83, 42.70, 27.50, 19.89, 14.37, 14.20. HRMS (FAB) m/z: 293.1179 ($M+H^+$); calc. for $C_{16}H_{18}FO_4$: 293.1189. $[\alpha]^{23}_D$ = –110.1 ± 2.0° (*c* 0.1, ethyl acetate).

Diethyl (2*R*,4*R*)-1-(4-chlorophenyl)bicyclo[1.1.0]butane-2,4-dicarboxylate (2c)

***E. coli* suspension in M9-N**				***D*-glucose in M9-N**	
OD_{600}	volume/mL	[PC]/μM	n_pro/μmol	volume/mL	[Glu]/mM
20	36.0	4.17	0.150	1.5	~10
alkyne (1c) stock in EtOH			**EDA stock in EtOH**		
stock/M	volume/μL	n_1/mmol	stock/M	volume/μL	n_2/mmol
1.0	200	0.20	2.0	400	0.80
purification eluent	**Product**				
Ethyl acetate in hexanes (0% to 10% gradient)	m[Pdt]/mg	n[Pdt]/mmol	yield	TTN	
	45.2	0.146	73%	980	

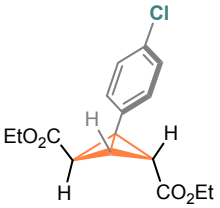

^{1}H NMR (400 MHz, $CDCl_3$) δ 7.28 (d, *J* = 8.9 Hz, 2H), 7.23 (d, *J* = 8.6 Hz, 2H), 4.14 (qd, *J* = 7.1, 2.4 Hz, 2H), 4.08 (qd, *J* = 7.1, 2.2 Hz, 2H), 3.24 (d, *J* = 0.6 Hz, 1H), 3.10 (d, *J* = 3.0 Hz, 1H), 3.08 (dd, *J* = 3.0, 0.5 Hz, 1H), 1.27 (t, *J* = 7.1 Hz, 3H), 1.16 (t, *J* = 7.1 Hz, 3H). ^{13}C NMR (101 MHz, $CDCl_3$) δ 170.06, 167.75, 133.48, 131.27, 129.93, 128.71, 61.10, 61.06, 44.77, 42.65, 27.47, 20.61, 14.36, 14.21. HRMS (FAB) m/z: 309.0902 ($M+H^+$); calc. for $C_{16}H_{18}ClO_4$: 309.0894. $[\alpha]^{23}_D$ = –141.5 ± 2.6° (*c* 0.1, ethyl acetate).

Diethyl (2*R*,4*R*)-1-(4-bromophenyl)bicyclo[1.1.0]butane-2,4-dicarboxylate (2d)

***E. coli* suspension in M9-N**				***D*-glucose in M9-N**	
OD_{600}	volume/mL	[PC]/μM	n_pro/μmol	volume/mL	[Glu]/mM
20	36.0	4.17	0.150	1.5	~10

alkyne (1d) stock in EtOH			**EDA stock in EtOH**		
stock/M	volume/μL	n_1/mmol	stock/M	volume/μL	n_2/mmol
1.0	150	0.15	2.0	300	0.60
purification eluent	**Product**				
Ethyl acetate in hexanes (0% to 10% gradient)	m[Pdt]/mg	n[Pdt]/mmol	yield	TTN	
	42.5	0.120	80%	800	

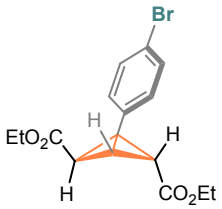

^{1}H NMR (400 MHz, $CDCl_3$) δ 7.43 (d, *J* = 8.7 Hz, 2H), 7.17 (d, *J* = 8.7 Hz, 2H), 4.14 (qd, *J* = 7.1, 2.4 Hz, 2H), 4.08 (qd, *J* = 7.1, 1.8 Hz, 2H), 3.24 (d, *J* = 0.6 Hz, 1H), 3.10 (d, *J* = 3.1 Hz, 1H), 3.09 (dd, *J* = 3.1, 0.5 Hz, 1H), 1.27 (t, *J* = 7.1 Hz, 3H), 1.16 (t, *J* = 7.1 Hz, 3H). ^{13}C NMR (101 MHz, $CDCl_3$) δ 170.02, 167.73, 131.84, 131.64, 130.22, 121.56, 61.11, 61.07, 44.74, 42.62, 27.53, 20.71, 14.36, 14.21. HRMS (FAB) m/z: 353.0399 ($M+H^+$); calc. for $C_{16}H_{18}BrO_4$: 353.0388 (^{79}Br). $[\alpha]^{23}_D$ = –128.4 ± 0.8° (*c* 0.1, ethyl acetate).

Diethyl (2*R*,4*R*)-1-(*p*-tolyl)bicyclo[1.1.0]butane-2,4-dicarboxylate (2e)

***E. coli* suspension in M9-N**				***D*-glucose in M9-N**	
OD_{600}	volume/mL	[PC]/μM	n_pro/μmol	volume/mL	[Glu]/mM
18	20.0	2.92	0.0584	1.0	~13
alkyne (1e) stock in EtOH			**EDA stock in EtOH**		
stock/M	volume/μL	n_1/mmol	stock/M	volume/μL	n_2/mmol
1.0	160	0.16	2.0	160	0.32
purification eluent	**Product**				
Ethyl acetate in hexanes (0% to 8% gradient)	m[Pdt]/mg	n[Pdt]/mmol	yield	TTN	
	29.6	0.103	64%	1760	

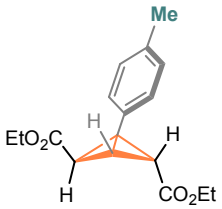

^{1}H NMR (400 MHz, $CDCl_3$) δ 7.19 (d, *J* = 8.2 Hz, 2H), 7.11 (d, *J* = 7.9 Hz, 2H), 4.18–4.03 (m, 4H), 3.23 (d, *J* = 0.6 Hz, 1H), 3.08 (dd, *J* = 3.0, 0.6 Hz, 1H), 3.06 (d, *J* = 3.0 Hz, 1H), 2.32 (s, 3H), 1.26 (t, *J* = 7.1 Hz, 3H), 1.15 (t, *J* = 7.1 Hz, 3H). ^{13}C NMR (101 MHz, $CDCl_3$) δ 170.48, 168.01, 137.37, 129.42, 129.22, 128.41, 60.94, 60.87, 44.62, 42.50, 28.09, 21.34, 20.07, 14.37, 14.20. HRMS (FAB) m/z: 289.1450 ($M+H^+$); calc. for $C_{17}H_{21}O_4$: 289.1440. $[\alpha]^{23}_D$ = –143.6 ± 1.0° (*c* 0.1, ethyl acetate).

Diethyl (2*R*,4*R*)-1-(4-ethylphenyl)bicyclo[1.1.0]butane-2,4-dicarboxylate (2f)

***E. coli* suspension in M9-N**				***D*-glucose in M9-N**	
OD_{600}	volume/mL	[PC]/μM	n_pro/μmol	volume/mL	[Glu]/mM
18	32.0	2.92	0.0934	1.5	~11
alkyne (1f) stock in EtOH			**EDA stock in EtOH**		
stock/M	volume/μL	n_1/mmol	stock/M	volume/μL	n_2/mmol
1.0	100	0.10	2.0	100	0.20
purification eluent	**Product**				
Ethyl acetate in hexanes	m[Pdt]/mg	n[Pdt]/mmol	yield	TTN	

(0% to 8% gradient)	16.8	0.0556	56%	600

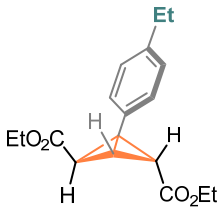

^{1}H NMR (400 MHz, $CDCl_3$) δ 7.22 (d, *J* = 8.3 Hz, 2H), 7.14 (d, *J* = 8.4 Hz, 2H), 4.20–4.01 (m, 4H), 3.23 (d, *J* = 0.6 Hz, 1H), 3.09 (dd, *J* = 3.0, 0.6 Hz, 1H), 3.07 (d, *J* = 3.0 Hz, 1H), 2.62 (q, *J* = 7.6 Hz, 2H), 1.26 (t, *J* = 7.1 Hz, 3H), 1.21 (t, *J* = 7.6 Hz, 3H), 1.14 (t, *J* = 7.1 Hz, 3H). ^{13}C NMR (101 MHz, $CDCl_3$) δ 170.49, 168.02, 143.73, 129.69, 128.46, 128.04, 60.93, 60.87, 44.57, 42.50, 28.72, 28.13, 20.14, 15.67, 14.38, 14.19. HRMS (FAB) m/z: 303.1588 ($M+H^+$); calc. for $C_{18}H_{23}O_4$: 303.1596. $[\alpha]^{23}_D$ = –133.7 ± 1.8° (*c* 0.1, ethyl acetate).

Diethyl (2*R*,4*R*)-1-(3-methoxyphenyl)bicyclo[1.1.0]butane-2,4-dicarboxylate (2g)

***E. coli* suspension in M9-N**				***D*-glucose in M9-N**	
OD_{600}	volume/mL	[PC]/μM	n_pro/μmol	volume/mL	[Glu]/mM
18	20.0	2.92	0.0584	1.0	~13
alkyne (1g) stock in EtOH			**EDA stock in EtOH**		
stock/M	volume/μL	n_1/mmol	stock/M	volume/μL	n_2/mmol
1.0	160	0.16	2.0	160	0.32
purification eluent	**Product**				
Ethyl acetate in hexanes (0% to 12% gradient)	m[Pdt]/mg	n[Pdt]/mmol	yield	TTN	
	27.2	0.0894	56%	1530	

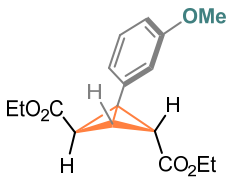

^{1}H NMR (400 MHz, $CDCl_3$) δ 7.24–7.19 (m, 1H), 6.88 (ddd, *J* = 7.6, 1.6, 1.0 Hz, 1H), 6.85–6.82 (m, 1H), 6.80 (ddd, *J* = 8.2, 2.6, 1.0 Hz, 1H), 4.20–4.01 (m, 4H), 3.78 (s, 3H), 3.25 (d, *J* = 0.6 Hz, 1H), 3.13 (dd, *J* = 3.0, 0.6 Hz, 1H), 3.09 (d, *J* = 3.0 Hz, 1H), 1.26 (t, *J* = 7.1 Hz, 3H), 1.15 (t, *J* = 7.1 Hz, 3H). ^{13}C NMR (101 MHz, $CDCl_3$) δ 170.31, 167.90, 159.67, 134.22, 129.54, 120.75, 114.01, 113.20, 61.01, 60.95, 55.35, 44.69, 42.58, 28.18, 20.69, 14.37, 14.20. HRMS (FAB) m/z: 305.1383 ($M+H^+$); calc. for $C_{17}H_{21}O_5$: 305.1389. $[\alpha]^{23}_D$ = –122.6 ± 1.5° (*c* 0.1, ethyl acetate).

Diethyl (2*R*,4*R*)-1-(3,5-dimethoxyphenyl)bicyclo[1.1.0]butane-2,4-dicarboxylate (2h)

***E. coli* suspension in M9-N**				***D*-glucose in M9-N**	
OD_{600}	volume/mL	[PC]/μM	n_pro/μmol	volume/mL	[Glu]/mM
16	45.0	2.54	0.114	3.0	~16
alkyne (1h) stock in EtOH			**EDA stock in EtOH**		
stock/M	volume/μL	n_1/mmol	stock/M	volume/μL	n_2/mmol
1.0	150	0.15	2.0	225	0.45
purification eluent	**Product**				
Ethyl acetate in hexanes (0% to 15% gradient)	m[Pdt]/mg	n[Pdt]/mmol	yield	TTN	
	19.8	0.0592	40%	520	

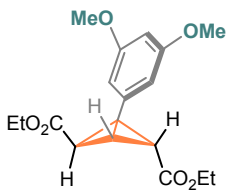

^{1}H NMR (400 MHz, $CDCl_3$) δ 6.44 (d, *J* = 2.2 Hz, 2H), 6.36 (t, *J* = 2.3 Hz, 1H), 4.15 (qd, *J* = 7.1, 2.5 Hz, 2H), 4.09 (qd, *J* = 7.1, 3.9 Hz, 2H),3.76 (s, 6H), 3.24 (s, 1H), 3.12 (d, *J* = 3.0 Hz, 1H), 3.09 (d, *J* = 3.0 Hz, 1H), 1.26 (t, *J* = 7.1 Hz, 3H), 1.17 (t, *J* = 7.1 Hz, 3H). ^{13}C NMR (101 MHz, $CDCl_3$) δ 170.14, 167.76, 160.71, 134.80, 106.29, 99.71, 60.88, 60.84, 55.33, 44.56, 42.45, 28.23, 20.67, 14.23, 14.11. HRMS (FAB) m/z: 335.1480 (M+H$^+$); calc. for $C_{18}H_{23}O_6$: 335.1495. $[\alpha]^{23}_D$ = –144.6 ± 3.5° (*c* 0.1, ethyl acetate).

Diethyl (2*R*,4*R*)-1-(3-hydroxyphenyl)bicyclo[1.1.0]butane-2,4-dicarboxylate (2i)

***E. coli* suspension in M9-N**				***D*-glucose in M9-N**	
OD_{600}	volume/mL	[PC]/μM	n_pro/μmol	volume/mL	[Glu]/mM
16	45.0	2.14	0.0963	3.0	~16
alkyne (1i) stock in EtOH			**EDA stock in EtOH**		
stock/M	volume/μL	n_1/mmol	stock/M	volume/μL	n_2/mmol
1.0	120	0.12	2.0	180	0.36
purification eluent	**Product**				
Ethyl acetate in hexanes (0% to 20% gradient)	m[Pdt]/mg	n[Pdt]/mmol	yield	TTN	
	10.4	0.0358	30%	370	

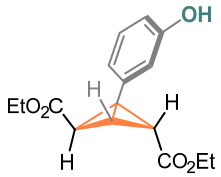

^{1}H NMR (400 MHz, $CDCl_3$) δ 7.15 (td, *J* = 8.1, 1.7 Hz, 1H), 6.87–6.83 (m, 1H), 6.78–6.74 (m, 1H), 6.73–6.68 (m, 1H), 5.06 (s, 1H), 4.21–4.02 (m, 4H), 3.23 (d, *J* = 0.6 Hz, 1H), 3.11 (dd, *J* = 3.1, 0.6 Hz, 1H), 3.09 (d, *J* = 3.0 Hz, 1H), 1.27 (t, *J* = 7.1 Hz, 3H), 1.15 (t, *J* = 7.1 Hz, 3H). ^{13}C NMR (101 MHz, $CDCl_3$) δ 170.22, 167.87, 155.59, 134.27, 129.62, 120.76, 115.15, 114.58, 60.94, 60.92, 44.54, 42.43, 27.86, 20.58, 14.23, 14.04. HRMS (FAB) m/z: 291.1237 (M+H$^+$); calc. for $C_{16}H_{19}O_5$: 291.1232.

Diethyl (2*R*,4*R*)-1-(thiophen-2-yl)bicyclo[1.1.0]butane-2,4-dicarboxylate (2j)

***E. coli* suspension in M9-N**				***D*-glucose in M9-N**	
OD_{600}	volume/mL	[PC]/μM	n_pro/μmol	volume/mL	[Glu]/mM
20	54.0	4.30	0.232	3.2	~14
alkyne (1j) stock in EtOH			**EDA stock in EtOH**		
stock/M	volume/μL	n_1/mmol	stock/M	volume/μL	n_2/mmol
1.0	100	0.10	2.0	200	0.40
purification eluent	**Product**				
Ethyl acetate in hexanes (0% to 8% gradient)	m[Pdt]/mg	n[Pdt]/mmol	yield	TTN	
	11.4	0.0407	41%	160	

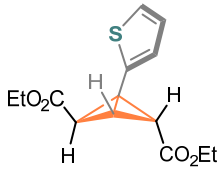

^{1}H NMR (400 MHz, $CDCl_3$) δ 7.20 (dd, *J* = 5.2, 1.2 Hz, 1H), 7.05 (dd, *J* = 3.5, 1.3 Hz, 1H), 6.94 (dd, *J* = 5.2, 3.5 Hz, 1H), 4.19–4.10 (m, 4H), 3.27 (s, 1H), 3.10 (d, *J* = 3.1 Hz, 1H), 3.06 (dd, *J* = 3.1, 0.6 Hz, 1H), 1.28 (t, *J* = 7.1 Hz, 3H), 1.20 (t, *J* = 7.1 Hz, 3H). ^{13}C NMR (101 MHz, $CDCl_3$) δ 169.92, 167.46, 135.29, 128.55, 126.97, 125.42, 61.14, 61.12, 45.87, 44.10, 23.88, 21.23, 14.37, 14.22. HRMS (FAB) m/z: 281.0839 (M+H$^+$); calc. for $C_{14}H_{17}O_4S$: 281.0848.

Diethyl (2*R*,4*R*)-1-(4-methoxyphenyl)bicyclo[1.1.0]butane-2,4-dicarboxylate (2k)

***E. coli* suspension in M9-N**				***D*-glucose in M9-N**	
OD_{600}	volume/mL	[PC]/μM	n_pro/μmol	volume/mL	[Glu]/mM
15	24.0	2.43	0.0583	1.0	~10
alkyne (1k) stock in EtOH			**EDA stock in EtOH**		
stock/M	volume/μL	n_1/mmol	stock/M	volume/μL	n_2/mmol
1.0	160	0.16	2.0	160	0.32
purification eluent	**Product**				
Ethyl acetate in hexanes (0% to 8% gradient)	m[Pdt]/mg	n[Pdt]/mmol	yield	TTN	
	32.4	0.107	67%	1830	

***E. coli* suspension in M9-N**				***D*-glucose in M9-N**	
OD_{600}	volume/mL	[PC]/μM	n_pro/μmol	volume/mL	[Glu]/mM
16	600	2.96	1.77	30	~12
alkyne (1k) stock in EtOH			**EDA stock in EtOH**		
stock/M	volume/mL	n_1/mmol	stock/mM	volume/mL	n_2/mmol
2.0	2.40	4.80	2.0	7.20	14.40
purification eluent	**Product**				
Ethyl acetate in hexanes (0% to 12% gradient)	m[Pdt]/mg	n[Pdt]/mmol	yield	TTN	
	680.4	2.34	47%	1260	

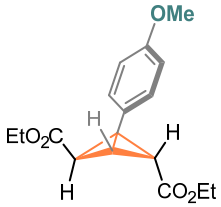

^{1}H NMR (400 MHz, $CDCl_3$) δ 7.25 (d, *J* = 8.7 Hz, 2H), 6.84 (d, *J* = 8.7 Hz, 2H), 4.20–3.99 (m, 4H), 3.79 (s, 3H), 3.21 (s, 1H), 3.04 (d, *J* = 2.9 Hz, 1H), 3.01 (d, *J* = 2.9 Hz, 1H), 1.27 (t, *J* = 7.1 Hz, 3H), 1.14 (t, *J* = 7.1 Hz, 3H). ^{13}C NMR (101 MHz, $CDCl_3$) δ 170.53, 168.01, 159.21, 130.03, 124.27, 113.99, 60.93, 60.85, 55.43, 44.68, 42.63, 27.90, 19.35, 14.38, 14.22. HRMS (FAB) m/z: 305.1375 ($M+H^+$); calc. for $C_{17}H_{21}O_5$: 305.1389. $[\alpha]^{23}_D$ = –138.2 ± 1.6° (*c* 0.1, ethyl acetate).

Diethyl (2*R*,4*R*)-1-(4-ethynylxyphenyl)bicyclo[1.1.0]butane-2,4-dicarboxylate (2l)

***E. coli* suspension in M9-N**				***D*-glucose in M9-N**	
OD_{600}	volume/mL	[PC]/μM	n_pro/μmol	volume/mL	[Glu]/mM
16	36.0	3.44	0.124	2.0	~13
alkyne (1l) stock in EtOH			**EDA stock in EtOH**		
stock/M	volume/μL	n_1/mmol	stock/M	volume/μL	n_2/mmol
1.0	150	0.15	2.0	225	0.45
purification eluent	**Product**				
Ethyl acetate in hexanes (0% to 8% gradient)	m[Pdt]/mg	n[Pdt]/mmol	yield	TTN	
	28.7	0.0962	64%	780	

***E. coli* suspension in M9-N**				***D*-glucose in M9-N**	
OD_{600}	volume/mL	[PC]/μM	n_pro/μmol	volume/mL	[Glu]/mM

18	600	3.03	1.82	30	~12
alkyne (1l) stock in EtOH			**EDA stock in EtOH**		
stock/M	volume/mL	n_1/mmol	stock/M	volume/mL	n_2/mmol
2.0	1.40	2.80	2.0	4.20	8.40
purification eluent	**Product**				
Ethyl acetate in hexanes (0% to 10% gradient)	m[Pdt]/mg	n[Pdt]/mmol	yield	TTN	
	393.7	1.32	47%	730	

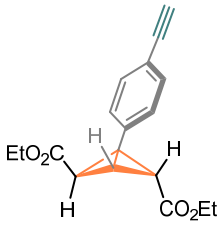

^{1}H NMR (400 MHz, $CDCl_3$) δ 7.45 (d, *J* = 8.5 Hz, 2H), 7.26 (d, *J* = 8.6 Hz, 2H), 4.17 (qd, *J* = 7.2, 2.9 Hz, 2H), 4.11 (qd, *J* = 7.1, 0.6 Hz, 2H), 3.29 (d, *J* = 0.6 Hz, 1H), 3.18 (dd, *J* = 3.1, 0.6 Hz, 1H), 3.15 (d, *J* = 3.1 Hz, 1H), 3.11 (s, 1H), 1.29 (t, *J* = 7.1 Hz, 3H), 1.17 (t, *J* = 7.1 Hz, 3H). ^{13}C NMR (101 MHz, $CDCl_3$) δ 170.04, 167.73, 133.79, 132.24, 128.28, 121.22, 83.47, 77.86, 61.12, 61.07, 44.73, 42.67, 27.88, 21.40, 14.36, 14.19. HRMS (FAB) m/z: 299.1282 ($M+H^+$); calc. for $C_{18}H_{19}O_4$: 299.1283. $[\alpha]^{23}_D$ = –152.6 ± 3.1° (*c* 0.1, ethyl acetate).

Diethyl (2*R*,4*R*)-1-(4-(hydroxymethyl)phenyl)bicyclo[1.1.0]butane-2,4-dicarboxylate (2m)

***E. coli* suspension in M9-N**				***D*-glucose in M9-N**	
OD_{600}	volume/mL	[PC]/μM	n_pro/μmol	volume/mL	[Glu]/mM
20	75.0	3.72	0.279	4.0	~13
alkyne (1m) stock in EtOH			**EDA stock in EtOH**		
stock/M	volume/μL	n_1/mmol	stock/M	volume/μL	n_2/mmol
1.0	360	0.36	2.0	540	1.08
purification eluent	**Product**				
Ethyl acetate in hexanes (0% to 25% gradient)	m[Pdt]/mg	n[Pdt]/mmol	yield	TTN	
	52.8	0.174	48%	630	

***E. coli* suspension in M9-N**				***D*-glucose in M9-N**	
OD_{600}	volume/mL	[PC]/μM	n_pro/μmol	volume/mL	[Glu]/mM
16	160	2.68	0.428	10	~15
alkyne (1m) stock in EtOH			**EDA stock in EtOH**		
stock/M	volume/mL	n_1/mmol	stock/M	volume/mL	n_2/mmol
1.0	1.00	1.00	2.0	2.00	4.00
purification eluent	**Product**				
Ethyl acetate in hexanes (0% to 25% gradient)	m[Pdt]/mg	n[Pdt]/mmol	yield	TTN	
	152.1	0.500	50%	580	

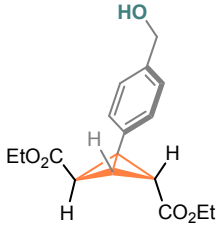

^{1}H NMR (400 MHz, $CDCl_3$) δ 7.30 (d, *J* = 2.5 Hz, 4H), 4.68 (d, *J* = 5.0 Hz, 2H), 4.14 (qd, *J* = 7.1, 2.3 Hz, 2H), 4.08 (qd, *J* = 7.1, 0.9 Hz, 2H), 3.26 (d, *J* = 0.5 Hz, 1H), 3.13 (dd, *J* = 3.1, 0.6 Hz, 1H), 3.10 (d, *J* = 3.0 Hz, 1H), 1.62 (t, *J* = 5.7 Hz, 1H), 1.27 (t, *J* = 7.1 Hz, 3H), 1.16 (t, *J* = 7.1 Hz, 3H). ^{13}C NMR (101 MHz, $CDCl_3$) δ 170.30, 167.93, 140.24, 132.11, 128.68, 127.15, 65.20, 61.02, 60.96, 44.72, 42.54, 27.96, 20.58, 14.37, 14.22. HRMS (FAB) m/z: 303.1230 (($M+H^+$)–H_2); calc. for $C_{17}H_{19}O_5$:

303.1232. $[\alpha]^{23}_D$ = –130.8 ± 1.2° (*c* 0.1, ethyl acetate).

A.5.2 Enzymatic synthesis of terminal cyclopropenes

All enzymatic reactions for cyclopropene formation in analytical scale were conducted following the general procedure described below and analyzed with gas chromatography (GC). All TTNs for the different products were determined using the GC standard curve of the corresponding racemic standard product made with $Rh_2(OAc)_4$.

All enzymatic reactions for cyclopropene formation in preparative scale were conducted following the general procedure described below and the corresponding cyclopropene products were isolated. Detailed conditions for preparative-scale reactions of different substrates are indicated separately.

General procedure for preparative-scale reactions:

To a 40 mL vial or 250 mL flask were added degassed suspension of *E. coli* expressing P411-**C6** or **K10** variant (OD_{600} = 10–60), alkyne (0.08–0.4 mmol, larger scales for **5a** and **5h**), EDA (1.0–4.0 equiv.), D-glucose (10–15 mM, 250 mM stock in M9-N), 1–5 vol% EtOH, M9-N buffer (pH 7.4) under anaerobic conditions. The vial or flask was capped and shaken (420 rpm for vials and 220 rpm for flasks) at room temperature for 12 h.

After the reaction was completed, every 30 mL portion of preparative-scale reaction mixture was transferred to a 50 mL Falcon centrifuge tube. The reaction container was washed with water (2 mL × 2) followed by mixed organic solvent (cyclohexane/ethyl acetate = 1:1, 2 mL × 3). The washing solution was combined to reaction mixture in centrifuge tubes. An additional 12 mL of cyclohexane/ethyl acetate solvent was added to every tube. After the tube (with ~45 mL mixture in total) was capped, it was vortexed (1 min × 3) and shaken vigorously, and centrifuged (14,000 × g, 5 min). The organic layer was separated and the aqueous layer was subjected to three more rounds of extraction. The organic layers were combined, dried over Na_2SO_4 and concentrated under reduced pressure. Purification by silica column chromatography with hexane/ethyl acetate as eluent afforded the desired cyclopropenes. Enantioselectivity was measured by chiral HPLC. TTNs were calculated based on measured protein concentration and isolated product yield.

Ethyl (*S*)-2-phenethylcycloprop-2-ene-1-carboxylate (*S*-6a)

Analysis Data (10 mM **5a**, P411-**K10**):

Entries	Pdt	Std	Pdt/Std	[Pdt]/mM	[PC]/μM	TTN	Avg. TTN	Avg. yield
6a-(1)	4637.1	590.6	7.852	6.24	1.93	3242		
6a-(2)	4639.5	592.1	7.836	6.23	1.93	3236		
6a-(3)	4797.4	582.9	8.230	6.54	1.93	3399		
6a-(4)	4674.5	588.0	7.950	6.32	1.93	3283	3290	63.3%

Preparative-scale reaction:

***E. coli* suspension expressing P411-K10 in M9-N**				***D*-glucose in M9-N**	
OD_{600}	volume/mL	[PC]/μM	n_pro/μmol	volume/mL	[Glu]/mM
20	28.0	3.12	0.0874	1.5	~13
alkyne (5a) stock in EtOH			**EDA stock in EtOH**		

stock/M	volume/μL	n_1/mmol	stock/M	volume/μL	n_2/mmol
0.80	500	0.40	0.80	500	0.40
purification eluent		**product**			
Ethyl acetate in hexanes (0% to 5% gradient)		m[Pdt]/mg	n[Pdt]/mmol	yield	TTN
		37.8	0.175	44%	2000

Ethyl (*R*)-2-phenethylcycloprop-2-ene-1-carboxylate (*R*-6a)

Analysis Data (10 mM **5a**, P411-**C6**):

Entries	Pdt	Std	Pdt/Std	[Pdt]/mM	[PC]/μM	TTN	Avg. TTN	Avg. yield
6a-(1)	4577.9	511.2	8.955	7.12	2.83	2518		
6a-(2)	4659.1	515.1	9.045	7.19	2.83	2543		
6a-(3)	4647.7	518.4	8.965	7.13	2.83	2521		
6a-(4)	4608.7	518.6	8.887	7.07	2.83	2499	2520	71.3%

Preparative-scale reaction:

***E. coli* suspension expressing P411-C6 in M9-N**				***D*-glucose in M9-N**	
OD_{600}	volume/mL	[PC]/μM	n_pro/μmol	volume/mL	[Glu]/mM
20	28.0	4.04	0.113	1.5	~13
alkyne (5a) stock in EtOH			**EDA stock in EtOH**		
stock/M	volume/μL	n_1/mmol	stock/M	volume/μL	n_2/mmol
0.80	500	0.40	0.80	500	0.40
purification eluent		**product**			
Ethyl acetate in hexanes (0% to 5% gradient)		m[Pdt]/mg	n[Pdt]/mmol	yield	TTN
		46.8	0.216	54%	1910

***E. coli* suspension expressing P411-C6 in M9-N**				***D*-glucose in M9-N**	
OD_{600}	volume/mL	[PC]/μM	n_pro/μmol	volume/mL	[Glu]/mM
24	800	5.35	4.28	50	~15
alkyne (5a) stock in EtOH			**EDA stock in EtOH**		
stock/M	volume/mL	n_1/mmol	stock/M	volume/mL	n_2/mmol
2.0	2.50	5.0	2.0	2.50 × 3	15.0
purification eluent		**product**			
Ethyl acetate in hexanes (0% to 5% gradient)		m[Pdt]/mg	n[Pdt]/mmol	yield	TTN
		824.1	3.81	76%	1780

(*S*)-**6a**: $[\alpha]^{23}_D$ = – 64.7 ± 3.6° (*c* 0.1, cyclohexane); (*R*)-**6a**: $[\alpha]^{23}_D$ = + 62.2 ± 2.5° (*c* 0.1, cyclohexane). Chiralpak IC, 5% *i*-PrOH in hexane, 1.0 mL/min, 210 nm

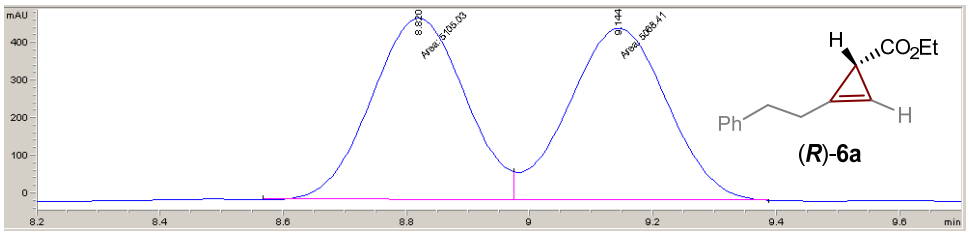

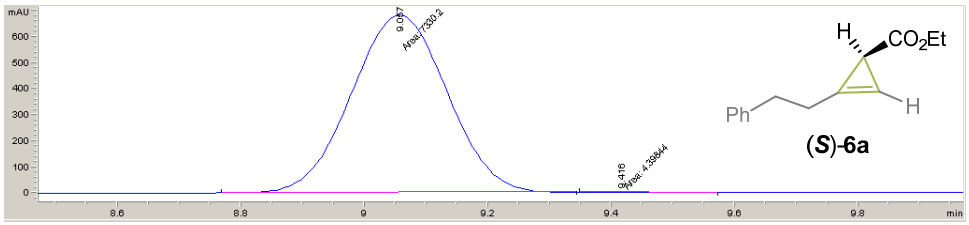

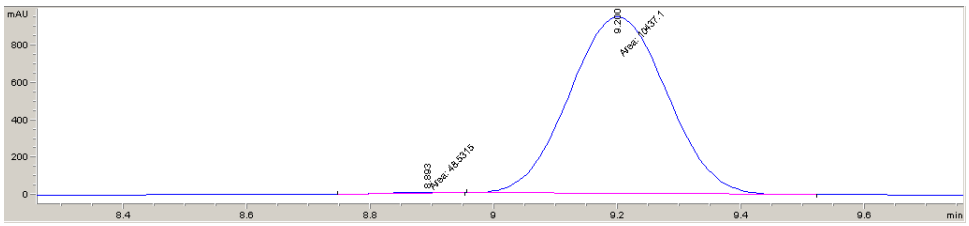

***rac*-6a**			***R*-6a**		
Retention Time (min)	Area (mAU*s)	Area %	Retention Time (min)	Area (mAU*s)	Area %
8.820	5105.03	50.19	9.057	7330.2	99.95
9.144	5066.41	49.81	9.416	4.4	0.05
Total	10171.44	100.00	Total	7334.6	100.00
***S*-6a**					
Retention Time (min)	Area (mAU*s)	Area %			
8.893	48.5	0.45			
9.200	10437.1	99.55			
Total	10485.6	100.00			

Ethyl (*R*)-2-octylcycloprop-2-ene-1-carboxylate (6b)

Analysis Data (10 mM **5b**, P411-**C6**):

Entries	Pdt	Std	Pdt/Std	[Pdt]/mM	[PC]/μM	TTN	Avg. TTN	Avg. yield
6b-(1)	1195.2	523.7	2.282	1.49	1.82	815		
6b-(2)	1128.3	528.7	2.134	1.39	1.82	763		
6b-(3)	1023.1	521.4	1.962	1.28	1.82	701	760	13.9%

Preparative-scale reaction:

***E. coli* suspension expressing P411-C6 in M9-N**				***D*-glucose in M9-N**	
OD_{600}	volume/mL	[PC]/μM	n_pro/μmol	volume/mL	[Glu]/mM
20	20.0 × 3	3.83	0.230	1.5	~12

alkyne (5b) stock in EtOH			**EDA stock in EtOH**		
stock/M	volume/μL	n_1/mmol	stock/M	volume/μL	n_2/mmol
0.80	250	0.20	0.80	250	0.20
purification eluent	**product**				
Ethyl acetate in hexanes (0% to 5% gradient)	m[Pdt]/mg	n[Pdt]/mmol	yield	TTN	
	27.2	0.121	61%	530	

(*R*)-**6b**: $[\alpha]^{23}_{D}$ = + 32.6 ± 1.8° (*c* 0.1, cyclohexane) [Note: (*S*)-**6b** (87% *ee*) was reported with $[\alpha]^{23}_{D}$ = – 30° (*c* 1.55, $CHCl_3$)[142]].

Chiralpak IC, 5% *i*-PrOH in hexane, 1.0 mL/min, 210 nm.

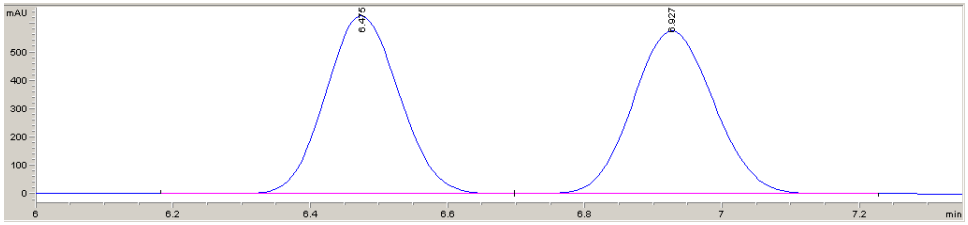

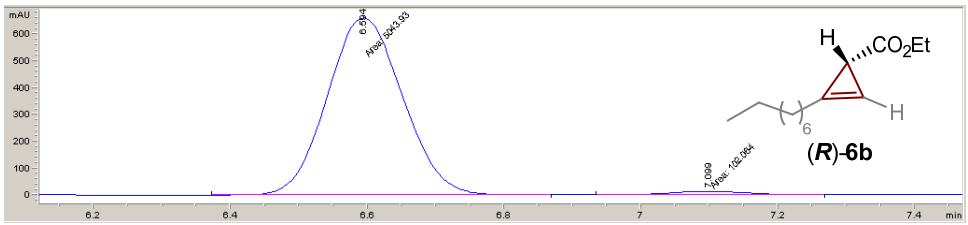

***rac*-6b**			***R*-6b**		
Retention Time (min)	Area (mAU*s)	Area %	Retention Time (min)	Area (mAU*s)	Area %
6.475	4707.7	49.89	6.594	5043.93	98.02
6.927	4729.1	50.11	7.099	102.06	1.98
Total	9436.8	100.00	Total	5145.99	100.00

Ethyl (*R*)-2-(hex-5-yn-1-yl)cycloprop-2-ene-1-carboxylate (6c)

Analysis Data (20 mM **5c**, P411-**C6**):

Entries	Pdt	Std	Pdt/Std	[Pdt]/mM	[PC]/μM	TTN	Avg. TTN	Avg. yield
6c-(1)	1084.2	344.6	3.146	2.39	1.67	1434		
6c-(2)	1164.4	407.1	2.860	2.17	1.67	1304		
6c-(3)	1079.9	385.7	2.800	2.13	1.67	1276		
6c-(4)	985.5	350.1	2.815	2.14	1.67	1283	1324	11.1%

Preparative-scale reaction:

***E. coli* suspension expressing P411-C6 in M9-N**				***D*-glucose in M9-N**	
OD_{600}	volume/mL	[PC]/μM	n_pro/μmol	volume/mL	[Glu]/mM
30	30.0	6.33	0.190	1.5	~12
alkyne (5c) stock in EtOH			**EDA stock in EtOH**		

stock/M	volume/μL	n_1/mmol	stock/M	volume/μL	n_2/mmol
0.80	500	0.40	0.80	500	0.40
purification eluent		**product**			
Ethyl acetate in hexanes (0% to 6% gradient)		m[Pdt]/mg	n[Pdt]/mmol	yield	TTN
		46.2	0.240	60%	1260

(*R*)-**6c**: $[\alpha]^{23}_{D}$ = + 52.2 ± 1.8° (*c* 0.1, cyclohexane).
Chiralpak IC, 5% *i*-PrOH in hexane, 1.0 mL/min, 210 nm

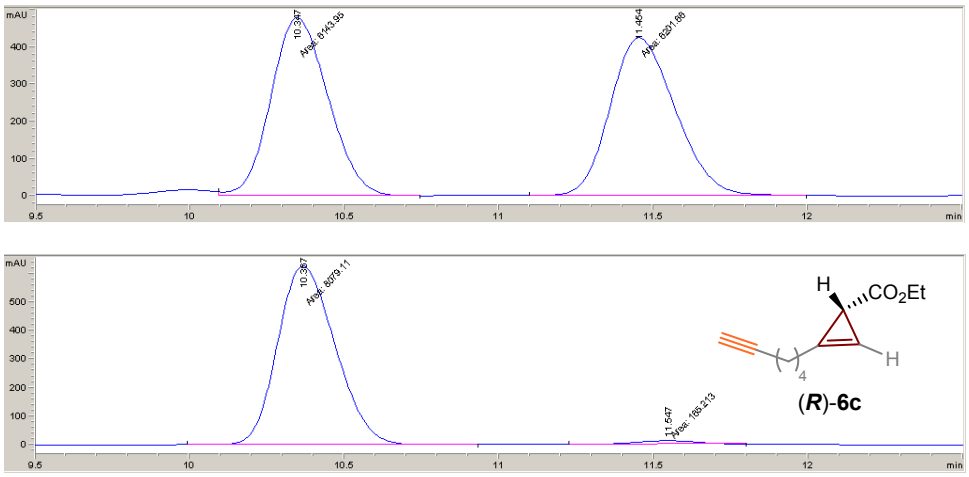

***rac*-6c**			***R*-6c**		
Retention Time (min)	Area (mAU*s)	Area %	Retention Time (min)	Area (mAU*s)	Area %
10.347	6143.95	49.77	10.367	8079.11	98.00
11.454	6201.66	50.23	11.547	165.21	2.00
Total	12345.61	100.00	Total	8244.32	100.00

(*R*)-6-(3-(Ethoxycarbonyl)cycloprop-1-en-1-yl)hexyl cyclobutanecarboxylate (6d)

Analysis Data (10 mM **5d**, P411-**C6**):

Entries	Pdt	Std	Pdt/Std	[Pdt]/mM	[PC]/μM	TTN	Avg. TTN	Avg. yield
6d-(1)	24642	4192	5.878	3.88	2.01	1930		
6d-(2)	22575	4190	5.388	3.56	2.01	1769		
6d-(3)	22572	4242	5.321	3.51	2.01	1747		
6d-(4)	24260	4249	5.710	3.77	2.01	1875	1831	36.8%

Preparative-scale reaction:

***E. coli* suspension expressing P411-C6 in M9-N**				***D*-glucose in M9-N**	
OD_{600}	volume/mL	[PC]/μM	n_pro/μmol	volume/mL	[Glu]/mM
32	25.0	6.48	0.162	1.5	~11
alkyne (5d) stock in EtOH			**EDA stock in EtOH**		
stock/M	volume/μL	n_1/mmol	stock/M	volume/μL	n_2/mmol
1.0	360	0.36	1.0	900	0.90

purification eluent	**product**			
Ethyl acetate in hexanes (0% to 12% gradient)	m[Pdt]/mg	n[Pdt]/mmol	yield	TTN
	56.7	0.193	54%	1190

(*R*)-**6d**: $[\alpha]^{23}_{D}$ = + 31.7 ± 1.7° (*c* 0.1, cyclohexane).

Chiralpak IC, 9% *i*-PrOH in hexane, 1.0 mL/min, 210 nm

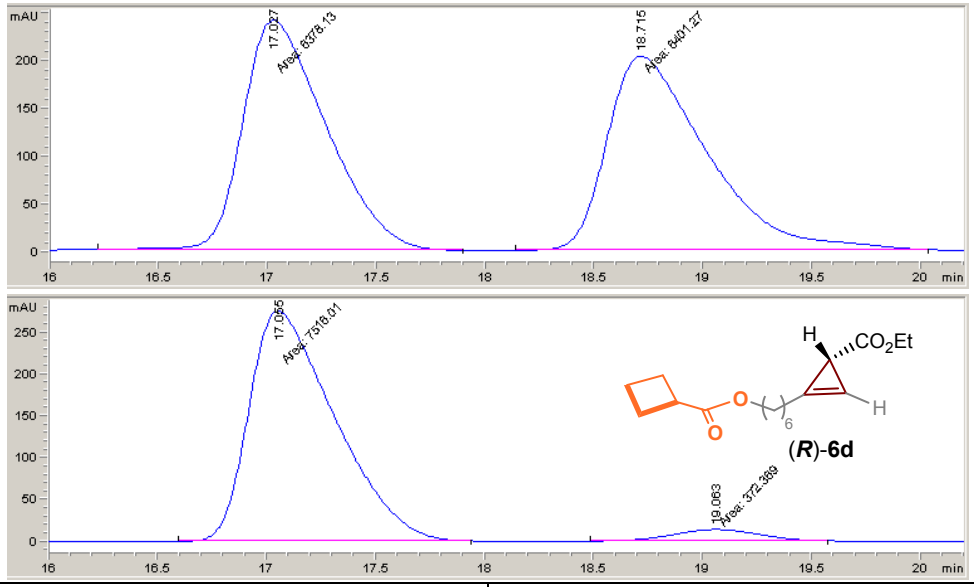

***rac*-6d**			***R*-6d**		
Retention Time (min)	Area (mAU*s)	Area %	Retention Time (min)	Area (mAU*s)	Area %
17.027	6378.13	49.91	17.055	7518.01	95.28
18.715	6401.27	50.09	19.063	372.37	4.72
Total	12779.4	100.00	Total	7890.38	100.00

Ethyl (*R*)-2-(5-(1,3-dioxolan-2-yl)pentyl)cycloprop-2-ene-1-carboxylate (6e)

Analysis Data (10 mM **5e**, P411-**C6**):

Entries	Pdt	Std	Pdt/Std	[Pdt]/mM	[PC]/μM	TTN	Avg. TTN	Avg. yield
6e-(1)	7788	4377	1.779	1.48	1.77	838		
6e-(2)	7579	4283	1.770	1.47	1.77	834		
6e-(3)	7654	4377	1.749	1.46	1.77	824		
6e-(4)	7263	4296	1.691	1.41	1.77	797	823	14.6%

Preparative-scale reaction:

***E. coli* suspension expressing P411-C6 in M9-N**				***D*-glucose in M9-N**	
OD_{600}	volume/mL	[PC]/μM	n_pro/μmol	volume/mL	[Glu]/mM
24	25.0 × 2	5.32	0.266	2.0	~10
alkyne (5e) stock in EtOH			**EDA stock in EtOH**		
stock/M	volume/μL	n_1/mmol	stock/M	volume/μL	n_2/mmol
1.0	240	0.24	1.0	720	0.72

purification eluent	product			
Ethyl acetate in hexanes (0% to 15% gradient)	m[Pdt]/mg	n[Pdt]/mmol	yield	TTN
	42.8	0.168	70%	630

(*R*)-**6e**: $[\alpha]^{23}_{D}$ = + 29.8 ± 1.3° (*c* 0.1, cyclohexane).

Chiralpak IC, 5% *i*-PrOH in hexane, 1.0 mL/min, 210 nm

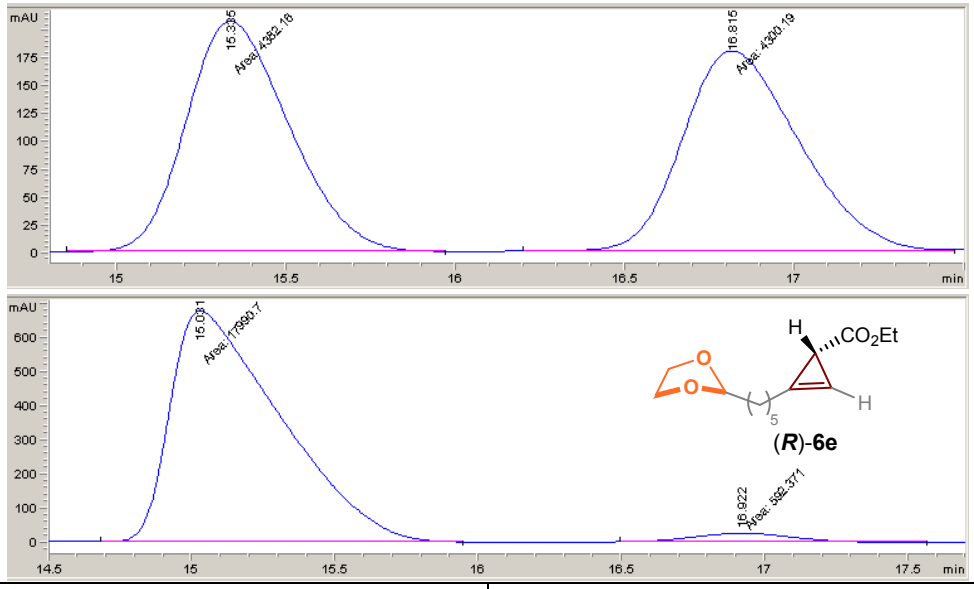

rac-**6e**			*R*-**6e**		
Retention Time (min)	Area (mAU*s)	Area %	Retention Time (min)	Area (mAU*s)	Area %
15.335	4382.18	50.47	15.031	17990.7	96.81
16.815	4300.19	49.53	16.922	592.4	3.19
Total	8682.37	100.00	Total	18583.1	100.00

Ethyl (*R*)-2-(3-isopropoxypropyl)cycloprop-2-ene-1-carboxylate (6f)

Analysis Data (10 mM **5f**, P411-**C6**):

Entries	Pdt	Std	Pdt/Std	[Pdt]/mM	[PC]/μM	TTN	Avg. TTN	Avg. yield
6f-(1)	212.9	504.7	0.422	0.38	1.82	207		
6f-(2)	289.9	514.0	0.564	0.50	1.82	276		
6f-(3)	252.4	511.2	0.494	0.44	1.82	242	242	4.4%

Preparative-scale reaction:

***E. coli* suspension expressing P411-C6 in M9-N**				***D*-glucose in M9-N**	
OD_{600}	volume/mL	[PC]/μM	n_pro/μmol	volume/mL	[Glu]/mM
30	40.0	6.27	0.251	2.0	~12
alkyne (5f) stock in EtOH			**EDA stock in EtOH**		
stock/mM	volume/μL	n_1/mmol	stock/mM	volume/μL	n_2/mmol
800	100	0.08	800	300	0.24
purification eluent			**product**		

Ethyl acetate in hexanes (0% to 8% gradient)	m[Pdt]/mg	n[Pdt]/mmol	yield	TTN
	13.6	0.0641	80%	260

Chiralpak IC, 5% *i*-PrOH in hexane, 1.0 mL/min, 210 nm

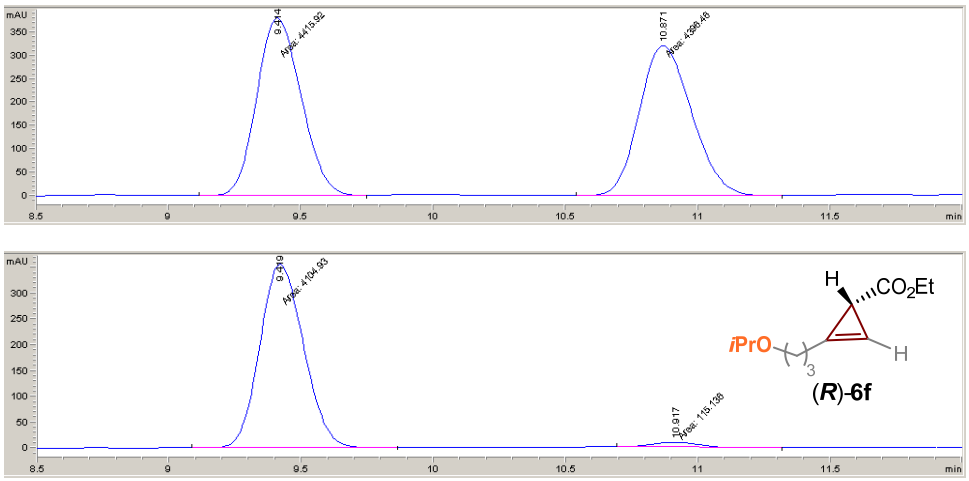

***rac*-6f**			***R*-6f**		
Retention Time (min)	Area (mAU*s)	Area %	Retention Time (min)	Area (mAU*s)	Area %
9.414	4415.92	50.11	9.419	4104.93	97.27
10.871	4396.46	49.89	10.917	115.14	2.73
Total	8812.38	100.00	Total	4220.07	100.00

Ethyl (*R*)-2-(cyclohexylmethyl)cycloprop-2-ene-1-carboxylate (6g)

Analysis Data (20 mM **5g**, P411-**C6**):

Entries	Pdt	Std	Pdt/Std	[Pdt]/mM	[PC]/μM	TTN	Avg. TTN	Avg. yield
6g-(1)	1044.5	704.1	1.483	0.97	1.67	585		
6g-(2)	903.7	654.8	1.380	0.91	1.67	544		
6g-(3)	1102.7	701.6	1.572	1.03	1.67	620		
6g-(4)	1105.0	726.7	1.521	1.00	1.67	600	587	4.9%

Preparative-scale reaction:

***E. coli* suspension expressing P411-C6 in M9-N**				***D*-glucose in M9-N**	
OD_{600}	volume/mL	[PC]/μM	n_pro/μmol	volume/mL	[Glu]/mM
20	20.0 × 3	3.83	0.230	1.5	~12
alkyne (5g) stock in EtOH			**EDA stock in EtOH**		
stock/M	volume/μL	n_1/mmol	stock/M	volume/μL	n_2/mmol
0.80	250	0.20	0.80	500	0.40
purification eluent		**product**			
Ethyl acetate in hexanes (0% to 5% gradient)		m[Pdt]/mg	n[Pdt]/mmol	yield	TTN
		23.1	0.111	55%	480

(*R*)-**6g**: $[\alpha]^{23}_{D}$ = + 53.4 ± 1.5° (*c* 0.1, cyclohexane).

Chiralpak IC, 5% *i*-PrOH in hexane, 1.0 mL/min, 210 nm

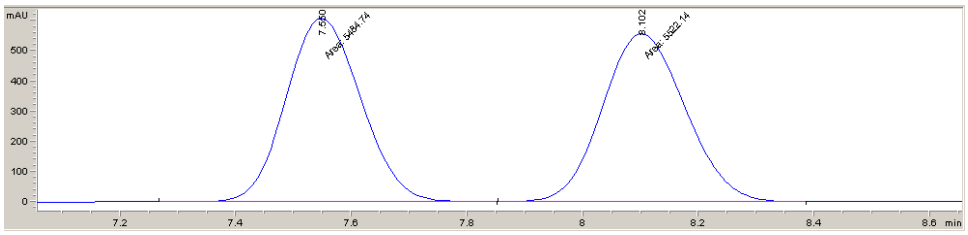

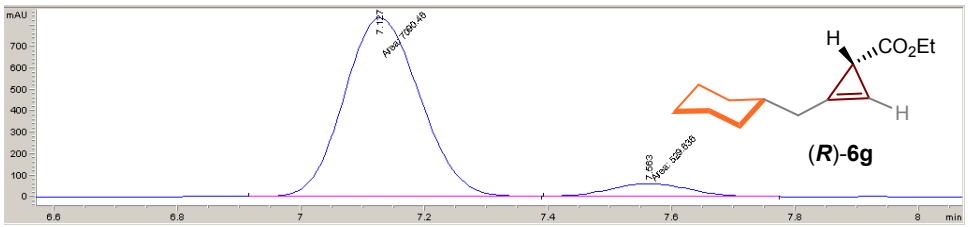

***rac*-6g**			***R*-6g**		
Retention Time (min)	Area (mAU*s)	Area %	Retention Time (min)	Area (mAU*s)	Area %
7.550	5484.74	49.83	7.127	7090.46	93.05
8.102	5522.14	50.17	7.563	529.64	6.95
Total	11006.88	100.00	Total	7620.10	100.00

Ethyl (*R*)-2-(6-((tetrahydro-2*H*-pyran-4-yl)methoxy)hexyl)cycloprop-2-ene-1-carboxylate (6h)

Analysis Data (10 mM **5h**, P411-**C6**):

Entries	Pdt	Std	Pdt/Std	[Pdt]/mM	[PC]/μM	TTN	Avg. TTN	Avg. yield
6h-(1)	40106	4085	9.818	7.31	1.77	4137		
6h-(2)	40775	4175	9.766	7.28	1.77	4115		
6h-(3)	39655	4125	9.613	7.16	1.77	4051		
6h-(4)	38780	4188	9.260	6.90	1.77	3902	4051	71.6%

Preparative-scale reaction:

***E. coli* suspension expressing P411-C6 in M9-N**				***D*-glucose in M9-N**	
OD_{600}	volume/mL	[PC]/μM	n_pro/μmol	volume/mL	[Glu]/mM
10	70.0	1.27	0.0886	3.0	~10
alkyne (5h) stock in EtOH			**EDA stock in EtOH**		
stock/M	volume/μL	n_1/mmol	stock/M	volume/mL	n_2/mmol
1.0	400	0.40	1.0	1.20	1.20
purification eluent	**product**				
Ethyl acetate in hexanes (0% to 12% gradient)	m[Pdt]/mg	n[Pdt]/mmol	yield	TTN	
	81.3	0.262	66%	2960	

***E. coli* suspension expressing P411-C6 in M9-N**	***D*-glucose in M9-N**

OD_{600}	volume/mL	[PC]/μM	n_pro/μmol	volume/mL	[Glu]/mM
20	200	4.84	0.968	12.0	~11
alkyne (5h) stock in EtOH			**EDA stock in EtOH**		
stock/M	volume/mL	n_1/mmol	stock/M	volume/mL	n_2/mmol
2.0	1.50	3.0	2.0	1.50 × 3	9.0
purification eluent		**product**			
Ethyl acetate in hexanes (0% to 12% gradient)		m[Pdt]/mg	n[Pdt]/mmol	yield	TTN
		872.4	2.81	94%	2900

(*R*)-**6h**: $[\alpha]^{23}_{D}$ = + 74.9 ± 1.8° (*c* 0.1, cyclohexane).

Chiralpak IC, 12% *i*-PrOH in hexane, 1.0 mL/min, 210 nm

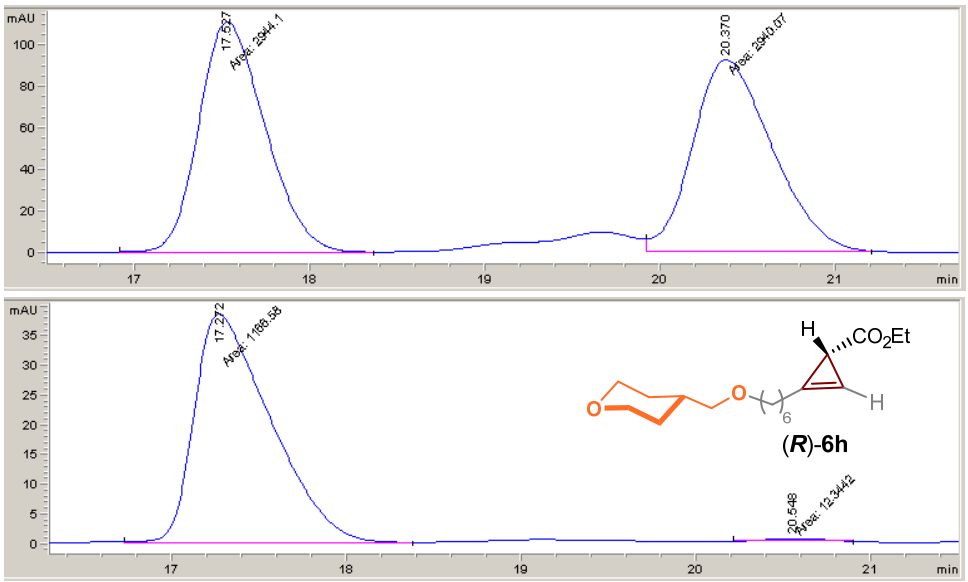

***rac*-6h**			***R*-6h**		
Retention Time (min)	Area (mAU*s)	Area %	Retention Time (min)	Area (mAU*s)	Area %
17.527	2944.10	50.03	17.272	1166.58	98.95
20.370	2940.07	49.97	20.548	12.34	1.05
Total	5884.17	100.00	Total	1178.92	100.00

Ethyl (*R*)-2-(6-(cyclopropylmethoxy)hexyl)cycloprop-2-ene-1-carboxylate (6i)

Analysis Data (10 mM **5i**, P411-**C6**):

Entries	Pdt	Std	Pdt/Std	[Pdt]/mM	[PC]/μM	TTN	Avg. TTN	Avg. yield
6i-(1)	26575	4144	6.413	4.44	2.01	2207		
6i-(2)	26599	4150	6.409	4.43	2.01	2206		
6i-(3)	26021	4086	6.368	4.40	2.01	2191		
6i-(4)	26300	4154	6.331	4.38	2.01	2179	2196	44.1%

Preparative-scale reaction:

***E. coli* suspension expressing P411-C6 in M9-N**	***D*-glucose in M9-N**

OD_{600}	volume/mL	[PC]/μM	n_pro/μmol	volume/mL	[Glu]/mM
32	25.0	6.48	0.162	1.5	~11
alkyne (5i) stock in EtOH			**EDA stock in EtOH**		
stock/M	volume/μL	n_1/mmol	stock/M	volume/μL	n_2/mmol
1.0	360	0.36	1.0	900	0.90
purification eluent		**product**			
Ethyl acetate in hexanes (0% to 10% gradient)		m[Pdt]/mg	n[Pdt]/mmol	yield	TTN
		61.8	0.232	64%	1430

(*R*)-**6i**: $[\alpha]^{23}_{D}$ = + 43.1 ± 1.5° (*c* 0.1, cyclohexane).

Chiralpak IC, 5% *i*-PrOH in hexane, 1.0 mL/min, 210 nm

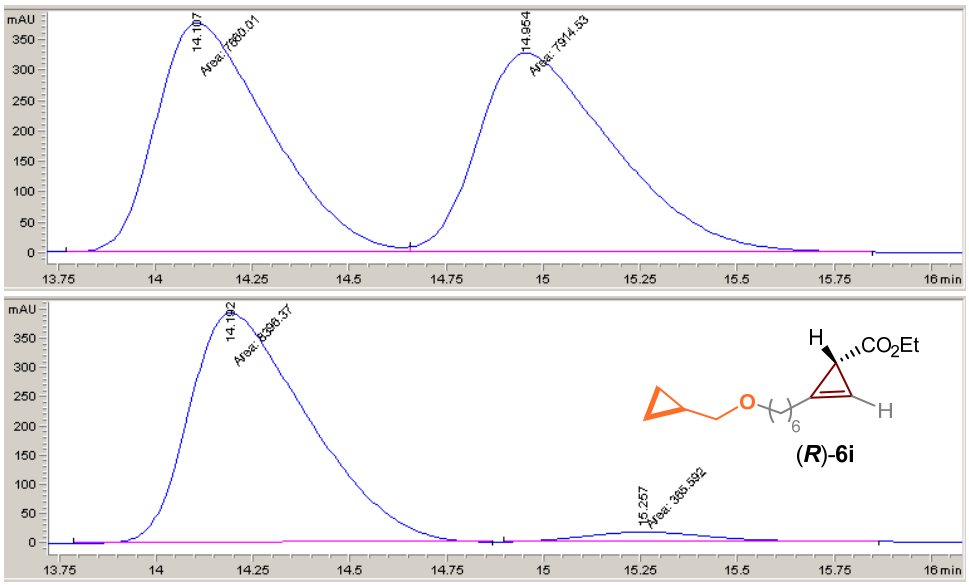

***rac*-6i**			***R*-6i**		
Retention Time (min)	Area (mAU*s)	Area %	Retention Time (min)	Area (mAU*s)	Area %
14.107	7660.01	49.18	14.192	8396.37	95.83
14.954	7914.53	50.82	15.257	365.59	4.17
Total	15574.54	100.00	Total	8761.96	100.00

Ethyl (*R* or *S*)-2-([1,1'-bi(cyclopropan)])-2-ene-1-carboxylate (*R* or *S*-6j)

Preparative-scale reaction:

***E. coli* suspension expressing P411-C6 in M9-N**				***D*-glucose in M9-N**	
OD_{600}	volume/mL	[PC]/μM	n_pro/μmol	volume/mL	[Glu]/mM
20	25.0	4.47	0.112	1.2	~11
alkyne (5j) stock in EtOH			**EDA stock in EtOH**		
stock/mM	volume/μL	n_1/mmol	stock/mM	volume/μL	n_2/mmol
400	250	0.10	400	375	0.15
purification eluent		**product**			
Ether in pentane		m[Pdt]/mg	n[Pdt]/mmol	yield	TTN

(0% to 20% gradient)	10.7	0.0703	70%	630

***E. coli* suspension expressing P411-K10 in M9-N**				***D*-glucose in M9-N**	
OD_{600}	volume/mL	[PC]/μM	n_pro/μmol	volume/mL	[Glu]/mM
20	25.0	3.07	0.0767	1.2	~11
alkyne (5j) stock in EtOH			**EDA stock in EtOH**		
stock/mM	volume/μL	n_1/mmol	stock/mM	volume/μL	n_2/mmol
400	250	0.10	400	375	0.15
purification eluent		**product**			
Ether in pentane (0% to 20% gradient)		m[Pdt]/mg	n[Pdt]/mmol	yield	TTN
		11.2	0.0736	74%	960

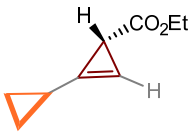

^{1}H NMR (600 MHz, Acetone-d_6) δ 6.47 (d, J = 1.6 Hz, 1H), 4.13 – 4.03 (m, 2H), 1.99 (d, J = 1.5 Hz, 1H), 1.91 (tt, J = 7.9, 4.6 Hz, 1H), 1.22 (t, J = 7.1 Hz, 3H), 1.01 – 0.94 (m, 2H), 0.84 – 0.80 (m, 1H), 0.61 – 0.58 (m, 1H). ^{13}C NMR (151 MHz, acetone) δ 175.54, 117.94, 92.45, 59.99, 18.65, 14.46, 6.79, 6.05, 5.78. HRMS (EI) m/z: 152.0865 ($M^{+\cdot}$); calc. for $C_9H_{12}O_2$: 152.0837.

Chiralpak IC, 5% *i*-PrOH in hexane, 1.0 mL/min, 210 nm

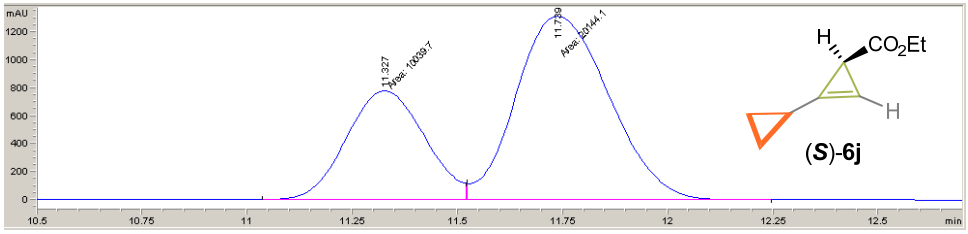

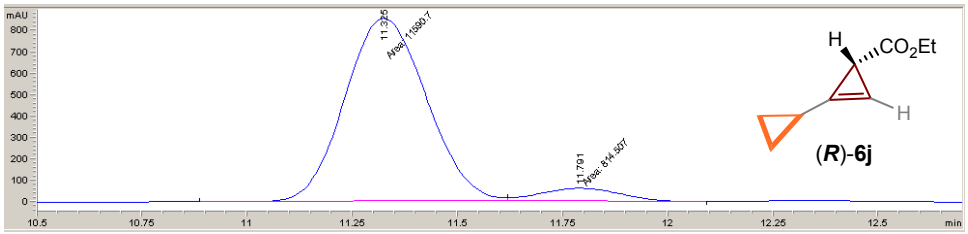

***S*-6j**			***R*-6j**		
Retention Time (min)	Area (mAU*s)	Area %	Retention Time (min)	Area (mAU*s)	Area %
11.327	10039.7	33.26	11.325	11590.7	93.43
11.739	20144.1	66.73	11.791	814.5	6.57
Total	30183.8	100.00	Total	12405.2	100.00

Ethyl (*R*)-2-(4-chlorobutyl)cycloprop-2-ene-1-carboxylate (6k)

Analysis Data (10 mM **5k**, P411-**C6**):

Entries	Pdt	Std	Pdt/Std	[Pdt]/mM	[PC]/μM	TTN	Avg. TTN	Avg. yield
6k-(1)	322.4	517.1	0.623	0.56	1.82	308		

6k-(2)	363.5	517.4	0.703	0.63	1.82	347		
6k-(3)	342.8	523.4	0.655	0.59	1.82	324	326	6.0%

Preparative-scale reaction:

***E. coli* suspension expressing P411-C6 in M9-N**				***D*-glucose in M9-N**	
OD_{600}	volume/mL	[PC]/μM	n_pro/μmol	volume/mL	[Glu]/mM
30	40.0	6.27	0.251	2.0	~12
alkyne (5k) stock in EtOH			**EDA stock in EtOH**		
stock/mM	volume/μL	n_1/mmol	stock/mM	volume/μL	n_2/mmol
800	125	0.10	800	375	0.30
purification eluent	**product**				
Ethyl acetate in hexanes (0% to 8% gradient)	m[Pdt]/mg	n[Pdt]/mmol	yield	TTN	
	17.6	0.0868	87%	340	

(*R*)-**6k**: $[\alpha]^{23}_{D}$ = + 25.7 ± 1.6° (*c* 0.1, cyclohexane).

Chiralpak IC, 5% *i*-PrOH in hexane, 1.0 mL/min, 210 nm

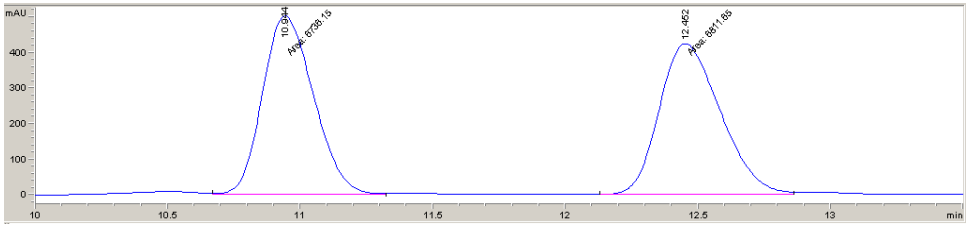

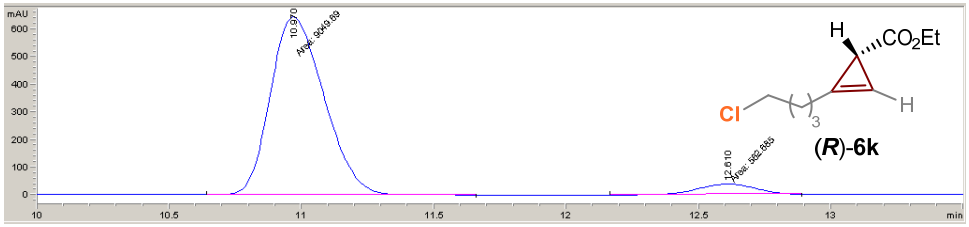

***rac*-6k**			***R*-6k**		
Retention Time (min)	Area (mAU*s)	Area %	Retention Time (min)	Area (mAU*s)	Area %
10.944	6736.15	49.72	10.970	9049.69	94.15
12.452	6811.65	50.28	12.610	562.69	5.85
Total	13547.8	100.00	Total	9612.38	100.00

Ethyl (*R*)-2-(6-((*trans*-4-(methoxymethyl)cyclohexyl)methoxy)hexyl)cycloprop-2-ene-1-carboxylate (6l)

Analysis Data (10 mM **5l**, P411-**C6**):

Entries	Pdt	Std	Pdt/Std	[Pdt]/mM	[PC]/μM	TTN	Avg. TTN	Avg. yield
6l-(1)	14861	4259	3.489	2.41	1.93	1252		
6l-(2)	13735	4274	3.214	2.22	1.93	1153		
6l-(3)	16271	4222	3.854	2.66	1.93	1383		

6l-(4)	13204	4323	3.054	2.11	1.93	1096	1221	23.5%

Preparative-scale reaction:

***E. coli* suspension expressing P411-C6 in M9-N**				***D*-glucose in M9-N**	
OD_{600}	volume/mL	[PC]/μM	n_pro/μmol	volume/mL	[Glu]/mM
10	35.0 × 2	1.27	0.0886	3.0	~10
alkyne (5l) stock in EtOH			**EDA stock in EtOH**		
stock/M	volume/μL	n_1/mmol	stock/M	volume/μL	n_2/mmol
1.0	180	0.18	1.0	540	0.54
purification eluent	**product**				
Ethyl acetate in hexanes (0% to 15% gradient)	m[Pdt]/mg	n[Pdt]/mmol	yield	TTN	
	22.1	0.0627	35%	710	

(*R*)-**6l**: $[\alpha]^{23}_{D}$ = + 62.6 ± 2.7° (*c* 0.1, cyclohexane).

Chiralpak IC, 7% *i*-PrOH in hexane, 1.0 mL/min, 210 nm

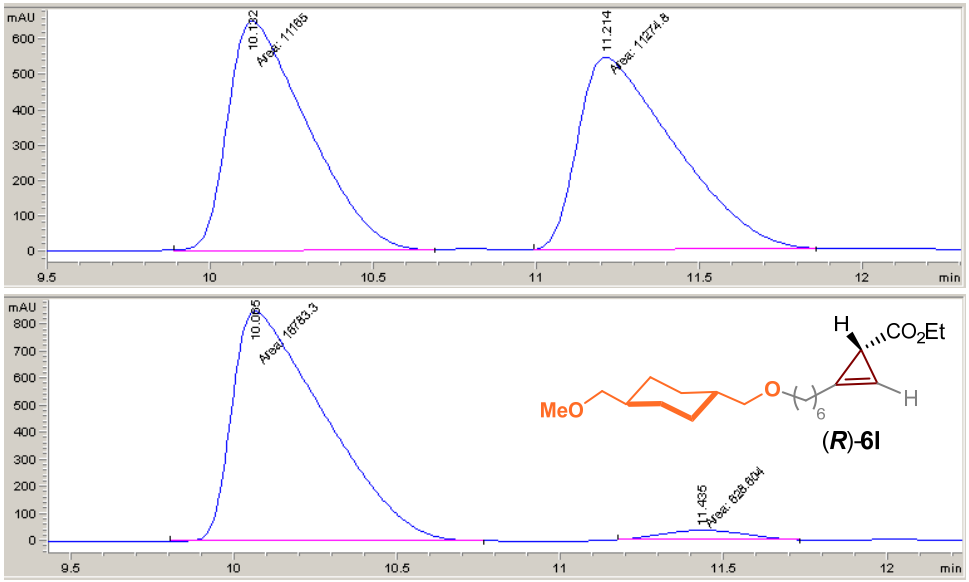

***rac*-6l**			***R*-6l**		
Retention Time (min)	Area (mAU*s)	Area %	Retention Time (min)	Area (mAU*s)	Area %
10.132	11165.0	49.76	10.065	16783.3	96.39
11.214	11274.8	50.24	11.435	628.6	3.61
Total	22439.8	100.00	Total	17411.9	100.00

Ethyl (*R*)-2-(6-hydroxyhexyl)cycloprop-2-ene-1-carboxylate (6m)

Preparative-scale reaction:

***E. coli* suspension expressing P411-C6 in M9-N**				***D*-glucose in M9-N**	
OD_{600}	volume/mL	[PC]/μM	n_pro/μmol	volume/mL	[Glu]/mM
30	40.0	6.80	0.272	1.5	~12
alkyne (5m) stock in EtOH			**EDA stock in EtOH**		
stock/M	volume/μL	n_1/mmol	stock/M	volume/μL	n_2/mmol

1.0	250	0.25	2.0	750	1.50
purification eluent		**product**			
Ethyl acetate in hexanes (0% to 25% gradient)		m[Pdt]/mg	n[Pdt]/mmol	yield	TTN
		38.2	0.193	80%	710

(*R*)-**6m**: $[\alpha]^{23}_{D}$ = + 80.1 ± 3.4° (*c* 0.1, ethyl acetate).
Chiralpak IC, 12% *i*-PrOH in hexane, 1.0 mL/min, 210 nm

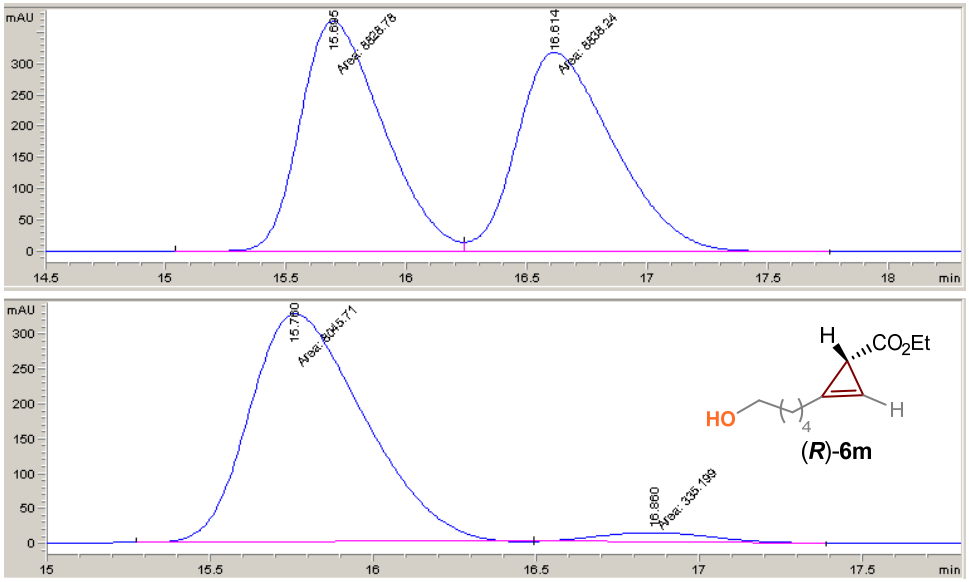

***rac*-6m**			***R*-6m**		
Retention Time (min)	Area (mAU*s)	Area %	Retention Time (min)	Area (mAU*s)	Area %
15.695	8828.78	49.97	15.760	8045.71	96.00
16.614	8838.24	50.03	16.860	335.20	4.00
Total	17667.02	100.00	Total	8380.91	100.00

A.5.3 Enzymatic synthesis of internal cyclopropenes

All enzymatic reactions for internal cyclopropene formation in analytical scale were conducted following the general procedure described below and analyzed with gas chromatography (GC). All TTNs for the different products were determined using the GC standard curves of the corresponding racemic standard products made with $Rh_2(OAc)_4$.

General procedure for preparative-scale reactions:

To a 500 mL flask were added a suspension of *E. coli* expressing P411-**C10** variant (OD_{600} = 15), alkyne (1.0 mmol), EDA (0.8 mmol, 0.8 equiv.), D-glucose (20 mM), M9-N buffer/EtOH (20:1 v/v) under anaerobic conditions. The flask was capped and shaken (300 rpm) inside the anaerobic chamber at room temperature for 2 h. The second portion of EDA (0.8 mmol, 0.8 equiv.) was added to the reaction before the reaction was shaken for another 2 h and a third portion of EDA (0.8 mmol, 0.8 equiv.) was then added. The reaction was shaken for another 20 h.

After the reaction was completed, the reaction mixture were transferred to 500 mL centrifuge bottle. The reaction flask was washed with water (3 mL × 3) followed by mixed organic solvent (hexane/ethyl acetate = 1:1, 5 mL × 3). The washing solution was combined with the reaction mixture

in the centrifuge bottle. An additional 100 mL of hexane/ethyl acetate solvent was added to the centrifuge bottle. After the bottle was capped, it was shaken vigorously and centrifuged (6,000 × g, 6 min). The organic layer was separated and the aqueous layer was subjected to three more rounds of extraction. The organic layers were combined, dried over Na_2SO_4 and concentrated under reduced pressure. Purification by silica column chromatography with hexane/ethyl acetate as eluents followed by C18 column reverse-phase chromatography using acetonitrile/water as eluents afforded the desired cyclopropenes. TTNs were calculated based on measured protein concentration and isolated product yield.

Ethyl 2-ethyl-3-phenylcycloprop-2-ene-1-carboxylate (9a)

Analysis Data (**WIRF**, OD_{600}=15):

Entries	Pdt	Std	Pdt/Std	[Pdt]/mM	[PC]/μM	TTN	Avg. TTN
9a-(1)	6839.6	806.9	8.476	6.03	2.26	2671	
9a-(2)	6587.7	776.4	8.485	6.03	2.26	2673	
9a-(3)	6650.3	779.8	8.528	6.06	2.26	2686	
9a-(4)	6678.4	789.6	8.458	6.01	2.26	2665	2674

Chiralpak IC, 4% isopropanol in hexane, 1.2 ml/min, 32 °C, 254nm

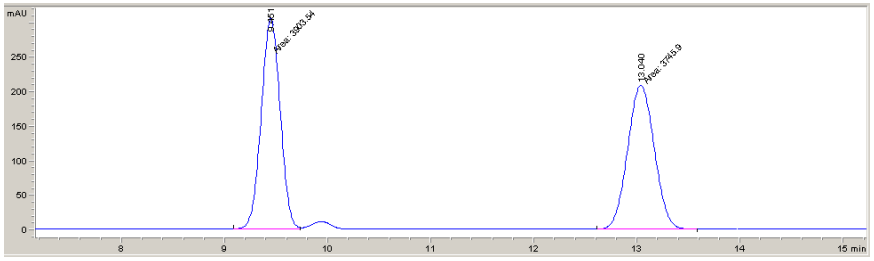

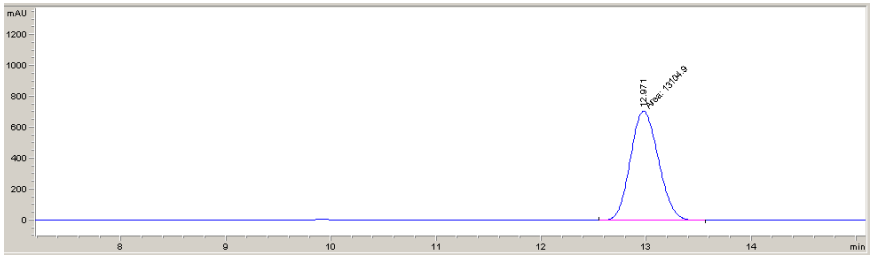

Racemic **9a**			Enzymatically produced **9a**		
Retention Time (min)	Area (mAU*s)	Area %	Retention Time (min)	Area (mAU*s)	Area %
9.45	3903.5	51.03	-	-	-
13.04	3745.9	48.97	12.97	13104.9	100.00
Total	7649.4	100.00	Total	13104.9	100.00

Ethyl 2-ethyl-3-(4-chorophenyl)cycloprop-2-ene-1-carboxylate (9b)

Analysis Data (**WIRF_GAK**, OD_{600}=20):

Entries	Pdt	Std	Pdt/Std	[Pdt]/mM	[PC]/μM	TTN	Avg.

							TTN
9b-(1)	6612.8	780.1	8.477	4.62	2.18	2124	
9b-(2)	6951.3	789.3	8.807	4.81	2.18	2210	
9b-(3)	6318.4	783.2	8.067	4.39	2.18	2018	
9b-(4)	6829.4	789.4	8.651	4.72	2.18	2169	2130

Chiralpak IC, 3% isopropanol in hexane, 1.2 ml/min, 32 °C, 254nm

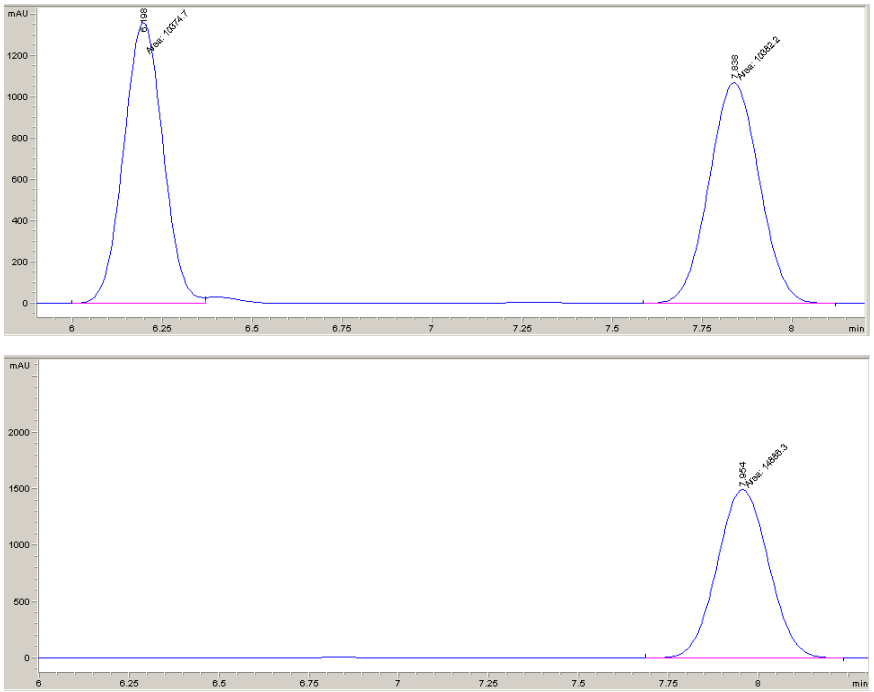

Racemic **9b**			Enzymatically produced **9b**		
Retention Time (min)	Area (mAU*s)	Area %	Retention Time (min)	Area (mAU*s)	Area %
6.20	10374.7	49.98	-	-	-
7.84	10382.2	50.02	7.95	14886.3	100.00
Total	20756.9	100.00	Total	14886.3	100.00

Ethyl 2-methyl-3-phenylcycloprop-2-ene-1-carboxylate (**9c**)

Analysis Data (**WIRF**, OD_{600}=15):

Entries	Pdt	Std	Pdt/Std	[Pdt]/mM	[PC]/μM	TTN	Avg. TTN
9c-(1)	6449.8	776.8	8.303	5.47	2.26	2426	
9c-(2)	6363.9	784.1	8.116	5.35	2.26	2370	
9c-(3)	5895.1	779.2	7.566	4.98	2.26	2207	
9c-(4)	6059.4	756.8	8.007	5.27	2.26	2338	2335

Chiralpak IC, 2.8% isopropanol in hexane, 1.2 ml/min, 32 °C, 254nm

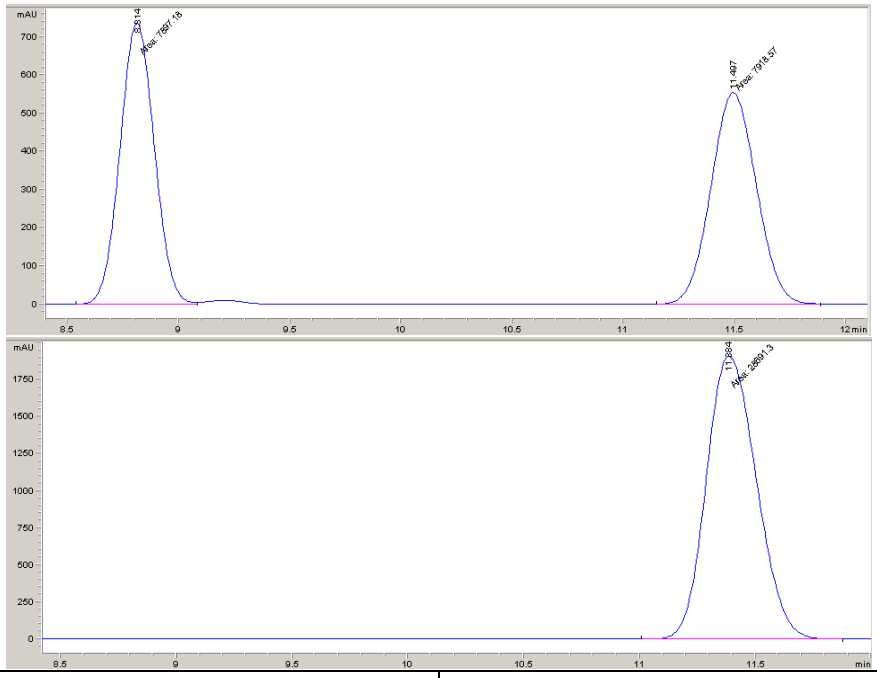

Racemic **9c**			Enzymatically produced **9c**		
Retention Time (min)	Area (mAU*s)	Area %	Retention Time (min)	Area (mAU*s)	Area %
8.81	7897.2	49.93	-	-	-
11.50	7918.6	50.07	11.88	28691.3	100.00
Total	15815.8	100.00	Total	28691.3	100.00

Ethyl 2-ethyl-3-(2-fluorophenyl)cycloprop-2-ene-1-carboxylate (9d)

Analysis Data (**WIRF**, OD_{600}=20):

Entries	Pdt	Std	Pdt/Std	[Pdt]/mM	[PC]/μM	TTN	Avg. TTN
9d-(1)	6031.1	769.7	7.836	3.83	3.01	1273	
9d-(2)	5341.5	767.4	6.961	3.40	3.01	1129	
9d-(3)	5778.2	778.0	7.427	3.63	3.01	1206	
9d-(4)	5862.0	793.9	7.384	3.61	3.01	1198	1201

Preparative-scale reaction:

***E. coli* suspension expressing WIRF in M9-N**				***D*-glucose**	
OD_{600}	volume/mL	[PC]/μM	n_pro/μmol	Mass/g	[Glu]/mM
15	200	3.11	0.621	0.75	~20
alkyne (8d) stock in EtOH			**EDA stock in EtOH**		
stock/M	volume/mL	n_1/mmol	stock/M	volume/mL	n_2/mmol
0.50	2.00	1.00	0.8	1.00 × 3	2.4
purification eluent		**Product**			
Silica column: EtOAc in hexanes (0% to 10% gradient) **C18 column**: MeCN in H_2O		m[Pdt]/mg	n[Pdt]/mmol	yield	TTN
		210.3	0.898	90%	1445

(0% to 100% gradient)				

Chiralpak IC, 3% isopropanol in hexane, 1.2 ml/min, 32 °C, 254nm

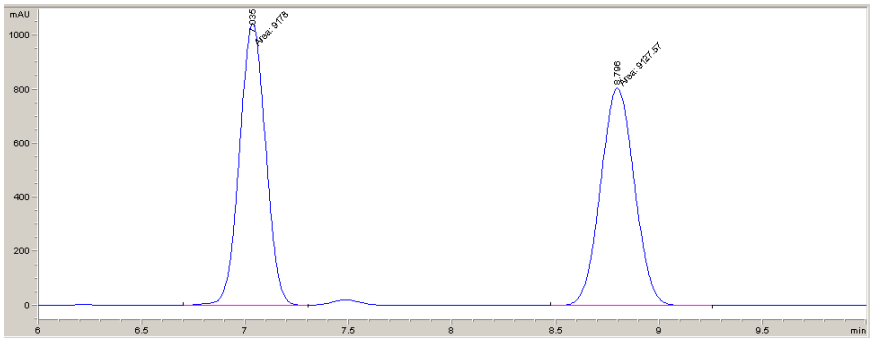

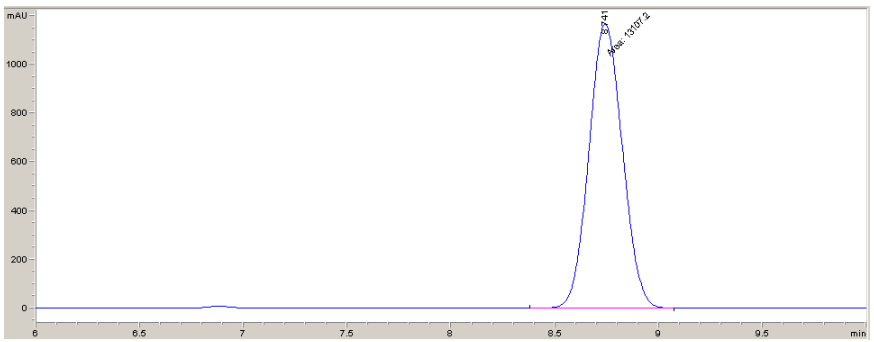

Racemic **9d**			Enzymatically produced **9d**		
Retention Time (min)	Area (mAU*s)	Area %	Retention Time (min)	Area (mAU*s)	Area %
7.04	9178.0	50.14	-	-	-
8.80	9127.6	49.86	8.74	13107.2	100.00
Total	18305.6	100.00	Total	13107.2	100.00

Ethyl 2-ethyl-3-(4-fluorophenyl)cycloprop-2-ene-1-carboxylate (9e)

Analysis Data (**WIRF_G**, OD_{600}=20):

Entries	Pdt	Std	Pdt/Std	[Pdt]/mM	[PC]/μM	TTN	Avg. TTN
9e-(1)	6531.9	788.0	8.289	4.27	2.69	1589	
9e-(2)	6825.3	801.1	8.520	4.39	2.69	1634	
9e-(3)	6455.4	793.5	8.135	4.19	2.69	1560	
9e-(4)	6645.0	772.6	8.601	4.43	2.69	1649	1608

Chiralpak IC, 3% isopropanol in hexane, 1.2 ml/min, 32 °C, 254nm

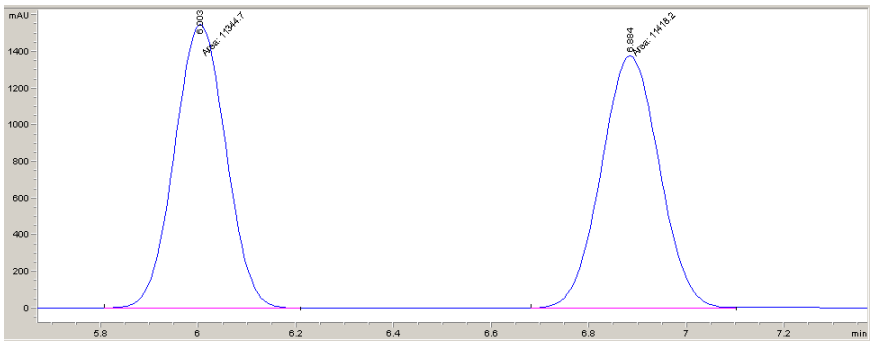

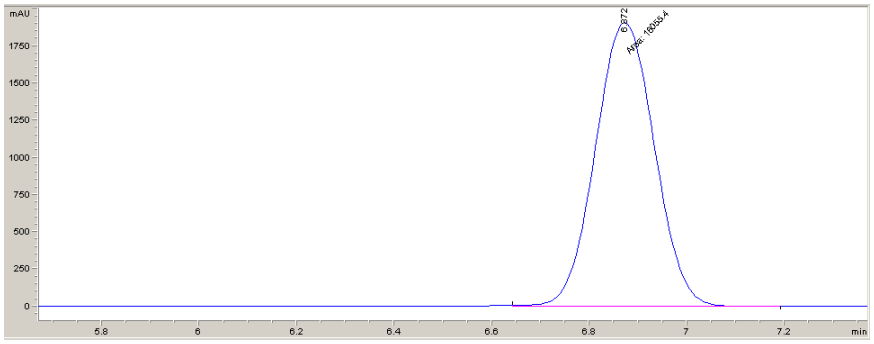

Racemic **9e**			Enzymatically produced **9e**		
Retention Time (min)	Area (mAU*s)	Area %	Retention Time (min)	Area (mAU*s)	Area %
6.00	11344.7	49.84	-	-	-
6.88	11418.2	50.16	6.87	16055.4	100.00
Total	22762.9	100.00	Total	16055.4	100.00

Ethyl 2-ethyl-3-(3-methoxyphenyl)cycloprop-2-ene-1-carboxylate (9f)

Analysis Data (**WIRF_G**, OD_{600}=20):

Entries	Pdt	Std	Pdt/Std	[Pdt]/mM	[PC]/μM	TTN	Avg. TTN
9f-(1)	2136.3	808.3	2.643	1.27	2.69	472	
9f-(2)	2365.8	793.6	2.981	1.43	2.69	533	
9f-(3)	2582.1	791.1	3.264	1.57	2.69	584	
9f-(4)	2161.4	798.1	2.708	1.30	2.69	484	519

Chiralpak IC, 3% isopropanol in hexane, 1.2 ml/min, 32 °C, 254nm

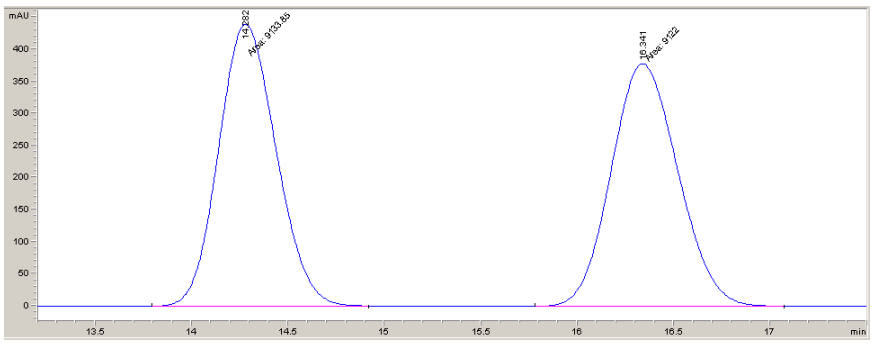

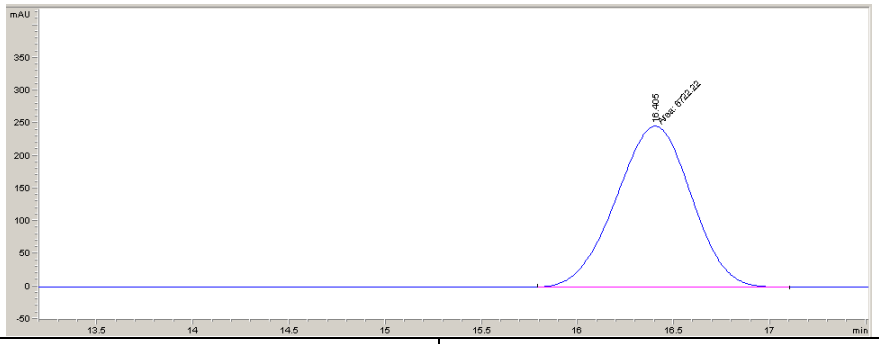

Racemic **9f**			Enzymatically produced **9f**		
Retention Time (min)	Area (mAU*s)	Area %	Retention Time (min)	Area (mAU*s)	Area %
14.28	9133.9	50.03	-	-	-
16.34	9122	49.97	16.41	6722.22	100.00
Total	18255.9	100.00	Total	6722.22	100.00

Ethyl 2-ethyl-3-(4-trifluoromethylphenyl)cycloprop-2-ene-1-carboxylate (9g)

Analysis Data (**WIRF_GAK**, OD_{600}=20):

Entries	Pdt	Std	Pdt/Std	[Pdt]/mM	[PC]/μM	TTN	Avg. TTN
9g-(1)	4817.3	781.3	6.166	3.13	2.18	1440	
9g-(2)	5442.6	810.4	6.716	3.41	2.18	1568	
9g-(3)	5254.5	795.8	6.603	3.36	2.18	1542	
9g-(4)	5083.1	790.7	6.429	3.27	2.18	1501	1513

Preparative-scale reaction:

***E. coli* suspension expressing WIRF_GAK in M9-N**				***D*-glucose**	
OD_{600}	volume/mL	[PC]/μM	n_pro/μmol	Mass/g	[Glu]/mM
15	200	1.75	0.351	0.75	~20
alkyne (8g) stock in EtOH			**EDA stock in EtOH**		
stock/M	volume/mL	n_1/mmol	stock/M	volume/mL	n_2/mmol
0.50	2.00	1.00	0.8	1.00 × 3	2.4
purification eluent		**Product**			
Silica column: EtOAc in hexanes (0% to 10% gradient) **C18 column**: MeCN in H_2O (0% to 100% gradient)		m[Pdt]/mg	n[Pdt]/mmol	yield	TTN
		245.8	0.865	87%	2465

Chiralpak IC, 2.2% isopropanol in hexane, 1.2 ml/min, 32 °C, 254nm

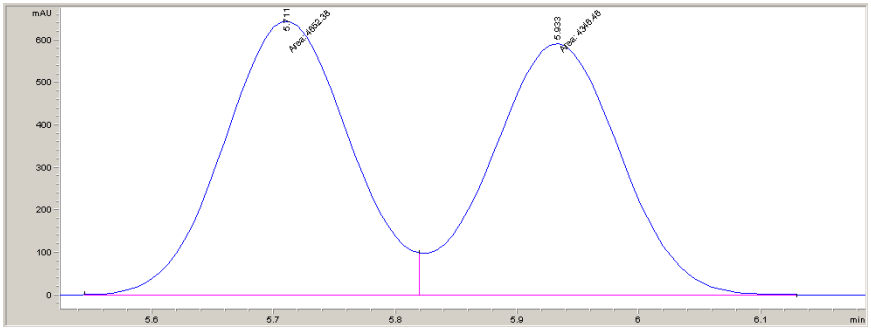

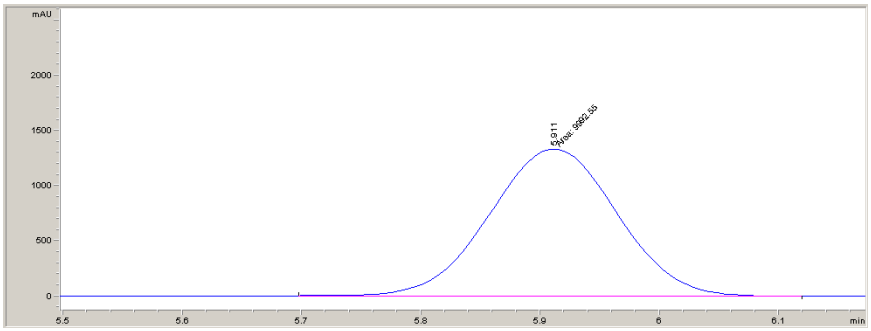

Racemic **9g**			Enzymatically produced **9g**		
Retention Time (min)	Area (mAU*s)	Area %	Retention Time (min)	Area (mAU*s)	Area %
5.71	4652.4	51.70	-	-	-
5.93	4346.5	48.30	5.91	9992.6	100.00
Total	8998.9	100.00	Total	9992.6	100.00

Ethyl 2-ethyl-3-(4-(difluoromethoxy)phenyl)cycloprop-2-ene-1-carboxylate (9h)

Analysis Data (**WIRF_GAK**, OD_{600}=20):

Entries	Pdt	Std	Pdt/Std	[Pdt]/mM	[PC]/μM	TTN	Avg. TTN
9h-(1)	6396.0	798.8	8.007	3.76	2.18	1728	
9h-(2)	5479.1	797.3	6.872	3.22	2.18	1481	
9h-(3)	5087.7	773.4	6.578	3.08	2.18	1417	
9h-(4)	5472.5	792.5	6.905	3.24	2.18	1488	1529

Chiralpak IC, 4% isopropanol in hexane, 1.2 ml/min, 32 °C, 254nm

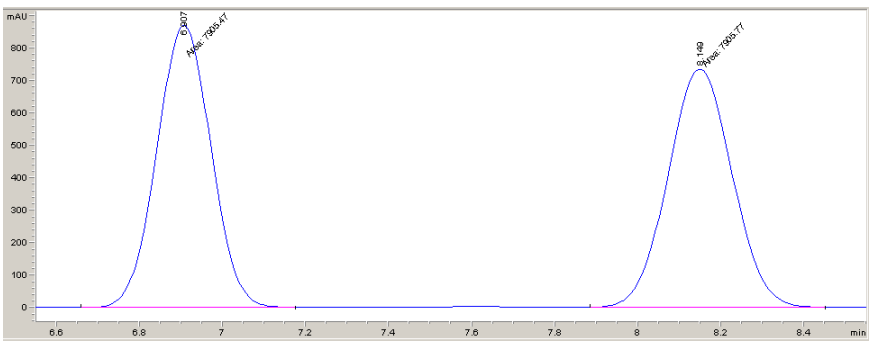

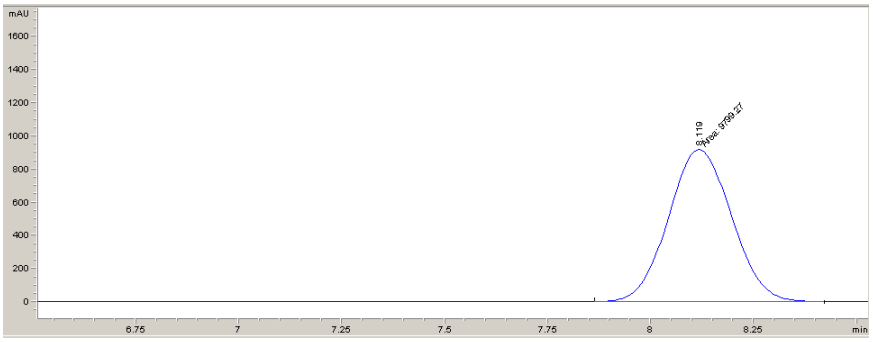

Racemic **9h**			Enzymatically produced **9h**		
Retention Time (min)	Area (mAU*s)	Area %	Retention Time (min)	Area (mAU*s)	Area %
6.91	7905.5	50.00	-	-	-
8.15	7905.8	50.00	8.12	9799.3	100.00
Total	15811.3	100.00	Total	9799.3	100.00

Ethyl 2-ethyl-3-(*p*-tolyl)cycloprop-2-ene-1-carboxylate (9i)

Analysis Data (**WIRF_GAK**, OD_{600}=15):

Entries	Pdt	Std	Pdt/Std	[Pdt]/mM	[PC]/μM	TTN	Avg. TTN
9i-(1)	11891.3	785.0	15.148	9.44	1.63	5782	
9i-(2)	11667.8	788.5	14.797	9.20	1.63	5639	
9i-(3)	12089.5	792.8	15.249	9.50	1.63	5823	
9i-(4)	11862.7	781.8	15.174	9.45	1.63	5792	5759

Chiralpak IC, 3% isopropanol in hexane, 1.2 ml/min, 32 °C, 254nm

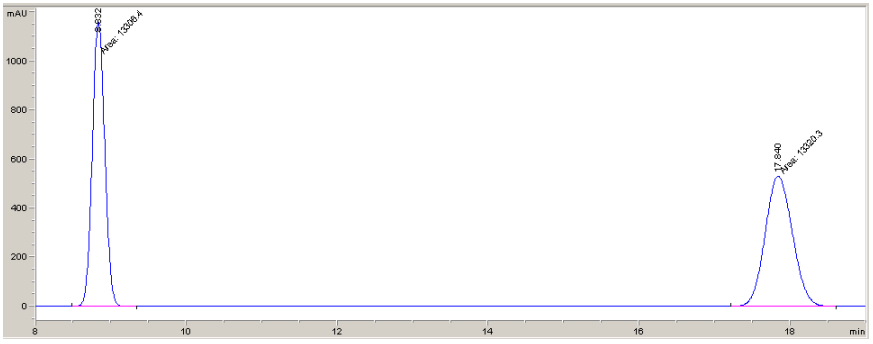

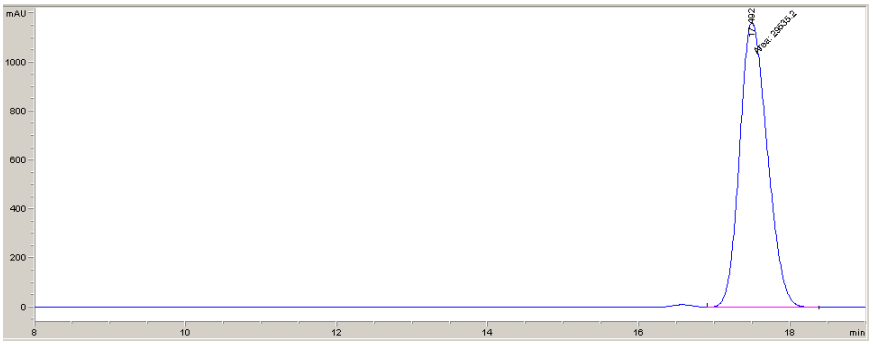

Racemic **9i**			Enzymatically produced **9i**		
Retention Time (min)	Area (mAU*s)	Area %	Retention Time (min)	Area (mAU*s)	Area %
8.83	13306.4	49.97	-	-	-
17.84	13320.3	50.03	17.49	29535.2	100.00
Total	26626.7	100.00	Total	29535.2	100.00

Ethyl 2-ethyl-3-(4-methoxyphenyl)cycloprop-2-ene-1-carboxylate (9j)

Analysis Data (**WIRF_GAK**, OD_{600}=15):

Entries	Pdt	Std	Pdt/Std	[Pdt]/mM	[PC]/μM	TTN	Avg. TTN
9j-(1)	10209.8	807.4	12.645	7.30	1.63	4470	
9j-(2)	10484.6	800.1	13.104	7.57	1.63	4639	
9j-(3)	10350.3	811.8	12.750	7.36	1.63	4509	
9j-(4)	9927.8	803.9	12.350	7.12	1.63	4361	4495

Chiralpak IC, 5% isopropanol in hexane, 1.2 ml/min, 32 °C, 254nm

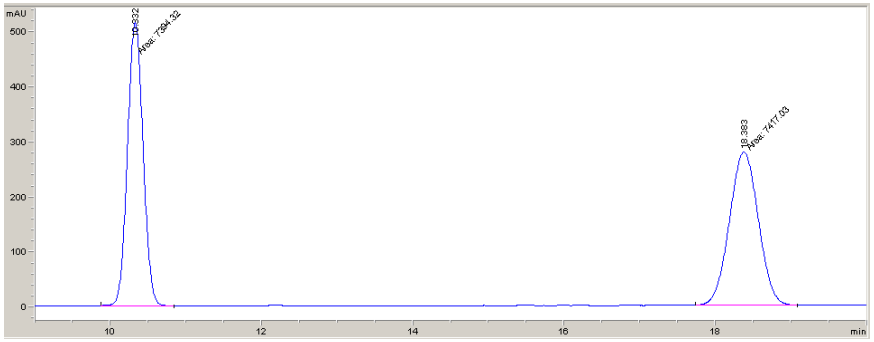

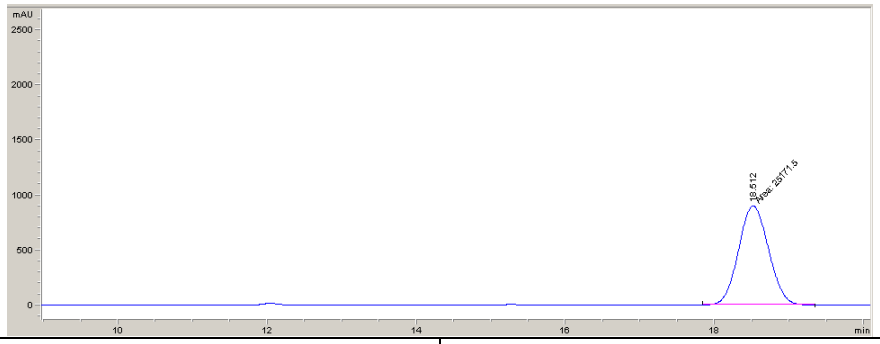

Racemic **9j**			Enzymatically produced **9j**		
Retention Time (min)	Area (mAU*s)	Area %	Retention Time (min)	Area (mAU*s)	Area %
10.33	7394.3	49.92	-	-	-
18.38	7417.0	50.08	18.51	25171.5	100.00
Total	14811.3	100.00	Total	25171.5	100.00

Ethyl 2-ethyl-3-(4-chloro-3-methylphenyl)cycloprop-2-ene-1-carboxylate (9k)

Analysis Data (**WIRF_GAK**, OD_{600}=20):

Entries	Pdt	Std	Pdt/Std	[Pdt]/mM	[PC]/μM	TTN	Avg. TTN
9k-(1)	4779.0	788.6	6.060	2.46	2.18	1131	
9k-(2)	4771.1	786.6	6.065	2.46	2.18	1132	
9k-(3)	4815.2	763.1	6.310	2.56	2.18	1178	
9k-(4)	4556.0	787.0	5.789	2.35	2.18	1080	1130

Chiralpak IC, 3% isopropanol in hexane, 1.2 ml/min, 32 °C, 254nm

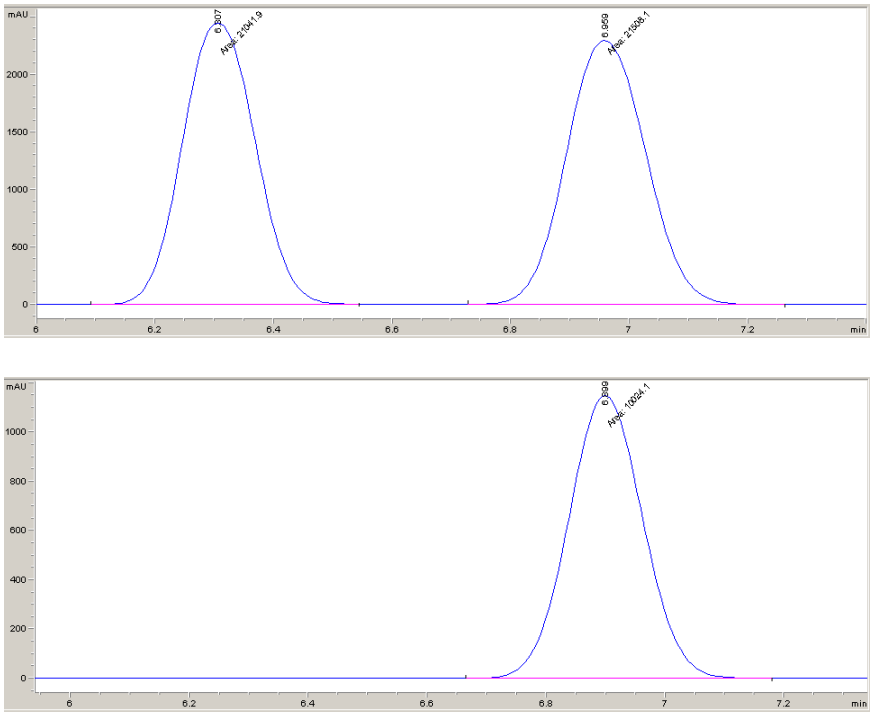

Racemic **9k**			Enzymatically produced **9k**		
Retention Time (min)	Area (mAU*s)	Area %	Retention Time (min)	Area (mAU*s)	Area %
6.31	21041.9	49.45	-	-	-
6.96	21508.1	50.55	6.90	10024.1	100.00
Total	42550.0	100.00	Total	10024.1	100.00

Ethyl 2-ethyl-3-(4-methoxy-3-methylphenyl)cycloprop-2-ene-1-carboxylate (9l)

Analysis Data (**WIRF_GAK**, OD_{600}=20):

Entries	Pdt	Std	Pdt/Std	[Pdt]/mM	[PC]/μM	TTN	Avg. TTN
9l-(1)	7021.1	797.6	8.803	3.73	2.18	1714	
9l-(2)	7502.1	809.4	9.269	3.94	2.18	1809	
9l-(3)	6806.2	807.3	8.431	3.56	2.18	1638	
9l-(4)	7147.9	807.5	8.852	3.75	2.18	1724	1721

Chiralpak IC, 5% isopropanol in hexane, 1.2 ml/min, 32 °C, 254nm

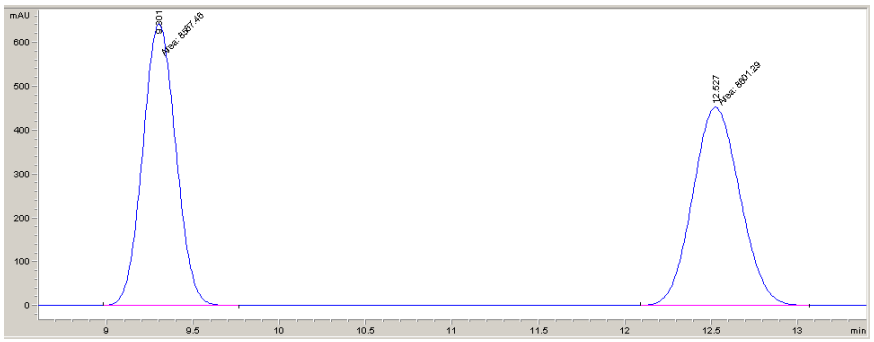

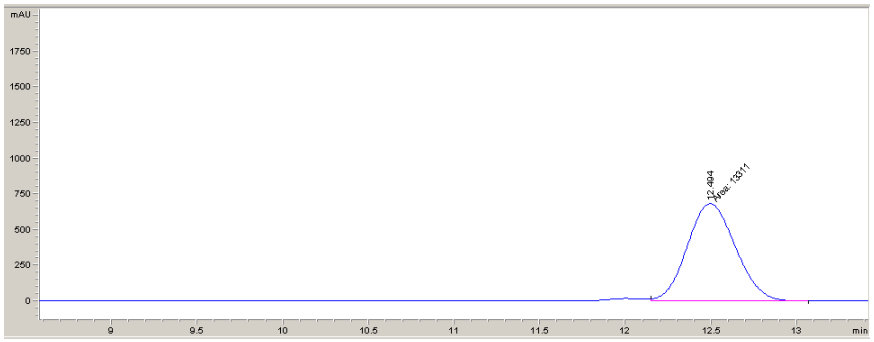

Racemic **9l**			Enzymatically produced **9l**		
Retention Time (min)	Area (mAU*s)	Area %	Retention Time (min)	Area (mAU*s)	Area %
9.30	8567.5	49.90	-	-	-
12.53	8601.3	50.10	12.49	13311.0	100.00
Total	17168.8	100.00	Total	13311.0	100.00

Ethyl 2-(2-ethoxyethyl)-3-ethylcycloprop-2-ene-1-carboxylate (9m)

Analysis Data (**C10**, OD_{600}=15):

Entries	Pdt	Std	Pdt/Std	[Pdt]/mM	[PC]/μM	TTN	Avg. TTN
9m-(1)	125.9	1066.5	0.118	0.11	2.34	46	
9m-(2)	123.4	1041.9	0.118	0.11	2.34	46	
9m-(3)	125.5	1032.3	0.122	0.11	2.34	47	
9m-(4)	118.2	1047.3	0.113	0.10	2.34	44	46

Analysis Data (**C10-T327V Q437L S332C**, OD_{600}=15):

Entries	Pdt	Std	Pdt/Std	[Pdt]/mM	[PC]/μM	TTN	Avg. TTN
9m-(1)	211.5	1039.4	0.203	0.17	2.57	64	
9m-(2)	217.2	1056.9	0.206	0.17	2.57	65	
9m-(3)	212.3	1055.3	0.201	0.16	2.57	64	
9m-(4)	208.6	1024.0	0.204	0.17	2.57	64	64

CycloSil-B, 88 °C isothermal for 92 min -> 2°C/min gradient -> 110°C isothermal for 3 min ->

60 °C/min gradient -> 240 °C isothermal for 5 min, flow rate 2.0 ml/min

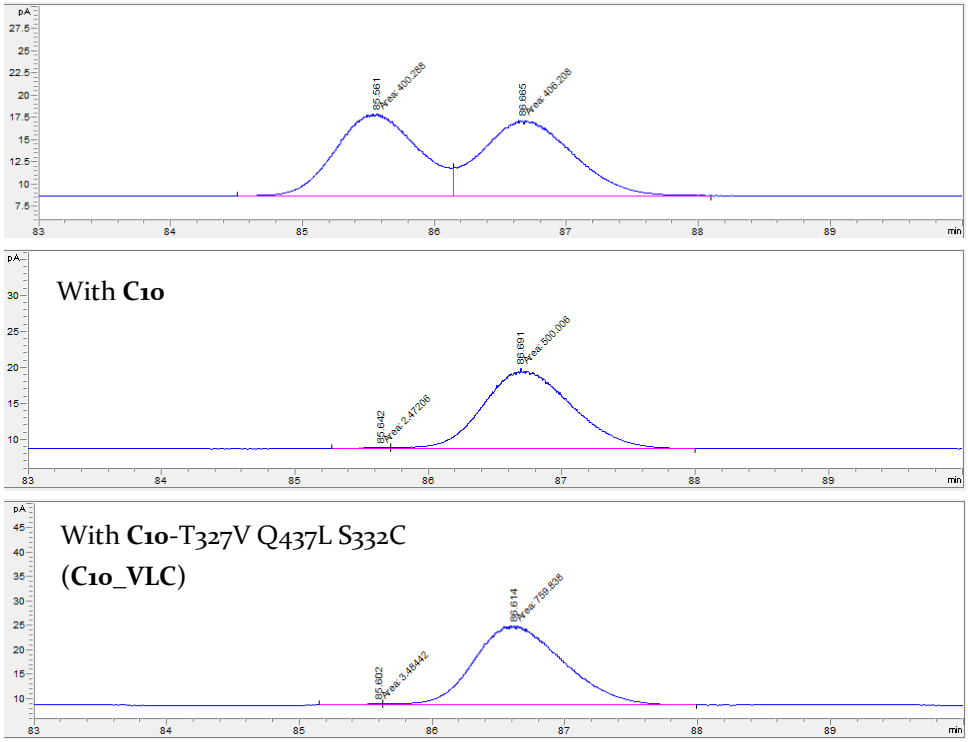

Racemic **9m**			**9m** produced by **C10**		
Retention Time (min)	Area (mAU*s)	Area %	Retention Time (min)	Area (mAU*s)	Area %
85.56	400.29	49.63	85.64	2.47	0.49
86.67	406.21	50.37	86.69	500.01	99.51
Total	806.50	100.00	Total	500.48	100.00
9m produced by **C10_VLC**					
Retention Time (min)	Area (mAU*s)	Area %			
85.60	3.48	0.46			
86.61	759.84	99.54			
Total	763.32	100.00			

Chemoselectivity in carbene transfer to internal alkyne **8n** with different P411 variants:

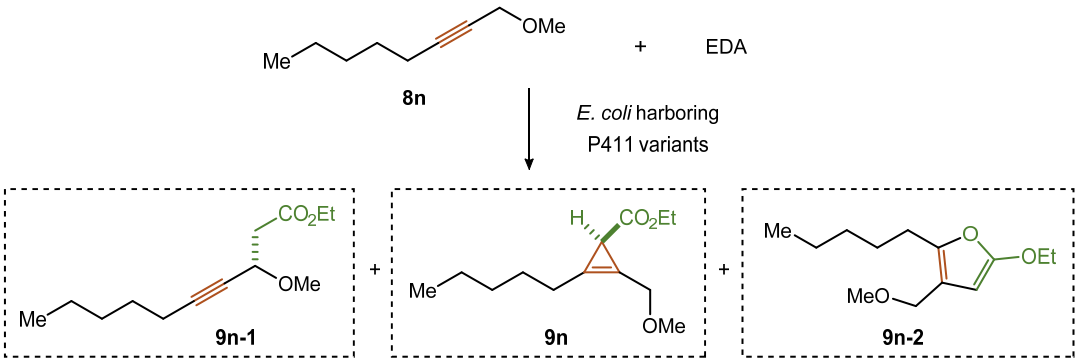

GC trace: HP5 column, 80 °C isothermal for 2 min -> 6°C/min gradient -> 180°C -> 60 °C/min gradient -> 250 °C isothermal for 2 min

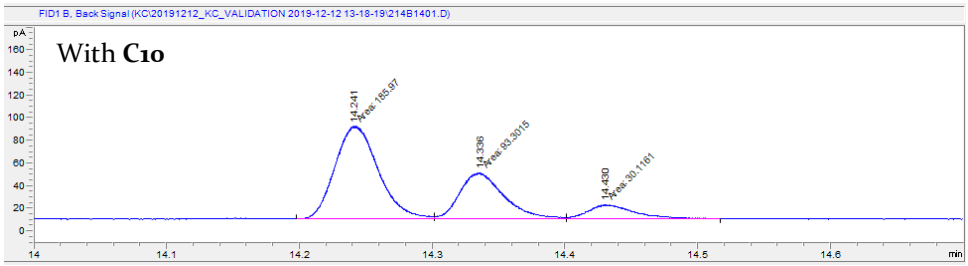

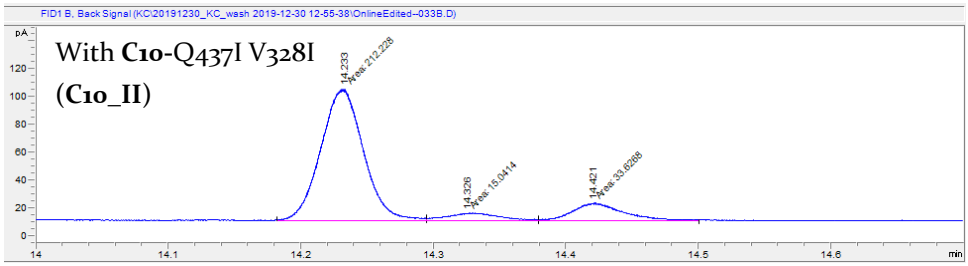

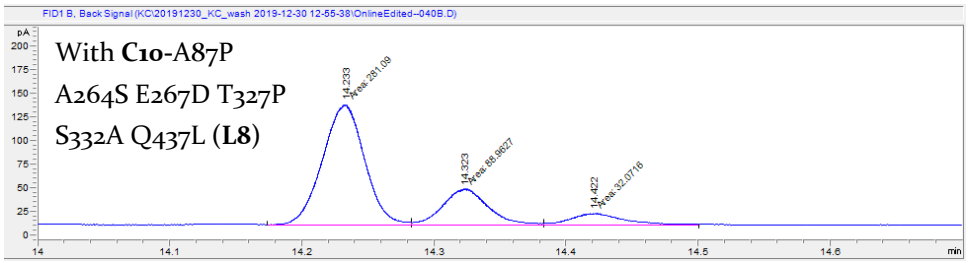

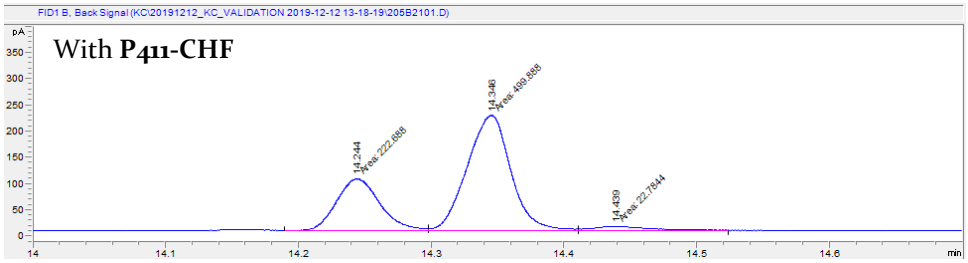

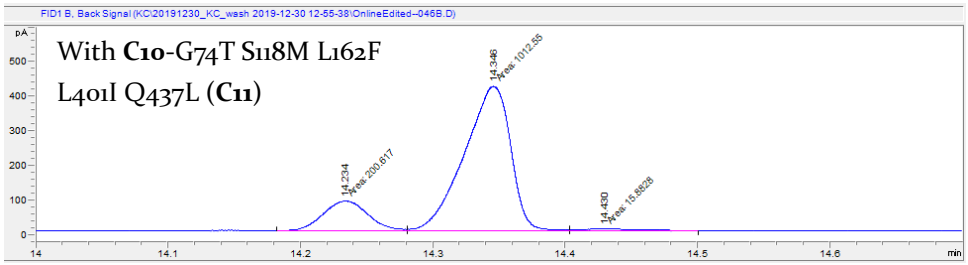

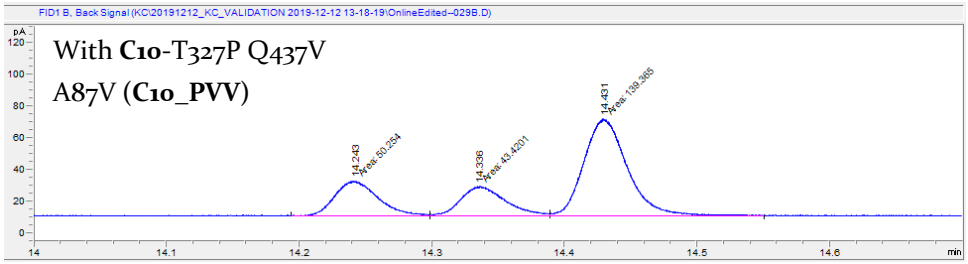

Product assignment:

Retention time	14.24 min	14.33 min	14.42 min
Compound #	**9n**	**9n-1**	**9n-2**
Compound structure	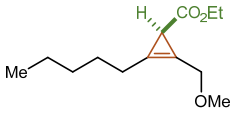	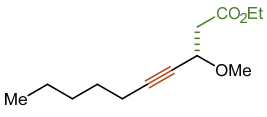	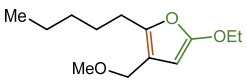

TTN for all products based on carbene transfer (OD_{600}=20 for **L8**, OD_{600}=15 for the rest):

Entries	Pdt	Std	Pdt/Std	[Pdt]/mM	[PC]/μM	TTN	Avg. TTN	Enzyme: **C10**
n-(1)	309.4	1026	0.302	0.24	2.72	90		
n-(2)	272.1	989.2	0.275	0.22	2.72	82		**9n-1**:**9n**:**9n-2**
n-(3)	283.4	1021.1	0.278	0.23	2.72	83		30:**60**:10
n-(4)	303.7	1005.6	0.302	0.25	2.72	90	86	

Entries	Pdt	Std	Pdt/Std	[Pdt]/mM	[PC]/μM	TTN	Avg. TTN	Enzyme: **C10_II**
n-(1)	272.7	1064.9	0.256	0.21	2.90	72		
n-(2)	259.5	988.2	0.263	0.21	2.90	74		**9n-1**:**9n**:**9n-2**
n-(3)	257.1	987.8	0.260	0.21	2.90	73		5:**80**:15
n-(4)	248.2	973.9	0.255	0.21	2.90	71	72	

Entries	Pdt	Std	Pdt/Std	[Pdt]/mM	[PC]/μM	TTN	Avg. TTN	Enzyme: **L8**
n-(1)	394.9	1028.2	0.384	0.31	2.34	133		
n-(2)	395.2	1015.3	0.389	0.32	2.34	135		**9n-1**:**9n**:**9n-2**
n-(3)	402.1	1010.6	0.398	0.32	2.34	138		22:**70**:8
n-(4)	382.2	994.3	0.384	0.31	2.34	133	135	

Entries	Pdt	Std	Pdt/Std	[Pdt]/mM	[PC]/μM	TTN	Avg. TTN	Enzyme: **CHF**
n-(1)	759	1002.5	0.757	0.61	2.20	278		
n-(2)	747.3	1006.1	0.743	0.60	2.20	272		**9n-1**:**9n**:**9n-2**
n-(3)	720.9	1008.8	0.715	0.58	2.20	262		**67**:30:3
n-(4)	745.4	1017.1	0.733	0.59	2.20	269	270	

Entries	Pdt	Std	Pdt/Std	[Pdt]/mM	[PC]/μM	TTN	Avg. TTN	Enzyme: **C11**
n-(1)	1221.8	1003.8	1.217	0.98	2.44	399		**9n-1**:**9n**:
n-(2)	1176.6	992.0	1.186	0.95	2.44	389		**9n-2**
n-(3)	1170.9	992.9	1.179	0.95	2.44	387		**82**:16:2

n-(4)	1182.0	991.1	1.193	0.96	2.44	391	392	

Entries	Pdt	Std	Pdt/Std	[Pdt]/mM	[PC]/μM	TTN	Avg. TTN	Enzyme: **C10_PVV**
n-(1)	227.5	1014.7	0.224	0.18	3.03	60		**9n-1**:**9n**: **9n-2** 18:22:**60**
n-(2)	229.3	1004.4	0.228	0.19	3.03	61		
n-(3)	224.9	991.0	0.227	0.18	3.03	61		
n-(4)	233.1	1016.0	0.229	0.19	3.03	62	61	

Chiral GC trace: CycloSil-B, 100 °C isothermal for 20 min -> 0.2°C/min gradient -> 120°C isothermal for 20 min -> 60 °C/min gradient -> 240 °C isothermal for 5 min, flow rate 2.0 ml/min

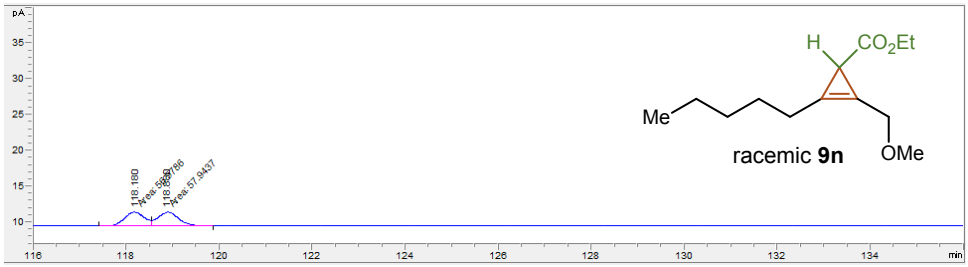

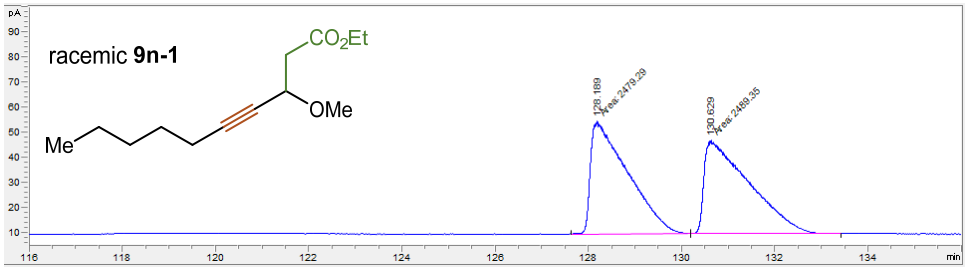

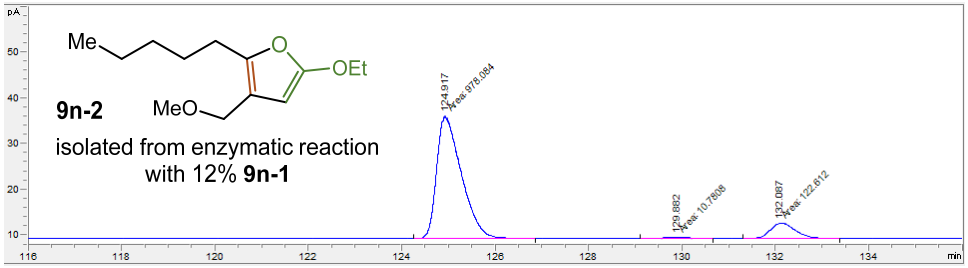

Racemic **9n**			Racemic **9n-1**		
Retention Time (min)	Area (mAU*s)	Area %	Retention Time (min)	Area (mAU*s)	Area %
118.18	58.08	50.06	128.19	2479.29	49.90
118.88	57.94	49.94	130.63	2489.35	50.10
Total	116.02	100.00	Total	4968.64	100.00

9n-2		
Retention Time (min)	Area (mAU*s)	Area %
124.92	978.08	100.00

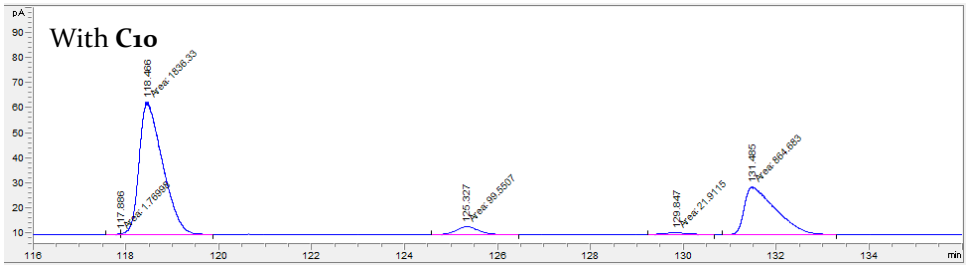

9n produced by **C10**			**9n-1** produced by **C10**		
Retention Time (min)	Area (mAU*s)	Area %	Retention Time (min)	Area (mAU*s)	Area %
117.89	1.77	0.10	129.85	21.91	2.47
118.47	1836.33	99.90	131.49	864.68	97.53
Total	1838.10	100.00	Total	886.59	100.00

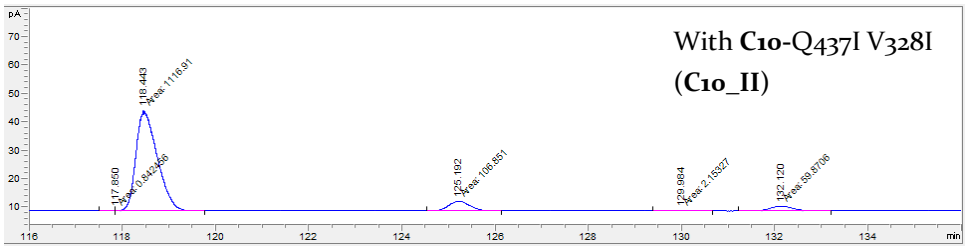

9n produced by **C10_II**			**9n-1** produced by **C10_II**		
Retention Time (min)	Area (mAU*s)	Area %	Retention Time (min)	Area (mAU*s)	Area %
117.85	0.84	0.08	129.98	2.15	3.41
118.44	1116.91	99.92	132.12	59.87	96.59
Total	1117.75	100.00	Total	63.02	100.00

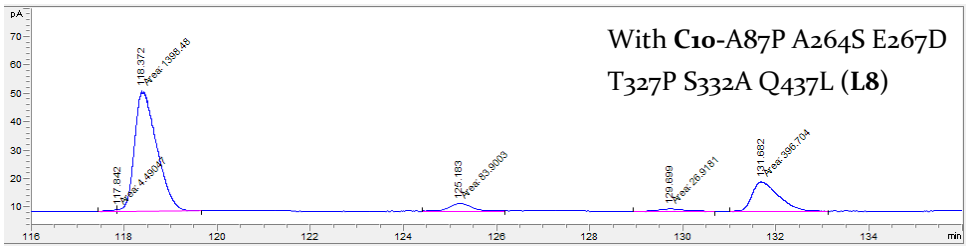

9n produced by **L8**			**9n-1** produced by **L8**		
Retention Time (min)	Area (mAU*s)	Area %	Retention Time (min)	Area (mAU*s)	Area %
117.84	4.49	0.32	129.70	26.91	6.35
118.37	1398.48	99.68	131.68	396.70	93.65
Total	1402.97	100.00	Total	423.61	100.00

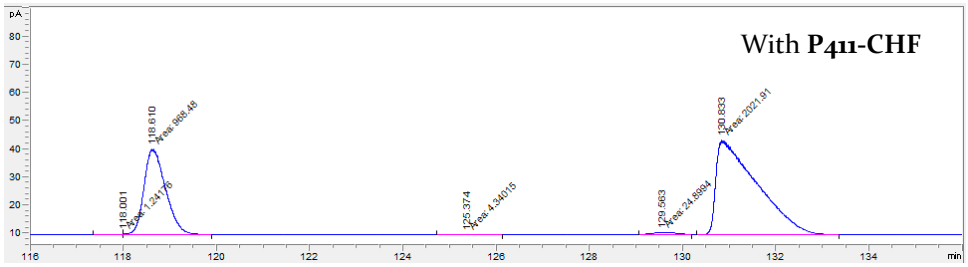

9n produced by **CHF**			**9n-1** produced by **CHF**		
Retention Time (min)	Area (mAU*s)	Area %	Retention Time (min)	Area (mAU*s)	Area %
118.00	1.24	0.13	129.56	24.90	1.22
118.61	968.48	99.87	130.83	2021.91	98.78
Total	969.72	100.00	Total	2046.81	100.00

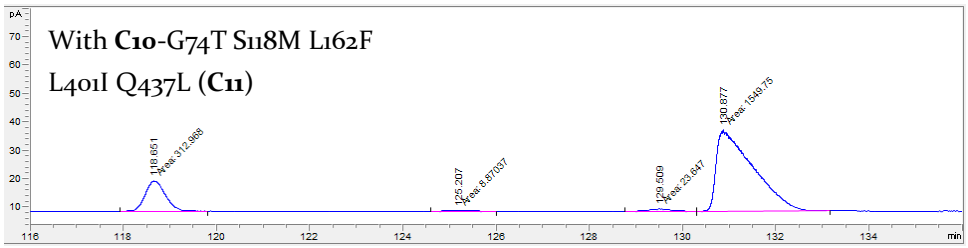

9n produced by **C11**			**9n-1** produced by **C11**		
Retention Time (min)	Area (mAU*s)	Area %	Retention Time (min)	Area (mAU*s)	Area %
-	-	-	129.51	23.65	1.50
118.65	312.97	100.00	130.88	1549.75	98.50
Total	969.72	100.00	Total	1573.40	100.00

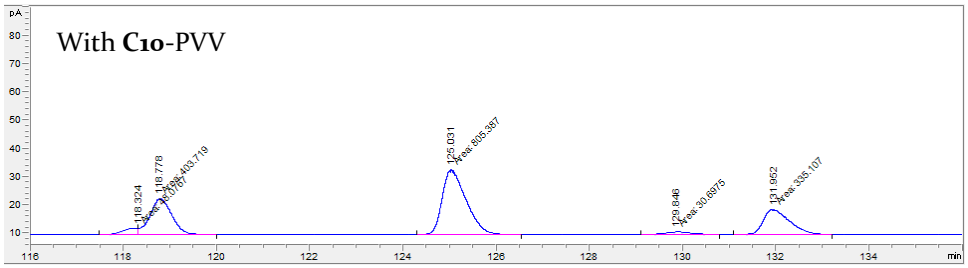

9n produced by **C10_PVV**			**9n-1** produced by **C10_PVV**		
Retention Time (min)	Area (mAU*s)	Area %	Retention Time (min)	Area (mAU*s)	Area %
118.32	48.08	10.64	129.85	30.70	8.39
118.78	403.71	89.36	131.95	335.11	91.61
Total	451.79	100.00	Total	365.81	100.00

5-Ethoxy-3-(methoxymethyl)-2-pentylfuran (9n-2)

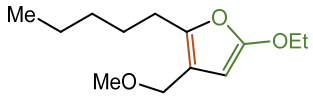

Compound **9n-2** was isolated from a large-scale enzymatic reaction using alkyne **8n** and EDA as substrates and **C10-PVV** as the enzyme variant. ^{1}H NMR (400 MHz, $CDCl_3$) δ 5.08 (s, 1H), 4.17 (s, 2H), 4.03 (q, *J* = 7.1 Hz, 2H), 3.32 (s, 3H), 2.50 (t, *J* = 7.5 Hz, 2H), 1.62–1.54 (m, 2H), 1.39 (t, *J* = 7.1 Hz, 3H), 1.35–1.22 (m, 4H), 0.88 (t, *J* = 7.0 Hz, 3H). ^{13}C NMR (101 MHz, $CDCl_3$) δ 159.24, 143.80, 116.69, 81.16, 66.73, 66.20, 57.73, 31.41, 28.57, 25.76, 22.54, 14.76, 14.16. HRMS (TOF) m/z: 227.1641 ($M+H^+$); calc. for [$C_{13}H_{22}O_3+H^+$]: 227.1642. The isolated furan adduct was identified to be the regio-isomer shown here, according to NOE signals.

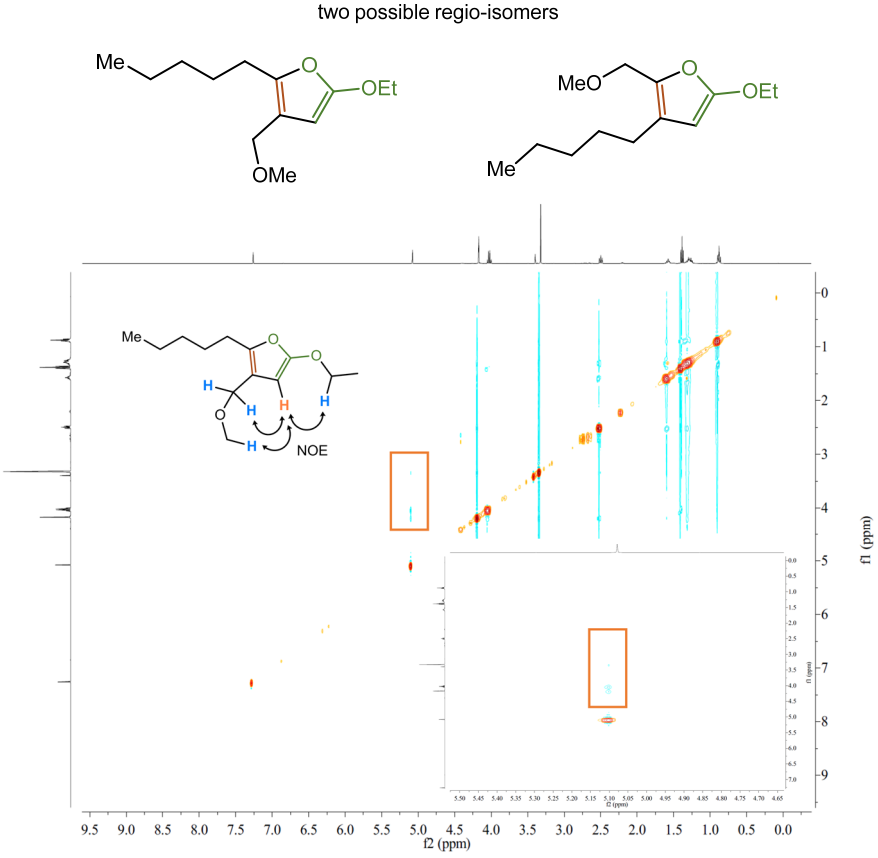

A.6 Derivatization of enzymatically produced strained carbocycles

Diethyl (2*R*,4*R*)-1-(4-(1-((4-acetamidophenyl)sulfonyl)-1*H*-1,2,3-triazol-4-yl)phenyl) bicyclo [1.1.0]butane-2,4-dicarboxylate (4a)

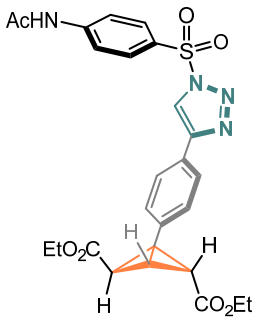

Bicyclobutane **2l** (41.6 mg, 0.139 mmol) was dissolved in toluene (3 mL) in a 20 mL vial. Copper(I) thiophene-2-carboxylate (CuTc, 3.2 mg, 12 mol%) was added. The mixture was kept stirring at 0 °C. A suspension of 4-acetamidobenzenesulfonyl azide (40.2 mg, 0.167 mmol) in toluene (5 mL) was added dropwise over 1 h. The resulting mixture was then allowed to warm to room temperature and stirred for 15 h. The reaction was diluted with ethyl acetate (15 mL), washed with NH_4Cl/NH_3 (2:1, 20 mL, aq.), and brine (50 mL), dried over $MgSO_4$, and then concentrated under reduced pressure. The crude

product was purified by silica column chromatography with hexane/ethyl acetate (4:1 to 1:3 gradient) to afford **4a** (69.2 mg, 0.129 mmol, 93%). ^{1}H NMR (400 MHz, $CDCl_3$) δ 8.32 (s, 1H), 8.10 (s, 1H), 8.00 (d, *J* = 9.0 Hz, 2H), 7.74 (dd, *J* = 12.8, 8.7 Hz, 4H), 7.34 (d, *J* = 8.6 Hz, 2H), 4.15 (dq, *J* = 7.1, 3.5 Hz, 2H), 4.08 (q, *J* = 7.1 Hz, 2H), 3.28 (d, *J* = 0.6 Hz, 1H), 3.19 (dd, *J* = 3.1, 0.6 Hz, 1H), 3.14 (d, *J* = 3.1 Hz, 1H), 2.20 (s, 3H), 1.27 (t, *J* = 7.2 Hz, 3H), 1.15 (t, *J* = 7.1 Hz, 3H). ^{13}C NMR (101 MHz, $CDCl_3$) δ 170.14, 169.15, 167.88, 147.11, 145.13, 134.03, 130.40, 129.53, 128.96, 127.92, 126.19, 119.62, 119.22, 61.17, 61.13, 44.75, 42.63, 27.84, 24.93, 21.39, 14.35, 14.21. HRMS (FAB) m/z: 539.1605 ($M+H^+$); calc. for $C_{26}H_{27}O_7SN_4$: 539.1600. $[\alpha]^{23}_D$ = –81.5 ± 2.1° (*c* 0.1, ethyl acetate).

Diethyl (2*R*,4*R*)-1-(4-(1-((*S*)-1-methoxy-1-oxo-3-phenylpropan-2-yl)-1*H*-1,2,3-triazol-4-yl) phenyl)bicyclo[1.1.0]butane-2,4-dicarboxylate (4b)

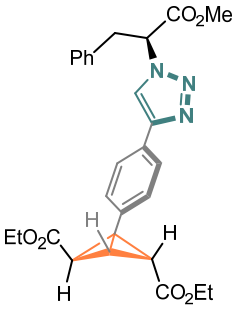

Sodium azide (7.02 g, 108 mmol) was dissolved in a mixture of water (30 mL) and DCM (15 mL) at 0 °C. Triflic anhydride (Tf_2O, 3 mL, 18 mmol) was added dropwise over 10 min. The reaction was then stirred for 2 h. The reaction was diluted with DCM (15 mL), washed by $NaHCO_3$ (50 mL, sat. aq.), and brine (50 mL), and dried over Na_2SO_4. A solution of triflic azide (TfN_3, ~15 mmol) in DCM was used for the next step.

Methyl *L*-phenylalaninate hydrochloride (1.73 g, 8.0 mmol), was dissolved in MeOH (16 mL). A aqueous solution of $CuSO_4$ (1.28 mL, 10 g/L, 1 mol%) and *N*,*N*-diisopropylethylamine (DIPEA, 2.09 mL, 12.0 mmol) were added. The resulting solution was stirred for 30 min before the dropwise addition of triflic azide (TfN_3, ~15 mmol in DCM) over 20 min. The reaction was stirred for 15 h. The reaction mixture was diluted with DCM (40 mL), washed by water (50 mL), HCl (50 mL, 5%, aq.), $NaHCO_3$ (50 mL, sat. aq.), and brine (50 mL), and dried over Na_2SO_4. After evaporation of solvent under reduced pressure, the product mixture was purified by silica column chromatography with hexane/ethyl acetate (1:0 to 12:1 gradient) to afford methyl (*S*)-2-azido-3-phenylpropanoate (1.65 g, 8.0 mmol, quantitative).

Bicyclobutane **2l** (49.5 mg, 0.166 mmol) was dissolved in THF/H_2O (1:1, 1.6 mL) in a 20 mL vial. An aqueous solution of $CuSO_4$ (17 µL, 1N, 10 mol%) and Cu powder (10.6 mg, 0.166 mmol) were added. The mixture was kept stirring at 0 °C. A solution of methyl (*S*)-2-azido- 3-phenylpropanoate (50.1 mg, 0.249 mmol) in THF (0.5 mL) was added dropwise over 5 min. The resulting mixture was then allowed to warm to room temperature and stirred for 24 h. The reaction was diluted with DCM (15 mL), washed with NH_4Cl (10 mL, aq. sat.), and brine (30 mL), dried over $MgSO_4$, and then concentrated under reduced pressure. The crude product was purified by silica column chromatography with hexane/ethyl acetate (8:1 to 2:1 gradient) to afford **4b** (82.5 mg, 0.164 mmol, 99%) as one major diastereomer determined by ^{1}H NMR. ^{1}H NMR (400 MHz, $CDCl_3$) δ 7.80 (s, 1H), 7.78–7.69 (m, 2H), 7.37–7.30 (m, 2H), 7.28–7.20 (m, 3H), 7.08–7.03 (m, 2H), 5.63 (dd, *J* = 8.1, 6.7 Hz, 1H), 4.15 (qd, *J* = 7.1, 2.6 Hz, 2H), 4.08 (q, *J* = 7.1 Hz, 2H), 3.77 (s, 3H), 3.52 (dd, *J* = 7.4, 3.2 Hz, 2H), 3.28 (d, *J* = 0.5 Hz, 1H), 3.17 (dd, *J* = 3.1, 0.6 Hz, 1H), 3.13 (d, *J* = 3.1 Hz, 1H), 1.27 (t, *J* = 7.1 Hz, 3H), 1.15 (t, *J* = 7.1 Hz, 3H). ^{13}C NMR (101 MHz, $CDCl_3$) δ 170.24, 168.84, 167.87, 147.40, 134.77, 132.77, 129.67, 129.08, 128.98, 128.84, 127.77, 125.80, 119.75, 64.17, 61.05, 61.01, 53.26, 44.71, 42.64, 39.12, 27.99, 20.89, 14.36, 14.22. HRMS (FAB) m/z: 504.2148 ($M+H^+$); calc. for $C_{28}H_{30}O_6N_3$: 504.2135. $[\alpha]^{23}_D$ = –278.7 ± 4.0° (*c* 0.0625, ethyl acetate).

Note: A diastereomer of **4b** was prepared through the same procedure using *D*-azido-phenylalanine. It was confirmed that the pair of diastereomers can be resolved on ^{1}H NMR at the α-C–H position of phenylalanine (splitting peaks: *D*-phenylalanine: 5.6410, 5.6242, 5.6208, 5.6041; *L*-phenylalanine: 5.6462, 5.6296, 5.6261, 5.6093; FWHM (full width at half maxima) = 0.0030 ppm; Δf1 = 0.0053 ppm, close to baseline separation).

Diethyl (2*R*,4*R*)-1-(4-((((*R*)-3,3,3-Trifluoro-2-methoxy-2-phenylpropanoyl)oxy)methyl) phenyl) bicyclo[1.1.0]butane-2,4-dicarboxylate (4c)

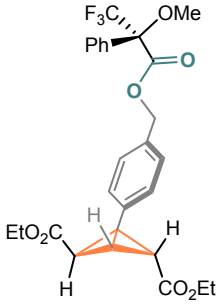

Bicyclobutane **2m** (16.1 mg, 0.053 mmol) and (*R*)-3,3,3-trifluoro-2- methoxy-2-phenylpropanoic acid (*R*-Mosher's acid, 30.4 mg, 0.13 mmol) were dissolved in dry DCM (2 mL) in a 10 mL vial. 1-Ethyl-3-(3-dimethylaminopropyl)carbodiimide hydrochloride (EDCI, 24.9 mg, 0.13 mmol), triethylamine (TEA, 18 µL, 0.13 mmol) and 4-dimethylaminopyridine (DMAP, 2.0 mg, 0.015 mmol) were added to the solution. The reaction mixture was then stirred at room temperature for 16 h. The reaction was diluted with DCM (5 mL), washed with water (10 mL), and brine (10 mL), dried over $MgSO_4$, and then concentrated under reduced pressure. The crude product was purified by silica column chromatography with hexane / ethyl acetate (1:0 to 4:1 gradient) to afford **4c** (25.2 mg, 0.048 mmol, 91%) as one major diastereomer determined by ^{1}H NMR. ^{1}H NMR (400 MHz, $CDCl_3$) δ 7.48–7.41 (m, 2H), 7.41–7.32 (m, 3H), 7.27 (s, 4H), 5.33 (d, *J* = 12.3 Hz, 1H), 5.29 (d, *J* = 12.2 Hz, 1H), 4.15 (qd, *J* = 7.2, 2.6 Hz, 2H), 4.07 (qd, *J* = 7.2, 2.0 Hz, 2H), 3.51 (q, $J_{H\text{-}F}$ = 1.2 Hz, 3H), 3.26 (d, *J* = 0.6 Hz, 1H), 3.14 (dd, *J* = 3.1, 0.6 Hz, 1H), 3.11 (d, *J* = 3.1 Hz, 1H), 1.27 (t, *J* = 7.1 Hz, 3H), 1.13 (t, *J* = 7.1 Hz, 3H). ^{13}C NMR (101 MHz, $CDCl_3$) δ 170.01, 167.67, 166.43, 133.67, 133.32, 132.11, 129.64, 128.54, 128.53, 128.42, 127.54, 127.28, 127.27, 124.68, 121.81, 118.94, 84.75, 67.60, 60.96, 60.88, 55.54, 44.61, 42.44, 27.66, 20.85, 14.23, 14.03 (CF_3, 127.54, 124.68, 121.81, 118.94, $J_{C\text{-}F}$ = 288.8 Hz;). HRMS (FAB) m/z: 519.1651 ((M+H$^+$)–H_2); calc. for $C_{27}H_{26}O_7F_3$: 519.1631. $[\alpha]^{23}_D$ = –43.2 ± 2.4° (*c* 0.1, ethyl acetate).

Note: A diastereomer of **4c** was prepared through the same procedure using *S*-Mosher's acid. It was confirmed that the pair of diastereomers can be resolved on ^{1}H NMR at one benzylic C–H position and ^{19}F NMR, albeit not perfectly (splitting peaks on ^{1}H NMR: *R*-Mosher's acid: 5.3027, 5.2721; *S*-Mosher's acid: 5.3044, 5.2737; FWHM = 0.0024–0.0029 ppm ppm; Δf1 = 0.0017 ppm; chemical shift on ^{19}F NMR: *R*-Mosher's acid: –71.665; *S*-Mosher's acid: –71.654; FWHM = 0.015 ppm ppm; Δf1 = 0.011 ppm).

((1*R*,2*R*)-1-(4-methoxyphenyl)bicyclo[1.1.0]butane-2,4-diyl)dimethanol (4d)

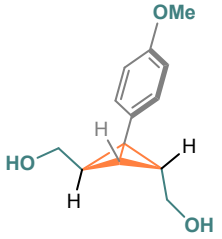

Bicyclobutane **2k** (101.3 mg, 0.33 mmol) was dissolved in anhydrous ether (10 mL) in a 50 mL flask. Dry methanol (67 µL, 1.67 mmol) was added to the solution, followed by the addition of lithium borohydride ($LiBH_4$, 2M in THF, 0.84 mL, 1.67 mmol). The reaction mixture was then heated up to a refluxing temperature, 45 °C, for 1 h, before ethyl acetate (0.5 mL) was added and the mixture was stirred at room temperature for 30 min. Then the reaction was quenched with NH_4Cl (10 mL, sat. aq.) and diluted with water (10 mL). The product was extracted

with ethyl acetate (20 mL × 6). The combined organic layer was dried over $MgSO_4$, and then concentrated under reduced pressure. White solid product crashed out during the removal of solvent. Collecting the solid product and recrystallization with acetone/hexane system afforded the diol **4d** (52.2 mg, 0.237 mmol, 71%). ^{1}H NMR (400 MHz, Acetone-d_6) δ 7.31 (d, J = 8.9 Hz, 2H), 6.85 (d, J = 8.8 Hz, 2H), 3.78 (s, 3H), 3.71–3.65 (m, 1H), 3.65 – 3.61 (m, 1H), 3.57–3.51 (m, 1H), 3.49–3.43 (m, 2H), 2.28 (t, J = 5.8 Hz, 1H), 1.92 (dd, J = 3.6, 1.0 Hz, 1H) (O–H protons are not resolved). ^{13}C NMR (101 MHz, Acetone) δ 158.07, 129.14, 129.08, 113.58, 60.27, 60.14 (splitting), 55.88, 55.75 (splitting), 54.56, 49.65, 49.61 (splitting), 46.08, 46.04 (splitting), 21.53, 16.55. (Note: the diol product might have two rotating conformations, resulting in splitting of 4 carbon peaks.) HRMS (FAB) m/z: 221.1168 ($M+H^+$); calc. for $C_{13}H_{17}O_3$: 221.1178. $[\alpha]^{23}_D$ = –50.8 ± 1.2° (*c* 0.1, acetone).

Crystal structure information of **4d**:

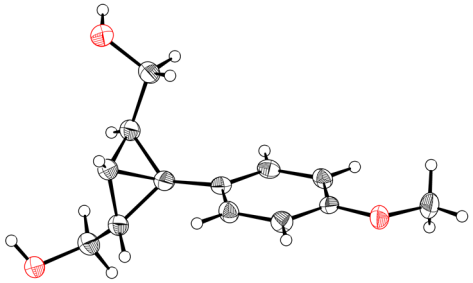

Identification code	p17505
Empirical formula	$C_{13}H_{16}O_3$
Formula weight	220.26
Temperature	175 K
Wavelength	1.54178 Å
Crystal system	Monoclinic
Space group	P 1 21 1
Unit cell dimensions	a = 5.3738(7) Å a= 90°
	b = 7.6719(8) Å b= 98.413(9)°
	c = 13.7357(19) Å g = 90°
Volume	560.19(12) Å^3
Z	2
Density (calculated)	1.306 Mg/m^3
Absorption coefficient	0.747 mm^{-1}
F(000)	236
Crystal size	0.22 x 0.18 x 0.06 mm^3
Theta range for data collection	3.252 to 79.483°.
Index ranges	-6<=h<=6, -9<=k<=9, -16<=l<=17
Reflections collected	17841
Independent reflections	2338 [R(int) = 0.0437]
Completeness to theta = 67.679°	99.9 %
Absorption correction	Semi-empirical from equivalents
Max. and min. transmission	1.0000 and 0.8812
Refinement method	Full-matrix least-squares on F^2

Data / restraints / parameters	2338 / 1 / 148
Goodness-of-fit on F2	1.111
Final R indices [I>2sigma(I)]	R1 = 0.0471, wR2 = 0.1225
R indices (all data)	R1 = 0.0482, wR2 = 0.1232
Absolute structure parameter	0.15(7)
Extinction coefficient	n/a
Largest diff. peak and hole	0.337 and -0.270 e.Å^{-3}

Ethyl (1*R*,2*R*)-4-(hydroxymethyl)-1-(4-methoxyphenyl)bicyclo[1.1.0]butane-2-carboxylate (4e)

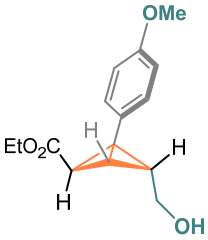

Mono-alcohol **4e** was obtained from the reduction of bicyclobutane **2k**. Collecting the mother liquor after recrystallization, evaporation of organic solvent followed by purification by silica column chromatography with hexane/ethyl acetate (5:1 to 3:1 gradient) afforded **4e** (14.6 mg, 0.056 mmol, 17%) with ~7:1 *r.r.* determined by ^{1}H NMR. ^{1}H NMR (400 MHz, Acetonitrile-d_3) δ 7.20 (d, *J* = 8.8 Hz, 2H), 6.88 (d, *J* = 8.8 Hz, 2H), 4.05 (qd, *J* = 7.1, 0.5 Hz, 2H), 3.78 (s, 3H), 3.43 (t, *J* = 6.3 Hz, 2H), 2.75 (tdd, *J* = 7.0, 3.3, 0.7 Hz, 1H), 2.70 (t, *J* = 5.9 Hz, 1H), 2.68 (s, 1H), 2.64 (d, *J* = 3.3 Hz, 1H), 1.14 (t, *J* = 7.1 Hz, 3H). ^{13}C NMR (101 MHz, CD_3CN) δ 168.54, 159.04, 129.70, 127.38, 114.20, 60.92, 56.42, 55.44, 47.23, 42.52, 24.86, 18.43, 13.99. MS (EI) m/z: 262 ($M^{+\cdot}$); calc. for $C_{15}H_{18}O_4$: 262.

(2-(4-Methoxyphenyl)cyclobut-1-ene-1,3-diyl)dimethanol (4f)

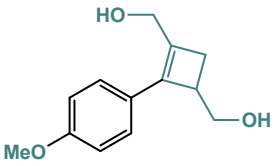

Bicyclobutane **2k** (54.7 mg, 0.18 mmol) was dissolved in anhydrous ether (5 mL) in a 20 mL vial and then cooled down to –78 °C. Lithium aluminium hydride (LAH, 13.7 mg, 0.36 mmol) was slowly added to the solution in portions. The reaction mixture was slowly warmed up to –20 °C over 2 h, before ethyl acetate (0.5 mL) was added and the mixture was stirred at –20 °C for another 30 min. Then the reaction was quenched with NH_4Cl (10 mL, sat. aq.) and diluted with water (10 mL). The product was extracted with ethyl acetate (20 mL × 3). The combined organic layer was dried over $MgSO_4$, and then concentrated under reduced pressure. The crude product was purified by silica column chromatography with hexane/ethyl acetate (2:1 to 1:2 gradient) to afford **4f** (18.1 mg, 0.082 mmol, 46%). ^{1}H NMR (400 MHz, Acetonitrile-d_3) δ 7.34 (d, *J* = 8.8 Hz, 2H), 6.92 (d, *J* = 8.9 Hz, 2H), 4.30 (d, *J* = 3.1 Hz, 2H), 3.80 (s, 5H), 3.57 (ddd, *J* = 11.2, 7.2, 4.3 Hz, 1H), 3.21–3.12 (m, 1H), 2.95 (t, *J* = 5.7 Hz, 1H), 2.70 (t, *J* = 5.5 Hz, 1H), 2.59 (dd, *J* = 13.7, 4.6 Hz, 1H). ^{13}C NMR (101 MHz, CD_3CN) δ 159.59, 140.27, 140.19, 128.91, 128.55, 114.63, 65.02, 59.23, 55.79, 42.11, 31.40. MS (EI) m/z: 220 ($M^{+\cdot}$); calc. for $C_{13}H_{16}O_3$: 220.

Ethyl (1*R*,2*R*,3*S*)-3-allyl-2-methyl-2-phenethylcyclopropane-1-carboxylate (7a)

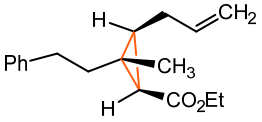

Cyclopropene (*R*)-**6a** (54.0 mg, 0.25 mmol) and CuI (5.0 mg, 0.026 mmol, 10 mol%) were dissolved in anhydrous ether (3 mL) to form a suspension in a 25 mL flask. Then the flask was charged with argon and cooled to –

78 °C. Methylmagnesium bromide (0.75 mL, 1M in ether, diluted from 3M solution in ether) was added dropwise to the reaction mixture over 10 min. The reaction was slowly warmed to –40 °C over 30 min and held at this temperature for another 1 h. A solution of allyl bromide (43 µL, 0.50 mmol) in ether (1 mL) was then added to the reaction dropwise over 5 min. The reaction was stirred at –40 °C for 1 h, before it was quenched with NH_4Cl/NH_3 (2:1, aq., 5 mL) at –20 °C. The aqueous layer was extracted twice with ether. The combined organic layers were washed with water (10 mL), and brine (10 mL), dried over $MgSO_4$, and then concentrated under reduced pressure. The crude product was purified by silica column chromatography with hexane/ethyl acetate (1:0 to 50:1 gradient) to afford **7a** (48.0 mg, 0.176 mmol, 71%) as a single diastereomer. ^{1}H NMR (400 MHz, $CDCl_3$) δ 7.23–7.17 (m, 2H), 7.13–7.07 (m, 3H), 5.73 (ddt, *J* = 17.3, 10.2, 6.2 Hz, 1H), 4.97 (dq, *J* = 17.2, 1.7 Hz, 1H), 4.89 (ddt, *J* = 10.2, 2.0, 1.4 Hz, 1H), 4.07–3.96 (m, 2H), 2.68–2.60 (m, 2H), 2.33 (ddt, *J* = 7.6, 6.2, 1.5 Hz, 2H), 1.57–1.51 (m, 2H), 1.40 (d, *J* = 8.9 Hz, 1H), 1.23 (s, 3H), 1.18 (t, *J* = 7.1 Hz, 3H), 1.09 (dt, *J* = 8.8, 7.4 Hz, 1H). ^{13}C NMR (101 MHz, $CDCl_3$) δ 171.68, 142.04, 137.72, 128.38, 128.33, 125.81, 114.58, 59.80, 45.06, 32.87, 31.77, 29.13, 27.89, 27.34, 14.39, 11.53. HRMS (FAB) m/z: 273.1849 ($M+H^+$); calc. for $C_{18}H_{25}O_2$: 273.1855. $[\alpha]^{23}_D$ = –61.3 ± 1.7° (*c* 0.1, ethyl acetate).

Ethyl (1*R*,6*R*,7*R*)-3,4-dimethyl-1-(6-((tetrahydro-2*H*-pyran-4-yl)methoxy)hexyl) bicyclo [4.1.0]hept-3-ene-7-carboxylate (7b)

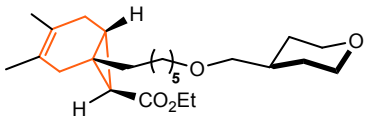

Cyclopropene (*R*)-**6g** (65.6 mg, 0.211 mmol) was dissolved 2,3-dimethylbutadiene (0.5 mL). Then the reaction was heated and stirred at 80 °C in a sealed tube for 23 h. After cooling to room temperature, the resulting mixture was concentrated under reduced pressure. The crude product was purified by silica column chromatography with hexane / ethyl acetate (1:0 to 6:1 gradient) to afford **7b** (81.1 mg, 0.207 mmol, 98%) as a single diastereomer. ^{1}H NMR (400 MHz, $CDCl_3$) δ 4.09 (qd, *J* = 7.1, 0.4 Hz, 2H), 4.01–3.90 (m, 2H), 3.45–3.32 (m, 4H), 3.24 (d, *J* = 6.6 Hz, 2H), 2.43–2.29 (m, 1H), 2.30–2.09 (m, 3H), 1.90–1.75 (m, 1H), 1.67–1.60 (m, 4H), 1.58–1.50 (m, 10H), 1.46–1.38 (m, 1H), 1.36–1.26 (m, 5H), 1.26–1.15 (m, 5H). ^{13}C NMR (101 MHz, $CDCl_3$) δ 173.76, 122.00, 121.77, 76.09, 71.37, 67.91, 60.21, 35.85, 35.60, 32.93, 32.16, 30.85, 30.20, 29.80, 29.69, 27.92, 26.89, 26.86, 26.33, 19.30, 19.09, 14.55. HRMS (FAB) m/z: 393.2992 ($M+H^+$); calc. for $C_{24}H_{41}O_4$: 393.3005. $[\alpha]^{23}_D$ = –48.2 ± 1.1° (*c* 0.1, ethyl acetate).

All-*cis* ethyl 2-ethyl-3-(2-fluorophenyl)cyclopropane-1-carboxylate (10a)

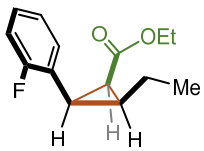

Product **9d** (46.9 mg, 0.2 mmol) from enzymatic reaction was dissolved in toluene (2 mL) in a vial and then Pd/C (10.6 mg, 10% palladium on carbon, 5 mol% Pd) was added to the solution. The vial was then capped, and the solution was degassed with H_2 using a H_2 balloon. The reaction was then stirred under H_2 atmosphere at room temperature for 12 h. After the reaction is completed, the organic solvent was removed under reduced pressure. Purification by silica column chromatography with hexane/ethyl acetate as eluents afforded the desired *all-cis* cyclopropane product **10a** (47.1 mg, >99% yield). ^{1}H NMR (400 MHz, $CDCl_3$) δ 7.25–7.15 (m, 2H), 7.05 (td, *J* = 7.5, 1.3 Hz, 1H), 6.99 (ddd, *J* = 9.9, 8.6, 1.3 Hz, 1H), 4.06 (qd, *J* = 7.2, 2.2 Hz, 2H), 2.48 (td, *J* = 8.8, 1.1 Hz, 1H), 2.13 (t, *J* = 8.6 Hz, 1H), 1.91 – 1.76 (m, 1H), 1.72 – 1.57 (m, 2H), 1.18 (t, *J* = 7.1 Hz, 3H), 0.95 (t, *J* = 7.1 Hz, 3H). ^{13}C NMR (101 MHz, $CDCl_3$)

δ 171.01, 162.63 (d, *J* = 246.9 Hz), 132.10 (d, *J* = 4.1 Hz), 128.40 (d, *J* = 8.4 Hz), 123.48 (d, *J* = 3.6 Hz), 122.86 (d, *J* = 15.1 Hz), 115.12 (d, *J* = 22.1 Hz), 60.09, 27.24, 23.39 (d, *J* = 1.8 Hz), 21.70 (d, *J* = 1.4 Hz), 17.47, 14.33, 14.04. HRMS (TOF) m/z: 237.1277 ($M+H^+$); calc. for [$C_{14}H_{17}FO_2+H^+$]: 237.1285.

All-*cis* (2-ethyl-3-(2-fluorophenyl)cyclopropyl)methanol (10b)

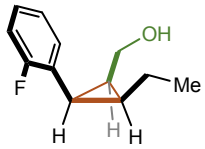

Cyclopropane **10a** (47.1 mg, 0.2 mmol) was dissolved in anhydrous THF (2 mL) in a 50 mL flask, which was then placed in an ice-water bath. $LiAlH_4$ (15.2 mg, 0.4 mmol, 2.0 equiv.) was slowly added to the solution. The reaction was allowed to slowly warm to room temperature over 1 h and then stirred for another 1h. NaOH (2 mL, 1M aq.) was added to quench the reaction. The crude product was extracted with ether (10 mL × 4). The combined organic layer was dried over Na_2SO_4 and concentrated under reduced pressure. Purification by silica column chromatography with hexane/ethyl acetate as eluents afforded the desired *all-cis* cyclopropane product **10b** (36.4 mg, 94% yield). ^{1}H NMR (400 MHz, $CDCl_3$) δ 7.34 (tdd, *J* = 7.6, 1.9, 1.1 Hz, 1H), 7.23–7.16 (m, 1H), 7.09–6.97 (m, 2H), 3.68 (d, *J* = 7.4 Hz, 2H), 2.13 (td, *J* = 8.8, 1.1 Hz, 1H), 1.65–1.51 (m, 3H), 1.34–1.25 (m, 1H), 1.17–1.02 (m, 4H). ^{13}C NMR (101 MHz, $CDCl_3$) δ 163.05 (d, *J* = 245.5 Hz), 132.44 (d, *J* = 4.2 Hz), 128.13 (d, *J* = 8.4 Hz), 124.47 (d, *J* = 15.5 Hz), 123.93 (d, *J* = 3.5 Hz), 115.43 (d, *J* = 22.7 Hz), 60.18 (d, *J* = 1.5 Hz), 21.93, 21.66, 18.60 (d, *J* = 2.8 Hz), 18.51, 14.70. HRMS (TOF) m/z: 177.1071 ($M+H^+-H_2O$); calc. for [$C_{12}H_{15}FO+H^+-H_2O$]: 177.1074.

Chapter 3

ENZYMATIC SYNTHESIS OF DIVERSE LACTONE DERIVATIVES: A LACTONE-CARBENE STRATEGY

Material for this chapter appears in: (1) **Chen, K.**[†]; Zhang, S.-Q.[†]; Brandenberg, O. F.; Hong, X.[*]; Arnold, F. H.[*], Alternate heme ligation steers activity and selectivity in engineered cytochrome P450-catalyzed carbene transfer reactions. *J. Am. Chem. Soc.* **140**, 16402–16407 (2018). (2) **Chen, K.**; Huang, X.; Zhang, S.-Q.; Kan, S. B. J.; Zhou, A. Z.; Hong, X.[*]; Arnold, F. H.[*], Engineered cytochrome *c*-catalyzed lactone-carbene B–H insertion. *Synlett* **30**, 378–382 (2019). (3) Zhou, A. Z.; **Chen, K.**[*]; Arnold, F. H.[*], Enzymatic lactone-carbene C–H insertion to build contiguous chiral centers. *ACS Catal.* **10**, 5393–5398 (2020).

3.1 Abstract

Lactones are a fundamental class of organic moieties that possess wide applications in fields varying from synthetic chemistry, to materials science, to medicinal chemistry. Nature employs different machineries to assemble these cyclic esters, however, with limitations in synthesizing structurally diverse lactone products. We therefore desired to expand nature's capacity for lactone formation using our enzymatic carbene-transfer strategy. Compared to *de novo* construction of cyclic esters, direct incorporation of lactone substructures to target molecules is an attractive approach, which can efficiently build lactone-based complex molecules and lead to broader structural diversity through a convergent biosynthetic scenario. Directed evolution significantly expanded the capacity of our enzymatic systems, enabling rapid and selective transfer of lactone-based carbenes to substrates with different functionalities. This newly demonstrated enzymatic platform allowed us to access a broad range of α-(heteroatom)substituted lactone and *spiro*-lactone derivatives with unprecedented efficiencies and selectivities.

3.2 Introduction

Lactones, as cyclic esters, belong to an important class of structural motifs that frequently appear in bioactive natural products[176-178], pharmaceuticals[179,180], agrochemicals[181] and aroma chemicals,[182] and are also intensively employed as building blocks for the production of other fine chemicals[183] as well as monomers for polyester synthesis[184]. For instance, 5-membered γ-lactones are widely distributed in the natural world, present in around 10% of natural products discovered to date[185]. Many of them have been found to display diverse biological profiles including antibiotic, antiviral, antifungal, anticancer, anti-inflammatory and cytostatic properties[186]. These unique biologically relevant activities have captured the great attention of biochemists to take them as promising lead structures for pharmaceutical development[187], as exemplified by the drug molecules shown in **Fig 3.1**.

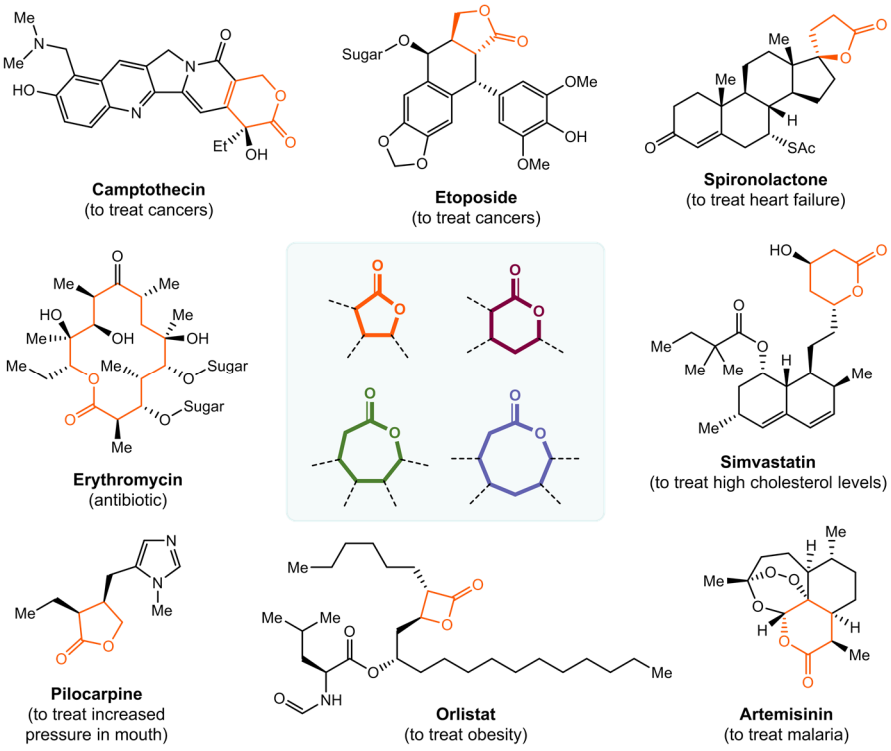

Figure 3.1. Representative examples of pharmaceutical compounds containing lactone structures. Some of these drugs are basically natural products, such as erythromycin, pilocarpine and artemisinin, or derivatives of natural products, such as etoposide and spironolactone.

Given the importance of lactones in different fields, chemists have devoted a great deal of effort to the development of synthetic methods for these cyclic ester structures[185,188]. Meanwhile, the widespread occurrence of lactone-based compounds in nature has also prompted chemists to visit nature's strategies for lactone formation. In fact, nature employs an array of machineries to assemble cyclic esters[189], among which three major approaches are intramolecular esterification of hydroxyl carboxylic acids by acyltransferases, oxidative lactonization of diols by alcohol dehydrogenases (ADHs)[190], and Baeyer-Villiger oxidation of cyclic ketones by monooxygenases (BVMOs)[191] (**Fig. 3.2.a**). In the recent decade, enzyme engineering, especially on ADHs and BVMOs, has expanded the scope of lactone products accessible to these native enzymatic systems[189]. Besides, fermentation processes employ fatty acids as substrates to synthesize lactones through hydroxylation by hydroxylases (*e.g.*, P450 or other metallo-oxidases) or hydratases and then intramolecular lactonization[192-194]. These native approaches, optimized by different engineering processes, have offered the synthetic community an alternative toolkit based on biocatalysis that can more selectively and efficiently produce desired lactone products compared to the existing chemical methods.

While seeing the promise of using biocatalysis for lactone synthesis, we also realized that there are still limitations in these native strategies. From the standpoint of retro-synthetic analysis, these natural enzymatic approaches are all based on C–O bond disconnection, which typically limits the

structural diversity of lactone products and renders the native strategies less versatile for broad synthetic purposes. Therefore, we desired to develop new enzymatic strategies using different disconnection modes for the synthesis of diverse lactone derivatives while taking advantage of enzymes' benefits with respect to efficiency and selectivity.

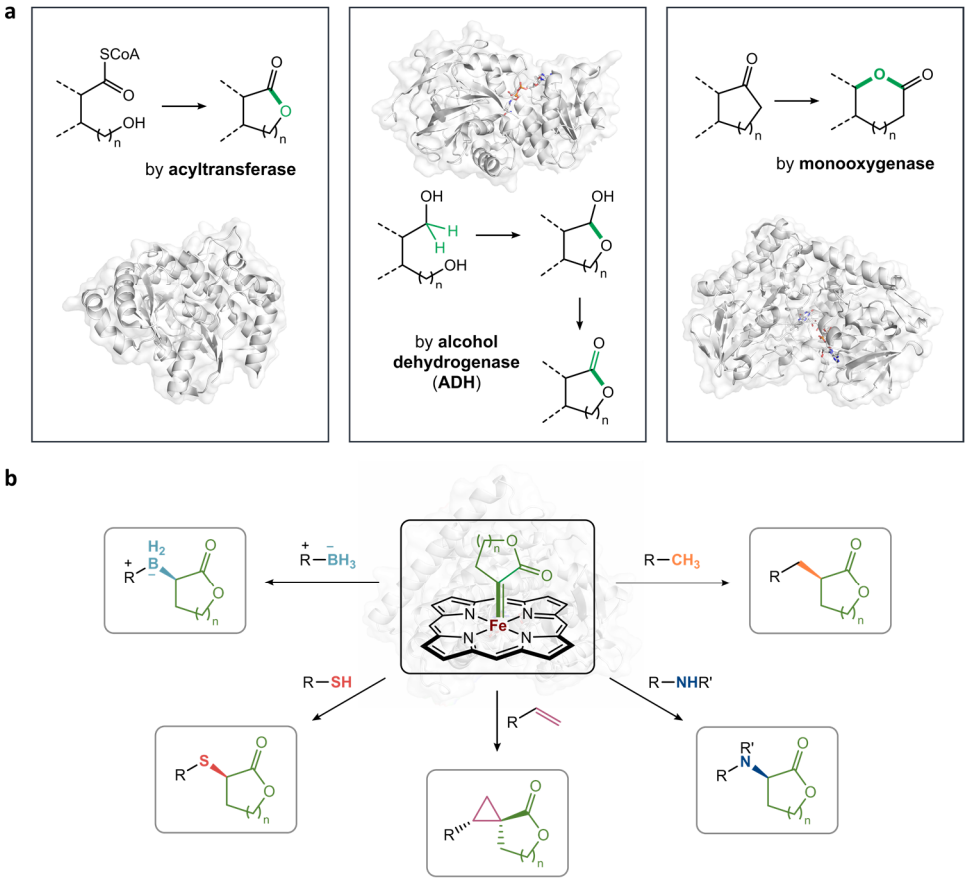

Figure 3.2. Enzymatic strategies for lactone assembly. a, Native strategies using acytransferase, alcohol dehydrogenase and flavin monooxygenase for lactone synthesis. **b**, Access to diverse lactone derivatives with a lactone-carbene strategy. Lactone-carbene X–H insertion (X = B, S, N and C) and cyclopropanation are presented here.

Our continuing effort on engineering hemeproteins for carbene chemistries thus inspired us to look at a new set of carbenes based on lactone structures for the transfer to different functionalities to assemble lactone derivatives (**Fig 3.2.b**). In fact, a few studies have demonstrated that α-diazo lactones can be utilized by rhodium complexes for carbene-transfer reactions[195,196]. However, these rhodium–carbenes are prone to β-hydride migration[197], which gives rise to undesired unsaturated lactones; optimization of the rhodium catalysts and cryogenic reaction conditions are thus required to attenuate these side reactions. Additionally, no enantioselective versions of these transformations have been reported. Our previous work on engineering hemeproteins for transfer of acyclic carbenes highlighted the power of directed evolution to shape protein active sites and greatly improve both reactivity and selectivity. We therefore speculated that aptly engineered hemeproteins would be capable of generating and stabilizing lactone-carbene intermediates,

circumventing unwanted β-hydride migration, and facilitating subsequent carbene-transfer reactions with exquisite stereocontrol. This proposed enzymatic approach would provide a concise route to a broad array of lactone-containing products.

3.3 Enzymatic cyclopropanation for *spiro*[2.4]lactone synthesis

We initially focused on constructing cyclopropane-containing *spiro*-lactones using α-diazo-γ-lactone (**LAD**) and styrene (**11a**) as substrates. Transferring a cyclic carbene to an olefin double bond is expected to form a *spiro*-carbon center. Quaternary stereogenic centers frequently occur in biologically relevant molecules and medicinal compounds[198], but are challenging to make due to the highly congested nature of these centers[199,200]. The anticipated reaction produces a strained, three-membered ring and furnishes two chiral centers in a stereoselective manner, which necessitates precise control of the three-dimensional orientation of two coupling partners. We believe this is a good challenge for an enzyme catalyst.

We began by testing a panel of cytochrome P411 variants expressed in *E. coli* and used as whole-cell catalysts, with **LAD** and **11a** as substrates (**Fig. 3.3**). Variant P411-**CIS**[61], previously engineered to react with EDA and transfer the corresponding α-mono-substituted carbene to styrene to forge a *cis*-cyclopropane, showed modest reactivity towards *spiro*-lactone formation, with 120 ± 10 total turnovers (TTN) and 90% de. Several P411 variants with various active site mutations (*e.g.*, T268A or T438S) were tested, but did not exhibit substantial improvements in reactivity. However, to our delight, P411-**CIS** double mutant L437F T438Q (referred to as P411-**G8**), previously evolved for carbene transfer to heteroatom-substituted olefins[63], was found to have 10-fold higher reactivity, providing 1320 ± 190 TTN while also showing improved stereoselectivity (97% de). A variant with two additional mutations, L75Y and L181I (referred to as P411-**G8S**), was an even better biocatalyst, furnishing the desired *spiro*-lactone product **12a** in 3090 ± 120 TTN, 99% de and >98% ee. Control experiments showed that free heme does not catalyze this reaction.

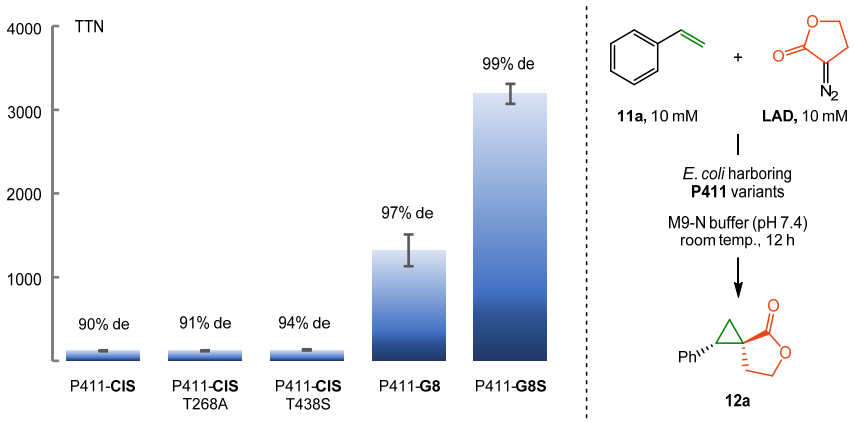

Figure 3.3. Comparison of P411 variants for forming *spiro*[2.4]-lactone 12a. Reactions were performed in

quadruplicate: suspensions of *E. coli* expressing P411 variants (OD_{600} = 30), 10 mM **11a**, 10 mM **LAD**, 25 mM D-glucose and 5 vol% EtOH in M9-N buffer at room temperature under anaerobic conditions for 12 h. Product formation was quantified by GC and TTNs were determined based on protein concentration.

To examine whether the serine axial ligand of this P411 variant played a significant role in promoting *in vivo* cyclopropanation activity, we mutated serine back to the canonical P450 axial ligand cysteine and found that the resulting P450-**G8S** variant synthesized **12a** with much lower activity (380 ± 20 TTN) but the same stereoselectivity (**Fig. 3.5**).

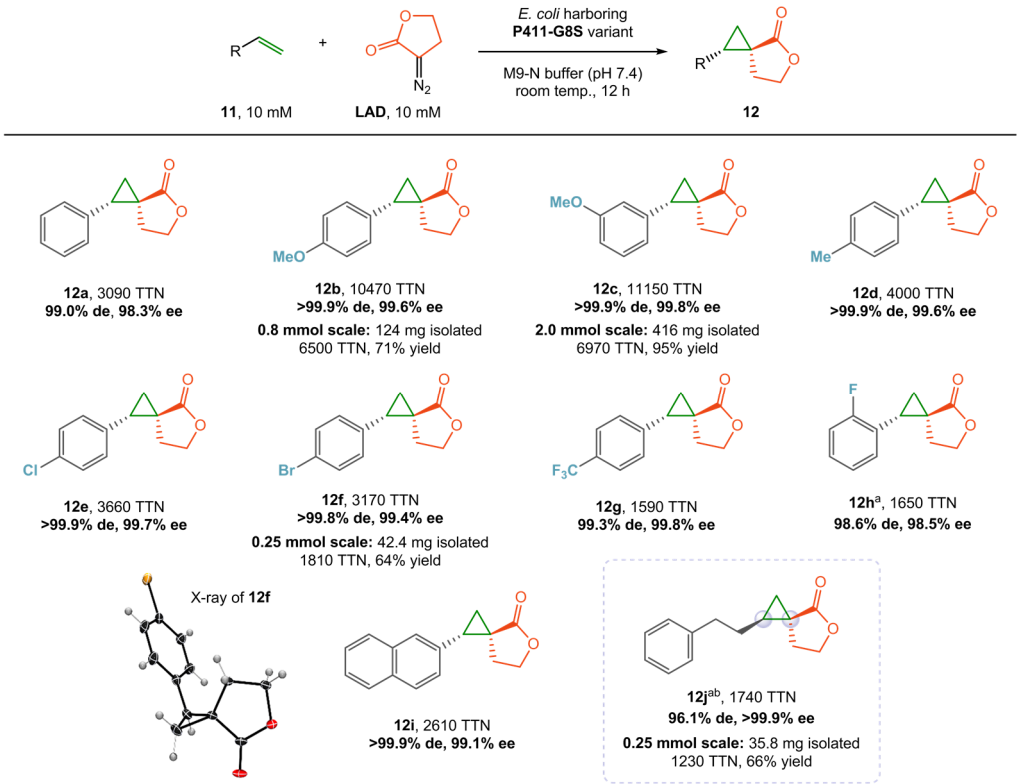

Figure 3.4. Scope of *spiro*[2.4]lactones with variant P411-G8S. Reactions were performed in quadruplicate: suspensions of *E. coli* expressing P411-**G8S** (OD_{600} = 15 or 30), 10 mM alkene, 10 mM **LAD**, 25 mM D-glucose and 5 vol% EtOH in M9-N buffer at room temperature under anaerobic conditions for 12 h. Product formation was quantified by GC and TTNs were determined based on protein concentration. [a]5 mM olefin, 5 mM **LAD**. [b]Absolute configuration not determined.

With the highly active and selective P411-**G8S** variant, we next explored the scope of olefin substrates for *spiro*-lactone construction (**Fig. 3.4**). Electron-rich styrenyl olefins (**11b** and **11c**) are particularly good substrates, with over 10,000 TTNs. Halides (**11e**, **11f** and **11h**) are also well-tolerated, offering opportunities for further derivatization through coupling methods. Fluorine-containing substrates, despite the strong electrondeficiency, are also accepted (*e.g.*, **11g**). Additionally, steric bulk (*e.g.*, 2-vinyl naphthalene **11i**) did not have a significant influence on reactivity. All tested styrenyl substrates gave (*E*)-*spiro*[2.4]lactone products with high-to-perfect stereoselectivity (98.6 to >99.9% de, and 98.3 to 99.8% ee). Unactivated aliphatic olefins such as 4-phenyl butene are also accepted by this biocatalytic system with 1740 TTN. Interestingly, NMR analysis revealed a (*Z*)-

configuration of product **12j**, which indicates potentially different binding modes for aromatic *vs*. aliphatic olefins in the enzyme's active site. The enzymatic reactions are also readily scalable and maintain stereoselectivity and high reactivity. Products **12b** and **12c** were prepared in hundred-milligram quantities with good isolated yields (71% yield, 6500 TTN and 95% yield, 6970 TTN). The absolute configurations of products **12b** and **12f** were unambiguously assigned as (1*S*, 2*S*) by X-ray crystallography.

3.4 Enzymatic S–H insertion for α-thio-γ-lactone synthesis

3.4.1 Enzymatic synthesis of α-thio-γ-lactones

Having established this biocatalytic platform for the efficient synthesis of *spiro*-lactones, we speculated that the active-site environment of P411-**G8S** may be especially suited to stabilize the iron-lactone-carbene intermediate. We were eager to examine whether this P411 variant can catalyze the transfer of this lactone-carbene to other functionalities, such as thiols. Carbene S–H insertion is poorly developed among carbene-transfer reactions; one challenge is that thiols can poison transition-metal catalysts through coordination. To date, only a few catalytic systems were developed for asymmetric carbene S–H insertion, and these exhibit limited catalytic efficiency[201] and/or low stereoselectivity[104,202-204]. Fasan and coworkers reported carbene S–H insertion with up to 49% ee by an engineered myoglobin[84]. Whereas carbene Si–H and N–H insertions with iron-porphyrin (bio)catalysts have been revealed to undergo concerted Si–H insertion[88] and nucleophilic attack by amine at the carbene center[205], the mechanism of carbene S–H insertion remains obscure[206]. We thus decided to take a closer look at lactone-carbene S–H insertion with the current enzymatic system.

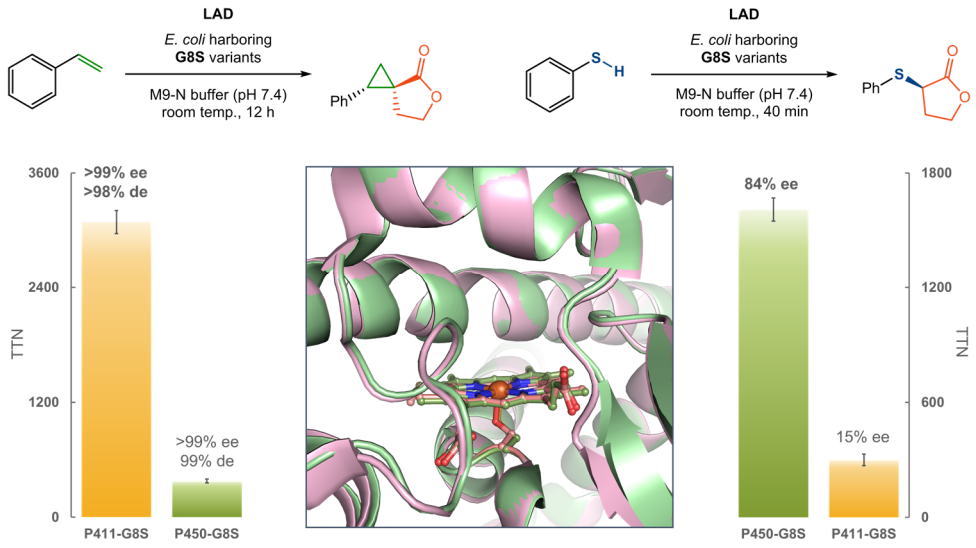

Figure 3.5. Comparison of P411-G8S and P450-G8S for lactone-carbene cyclopropanation and S–H insertion. Reactions were performed in quadruplicate: suspensions of *E. coli* expressing P411 or P450-**G8S**

(OD_{600} = 15 or 30), 10 mM **11a** or **13a**, 10 mM **LAD**, 25 mM D-glucose and 5 vol% EtOH in M9-N buffer at room temperature under anaerobic conditions for 12 h (for cyclopropanation) and 40 min (for S–H insertion). Product formation was quantified by GC and TTNs were determined based on protein concentration. The overlay of P450-**CIS** (PDB: 4h24, in green) and P411-**CIS** (PDB: 4h23, in pink) active-site structures is shown as analogy to P450/P411-**G8S**.

Using P411-**G8S** as a whole-cell catalyst, thiophenol **13a** reacted with **LAD** to give the desired α-thio-γ-lactone product **14a** in 300 ± 30 TTN, but with poor enantioselectivity (15 ± 2% ee). In an effort to improve reactivity and selectivity, we wanted to explore how the identity of the heme axial ligand[62,64,111,207,208] affected the S–H insertion process. We thus tested this reaction with a library of mutant enzymes made by site-saturation mutagenesis of the axial-ligand residue S400 in P411-**G8S**. To our delight, simply replacing the axial serine with cysteine (the native ligating residue in P450s) substantially improved reactivity and selectivity, to 1610 ± 60 TTN and 84 ± 1% ee (**Fig. 3.5**).

We next evaluated the substrate range of this cysteine-ligated P450-**G8S** variant for lactone-carbene S–H insertion (**Fig. 3.6**). Thiophenols with *meta*-OMe and *para*-halide substituents were successfully converted into the corresponding α-thio-γ-lactone products (**14b** to **14e**) with good TTNs and enantioselectivities. However, *para*-(fluorinated)alkyl groups (**13f** to **13h**) or a bulkier aromatic ring (**13j**) gave lower reactivity and selectivity, suggesting that steric hindrance may affect substrate orientation. Products **14d** and **14e** were also synthesized in hundred-milligram scale under modified conditions; good isolated yields were obtained with slightly improved enantioselectivity.

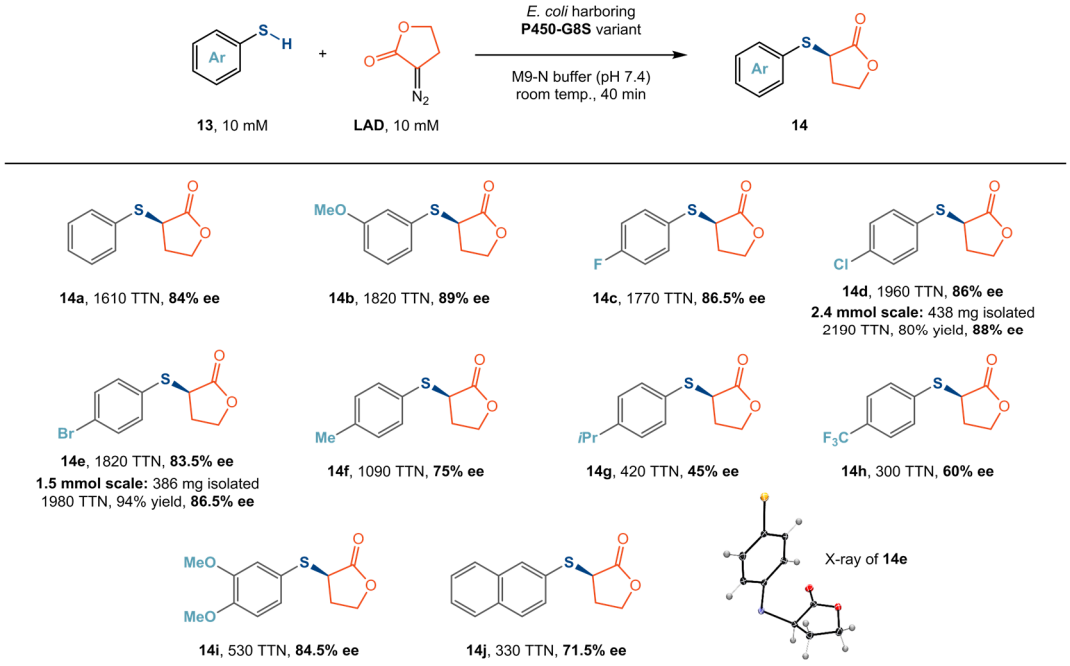

Figure 3.6. Scope of α-thio-γ-lactones with variant P450-G8S. Reactions were performed in quadruplicate: suspensions of *E. coli* expressing P450-**G8S** (OD_{600} = 15 or 30), 10 mM thiol, 10 mM **LAD**, 25 mM D-glucose and 5 vol% EtOH in M9-N buffer at room temperature under anaerobic conditions for 40 min. Product formation was quantified by GC and TTNs were determined based on protein concentration. *For preparative-scale reaction: 2.0 equiv. thiol, 2 h.

3.4.2 Mechanistic study of enzymatic S–H insertion

It struck us as interesting that the P411/P450-**G8S** variants behaved so differently in the S–H insertion and cyclopropanation reactions (**Fig 3.5**; **Table B-2** and **B-4** in **Appendix B**). According to a previous structural study of P411-**CIS** and P450-**CIS** variants that also differed solely at the axial-ligand residue, the cysteine-to-serine mutation maintains almost identical active-site geometries. As also demonstrated in previous work on *in vivo* reactions using P411 variants, the endogenous reductant NADPH can act as an electron donor to reduce Fe^{III} to Fe^{II}, which is required for the iron center to activate diazo compounds to form iron-carbenoid intermediates[62]. Cysteine-ligated heme, on the other hand, has a lower reduction potential of the ferric state and thus results in poor reduction efficiency of the iron center by NADPH. Consequently, P411-**G8S** exhibits significantly higher cyclopropanation activity compared to P450-**G8S**, though both show similar selectivities. However, for carbene S–H insertion, thiol substrates can also serve as a strong reductant and enable P450 variants to form iron-carbenes. But this did not explain the significant disparity between P411-**G8S** and P450-**G8S** in both reactivity and selectivity, causing us to speculate that the axial ligand was exerting a heretofore unobserved effect on the reaction mechanism.

To explore the effects of axial coordination on the S–H insertion reaction in more detail, we used DFT calculations. The generation of iron-carbenoid species is reasonably facile, according to previous experimental and computational studies[88,209,210]. Our computational investigations thus focused on the insertion steps. Simplified iron-porphyrin models (**cat1** and **cat2**) were used, where SMe and OMe were chosen to mimic deprotonated Cys and Ser ligands.

The free energy diagram of the most favorable pathway for S–H insertion is shown in **Fig. 3.7**. The insertion occurs in a stepwise fashion, involving one hydrogen-atom-transfer (HAT) step and subsequent C–S bond formation with a thiyl radical. Both **cat1** and **cat2** showed similar reactivities for S–H bond insertion, with free energy barriers of 19.4 kcal/mol and 18.5 kcal/mol, respectively. However, we found that the iron-alkyl intermediates (**int2**$^{\mathbf{SMe}}$ and **int2**$^{\mathbf{OMe}}$) can undergo a reversible C–Fe bond homolytic cleavage (via **TS3**$^{\mathbf{SMe}}$ and **TS3**$^{\mathbf{OMe}}$), which erodes the enantioenriched alkyl-substituted stereocenter. The two pathways, radical rebound and C–Fe bond cleavage, are differentiated by the axial coordination. With SMe ligation, C–S bond formation is more favorable than C–Fe bond homolytic cleavage (**TS2**$^{\mathbf{SMe}}$, $\Delta G^{\neq}$ = 6.7 kcal/mol *vs*. **TS3**$^{\mathbf{SMe}}$, $\Delta G^{\neq}$ = 10.4 kcal/mol), while the opposite is true for the OMe-ligated intermediate **int2**$^{\mathbf{OMe}}$ (**TS2**$^{\mathbf{OMe}}$, $\Delta G^{\neq}$ = 7.3 kcal/mol *vs*. **TS2**$^{\mathbf{SMe}}$, $\Delta G^{\neq}$ = 6.2 kcal/mol). These results indicate that Cys-ligated P450 enzymes should achieve much higher enantioselectivities than Ser-ligated P411 enzymes, which matches the experimental observations. The axial coordination has a limited effect on C–S rebound, but strongly controls the feasibility of C–Fe bond dissociation[211-213]. Since oxygen has a much higher electronegativity than sulfur, the anionic **cat2** is more stable than the sulfur-coordinated **cat1**. Therefore, C–Fe homolytic cleavage with OMe ligation, which releases **cat2**, has a lower activation barrier and is more

exothermic than that with sulfur coordination. The difference in exothermicity drives the change in reaction barrier, which eventually leads to the difference in enantioselectivities of the two catalysts.

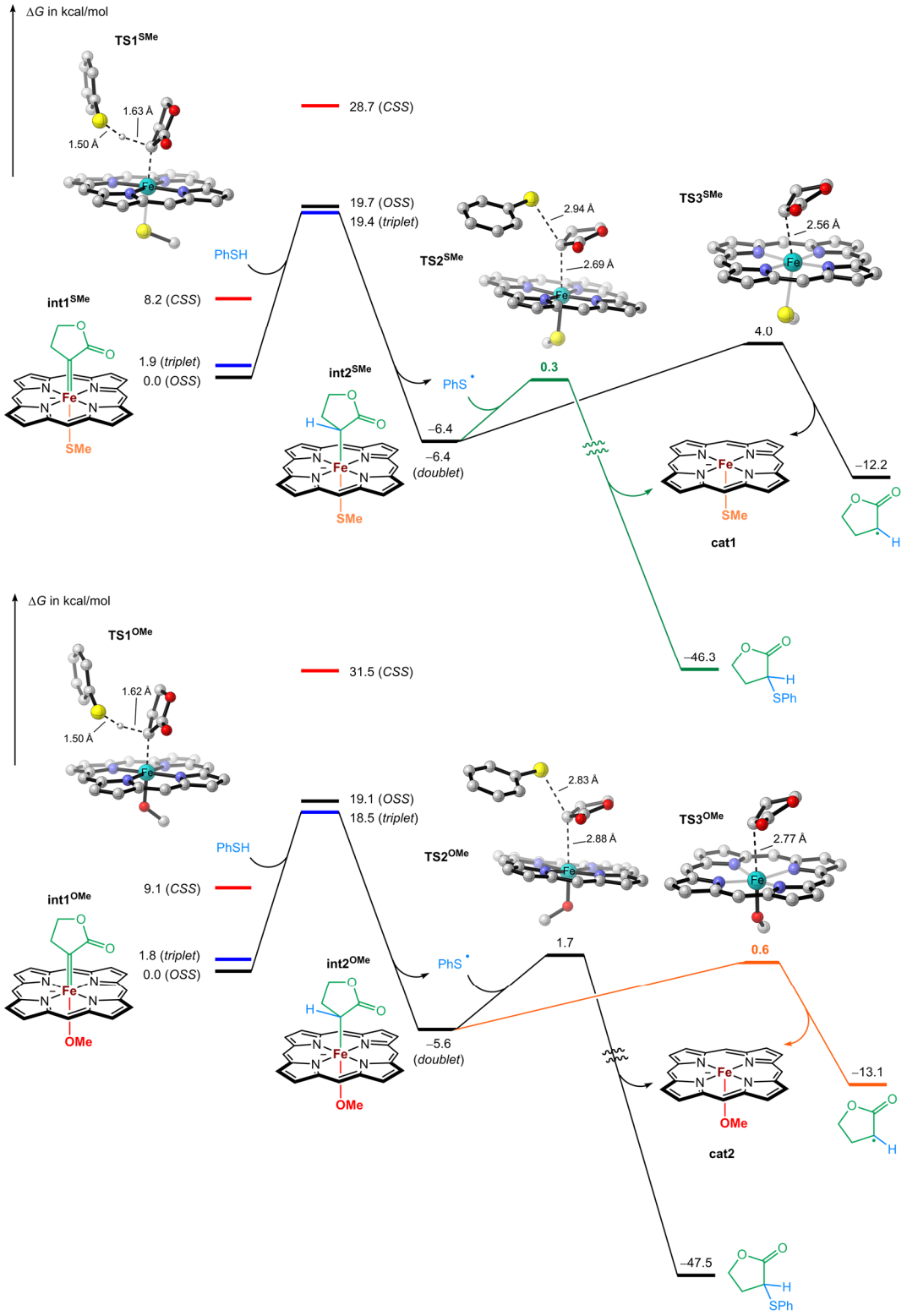

Figure 3.7. Free energy diagrams for the most favorable reaction pathways of S–H insertion with model catalysts. Gibbs free energy obtained at the B3LYP/def2-TZVP//B3LYP/6-31G(d)-LANL2DZ level. The most stable spin states are shown in parentheses. OSS is open-shell singlet; CSS is closed-shell singlet.

3.5 Enzymatic C–H insertion for β-amino lactone synthesis

3.5.1 Identification and evolution of P411 enzymes for lactone-carbene C–H insertion

Enantioselective C(sp^3)–H alkylation via carbene insertion into C–H bonds provides a powerful strategy for C(sp^3)–C(sp^3) bond formation to build diverse molecular skeletons and for late-stage modification of complex molecules[214-216]. Transition-metal catalysts based on rhodium[217-221], iridium[222-225], cobalt[226,227], copper[228,229], and other metals[230-235] have been shown to catalyze carbene insertion into C–H bonds. In most reported methods, carbenes bearing one electron-donating aryl/alkenyl group and one electron-withdrawing group ('donor-acceptor carbenes')[236,237] have been demonstrated to be superior for intermolecular C–H insertions, with control over reactivity and selectivity in these catalytic systems[238-242]. Other carbenes, however, such as acceptor-only carbenes, are less explored for C–H insertion reactions[223]; acceptor-only carbenes with an additional alkyl substituent at the α-position are even more challenging to use in these systems due to competitive β-hydride migration upon the formation of the metallo-carbene species[195].

Recently, we reported the engineering of cytochromes P411 for the transfer of carbene moieties to C–H bonds using diazo compounds bearing a single electron-withdrawing substituent and the establishment of this enzymatic platform for stereoselective C–C bond assembly with a chiral center formed at the β-position[77,78]. We thus anticipated that the P411 enzymes could be evolved further to adopt branched carbenes for C–H insertion, which would enable them to build a chiral center at α-position or even contiguous chiral centers at both α and β-positions. With our previous success on using lactone-based carbenes for cyclopropanation and S–H insertion, we would like to further explore these cyclic carbenes for C–H functionalization rather than the well-studied donor-acceptor carbenes.

We initiated this investigation of carbene C–H insertion with α-diazo-γ-lactone (**LAD**) and 4,*N*,*N*-trimethylaniline (**15a**) as substrates (**Fig. 3.8**). The expected carbene transfer reaction leads to the formation of a β-amino lactone product, **16a**, through carbene insertion into an α-amino C–H bond with a chiral center generated at the α-position. Such β-amino lactone products are analogs of sesquiterpene-lactone amino derivatives, which possess desirable pharmaceutical properties[243]. Screening various hemeproteins, including P450 variants, P411s, and cytochromes *c* in the form of whole *E. coli* cell catalysts identified a P411 variant, P411-**C10**, capable of the desired C–H insertion transformation. P411-**C10**, previously found with activity for internal cyclopropene formation, catalyzed the C–H insertion reaction using a cyclic carbene with modest efficiency (105 TTN) and stereoselectivity (47% ee).

To enhance enzyme activity and selectivity by directed evolution, we targeted active-site residues for site-saturation mutagenesis and screening (**Fig. 3.8**). Loop residues in the enzyme's active site were tested first, and beneficial mutations T327V and Q437L together increased total

turnovers 9-fold. However, enantioselectivity decreased to 40% ee after three rounds of evolution. As substrate **15a** is symmetric, we hypothesized that it might bind with different orientations relative to the carbene intermediate, which would lead to the diminished stereoselectivity. To address this, we next targeted amino acids previously shown to dramatically affect stereoselectivity in either native or non-native functions of this P450, such as sites 87, 264, 268, and 328[61,63,75,244-247]. Screening a site-saturation library at site 87 for increased enantioselectivity resulted in discovery of a proline mutation giving 56% ee, albeit with decreased TTN. Residue 264 is the closest residue to the iron center, which may also influence binding of substrate or the orientation of the carbene intermediate. The A264S mutation improved both activity and enantioselectivity. Revisiting site 327 identified another proline mutation, which boosted the ee to 75%. The three mutations A87P, A264S, and V327P may have improved enantioselectivity by providing a more restricted binding mode for substrate **1a** in the enzyme.

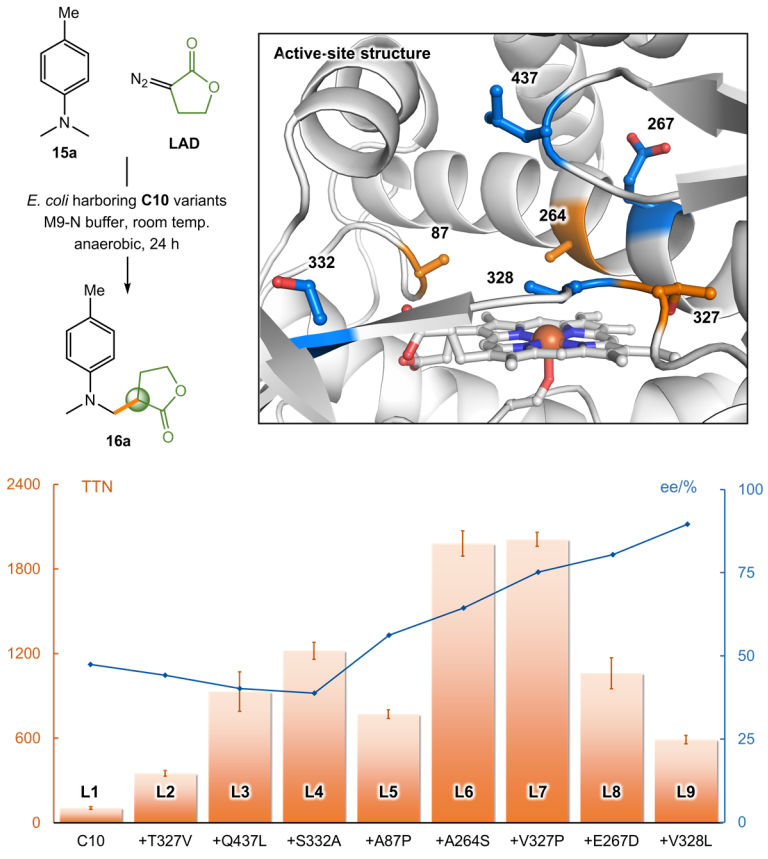

Figure 3.8. Directed evolution of P411-C10 for lactone-carbene insertion into α-amino C–H bonds. Reactions were performed in quadruplicate under the following conditions: 10 mM 4,*N*,*N*-trimethyl aniline (**15a**), 10 mM **LAD**, *E. coli* harboring P411-**C10** variants (OD_{600} = 15 to 60), D-glucose (25 mM), M9-N buffer/EtOH (19:1), anaerobic, 24 h. Product formation was quantified by HPLC, TTNs were determined based on protein concentration, and enantioselectivity was measured using chiral HPLC. The active-site structure of P411-**E10** variant (pdb: 5UCW) was used to guide site-saturation mutagenesis.

Further rounds of evolution accumulated two more mutations, E264D and V328L, to give final variant **L9** that produces **16a** with 90% ee. Although the TTN of **L9** dropped to approximately 600

under screening conditions, optimization of enzyme expression and reaction conditions improved TTN 1.5- to 2.5-fold (**Fig. 3.9**, entry **16a**; and **Table B-6** in **Appendix B**). Another variant, **L10**, with a V328R mutation obtained from the 328X site-saturation library, showed the opposite stereo-preference (–68% ee) for this C–H insertion reaction, suggesting that this biocatalytic platform may be tunable for enantio-divergent synthesis[63,169,248].

3.5.2 Scope evaluation of enzymatic lactone-carbene C–H insertion

As different variants in the enzyme lineage (**L1** to **L10**) showed different levels of activity or selectivity for the C–H insertion reaction, we selected representative variants (**L6** to **L10**) with which to evaluate the transformation of various *N*,*N*-dialkyl aniline derivatives, as shown in **Fig. 3.9.a**. Substituents on the phenyl ring, including methyl, methoxyl or halide, are all compatible with the biocatalytic system, giving TTNs ranging from 410 to 2920. Variants **L9** and **L10** showed consistently opposite stereo-preference for diverse substrates (*e.g.*, for **16d** and **16e**, 84% ee and 75% ee with **L9**, –55% and –86.5% ee with **L10**), whereas activity had different trends in some cases (*e.g.*, for **16d** and **16e**, 1410 TTN and 410 TTN with **L9**, 720 TTN and 1800 TTN with **L10**). Interestingly, with *N*-methyl, *N*-ethyl aniline (**15g**), **L9** only synthesized the primary C–H insertion product **16g** with high efficiency (1710 TTN) and high enantioselectivity (95% ee); **L10**, in contrast, gave a mixture of the primary and secondary C–H insertion products, **16g** and **16g'**, with a ratio of 71:29, where product **16g'** was found to be mainly a single diastereomer and enantiomer (>95:5 d.r. and 97.5% ee). Based on this result, we anticipated that this enzyme lineage may have the potential to functionalize secondary C–H bonds to build contiguous chiral centers.

To explore the enzymes' ability to insert the lactone-carbene into secondary C–H bonds, we selected dialkyl-aniline, pyrrolidine, azetidine, and other *N*-aryl amine derivatives as substrates. We first screened the entire enzyme lineage with more than 10 substrates in 96-well plates (**Table B-6** and **B-7** in **Appendix B**). We were pleasantly surprised to see that many of the reactions formed the corresponding C–H insertion products. We picked the most promising combinations of enzyme variants and substrates for validation and further confirmation of the products. As shown in **Fig. 3.9.b**, the enzymes are particularly efficient toward carbene insertion into secondary C–H bonds, giving up to 4000 TTN. The final two variants, **L9** and **L10**, gave good to high diastereoselectivities and enantioselectivities. For instance, **L9** and **L10** formed the same diastereomer with diethyl aniline (**15h**), giving 94:6 d.r. and 99:1 d.r., respectively; however, the diastereomers were obtained with opposite enantioselectivity (81% ee and –94.5% ee, respectively). The same trend was observed with *N*-phenyl pyrrolidine (**15i**). With 2,3-dimethyl phenylpyrrolidine (**15k**), only moderate diastereoselectivity was achieved with the selected variants, but the diastereomers can be separated easily by chromatography, and high enantioselectivity was observed for both diastereomers (up to 96% ee and 99% ee, respectively). Finally, *N*-phenyl azetidine (**15m**), which has a higher C–H bond

dissociation energy on a strained ring, was also active for C–H insertion, but only poor enantioselectivity was achieved (>95:5 d.r. and 13% ee for product **16m**), presumably reflecting its distinct structure from that of substrate **15a** used for evolution.

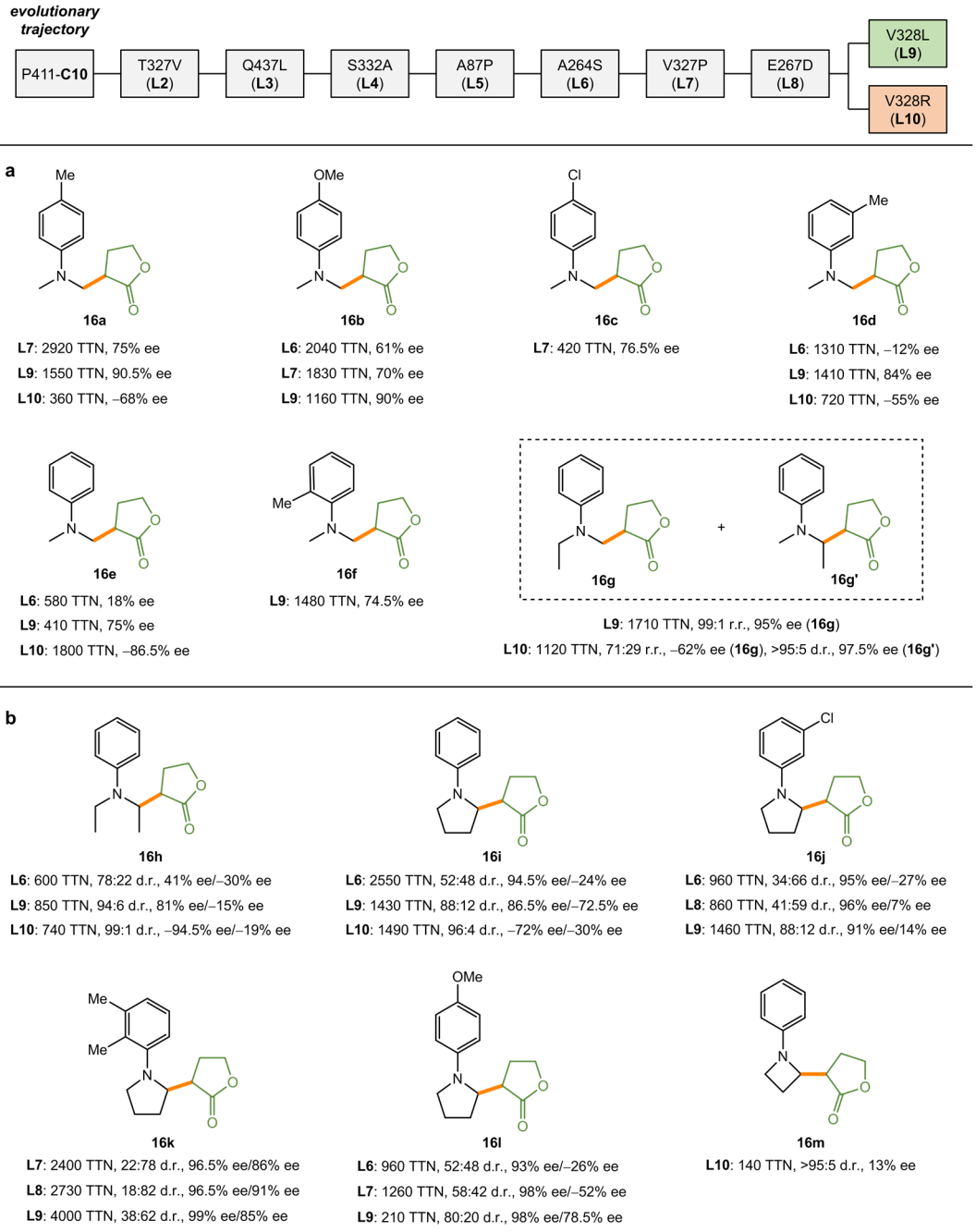

Figure 3.9. Scope of lactone-carbene insertion into α-amino C–H bonds. a, Primary C–H bond insertion. **b**, Secondary C–H bond insertion. Reactions were performed in triplicate or quadruplicate under the following conditions: 12 mM aniline derivatives, 12 mM **LAD**, *E. coli* harboring P411-**C10** variants (OD_{600} = 30 or 60), D-glucose (25 mM), M9-N buffer/EtOH (19:1), anaerobic, 24 h. Product formation was quantified by HPLC and TTNs were determined based on protein concentration. Enantioselectivity was measured using chiral HPLC; diastereoselectivity and regioselectivity were determined by HPLC and NMR.

It is worth revisiting the cases where **L9** and **L10** formed the same major diastereomer but the

opposite enantiomer in carbene insertion into secondary C–H bonds. This suggests that the single mutation going from **L9** to **L10**, L328R, inverted two chiral centers simultaneously. As leucine and arginine possess very distinct features, we reasoned that the two residues might drive opposite orientations of the carbene intermediates with the hydrophobic side facing L328 and the hydrophilic side facing R328 (**Fig. 3.10**). Then C–H insertion might take place with the substrate approaching from different sides to give the opposite enantiomers. The detailed mechanism of C–H insertion, however, is still elusive--the reaction can undergo a radical pathway of hydrogen atom abstraction followed by radical rebound[225-227,230] or a concerted insertion pathway[249-251], which may further affect the stereochemistry of the α-chiral center[252]. Mechanistic studies are ongoing to gain further insights into the C–H insertion reactions.

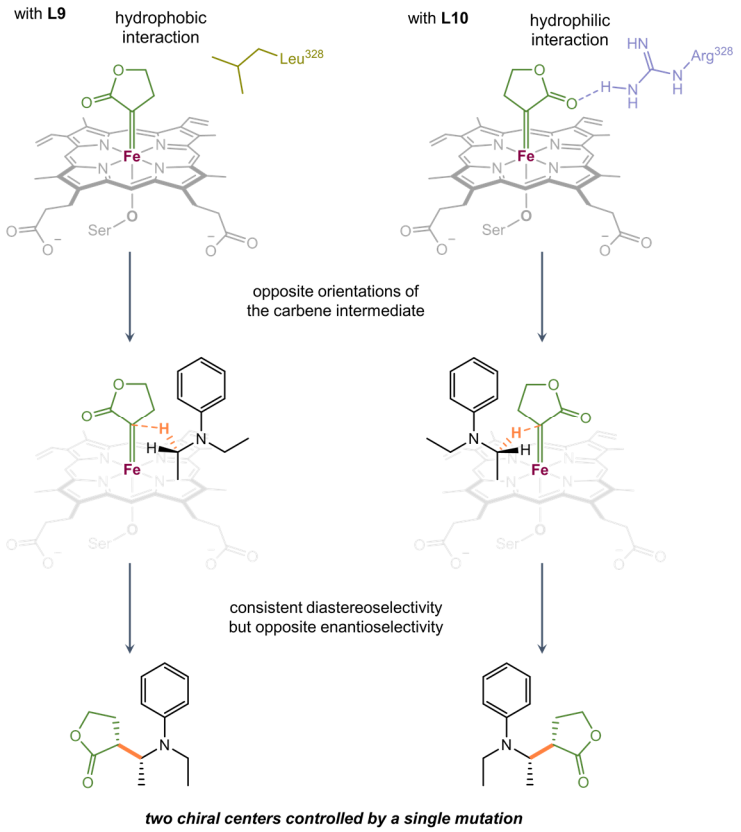

Figure 3.10. Possible explanation for stereocontrol in lactone-carbene insertion into secondary C–H bonds.

3.6 Enzymatic N–H insertion for α-amino lactone synthesis

Carbene insertion into N–H bonds represents one powerful method to forge C–N bonds[253,254]. For instance, rhodium-catalyzed carbene N–H insertion is employed in the synthesis of thienamycin, one of the most potent naturally produced antibiotics till now[255,256]. In the recent two decades, a variety of chiral catalytic scaffolds based on different transition metals have been developed for the enantioselective version of carbene N–H insertion using anilines [257 - 261],

amides[262,263], imines[264] and even aliphatic amines[265] as the nitrogen sources. Recent advances with metalloenzymes have also revealed that hemeproteins, such as P450s[82] or myoglobins[83,266], are also capable of transferring carbenes to amine functionalities. Computational studies have disclosed a formal N–H insertion mechanism[205] with hemeproteins via nucleophilic attack, ylide rearrangement followed by enol tautomerization, where the final proton shift step leads to the formation of α-chiral centers (**Fig. 3.11.a**). Unlike a lot of synthetic methods using chiral H-bonding catalysts to promote enantioselective proton transfer[263-265], the enol intermediate released from the heme cofactor inside enzymes' active sites is surrounded by numerous proton sources, including backbone amides, protic side chains and free water molecules. Therefore, the major challenge in this category of transformations lies on how to leverage the enzyme scaffolds to induce desired stereo-control on the proton transfer process.

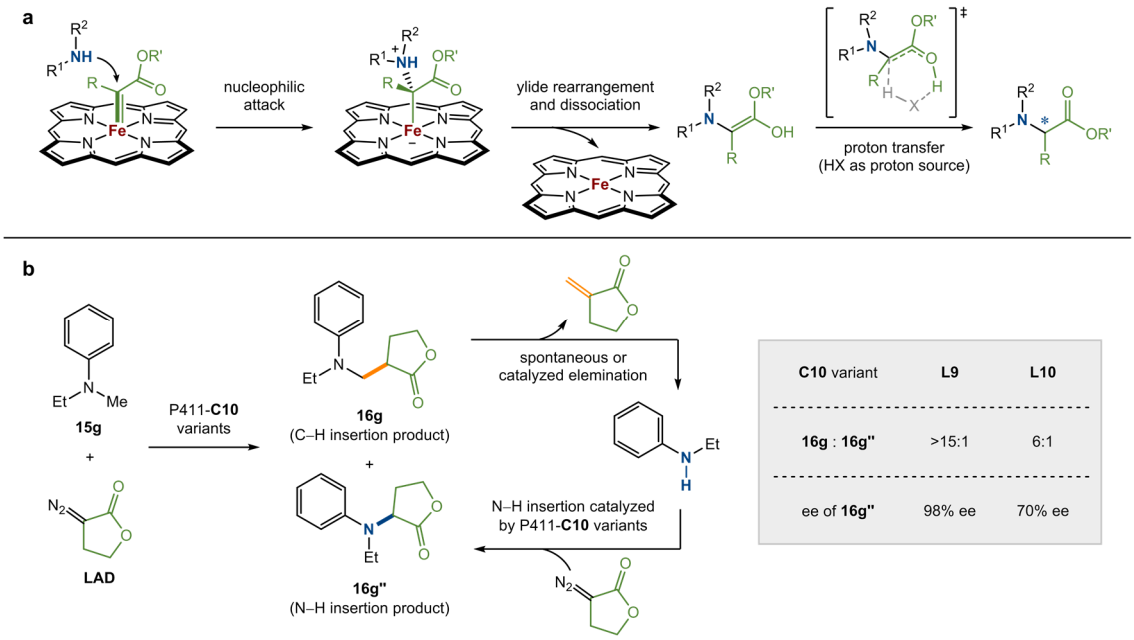

Figure 3.11. Carbene N–H insertion catalyzed by hemeproteins. a, Mechanism of iron-porphyrin-catalyzed carbene N–H insertion. **b**, N–H insertion as a side reaction in lactone-carbene C–H insertion.

Lactone-carbene N–H insertion is expected to produce α-amino lactones, a class of structural motifs found in numerous biologically active natural products as well as pharmaceuticals and also used as versatile precursors for α-amino acid derivative preparation[267-269]. Although rhodium catalysts have been reported for N–H insertion with lactone-carbenes[197], enantioselective versions have yet to be documented. As our P411 enzymes have shown the potential to accommodate lactone-carbenes for the transfer to different functionalities, we surmised that these specifically engineered P411 variants may have reorganized their active sites to impose unique binding modes for the lactone moieties. This would be a desirable feature to effect chiral induction in the proton transfer process for enantioselective N–H insertion.

In fact, we observed small amount of N–H insertion products in our lactone-carbene C–H

insertion reactions when using aniline derivatives as substrates (**Fig. 3.11.b**). We rationalized that elimination of α-methylene-γ-butyrolactone from the C–H insertion product **16g** led to a demethylated amine, which could further couple with another lactone-carbene and then release the amine insertion product **16g''** in the presence of P411 lactone-carbene transferase. And surprisingly, the 'side' product **16g''** by N–H insertion was determined with moderate to high enantioselectivities (98% ee with **L9** and 70% ee with **L10**), which provides a strong evidence for our hypothesis that the engineered P411 enzymes could also exert requisite stereo-control on N–H insertion reactions.

Based on this result, we would like to examine whether the enzyme lineage evolved from P411-**C10** (**L1** to **L10**, initially for lactone-carbene C–H insertion) could also provide a generalized platform for enantioselective N–H insertion reactions. We screened the entire enzyme lineage against various amine substrates, including anilines, *N*-alkyl anilines, indoline, tetrahydroquinoline and even aliphatic amines, in 96-well plates, and used chiral HPLC to determine reaction conversion (enzyme activity) and enantioselectivity. The screening result established that the desired N–H insertion reactions could proceed smoothly with all the tested amines, giving decent to excellent reactivities with different P411 variants in this enzyme lineage, as summarized in **Fig. 3.12**. Anilines (**17a** to **17c**) were found to be highly reactive, affording 100% conversion to the N–H insertion products in a stereodivergent way, where variants **L4** and **L5** displayed the opposite stereo-preference compared to **L6** to **L9**. Electronically-deficient aniline **17d** showed relatively low reactivity but maintained good enantioselectivity with variants **L6** and **L7**. *N*-alkyl anilines (**17e** to **17h**) also served as superior amine substrates in terms of both reactivity and enantioselectivity; by selecting suitable enzyme variants for each substrate, products **18e** to **18h** could be synthesized in high enantiopurity (95% to 98% ee). Cyclic amines (**17i** and **17j**) were also successfully coupled with the lactone carbene in an enantioselective manner when using variants **L6** and **L7**; on the other side, **L8** and **L9** displayed nonetheless higher activities for these substrates, but only delivered low to modest selectivities. Again, it would be important to choose the right enzyme variant for each substrate featuring different steric or electronic properties.

In addition to aniline derivatives, aliphatic amines, such as benzylamine (**17k**) or phenethylamine (see **Table B-9** in **Appendix B**), were also compatible with this biocatalytic system for lactone-carbene N–H insertion, giving >98% ee for **18k** using variants **L6** to **L8**, albeit with limited activity. Interestingly, a reaction using a non-lactone-type carbene (Me-EDA, with substitutions of a methyl group and an ester group at α-position) also produced the desired N–H insertion product **18l** in 53% ee using variant **L10**, which further demonstrated the possibility of extending this enzymatic N–H insertion platform to more different types of carbene partners.

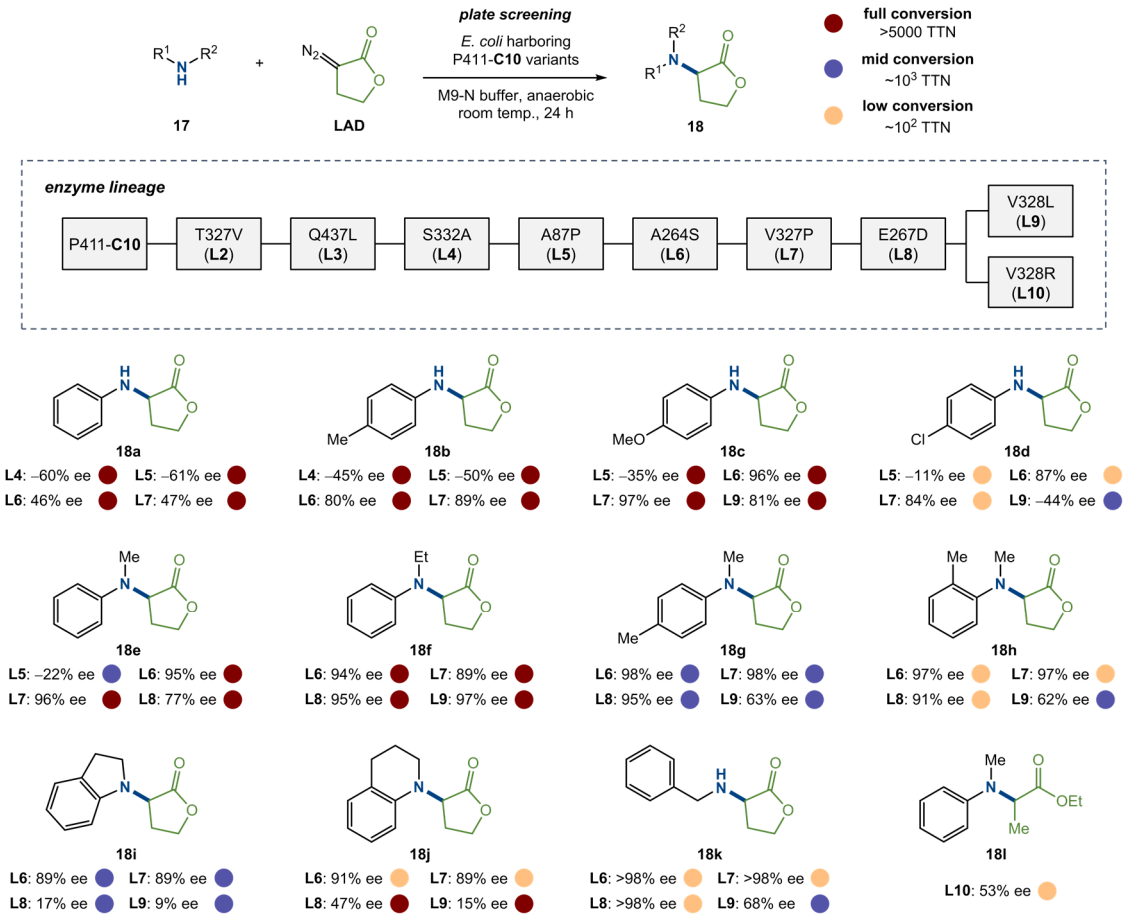

Figure 3.12. Lactone-carbene N–H insertion with P411-C10 lineage. Results were obtained from plate screening under the following conditions: 10 mM amine, 10 mM **LAD**, *E. coli* harboring P411-**C10** variants, D-glucose (25 mM), M9-N buffer/EtOH (19:1), anaerobic, 24 h. Enantioselectivity and substrate conversion were determined by chiral HPLC; TTNs were estimated based on substrate conversion and expression level of **C10** variants.

3.7 Enzymatic B–H insertion for α-boryl lactone synthesis

The broad applications of organoboron compounds[270-273] have prompted chemists to develop efficient, selective and modular synthetic platforms for installing boron motifs onto carbon backbones[274-276]. One major class of methods for forming carbon–boron (C–B) bonds relies on transition metal-catalyzed B–H bond insertion of carbenes[277-283], as first introduced by Curran and co-workers. Recently, our lab developed the first biocatalytic system for this transformation using engineered variants of cytochrome *c* from the Gram-negative, thermohalophilic bacterium *Rhodothermus marinus* (*Rma* cyt *c*)[86]. The laboratory-evolved enzymes exhibited very high efficiency (up to 15,300 turnovers and 6,100 h^{-1} turnover frequency) and enantioselectivity (up to 98% ee) with different carbenes and boranes. To expand the catalytic range of this enzymatic C–B bond-forming platform, we engineered *Rma* cyt *c* to accept structurally different carbenes. In previous work, we typically used α-ester-substituted diazo compounds as carbene precursors;

recently, we also demonstrated that *Rma* cyt *c* mutants can be evolved to use a spectrum of α-trifluoromethyl-α-alkyl carbenes to furnish a wide array of chiral α-trifluoromethylated organoborons[87]. We were curious whether cyclic carbenes can also be used by *Rma* cyt *c*, despite significant structural differences compared to the acyclic carbenes used in previous work.

We therefore started to explore the borylation reaction using the lactone diazo **LAD** and an *N*-heterocyclic carbene (NHC)-stabilized borane as substrates in the presence of whole *E. coli* bacteria expressing *Rma* cyt *c* variants (**Fig. 3.13**). We first tested the variants obtained during directed evolution for borylation with acyclic carbene precursors (*e.g.*, Me-EDA) (**Table B-10** in **Appendix B**). We were pleasantly surprised to see that wild-type *Rma* cyt *c* exhibited high efficiency for lactone carbene B–H insertion, with 960 total turnovers (TTN) and 70% GC yield. The enantioselectivity, however, was poor, with only 36% ee. A distal axial-ligand M100D mutation, previously discovered to facilitate both carbene Si–H and B–H insertion, improved the yield, but did not improve the enantio-control of this reaction. Residue V75 in an α-helix region was previously shown to affect carbene orientation. Screening of M100D variants containing mutations at V75 identified M100D V75R as the most selective, with 87% ee, whereas V75T/C/K/P/G mutations resulted in poor to moderate enantioselectivities. An additional M103V mutation led to more precise stereo-control, giving 90% ee.

To further increase the enantioselectivity of lactone-carbene B–H insertion, we subjected the *Rma* cyt *c* V75R M100D M103V (RDV) variant to site-saturation mutagenesis, targeting active-site amino acid residues which are close to the iron center in wild-type *Rma* cyt *c* (within 10 Å) (**Fig. 3.13**). It is known that the residues residing on the flexible front loop are important for controlling the structure of the heme pocket[88], which is presumably the active site for this novel function. Consequently, introducing suitable mutations on this loop may help to orient the iron-carbene intermediate or tune the approach of the borane substrate and thus lead to desired enantioselectivity. A double-site-saturation mutagenesis library at residues M99 and T101 was cloned and screened as whole-cell catalysts in four 96-well plates for improved borylation enantioselectivity. Double mutant M99Q T101Y (**BOR^{LAC}**) was finally identified to exhibit higher selectivity 92.5% ee and good catalytic efficiency (970 TTN, 80% GC yield).

With an efficient and selective borylating variant **BOR^{LAC}** in hand, we then assessed the scope of boranes that this platform can use (**Fig. 3.14.a**). Boranes without stabilizing groups are highly reactive and unstable in aqueous conditions. Lewis bases, such as ethers, amines, phosphines and NHCs, are generally used as good stabilizing groups for free boranes[284]. Considering the biocompatibility and cell permeability of the borane reagents, NHC-stabilized boranes turned out to be suitable candidates for this borylation platform[285]. Indeed, borane complexes stabilized by NHCs featuring different electronic properties, steric hindrance and/or lipophilicity all served as good substrates for the target borylation reaction, furnishing the desired products with up to 1160

TTN and enantioselectivities up to 94% ee. For instance, fluorine-containing alkyl groups (*e.g.*, **20c**), which are electron-withdrawing and usually exhibit very different lipophilicity and hydrophilicity relative to general aliphatic alkyl groups, were found to be compatible with the whole-cell reaction conditions.

a Whole protein structure and active-site structure of wild-type *Rma* cyt *c*

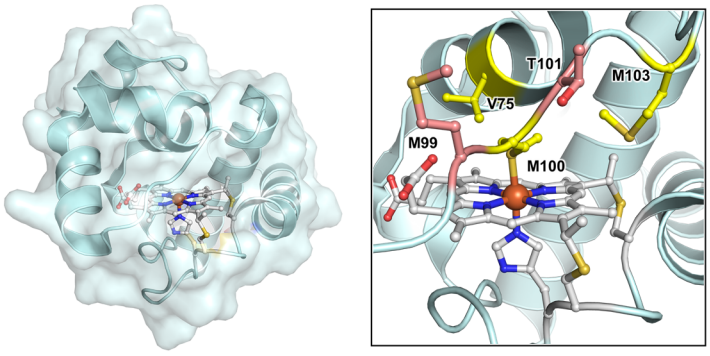

b Lactone-carbene B–H insertion with *Rma* cyt *c* variants

variant	yield	TTN	ee
Rma* cyt *c wild-type	70%	960	36%
Rma* cyt *c M100D	76%	1280	36%
Rma* cyt *c V75R M100D	96%	1640	87%
Rma* cyt *c V75R M100D M103V	75%	1270	90%
Rma* cyt *c V75R M99Q M100D T101Y M103V (**BOR^{LAC}**)	80%	970	**92.5%**

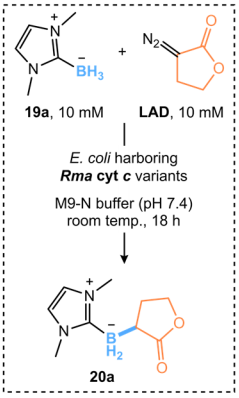

Figure 3.13. Directed evolution of *Rma* cyt *c* for lactone-carbene B–H insertion. a, Whole protein structure and active-site structure of wild-type *Rma* cyt *c* (PDB: 3CP5). **b,** Yields and ee's of selected *Rma* cyt *c* variants for B–H insertion. Reactions were conducted in quadruplicate: suspensions of *E. coli* expressing *Rma* cyt *c* variants (OD_{600} = 20), 10 mM borane **19a**, 10 mM **LAD**, and 5 vol% acetonitrile in M9-N buffer (pH 7.4) at room temperature under anaerobic conditions for 18 hours. TTN refers to the molar ratio of total desired product, as quantified by gas GC-MS, to total heme protein. Enantioselectivity was determined by chiral HPLC.

To explore the longevity of the biocatalyst, we tried portion-wise addition of the two substrates (**Fig. 3.14.c**). Every 1.5 hours, we added an additional aliquot corresponding to 12.5 mM of each substrate to the reaction. Over 20 additions, we observed continuous and steadily increasing product formation, which indicates that the catalyst maintained function over 30 hours. However, we did notice that enantioselectivities decreased. Covalent modification of the protein backbone by carbene species and non-covalent binding of borane substrate or product to the protein may cause structural changes that compromise stereo-control[175]. Further reaction engineering and optimization, such as using a flow system to maintain consistent concentrations of reagents, may be able to address this selectivity drop.

Given that the 5-membered cyclic lactone-carbene worked so well for this biocatalytic B–H

insertion, we wondered whether other cyclic carbenes, particularly lactone-carbenes with different ring sizes, would also be accepted (**Fig. 3.14.a**). 6- and 7-membered lactone diazos (**LAD-2** and **LAD-3**) were readily prepared from corresponding lactones and used as cyclic carbene precursors for testing B–H insertion using variant **BOR^{LAC}**. The 6-membered lactone-carbene showed high reactivities (up to 1190 TTN and 92% ee) for the desired borylation with three different borane substrates. Additionally, enzymatic borylation with both 5- and 6-membered lactone carbenes was readily scalable to millimole level, affording the desired products in high isolated yields (**Fig. 3.14.b**). However, with one additional carbon in the ring, the 7-membered lactone-carbene behaved in a completely different manner: **BOR^{LAC}** exhibited only low activity with this carbene precursor (< 50 TTN).

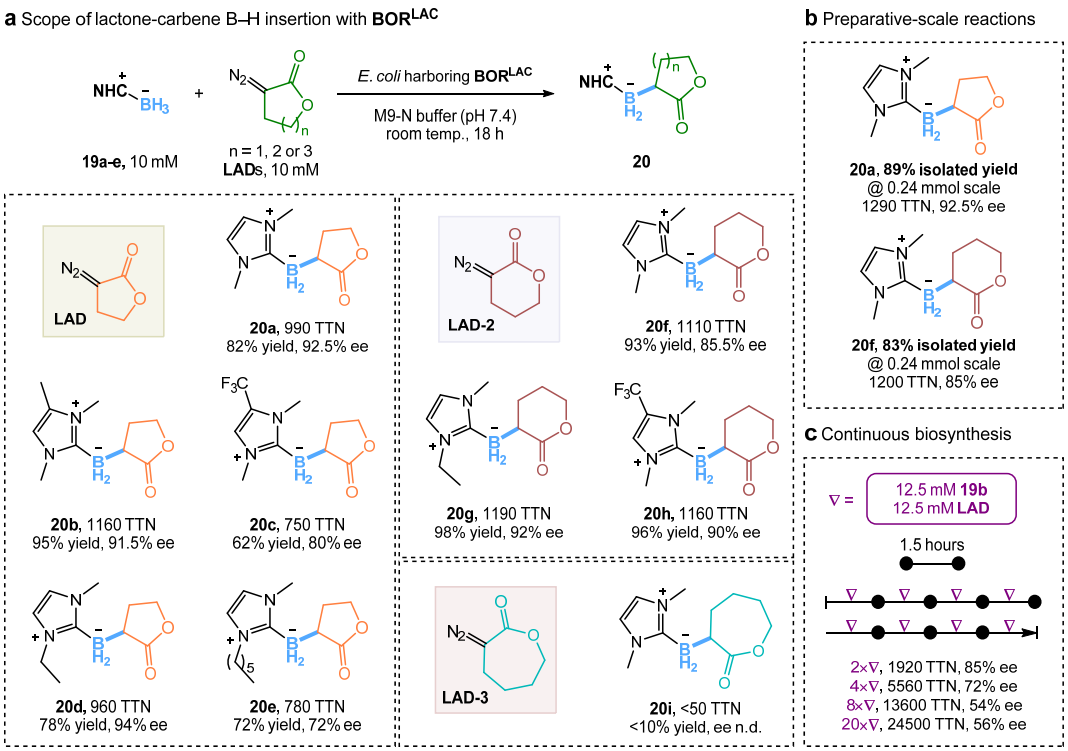

Figure 3.14. BOR^{LAC}–catalyzed for lactone-carbene B–H insertion. a, Scope of lactone-carbene B–H insertion with **BOR^{LAC}**. Reactions were conducted in quadruplicate: suspensions of *E. coli* expressing *Rma* cyt *c* variants (OD_{600} = 20), 10 mM borane **2**, 10 mM lactone diazo **1**, **4** or **6**, and 5 vol% acetonitrile in M9-N buffer (pH 7.4) at room temperature under anaerobic conditions for 18 hours. **b**, Preparative-scale synthesis of organoborons. Reaction conditions: suspensions of *E. coli* expressing *Rma* cyt *c* variants (OD_{600} = 20), 12 mM borane **19a**, 12 mM lactone diazo **LAD** or **LAD-2**, and 5 vol% acetonitrile in M9-N buffer (pH 7.4) at room temperature under anaerobic conditions for 18 hours. **c**, Enzymatic synthesis of organoborons with portion-wise addition of substrates. Reactions were conducted in duplicate using the standard reaction conditions except for using 2.5 M solution stocks of borane **19b** and **LAD** (one portion = 2 μL of each substrate stock).

To understand the origins of this dramatic impact of ring size on *Rma* cyt *c*-catalyzed lactone-carbene B–H insertion chemistry, we employed DFT calculations to compare the structures and the electronic properties of three lactone-type IPCs. Unlike 5-membered lactone-based **IPC2,** which

takes on a rigid planar structure, 6-membered lactone-carbene **IPC3** showed a slightly flexible structure with a dihedral angle d(Fe-C-C-O) of 46° in the ground OSS state, while its triplet state still possesses a near-planar geometry (**Fig. B-2** in **Appendix B**). However, 7-membered lactone **IPC4** takes on highly twisted conformations with d(Fe-C-C-O) from 47° to 73° in all electronic states[197]. It is apparent that none of the electronic states in **IPC4** shares a similar structure with **IPC2**. This may explain why **BOR^{LAC}**, which was evolved for the 5-membered lactone carbene, did not exhibit high reactivity towards borylation with the 7-membered lactone carbene. But this does not necessarily mean that *Rma* cyt *c* cannot be engineered to accommodate the 7-membered lactone carbene for B–H insertion; further engineering using **BOR^{LAC}** as a starting template could well lead to variants with improved reactivity on this 7-membered lactone carbene.

3.8 Conclusion

By establishing five biocatalytic methods, we now have expanded our enzymatic platform based on hemeprotein carbene transferases to assemble a broad array of structurally diverse lactone derivatives, including α-thio/amino/alkyl/boryl lactones and *spiro*[2.4]lactones. These demonstrations have provided a convergent biosynthetic scheme, offering a succinct method to construct complex lactone-based structures, as an alternative to nature's strategy of *de novo* assembly of lactone moieties. Enzyme engineering starting from the same original cytochrome P450$_{BM3}$, quickly diverted its catalytic capability to new functions, including lactone-carbene C–H/N–H/S–H insertions and cyclopropanation, which once again speaks to the superior plasticity of the P450 (or P411) scaffolds and the immense potential to direct the construction of complex molecular structures.

In the development of the first two methods, it is interesting to note that simply altering the heme ligation (serine or cysteine) in the cytochrome P450 variants was able to rapidly optimize the two carbene-transfer reactions, cyclopropanation and S–H insertion, with unprecedented levels of efficiency and stereo-control (up to 11150 TTN and >99.9% ee). To understand how axial ligation affects both selectivity and reactivity in carbene S–H insertion, we conducted a DFT study and described two mechanistic pathways involving a radical coupling process between a thiyl radical and a heme-bound alkyl species or a free alkyl radical. The different electronic properties of serine and cysteine ligands lead to opposite preferences in the reaction pathways and distinct product profiles. The development of novel reactions combined with thorough mechanistic analyses does not only expand the biocatalytic repertoire of hemeproteins but also provides valuable insights into how these enzymes can be tuned for further exploration of new chemistries.

The engineered platform for lactone-carbene C–H insertion allowed us to functionalize primary or secondary C–H bonds at α-amino positions. The biocatalytic system was rapidly evolved

to take *N*,*N*-dialkylaniline derivatives as substrates to furnish chiral β-amino lactone products with high catalytic efficiency (up to 4000 TTN) and in a stereo-divergent manner. A single mutation can control the stereoselectivity of carbene insertion into secondary C–H bonds, inverting the two contiguous chiral centers and leading to the opposite enantiomers of the same major diastereomers. And interestingly, the enzyme lineage obtained in the C–H insertion study was also able to carry out highly efficient and selective lactone-carbene N–H insertion reactions with a broad range of amines, setting up a powerful system to build diverse α-amino lactones. These results have again highlighted the promiscuity of our enzymes especially when engineered to accommodate the same or similar types of substrates or intermediates. We could anticipate that these newly evolved P411 variants would probably serve as potential engineering templates for the further development of more challenging carbene- or nitrene-transfer reactions.

Not limited to P450 enzymes, the biocatalytic platform based on *Rma* cyt *c* hemeproteins has also been demonstrated with extended capacity on using cyclic lactone carbenes for B–H insertion reactions. A range of organoborons were accessed at preparative scales and with unprecedented catalytic efficiencies (up to 24,500 TTN) and high enantioselectivities (up to 94% ee).

The new chemistries in the chapter have presented a good example of how to systematically explore the new functions that natural enzymes can potentially take on. We believe that exploiting the catalytic promiscuity of native enzymes coupled with evolutionary strategies will further open the chemical space of genetically encoded biocatalysts to fulfill increasing demands in the synthetic world.

3.9 Experimental methods

See **Appendix B** for supporting tables and figures, synthesis and characterization of compounds, assignment of absolute stereochemistry, and determination of enantioselectivity. NMR spectra and calibration curves are in the Supporting Information of the published paper, but not included here.

3.9.1 General information

Unless otherwise noted, all chemicals and reagents were obtained from commercial suppliers (Sigma-Aldrich, VWR, Alfa Aesar, Acros, Combi-Blocks, TCI and Ark Pharm) and used without further purification. Silica gel chromatography was carried out using AMD Silica Gel 60, 230-400 mesh. ^{1}H and ^{13}C NMR spectra were taken using a Bruker Prodigy 400 MHz instrument and are internally referenced to the residual solvent peak (chloroform). Data for ^{1}H NMR are reported as follows: chemical shift (δ ppm), multiplicity (s = singlet, d = doublet, t = triplet, q = quartet, p =

pentet, m = multiplet, dd = doublet of doublets, dt = doublet of triplets, ddd = doublet of doublet of doublets), coupling constant (Hz), integration. Sonication was performed using a Qsonica Q500 sonicator. High-resolution mass spectra were obtained at the California Institute of Technology Mass Spectral Facility. Synthetic reactions were monitored using thin layer chromatography (Merck 60 gel plates) using a UV-lamp for visualization.

3.9.2 Chromatography

Analytical reversed-phase high-performance liquid chromatography (HPLC) was carried out using an Agilent 1200 series instrument and a Kromasil 100 C18 column (4.6 × 50 mm, 5 μm) with water and acetonitrile as the mobile phase and visualization at 210 nm for library screening. Analytical normal-phase HPLC was carried out using an Agilent 1200 series instrument and chiral columns Chiralpak IC (4.6 mm × 25 cm), IA (4.6 mm × 25 cm), AS-H (4.6 mm × 25 cm) and OJ-H (4.6 mm × 25 cm) with *n*-hexane and isopropanol as the mobile phase and visualization at 210 nm for chiral separation. Gas chromatography (GC) analyses were carried out using an Agilent 7820A or Shimadzu GC-17A gas chromatograph, FID detector, a J&W HP-5 column (30 m × 0.32 mm, 0.25 μm film) and CycloSil-B column (30 m × 0.25 mm, 0.25 μm film). Gas chromatography-mass spectrometry (GC-MS) analyses were carried out using a Shimadzu GCMS-QP2010SE system and J&W HP-5m column.

3.9.3 Cloning and site-saturation mutagenesis

pET22b(+) containing a C-terminal 6x-His tag was used as a cloning and expression vector for all enzymes described in this study. Site-saturation mutagenesis was performed using a modified QuikChange™ mutagenesis protocol[170]. Primer sequences are available upon request. The PCR products were digested with DpnI, gel purified, and fragments were assembled using Gibson Mix[171]. The ligation mixture was used to directly transform *E. coli* strain BL21 *E. cloni*® (Lucigen). Cells were grown using Luria-Bertani medium (LB) or Hyperbroth (AthenaES) (HB) with 0.1 mg/mL ampicillin (LB_{amp} or HB_{amp}) for P411 or P450; cells expressing cyt *c* requires an additional antibiotic 20 μg/mL chloramphenicol ($LB_{amp/chlor}$). Electrocompetent *E. coli* cells were prepared following the protocol of Sambrook *et al*[172]. T5 exonuclease, Phusion polymerase, and Taq ligase were purchased from New England Biolabs (NEB, Ipswich, MA). M9-N minimal medium (abbreviated as M9-N buffer; pH 7.4) was used as a buffering system for whole cells, lysates, and purified proteins, unless otherwise specified. M9-N buffer was used without a carbon source; it contains 47.7 mM Na_2HPO_4, 22.0 mM KH_2PO_4, 8.6 mM NaCl, 2.0 mM $MgSO_4$, and 0.1 mM $CaCl_2$.

3.9.4 Determination of hemeprotein concentration

1. **Preparation of cell lysate**: Aliquots of ~3 mL OD_{600} = 60 cells were prepared in 15 mL conical tubes, which were then placed on wet ice. Cells were lysed by sonication following the program below: sonication for 4 min, 1 second on - 1 second off, 35% amplitude. The sonicated samples were then transferred to two Eppendorf tubes, and then centrifuged down (14,000 rpm, 15 min, 4 °C). The supernatants (~2.5 mL) were then collected to a 5-mL glass vial for analysis.

2. **Hemechrome assay for protein concentration measurement**:

Method 1 (used for **3.3** and **3.4**): A solution of sodium dithionite (10 mg/mL) was prepared in M9-N buffer. Separately, a solution of 1 M NaOH (0.4 mL) was mixed with pyridine (1 mL), followed by centrifugation (10,000 × g, 30 s) to separate the excess aqueous layer to give a pyridine-NaOH solution. To a cuvette containing 700 µL protein solution (purified protein or lysate) in M9-N buffer, 50 µL of dithionite solution (0.1 M in M9-N) and 250 µL pyridine-NaOH solution were added. The cuvette was sealed with Parafilm, and the UV-Vis spectrum of the reduced Fe^{II} state was recorded immediately. To another cuvette containing 700 µL protein solution (purified protein or lysate) in M9-N buffer, 50 µL of potassium ferricyanide (0.1 M in M9-N) and 250 µL pyridine-NaOH solution were added. The cuvette was sealed with Parafilm, and the UV-Vis spectrum of the oxidized Fe^{III} state was recorded immediately. The protein concentration was determined using $\varepsilon\_[557_{reduced} - 540_{oxidized}] = 23.98\ mM^{-1}cm^{-1}$ (ref 173).

Method 2 (used for **3.5**): A solution of NaOH/pyridine was prepared by mixing 1 mL of NaOH aqueous solution (1 M), 2 mL of water and 2 mL of pyridine. To 4.5 mL of NaOH/pyridine solution, 22.5 µL of $K_3Fe(CN)_6$ aqueous solution (0.1 M) was added to make **solution 1**. A **background solution** was prepared by mixing 500 µL M9-N and 500 µL of the NaOH/pyridine solution, which was used for UV background subtraction. When measuring samples with a UV spectrometer, a spectrum of a mixed solution (oxidized spectrum) with 500 µL cell lysate + 500 µL **solution 1** was taken at the wavelength range 380 nm to 650 nm. Subsequently, 5 µL of dithionite solution (0.5 M in 0.1 M NaOH solution) was added to the same sample and mixed by pipetting; a spectrum of this solution (reduced spectrum) was taken at 380 nm to 650 nm. The protein concentration was calculated using the extinction coefficient and dilution factor (2× dilution in volume): $\varepsilon\_[557_{reduced} - 540_{oxidized}] = 23.98\ mM^{-1}cm^{-1}$.

Method 3 (used for **3.7**): A solution of 0.5 M sodium dithionite in 0.5 M NaOH was first prepared. Separately, a solution of 1 M NaOH (0.4 mL) was mixed with pyridine (1 mL), followed by centrifugation (10,000 × g, 30 seconds) to separate the excess aqueous layer and give a pyridine-NaOH solution. To a cuvette containing 400 µL protein solution (purified protein or heat-treated lysate) in M9-N buffer, 400 µL pyridine-NaOH solution was added and mixed thoroughly. 2 µL of sodium dithionite solution was added to the solution and the cuvette was sealed with Parafilm, and

the UV-Vis spectrum was recorded immediately. Cytochrome *c* concentration was determined using ε_{550} = 30.27 $mM^{-1}cm^{-1}$ (ref 173).

3.9.5 Expression of P450, P411 and cyt *c* proteins

(1) P450 and P411 enzymes: *E. coli* BL21 *E. cloni*® cells carrying a plasmid encoding a P450 or P411 variant were grown overnight in 5 mL LB_{amp} (37 °C, 250 rpm). The pre-culture was used to inoculate 45 mL of HB_{amp} in a 125 mL Erlenmeyer flask; this culture was incubated at 37 °C, 220 rpm for 2 h and 15 min. Cultures were then cooled on ice (20–40 min), and expression was induced with IPTG and ALA with final concentrations of 0.5 mM and 1.0 mM, respectively. Expression was conducted at 24 °C, at 140 rpm, for 20 h (± 20 min). Cultures were then centrifuged (4,500 × g, 5 min, 4 °C), and the pellets were resuspended to an OD_{600} of 60 or 30 in M9-N minimal medium (no nitrogen). Aliquots of the cell suspension (3–4 mL) were used to determine the P450 and P411 expression level after lysis by sonication. The expression level in OD_{600} = 60 lysates is typically in the range of 16–24 µM for P450-**G8S**, 2.4–6 µM for P411-**G8S** and 3–13 µM for P411-**C10** variants.

(2) Cyt *c* proteins: (a) **Plasmid construction**. All variants described in this paper were cloned and expressed using the pET22b(+) vector (Novagen). The gene encoding *Rma* cyt *c* (UNIPROT ID B3FQS5) was obtained as a single gBlock (IDT), codon-optimized for *E. coli*, and cloned using Gibson assembly into pET22b(+) (Novagen) between restriction sites *Nde*I and *Xho*I in frame with an *N*-terminal pelB leader sequence (to ensure periplasmic localization and proper maturation; MKYLLPTAAAGLLLLAAQPAMA) and a *C*-terminal 6xHis-tag. This plasmid was co-transformed with the cytochrome *c* maturation plasmid pEC86 into *E. cloni*® EXPRESS BL21(DE3) cells (Lucigen). (b) **Expression of cytochrome *c* variants.** 25 mL $HB_{amp/chlor}$ in a 125 mL flask was inoculated with an overnight culture (0.5 mL, $LB_{amp/chlor}$) of recombinant *E.* cloni® EXPRESS BL21(DE3) cells containing a pET22b(+) plasmid encoding the cytochrome *c* variant, and the pEC86 plasmid. The culture was shaken at 37 °C and 230 rpm (no humidity control) until the OD_{600} was 0.7 (approximately 3 hours). The culture was placed on ice for 30 minutes, and IPTG and ALA were added to final concentrations of 20 µM and 200 µM, respectively. The incubator temperature was reduced to 20 °C, and the culture was allowed to shake for 22 hours at 160 rpm. Cells were harvested by centrifugation (4 °C, 5 min, 4,000 × g). The cell pellet was resuspended in M9-N buffer to an OD_{600} of 60 or 30 in M9-N minimal medium (no nitrogen). Aliquots of the cell suspension (3–4 mL) were used to determine the cyt *c* expression level after lysis by sonication. The expression level in OD_{600} = 30 lysates is typically in the range of 12–20 µM.

3.9.6 Biotransformations

The cell suspension in M9-N (with a certain OD_{600}) was degassed by sparging with argon in

sealed vials or flasks for 30 min (no degassing process for **3.5** to **3.7**). Separately, a glucose solution (250 mM in M9-N) was degassed by sparging with argon for 30 minutes. All solutions were uncapped and transferred into an anaerobic chamber (oxygen level: < 40 ppm). Resuspended cells (340 µL) were added to 2 mL vials, followed by D-glucose (40 µL, 250 mM in M9-N), substrate (10 µL of an EtOH stock), and **LAD** (10 µL of an EtOH stock). Final concentrations were typically 10.0 mM substrate, 10.0 mM **LAD** (substrate:**LAD** = 1:1), and 25 mM glucose; final reaction volume was 400 µL. The vials were sealed and shaken inside the anaerobic chamber at room temperature and 560 or 600 rpm for a set time.

(1) For **3.3**, **3.4** and **3.7**: After the reaction was completed and the vials removed from the anaerobic chamber, internal standard 1,3,5-trimethoxybenzene, 1,2,3-trimethoxybenzene or ethyl 2-phenylacetate (20 µL of 20 mM stock solution in toluene) was added followed by mixed solvent (hexane/ethyl acetate = 1:1, 1.0 mL). The mixture was transferred to a 1.7 mL Eppendorf tube, and then subjected to vortexing (15 s × 3) and centrifugation (14,000 rpm, 5 min) to completely separate the organic and aqueous layers. A sample of the organic layer (0.8 mL) was transferred to a vial for GC analysis.

(2) For **3.5**: After the reaction was completed and the vials removed from the anaerobic chamber, internal standard 1,3,5-trimethoxybenzene (1,3,5-TMOB), *p*-methyl anisole (pMe-anisole), ethyl 2-phenylacetate (PhEA), or allyl phenyl ether (AllylOPh) (20 µL of 20 mM stock solution in acetonitrile) was added followed by acetonitrile (0.58 mL). The mixture was transferred to a 1.7-mL Eppendorf tube, and then subjected to vortexing (15 s × 3) and centrifugation (14,000 rpm, 5 min, 4 °C). A sample of the supernatant (0.8 mL) was transferred to a vial for reverse-phase HPLC analysis.

The procedures for preparative-scale enzymatic reactions are outlined in detail (See **Appendix B**).

3.9.7 Reaction screening in 96-well plate format

Enzyme libraries (single/double-site-saturation libraries generated employing the "22c-trick" method or collections of heme protein variants) were screened in 96-well plates.

E. coli libraries for P411 variants were cultured in LB_{amp} (300 µL/well) at 37 °C, 250 rpm and 80% relative humidity overnight. HB_{amp} (950 µL/well) was inoculated with the pre-culture (50 µL/well) and incubated at 37 °C, 230 rpm, 80% humidity for 2 h and 45 min. The plates were cooled on ice for 30 minutes, and expression was induced with 0.5 mM IPTG and 1.0 mM ALA (final concentrations). Expression was conducted: (1) at 24 °C and 200 rpm for 20–24 h (for **3.3** and **3.4**); (2) at 22 °C and 220 rpm for 20 h (for **3.5** and **3.6**).

E. coli libraries for *Rma* cytochrome *c* variants were cultured in $LB_{amp/chlor}$ (400 µL/well) at 37 °C,

250 rpm and 80% relative humidity overnight. $HB_{amp/chlor}$ (950 µL/well) was inoculated with the pre-culture (30 µL/well) and incubated at 37 °C, 250 rpm, 80% humidity for 2 h and 45 min. The plates were cooled on ice for 30 minutes, and expression was induced with 20 µM IPTG and 0.2 mM 5-aminolevulinic acid (final concentrations). Expression was conducted at 24 °C and 200 rpm for 20–24 h.

The cells were pelleted (4,500 × g, 5 min, 4 °C) and resuspended with M9-N buffer (340 µL/well) and D-glucose solution (40 µL/well, in M9-N). The 96-well plate was then transferred to an anaerobic chamber. In the anaerobic chamber, substrate (10 µL/well, 400 mM in EtOH) and **LAD** (10 µL/well, 400 mM in EtOH) were added to the plate. The plate was sealed with an aluminum foil, removed from the anaerobic chamber, and shaken at 600 rpm.

Cyclopropanation screening. After 12 h, the seal was removed and acetonitrile (580 µL/well) and internal standard ethyl phenylacetate (PhEA, 20 mM in acetonitrile, 20 µL/well) were added. The plate was tightly sealed with a reusable silicone mat, vortexed (15 s × 3) and centrifuged (4,500 × g, 5 min). The supernatant (200 µL/well) was filtered through an AcroPrep 96-well filter plate (0.2 µm) into a shallow-well plate for reversed-phase HPLC analysis (C18 poroshell column, MeCN:H_2O = 50:50, 1.2 mL/min flow, 2.95 min, 210 nm).

S–H insertion screening. After 8 h, the seal was removed and mixed solvent (hexane/ethyl acetate = 1:1, 600 µL/well) was added. The plate was tightly sealed with a reusable silicone mat, vortexed (15 s × 3) and centrifuged (4,500 × g, 5 min) to completely separate the organic and aqueous layers. The organic layers (200 µL/well) were transferred to 300 µL vial inserts, which were then placed in 2 mL vials for normal-phase chiral HPLC analysis (OJ-H chiral column, hexane:^{i}PrOH = 60:40, 1.35 mL/min flow, 12.5 min, 220 nm).

C–H insertion screening. After 24 h, the seal was removed and acetonitrile (580 µL/well) and internal standard (1,3,5-trimethoxybenzene, *p*-methyl anisole, ethyl 2-phenylacetate or allyl phenyl ether; 20 mM in acetonitrile; 20 µL/well) were added. The plate was tightly sealed with a reusable silicone mat, vortexed (15 s × 3) and centrifuged (4,500 × g, 5 min). The supernatant (200 µL/well) was filtered through an AcroPrep 96-well filter plate (0.2 µm) into a shallow-well plate for reversed-phase HPLC analysis (C18 Kromasil column, MeCN:H_2O gradient from 40:60 to 100:0, 1.2 mL/min flow, 230 or 254 nm).

N–H insertion screening. After 24 h, the seal was removed and mixed solvent (hexane/ethyl acetate = 1:1, 600 µL/well) was added. The plate was tightly sealed with a reusable silicone mat, vortexed (15 s × 3) and centrifuged (4,500 × g, 5 min) to completely separate the organic and aqueous layers. The organic layers (200 µL/well) were transferred to 300 µL vial inserts, which were then placed in 2 mL vials for normal-phase chiral HPLC analysis (IC chiral column, hexane:^{i}PrOH = 85:15, 1.2 mL/min flow, 15 min, 254 nm).

B–H insertion screening. After 12 h, the seal was removed and mixed solvent (hexanes/ethylacetate = 4:6, 600 µL/well) was added followed by the addition of internal standard (20 µL of 20 mM 1,3,5-trimethoxybenzene in toluene). The plates were tightly sealed with reusable silicone mats and shaken vigorously to thoroughly mix the organic and aqueous layers. The plates were centrifuged (4,000 × g, 5 min) and the organic layer (300 µL) was transferred to autosampler vials with inserts for chiral HPLC analysis (IC chiral column, hexane:^{i}PrOH = 60:40, 1.5 mL/min flow, 15 min, 235 nm).

3.9.8 Protein purification

To obtain purified protein of P411 and P450 variants, single colonies of *E. coli* BL21(DE3) freshly transformed with plasmid encoding either of the two variants were used to inoculate 30 mL LB_{amp} broth and cultures were grown at 37 °C, 250 rpm for 14h. Subsequently, 950 mL of HB_{amp} broth in a 2.8 L flask were inoculated with 15 mL of the precultures and incubated at 37 °C, 180 rpm for 2.5 h (to OD_{600}~1.5). Cultures were then cooled in an ice-water bath for 20 min and induced with 0.5 mM IPTG and 1.0 mM ALA (final concentrations). Expression was conducted at 24 °C, 150 rpm, for 18 h. Cultures were then centrifuged (5,000 × g, 5 min, 4 °C), the supernatant was discarded, and the cell pellets were frozen on dry ice and stored at –20 °C. For protein purification, frozen cells were thawed on ice and resuspended in buffer A (25 mM tris, 20 mM imidazole, 100 mM NaCl, pH 7.5; 4 mL buffer per g of wet cell weight). The cell suspension was supplemented with 1 mg/mL lysozyme, 0.1 mg/mL DNAse I, and one protease inhibitor tablet (Pierce Protease Inhibitor Tablets, Thermo Scientific). The cell suspension was lysed by sonication (QSonica sonicator, 1 min total time, 1 s on / off cycles, 40% output). To pellet insoluble material, lysates were centrifuged (20,000 × g, 20 min, 4 °C), and the cleared lysate was filtered through a 0.45 µm filter unit. His-tagged P411 or P450 proteins were purified from the lysate using a nickel NTA column (1 mL HisTrap HP, GE Healthcare) using an AKTAxpress purifier FPLC system (GE healthcare). Proteins were eluted on a stepwise gradient from 100% buffer A to 100% buffer B (25 mM tris, 300 mM imidazole, 100 mM NaCl, pH 7.5): 0 to 35 % buffer B over 5 column volumes (CV), held at 35% buffer B for 5 CV, and 35 to 100 % buffer B over 3 CV. P411 or P450 variants were eluted at 30–35 % buffer B. Fractions containing eluted protein were pooled and subjected to three rounds of buffer exchange to storage buffer (25 mM Tris-HCl, 100 mM NaCl, pH 7.5) using centrifugal spin filters (30 kDa molecular weight cut-off, Amicon Ultra, Merck Millipore). Subsequently, the concentrated protein was aliquoted, flash-frozen on powdered dry ice, and stored at –20 °C. Protein concentrations were determined via the pyridine/hemochrome assay specified above prior to setting up biocatalytic reactions.

Appendix B

SUPPLEMENTARY INFORMATION FOR CHAPTER 3

Material for this chapter appears in: (1) **Chen, K.**[†]; Zhang, S.-Q.[†]; Brandenberg, O. F.; Hong, X.[*]; Arnold, F. H.[*], Alternate heme ligation steers activity and selectivity in engineered cytochrome P450-catalyzed carbene transfer reactions. *J. Am. Chem. Soc.* **140**, 16402–16407 (2018). (2) **Chen, K.**; Huang, X.; Zhang, S.-Q.; Kan, S. B. J.; Zhou, A. Z.; Hong, X.[*]; Arnold, F. H.[*], Engineered cytochrome *c*-catalyzed lactone-carbene B–H insertion. *Synlett* **30**, 378–382 (2019). (3) Zhou, A. Z.; **Chen, K.**[*]; Arnold, F. H.[*], Enzymatic lactone-carbene C–H insertion to build contiguous chiral centers. *ACS Catal.* **10**, 5393–5398 (2020).

B.1 Supporting Tables B-1 to B-11

Table B-1. Summary of different heme proteins tested for *spiro*[2.4]-lactone formation.

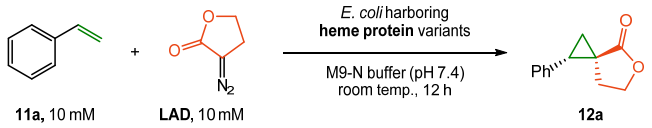

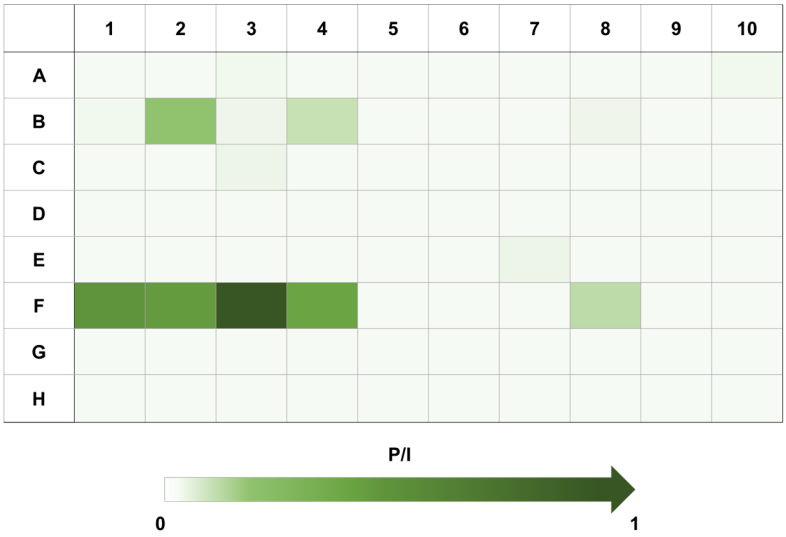

location	name	Mutations
A1	P450$_{BM3}$-wild type (WT, CYP102A1)	-
A2	P450-C400S	C400S (relative to P450-WT)
A3	P411-CIS	V78A F87V P142S T175I A184V S226R H236Q E252G T268A A290V L353V I366V C400S E442K (relative to P450-WT)
A4	P450-CIS	S400C (relative to P411-CIS)
A5	P450-CIS C400H	C400H (relative to P450-CIS)
A6	P411-**A10**	T438S I263F A328V L437V (relative to P411-**CIS**)
A7	P450-**A10**	S400C (relative to P411-**A10**)
A8	P450-**A10** C400H	C400H (relative to P450-**A10**)

A9	P450-**A10** C400A	C400A (relative to P450-**A10**)
A10	P411-**CIS** T438S (**P**)	T438S (relative to P411-**CIS**)
B1	P411-**CIS** T268A	T268A (relative to P411-**CIS**)
B2	P411-**CIS** T268A F87V	T268A F87V (relative to P411-**CIS**)
B3	P411-**CIS** T268A F87A	T268A F87A (relative to P411-**CIS**)
B4	P411- **CIS** I263F T438S (**P1**)	I263F T438S (relative to P411-**CIS**)
B5	P411- **CIS** I263Y T438S	I263Y T438S (relative to P411-**CIS**)
B6	P411- **CIS** I263M T438S	I263M T438S (relative to P411-**CIS**)
B7	P411-**CIS** L75A L181A	L75A L181A (relative to P411-**CIS**)
B8	P411-**CIS** L75A I263A L437A	L75A I263A L437A (relative to P411-**CIS**)
B9	P411-**P2**	A328V (relative to P411-"I263F")
B10	P411-**P3**	A328V V87A (relative to P411-"I263F")
C1	P411-**P4**	V87A A268G A328V (relative to P411-"I263F")
C2	P11-"A82L"	V87A A268G A328V A82L (relative to P411-"I263F")
C3	P11-**P5**	V87A A268G A328V A82I (relative to P411-"I263F")
C4	P411-**E10**	A78V F263L (relative to P411-"A82L")
C5	P411-**E10** E267D	E267D (relative to P411-**E10**)
C6	P411-**E10** S438A	S438A (relative to P411-**E10**)
C7	P411-**E10** V78F	V78F (relative to P411-**E10**)
C8	P411-**E10** V78Y	V78Y (relative to P411-**E10**)
C9	P411-**E10** V78F S438A	V78F S438A (relative to P411-**E10**)
C10	P411-**E10** V78Y S438A	V78Y S438A (relative to P411-**E10**)
D1	P411-**K1**	A87F (relative to P411-**P4**)
D2	P411-**C1**	A87W (relative to P411-**P4**)
D3	P411-**P4** A87I	A87I (relative to P411-**P4**)
D4	P411-**C2**	L437G (relative to P411-**C1**)
D5	P411-**C3**	V328Y (relative to P411-**C2**)
D6	P411-**C4**	T328V (relative to P411-**C3**)
D7	P411-**C6**	F261M T436H (relative to P411-**C4**)
D8	P411-**K3**	F261G T327P (relative to P411-**K1**)
D9	P411-**K5**	S72W L437F (relative to P411-**K3**)
D10	P411-**K6**	T269L (relative to P411-**K5**)
E1	P411-**K8**	A78S A330V (relative to P411-**K6**)
E2	P411-**K10**	L188C T436M (relative to P411-**K8**)
E3	P411-**P4** F261M	F261M (relative to P411-**P4**)
E4	P411-**P4** F261M T269L	F261M T269L (relative to P411-**P4**)
E5	P411-**P4** A87F F261C	A87F F261C (relative to P411-**P4**)
E6	P411-**P4** F81V	F81V (relative to P411-**P4**)
E7	P411-"A82L" F263Y A78L T327L	F263Y A78L T327L (relative to P411-"A82L")
E8	P411-"M177L" H266V N70E A330Y ΔFAD	N70E A74G A78L A82L M177L F263Y H266V T327I A330Y T436L L437Q S438T (relative to P411-**P4**) with FAD domain truncated
E9	P411-"L437Q" S438T T436L V178E	A74G A78L A82L V178E F263Y T327I T436L L437Q

	ΔFAD	S438T (relative to P411-**P4**) with FAD domain truncated
E10	P411-"A82L" F263Y A78L T327I	F263Y A78L T327I (relative to P411-**A82L**)
F1	P411-**G8**	L437F T438Q (relative to P411-**CIS**)
F2	P411-**G8** L75Y	L75Y (relative to P411-**G8**)
F3	P411-**G8S** (or P411-**VAC**$_{cis}$)	L75Y L181I (relative to P411-**G8**)
F4	P411-**G8** L181V	L181V (relative to P411-**G8**)
F5	P411-**E12**	I263G L437F (relative to P411-**CIS**)
F6	P411-**E12** V87L	V87L (relative to P411-**E12**)
F7	P411-**E12** V87L L181R	V87L L181R (relative to P411-**E12**)
F8	P411-**F3**	V87T T438C (relative to P411-**CIS**)
F9	P411-**H9**	I263G L437F (relative to P411-**F3**)
F10	P411-**6C9**	V87T L181G I263M V281L T438C (relative to P411-**CIS**) with FAD domain truncated
G1	*Rma* cyt *c*-wild type (WT)	-
G2	*Rma* cyt *c*-M100D	M100D (relative to *Rma* cyt *c*-WT)
G3	*Rma* cyt *c*-V75K M100D	V75K M100D (relative to *Rma* cyt *c*-WT)
G4	*Rma* cyt *c*-V75P M100D	V75P M100D (relative to *Rma* cyt *c*-WT)
G5	*Rma* cyt *c*-V75G M100D	V75G M100D (relative to *Rma* cyt *c*-WT)
G6	*Rma* cyt *c*-V75C M100D	V75C M100D (relative to *Rma* cyt *c*-WT)
G7	*Rma* cyt *c*-V75T M100D M103E	V75T M100D M103E (relative to *Rma* cyt *c*-WT)
G8	*Rma* cyt *c*-V75T M100D M103D	V75T M100D M103D (relative to *Rma* cyt *c*-WT)
G9	*Rma* cyt *c*-V75T M100D M103N	V75T M100D M103N (relative to *Rma* cyt *c*-WT)
G10	*Rma* cyt *c*-V75T M100D M103A	V75T M100D M103A (relative to *Rma* cyt *c*-WT)
H1	*Rma* cyt *c*-R66Y V75G M100D	R66Y V75G M100D (relative to *Rma* cyt *c*-WT)
H2	*Rma* cyt *c*-V75G M89H M100D	V75G M89H M100D (relative to *Rma* cyt *c*-WT)
H3	*Rma* cyt *c*-V75K M100D M103V	V75K M100D M103V (relative to *Rma* cyt *c*-WT)
H4	*Rma* cyt *c*-V75K M100D T101C M103A	V75K M100D T101C M103A (relative to *Rma* cyt *c*-WT)
H5	*Rma* cyt *c*-V75R M99C M100D M103D	V75R M99C M100D M103D (relative to *Rma* cyt *c*-WT)
H6	*Rma* cyt *c*-V75R M100D T101Q M103D	V75R M100D T101Q M103D (relative to *Rma* cyt *c*-WT)
H7	*Rma* cyt *c*-V75P M99Y M100D	V75P M99Y M100D (relative to *Rma* cyt *c*-WT)
H8	*Rma* cyt *c*-V75P M99Y M100D T101W	V75P M99Y M100D T101W (relative to *Rma* cyt *c*-WT)
H9	*Rma* cyt *c*-R67W V75G M100D	R67W V75G M100D (relative to *Rma* cyt *c*-WT)
H10	*Rma* cyt *c*-R67P V75G M100D	R67P V75G M100D (relative to *Rma* cyt *c*-WT)

Note: P/I value refers to the peak area ratio of cyclopropane products to internal standard based on the absorbance at wavelength of 210 nm by HPLC screening.

Table B-2. Comparison of P450-**G8S** and P411-**G8S** for cyclopropanation and S–H insertion.

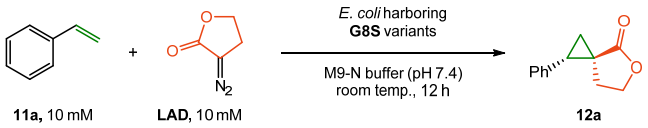

G8S variant	**TTN**	**de**	**ee**
P411-G8S	3090 ± 120	>99%	>98.5%
P450-G8S	380 ± 20	>99%	99%

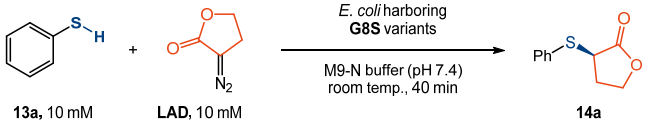

G8S variant	**TTN**	**ee**
P411-G8S	1610 ± 120	84 ± 1%
P450-G8S	300 ± 30	15 ± 2%

Note: Analytical reactions using whole-cell catalysts were set up in quadruplicate and were analyzed by GC. The TTNs for *spiro*[2.4]-lactone formation were obtained using cell suspensions at OD_{600} = 30 for both variants; the TTNs for S–H insertion were obtained using cell suspensions at OD_{600} = 30 for P411-**G8S** variant and OD_{600} = 15 for P450-**G8S**. The errors in all tables are standard deviations. Diastereoselectivity and enantioselectivity were determined by chiral HPLC.

Table B-3. Comparison of **G8S** variants for cyclopropanation and S–H insertion in different forms.

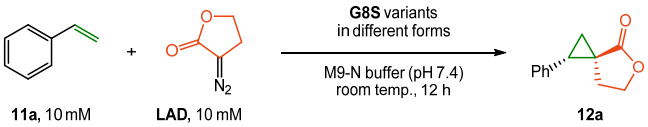

G8S variant	relative activity	**de**	**ee**
P411-**G8S** whole cell	1.000 ± 0.013	>99%	98.6%
P411-**G8S** lysate	0.0063 ± 0.0003	n.d.	n.d.
P411-**G8S** purified protein	0.0077 ± 0.0007	n.d.	n.d.
P450-**G8S** whole cell	0.183 ± 0.010	>99.5%	>99%
P450-**G8S** lysate	0.028 ± 0.001	>99.5%	99%
P450-**G8S** purified protein	0.037 ± 0.001	>99.5%	99%

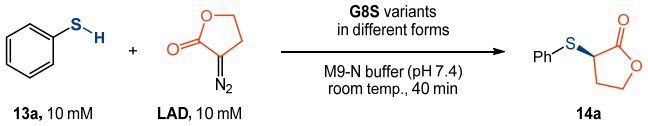

G8S variant	relative activity	**ee**
P450-**G8S** whole cell	1.000 ± 0.019	85%
P450-**G8S** lysate	0.481 ± 0.019	78%
P450-**G8S** purified protein	0.571 ± 0.010	80%
P411-**G8S** whole cell	0.167 ± 0.006	13%
P411-**G8S** lysate	0.022 ± 0.001	n.d.

P411-**G8S** purified protein	0.035 ± 0.001	n.d.

Note: Analytical reactions were set up in triplicate using protein catalysts in forms of whole cell, lysate and purified protein, and were analyzed by GC. Protein concentration of P450-**G8S** catalyst was adjusted to 4.25 μM, and that of P411-**G8S** catalyst was adjusted to 1.70 μM in the analytical reactions. Relative activity was normalized by protein concentration. The errors in all tables are standard deviations. Diastereoselectivity and enantioselectivity were determined by chiral HPLC. n.d. = not determined.

Table B-4. Competition reactions (cyclopropanation *vs* S–H insertion) with **G8S** variants.

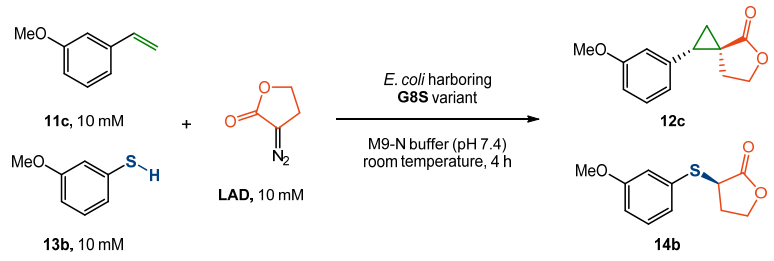

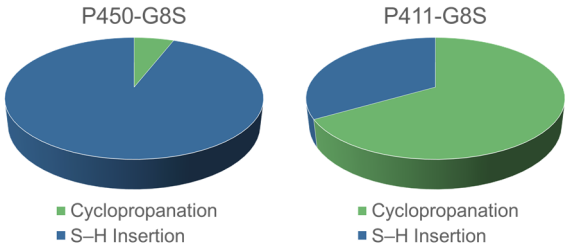

G8S variant	TTN for S–H insertion	TTN for cyclopropanation	S–H insertion: cyclopropanation
P450-**G8S**	1330 ± 10	84 ± 16	16 : 1
P411-**G8S**	1100 ± 80	2200 ± 40	1 : 2

Note: Analytical reactions were set up in triplicate using whole-cell catalyst (P411-**G8S** at OD_{600} = 30 and P450-**G8S** at OD_{600} = 15) and were analyzed by GC. The errors in the table are standard deviations.

Table B-5. Directed evolution of P411-**C10** for lactone-carbene C–H insertion.

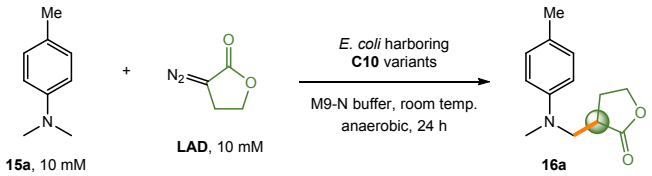

P411-**C10** variant	**TTN**	**ee**
C10 (L1)	105 ± 10	47%
C10-T327V (**L2**)	350 ± 20	44%
C10-T327V Q437L (**L3**)	930 ± 140	40%
C10-T327V Q437L S332A (**L4**)	1220 ± 60	39%
C10-T327V Q437L S332A A87P (**L5**)	770 ± 30	56%
C10-T327V Q437L S332A A87P A264S (**L6**)	1980 ± 90	64.5%

C10-T327P Q437L S332A A87P A264S (**L7**)	2010 ± 50	75%
C10-T327P Q437L S332A A87P A264S E267D (**L8**)	1060 ± 110	80.5%
C10-T327P Q437L S332A A87P A264S E267D V328L (**L9**)	590 ± 30	90%
C10-T327P Q437L S332A A87P A264S E267D V328R (**L10**)	180 ± 15	–66%

Note: Analytical reactions were set up in quadruplicate using whole *E. coli* cells harboring P411-**C10** variants (OD_{600} = 60 for **L1**, **L5** and **L10**, OD_{600} = 30 for the rest). Product formation was quantified by HPLC and TTNs were determined based on protein concentration. Enantioselectivity was determined by chiral HPLC.

Table B-6. Optimization of expression and reaction conditions for lactone-carbene C–H insertion.

Variant	Enzyme expression conditions (**1**) + Reaction conditions (**1**)	Enzyme expression conditions (**2**) + Reaction conditions (**2**)
L6	OD_{600} = 30 2070 TTN, 72% yield, 64.5% ee	OD_{600} = 60 2760 TTN, 82% yield, 63% ee
L7	OD_{600} = 30 1960 TTN, 86% yield, 75% ee	OD_{600} = 30 2920 TTN, >99% yield, 74.5% ee
L9	OD_{600} = 30 610 TTN, 16% yield, 90% ee	OD_{600} = 60 1380 TTN, 61% yield, 90.5% ee
L10	OD_{600} = 60 180 TTN, 6% yield, –66% ee	OD_{600} = 60 360 TTN, 8% yield, –68% ee

Enzyme expression conditions (**1**) for **Table S1**: 22 °C, at 150 rpm, for 20 h (± 20 min).
Enzyme expression conditions (**2**): 24 °C, at 140 rpm, for 20 h (± 20 min).
Reaction conditions (**1**): 10 mM **15a**, 10 mM LAD, *E. coli* harboring P411-**C10** variants (OD_{600} = 60 for **L1**, **L5** and **L10**, OD_{600} = 30 for the rest), D-glucose (25 mM), M9-N buffer/EtOH (19:1), anaerobic, 24 h.
Reaction conditions (**2**): 12 mM **15a**, 12 mM LAD, *E. coli* harboring P411-**C10** variants (OD_{600} = 30 for **L7**, OD_{600} = 60 for the rest), D-glucose (25 mM), M9-N buffer/EtOH (19:1), anaerobic, 24 h.

Table B-7. Different substrates tested for lactone-carbene C–H insertion.

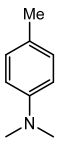	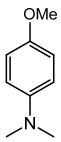	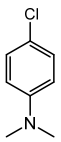	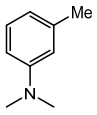	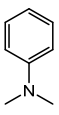	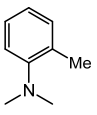	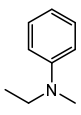
pMe-DMA (**15a**)	pOMe-DMA (**15b**)	pCl-DMA (**15c**)	mMe-DMA (**15d**)	DMA (**15e**)	oMe-DMA (**15f**)	Me,Et-Ani (**15g**)
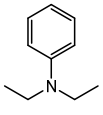	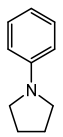	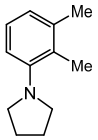	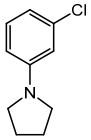	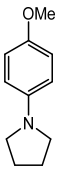	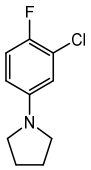	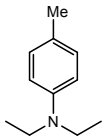
DEA (**15h**)	Ph-pyr (**15i**)	diMePh-pyr (**15j**)	mClPh-pyr (**15k**)	pOMe-pyr (**15l**)	pFmCl-pyr (**15n**)	pMe-DEA

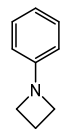	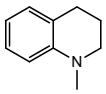	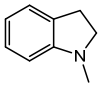	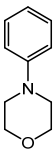	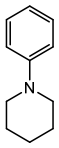	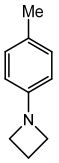
Ph-aze (**15m**)	THQ	indoline	Ph-mor	Ph-pip	pTol-aze

Table B-8. Substrate screening results for lactone-carbene C–H insertion.

yield 0% 0–0.5% 0.5–2% 2–10% 10–20% 20–50% 50–100%

	L1	L2	L3	L4	L5	L6	L7	L8	L9	L10
16a	1.1%	4.2%	11.8%	12.0%	16.0%	62.7%	74.9%	29.6%	27.0%	13.4%
16b	2.2%	10.0%	12.2%	12.3%	11.9%	45.4%	34.9%	8.5%	22.1%	9.7%
16c	0.1%	0.5%	1.5%	2.0%	1.5%	5.5%	7.0%	2.4%	1.7%	0.8%
16d	0.1%	0.1%	0.2%	0.5%	1.0%	16.0%	9.1%	10.1%	23.8%	16.9%
16e	0.1%	0.3%	0.7%	1.0%	3.6%	23.8%	7.0%	9.0%	15.8%	35.5%
16f	0.0%	0.0%	0.0%	0.0%	0.9%	2.0%	1.0%	1.0%	38.1%	1.0%
16g	0.0%	1.0%	2.2%	2.5%	2.8%	12.1%	7.4%	5.3%	49.1%	23.7%
16h	0.0%	0.1%	0.2%	0.0%	0.9%	6.2%	2.8%	2.9%	12.5%	10.1%
16i	0.7%	1.7%	3.4%	3.7%	7.6%	25.7%	30.4%	14.0%	32.1%	22.7%
16j	2.6%	20.4%	31.5%	25.1%	19.4%	23.6%	56.2%	53.0%	82.1%	3.8%
16k	0.0%	0.9%	3.0%	3.9%	6.8%	25.6%	29.1%	29.5%	43.2%	9.3%
16l	2.3%	8.3%	6.9%	6.9%	12.1%	30.9%	33.1%	6.9%	9.4%	15.4%
16m	0.0%	0.0%	0.0%	0.0%	0.0%	0.0%	0.0%	0.0%	0.4%	2.5%
16n	0.1%	0.2%	0.7%	0.7%	1.0%	4.0%	3.6%	3.4%	3.2%	2.6%

Substrate screening was carried out in two rounds:

(1) Rapid screening (without accurate quantification):

The enzyme lineage **L1** to **L10** was expressed in each line of a 96-well plate (column 2 to column 11 with variants **L1** to **L10**, respectively). Enzymatic reactions were set up with substrate concentration of 10 mM for both **LAD** and aniline derivative (one substrate in one line). After the reactions were completed, acetonitrile (600 µL/well) was added to reaction plates. The plates were tightly sealed with a reusable silicone mat, vortexed (15 s × 3) and centrifuged (4,500 × g, 5 min). The supernatant (200 µL/well) was filtered through an AcroPrep 96-well filter plate (0.2 µm) into a shallow-well plate for reversed-phase HPLC analysis (C18 Kromasil column, MeCN:H_2O gradient from 40:60 to 100:0, 1.2 mL/min flow, 230 or 254 nm). Promising substrates were then identified with new compound peaks observed on HPLC followed by further confirmation of products with NMR based on reaction scale-up and product isolation.

Note: Substrates Ph-mor, Ph-pip and pTol-aze were found inactive towards lactone-carbene C–H insertion using variants **L1** to **L10**. Substrates THQ and indoline were found to generate mixtures of C–H insertion products at multiple sites of the molecules (with poor regio- and stereo-selectivities).

(2) Plate re-screening (with accurate quantification):

The re-screening was performed with the substrates identified with promising products, following the procedure used for rapid screening but with internal standard for quantification and using specific HPLC methods developed for each substrate.

Notes: (1) The products quantified here correspond to the sum of all the products when different diastereomers or regio-isomers were formed. (2) Some diastereomers or regio-isomers could be separated from each other on HPLC, while others did not show separation. (3) Expression level of enzyme variants in plate may be different from that in flasks for validation.

Table B-9. Substrates tested for carbene N–H insertion.

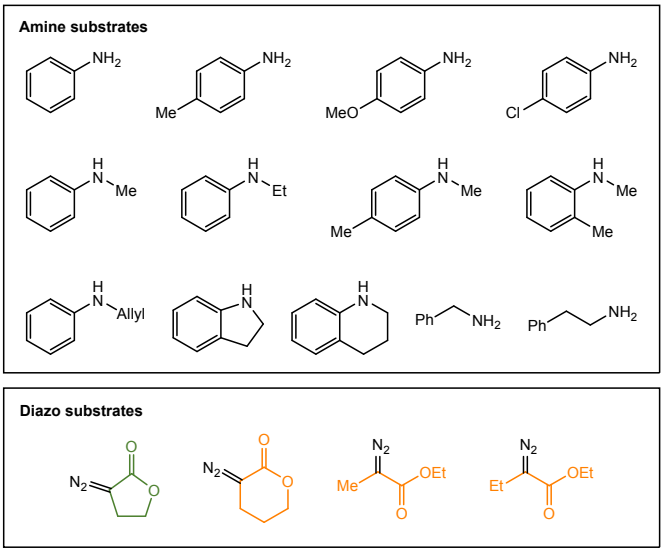

Notes: 6-membered lactone diazo was inactive towards N–H insertion; Me-EDA and Et-EDA showed promising reactivities with late variants in the enzyme lineage from **L1** to **L10**.

Table B-10. Enantioselectivity screening of *Rma* cyt *c* variants-catalyzed lactone-carbene B–H insertion.

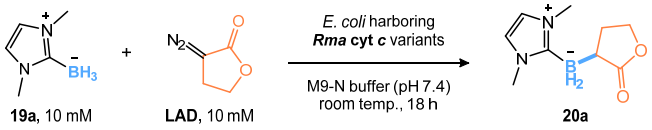

	2	3	4	5	6	7	8	9	10	11
B	58.9	29.3	43.2	76.7	26.4	6.9	57.0	8.8	21.0	51.8
C	58.1	55.0	59.4	54.8	25.0	57.3	37.5	14.1	29.1	85.9
D	84.3	84.8	85.0	84.1	83.0	78.6	85.9	87.0	85.5	86.8
E	87.3	86.3	87.4	81.4	83.7	4.8	22.0	23.3	5.3	30.2
F	18.0	18.8	-16.5	5.4	-29.2	-7.9	-12.9	-1.3	-6.5	14.2
G	8.2	-9.0	26.2	29.9	54.5	47.3	4.2	50.1	56.9	57.9

well	Mutations at specific sites							
location	site 66	site 67	site 75	site 89	site 99	site 100	site 101	site 103
B2	-	-	V75K	-	-	M100D	T101Y	M103A
B3	-	-	-	-	-	M100D	-	-
B4	-	-	V75K	-	-	M100D	-	-
B5	-	-	V75R	-	-	M100D	-	-
B6	-	-	V75P	-	-	M100D	-	-

B7	-	-	V75C	-	-	M100D	-	-
B8	-	-	V75G	-	-	M100D	-	-
B9	-	-	V75T	-	-	M100D	-	-
B10	-	-	V75K	-	-	M100D	-	M103V
B11	-	-	V75K	-	-	M100D	-	M103N
C2	-	-	V75K	-	-	M100D	-	M103Q
C3	-	-	V75K	-	-	M100D	-	M103T
C4	-	-	V75K	-	-	M100D	-	M103A
C5	-	-	V75K	-	-	M100D	-	M103S
C6	-	-	V75K	-	-	M100D	-	M103Y
C7	-	-	V75K	-	-	M100D	T101C	M103A
C8	-	-	V75K	-	-	M100D	T101M	M103A
C9	-	-	V75K	-	-	M100D	T101F	M103A
C10	-	-	V75R	-	-	M100D	-	M103Q
C11	-	-	V75R	-	-	M100D	-	M103K
D2	-	-	V75R	-	-	M100D	-	M103F
D3	-	-	V75R	-	-	M100D	-	M103I
D4	-	-	V75R	-	-	M100D	-	M103V
D5	-	-	V75R	-	-	M100D	-	M103D
D6	-	-	V75R	-	-	M100D	-	M103G
D7	-	-	V75R	-	-	M100D	T101G	M103D
D8	-	-	V75R	-	-	M100D	T101V	M103D
D9	-	-	V75R	-	-	M100D	T101Q	M103D
D10	-	-	V75R	-	M99W	M100D	-	M103D
D11	-	-	V75R	-	M99C	M100D	-	M103D
E2	-	-	V75R	-	M99P	M100D	-	M103D
E3	-	-	V75R	-	M99Y	M100D	-	M103D
E4	-	-	V75R	-	M99V	M100D	-	M103D
E5	-	-	V75R	M89L	-	M100D	-	M103D
E6	-	-	V75R	M89K	-	M100D	-	M103D
E7	-	-	V75P	-	M99C	M100D	-	-
E8	-	-	V75P	-	M99Y	M100D	-	-
E9	-	-	V75P	-	M99P	M100D	-	-
E10	-	-	V75P	-	M99K	M100D	-	-
E11	-	-	V75P	-	M99L	M100D	-	-
F2	-	-	V75P	-	M99Y	M100D	T101W	-
F3	-	-	V75P	-	M99Y	M100D	T101A	-
F4	-	-	V75P	-	M99Y	M100D	T101Y	-
F5	-	-	V75P	-	-	M100D	-	M103N
F6	-	-	V75P	-	-	M100D	-	M103S
F7	-	-	V75P	-	-	M100D	-	M103A
F8	-	-	V75P	-	-	M100D	-	M103L
F9	-	-	V75P	-	-	M100D	-	M103D

F10	-	-	V75P	-	-	M100D	-	M103E
F11	-	-	V75T	-	-	M100D	-	M103E
G2	-	-	V75T	-	-	M100D	-	M103I
G3	-	-	V75T	-	-	M100D	-	M103L
G4	-	-	V75T	-	-	M100D	-	M103V
G5	-	-	V75T	-	-	M100D	-	M103Q
G6	R66Y	-	V75G	-	-	M100D	-	-
G7	-	R67L	V75G	-	-	M100D	-	-
G8	-	R67P	V75G	-	-	M100D	-	-
G9	-	R67W	V75G	-	-	M100D	-	-
G10	-	-	V75G	M89F	-	M100D	-	-
G11	-	-	V75G	M89H	-	M100D	-	-

Notes: numbers in the heat-map table are the ee values (in %) of the B–H insertion products produced by the corresponding *Rma* cyt *c* variants in the 96-well plate.

Table B-11. List of mutations in P411, P450 and *Rma* cyt *c* variants involved in Chapter 3.

P411 variant	**Mutations relative to wild-type protein ($P450_{BM3}$ or *Rma* cyt *c*)**
P411-**G8S**	L75Y V78A F87V P142S T175I L181I A184V S226R H236Q E252G T268A A290V L353V I366V C400S L437F T438Q E442K (relative to P450-WT)
P450-**G8S**	L75Y V78A F87V P142S T175I L181I A184V S226R H236Q E252G T268A A290V L353V I366V L437F T438Q E442K (relative to P450-WT)
P411-**C10** (**L1**)	N70E A74G V78L A82L F87A M118S P142S F162L T175I M177L A184V S226R H236Q E252G I263Y H266V T268G A290V A328V A330Y L353V I366V C400S I401L T436L L437Q E442K ΔFAD (relative to P450-WT)
L2	N70E A74G V78L A82L F87A M118S P142S F162L T175I M177L A184V S226R H236Q E252G I263Y H266V T268G A290V **T327V** A328V A330Y L353V I366V C400S I401L T436L L437Q E442K ΔFAD (relative to P450-WT)
L3	N70E A74G V78L A82L F87A M118S P142S F162L T175I M177L A184V S226R H236Q E252G I263Y H266V T268G A290V **T327V** A328V A330Y L353V I366V C400S I401L T436L E442K ΔFAD (relative to P450-WT)
L4	N70E A74G V78L A82L F87A M118S P142S F162L T175I M177L A184V S226R H236Q E252G I263Y H266V T268G A290V **T327V** A328V A330Y **S332A** L353V I366V C400S I401L T436L E442K ΔFAD (relative to P450-WT)
L5	N70E A74G V78L A82L **F87P** M118S P142S F162L T175I M177L A184V S226R H236Q E252G I263Y H266V T268G A290V **T327V** A328V A330Y **S332A** L353V I366V C400S I401L T436L E442K ΔFAD (relative to P450-WT)
L6	N70E A74G V78L A82L **F87P** M118S P142S F162L T175I M177L A184V S226R H236Q E252G I263Y **A264S** H266V T268G A290V **T327V** A328V A330Y **S332A** L353V I366V C400S I401L T436L E442K ΔFAD (relative to P450-WT)
L7	N70E A74G V78L A82L **F87P** M118S P142S F162L T175I M177L A184V S226R H236Q E252G I263Y **A264S** H266V T268G A290V **T327P** A328V A330Y **S332A** L353V I366V C400S I401L T436L E442K ΔFAD (relative to P450-WT)

L8	N70E A74G V78L A82L **F87P** M118S P142S F162L T175I M177L A184V S226R H236Q E252G I263Y **A264S** H266V **E267D** T268G A290V **T327P** A328V A330Y **S332A** L353V I366V C400S I401L T436L E442K ΔFAD (relative to P450-WT)
L9	N70E A74G V78L A82L **F87P** M118S P142S F162L T175I M177L A184V S226R H236Q E252G I263Y **A264S** H266V **E267D** T268G A290V **T327P A328L** A330Y **S332A** L353V I366V C400S I401L T436L E442K ΔFAD (relative to P450-WT)
L10	N70E A74G V78L A82L **F87P** M118S P142S F162L T175I M177L A184V S226R H236Q E252G I263Y **A264S** H266V **E267D** T268G A290V **T327P A328R** A330Y **S332A** L353V I366V C400S I401L T436L E442K ΔFAD (relative to P450-WT)
Rma cyt *c*-D	M100D (relative to *Rma* cyt *c*-WT)
Rma cyt *c*-RD	V75R M100D (relative to *Rma* cyt *c*-WT)
Rma cyt *c*-RDV	V75R M100D M103V (relative to *Rma* cyt *c*-WT)
Rma cyt *c*-**BOR**$^{\mathbf{Lac}}$	V75R M99Q M100D T101Y M103V (relative to *Rma* cyt *c*-WT)

Note: ΔFAD means FAD domain truncation. See the publications for the nucleotide and amino acid sequences of the hemeprotein variants.

B.2 Supporting Figures B-1 to B-2

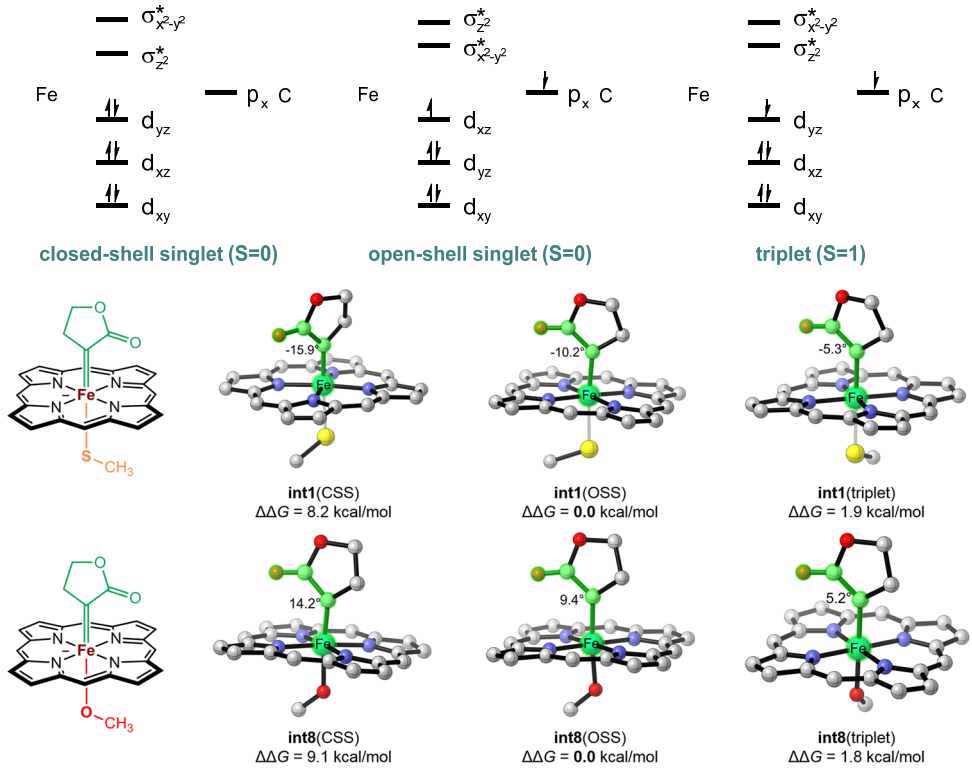

Figure B-1. Comparison of the iron-carbene intermediates with different axial ligands by DFT. Gibbs free energy obtained at the B3LYP/def2-TZVP//B3LYP/6-31G(d)-LANL2DZ level. OSS is open-shell singlet; CSS is closed-shell singlet. *Note: No major difference in electronic state distribution, energy level or structural geometry is observed.

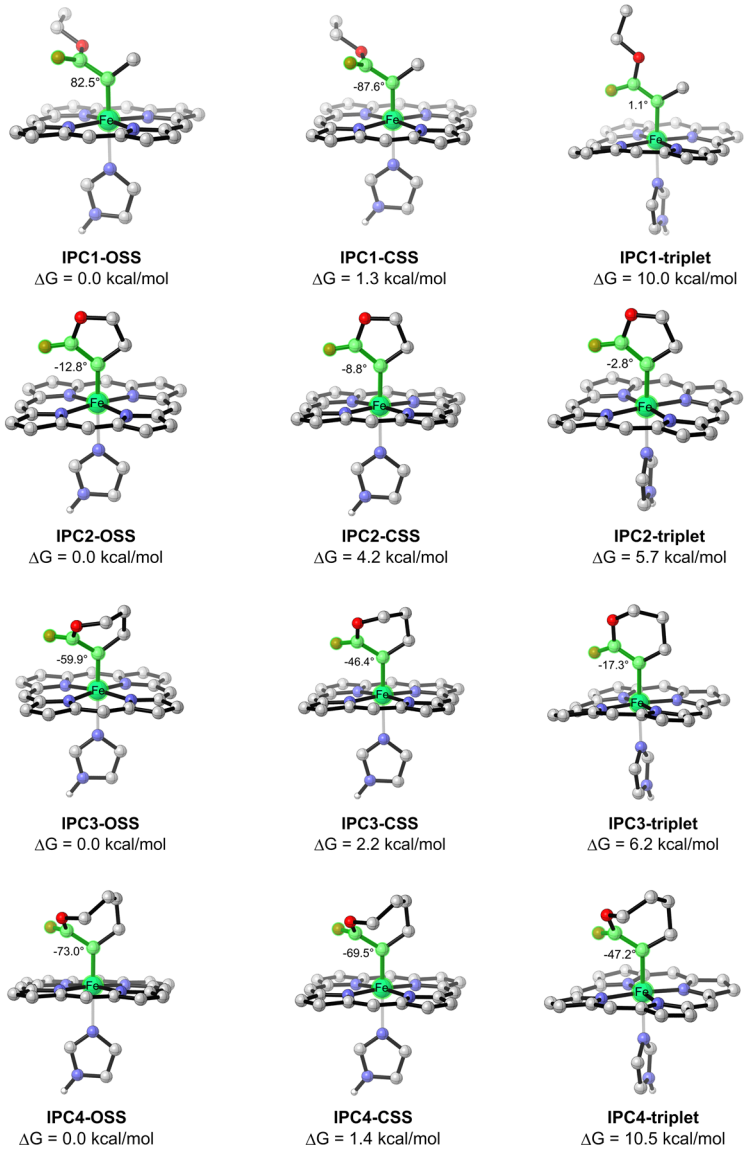

Figure B-2. Comparison of the electronic states of iron-porphyrin carbene intermediates. The Gibbs free energies were obtained at B3LYP-D3(BJ)/def2-TZVPP//B3LYP/def2-SVP level.

A.3 Preparation of lactone-diazo substrates

3-Diazodihydrofuran-2(3*H*)-one (LAD)

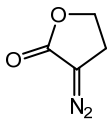

The preparation of the title compound **1** followed a modified procedure reported by Sattely *et al*. Sodium azide (4.83 g, 74.3 mmol, 4 equiv.), sodium hydroxide (80 mL of 2 M in water, 160 mmol), tetrabutylammonium bromide (60.0 mg, 0.190 mmol, 0.01 equiv.), and hexane (80 mL) were combined in a 500-mL flask with magnetic stir bar open to the air and cooled to 0 °C. With vigorous stirring, triflic anhydride (6.20 mL, 37.1 mmol, 2 equiv.) was added dropwise. After 15 min, a solution of 2-acetyl-butyrolactone (2.00 mL, 18.6 mmol) in acetonitrile (70 mL) was poured into the vessel through a funnel, followed by an additional 10 mL of acetonitrile to complete the transfer. The initially colorless reaction mixture immediately turned yellow. After stirring for 20 min at 0 °C, the mixture was diluted with ice water (50 mL) and chilled EtOAc (50

mL) and transferred to a separatory funnel. After phase separation and removal of the organic fraction, the aqueous layer was washed with chilled EtOAc (50 mL × 5). The combined organic layer was dried over Na_2SO_4, filtered, and concentrated under reduced pressure. The resulting crude product was purified through a silica column using hexane: ethyl acetate (3:1 to 2:1) as eluents. The yellow-colored fractions were concentrated to afford the product as a bright yellow crystalline solid (1.2 – 1.6 g, 60 – 75% yield).

3-Diazotetrahydro-2*H*-pyran-2-one (**LAD-2**) and **3-diazooxepan-2-one** (**LAD-3**)

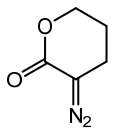
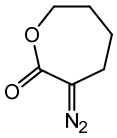

The preparation of the title compounds **LAD-2** and **LAD-3** followed a modified procedure reported by DeAngelis *et al*. A flame-dried round-bottomed flask was charged with diisopropylamine (1.88 mL, 13.41 mmol) under a nitrogen atmosphere. Anhydrous THF (40mL) was added and the flask was cooled to 0 °C. A solution of *n*-butyllithium (5.36 mL, 13.4 mmol) (2.5M solution in hexanes) was added dropwise and the mixture was stirred for 30 min and subsequently cooled to –78 °C by a bath of dry ice/acetone. A solution of tetrahydro-2*H*-pyran-2-one or oxepan-2-one (11.2 mmol) in 27 mL of anhydrous THF was added dropwise and the reaction was stirred at –78 °C for 15 minutes. 2,2,2-Trifluoroethyl trifluoroacetate (TFEA) (2.24 mL, 16.8 mmol) was then added dropwise and the reaction was stirred at –78 °C for 30 minutes and then allowed to warm to room temperature over 1 hour. The reaction was quenched with 50 mL of 10% HCl and extracted with Et_2O (50 mL × 3). The combined organic layer was washed with brine, dried over anhydrous $MgSO_4$, and concentrated under reduced pressure. The crude product 3-(2,2,2-trifluoroacetyl)tetrahydro-2*H*- pyran-2-one or 3-(2,2,2-trifluoroacetyl)oxepan-2-one was used for the next step without further purification.

The crude product was dissolved in anhydrous CH_2Cl_2 (110 mL), and *o*-nitrobenzenesulfonyl azide (*o*-NBSA) (3.21 g, 14.1 mmol) was added followed by dropwise addition of 1,8-diazabicyclo(5.4.0)undec-7-ene (DBU, 2.39 mL, 16 mmol) and the reaction was stirred at room temperature for 3 hours. The reaction was quenched by water (50 mL) and the product was extracted by ether (40 mL × 7). The combined organic layer was washed with brine, dried over anhydrous $MgSO_4$, and concentrated under reduced pressure. The resulting crude product was purified through a silica column using hexane: ethyl acetate (2:1 to 1:2) as eluents. The yellow-colored fractions were concentrated to afford product **LAD-2** as a bright yellow crystalline solid (1.06 g, 75% yield) and product **LAD-3** as an orange oil (1.28 g, 82% yield).

B.4 Preparation of racemic standard products

General procedure for the synthesis of *spiro*[2.4]-lactone standard products:

To a 20 mL vial was added olefin (1.0 mmol, 2.0 equiv.), $Rh_2(OAc)_4$ (2.2 mg, 1 mol%) and DCM (5 mL). The mixture was cooled to –78 °C, and a solution of **LAD** (0.5 mmol, 1.0 equiv.) in DCM (3 mL) was added dropwise to the reaction mixture over 2 hours through a syringe pump. The reaction was allowed to slowly warm up to room temperature over 8 hours and stirred at room temperature for another 8 hours. Evaporation of the organic solvent and purification by silica column chromatography using hexane and ethyl acetate as eluents afforded racemic cyclopropane products in 20–60% yields (diastereomers can be separated).

(*E*)-1-Phenyl-5-oxaspiro[2.4]heptan-4-one ((*E*)-12a)

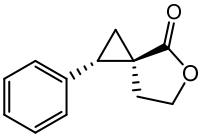

^{1}H NMR (400 MHz, $CDCl_3$) δ 7.39–7.30 (m, 2H), 7.30–7.23 (m, 1H), 7.18–7.08 (m, 2H), 4.40 (td, *J* = 8.9, 5.6 Hz, 1H), 4.27 (td, *J* = 8.9, 6.7 Hz, 1H), 2.76 (dd, *J* = 9.4, 7.1 Hz, 1H), 2.15 (ddd, *J* = 13.1, 8.9, 6.8 Hz, 1H), 1.90 (ddd, *J* = 13.0, 8.8, 5.6 Hz, 1H), 1.80 (dd, *J* = 9.4, 5.1 Hz, 1H), 1.47 (dd, *J* = 7.1, 5.1 Hz, 1H). ^{13}C NMR (101 MHz, $CDCl_3$) δ 179.50, 136.11, 128.74, 128.17, 127.24, 66.01, 31.10, 27.53, 25.51, 18.53.

(*Z*)-1-Phenyl-5-oxaspiro[2.4]heptan-4-one ((*Z*)-12a)

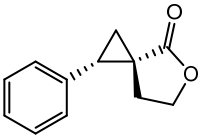

^{1}H NMR (400 MHz, $CDCl_3$) δ 7.34–7.19 (m, 5H), 4.51–4.36 (m, 2H), 2.74–2.54 (m, 2H), 2.27 (ddd, *J* = 12.7, 7.2, 2.9 Hz, 1H), 1.93 (dd, *J* = 7.7, 5.3 Hz, 1H), 1.54 (dd, *J* = 8.9, 5.3 Hz, 1H). ^{13}C NMR (101 MHz, $CDCl_3$) δ 175.97, 135.38, 129.02, 128.24, 127.19, 65.66, 34.76, 32.10, 27.83, 17.33.

HRMS (TOF) m/z: 189.0917 ($M+H^+$); calc. for $C_{12}H_{13}O_2$: 189.0916.

(*E*)-1-(4-Methoxyphenyl)-5-oxaspiro[2.4]heptan-4-one ((*E*)-12b)

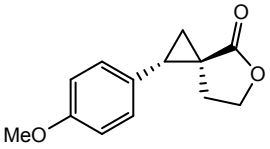

^{1}H NMR (400 MHz, $CDCl_3$) δ 7.05 (d, *J* = 8.4 Hz, 2H), 6.87 (d, *J* = 8.8 Hz, 2H), 4.40 (td, *J* = 9.0, 5.5 Hz, 1H), 4.26 (td, *J* = 8.9, 6.9 Hz, 1H), 3.80 (s, 3H), 2.71 (dd, *J* = 9.4, 7.1 Hz, 1H), 2.12 (ddd, *J* = 13.0, 8.9, 6.9 Hz, 1H), 1.88 (ddd, *J* = 13.0, 8.7, 5.5 Hz, 1H), 1.77 (dd, *J* = 9.4, 5.1 Hz, 1H), 1.40 (dd, *J* = 7.1, 5.1 Hz, 1H). ^{13}C NMR (101 MHz, $CDCl_3$) δ 179.66, 158.84, 129.31, 127.99, 114.18, 66.02, 55.44, 30.64, 27.29, 25.56, 18.52.

(*Z*)-1-(4-Methoxyphenyl)-5-oxaspiro[2.4]heptan-4-one ((*Z*)-12b)

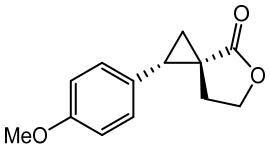

^{1}H NMR (400 MHz, $CDCl_3$) δ 7.17 (d, *J* = 8.3 Hz, 2H), 6.82 (d, *J* = 8.8 Hz, 2H), 4.46 (td, *J* = 9.0, 2.9 Hz, 1H), 4.40 (ddd, *J* = 9.8, 9.0, 7.3 Hz, 1H), 3.77 (s, 3H), 2.61 (dt, *J* = 12.1, 9.1 Hz, 2H), 2.25 (ddd, *J* = 12.7, 7.1, 2.8 Hz, 1H), 1.87 (dd, *J* = 7.6, 5.2 Hz, 1H), 1.51 (dd, *J* = 8.9, 5.2 Hz, 1H). ^{13}C NMR (101 MHz, $CDCl_3$) δ 176.15, 158.69, 130.04, 127.42, 113.70, 65.67, 55.34, 34.27, 32.05, 27.66, 17.47.

HRMS (TOF) m/z: 219.1024 ($M+H^+$); calc. for $C_{13}H_{15}O_3$: 219.1021.

(*E*)-1-(3-Methoxyphenyl)-5-oxaspiro[2.4]heptan-4-one ((*E*)-12c)

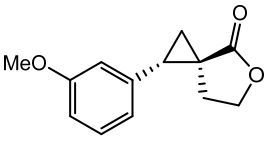

^{1}H NMR (400 MHz, $CDCl_3$) δ 7.22–7.15 (m, 1H), 6.74 (ddd, *J* = 8.3, 2.6, 0.9 Hz, 1H), 6.64 (dp, *J* = 7.7, 0.8 Hz, 1H), 6.62 – 6.57 (m, 1H), 4.34 (td, *J* = 8.9, 5.7 Hz, 1H), 4.21 (td, *J* = 8.9, 6.7 Hz, 1H), 3.74 (s, 3H), 2.66 (dd, *J* = 9.3, 7.1 Hz, 1H), 2.09 (ddd, *J* = 13.1, 8.9, 6.8 Hz, 1H), 1.86 (ddd, *J* = 13.0, 8.8, 5.7 Hz, 1H), 1.71 (dd, *J* = 9.3, 5.1 Hz, 1H), 1.38 (dd, *J* = 7.1, 5.1 Hz, 1H). ^{13}C NMR (101 MHz, $CDCl_3$) δ 179.38, 159.80, 137.67, 129.64, 120.28, 114.14, 112.24, 65.96, 55.25, 31.01, 27.44, 25.46, 18.47.

(*Z*)-1-(3-Methoxyphenyl)-5-oxaspiro[2.4]heptan-4-one ((*Z*)-12c)

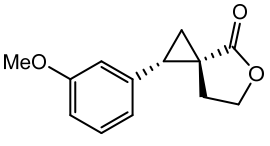

^{1}H NMR (400 MHz, $CDCl_3$) δ 7.13 (t, *J* = 7.9 Hz, 1H), 6.77 (ddd, *J* = 6.9, 1.5, 0.8 Hz, 1H), 6.73 (t, *J* = 2.1 Hz, 1H), 6.69 (dd, *J* = 8.2, 2.5 Hz, 1H), 4.43 – 4.30 (m, 2H), 3.72 (s, 3H), 2.63–2.48 (m, 2H), 2.19 (ddd, *J* = 12.9, 7.1, 2.9

Hz, 1H), 1.84 (dd, *J* = 7.7, 5.3 Hz, 1H), 1.46 (dd, *J* = 8.8, 5.3 Hz, 1H). ^{13}C NMR (101 MHz, $CDCl_3$) δ 175.79, 159.33, 136.89, 129.08, 121.31, 114.89, 112.34, 65.53, 55.17, 34.63, 32.02, 27.77, 17.33.
HRMS (TOF) m/z: 219.1021 ($M+H^+$); calc. for $C_{13}H_{15}O_3$: 219.1021.

(*E*)-1-(4-Tolyl)-5-oxaspiro[2.4]heptan-4-one ((*E*)-12d)

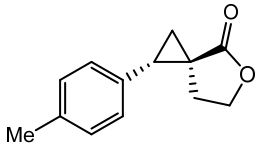

^{1}H NMR (400 MHz, $CDCl_3$) δ 7.14 (d, *J* = 7.9 Hz, 2H), 7.01 (d, *J* = 8.1 Hz, 2H), 4.40 (td, *J* = 8.9, 5.6 Hz, 1H), 4.26 (td, *J* = 8.9, 6.8 Hz, 1H), 2.72 (dd, *J* = 9.4, 7.1 Hz, 1H), 2.34 (s, 3H), 2.14 (ddd, *J* = 13.0, 8.9, 6.8 Hz, 1H), 1.89 (ddd, *J* = 12.9, 8.7, 5.5 Hz, 1H), 1.78 (dd, *J* = 9.3, 5.1 Hz, 1H), 1.43 (dd, *J* = 7.1, 5.1 Hz, 1H). ^{13}C NMR (101 MHz, $CDCl_3$) δ 179.63, 136.96, 132.99, 129.44, 128.09, 66.03, 30.94, 27.40, 25.54, 21.19, 18.47.

(*Z*)-1-(4-Tolyl)-5-oxaspiro[2.4]heptan-4-one ((*Z*)-12d)

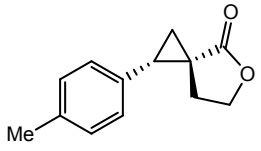

^{1}H NMR (400 MHz, $CDCl_3$) δ 7.12 (q, *J* = 8.1 Hz, 4H), 4.49–4.37 (m, 2H), 2.69–2.54 (m, 2H), 2.30 (s, 3H), 2.24 (dd, *J* = 7.1, 2.9 Hz, 1H), 1.90 (dd, *J* = 7.7, 5.2 Hz, 1H), 1.51 (dd, *J* = 8.9, 5.3 Hz, 1H). ^{13}C NMR (101 MHz, $CDCl_3$) δ 176.09, 136.79, 132.33, 129.01, 128.88, 65.66, 34.57, 32.12, 27.73, 21.27, 17.34.
HRMS (TOF) m/z: 203.1074 ($M+H^+$); calc. for $C_{13}H_{15}O_2$: 203.1072

(*E*)-1-(4-Chlorophenyl)-5-oxaspiro[2.4]heptan-4-one ((*E*)-12e)

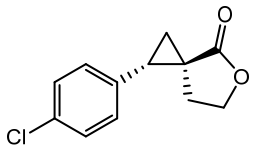

^{1}H NMR (400 MHz, $CDCl_3$) δ 7.31 (d, *J* = 8.5 Hz, 2H), 7.06 (d, *J* = 8.1 Hz, 2H), 4.41 (td, *J* = 9.0, 5.8 Hz, 1H), 4.28 (td, *J* = 8.9, 6.5 Hz, 1H), 2.72 (dd, *J* = 9.3, 7.1 Hz, 1H), 2.14 (ddd, *J* = 13.1, 8.9, 6.5 Hz, 1H), 1.88 (ddd, *J* = 13.0, 8.8, 5.8 Hz, 1H), 1.80 (dd, *J* = 9.3, 5.2 Hz, 1H), 1.42 (dd, *J* = 7.1, 5.2 Hz, 1H). ^{13}C NMR (101 MHz, $CDCl_3$) δ 179.19, 134.71, 133.12, 129.50, 128.96, 65.98, 30.34, 27.61, 25.49, 18.70.

(*Z*)-1-(4-Chlorophenyl)-5-oxaspiro[2.4]heptan-4-one ((*Z*)-12e)

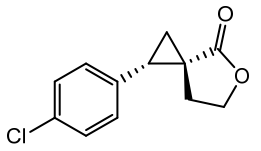

^{1}H NMR (400 MHz, $CDCl_3$) δ 7.25 (d, *J* = 8.5 Hz, 2H), 7.18 (d, *J* = 8.3 Hz, 2H), 4.47 (td, *J* = 9.0, 3.0 Hz, 1H), 4.40 (ddd, *J* = 9.6, 9.0, 7.4 Hz, 1H), 2.68–2.54 (m, 2H), 2.28 (ddd, *J* = 12.7, 7.3, 2.9 Hz, 1H), 1.89 (dd, *J* = 7.7, 5.3 Hz, 1H), 1.55 (dd, *J* = 8.9, 5.4 Hz, 1H). ^{13}C NMR (101 MHz, $CDCl_3$) δ 175.85, 133.89, 133.00, 130.37, 128.41, 65.69, 33.93, 31.91, 27.92, 17.61.
HRMS (TOF) m/z: 223.0542 ($M+H^+$); calc. for $C_{12}H_{12}O_2Cl$: 223.0526.

(*E*)-1-(4-Bromophenyl)-5-oxaspiro[2.4]heptan-4-one ((*E*)-12f)

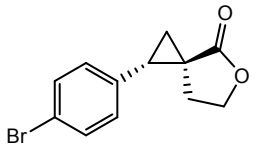

^{1}H NMR (400 MHz, $CDCl_3$) δ 7.46 (d, *J* = 8.4 Hz, 2H), 7.00 (d, *J* = 8.5 Hz, 2H), 4.41 (td, *J* = 9.0, 5.8 Hz, 1H), 4.28 (td, *J* = 8.9, 6.6 Hz, 1H), 2.77–2.63 (m, 1H), 2.14 (ddd, *J* = 13.1, 8.9, 6.5 Hz, 1H), 1.88 (ddd, *J* = 13.2, 8.8, 5.8 Hz, 1H), 1.80 (dd, *J* = 9.3, 5.2 Hz, 1H), 1.42 (dd, *J* = 7.1, 5.2 Hz, 1H). ^{13}C NMR (101 MHz, $CDCl_3$) δ 179.15, 135.25, 131.90, 129.85, 121.17, 65.98, 30.40, 27.61, 25.48, 18.66.

(*Z*)-1-(4-Bromophenyl)-5-oxaspiro[2.4]heptan-4-one ((*Z*)-12f)

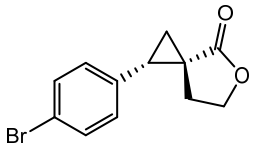

^{1}H NMR (400 MHz, $CDCl_3$) δ 7.40 (d, *J* = 8.4 Hz, 2H), 7.12 (d, *J* = 8.1 Hz, 2H), 4.47 (td, *J* = 9.0, 3.0 Hz, 1H), 4.40 (ddd, *J* = 9.6, 9.0, 7.4 Hz, 1H), 2.66 – 2.54 (m, 2H), 2.28 (ddd, *J* = 13.0, 7.5, 3.2 Hz, 1H), 1.88 (dd, *J* = 7.7, 5.4 Hz, 1H), 1.55 (dd, *J* = 8.8, 5.4 Hz, 1H). ^{13}C NMR (101 MHz, $CDCl_3$) δ 175.84, 134.43, 131.33, 130.73, 121.14, 65.69, 33.97, 31.89, 27.91, 17.56.

HRMS (TOF) m/z: 267.0044 ($M+H^+$); calc. for $C_{12}H_{12}O_2Br$: 267.0021.

(*E*)-1-((4-(Trifluoromethyl)phenyl))-5-oxaspiro[2.4]heptan-4-one ((*E*)-12g)

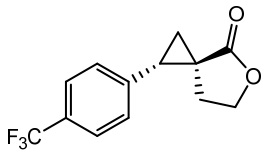

^{1}H NMR (400 MHz, $CDCl_3$) δ 7.60 (d, *J* = 7.9 Hz, 2H), 7.24 (d, *J* = 8.7 Hz, 2H), 4.43 (td, *J* = 9.0, 5.9 Hz, 1H), 4.29 (td, *J* = 9.0, 6.4 Hz, 1H), 2.80 (dd, *J* = 9.3, 7.1 Hz, 1H), 2.17 (ddd, *J* = 13.1, 8.9, 6.4 Hz, 1H), 1.94–1.82 (m, 2H), 1.51 (dd, *J* = 7.1, 5.2 Hz, 1H). ^{13}C NMR (101 MHz, $CDCl_3$) δ 178.94, 140.47, 129.54 (130.02, 129.70, 129.37, 129.05, q, *J* = 32.5 Hz), 128.45, 125.73 (125.79, 125.75, 125.71, 125.67, q, *J* =3.8 Hz), 124.16 (128.21, 125.51, 122.81, 120.11, q, *J* = 271.8 Hz), 65.98, 30.48, 28.00, 25.46, 18.91.

(*Z*)-1-((4-(Trifluoromethyl)phenyl))-5-oxaspiro[2.4]heptan-4-one ((*Z*)-12g)

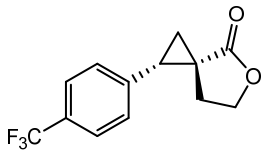

^{1}H NMR (400 MHz, $CDCl_3$) δ 7.54 (d, *J* = 8.1 Hz, 2H), 7.37 (d, *J* = 8.6 Hz, 2H), 4.49 (td, *J* = 9.0, 3.1 Hz, 1H), 4.42 (td, *J* = 9.3, 7.4 Hz, 1H), 2.74 – 2.57 (m, 2H), 2.32 (ddd, *J* = 12.8, 7.3, 3.1 Hz, 1H), 1.96 (dd, *J* = 7.7, 5.4 Hz, 1H), 1.61 (dd, *J* = 8.8, 5.4 Hz, 1H). ^{13}C NMR (101 MHz, $CDCl_3$) δ 175.69, 139.45, 129.39, 129.33 (129.81, 129.49, 129.16, 128.84, q, *J* = 32.5 Hz), 125.19 (125.24, 125.21, 125.17, 125.13, q, *J* = 3.8 Hz), 124.29 (128.34, 125.64, 122.94, 120.22, q, *J* = 271.9 Hz), 65.73, 34.06, 31.89, 28.23, 17.69.

HRMS (TOF) m/z: 257.0796 ($M+H^+$); calc. for $C_{13}H_{12}O_2F_3$: 257.0789.

(*E*)-1-(2-Fluorophenyl)-5-oxaspiro[2.4]heptan-4-one ((*E*)-12h)

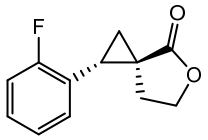

^{1}H NMR (400 MHz, $CDCl_3$) δ 7.31–7.23 (m, 1H), 7.12 (td, *J* = 7.5, 1.1 Hz, 1H), 7.10–7.02 (m, 2H), 4.41 (dtd, *J* = 8.9, 4.9, 0.3 Hz, 1H), 4.34 (td, *J* = 8.6, 7.5 Hz, 1H), 2.84–2.70 (m, 1H), 2.15 (ddd, *J* = 13.0, 9.0, 7.4 Hz, 1H), 1.84–1.74 (m, 2H), 1.45 (dd, *J* = 7.2, 5.0 Hz, 1H). ^{13}C NMR (101 MHz, $CDCl_3$) δ 179.32, 162.49 (163.72, 161.27, d, *J* = 248.2 Hz), 129.39 (129.41, 129.38, d, *J* = 3.7 Hz), 129.18 (129.22, 129.14, d, *J* = 8.2 Hz), 124.39 (124.40, 124.37, d, *J* = 3.7 Hz), 123.73 (123.80, 123.66, d, *J* = 14.7 Hz), 115.62 (115.73, 115.51, d, *J* = 21.5 Hz), 66.15, 26.49, 25.89, 25.50 (25.52, 25.48, d, *J* = 3.7 Hz), 17.43 (17.43, 17.42, d, *J* = 1.5 Hz).

(*Z*)-1-(2-Fluorophenyl)-5-oxaspiro[2.4]heptan-4-one ((*Z*)-12h)

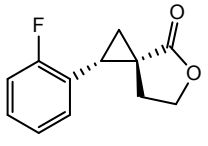

^{1}H NMR (400 MHz, $CDCl_3$) δ 7.26–7.17 (m, 2H), 7.09 (td, *J* = 7.5, 1.1 Hz, 1H), 6.99 (ddd, *J* = 9.6, 8.3, 1.2 Hz, 1H), 4.52–4.44 (m, 2H), 2.68–2.54 (m, 2H), 2.33 (ddd, *J* = 12.7, 6.3, 4.0 Hz, 1H), 1.86 (dd, *J* = 7.7, 5.3 Hz, 1H), 1.54 (dd, *J* = 8.7, 5.3 Hz, 1H). ^{13}C NMR (101 MHz, $CDCl_3$) δ 176.26, 162.33 (163.54, 161.11, d, *J* = 245.9 Hz), 130.43 (130.45, 130.41, d, *J* = 3.7 Hz), 128.97 (129.01, 128.93, d, *J* = 8.3 Hz), 123.90 (123.92, 123.88, d, *J* = 3.5 Hz), 123.15 (123.22, 123.07, d, *J* = 14.8 Hz), 114.94 (115.04, 114.83, d, *J* = 21.4 Hz), 65.92, 31.56, 28.11 (28.13, 28.09, d, *J* = 3.8 Hz), 26.95, 16.51.

HRMS (TOF) m/z: 207.0842 ($M+H^+$); calc. for $C_{12}H_{12}O_2F$: 207.0821.

(*E*)-1-(Naphthalen-2-yl)-5-oxaspiro[2.4]heptan-4-one ((*E*)-12i)

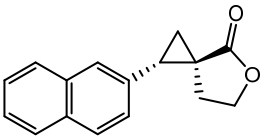

^{1}H NMR (400 MHz, $CDCl_3$) δ 7.87–7.76 (m, 3H), 7.60–7.55 (m, 1H), 7.53–7.44 (m, 2H), 7.26 (dd, *J* = 8.4, 1.8 Hz, 1H), 4.40 (td, *J* = 9.0, 5.5 Hz, 1H), 4.26 (td, *J* = 8.9, 6.8 Hz, 1H), 2.92 (dd, *J* = 9.2, 7.2 Hz, 1H), 2.18 (ddd, *J* = 13.1, 8.9, 6.8 Hz, 1H), 1.95–1.82 (m, 2H), 1.63 (dd, *J* = 7.2, 5.2 Hz, 1H). ^{13}C NMR (101 MHz, $CDCl_3$) δ 179.48, 133.70, 133.47, 132.64, 128.47, 127.82, 127.70, 126.70, 126.58, 126.50, 126.11, 66.07, 31.36, 27.80, 25.61, 18.53.

(*Z*)-1-(Naphthalen-2-yl)-5-oxaspiro[2.4]heptan-4-one ((*Z*)-12i)

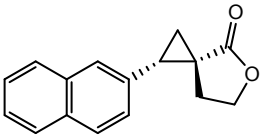

^{1}H NMR (400 MHz, $CDCl_3$) δ 7.81–7.74 (m, 3H), 7.71 (dd, *J* = 1.9, 1.0 Hz, 1H), 7.47–7.39 (m, 2H), 7.37 (dd, *J* = 8.5, 1.8 Hz, 1H), 4.52–4.42 (m, 2H), 2.80 (t, *J* = 8.3 Hz, 1H), 2.67 (dt, *J* = 12.5, 9.3 Hz, 1H), 2.34 (ddd, *J* = 12.7, 6.9, 3.3 Hz, 1H), 2.07 (dd, *J* = 7.7, 5.3 Hz, 1H), 1.62 (dd, *J* = 8.8, 5.3 Hz, 1H). ^{13}C NMR (101 MHz, $CDCl_3$) δ 175.97, 133.31, 132.89, 132.72, 127.91, 127.87, 127.85, 127.75, 127.14, 126.13, 125.81, 65.71, 34.97, 32.15, 17.60.
HRMS (TOF) m/z: 239.1079 ($M+H^+$); calc. for $C_{16}H_{15}O_2$: 239.1072.

(*E*)-1-Phenethyl-5-oxaspiro[2.4]heptan-4-one ((*E*)-12j)

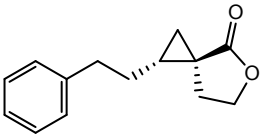

^{1}H NMR (400 MHz, $CDCl_3$) δ 7.31–7.26 (m, 2H), 7.23–7.13 (m, 3H), 4.36 (td, *J* = 9.0, 3.5 Hz, 1H), 4.18 (q, *J* = 8.6 Hz, 1H), 2.79–2.54 (m, 2H), 2.39 (dt, *J* = 12.5, 9.0 Hz, 1H), 2.09–1.83 (m, 3H), 1.30 (p, *J* = 7.4 Hz, 1H), 1.23–1.10 (m, 2H). ^{13}C NMR (101 MHz, $CDCl_3$) δ 178.51, 141.60, 128.71, 128.48, 126.02, 65.79, 35.82, 31.87, 30.36, 28.56, 24.18, 20.22.

(*Z*)-1-Phenethyl-5-oxaspiro[2.4]heptan-4-one ((*Z*)-12j)

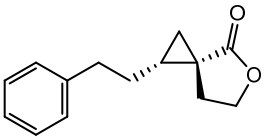

^{1}H NMR (400 MHz, $CDCl_3$) δ 7.32–7.26 (m, 2H), 7.24–7.15 (m, 3H), 4.37 (td, *J* = 8.6, 6.7 Hz, 1H), 4.20 (td, *J* = 8.7, 6.4 Hz, 1H), 2.83–2.68 (m, 2H), 2.17–2.05 (m, 2H), 1.74–1.59 (m, 2H), 1.51 (dq, *J* = 9.1, 6.8 Hz, 1H), 1.40 (dd, *J* = 9.1, 4.2 Hz, 1H), 0.60 (dd, *J* = 6.7, 4.2 Hz, 1H). ^{13}C NMR (101 MHz, $CDCl_3$) δ 180.22, 141.31, 128.51, 128.48, 126.13, 65.92, 35.64, 31.89, 25.59, 25.52, 24.17, 21.13.
HRMS (TOF) m/z: 217.1233 ($M+H^+$); calc. for $C_{14}H_{17}O_2$: 217.1229.

General procedure for the synthesis of α-thio-γ-lactone standard products:

To a 100 mL round-bottom flask was added (substituted) thiophenol (2.0 mmol, 1.0 equiv.), NaOMe (162 mg, 3.0 mmol, 1.5 equiv.) and dry MeOH (30 mL). The mixture was stirred at room temperature for 1 hour before 3-bromodihydrofuran-2(3*H*)-one (214 μL, 1.3 equiv.) was added in one portion. The reaction was stirred at room temperature for another 24 hours. Methanol was evaporated under reduced pressure. The crude mixture was then dissolved in DCM and washed with water. The aqueous phase was extracted by DCM (30 mL × 3). The combined organic layer was dried over Na_2SO_4, filtered, and concentrated under reduced pressure. Purification by silica column chromatography using hexane and ethyl acetate as eluents afforded racemic α-thio-γ-lactones in

50–80% yields.

3-(Phenylthio)dihydrofuran-2(3*H*)-one (14a)

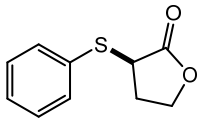

^{1}H NMR (400 MHz, $CDCl_3$) δ 7.61–7.50 (m, 2H), 7.39–7.29 (m, 3H), 4.31–4.17 (m, 2H), 3.86 (dd, *J* = 8.6, 6.2 Hz, 1H), 2.67 (dddd, *J* = 13.4, 8.7, 7.7, 6.6 Hz, 1H), 2.27 (ddt, *J* = 13.5, 7.4, 6.1 Hz, 1H). ^{13}C NMR (101 MHz, $CDCl_3$) δ 175.10, 133.73, 131.81, 129.40, 128.86, 66.62, 44.54, 30.10. HRMS (TOF) m/z: 195.0468 ($M+H^+$); calc. for $C_{10}H_{11}O_2S$: 195.0480.

3-((3-Methoxyphenyl)thio)dihydrofuran-2(3*H*)-one (14b)

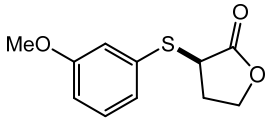

^{1}H NMR (400 MHz, $CDCl_3$) δ 7.28–7.21 (m, 1H), 7.12 (dt, *J* = 7.4, 1.6 Hz, 2H), 6.87 (ddd, *J* = 8.4, 2.3, 1.3 Hz, 1H), 4.31–4.20 (m, 2H), 3.88 (dd, *J* = 8.7, 6.4 Hz, 1H), 3.80 (s, 3H), 2.68 (dddd, *J* = 13.5, 8.7, 7.5, 6.6 Hz, 1H), 2.28 (ddt, *J* = 13.6, 7.4, 6.3 Hz, 1H). ^{13}C NMR (101 MHz, $CDCl_3$) δ 175.12, 160.00, 133.04, 130.17, 125.53, 118.46, 114.82, 66.65, 55.51, 44.53, 30.17. HRMS (TOF) m/z: 225.0564 ($M+H^+$); calc. for $C_{11}H_{13}O_3S$: 225.0585.

3-((4-Fluorophenyl)thio)dihydrofuran-2(3*H*)-one (14c)

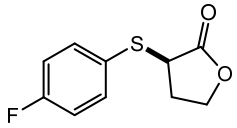

^{1}H NMR (400 MHz, $CDCl_3$) δ 7.57 (dd, *J* = 8.9, 5.3 Hz, 2H), 7.05 (dd, *J* = 8.9, 8.5 Hz, 2H), 4.31–4.17 (m, 2H), 3.77 (dd, *J* = 8.7, 6.2 Hz, 1H), 2.66 (dddd, *J* = 13.5, 8.7, 7.7, 6.6 Hz, 1H), 2.25 (ddt, *J* = 13.5, 7.4, 6.1 Hz, 1H). ^{13}C NMR (101 MHz, $CDCl_3$) δ 174.80, 163.41 (164.66, 162.17, d, *J* = 150.8 Hz), 136.72 (136.76, 136.67, d, *J* = 8.5 Hz), 126.49 (126.51, 126.48, d, *J* = 3.6 Hz), 116.49 (116.60, 116.39, d, *J* = 22.1 Hz), 66.43, 44.82 (44.83, 44.81, d, *J* = 1.4 Hz), 29.73. HRMS (FAB) m/z: 213.0386 ($M+H^+$); calc. for $C_{10}H_{10}O_2SF$: 213.0396.

3-((4-Chlorophenyl)thio)dihydrofuran-2(3*H*)-one (14d)

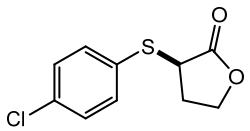

^{1}H NMR (400 MHz, $CDCl_3$) δ 7.50 (d, *J* = 8.6 Hz, 2H), 7.31 (d, *J* = 8.5 Hz, 2H), 4.27 (t, *J* = 6.9 Hz, 2H), 3.82 (dd, *J* = 8.7, 6.3 Hz, 1H), 2.74–2.62 (m, 1H), 2.25 (td, *J* = 13.4, 6.5 Hz, 1H). ^{13}C NMR (101 MHz, $CDCl_3$) δ 174.83, 135.31, 135.12, 130.26, 129.59, 66.59, 44.55, 29.93. HRMS (TOF) m/z: 229.0080 ($M+H^+$); calc. for $C_{10}H_{10}O_2SCl$: 229.0090.

3-((4-Bromophenyl)thio)dihydrofuran-2(3*H*)-one (14e)

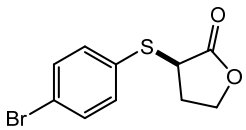

^{1}H NMR (400 MHz, $CDCl_3$) δ 7.53–7.36 (m, 4H), 4.28 (td, *J* = 7.0, 1.0 Hz, 2H), 3.83 (dd, *J* = 8.7, 6.4 Hz, 1H), 2.68 (ddtd, *J* = 14.1, 8.7, 7.0, 0.6 Hz, 1H), 2.25 (dqd, *J* = 13.4, 6.7, 1.1 Hz, 1H). ^{13}C NMR (101 MHz, $CDCl_3$) δ 174.81, 135.20, 132.54, 130.98, 123.40, 66.60, 44.43, 29.95. HRMS (TOF) m/z: 271.9518 ($M+H^+$); calc. for $C_{10}H_9O_2SBr$: 271.9507.

3-((4-Tolyl)thio)dihydrofuran-2(3*H*)-one (14f)

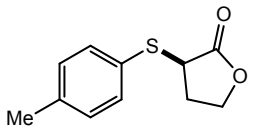

^{1}H NMR (400 MHz, $CDCl_3$) δ 7.46 (d, *J* = 8.1 Hz, 2H), 7.15 (d, *J* = 7.9 Hz, 2H), 4.27–4.15 (m, 2H), 3.78 (dd, *J* = 8.7, 6.0 Hz, 1H), 2.64 (dddd, *J* = 13.5, 8.7, 7.8, 6.7 Hz, 1H), 2.35 (s, 3H), 2.31–2.21 (m, 1H). ^{13}C NMR (101 MHz, $CDCl_3$) δ 175.19, 139.44, 134.52, 130.22, 127.85, 66.62, 44.82, 29.99, 21.38. HRMS (TOF) m/z: 209.0631 ($M+H^+$); calc. for $C_{11}H_{13}O_2S$: 209.0636.

3-((4-Isopropylphenyl)thio)dihydrofuran-2(3*H*)-one (14g)

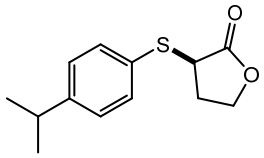

^{1}H NMR (400 MHz, $CDCl_3$) δ 7.49 (d, *J* = 8.3 Hz, 2H), 7.20 (d, *J* = 8.1 Hz, 2H), 4.28–4.14 (m, 2H), 3.80 (dd, *J* = 8.7, 6.1 Hz, 1H), 2.90 (hept, *J* = 7.0 Hz, 1H), 2.65 (dddd, *J* = 13.5, 8.7, 7.7, 6.6 Hz, 1H), 2.27 (ddt, *J* = 13.5, 7.4, 6.0 Hz, 1H), 1.24 (d, *J* = 7.0 Hz, 6H). ^{13}C NMR (101 MHz, $CDCl_3$) δ 175.25, 150.17, 134.42, 128.26, 127.60, 66.61, 44.80, 33.97, 30.10, 23.95. HRMS (TOF) m/z: 237.0931 ($M+H^+$); calc. for $C_{13}H_{17}O_2S$: 237.0949.

3-((4-(Trifluoromethyl)phenyl)thio)dihydrofuran-2(3*H*)-one (14h)

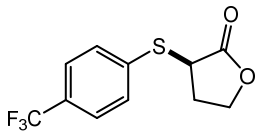

^{1}H NMR (400 MHz, $CDCl_3$) δ 7.63 (d, *J* = 8.3 Hz, 2H), 7.58 (d, *J* = 8.3 Hz, 2H), 4.36 (qdd, *J* = 9.1, 7.5, 6.2 Hz, 2H), 3.98 (dd, *J* = 8.7, 6.5 Hz, 1H), 2.75 (dddd, *J* = 13.7, 8.7, 7.5, 6.4 Hz, 1H), 2.29 (ddt, *J* = 13.7, 7.5, 6.3 Hz, 1H). ^{13}C NMR (101 MHz, $CDCl_3$) δ 174.48, 137.51, 131.68, 130.02 (130.51, 130.18, 129.86, 129.53, q, *J* = 32.3 Hz), 126.04 (126.09, 126.06, 126.02, 125.98, q, *J* = 3.8 Hz), 123.85 (127.90, 125.20, 122.49, 119.79, q, *J* = 273.1 Hz), 66.53, 43.48, 29.98. HRMS (FAB) m/z: 263.0347 ($M+H^+$); calc. for $C_{11}H_{10}O_2SF_3$: 263.0354.

3-((3,4-Dimethoxyphenyl)thio)dihydrofuran-2(3*H*)-one (14i)

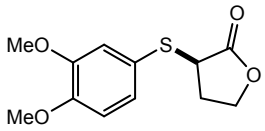

^{1}H NMR (400 MHz, $CDCl_3$) δ 7.19 (dd, *J* = 8.3, 2.1 Hz, 1H), 7.15 (d, *J* = 2.1 Hz, 1H), 6.85 (d, *J* = 8.3 Hz, 1H), 4.24 (ddd, *J* = 8.9, 7.8, 5.8 Hz, 1H), 4.15 (ddd, *J* = 8.9, 7.6, 6.5 Hz, 1H), 3.90 (s, 6H), 3.75 (dd, *J* = 8.8, 6.2 Hz, 1H), 2.66 (dddd, *J* = 13.4, 8.7, 7.8, 6.5 Hz, 1H), 2.28 (ddt, *J* = 13.5, 7.6, 6.0 Hz, 1H). ^{13}C NMR (101 MHz, $CDCl_3$) δ 175.41, 150.38, 149.20, 128.46, 121.81, 117.98, 111.50, 66.57, 56.16, 56.03, 45.26, 29.73. HRMS (TOF) m/z: 255.0707 ($M+H^+$); calc. for $C_{12}H_{15}O_4S$: 255.0691.

3-(Naphthalen-2-ylthio)dihydrofuran-2(3*H*)-one (14j)

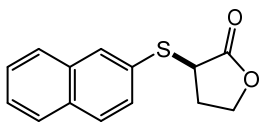

^{1}H NMR (400 MHz, Chloroform-*d*) δ 8.06 (d, *J* = 1.7 Hz, 1H), 7.85–7.78 (m, 3H), 7.60 (dd, *J* = 8.6, 1.9 Hz, 1H), 7.55–7.47 (m, 2H), 4.30–4.21 (m, 2H), 3.96 (dd, *J* = 8.7, 6.3 Hz, 1H), 2.74–2.64 (m, 1H), 2.36–2.27 (m, 1H). ^{13}C NMR (101 MHz, $CDCl_3$) δ 175.10, 133.67, 133.16, 133.07, 130.24, 129.13, 129.08, 127.86, 127.02, 126.89, 66.67, 44.58, 30.11. HRMS (TOF) m/z: 245.0619 ($M+H^+$); calc. for $C_{14}H_{13}O_2S$: 245.0636.

General procedure for the synthesis of organoborane standard products:

The preparation of racemic organoborane standard products follows the reported protocol

using rhodium acetate[277] or iodine[283] as catalyst for carbene B–H insertion. Iodine (10 mol%) or $Rh_2(OAc)_4$ (2 mol%) was added to the solution of NHC-BH_3 (1.0 equiv) in dichloromethane. The mixture was allowed to stir for 5 min. A solution of diazo compound (1.2 equiv) in dichloromethane was then added through a syringe pump. The reaction mixture was allowed to stir for 10 h. Quick filtration and further purification through a silica column using hexane:ethyl acetate (2:1 to 0:1) or hexane:(ethyl acetate:acetone 5:5) (2:1 to 0:1) elution system afforded the organoborane standard products.

Note: The ^{1}H NMR resonances of the B–H protons are broad (due to geminal coupling with boron) and generally in the range of 0.4–1.6 ppm. The ^{13}C NMR resonances of the boron-binding NHC quaternary carbons usually appear at around 170 ppm and are typically broad (due to germinal coupling with boron) and weak; these signals are sometimes not visible in the ^{13}C NMR spectra.

(1,3-Dimethyl-1*H*-imidazol-3-ium-2-yl)(2-oxotetrahydrofuran-3-yl)dihydroborate (20a)

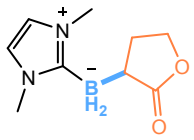

^{1}H NMR (400 MHz, $CDCl_3$) δ 6.83 (s, 2H), 4.45 (dddd, *J* = 10.7, 8.1, 6.8, 1.0 Hz, 1H), 4.27 (tq, *J* = 9.0, 1.1 Hz, 1H), 3.83–3.69 (m, 6H), 2.53–2.25 (m, 1H), 2.01–1.93 (m, 1H), 1.88–1.80 (m, 1H), 1.79–1.16 (m, 2H); ^{13}C NMR (101 MHz, $CDCl_3$) δ 187.91, 120.62, 67.86, 36.15, 30.86; ^{11}B NMR (128 MHz, $CDCl_3$) δ -27.08 (t, *J* = 89.6Hz). HRMS (FAB+) m/z: 193.1144 ((M+H$^+$)–H_2); calc. for $C_9H_{14}O_2N_2B$: 193.1148.

(2-Oxotetrahydrofuran-3-yl)(1,3,5-trimethyl-1*H*-imidazol-3-ium-2-yl)dihydroborate (20b)

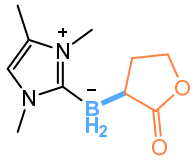

^{1}H NMR (400 MHz, $CDCl_3$) δ 6.57 (q, *J* = 1.1 Hz, 1H), 4.47 (ddd, *J* = 10.8, 8.2, 6.8 Hz, 1H), 4.28 (ddd, *J* = 9.0, 8.2, 1.8 Hz, 1H), 3.70 (s, 3H), 3.64 (s, 3H), 2.45–2.33 (m, 1H), 2.18 (d, *J* = 1.2 Hz, 3H), 2.00–1.92 (m, 1H), 1.89–1.59 (m, 2H), 1.49 – 1.11 (m, 1H); ^{13}C NMR (101 MHz, $CDCl_3$) δ 165.20, 128.29, 117.79, 67.89, 35.77, 32.59, 30.95, 9.67; ^{11}B NMR (128 MHz, $CDCl_3$) δ -26.77 (t, *J* = 89.4 Hz). HRMS (FAB+) m/z: 207.1317 ((M+H$^+$)–H_2); calc. for $C_{10}H_{16}O_2N_2B$: 207.1305.

(1,3-Dimethyl-5-(trifluoromethyl)-1*H*-imidazol-3-ium-2-yl)(2-oxotetrahydrofuran-3-yl)dihydroborate (20c)

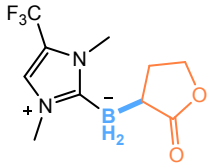

^{1}H NMR (400 MHz, $CDCl_3$) δ 7.28 (q, *J* = 1.3 Hz, 1H), 4.45 (ddd, *J* = 10.4, 8.3, 7.0 Hz, 1H), 4.29 (ddd, *J* = 8.9, 8.3, 2.2 Hz, 1H), 3.87 (d, *J* = 0.8 Hz, 3H), 3.81 (s, 3H), 2.51–2.32 (m, 1H), 2.07–1.65 (m, 3H), 1.59–1.10 (m, 1H); ^{13}C NMR (101 MHz, $CDCl_3$) δ 187.70, 122.82 (q, *J* = 4.2 Hz), 122.52 (q, *J* = 41.1 Hz), 119.39 (q, *J* = 268.7 Hz), 68.00, 36.81, 34.25, 34.23, 34.21, 34.19, 30.65; ^{11}B NMR (128 MHz, $CDCl_3$) δ -27.15 (t, *J* = 90.7 Hz). HRMS (FAB+) m/z: 261.1030 ((M+H$^+$)–H_2); calc. for $C_{10}H_{13}O_2N_2F_3B$: 261.1022.

(1-Ethyl-3-methyl-1*H*-imidazol-3-ium-2-yl)(2-oxotetrahydrofuran-3-yl)dihydroborate (20d)

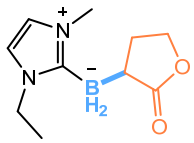

^{1}H NMR (400 MHz, $CDCl_3$) δ 6.88 (d, *J* = 2.0 Hz, 1H), 6.84 (d, *J* = 2.0 Hz, 1H), 4.45 (ddd, *J* = 10.8, 8.2, 6.8 Hz, 1H), 4.27 (ddd, *J* = 8.9, 8.2, 1.8 Hz, 1H), 4.24–4.09 (m, 2H), 3.76 (s, 3H), 2.50–2.29 (m, 1H), 2.02–1.66 (m, 3H), 1.61–1.13 (m, 1H), 1.40

(t, *J* = 7.3 Hz, 3H); ^{13}C NMR (101 MHz, $CDCl_3$) δ 187.77, 121.00, 118.45, 67.82, 43.72, 36.07, 30.93, 15.90; ^{11}B NMR (128 MHz, $CDCl_3$) δ -27.10 (t, *J* = 89.6 Hz). HRMS (FAB+) m/z: 207.1296 ((M+H$^+$)–H_2); calc. for $C_{10}H_{16}O_2N_2B$: 207.1305.

(3-Hexyl-1-methyl-1*H*-imidazol-3-ium-2-yl)(2-oxotetrahydrofuran-3-yl)dihydroborate (20e)

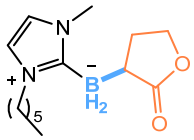

^{1}H NMR (400 MHz, $CDCl_3$) δ 6.86 (d, *J* = 1.9 Hz, 1H), 6.83 (d, *J* = 1.9 Hz, 1H), 4.45 (ddd, *J* = 10.8, 8.2, 6.8 Hz, 1H), 4.27 (ddd, *J* = 8.9, 8.2, 1.8 Hz, 1H), 4.17–4.01 (m, 2H), 3.76 (s, 3H), 2.48–2.31 (m, 1H), 2.13–1.64 (m, 5H), 1.58–1.14 (m, 7H), 0.88 (t, *J* = 7.0 Hz, 3H); ^{13}C NMR (101 MHz, $CDCl_3$) δ 187.77, 120.82, 119.03, 67.82, 48.85, 36.12, 31.46, 30.95, 30.65, 26.36, 22.61, 14.12; ^{11}B NMR (128 MHz, $CDCl_3$) δ -27.09 (t, *J* = 90.3 Hz). HRMS (FAB+) m/z: 263.1927 ((M+H$^+$)–H_2); calc. for $C_{14}H_{24}O_2N_2B$: 263.1931.

(1,3-Dimethyl-1*H*-imidazol-3-ium-2-yl)(2-oxotetrahydro-2*H*-pyran-3-yl)dihydroborate (20f)

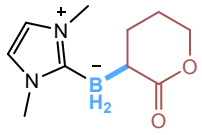

^{1}H NMR (400 MHz, $CDCl_3$) δ 6.80 (s, 2H), 4.46 (dddd, *J* = 11.0, 7.4, 3.7, 1.0 Hz, 1H), 4.26–4.19 (m, 1H), 3.74 (s, 6H), 2.14–1.95 (m, 3H), 1.89–1.75 (m, 1H), 1.71–1.55 (m, 2H), 1.51–1.15 (m, 1H); ^{13}C NMR (101 MHz, $CDCl_3$) δ 181.58, 120.48, 69.44, 36.10, 27.17, 22.39; ^{11}B NMR (128 MHz, $CDCl_3$) δ -24.71 (t, *J* = 90.4 Hz). HRMS (FAB+) m/z: 207.1330 ((M+H$^+$)–H_2); calc. for $C_{10}H_{16}O_2N_2B$: 207.1305.

(1-Ethyl-3-methyl-1*H*-imidazol-3-ium-2-yl)(2-oxotetrahydro-2*H*-pyran-3-yl)dihydroborate (20g)

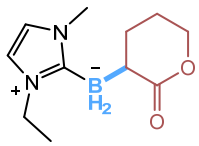

^{1}H NMR (400 MHz, $CDCl_3$) δ 6.86 (d, *J* = 2.0 Hz, 1H), 6.82 (d, *J* = 1.9 Hz, 1H), 4.46 (dddd, *J* = 10.8, 7.4, 3.7, 1.0 Hz, 1H), 4.26–4.10 (m, 3H), 3.75 (s, 3H), 2.14–1.94 (m, 3H), 1.86–1.74 (m, 1H), 1.70–1.10 (m, 3H), 1.43–1.38 (m, 3H); ^{13}C NMR (101 MHz, $CDCl_3$) δ 181.45, 120.88, 118.29, 69.42, 43.64, 36.02, 27.22, 22.40, 15.88; ^{11}B NMR (128 MHz, $CDCl_3$) δ -24.73 (t, *J* = 90.4 Hz). HRMS (FAB+) m/z: 221.1452 ((M+H$^+$)–H_2); calc. for $C_{11}H_{18}O_2N_2B$: 221.1461.

(1,3-Dimethyl-5-(trifluoromethyl)-1*H*-imidazol-3-ium-2-yl)(2-oxotetrahydro-2*H*-pyran-3-yl)dihydroborate (20h)

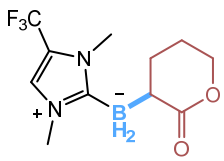

^{1}H NMR (400 MHz, $CDCl_3$) δ 7.26 (s, 1H), 4.43 (dddd, *J* = 10.7, 7.1, 3.7, 1.1 Hz, 1H), 4.30–4.19 (m, 1H), 3.90–3.82 (m, 3H), 3.79 (s, 3H), 2.13–1.96 (m, 3H), 1.90–1.59 (m, 3H), 1.54–1.11 (m, 1H); ^{13}C NMR (101 MHz, $CDCl_3$) δ 181.22, 122.70 (q, *J* = 4.1 Hz), 122.32 (q, *J* = 40.8 Hz), 119.44 (q, *J* = 267.6 Hz), 69.76, 36.71, 34.14, 34.12, 27.29, 22.32; ^{11}B NMR (128 MHz, $CDCl_3$) δ -24.93 (t, *J* = 91.3 Hz). HRMS (FAB+) m/z: 275.1170 ((M+H$^+$)–H_2); calc. for $C_{11}H_{15}O_2N_2F_3B$: 275.1179.

B.5 Enzymatic preparation of lactone-carbene C–H insertion products

General procedure for enzymatic synthesis of β-amino lactone products:

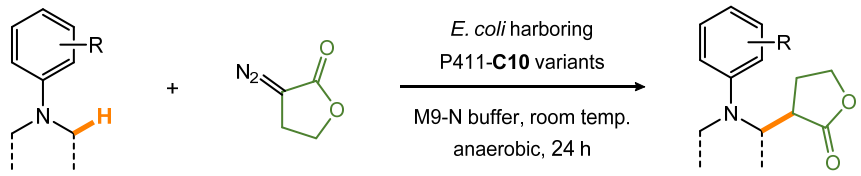

To 50-mL falcon tubes were added a suspension of *E. coli* expressing P411-**C10** variant (OD_{600} = 60, 30 mL), **LAD** (0.1–0.5 mmol), aniline derivative (1.2 equiv.), D-glucose (~20 mM), M9-N buffer/EtOH (~20:1 v/v) under anaerobic conditions. The tubes were capped and shaken (600 rpm) inside an anaerobic chamber at room temperature for 20–24 h. After the reaction was completed, the reaction mixture was transferred to 500 mL centrifuge bottle, and ~100 mL of hexane/ethyl acetate (1:1) mixed solvent was added. After the bottle was capped, it was shaken vigorously and centrifuged (6,000 × g, 6 min). The organic layer was separated, and the aqueous layer was subjected to three more rounds of extraction. The organic layers were combined, dried over Na_2SO_4 and concentrated under reduced pressure. Purification by silica column chromatography with hexane/ethyl acetate afforded the desired β-amino lactone products.

Notes: 1. **C10** variants (usually the most active and/or selective ones) were chosen for each substrate according to the plate screening result, and substrate loading in each reaction was based on rough estimation of the enzymes' activity in plate screening. 2. Total turnovers or yields were not accurately quantified (yields are in the range of 30–80%). The products isolated from these preparative-scale enzymatic reactions were further used for HPLC calibration curves and quantification of analytical-scale reactions. 3. The absolute configuration of the β-amino lactone products was not determined.

3-((Methyl(*p*-tolyl)amino)methyl)dihydrofuran-2(3*H*)-one (16a)

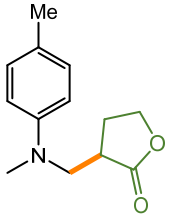

Product **16a** was synthesized using variant **L4**. ^{1}H NMR (400 MHz, $CDCl_3$) δ 7.07 (d, *J* = 8.2 Hz, 2H), 6.68 (d, *J* = 8.7 Hz, 2H), 4.35 (td, *J* = 8.8, 2.6 Hz, 1H), 4.15 (ddd, *J* = 10.0, 9.1, 6.6 Hz, 1H), 3.94 (dd, *J* = 15.1, 4.5 Hz, 1H), 3.43 (dd, *J* = 15.1, 8.0 Hz, 1H), 2.96 (s, 3H), 2.91 (dddd, *J* = 10.6, 8.6, 8.0, 4.5 Hz, 1H), 2.34 (dddd, *J* = 12.7, 9.0, 6.6, 2.6 Hz, 1H), 2.26 (s, 3H), 2.12 (dtd, *J* = 12.7, 10.2, 8.6 Hz, 1H). ^{13}C NMR (101 MHz, $CDCl_3$) δ 178.48, 146.77, 130.03, 126.65, 113.06, 66.74, 53.31, 39.56, 38.67, 28.10, 20.36. HRMS (TOF) m/z: 220.1311 ($M+H^+$); calc. for [$C_{13}H_{17}NO_2+H^+$]: 220.1332.

3-(((4-Methoxyphenyl)(methyl)amino)methyl)dihydrofuran-2(3*H*)-one (16b)

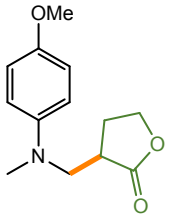

Product **16b** was synthesized using variant **L6**. ^{1}H NMR (400 MHz, $CDCl_3$) δ 6.85 (d, *J* = 9.1 Hz, 2H), 6.75 (d, *J* = 7.9 Hz, 2H), 4.34 (td, *J* = 8.8, 2.6 Hz, 1H), 4.15 (ddd, *J* = 9.8, 9.1, 6.7 Hz, 1H), 3.86 (dd, *J* = 14.8, 4.3 Hz, 1H), 3.76 (s, 3H), 3.37 (dd, *J* = 14.8, 8.3 Hz, 1H), 2.92 (s, 3H), 2.90–2.82 (m, 1H), 2.34 (dddd, *J* = 11.3, 8.9, 6.7, 2.6 Hz, 1H), 2.18–2.04 (m, 1H). ^{13}C NMR (101 MHz, $CDCl_3$) δ 178.48, 118.03, 115.22, 115.00, 114.74, 66.74, 55.86, 54.34, 40.16, 38.56, 28.23. HRMS (TOF) m/z: 236.1288 ($M+H^+$); calc. for [$C_{13}H_{17}NO_3+H^+$]: 236.1281.

3-(((4-Chlorophenyl)(methyl)amino)methyl)dihydrofuran-2(3*H*)-one (16c)

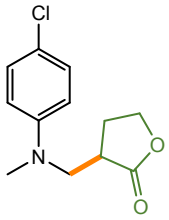

Product **16c** was synthesized using variant **L7**. ^{1}H NMR (400 MHz, $CDCl_3$) δ 7.18 (d, *J* = 9.1 Hz, 2H), 6.65 (d, *J* = 9.1 Hz, 2H), 4.35 (td, *J* = 8.8, 2.4 Hz, 1H), 4.16 (ddd, *J* = 10.1, 9.1, 6.6 Hz, 1H), 3.93 (dd, *J* = 15.3, 4.7 Hz, 1H), 3.46 (dd, *J* = 15.2, 7.7 Hz, 1H), 2.97 (s, 3H), 2.89 (dddd, *J* = 10.8, 8.8, 7.7, 4.8 Hz, 1H), 2.35 (dddd, *J* = 12.6, 8.8, 6.5, 2.4 Hz, 1H), 2.09 (dddd, *J* = 12.6, 10.8, 10.1, 8.6 Hz, 1H). ^{13}C NMR (101 MHz, $CDCl_3$) δ 178.13, 147.35, 129.25, 122.10, 113.70, 66.67, 53.01, 39.51, 38.65, 27.96. HRMS (TOF) m/z: 240.0785 ($M+H^+$); calc. for [$C_{12}H_{14}ClNO_2+H^+$]: 240.0786.

3-((Methyl(*m*-tolyl)amino)methyl)dihydrofuran-2(3*H*)-one (16d)

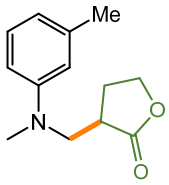

Product **16d** was synthesized using variant **L9**. ^{1}H NMR (400 MHz, $CDCl_3$) δ 7.14 (dd, *J* = 9.1, 7.4 Hz, 1H), 6.67–6.52 (m, 3H), 4.36 (td, *J* = 8.8, 2.5 Hz, 1H), 4.16 (ddd, *J* = 10.0, 9.1, 6.6 Hz, 1H), 3.98 (dd, *J* = 15.2, 4.6 Hz, 1H), 3.46 (dd, *J* = 15.2, 7.9 Hz, 1H), 2.99 (s, 3H), 2.94 (dddd, *J* = 10.7, 8.8, 8.0, 4.6 Hz, 1H), 2.41–2.33 (m, 1H), 2.32 (s, 3H), 2.13 (dddd, *J* = 12.7, 10.7, 10.0, 8.5 Hz, 1H). ^{13}C NMR (101 MHz, $CDCl_3$) δ 178.40, 148.86, 139.25, 129.35, 118.19, 113.36, 109.84, 66.72, 52.94, 39.42, 38.77, 28.02, 22.07. HRMS (TOF) m/z: 220.1341 ($M+H^+$); calc. for [$C_{13}H_{17}NO_2+H^+$]: 220.1332.

3-((Methyl(phenyl)amino)methyl)dihydrofuran-2(3*H*)-one (16e)

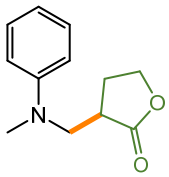

Product **16e** was synthesized using variant **L6**. ^{1}H NMR (400 MHz, $CDCl_3$) δ 7.29–7.22 (m, 3H), 6.75 (dtt, *J* = 7.3, 1.9, 1.0 Hz, 3H), 4.36 (td, *J* = 8.8, 2.6 Hz, 1H), 4.16 (ddd, *J* = 9.9, 9.1, 6.6 Hz, 1H), 3.98 (dd, *J* = 15.2, 4.5 Hz, 1H), 3.48 (dd, *J* = 15.2, 7.8 Hz, 1H), 3.00 (s, 3H), 2.93 (dddd, *J* = 10.8, 8.8, 7.9, 4.6 Hz, 1H), 2.36 (dddd, *J* = 12.6, 8.9, 6.6, 2.5 Hz, 1H), 2.13 (dddd, *J* = 12.7, 10.7, 10.0, 8.5 Hz, 1H). ^{13}C NMR (101 MHz, $CDCl_3$) δ 178.37, 148.79, 129.52, 117.24, 112.61, 66.73, 52.96, 39.38, 38.78, 28.03. HRMS (TOF) m/z: 206.1167 ($M+H^+$); calc. for [$C_{12}H_{15}NO_2+H^+$]: 206.1176.

3-((Methyl(*o*-tolyl)amino)methyl)dihydrofuran-2(3*H*)-one (16f)

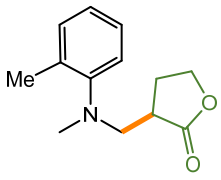

Product **16f** was synthesized using variant **L9**. ^{1}H NMR (400 MHz, $CDCl_3$) δ 7.24–7.17 (m, 2H), 7.14 (d, *J* = 7.8 Hz, 1H), 7.04 (td, *J* = 7.3, 1.5 Hz, 1H), 4.35 (td, *J* = 8.8, 3.0 Hz, 1H), 4.17 (ddd, *J* = 9.6, 9.1, 6.9 Hz, 1H), 3.62 (dd, *J* = 12.9, 4.2 Hz, 1H), 3.00 (dd, *J* = 12.9, 10.3 Hz, 1H), 2.78 (tdd, *J* = 10.1, 8.8, 4.3 Hz, 1H), 2.69 (s, 3H), 2.33 (s, 3H), 2.32 – 2.24 (m, 1H), 2.12 (dtd, *J* = 12.9, 9.8, 8.6 Hz, 1H). ^{13}C NMR (101 MHz, $CDCl_3$) δ 178.66, 150.84, 133.89, 131.35, 126.82, 124.10, 120.95, 66.97, 55.95, 43.43, 38.63, 28.13, 18.12. HRMS (TOF) m/z: 220.1332 ($M+H^+$); calc. for [$C_{13}H_{17}NO_2+H^+$]: 220.1332.

3-((Ethyl(pheny)amino)methyl)dihydrofuran-2(3*H*)-one (16g)

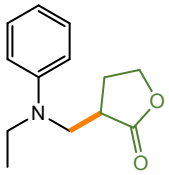

Product **16g** was synthesized using variants **L9** and **L10**. ^{1}H NMR (400 MHz, $CDCl_3$) δ 7.29 – 7.20 (m, 3H), 6.82–6.64 (m, 3H), 4.36 (td, *J* = 8.8, 2.5 Hz, 1H), 4.16 (ddd, *J* = 9.9, 9.1, 6.6 Hz, 1H), 3.91 (dd, *J* = 15.1, 4.6 Hz, 1H), 3.55–3.30 (m, 3H), 2.93 (tdd, *J* = 10.8, 8.3, 4.6 Hz, 1H), 2.38 (dddd, *J* = 12.5, 8.9, 6.6, 2.5 Hz, 1H), 2.13 (dtd, *J* = 12.6, 10.3, 8.7 Hz, 1H), 1.15 (t, *J* = 7.0 Hz, 3H). ^{13}C NMR (101 MHz, $CDCl_3$) δ 178.47, 147.63, 129.56, 117.01, 112.97, 66.77, 50.65, 46.17, 39.10, 28.00, 12.21. HRMS (TOF) m/z: 220.1311 ($M+H^+$); calc. for [$C_{13}H_{17}NO_2+H^+$]: 220.1332.

3-(1-(Methyl(phenyl)amino)ethyl)dihydrofuran-2(3*H*)-one (16g')

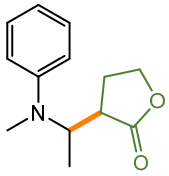

Product **16g'** was observed in the enzymatic reaction using variant **L10** and was obtained in a mixture form with a side product **16g"** (via N–H insertion after demethylation, see **Fig. 3.11.b**). ^{1}H NMR (400 MHz, $CDCl_3$) δ 7.31–7.21 (m, 2H), 6.91–6.70 (m, 3H), 4.57 (dd, *J* = 8.8, 11.1 Hz, 2H), 4.35 (td, *J* = 8.7, 3.1 Hz, 1H), 4.14 (td, *J* = 9.2, 7.1 Hz, 1H), 2.91 (td, *J* = 9.8, 3.9 Hz, 1H), 2.80 (s, 3H), 2.37–2.18 (m, 2H), 1.31 (d, *J* = 6.9 Hz, 3H). HRMS (TOF) m/z: 220.1342 ($M+H^+$); calc. for [$C_{13}H_{17}NO_2+H^+$]: 220.1332.

3-(1-(Ethyl(phenyl)amino)ethyl)dihydrofuran-2(3*H*)-one (16h)

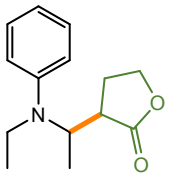

Product **16h** was synthesized with a diastereomeric ratio of 16:1 using variant **L9**. Further silica column purification using dichloromethane/acetone/hexane as eluent was able to afford the pure major diastereomer. ^{1}H NMR (400 MHz, $CDCl_3$) δ 7.30–7.21 (m, 3H), 6.85 (dd, *J* = 9.0, 1.1 Hz, 2H), 6.76 (tt, *J* = 7.3, 1.0 Hz, 1H), 4.51 (qd, *J* = 6.9, 3.7 Hz, 1H), 4.35 (td, *J* = 8.8, 2.6 Hz, 1H), 4.13 (ddd, *J* = 9.8, 8.9, 6.9 Hz, 1H), 3.37 – 3.18 (m, 2H), 2.93 (ddd, *J* = 10.8, 9.1, 3.7 Hz, 1H), 2.37–2.25 (m, 1H), 2.25–2.15 (m, 1H), 1.31 (d, *J* = 6.9 Hz, 3H), 1.15 (t, *J* = 7.0 Hz, 3H). ^{13}C NMR (101 MHz, $CDCl_3$) δ 178.12, 147.76, 129.57, 117.65, 114.35, 66.51, 52.38, 42.43, 39.62, 24.27, 14.65, 14.55. HRMS (TOF) m/z: 234.1483 ($M+H^+$); calc. for [$C_{14}H_{19}NO_2+H^+$]: 234.1489.

3-(1-Phenylpyrrolidin-2-yl)dihydrofuran-2(3*H*)-one (16i)

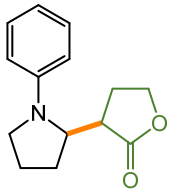

Product **16i** was synthesized with a diastereomeric ratio of 9:1 using variant **L9**. The major diastereomer: ^{1}H NMR (400 MHz, $CDCl_3$) δ 7.33–7.22 (m, 2H), 6.81–6.62 (m, 3H), 4.47 (dt, *J* = 7.9, 3.7 Hz, 1H), 4.38 (ddd, *J* = 9.0, 6.5, 4.6 Hz, 1H), 4.17–4.08 (m, 1H), 3.57 (ddd, *J* = 9.2, 6.9, 5.6 Hz, 1H), 3.41 (td, *J* = 9.9, 3.9 Hz, 1H), 3.34–3.25 (m, 1H), 2.36–2.19 (m, 1H), 2.18–1.99 (m, 4H), 1.81 (dtd, *J* = 12.7, 6.2, 3.5 Hz, 1H). ^{13}C NMR (101 MHz, $CDCl_3$) δ 178.13, 146.67, 129.55, 116.89, 112.90, 66.73, 56.78, 49.63, 41.16, 27.89, 24.36, 23.91. HRMS (TOF) m/z: 232.1321 ($M+H^+$); calc. for [$C_{14}H_{17}NO_2+H^+$]: 232.1332.

3-(1-(3-Chlorophenyl)pyrrolidin-2-yl)dihydrofuran-2(3*H*)-one (16j)

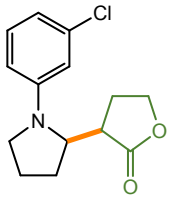

Product **16j** was synthesized with a diastereomeric ratio of 9:1 using variant **L9**. The major diastereomer: ^{1}H NMR (400 MHz, $CDCl_3$) δ 7.14 (t, *J* = 8.1 Hz, 1H), 6.69 (ddd, *J* = 7.8, 1.9, 0.8 Hz, 1H), 6.62 (t, *J* = 2.2 Hz, 1H), 6.54 (ddd, *J* = 8.4, 2.5, 0.8 Hz, 1H), 4.44–4.38 (m, 1H), 4.38–4.25 (m, 1H), 4.13 (td, *J* = 9.0, 8.0 Hz, 1H), 3.50 (ddd, *J* = 9.3, 7.0, 5.7 Hz, 1H), 3.34 (td, *J* = 10.0, 4.0 Hz, 1H), 3.26 (dt, *J* = 9.3, 7.4 Hz, 1H), 2.36–2.18 (m, 1H), 2.16–1.95 (m, 4H), 1.83–1.74 (m, 1H). ^{13}C NMR (101 MHz, $CDCl_3$) δ 177.81, 147.66, 135.38, 130.42, 116.75, 112.78, 111.00, 66.67, 56.85, 49.65, 41.04, 27.90, 24.25, 23.86. HRMS (TOF) m/z: 266.0937 ($M+H^+$); calc. for [$C_{14}H_{16}ClNO_2+H^+$]: 266.0942.

3-(1-(2,3-Dimethylphenyl)pyrrolidin-2-yl)dihydrofuran-2(3*H*)-one (16k)

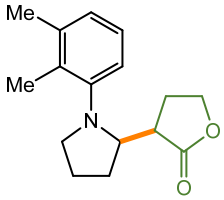

Product **16k** was synthesized with a diastereomeric ratio of 1:1.6 using variant **L9**. The diastereomers can be easily separated by silica chromatography.

Major diastereomer (**16k2**): ^{1}H NMR (400 MHz, $CDCl_3$) δ 7.04 (d, *J* = 4.6 Hz, 2H), 6.88 (t, *J* = 4.3 Hz, 1H), 4.14–4.02 (m, 3H), 3.51–3.42 (m, 1H), 2.77–2.68 (m, 1H), 2.62 (td, *J* = 9.0, 5.3 Hz, 1H), 2.39–2.27 (m, 1H), 2.26 (s, 3H), 2.23 (s, 3H), 2.19–2.04 (m, 2H), 2.00–1.82 (m, 3H). ^{13}C NMR (101 MHz, $CDCl_3$) δ 178.08, 149.05, 138.00, 132.78, 125.94, 125.31, 118.85, 66.71, 60.32, 56.02, 44.40, 31.13, 25.56, 24.45, 20.83, 14.59. HRMS (TOF) m/z: 260.1631 ($M+H^+$); calc. for [$C_{16}H_{21}NO_2+H^+$]: 260.1645.

Minor diastereomer (**16k1**): ^{1}H NMR (400 MHz, $CDCl_3$) δ 7.12–7.02 (m, 2H), 6.91 (dd, *J* = 6.7, 1.7 Hz, 1H), 4.29 (td, *J* = 9.1, 3.0 Hz, 1H), 4.14 (ddd, *J* = 8.0, 7.3, 4.7 Hz, 1H), 4.08 (td, *J* = 9.3, 7.4 Hz, 1H), 3.45 (ddd, *J* = 9.1, 7.3, 5.5 Hz, 1H), 2.91 (td, *J* = 9.7, 4.6 Hz, 1H), 2.65 (ddd, *J* = 9.1, 7.9, 6.6 Hz, 1H), 2.27 (s, 3H), 2.23–2.05 (m, 5H), 1.99–1.82 (m, 3H), 1.71–1.61 (m, 1H). ^{13}C NMR (101 MHz, $CDCl_3$) δ 178.88, 146.87, 138.26, 132.69, 126.03, 125.29, 117.37, 67.16, 58.57, 54.78, 40.52, 26.16, 23.61, 23.02, 20.80, 14.36. HRMS (TOF) m/z: 260.1628 ($M+H^+$); calc. for [$C_{16}H_{21}NO_2+H^+$]: 260.1645.

3-(1-(4-Methoxyphenyl)pyrrolidin-2-yl)dihydrofuran-2(3*H*)-one (16l)

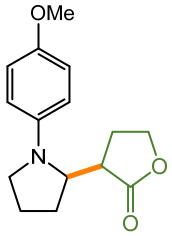

Product **16l** was synthesized using variant **L7** (with a diastereomeric ratio of 1.4:1) and **L9** (with a diastereomeric ratio of 4:1). The major diastereomer: ^{1}H NMR (400 MHz, $CDCl_3$) δ 6.86 (d, *J* = 9.1 Hz, 2H), 6.65 (d, *J* = 9.1 Hz, 2H), 4.35 (ddd, *J* = 8.7, 7.1, 4.4 Hz, 2H), 4.17–4.07 (m, 1H), 3.76 (s, 3H), 3.53 (ddd, *J* = 8.9, 6.7, 5.6 Hz, 1H), 3.32 (td, *J* = 9.9, 4.0 Hz, 1H), 3.19 (dt, *J* = 8.8, 7.4 Hz, 1H), 2.33–1.91 (m, 5H), 1.81–1.70 (m, 1H). ^{13}C NMR (101 MHz, $CDCl_3$) δ 178.33, 151.78, 141.48, 115.21, 114.20, 66.79, 57.28, 55.99, 50.53, 41.28, 27.85, 24.44, 23.82. HRMS (TOF) m/z: 262.1421 ($M+H^+$); calc. for [$C_{15}H_{19}NO_3+H^+$]: 262.1438.

3-(1-Phenylazetidin-2-yl)dihydrofuran-2(3*H*)-one (16m)

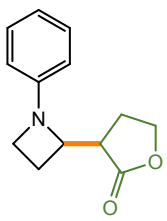

Product **16m** was synthesized with a diastereomeric ratio of >20:1 using variant **L10**. ^{1}H NMR (400 MHz, $CDCl_3$) δ 7.25–7.19 (m, 2H), 6.78 (tt, *J* = 7.4, 1.1 Hz, 1H), 6.57–6.42 (m, 2H), 4.63 (ddd, *J* = 8.3, 7.0, 5.0 Hz, 1H), 4.45 (td, *J* = 9.0, 3.0 Hz, 1H), 4.29 (td, *J* = 9.3, 7.2 Hz, 1H), 3.95 (ddd, *J* = 8.9, 7.1, 4.1 Hz, 1H), 3.67 (dt, *J* = 8.8, 7.3 Hz,

1H), 3.30 (td, *J* = 9.7, 5.1 Hz, 1H), 2.63–2.51 (m, 1H), 2.43–2.31 (m, 2H), 2.21 (ddt, *J* = 11.4, 8.8, 7.2 Hz, 1H). ^{13}C NMR (101 MHz, $CDCl_3$) δ 176.93, 151.30, 129.28, 118.40, 111.82, 67.28, 62.19, 50.18, 43.12, 23.63, 18.92. HRMS (TOF) m/z: 218.1183 ($M+H^+$); calc. for [$C_{13}H_{15}NO_2+H^+$]: 218.1176.

3-(1-(3-Chloro-4-fluorophenyl)pyrrolidin-2-yl)dihydrofuran-2(3*H*)-one (16n)

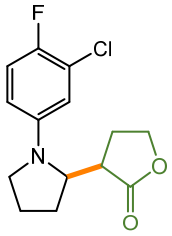

Product **16n** was synthesized with a diastereomeric ratio of 13:1 using variant **L9**. The major diastereomer: ^{1}H NMR (400 MHz, $CDCl_3$) δ 7.01 (t, *J* = 8.9 Hz, 1H), 6.63 (dd, *J* = 6.1, 3.0 Hz, 1H), 6.48 (dt, *J* = 9.1, 3.4 Hz, 1H), 4.40–4.31 (m, 2H), 4.14 (td, *J* = 8.9, 7.9 Hz, 1H), 3.49 (ddd, *J* = 9.1, 7.1, 5.5 Hz, 1H), 3.28 (td, *J* = 9.9, 4.0 Hz, 1H), 3.21 (dt, *J* = 9.1, 7.4 Hz, 1H), 2.30–2.18 (m, 1H), 2.13–1.97 (m, 4H), 1.83–1.73 (m, 1H). ^{13}C NMR (101 MHz, $CDCl_3$) δ 177.80, 150.72 (d, *J* = 239.4 Hz), 143.81 (d, *J* = 2.0 Hz), 121.48 (d, *J* = 18.4 Hz), 117.05 (d, *J* = 21.8 Hz), 114.02, 111.82 (d, *J* = 6.1 Hz), 66.69, 57.22, 50.19, 41.06, 27.98, 24.36, 23.81. HRMS (TOF) m/z: 284.0839 ($M+H^+$); calc. for [$C_{14}H_{15}FClNO_2+H^+$]: 284.0848.

B.5 Analysis of biotransformations for strained carbocycle construction

B.5.1 Enzymatic synthesis of *spiro*[2.4]lactones

All enzymatic reactions for *spiro*[2.4]-lactone formation in analytical scale were conducted following the general procedure described below and analyzed with gas chromatography (GC). All TTNs for the different products were determined using the GC standard curve of the corresponding racemic standard product made with $Rh_2(OAc)_4$.

All enzymatic reactions for *spiro*[2.4]-lactone formation in preparative scale were conducted following the general procedure described below and the corresponding *spiro*[2.4]-lactone products were isolated. Detailed conditions for preparative-scale reactions of different substrates are indicated separately.

General procedure for preparative-scale reactions:

To a 40 mL vial or 250 mL flask were added degassed suspension of *E. coli* expressing P411-**G8S** variant (OD_{600} = 20–30), olefin (0.25–2.0 mmol), **LAD** (1.0 equiv.), D-glucose (10–15 mM, 250 mM stock in M9-N), 1–5 vol% EtOH, M9-N buffer (pH 7.4) under anaerobic conditions. The vial or flask was capped and shaken (420 rpm for vials and 250 rpm for flasks) at room temperature for 12 h.

After the reaction was completed, 35 mL portions of preparative-scale reaction mixture were transferred to 50 mL centrifuge tubes. The reaction container was washed with water (2 mL × 2) followed by mixed organic solvent (hexane/ethyl acetate = 1:1, 2 mL × 3). The washing solution was combined with the reaction mixture in the centrifuge tubes. An additional 12 mL of hexane / ethyl acetate solvent was added to every tube. After the tube (with ~48 mL mixture in total) was capped, it was vortexed (1 min × 3) and shaken vigorously, and centrifuged (12,000 × g, 5 min). The organic layer was separated and the aqueous layer was subjected to three more rounds of extraction. The organic layers were combined, dried over Na_2SO_4 and concentrated under reduced pressure. Purification by silica column chromatography with hexane/ethyl acetate as eluent afforded the desired *spiro*[2.4]-lactones. TTNs were calculated based on measured protein concentration and isolated product yield.

(1*S*, 2*S*)-1-Phenyl-5-oxaspiro[2.4]heptan-4-one (12a)

Analysis Data (10 mM **11a**):

Entries	Pdt	Std	Pdt/Std	[Pdt]/mM	[PC]/μM	TTN	Avg. TTN
12a-(1)	6096.9	679.8	8.969	4.54	1.32	3445	
12a-(2)	5411.4	645.4	8.384	4.25	1.32	3230	
12a-(3)	5192.7	627.3	8.278	4.20	1.32	3191	
12a-(4)	5137.1	619.8	8.288	4.21	1.32	3194	3265
12a-(5)	31945	3196	9.995	5.03	1.62	3103	
12a-(6)	29685	3210	9.248	4.67	1.62	2882	
12a-(7)	28300	3177	8.908	4.51	1.62	2781	
12a-(8)	28124	3037	9.260	4.68	1.62	2886	2913

Chiralpak OJ-H, 20% *i*-PrOH in hexane, 1.0 mL/min, 24 °C, 235 nm

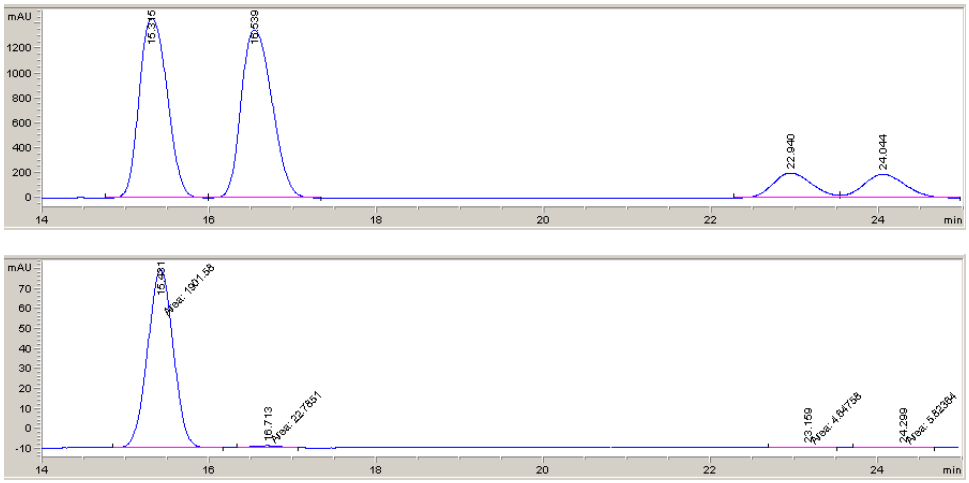

***rac*-*Z*- and *E*-12a**			**(1*S*, 2*S*)-12a**		
Retention Time (min)	Area (mAU*s)	Area %	Retention Time (min)	Area (mAU*s)	Area %
15.315 (*E*)	33379.8	41.30	15.431	1901.6	98.60
16.539 (*E*)	34416.7	42.58	16.713	16.7	0.86
22.940 (*Z*)	6497.4	8.04	23.159	4.6	0.24
24.044 (*Z*)	6536.8	8.08	24.299	5.8	0.30
Total	80830.7	100.00	Total	1928.7	100.00

(1*S*, 2*S*)-1-(4-Methoxyphenyl)-5-oxaspiro[2.4]heptan-4-one (12b)

Analysis Data (10 mM **11b**):

Entries	Pdt	Std	Pdt/Std	[Pdt]/mM	[PC]/μM	TTN	Avg. TTN
12b-(1)	46399	2981	15.565	8.53	0.81	10524	
12b-(2)	48120	2993	16.078	8.78	0.81	10838	
12b-(3)	46572	3013	15.457	8.47	0.81	10457	
12b-(4)	46397	3128	14.833	8.16	0.81	10072	10473

Preparative-scale reaction:

***E. coli* suspension expressing P411-G8S in M9-N**				***D*-glucose in M9-N**	
OD_{600}	volume/mL	[PC]/μM	n_pro/μmol	volume/mL	[Glu]/mM
28	32.0	2.618	0.0877	2.0	~15
olefin (11b) stock in EtOH			**LAD stock in EtOH**		
stock/M	volume/μL	n_1/mmol	stock/M	volume/μL	n_2/mmol
2.0	400	0.80	1.0	800	0.80
purification eluent		**Product**			
Ethyl acetate in hexanes (0% to 25% gradient)		m[Pdt]/mg	n[Pdt]/mmol	yield	TTN
		124.3	0.600	71%	6500

Note: [PC] = protein concentration in original cell suspension, n_pro = amount of protein in the reaction, [Glu] = *D*-glucose concentration in reaction mixture, n_1 = amount of olefin in the reaction, n_2 = amount of **LAD** in the reaction, m[Pdt] = mass of product isolated, n[Pdt] = amount of product. The same for the following tables.

Optical rotation: $[\alpha]^{23}_{D} = -159.9 \pm 0.3°$ (*c* 0.6, ethyl acetate).

Chiralpak IA, 8% *i*-PrOH in hexane, 1.2 mL/min, 32 °C, 235 nm

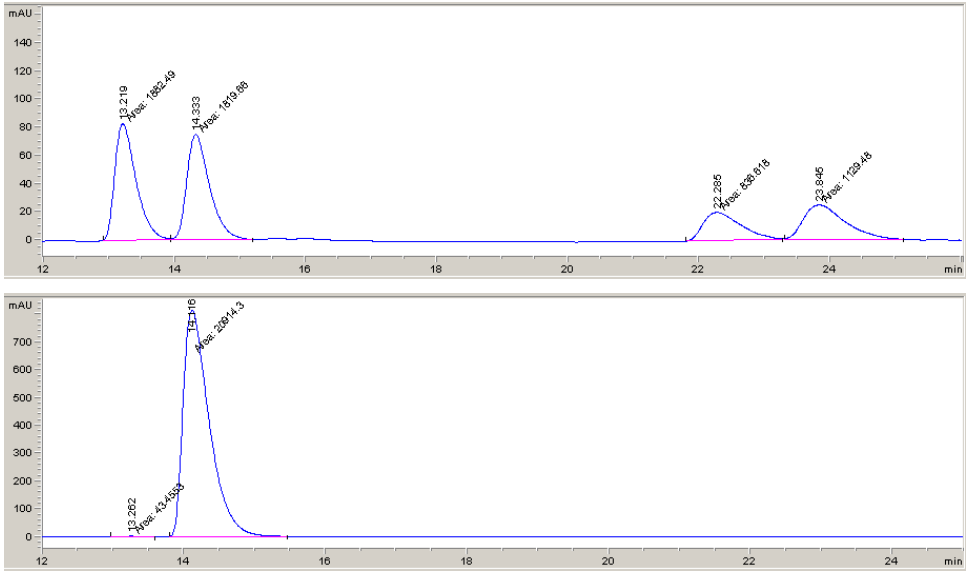

***rac*-*Z*- and *E*-12b**			**(1*S*, 2*S*)-12b**		
Retention Time (min)	Area (mAU*s)	Area %	Retention Time (min)	Area (mAU*s)	Area %
13.219 (*E*)	1862.5	32.97	13.262	43.5	0.20
14.333 (*E*)	1819.7	32.22	14.116	20914.3	99.80
22.285 (*Z*)	836.6	14.81	-	-	-
23.845 (*Z*)	1129.5	20.00	-	-	-
Total	5648.3	100.00	Total	20957.8	100.00

Crystal structure information of **12b**:

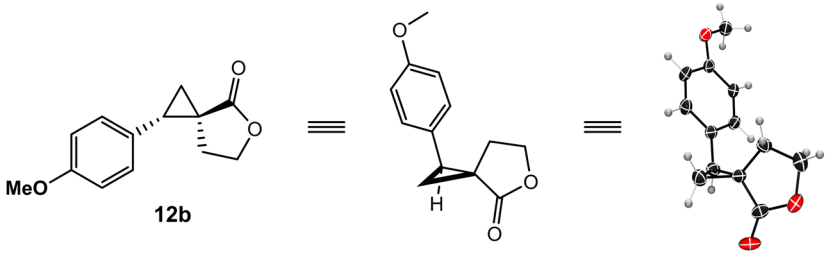

Identification code	v18081
Empirical formula	$C_{13}H_{14}O_3$
Formula weight	218.24
Temperature	175 K
Wavelength	1.54178 Å
Crystal system	Orthorhombic
Space group	$P2_12_12_1$
Unit cell dimensions	a = 6.2610(7) Å α = 90°
	b = 7.4076(8) Å β = 90°
	c = 24.242(2) Å γ = 90°
Volume	1124.3(2) $Å^3$
Z	4
Density (calculated)	1.289 g/cm^3
Absorption coefficient	0.744 mm^{-1}
F(000)	464
Crystal size	0.26 x 0.21 x 0.15 mm^3
Theta range for data collection	3.646 to 80.268°.
Index ranges	-7<=h<=7, -9<= k<= 9, -30<= l<= 30
Reflections collected	28343
Independent reflections 2423	[R(int) = 0.0298]
Completeness to theta = 67.679°	100.0 %
Absorption correction	Semi-empirical from equivalents
Max. and min. transmission	1.0000 and 0.9262
Refinement method	Full-matrix least-squares on F2
Data / restraints / parameters	2423 / 0 / 147
Goodness-of-fit on F2	1.092
Final R indices [I>2sigma(I)]	R1 = 0.0261, wR2 = 0.0678
R indices (all data)	R1 = 0.0261, wR2 = 0.0679
Absolute structure parameter [Flack]	0.03(3)
Absolute structure parameter [Hooft]	0.05(3)
Extinction coefficient	0.0083(9)
Largest diff. peak and hole	0.179 and -0.132 $e.Å^{-3}$

(1*S*, 2*S*)-1-(3-Methoxyphenyl)-5-oxaspiro[2.4]heptan-4-one (12c)

Analysis Data (10 mM **11c**):

Entries	Pdt	Std	Pdt/Std	[Pdt]/mM	[PC]/μM	TTN	Avg. TTN
12c-(1)	50973	3011	16.929	9.60	0.81	11854	
12c-(2)	50742	2986	16.993	9.64	0.81	11895	
12c-(3)	48424	3070	15.773	9.00	0.81	11112	
12c-(4)	41983	3068	13.684	7.90	0.81	9746	11152

Preparative-scale reaction:

***E. coli* suspension expressing P411-G8S in M9-N**				***D*-glucose in M9-N**	
OD_{600}	volume/mL	[PC]/μM	n_pro/μmol	volume/mL	[Glu]/mM
27	85.0	3.218	0.2734	5	~13
olefin (11c) stock in EtOH			**LAD stock in EtOH**		
stock/M	volume/μL	n_1/mmol	stock/M	volume/μL	n_2/mmol
2.0	1000	2.0	1.0	2000	2.0
purification eluent	**Product**				
Ethyl acetate in hexanes (0% to 25% gradient)	m[Pdt]/mg	n[Pdt]/mmol	yield	TTN	
	415.8	1.91	95%	6970	

Optical rotation: $[\alpha]^{23}_{D} = -138.0 \pm 0.3°$ (*c* 0.8, ethyl acetate).

Chiralpak OD-H, 12% *i*-PrOH in hexane, 1.2 mL/min, 32 °C, 235 nm

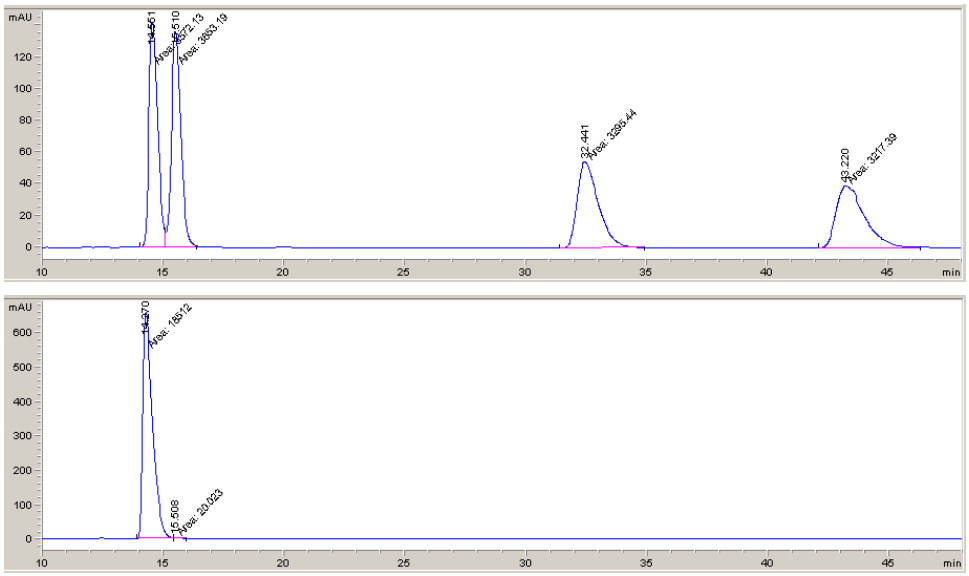

***rac*-*Z*- and *E*-12c**			**(1*S*, 2*S*)-12c**		
Retention Time (min)	Area (mAU*s)	Area %	Retention Time (min)	Area (mAU*s)	Area %
14.561 (*E*)	3572.1	26.00	14.370	18512.0	99.89
15.510 (*E*)	3653.2	26.59	15.508	20.0	0.11
32.441 (*Z*)	3295.4	23.99	-	-	-
43.220 (*Z*)	3217.4	23.42	-	-	-
Total	13738.1	100.00	Total	18532.0	100.00

(1*S*, 2*S*)-1-(4-Tolyl)-5-oxaspiro[2.4]heptan-4-one (12d)

Analysis Data (10 mM **11d**):

Entries	Pdt	Std	Pdt/Std	[Pdt]/mM	[PC]/μM	TTN	Avg. TTN
12d-(1)	37022	3016	12.275	6.83	1.62	4216	
12d-(2)	31892	3006	10.609	5.98	1.62	3693	
12d-(3)	39781	3192	12.463	6.93	1.62	4274	
12d-(4)	33482	3047	10.989	6.18	1.62	3814	3999

Chiralpak IA, 8% *i*-PrOH in hexane, 1.2 mL/min, 32 °C, 235 nm

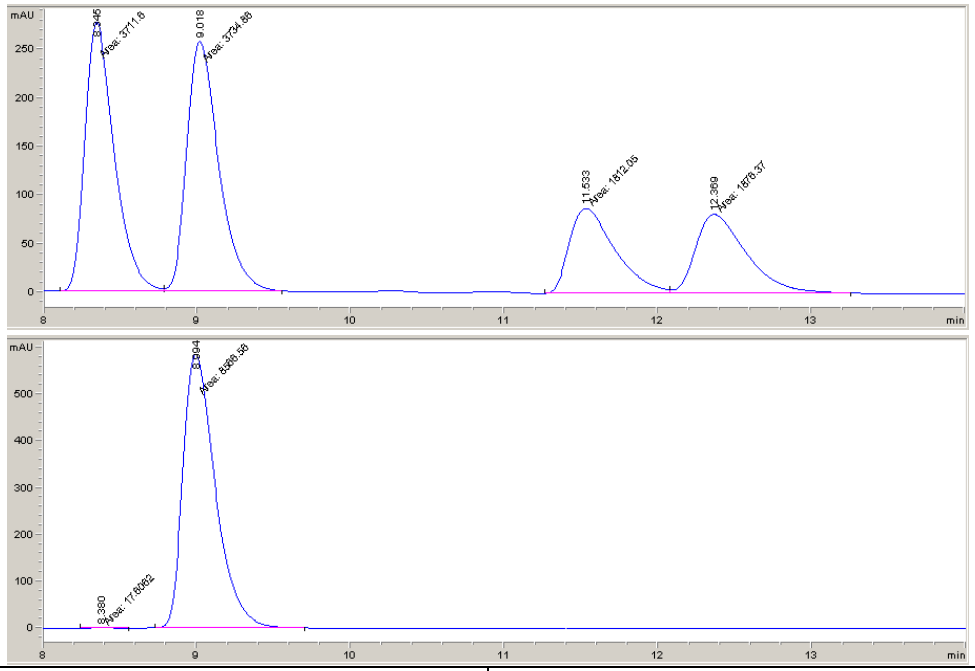

***rac*-*Z*- and *E*-12d**			**(1*S*, 2*S*)-12d**		
Retention Time (min)	Area (mAU*s)	Area %	Retention Time (min)	Area (mAU*s)	Area %
8.345 (*E*)	3711.6	33.33	8.380	17.6	0.20
9.018 (*E*)	3734.9	33.54	8.994	8588.6	99.80
11.533 (*Z*)	1812.1	16.27	-	-	-
13.369 (*Z*)	1878.4	16.87	-	-	-
Total	11137.0	100.00	Total	8606.2	100.00

(1*S*, 2*S*)-1-(4-Chlorophenyl)-5-oxaspiro[2.4]heptan-4-one (12e)

Analysis Data (10 mM **11e**):

Entries	Pdt	Std	Pdt/Std	[Pdt]/mM	[PC]/μM	TTN	Avg. TTN
12e-(1)	36851	3058	12.051	6.73	1.62	4153	
12e-(2)	32339	3091	10.462	5.87	1.62	3623	
12e-(3)	29981	3095	9.687	5.45	1.62	3362	

12e-(4)	30644	3032	10.107	5.68	1.62	3504	3660

Chiralpak IA, 8% *i*-PrOH in hexane, 1.2 mL/min, 32 °C, 235 nm

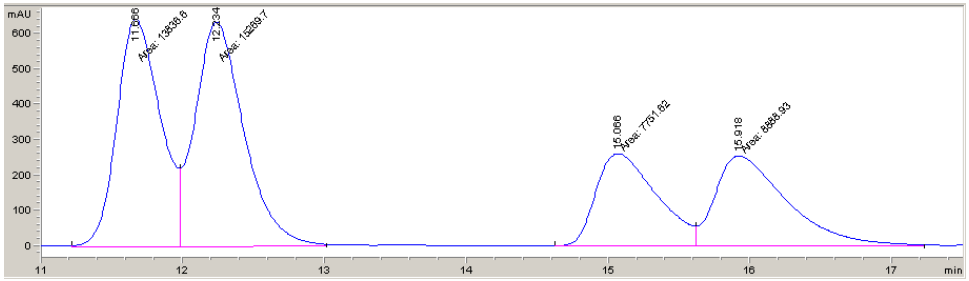

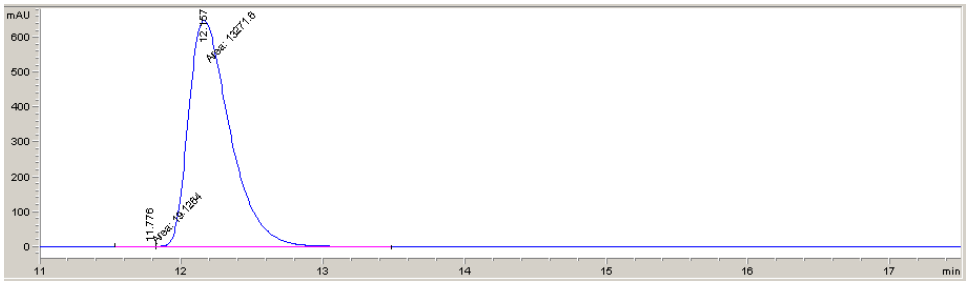

***rac*-*Z*- and *E*-12e**			**(1*S*, 2*S*)-12e**		
Retention Time (min)	Area (mAU*s)	Area %	Retention Time (min)	Area (mAU*s)	Area %
11.666 (*E*)	13836.6	30.27	11.776	19.1	0.14
12.234 (*E*)	15269.7	33.40	12.157	13271.6	99.86
15.066 (*Z*)	7751.6	16.96	-	-	-
15.918 (*Z*)	8858.9	19.38	-	-	-
Total	45716.8	100.00	Total	13290.7	100.00

(1*S*, 2*S*)-1-(4-Bromophenyl)-5-oxaspiro[2.4]heptan-4-one (12f)

Analysis Data (10 mM **11f**):

Entries	Pdt	Std	Pdt/Std	[Pdt]/mM	[PC]/μM	TTN	Avg. TTN
12f-(1)	27512	3015	9.125	5.20	1.62	3207	
12f-(2)	28599	3090	9.255	5.27	1.62	3251	
12f-(3)	28701	2984	9.618	5.47	1.62	3374	
12f-(4)	24259	2994	8.103	4.63	1.62	2860	3173

Preparative-scale reaction:

***E. coli* suspension expressing P411-G8S in M9-N**				**D-glucose in M9-N**	
OD_{600}	volume/mL	[PC]/μM	n_pro/μmol	volume/mL	[Glu]/mM
28	32.0	2.618	0.0877	2	~15
olefin (11f) stock in EtOH			**LAD stock in EtOH**		
stock/M	volume/μL	n_1/mmol	stock/M	volume/μL	n_2/mmol
1.0	250	0.25	1.0	250	0.25
purification eluent		**Product**			

Ethyl acetate in hexanes (0% to 25% gradient)	m[Pdt]/mg	n[Pdt]/mmol	yield	TTN
	42.4	0.159	64%	1810

Optical rotation: $[\alpha]^{23}_{D} = -139.7 \pm 0.5°$ (*c* 0.3, ethyl acetate).

Chiralpak IA, 8% *i*-PrOH in hexane, 1.2 mL/min, 32 °C, 235 nm

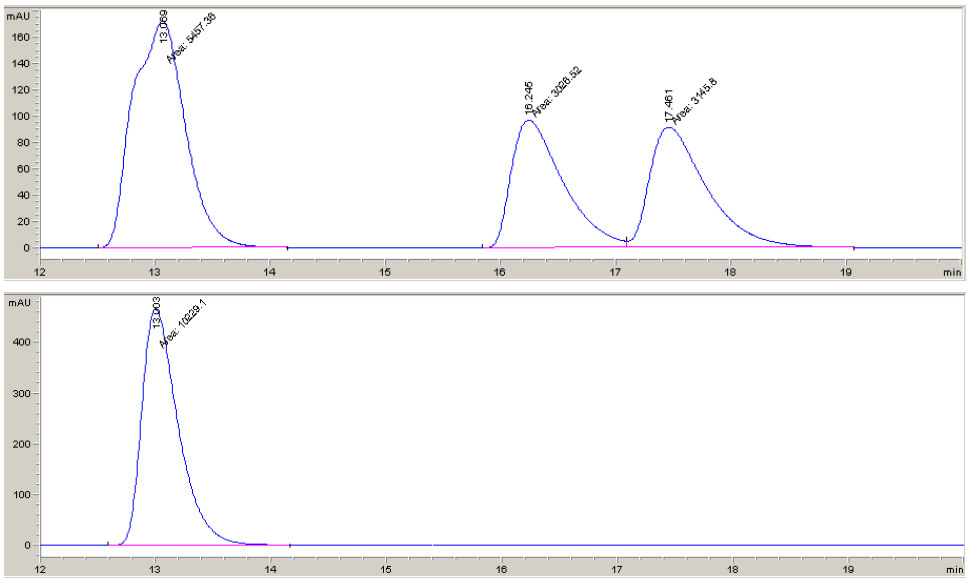

***rac*-*Z*- and *E*-12f**			**(1*S*, 2*S*)-12f**		
Retention Time (min)	Area (mAU*s)	Area %	Retention Time (min)	Area (mAU*s)	Area %
13.069 (*E*)	5457.4	46.93	13.003	10229.1	100.00
16.245 (*Z*)	3026.5	26.02	-	-	-
17.461 (*Z*)	3145.8	27.05	-	-	-
Total	11629.4	100.00	Total	10229.1	100.00

Chiralpak OD-H, 10% *i*-PrOH in hexane, 1.2 mL/min, 40 °C, 235 nm

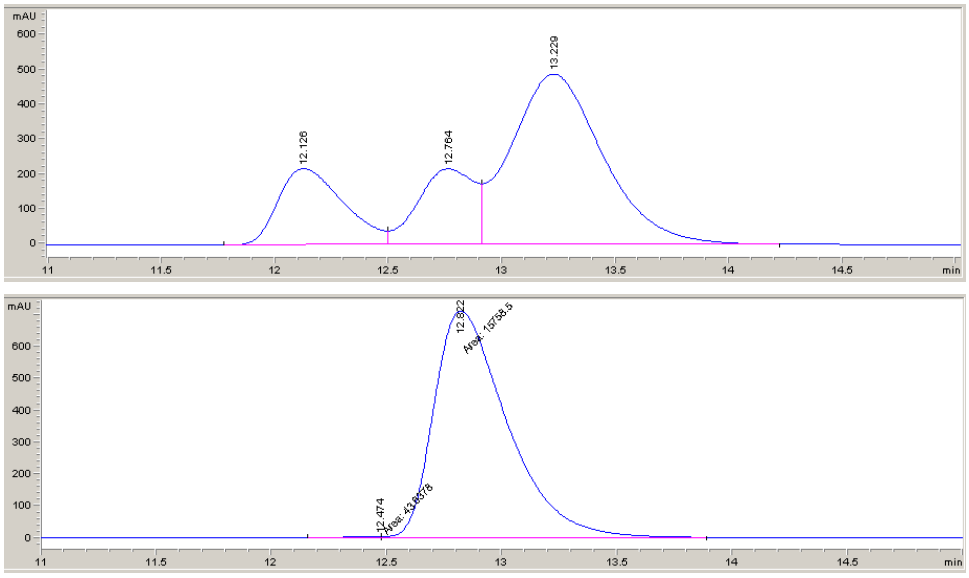

***rac*-*Z*- and *E*-12f**			**(1*S*, 2*S*)-12f**		
Retention Time (min)	Area (mAU*s)	Area %	Retention Time (min)	Area (mAU*s)	Area %
12.126 (*E*)	4399.4	20.03	12.474	43.6	0.28

12.764 (*E*)	3765.8	17.14	12.822	15758.5	99.72
13.229 (*Z*)	13800.5	62.83	-	-	-
Total	21965.7	100.00	Total	15802.1	100.00

Crystal structure information of **12f**:

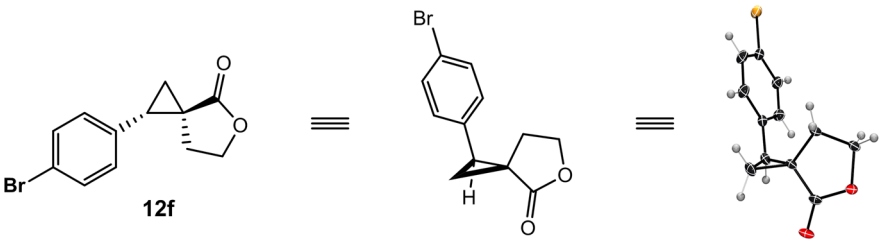

Identification code	v18091
Empirical formula	$C_{12}H_{11}BrO_2$
Formula weight	267.12
Temperature	100 K
Wavelength	0.71073 Å
Crystal system	Orthorhombic
Space group	$P2_12_12_1$
Unit cell dimensions	a = 6.3854(18) Å α = 90°
	b = 6.702(2) Å β = 90°
	c = 25.222(5) Å γ = 90°
Volume	1079.4(5) Å^3
Z	4
Density (calculated)	1.644 g/cm^3
Absorption coefficient	3.783 mm^{-1}
F(000)	536
Crystal size	0.30 x 0.26 x 0.14 mm^3
Theta range for data collection	3.145 to 45.297°.
Index ranges	-12<= h<= 10, -13<= k<= 13, -50<= l<= 50
Reflections collected	65957
Independent reflections 8908	[R(int) = 0.0351]
Completeness to theta = 25.242°	99.9 %
Absorption correction	Semi-empirical from equivalents
Max. and min. transmission	1.0000 and 0.8289
Refinement method	Full-matrix least-squares on F2
Data / restraints / parameters	8908 / 0 / 137
Goodness-of-fit on F2	1.025
Final R indices [I>2sigma(I)]	R1 = 0.0210, wR2 = 0.0533
R indices (all data)	R1 = 0.0262, wR2 = 0.0542
Absolute structure parameter [Flack]	0.028(4)
Absolute structure parameter [Hooft]	0.046(3)
Extinction coefficient	n/a
Largest diff. peak and hole	0.633 and -0.799 e.Å^{-3}

(1*S*, 2*S*)-1-((4-(Trifluoromethyl)phenyl))-5-oxaspiro[2.4]heptan-4-one (12g)

Analysis Data (10 mM **11g**):

Entries	Pdt	Std	Pdt/Std	[Pdt]/mM	[PC]/μM	TTN	Avg. TTN
12g-(1)	12126	3113	3.895	2.60	1.62	1605	
12g-(2)	12245	2903	4.218	2.81	1.62	1734	
12g-(3)	10252	2928	3.501	2.35	1.62	1448	
12g-(4)	11080	2887	3.838	2.56	1.62	1583	1592

Chiral HPLC trace:

Chiralpak IA, 8% *i*-PrOH in hexane, 1.2 mL/min, 32 °C, 235 nm

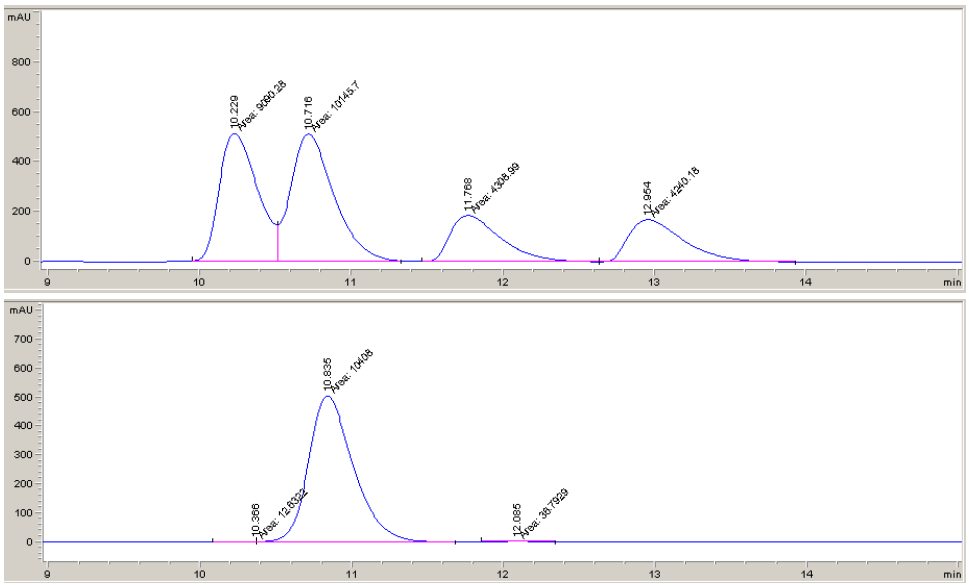

***rac*-*Z*- and *E*-12g**			**(1*S*, 2*S*)-12g**		
Retention Time (min)	Area (mAU*s)	Area %	Retention Time (min)	Area (mAU*s)	Area %
10.229 (*E*)	9090.3	32.72	10.366	12.6	0.12
10.716 (*E*)	10145.7	36.51	10.835	10408.0	99.53
11.768 (*Z*)	4309.0	15.51	12.085	36.8	0.35
12.954 (*Z*)	4240.2	15.26	-	-	-
Total	27785.2	100.00	Total	10457.4	100.00

(1*S*, 2*S*)-1-(2-Fluorophenyl)-5-oxaspiro[2.4]heptan-4-one (12h)

Analysis Data (5 mM **11h**):

Entries	Pdt	Std	Pdt/Std	[Pdt]/mM	[PC]/μM	TTN	Avg. TTN
12h-(1)	9723	3063	3.174	1.92	1.16	1651	
12h-(2)	9766	3134	3.116	1.89	1.16	1621	
12h-(3)	9697	3044	3.186	1.93	1.16	1657	
12h-(4)	9879	3059	3.229	1.96	1.16	1679	1652

Chiralpak OD-H, 10% *i*-PrOH in hexane, 1.2 mL/min, 40 °C, 235 nm

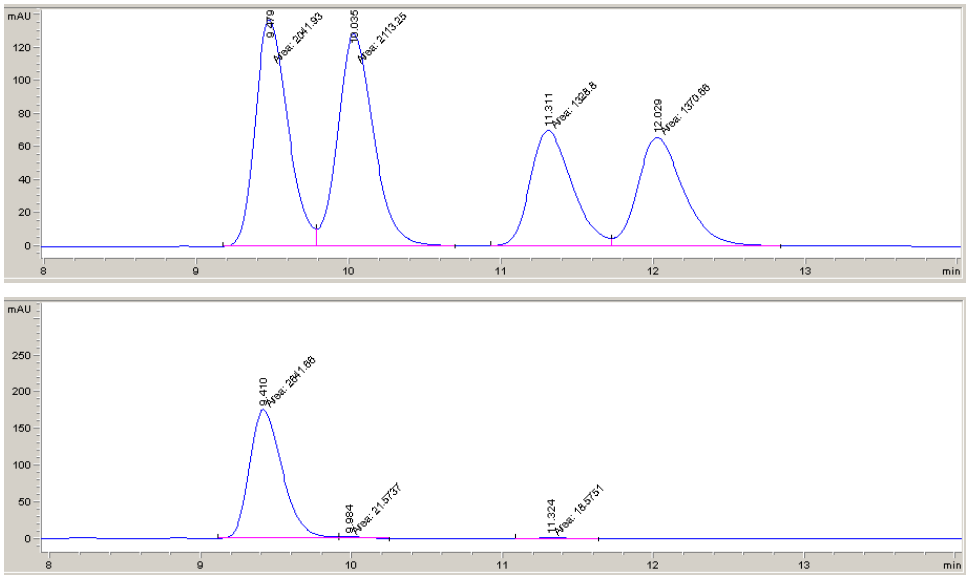

***rac*-*Z*- and *E*-12h**			**(1*S*, 2*S*)-12h**		
Retention Time (min)	Area (mAU*s)	Area %	Retention Time (min)	Area (mAU*s)	Area %
9.479 (*E*)	2041.9	29.79	9.410	2641.7	98.50
10.035 (*E*)	2113.2	30.83	9.984	21.6	0.81
11.311 (*Z*)	1328.8	19.38	11.324	18.6	0.69
12.029 (*Z*)	1370.7	20.00	-	-	-
Total	6854.6	100.00	Total	2681.9	100.00

(1*S*, 2*S*)-1-(Naphthalen-2-yl)-5-oxaspiro[2.4]heptan-4-one (12i)

Analysis Data (10 mM **11i**):

Entries	Pdt	Std	Pdt/Std	[Pdt]/mM	[PC]/μM	TTN	Avg. TTN
12i-(1)	27834	3149	8.839	4.73	1.62	2916	
12i-(2)	28556	3193	8.943	4.78	1.62	2949	
12i-(3)	23350	3223	7.245	3.90	1.62	2410	
12i-(4)	25288	3386	7.468	4.02	1.62	2481	2613

Chiralpak IA, 8% *i*-PrOH in hexane, 1.2 mL/min, 32 °C, 235 nm

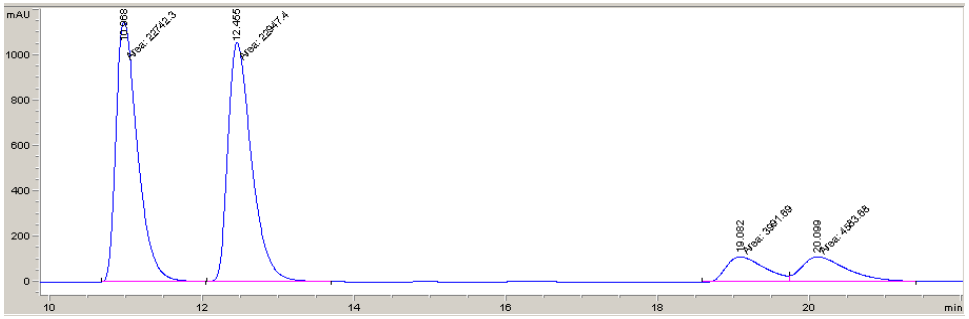

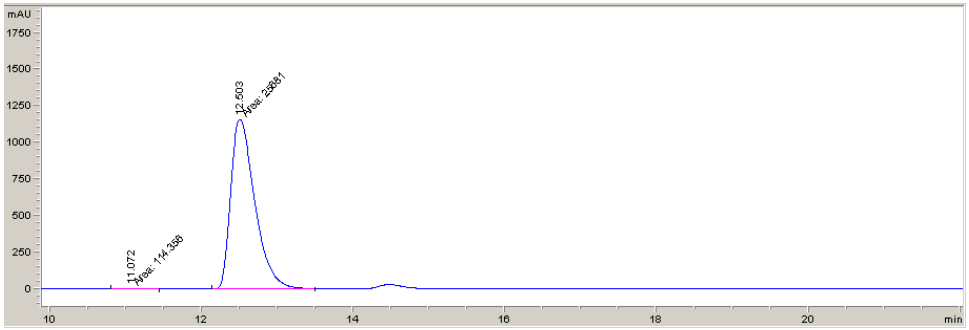

***rac*-*Z* and *E*-12i**			**(1*S*, 2*S*)-12i**		
Retention Time (min)	Area (mAU*s)	Area %	Retention Time (min)	Area (mAU*s)	Area %
10.968 (*E*)	22742.3	41.91	11.072	114.4	0.44
12.455 (*E*)	22947.4	42.28	12.503	25881.0	99.56
19.082 (*Z*)	3991.7	7.36	-	-	-
20.099 (*Z*)	4583.7	8.45	-	-	-
Total	54265.1	100.00	Total	25995.4	100.00

(–)-(*Z*)-**1-Phenethyl-5-oxaspiro[2.4]heptan-4-one (12j)**

Analysis Data (5 mM **11j**):

Entries	Pdt	Std	Pdt/Std	[Pdt]/mM	[PC]/μM	TTN	Avg. TTN
12j-(1)	11942	2840	4.205	2.14	1.16	1835	
12j-(2)	12393	3173	3.906	1.99	1.16	1707	
12j-(3)	12453	3189	3.905	1.99	1.16	1706	
12j-(4)	11944	3062	3.901	1.99	1.16	1704	
12j-(5)	12213	3030	4.031	2.05	1.16	1760	1743

Preparative-scale reaction:

***E. coli* suspension expressing P411-G8S in M9-N**				***D*-glucose in M9-N**	
OD_{600}	volume/mL	[PC]/μM	n_pro/μmol	volume/mL	[Glu]/mM
24	98	1.37	0.1343	5	~12
olefin (11j) stock in EtOH			**LAD stock in EtOH**		
stock/M	volume/μL	n_1/mmol	stock/M	volume/μL	n_2/mmol
1.0	250	0.25	1.0	250	0.25
purification eluent		**Product**			
Ethyl acetate in hexanes (0% to 25% gradient)		m[Pdt]/mg	n[Pdt]/mmol	yield	TTN
		35.8	0.166	66%	1230

Optical rotation: $[\alpha]^{23}_{D} = -55.0 \pm 0.6°$ (*c* 0.2, ethyl acetate).

Chiralpak OD-H, 10% *i*-PrOH in hexane, 1.2 mL/min, 40 °C, 220 nm

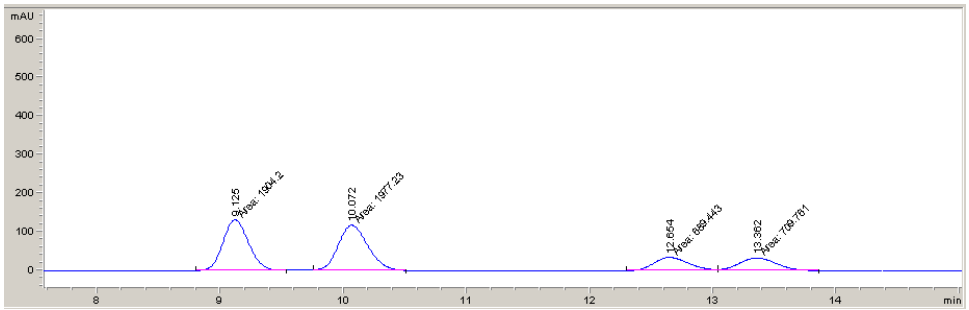

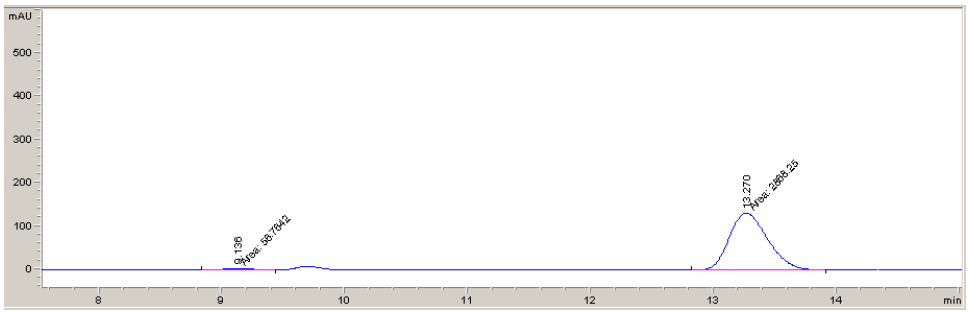

***rac*-*Z*- and *E*-12j**			**(–)-*Z*-12j**		
Retention Time (min)	Area (mAU*s)	Area %	Retention Time (min)	Area (mAU*s)	Area %
9.125 (*E*)	1904.2	36.06	9.135	56.8	1.94
10.072 (*E*)	1977.2	37.44	-	-	-
12.654 (*Z*)	689.4	13.06	-	-	-
13.362 (*Z*)	709.8	13.44	13.270	2868.3	98.06
Total	5280.6	100.00	Total	2925.1	100.00

B.5.2 Enzymatic synthesis of α-thio-γ-lactones

All enzymatic reactions for α-thio-γ-lactone synthesis in analytical scale were conducted following the general procedure described below and analyzed with gas chromatography (GC). All TTNs for the different products were determined using the GC standard curve of the corresponding racemic standard products.

All enzymatic reactions for α-thio-γ-lactone synthesis in preparative scale were conducted following the general procedure described below and the corresponding α-thio-γ-lactone products were isolated. Detailed conditions for preparative-scale reactions of different substrates are indicated separately.

General procedure for preparative-scale reactions:

To a 40 mL vial or 250 mL flask were added degassed suspension of *E. coli* expressing P450-**G8S** variant (OD_{600} = 15–20), thiol (1.5 equiv.), LAD (1.5 or 2.4 mmol.), *D*-glucose (10–15 mM, 250 mM stock in M9-N), 1–5 vol% EtOH, M9-N buffer (pH 7.4) under anaerobic conditions. The flask was capped and shaken (250 rpm) at room temperature for 2 h.

After the reaction was completed, 35 mL portions of preparative-scale reaction mixture were transferred to 50 mL centrifuge tubes. The reaction container was washed with water (2 mL × 2) followed by mixed organic solvent (hexane/ethyl acetate = 1:1, 2 mL × 3). The washing solution was combined with the reaction mixture in the centrifuge tubes. An additional 12 mL of hexane / ethyl

acetate solvent was added to every tube. After the tube (with ~48 mL mixture in total) was capped, it was vortexed (1 min × 3) and shaken vigorously, and centrifuged (12,000 × g, 5 min). The organic layer was separated and the aqueous layer was subjected to three more rounds of extraction. The organic layers were combined, dried over Na_2SO_4 and concentrated under reduced pressure. Purification by silica column chromatography with hexane/ethyl acetate as eluent afforded the desired α-thio-γ-lactones. Enantioselectivity was measured by chiral HPLC. TTNs were calculated based on measured protein concentration and isolated product yield.

(*R*)-3-(Phenylthio)dihydrofuran-2(3*H*)-one (14a)

Analysis Data:

Entries	Pdt	Std	Pdt/Std	[Pdt]/mM	[PC]/μM	TTN	Avg. TTN
14a-(1)	25062	3496	7.169	6.54	4.21	1552	
14a-(2)	27038	3413	7.922	7.22	4.21	1715	
14a-(3)	28412	3453	8.228	7.50	4.21	1782	
14a-(4)	26034	3429	7.592	6.92	4.21	1644	1673
14a-(5)	24779	3388	7.314	6.67	4.28	1558	
14a-(6)	23497	3388	6.935	6.32	4.28	1478	
14a-(7)	24733	3275	7.552	6.89	4.28	1609	
14a-(8)	24427	3373	7.242	6.60	4.28	1543	1547

Chiralpak OJ-H, 24% *i*-PrOH in hexane, 1.2 mL/min, 24 °C, 235 nm

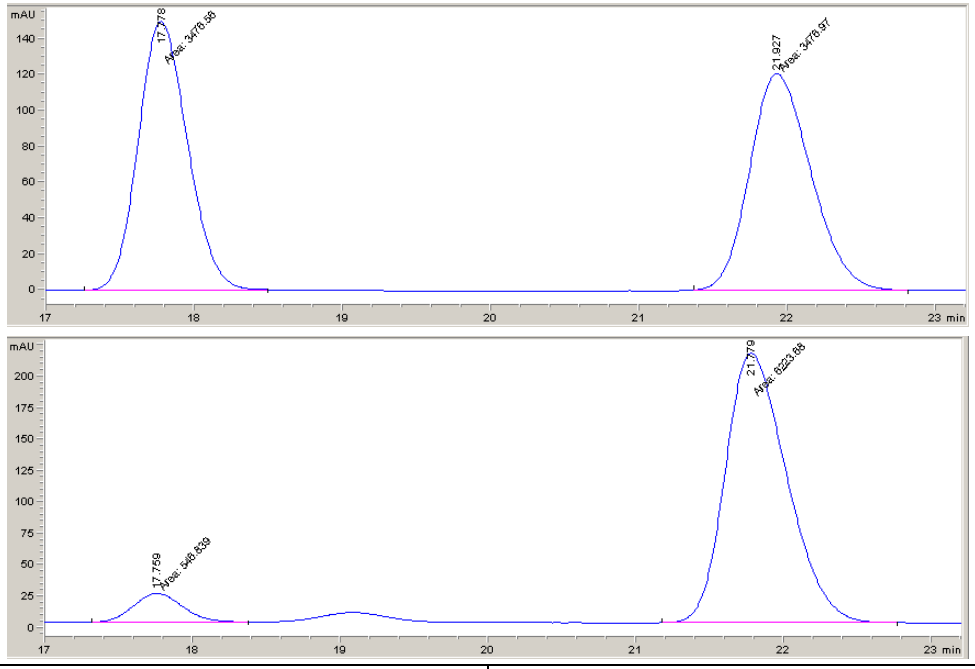

***rac*-14a**			***R*-14a**		
Retention Time (min)	Area (mAU*s)	Area %	Retention Time (min)	Area (mAU*s)	Area %
17.778	3476.6	49.99	17.759	546.8	8.08
21.927	3477.0	50.01	21.779	6223.7	91.92

Total	6953.6	100.00	Total	6770.5	100.00

(*R*)-3-((3-Methoxyphenyl)thio)dihydrofuran-2(3*H*)-one (14b)

Analysis Data:

Entries	Pdt	Std	Pdt/Std	[Pdt]/mM	[PC]/μM	TTN	Avg. TTN
14b-(1)	33529	3364	9.967	7.91	4.28	1849	
14b-(2)	33478	3418	9.795	7.78	4.28	1818	
14b-(3)	32920	3379	9.743	7.74	4.28	1809	
14b-(4)	33936	3458	9.814	7.79	4.28	1822	1824

Chiralpak OD-H, 12% *i*-PrOH in hexane, 1.2 mL/min, 32 °C, 235 nm

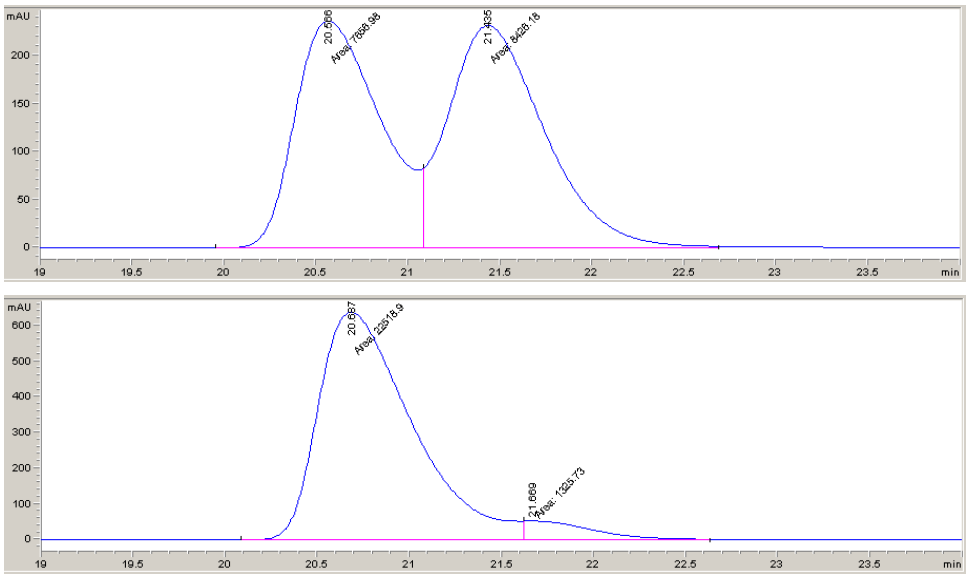

***rac*-14b**			***R*-14b**		
Retention Time (min)	Area (mAU*s)	Area %	Retention Time (min)	Area (mAU*s)	Area %
20.566	7657.0	47.61	20.687	22518.9	94.44
21.435	8426.2	52.39	21.669	1325.7	5.56
Total	16083.2	100.00	Total	23844.6	100.00

(*R*)-3-((4-Fluorophenyl)thio)dihydrofuran-2(3*H*)-one (14c)

Analysis Data:

Entries	Pdt	Std	Pdt/Std	[Pdt]/mM	[PC]/μM	TTN	Avg. TTN
14c-(1)	44068	5404	8.155	8.09	4.43	1826	
14c-(2)	42946	5518	7.782	7.73	4.43	1745	
14c-(3)	42540	5443	7.816	7.76	4.43	1752	
14c-(4)	42676	5503	7.755	7.70	4.43	1739	1765

Chiralpak OD-H, 10% *i*-PrOH in hexane, 1.2 mL/min, 40 °C, 235 nm

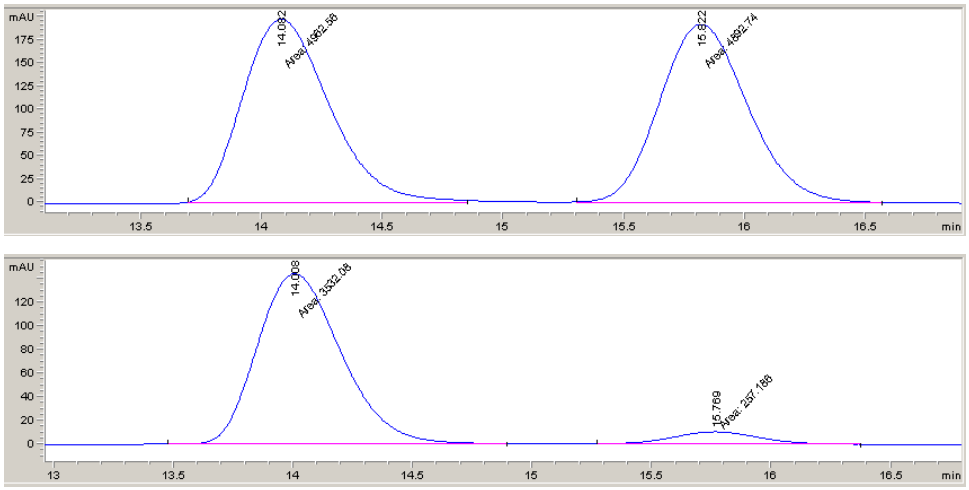

***rac*-14c**			***R*-14c**		
Retention Time (min)	Area (mAU*s)	Area %	Retention Time (min)	Area (mAU*s)	Area %
14.082	4962.6	50.35	14.008	3532.1	93.21
15.822	4892.7	49.65	15.769	257.2	6.79
Total	9855.3	100.00	Total	3789.3	100.00

(*R*)-3-((4-Chlorophenyl)thio)dihydrofuran-2(3*H*)-one (14d)

Analysis Data:

Entries	Pdt	Std	Pdt/Std	[Pdt]/mM	[PC]/μM	TTN	Avg. TTN
14d-(1)	35908	3306	10.861	8.18	4.28	1913	
14d-(2)	37309	3237	11.526	8.65	4.28	2023	
14d-(3)	37284	3289	11.336	8.52	4.28	1991	
14d-(4)	36890	3390	10.882	8.20	4.28	1916	1961

Preparative-scale reaction:

***E. coli* suspension expressing P450-G8S in M9-N**				***D*-glucose in M9-N**	
OD_{600}	volume/mL	[PC]/μM	n_pro/μmol	volume/mL	[Glu]/mM
20	150	4.506	0.8757	10	~15
thiol (13d) stock in EtOH			**LAD stock in EtOH**		
stock/M	volume/μL	n_1/mmol	stock/M	volume/μL	n_2/mmol
2.0	1800	3.60	1.0	2400	2.40
purification eluent		**Product**			
Ethyl acetate in hexanes (0% to 25% gradient)		m[Pdt]/mg	n[Pdt]/mmol	yield	TTN
		438.3	1.92	80%	2190

Optical rotation: $[\alpha]^{23}_{D} = -45.6 \pm 0.2°$ (*c* 0.8, ethyl acetate).

Chiralpak IA, 8% *i*-PrOH in hexane, 1.2 mL/min, 32 °C, 235 nm

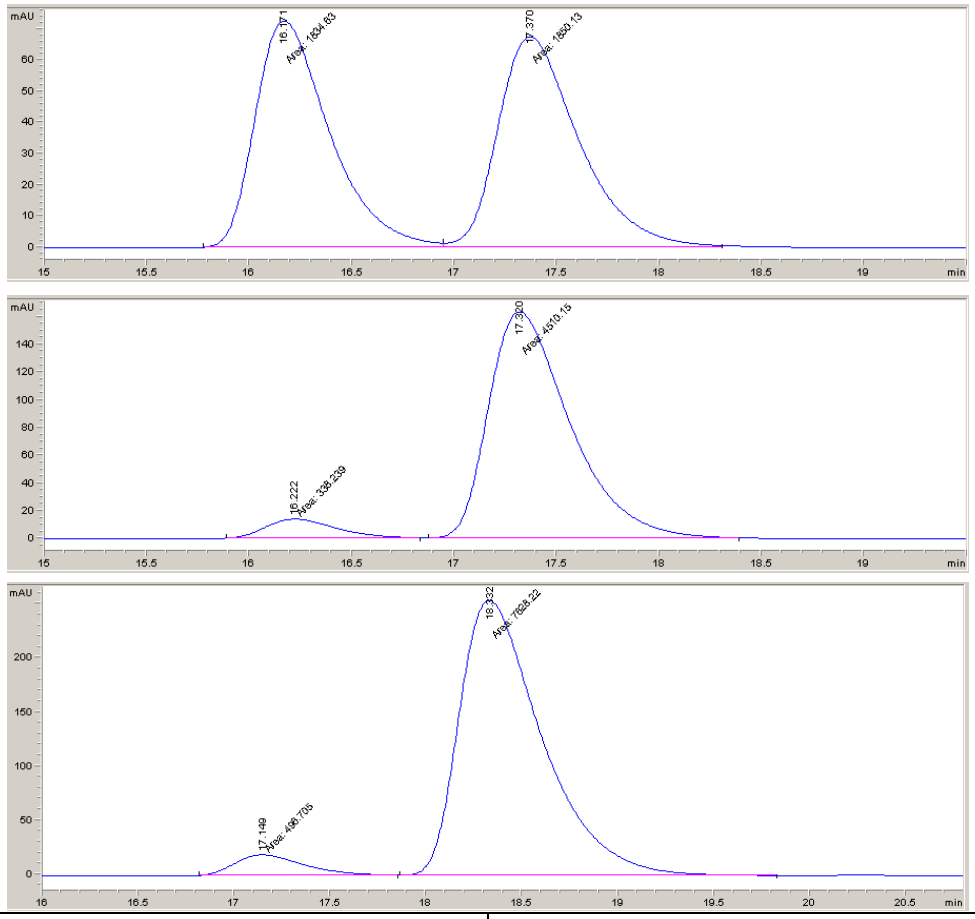

***rac*-14d**			***R*-14d**		
Retention Time (min)	Area (mAU*s)	Area %	Retention Time (min)	Area (mAU*s)	Area %
16.171	1834.6	49.77	16.222	338.2	6.98
17.370	1850.1	50.23	17.320	4510.2	93.02
Total	3684.7	100.00	Total	4848.4	100.00
***R*-14d_scale-up**					
Retention Time (min)	Area (mAU*s)	Area %			
17.149	496.7	6.11			
18.332	7628.2	93.89			
Total	8124.9	100.00			

(*R*)-3-((4-Bromophenyl)thio)dihydrofuran-2(3*H*)-one (14e)

Analysis Data:

Entries	Pdt	Std	Pdt/Std	[Pdt]/mM	[PC]/μM	TTN	Avg. TTN
14e-(1)	36496	3382	10.791	7.98	4.28	1866	
14e-(2)	34803	3354	10.377	7.70	4.28	1799	
14e-(3)	34274	3318	10.330	7.67	4.28	1792	
14e-(4)	35519	3357	10.581	7.84	4.28	1832	1822

Preparative-scale reaction:

***E. coli* suspension expressing P450-G8S in M9-N**				***D*-glucose in M9-N**	
OD_{600}	volume/mL	[PC]/μM	n_pro/μmol	volume/mL	[Glu]/mM
15	160	3.320	0.7149	10	~15
thiol (13e) stock in EtOH			**LAD stock in EtOH**		
stock/M	volume/μL	n_1/mmol	stock/M	volume/μL	n_2/mmol
1.0	2250	2.25	1.0	1500	1.50
purification eluent		**Product**			
Ethyl acetate in hexanes (0% to 25% gradient)		m[Pdt]/mg	n[Pdt]/mmol	yield	TTN
		386.5	1.42	94%	1980

Optical rotation: $[\alpha]^{23}_{D} = -41.7 \pm 0.2°$ (*c* 0.8, ethyl acetate).

Chiralpak IA, 8% *i*-PrOH in hexane, 1.2 mL/min, 32 °C, 235 nm

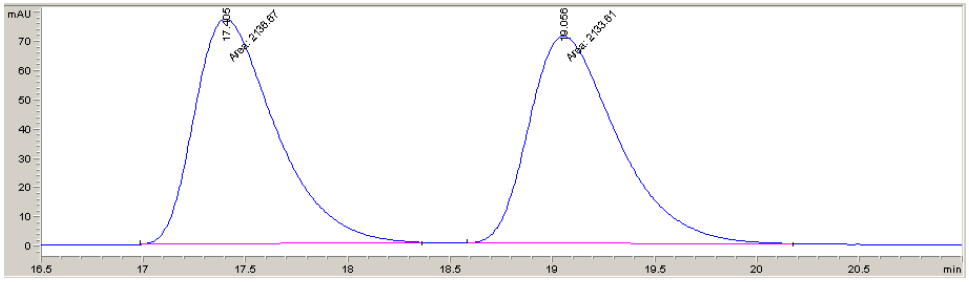

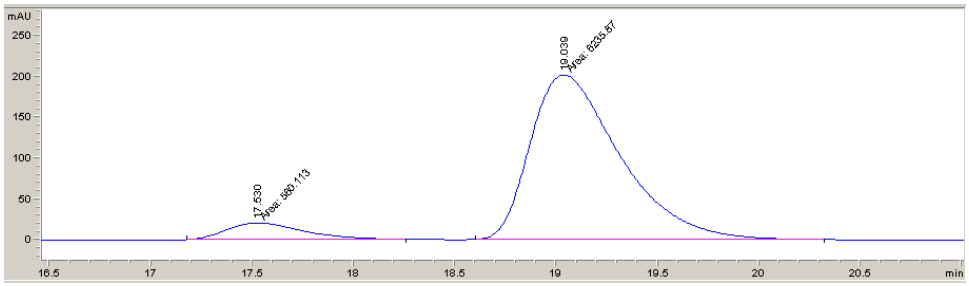

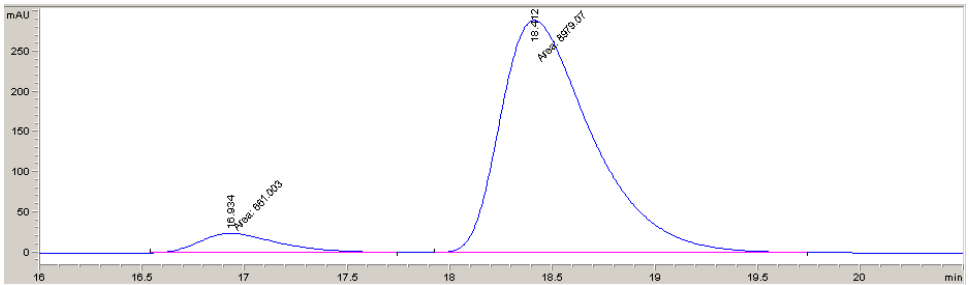

***rac*-14e**			***R*-14e**		
Retention Time (min)	Area (mAU*s)	Area %	Retention Time (min)	Area (mAU*s)	Area %
17.405	2136.7	50.02	17.530	560.1	8.24
19.056	2133.6	49.98	19.039	6235.9	91.76
Total	4270.3	100.00	Total	6796.6	100.00

***R*-14e_scale-up**		
Retention Time (min)	Area (mAU*s)	Area %

16.934	661.0	6.86
18.412	8979.1	93.14
Total	9640.1	100.00

Crystal structure information of **14e**:

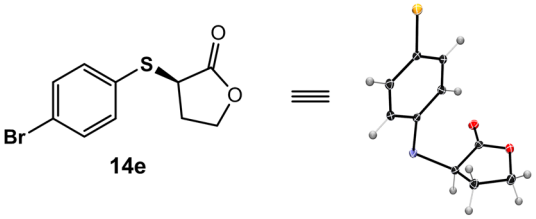

14e

Identification code	V18160
Empirical formula	$C_{10}H_9BrO_2S$
Formula weight	273.14
Temperature	100(2) K
Wavelength	0.71073 Å
Crystal system	Monoclinic
Space group	$P2_1$
Unit cell dimensions	a = 5.7304(6) Å α = 90°. b = 8.3275(7) Å β = 92.034(3)°. c = 10.4712(8) Å γ = 90°.
Volume	499.37(8) $Å^3$
Z	2
Density (calculated)	1.817 Mg/m^3
Absorption coefficient	4.292 mm^{-1}
F(000)	272
Crystal size	0.250 x 0.150 x 0.150 mm^3
Theta range for data collection	3.126 to 36.330°.
Index ranges	-9<=h<=9, -13<=k<=13, -17<=l<=17
Reflections collected	13036
Independent reflections 4669	[R(int) = 0.0244]
Completeness to theta = 25.242°	99.6 %
Absorption correction	Semi-empirical from equivalents
Max. and min. transmission	0.7471 and 0.6420
Refinement method	Full-matrix least-squares on F2
Data / restraints / parameters	4669 / 1 / 127
Goodness-of-fit on F2	0.859
Final R indices [I>2sigma(I)]	R1 = 0.0163, wR2 = 0.0408
R indices (all data)	R1 = 0.0175, wR2 = 0.0412
Absolute structure parameter	0.030(4)
Extinction coefficient	n/a
Largest diff. peak and hole	0.388 and -0.336 $e.Å^{-3}$

(*R*)-3-((4-Tolyl)thio)dihydrofuran-2(3*H*)-one (14f)

Analysis Data:

Entries	Pdt	Std	Pdt/Std	[Pdt]/mM	[PC]/μM	TTN	Avg. TTN
14f-(1)	23458	3376	6.948	4.61	4.28	1077	
14f-(2)	22953	3235	7.095	4.70	4.28	1099	
14f-(3)	23421	3341	7.010	4.65	4.28	1086	
14f-(4)	23731	3351	7.082	4.69	4.28	1097	1089

Chiralpak OJ-H, 24% *i*-PrOH in hexane, 1.2 mL/min, 28 °C, 220 nm

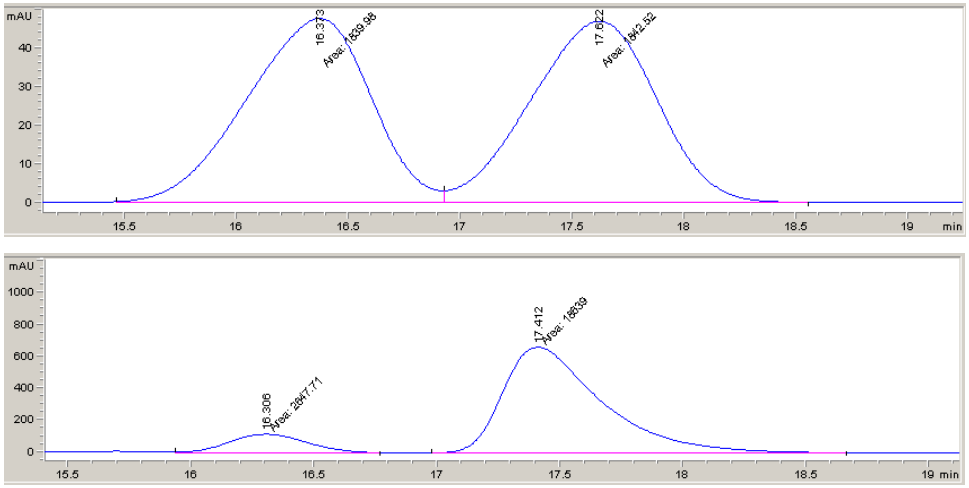

***rac*-14f**			***R*-14f**		
Retention Time (min)	Area (mAU*s)	Area %	Retention Time (min)	Area (mAU*s)	Area %
16.373	1840.0	49.97	16.306	2647.7	12.44
17.622	1842.5	50.03	17.412	18639.0	87.56
Total	3682.5	100.00	Total	21286.7	100.00

(*R*)-3-((4-Isopropylphenyl)thio)dihydrofuran-2(3*H*)-one (14g)

Analysis Data:

Entries	Pdt	Std	Pdt/Std	[Pdt]/mM	[PC]/μM	TTN	Avg. TTN
14g-(1)	9404	3133	3.002	1.80	4.28	422	
14g-(2)	9015	2968	3.037	1.83	4.28	427	
14g-(3)	9040	3255	2.777	1.67	4.28	391	
14g-(4)	9319	2983	3.124	1.88	4.28	439	420

Chiralpak OD-H, 10% *i*-PrOH in hexane, 1.2 mL/min, 40 °C, 235 nm

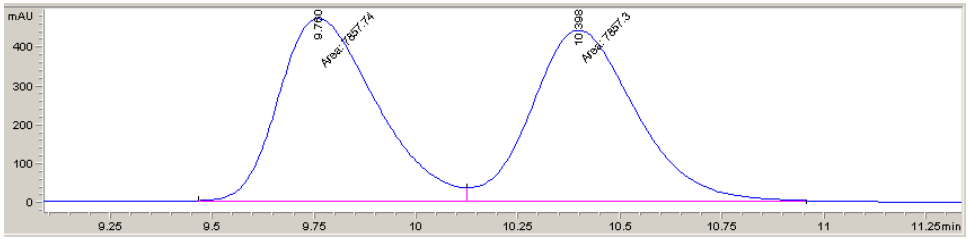

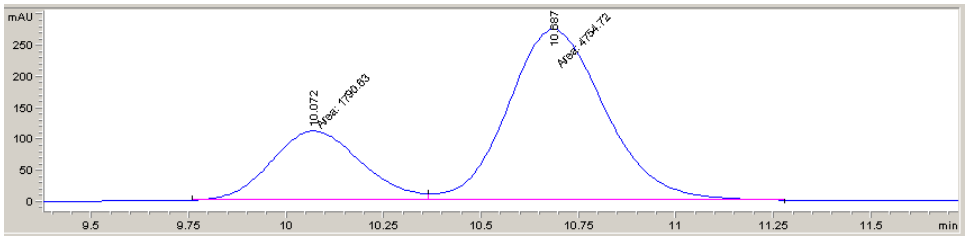

***rac*-14g**			***R*-14g**		
Retention Time (min)	Area (mAU*s)	Area %	Retention Time (min)	Area (mAU*s)	Area %
9.760	7857.7	50.00	10.072	1790.6	27.36
10.398	7857.3	50.00	10.687	4754.7	72.64
Total	15715.0	100.00	Total	6545.3	100.00

(*R*)-3-((4-Trifluoromethylphenyl)thio)dihydrofuran-2(3*H*)-one (14h)

Analysis Data:

Entries	Pdt	Std	Pdt/Std	[Pdt]/mM	[PC]/μM	TTN	Avg. TTN
14h-(1)	1062	678.8	1.565	1.32	4.81	275	
14h-(2)	1124.1	681.5	1.649	1.39	4.81	290	
14h-(3)	1211.8	678.9	1.785	1.51	4.81	314	
14h-(4)	1236.2	674.1	1.834	1.55	4.81	322	300

Chiralpak IA, 8% *i*-PrOH in hexane, 1.2 mL/min, 32 °C, 235 nm

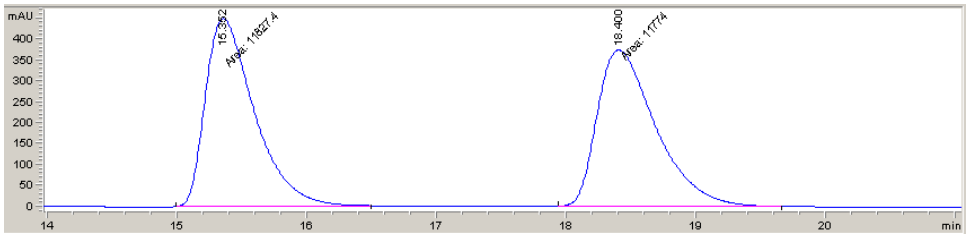

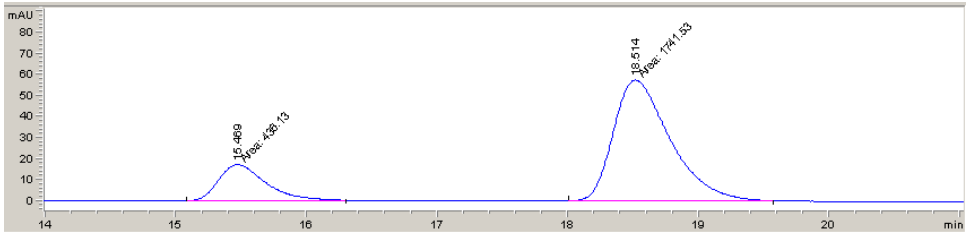

***rac*-14h**			***R*-14h**		
Retention Time	Area (mAU*s)	Area %	Retention Time	Area (mAU*s)	Area %

(min)			(min)		
15.352	11827.4	50.11	15.469	436.1	20.03
18.400	11774.0	49.89	18.514	1741.5	79.97
Total	23601.4	100.00	Total	2177.6	100.00

(*R*)-3-((3,4-Dimethoxyphenyl)thio)dihydrofuran-2(3*H*)-one (14i)

Analysis Data:

Entries	Pdt	Std	Pdt/Std	[Pdt]/mM	[PC]/μM	TTN	Avg. TTN
14i-(1)	9814	3203	3.064	2.64	4.28	617	
14i-(2)	9941	4040	2.461	2.13	4.28	499	
14i-(3)	10085	4349	2.319	2.01	4.28	471	
14i-(4)	10000	3671	2.724	2.36	4.28	551	534

Chiralpak OD-H, 12% *i*-PrOH in hexane, 1.2 mL/min, 32 °C, 235 nm

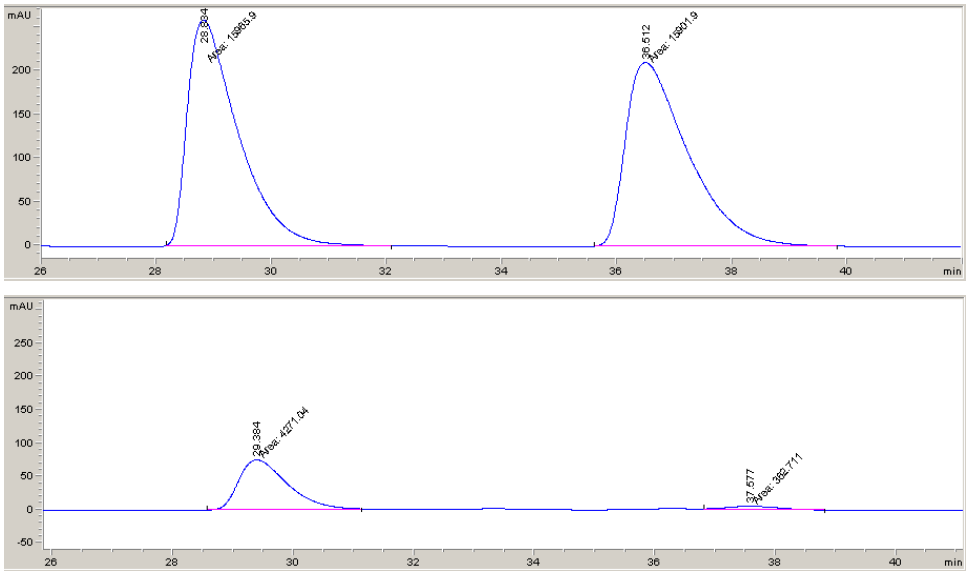

Area% report for ***rac*-14i**:

***rac*-14i**			***R*-14i**		
Retention Time (min)	Area (mAU*s)	Area %	Retention Time (min)	Area (mAU*s)	Area %
28.834	15965.9	50.10	29.384	4271.0	92.17
36.512	15901.9	49.90	37.577	362.7	7.82
Total	31867.8	100.00	Total	4633.7	100.00

(*R*)-3-(Naphthalen-2-ylthio)dihydrofuran-2 (3*H*)-one (14j)

Analysis Data:

Entries	Pdt	Std	Pdt/Std	[Pdt]/mM	[PC]/μM	TTN	Avg. TTN
14j-(1)	6820	3552	1.920	1.17	4.28	273	

14j-(2)	6843	3267	2.095	1.27	4.28	298	
14j-(3)	8152	3195	2.551	1.55	4.28	361	
14j-(4)	7779	3394	2.292	1.39	4.28	325	328

Chiralpak IA, 8% *i*-PrOH in hexane, 1.2 mL/min, 32 °C, 235 nm

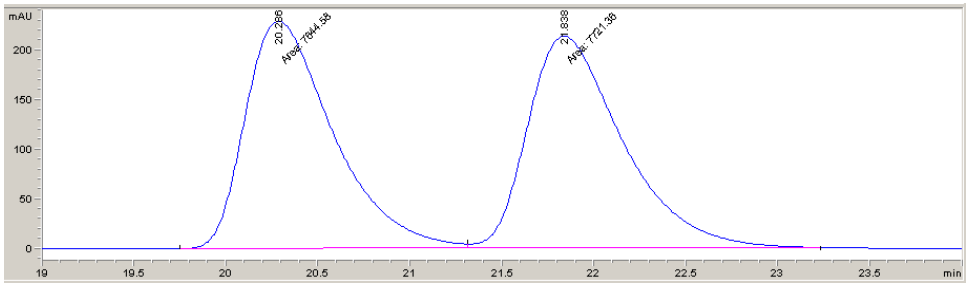

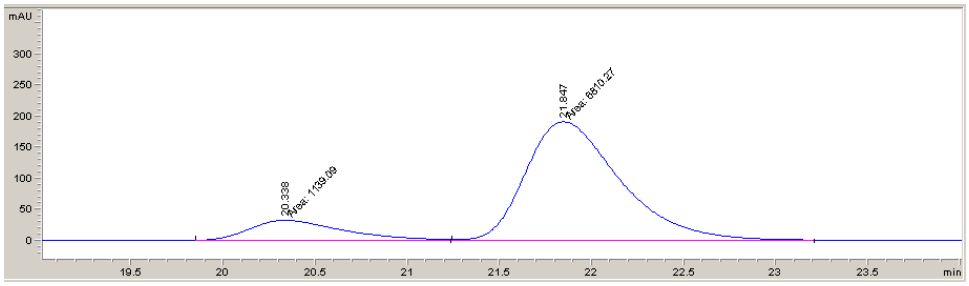

***rac*-14j**			***R*-14j**		
Retention Time (min)	Area (mAU*s)	Area %	Retention Time (min)	Area (mAU*s)	Area %
20.286	7644.6	49.75	20.338	1139.1	14.33
21.838	7721.4	50.25	21.847	6810.3	85.67
Total	15366.0	100.00	Total	7949.4	100.00

B.5.3 Enzymatic synthesis of α-alkyl-γ-lactones

All enzymatic reactions for lactone-carbene C–H insertion in analytical scale were conducted following the general procedure described below and analyzed with HPLC. All TTNs for different products were determined using the HPLC standard curves of the corresponding products obtained from the preparative-scale enzymatic reactions.

3-((Methyl(*p*-tolyl)amino)methyl)dihydrofuran-2(3*H*)-one (16a)

Analysis Data:

L6 OD_{600} = 60	Pdt	Std	Pdt/Std	[Pdt]/mM	[PC]/μM	TTN	Avg. TTN
16a-L6_a	6946.0	1177.9	5.8969	9.6049	3.57	2694	
16a-L6_b	7124.5	1181.0	6.0326	9.8259	3.57	2756	
16a-L6_c	7387.5	1191.3	6.2012	10.1005	3.57	2833	2761

L7 OD_{600} = 30	Pdt	Std	Pdt/Std	[Pdt]/mM	[PC]/μM	TTN	Avg. TTN
16a-L7_a	8503.9	1178.9	7.2134	11.7492	4.10	2865	

16a-L7_b	8814.0	1180.6	7.4657	12.1601	4.10	2965	
16a-L7_c	8693.1	1201.0	7.2382	11.7896	4.10	2875	
16a-L7_d	8801.1	1170.2	7.5210	12.2502	4.10	2987	2923

L9 OD_{600} = 60	Pdt	Std	Pdt/Std	[Pdt]/mM	[PC]/μM	TTN	Avg. TTN
16a-L9_a	5770.5	1207.4	4.7793	7.7845	5.18	1502	
16a-L9_b	5860.1	1146.8	5.1100	8.3231	5.18	1606	
16a-L9_c	5807.0	1173.3	4.9493	8.0614	5.18	1556	1555

L10 OD_{600} = 60	Pdt	Std	Pdt/Std	[Pdt]/mM	[PC]/μM	TTN	Avg. TTN
16a-L10_a	757.5	1282.2	0.5908	0.9623	2.71	355	
16a-L10_b	781.0	1303.6	0.5991	0.9758	2.71	360	
16a-L10_c	767.1	1260.3	0.6087	0.9914	2.71	366	361

Chiralpak OD-H, 6% IPA in hexane, 1.0 ml/min, 32 °C, 254nm

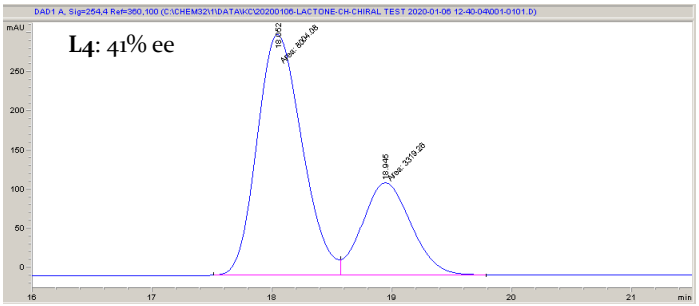

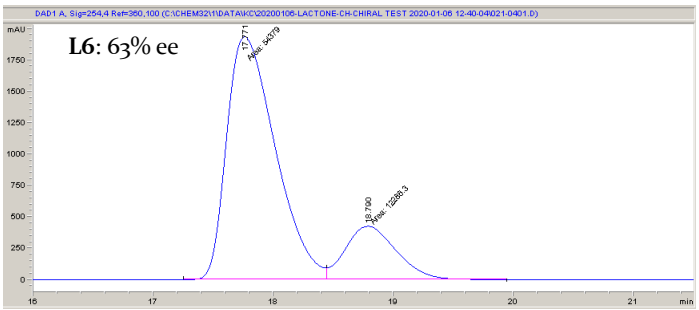

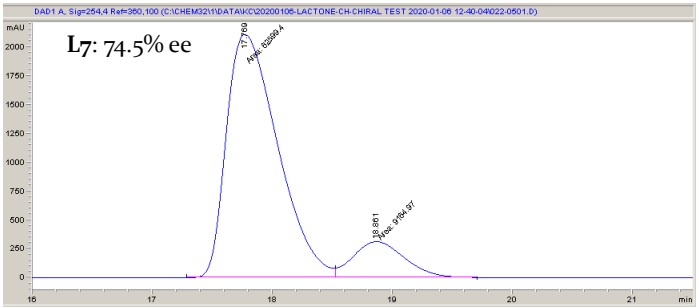

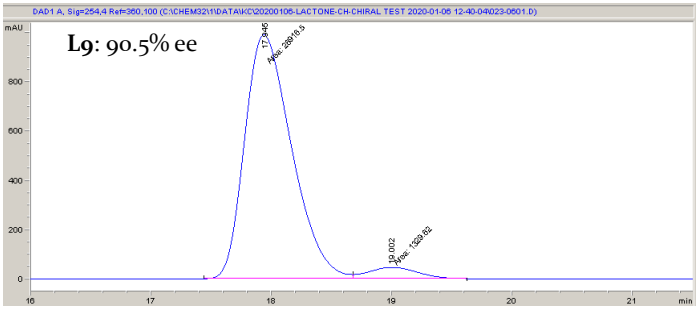

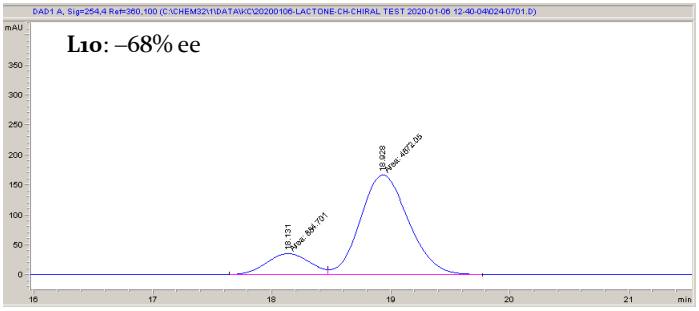

16a by variant **L4**			**16a** by variant **L6**		
Retention Time (min)	Area (mAU*s)	Area %	Retention Time (min)	Area (mAU*s)	Area %
18.05	8004.1	70.69	17.77	54379	81.57
18.95	3319.3	29.31	18.79	12286.3	18.43
Total	11323.4	100.00	Total	66665.3	100.00
16a by variant **L7**			**16a** by variant **L9**		
Retention Time (min)	Area (mAU*s)	Area %	Retention Time (min)	Area (mAU*s)	Area %
17.77	62599.4	87.23	17.95	26916.5	95.29
18.86	9165.0	12.77	19.00	1329.6	4.71
Total	71764.4	100.00	Total	28246.1	100.00
16a by variant **L10**					
Retention Time (min)	Area (mAU*s)	Area %			
18.13	884.7	15.92			
18.93	4672.1	84.08			
Total	5556.8	100.00			

3-(((4-Methoxyphenyl)(methyl)amino)methyl)dihydrofuran-2(3*H*)-one (16b)

Analysis Data:

L6 OD_{600} = 60	Pdt	Std	Pdt/Std	[Pdt]/mM	[PC]/μM	TTN	Avg. TTN
16b-L6_a	7269.6	1175.4	6.1848	7.2473	3.57	2032	
16b-L6_b	7306.7	1168.5	6.2531	7.3273	3.57	2055	
16b-L6_c	7300.7	1173.5	6.2213	7.2901	3.57	2044	2044

L7 OD_{600} = 30	Pdt	Std	Pdt/Std	[Pdt]/mM	[PC]/μM	TTN	Avg. TTN
16b-L7_a	8352.8	1184.0	7.0547	8.2667	4.40	1878	
16b-L7_b	8083.9	1180.5	6.8479	8.0243	4.40	1823	
16b-L7_c	8109.2	1200.5	6.7549	7.9153	4.40	1798	1833

L9 OD_{600} = 60	Pdt	Std	Pdt/Std	[Pdt]/mM	[PC]/μM	TTN	Avg. TTN
16b-L9_a	5711.2	1165.9	4.8985	5.7401	5.18	1108	
16b-L9_b	6011.9	1184.9	5.0738	5.9454	5.18	1147	
16b-L9_c	6498.1	1203.1	5.4011	6.3290	5.18	1221	1159

Chiralpak OD-H, 6% IPA in hexane, 1.0 ml/min, 32 °C, 254nm

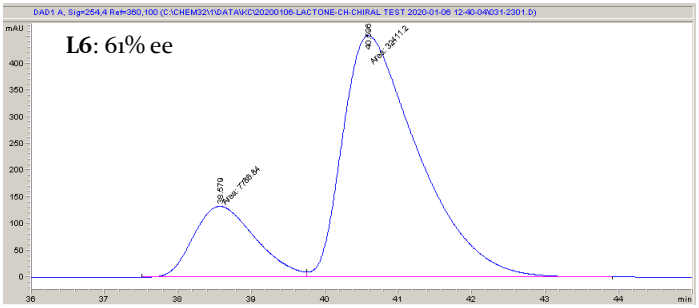

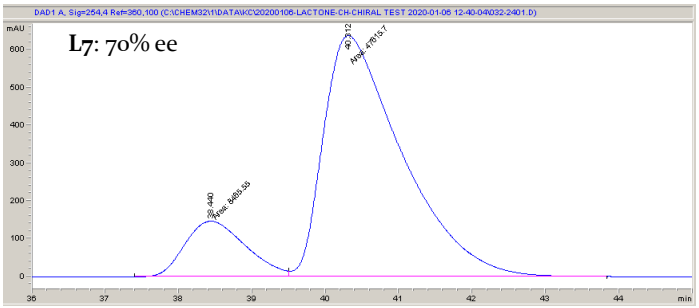

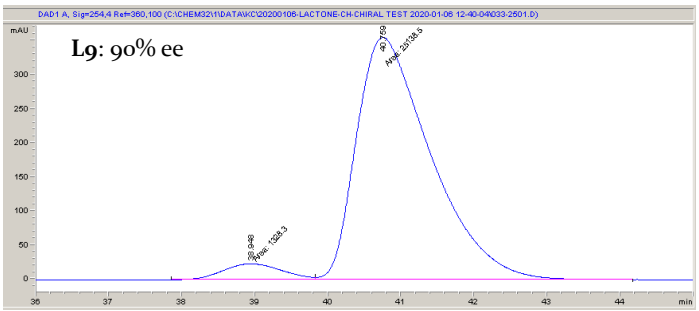

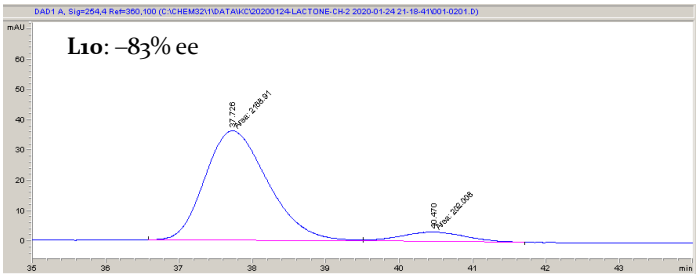

16b by variant **L6**			**16b** by variant **L7**		
Retention Time (min)	Area (mAU*s)	Area %	Retention Time (min)	Area (mAU*s)	Area %
38.58	7786.8	19.37	38.44	8465.6	15.10
40.60	32411.2	80.63	40.31	47615.7	84.90
Total	40198.0	100.00	Total	56081.3	100.00
16b by variant **L9**			**16b** by variant **L10**		
Retention Time (min)	Area (mAU*s)	Area %	Retention Time (min)	Area (mAU*s)	Area %
38.95	1328.3	5.02	37.73	2168.9	91.48
40.76	25138.5	94.98	40.47	202.0	8.52
Total	26466.8	100.00	Total	2370.9	100.00

3-(((4-Chlorophenyl)(methyl)amino)methyl)dihydrofuran-2(3*H*)-one (16c)

Analysis Data:

L7 OD_{600} = 60	Pdt	Std	Pdt/Std	[Pdt]/mM	[PC]/µM	TTN	Avg. TTN
16c-L7_a	2074.3	1354.6	1.5313	3.6794	8.80	418	
16c-L7_b	2092.0	1363.4	1.5344	3.6869	8.80	419	
16c-L7_c	2131.2	1366.2	1.5599	3.7482	8.80	426	421

Chiralpak IA, 3% IPA in hexane, 1.2 ml/min, 32 °C, 254nm

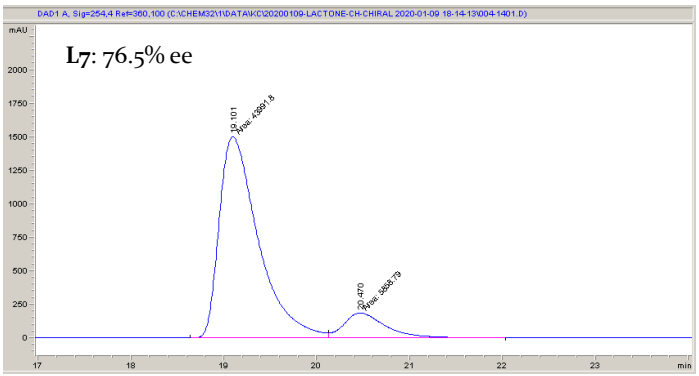

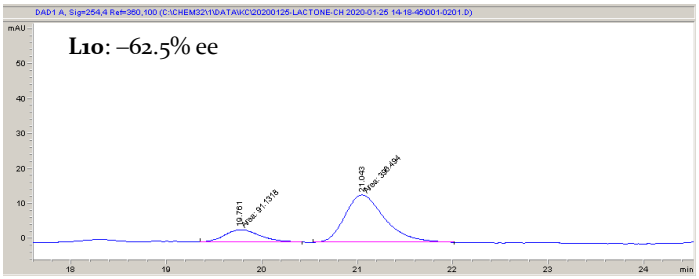

16c by variant **L7**			**16c** by variant **L10**		
Retention Time (min)	Area (mAU*s)	Area %	Retention Time (min)	Area (mAU*s)	Area %
19.10	43991.8	88.25	19.76	91.1	18.68
20.47	5858.8	11.75	21.04	396.5	81.32
Total	49850.6	100.00	Total	487.6	100.00

3-((Methyl(*m*-tolyl)amino)methyl)dihydrofuran-2(3*H*)-one (16d)

Analysis Data:

L6 OD_{600} = 60	Pdt	Std	Pdt/Std	[Pdt]/mM	[PC]/µM	TTN	Avg. TTN
16d-L6_a	2184.8	1198.0	1.8237	4.5611	3.57	1279	
16d-L6_b	2292.9	1197.8	1.9143	4.7876	3.57	1343	
16d-L6_c	2234.6	1204.8	1.8547	4.6387	3.57	1301	1308

L9 OD_{600} = 60	Pdt	Std	Pdt/Std	[Pdt]/mM	[PC]/µM	TTN	Avg. TTN
16d-L9_a	3309.9	1166.7	2.8370	7.0953	5.18	1369	
16d-L9_b	3557.4	1191.0	2.9869	7.4702	5.18	1442	
16d-L9_c	3516.9	1195.6	2.9415	7.3568	5.18	1420	1410

L10 OD_{600} = 60	Pdt	Std	Pdt/Std	[Pdt]/mM	[PC]/µM	TTN	Avg. TTN
16d-L10_a	975.1	1273.6	0.7656	1.9148	2.71	707	
16d-L10_b	992.8	1264.3	0.7853	1.9639	2.71	725	
16d-L10_c	979.1	1252.8	0.7815	1.9546	2.71	722	718

Chiralpak OD-H, 6% IPA in hexane, 1.0 ml/min, 32 °C, 254nm

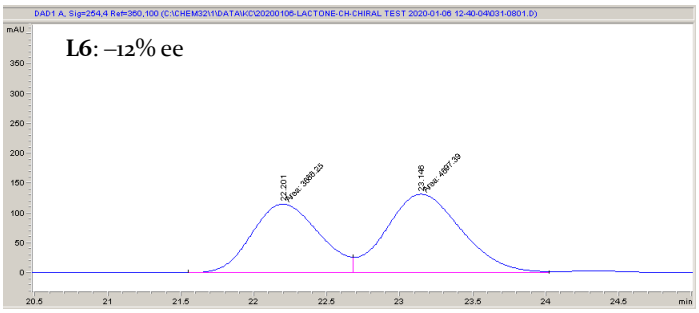

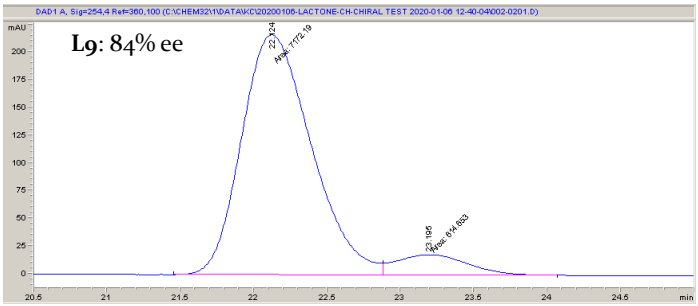

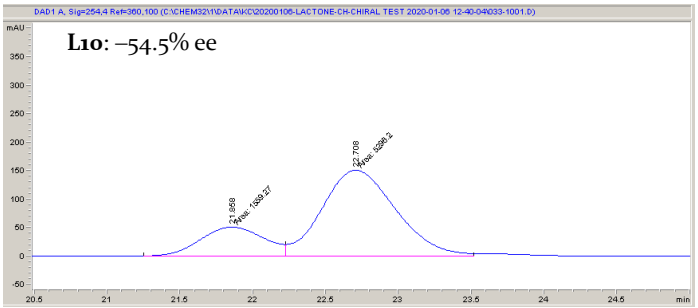

16d by variant **L6**			**16d** by variant **L9**		
Retention Time (min)	Area (mAU*s)	Area %	Retention Time (min)	Area (mAU*s)	Area %
22.20	3686.3	43.97	22.12	7172.2	92.11
23.15	4697.4	56.03	23.20	614.7	7.89
Total	8383.7	100.00	Total	7786.9	100.00
16d by variant **L10**					
Retention Time (min)	Area (mAU*s)	Area %			
21.86	1559.3	22.75			
22.71	5296.2	77.25			
Total	6855.5	100.00			

3-((Methyl(phenyl)amino)methyl)dihydrofuran-2(3*H*)-one (16e)

Analysis Data:

L6 OD_{600} = 60	Pdt	Std	Pdt/Std	[Pdt]/mM	[PC]/μM	TTN	Avg. TTN
16e-L6_a	2614.2	2092.9	1.2491	2.2205	3.57	623	
16e-L6_b	2254.9	2094.7	1.0765	1.9137	3.57	537	
16e-L6_c	2440.0	2083.2	1.1713	2.0822	3.57	584	581

L9 OD_{600} = 60	Pdt	Std	Pdt/Std	[Pdt]/mM	[PC]/μM	TTN	Avg. TTN
16e-L9_a	2284.6	2141.1	1.0670	1.8968	5.18	366	
16e-L9_b	2652.9	2066.7	1.2836	2.2819	5.18	440	
16e-L9_c	2555.8	2037.2	1.2546	2.2302	5.18	430	412

L10 OD_{600} = 60	Pdt	Std	Pdt/Std	[Pdt]/mM	[PC]/μM	TTN	Avg. TTN
16e-L10_a	5067.8	2157.2	2.3492	4.1763	2.71	1542	
16e-L10_b	5809.1	2190.8	2.6516	4.7137	2.71	1741	
16e-L10_c	5639.4	2190.4	2.5746	4.5769	2.71	1690	1658

Chiralpak OD-H, 6% IPA in hexane, 1.0 ml/min, 32 °C, 254nm

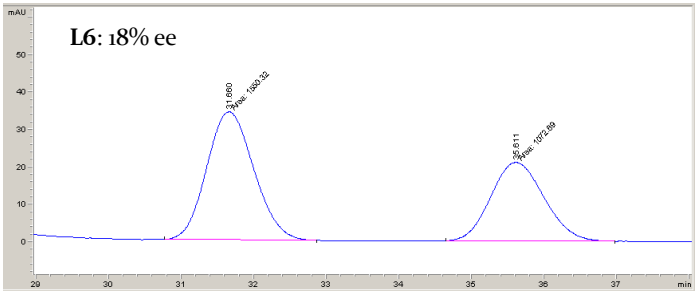

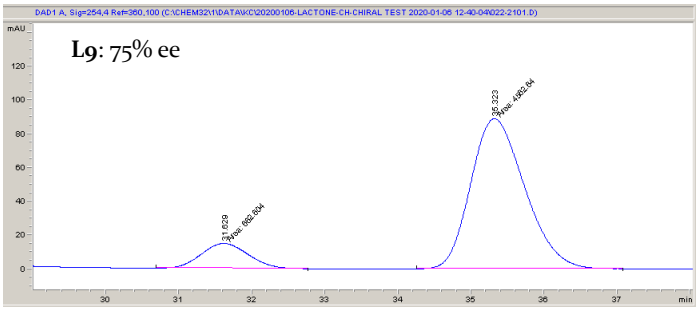

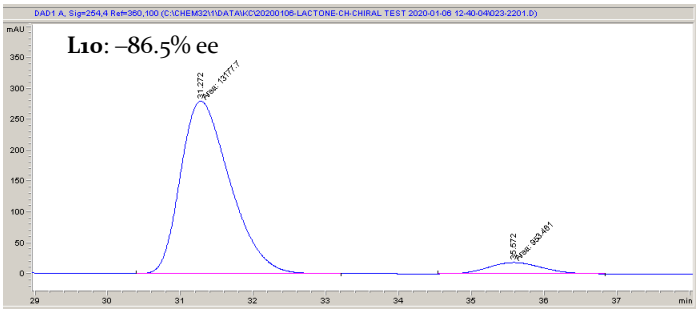

16e by variant **L6**			**16e** by variant **L9**		
Retention Time (min)	Area (mAU*s)	Area %	Retention Time (min)	Area (mAU*s)	Area %
31.66	1550.3	59.10	31.63	662.6	12.68
35.61	1072.7	40.90	35.32	4562.6	87.32
Total	2623.0	100.00	Total	5225.2	100.00

16e by variant **L10**		
Retention Time (min)	Area (mAU*s)	Area %
31.27	13177.7	93.25
35.57	953.5	6.75
Total	14131.2	100.00

3-((Methyl(*o*-tolyl)amino)methyl)dihydrofuran-2(3*H*)-one (16f)

Analysis Data:

L9 OD_{600} = 60	Pdt	Std	Pdt/Std	[Pdt]/mM	[PC]/μM	TTN	Avg. TTN
16f-L7_a	4037.9	1292.2	3.1248	7.4890	5.18	1445	
16f-L7_b	4090.4	1278.3	3.1999	7.6688	5.18	1480	
16f-L7_c	4210.4	1286.0	3.2740	7.8465	5.18	1514	1480

Chiralpak IC, 6% IPA in hexane, 1.2 ml/min, 32 °C, 254nm

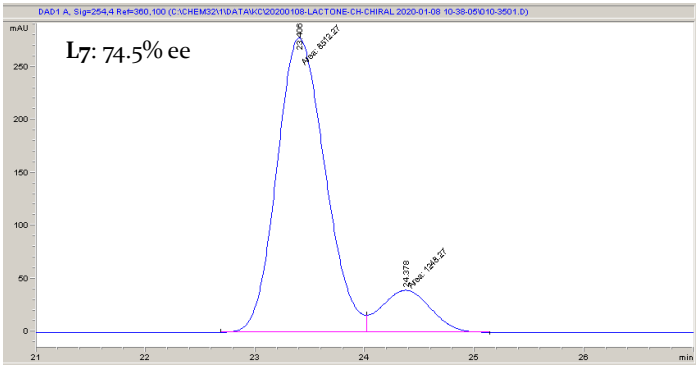

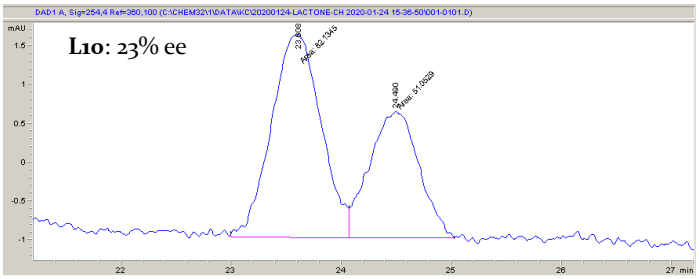

16f by variant **L9**			**16f** by variant **L10**		
Retention Time (min)	Area (mAU*s)	Area %	Retention Time (min)	Area (mAU*s)	Area %
23.41	8512.3	87.21	23.61	82.1	61.64
24.38	1248.3	12.79	24.49	51.1	38.36
Total	9760.6	100.00	Total	133.2	100.00

Note: Variant **L10** is not able to give good activity or reverse the enantioselectivity (compared to that with **L9**) when using substrates bearing an *ortho*-substituent on the phenyl ring (*e.g.*, substrates **15f** and **15k**).

3-((Ethyl(pheny)amino)methyl)dihydrofuran-2(3*H*)-one (16g)
3-(1-(Methyl(phenyl)amino)ethyl)dihydrofuran-2(3*H*)-one (16g')

Analysis Data:

L6 OD_{600} = 60	Pdt-**16g**	Pdt-**16g'**	Std	Pdt/Std	[Pdt]/mM	[PC]/μM	TTN	Avg. TTN
16g/g'-L6_a	2871.8	77.7	1247.7	2.3639	4.2603	3.57	1195	
16g/g'-L6_b	2911.5	79.1	1241.2	2.4094	4.3423	3.57	1218	
16g/g'-L6_c	2889.4	80.9	1253.4	2.3698	4.2708	3.57	1198	1203

L9 OD_{600} = 60	Pdt-**16g**	Pdt-**16g'**	Std	Pdt/Std	[Pdt]/mM	[PC]/μM	TTN	Avg. TTN
16g/g'-L9_a	6070.1	84.9	1250.8	4.9209	8.8684	5.18	1711	
16g/g'-L9_b	6498.3	84.5	1292.6	5.0927	9.1780	5.18	1771	
16g/g'-L9_c	6185.2	85.3	1323.9	4.7364	8.5359	5.18	1647	1710

L10 OD_{600} = 60	Pdt-**16g**	Pdt-**16g'**	Std	Pdt/Std	[Pdt]/mM	[PC]/μM	TTN	Avg. TTN
16g/g'-L10_a	1606.2	672.3	1414.3	1.6110	2.9034	2.71	1072	
16g/g'-L10_b	1701.5	712.6	1404.6	1.7187	3.0975	2.71	1144	
16g/g'-L10_c	1698.3	712.0	1395.3	1.7274	3.1132	2.71	1150	1122

Chiralpak IC, 8% IPA in hexane, 1.2 ml/min, 32 °C, 254nm

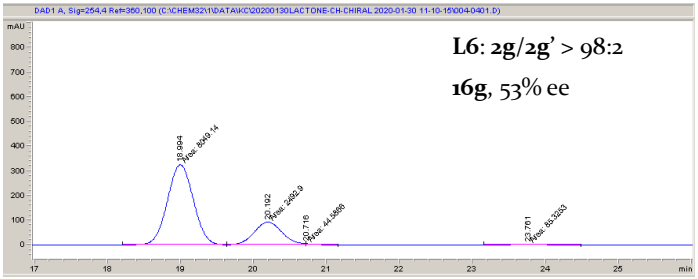

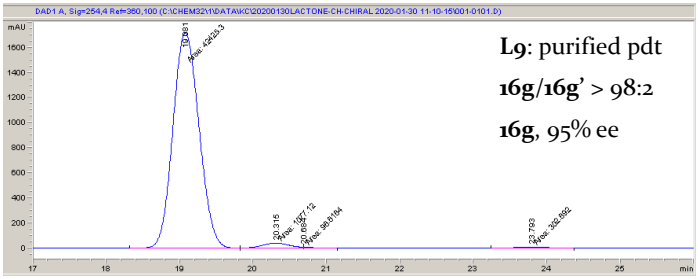

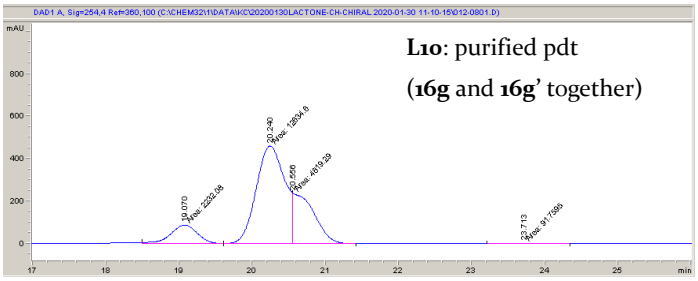

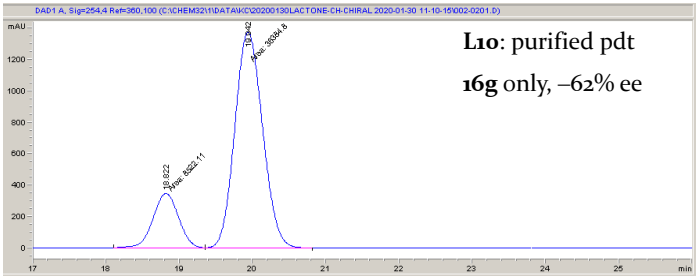

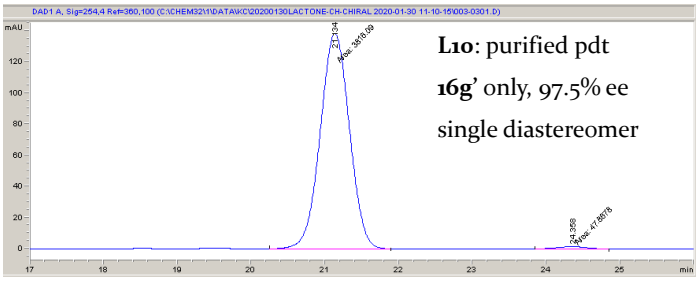

16g by variant **L6**			**16g** by variant **L9**		
Retention Time (min)	Area (mAU*s)	Area %	Retention Time (min)	Area (mAU*s)	Area %
18.99	8049.1	76.35	19.08	42425.3	97.52
20.19	2492.9	23.65	20.32	1077.1	2.48
Total	10542.0	100.00	Total	43502.4	100.00
16g by variant **L10**			**16g'** by variant **L10**		
Retention Time (min)	Area (mAU*s)	Area %	Retention Time (min)	Area (mAU*s)	Area %
18.82	8522.1	18.98	21.13	3816.1	98.76
19.94	36384.8	81.02	24.36	47.9	1.24
Total	44906.9	100.00	Total	3864	100.00

Note: The ee of **16g'** with variants **L6** and **L9** here cannot be accurately determined due to the peak overlap between one enantiomer of **2g** and one enantiomer of **16g'** (which is also very obvious in the situation of **L10**). Silica chromatography partially separated **16g** and **16g'**, which allowed the ee determination of **2g** and **2g'** with **L10**. Additionally, the confirmed side product **16g"** had no effect on the ee determination of **16g** and **16g'** due to a very different retention time on chiral HPLC.

3-(1-(Ethyl(phenyl)amino)ethyl)dihydrofuran-2(3*H*)-one (16h)

Analysis Data:

L6 OD_{600} = 60	Pdt-**16h1**	Pdt-**16h2**	Std	Pdt/Std	[Pdt]/mM	[PC]/μM	TTN	Avg. TTN
16h-L6_a	3483.2	984.7	2133.1	2.0946	2.0740	3.57	582	
16h-L6_b	3664.9	1031.0	2107.2	2.2285	2.2067	3.57	619	
16h-L6_c	3645.1	1021.7	2127.3	2.1938	2.1723	3.57	609	603

L9 OD_{600} = 60	Pdt-**16h1**	Pdt-**16h2**	Std	Pdt/Std	[Pdt]/mM	[PC]/μM	TTN	Avg. TTN
16h-L9_a	8696.2	583.0	2114.0	4.3894	4.3464	5.18	839	
16h-L9_b	8734.5	572.4	2112.3	4.4061	4.3629	5.18	842	
16h-L9_c	9017.8	591.4	2112.6	4.5485	4.5039	5.18	869	850

L10 OD_{600} = 60	Pdt-**16h1**	Pdt-**16h2**	Std	Pdt/Std	[Pdt]/mM	[PC]/μM	TTN	Avg. TTN
16h-L10_a	4435.5	56.4	2218.1	2.0251	2.0053	2.71	740	
16h-L10_b	4492.9	59.2	2209.8	2.0600	2.0398	2.71	753	

16h-L10_c	4288.2	56.5	2211.3	1.9648	1.9455	2.71	718	737

Chiralpak IC, 4.5% IPA in hexane, 1.1 ml/min, 28 °C, 254nm

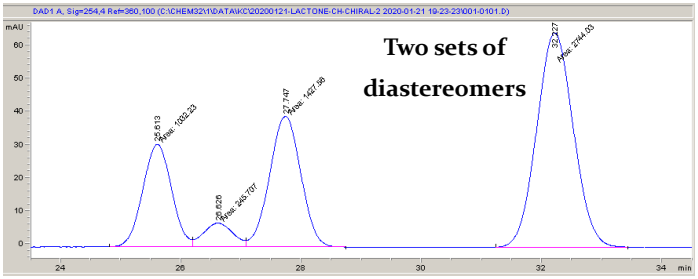

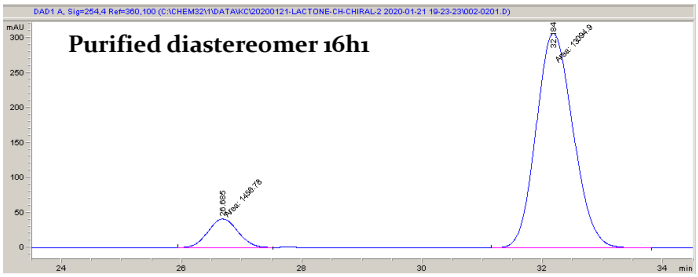

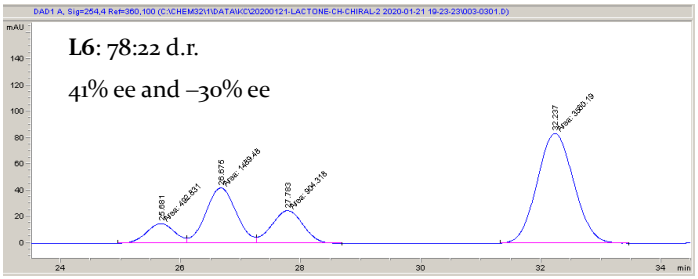

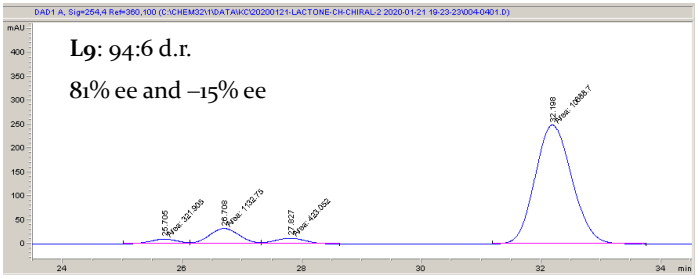

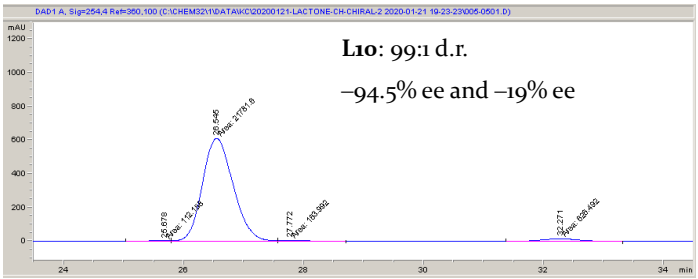

16h1 by variant **L6**			**16h2** by variant **L6**		
Retention Time (min)	Area (mAU*s)	Area %	Retention Time (min)	Area (mAU*s)	Area %
26.68	1489.5	29.50	25.68	492.8	35.27
32.24	3560.2	70.50	27.78	904.3	64.73
Total	5049.7	100.00	Total	1397.1	100.00

16h1 by variant **L9**			**16h2** by variant **L9**		
Retention Time (min)	Area (mAU*s)	Area %	Retention Time (min)	Area (mAU*s)	Area %
26.71	1132.8	9.58	25.71	321.9	43.27
32.20	10688.7	90.42	27.83	423.1	56.73
Total	11821.5	100.00	Total	744.0	100.00
16h1 by variant **L10**			**16h2** by variant **L10**		
Retention Time (min)	Area (mAU*s)	Area %	Retention Time (min)	Area (mAU*s)	Area %
26.55	21781.6	97.20	25.68	112.2	40.62
32.27	626.5	2.80	27.77	164.0	59.38
Total	22408.1	100.00	Total	276.2	100.00

3-(1-Phenylpyrrolidin-2-yl)dihydrofuran-2(3*H*)-one (16i)

Analysis Data:

L6 OD_{600} = 60	Pdt	Std	Pdt/Std	[Pdt]/mM	[PC]/μM	TTN	Avg. TTN
16i-L6_a	5487.8	1314.6	4.1745	9.1104	3.57	2555	
16i-L6_b	5440.1	1301.8	4.1789	9.1200	3.57	2558	
16i-L6_c	5450.8	1308.0	4.1673	9.0947	3.57	2550	2554

L7 OD_{600} = 60	Pdt	Std	Pdt/Std	[Pdt]/mM	[PC]/μM	TTN	Avg. TTN
16i-L7_a	6040.7	1293.6	4.6697	10.1911	8.80	1157	
16i-L7_b	6051.7	1295.3	4.6720	10.1963	8.80	1158	
16i-L7_c	6017.4	1281.8	4.6945	10.2453	8.80	1164	1160

L9 OD_{600} = 60	Pdt	Std	Pdt/Std	[Pdt]/mM	[PC]/μM	TTN	Avg. TTN
16i-L9_a	4648.3	1371.8	3.3885	7.3950	5.27	1404	
16i-L9_b	4805.3	1370.5	3.5062	7.6520	5.27	1453	
16i-L9_c	4844.6	1402.7	3.4538	7.5375	5.27	1431	1429

L10 OD_{600} = 60	Pdt	Std	Pdt/Std	[Pdt]/mM	[PC]/μM	TTN	Avg. TTN
16i-L10_a	2388.6	1356.8	1.7605	3.8420	2.71	1419	
16i-L10_b	2507.7	1307.3	1.9182	4.1863	2.71	1546	
16i-L10_c	2576.4	1373.3	1.8761	4.0943	2.71	1512	1492

Chiralpak IC, 6% IPA in hexane, 1.2 ml/min, 32 °C, 254nm

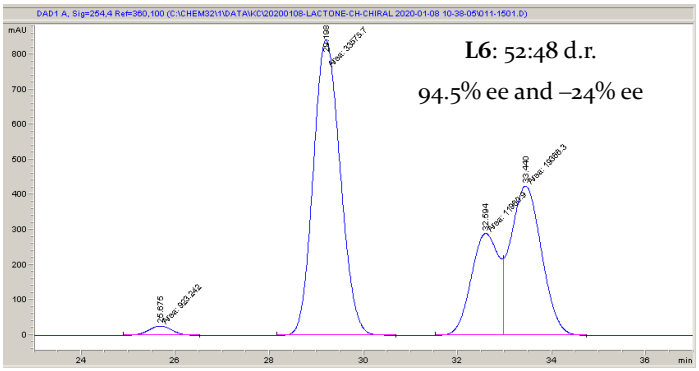

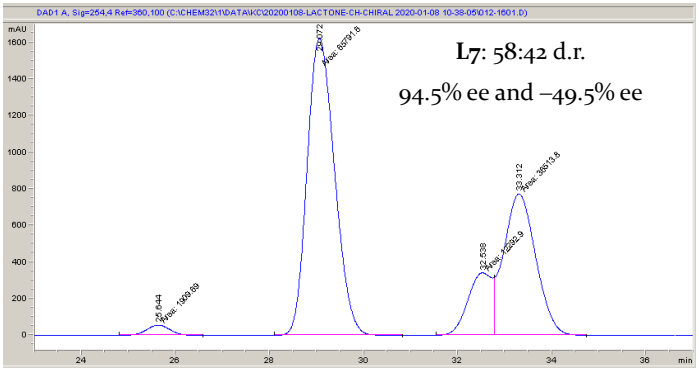

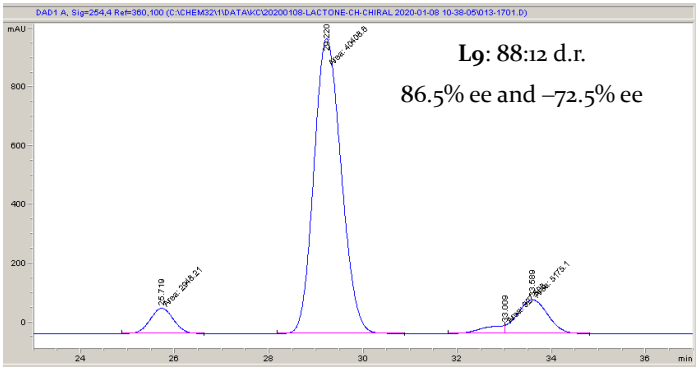

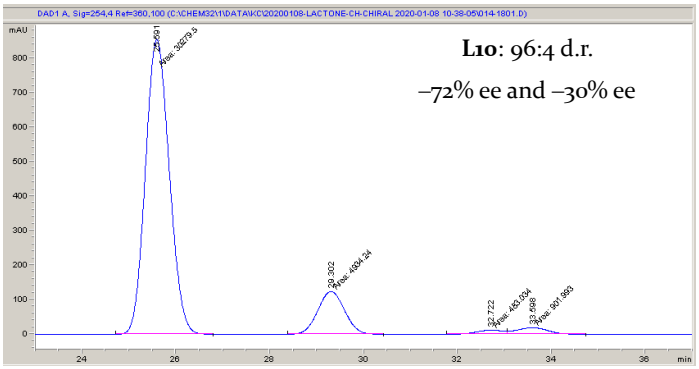

16i1 by variant **L6**			**16i2** by variant **L6**		
Retention Time (min)	Area (mAU*s)	Area %	Retention Time (min)	Area (mAU*s)	Area %
25.68	923.2	2.68	32.59	11960.9	38.18
29.20	33575.7	97.32	33.44	19366.3	61.82
Total	34498.9	100.00	Total	31327.2	100.00
16i1 by variant **L7**			**16i2** by variant **L7**		
Retention Time	Area (mAU*s)	Area %	Retention Time	Area (mAU*s)	Area %

(min)			(min)		
25.64	1909.7	2.82	32.54	12292.9	25.19
29.07	65791.6	97.18	33.31	36513.8	74.81
Total	67701.3	100.00	Total	48806.7	100.00
16i1 by variant **L9**			**16i2** by variant **L9**		
Retention Time (min)	Area (mAU*s)	Area %	Retention Time (min)	Area (mAU*s)	Area %
25.71	2948.2	6.80	33.01	827.6	13.79
29.22	40408.6	93.20	33.59	5175.1	86.21
Total	43356.8	100.00	Total	6002.7	100.00
16i1 by variant **L10**			**16i2** by variant **L10**		
Retention Time (min)	Area (mAU*s)	Area %	Retention Time (min)	Area (mAU*s)	Area %
25.59	30279.5	85.99	32.72	483.0	34.87
29.30	4934.2	14.01	33.60	902.0	65.13
Total	35213.7	100.00	Total	1385.0	100.00

3-(1-(3-Chlorophenyl)pyrrolidin-2-yl)dihydrofuran-2(3*H*)-one (16j)

Analysis Data:

L6 OD_{600} = 60	Pdt	Std	Pdt/Std	[Pdt]/mM	[PC]/μM	TTN	Avg. TTN
16j-L6_a	3072.0	1337.8	2.2963	3.4116	3.45	990	
16j-L6_b	2853.6	1324.3	2.1548	3.2014	3.45	929	
16i-L6_c	2911.2	1312.4	2.2182	3.2956	3.45	957	959

L7 OD_{600} = 60	Pdt	Std	Pdt/Std	[Pdt]/mM	[PC]/μM	TTN	Avg. TTN
16j-L7_a	4395.6	1188.0	3.7000	5.4971	8.80	624	
16j-L7_b	3527.1	1067.0	3.3056	4.9112	8.80	558	
16j-L7_c	5181.6	1248.0	4.1519	6.1685	8.80	701	628

L8 OD_{600} = 60	Pdt	Std	Pdt/Std	[Pdt]/mM	[PC]/μM	TTN	Avg. TTN
16j-L8_a	4296.0	1189.8	3.6107	5.3644	6.43	834	
16j-L8_b	4214.8	1189.6	3.5430	5.2639	6.43	819	
16j-L8_c	4289.5	1180.8	3.6327	5.3971	6.43	839	
16j-L8_d	4790.6	1193.6	4.0136	5.9630	6.43	927	855

L9 OD_{600} = 60	Pdt	Std	Pdt/Std	[Pdt]/mM	[PC]/μM	TTN	Avg. TTN
16j-L9_a	5079.1	1171.5	4.3356	6.4413	5.19	1241	
16j-L9_b	6388.1	1177.2	5.4265	8.0622	5.19	1554	

16j-L9_c	5941.2	1160.0	5.1217	7.6093	5.19	1466	
16j-L9_d	6305.6	1154.1	5.4637	8.1173	5.19	1564	1456

Chiralpak IA, 3% IPA in hexane, 1.2 ml/min, 32 °C, 254nm

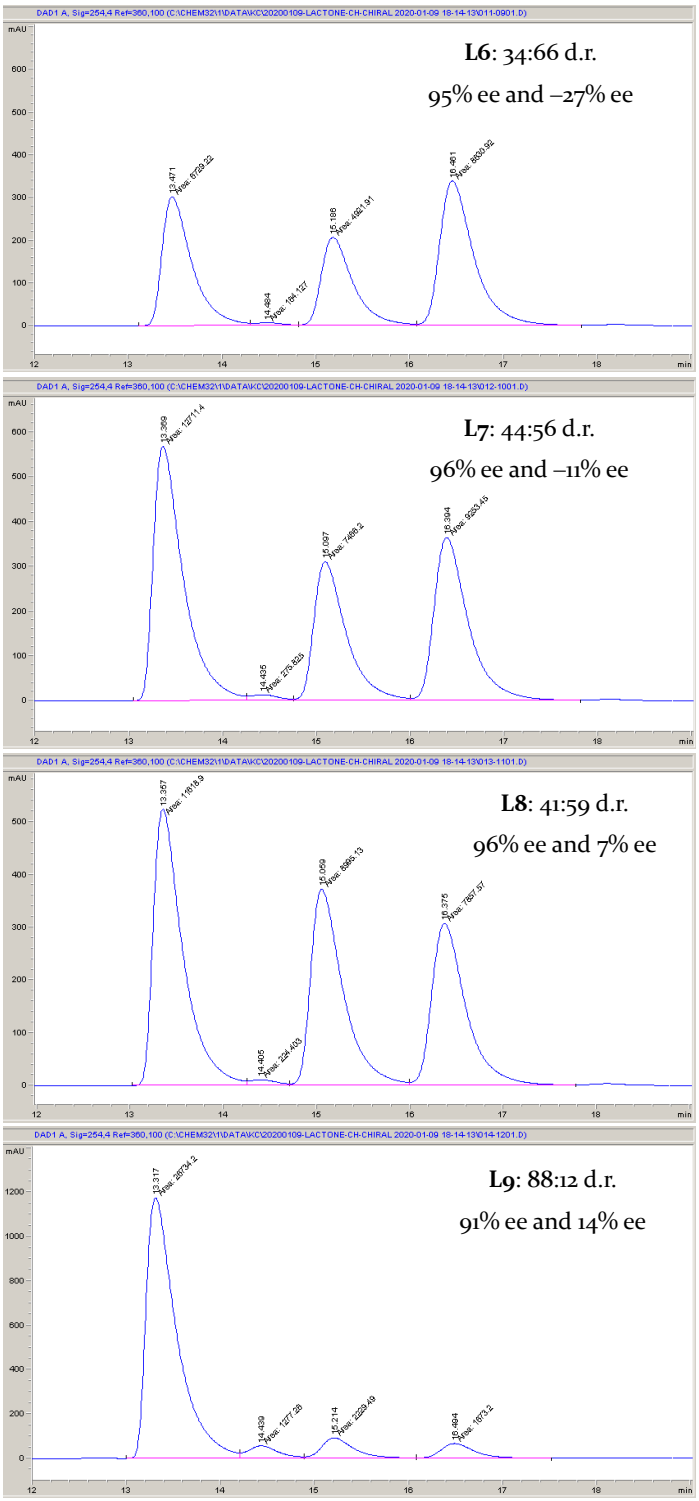

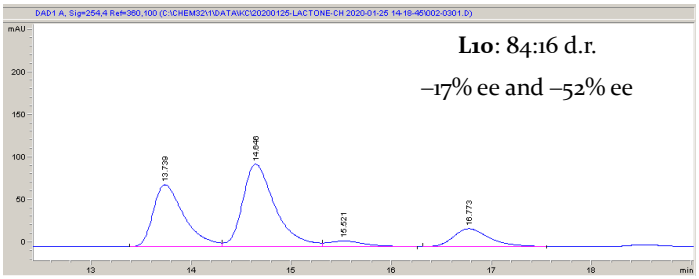

16j1 by variant **L6**			**16j2** by variant **L6**		
Retention Time (min)	Area (mAU*s)	Area %	Retention Time (min)	Area (mAU*s)	Area %
13.47	6729.2	97.62	15.17	4921.9	36.32
14.48	164.1	2.38	16.46	8630.9	63.68
Total	6893.3	100.00	Total	13552.8	100.00
16j1 by variant **L7**			**16j2** by variant **L7**		
Retention Time (min)	Area (mAU*s)	Area %	Retention Time (min)	Area (mAU*s)	Area %
13.37	12711.4	97.88	15.10	7466.2	44.66
14.44	275.8	2.12	16.39	9253.5	55.34
Total	12987.2	100.00	Total	16719.7	100.00
16j1 by variant **L8**			**16j2** by variant **L8**		
Retention Time (min)	Area (mAU*s)	Area %	Retention Time (min)	Area (mAU*s)	Area %
13.36	11618.9	98.11	15.06	8995.1	53.37
14.41	224.4	1.89	16.38	7857.6	46.63
Total	11843.3	100.00	Total	16852.7	100.00
16j1 by variant **L9**			**16j2** by variant **L9**		
Retention Time (min)	Area (mAU*s)	Area %	Retention Time (min)	Area (mAU*s)	Area %
13.32	26734.2	95.44	15.21	2229.5	57.13
14.44	1277.3	4.56	16.49	1673.2	42.87
Total	28011.5	100.00	Total	3902.7	100.00
16j1 by variant **L10**			**16j2** by variant **L10**		
Retention Time (min)	Area (mAU*s)	Area %	Retention Time (min)	Area (mAU*s)	Area %
13.74	1563.6	41.66	15.52	168.3	23.88
14.65	2189.9	58.34	16.77	536.6	76.12
Total	3753.5	100.00	Total	704.9	100.00

3-(1-(2,3-Dimethylphenyl)pyrrolidin-2-yl)dihydrofuran-2(3*H*)-one (16k)

Analysis Data:

L7 OD_{600} = 30	Pdt-**16k1**	Pdt-**16k2**	Std	Pdt/Std	[Pdt]/mM	[PC]/μM	TTN	Avg. TTN
16k-L7_a	6348.1	1742.6	1185.9	6.8224	10.3360	4.40	2348	

16k-L7_b	6633.2	1820.7	1210.0	6.9867	10.5848	4.40	2404	
16k-L7_c	6673.6	1839.2	1197.0	7.1118	10.7743	4.40	2447	2400

L8 OD_{600} = 30	Pdt-**16k1**	Pdt-**16k2**	Std	Pdt/Std	[Pdt]/mM	[PC]/μM	TTN	Avg. TTN
16k-L8_a	5871.2	1294.8	1138.0	6.2970	9.5400	3.51	2716	
16k-L8_b	5708.7	1247.3	1152.8	6.0340	9.1415	3.51	2602	
16k-L8_c	5912.4	1280.9	1132.5	6.3517	9.6228	3.51	2739	
16k-L8_d	6284.3	1359.8	1149.4	6.6505	10.0755	3.51	2868	2731

L9 OD_{600} = 30	Pdt-**16k1**	Pdt-**16k2**	Std	Pdt/Std	[Pdt]/mM	[PC]/μM	TTN	Avg. TTN
16k-L9_a	5705.5	3229.5	1257.1	7.1076	10.7681	2.63	4089	
16k-L9_b	5650.4	3192.2	1286.2	6.8750	10.4156	2.63	3955	
16k-L9_c	5418.3	3073.9	1233.8	6.8830	10.4277	2.63	3959	4001

Chiralpak OD-H, 4% IPA in hexane, 1.2 ml/min, 32 °C, 254nm

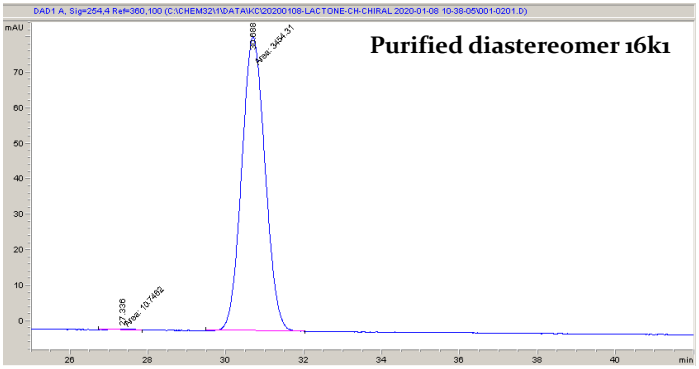

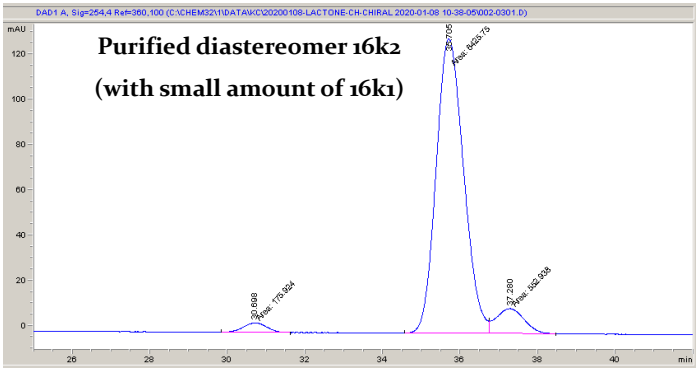

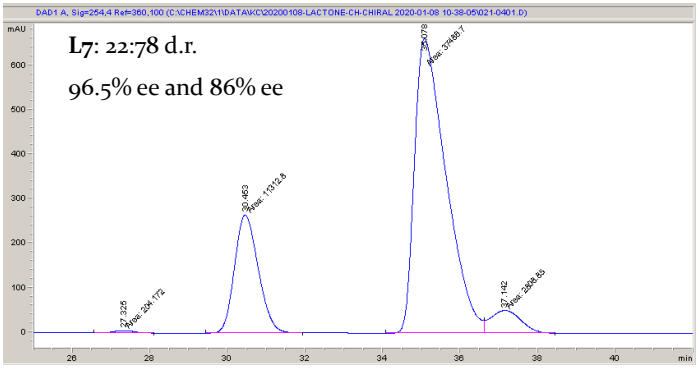

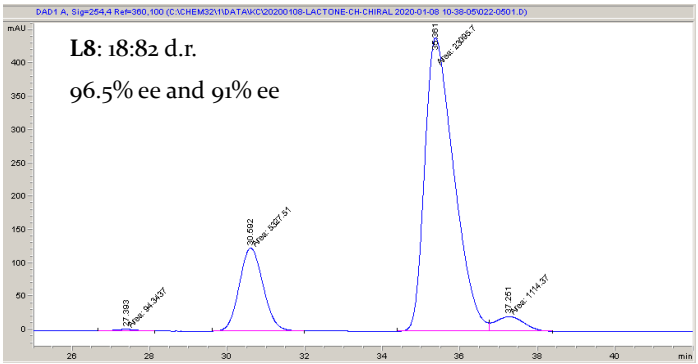

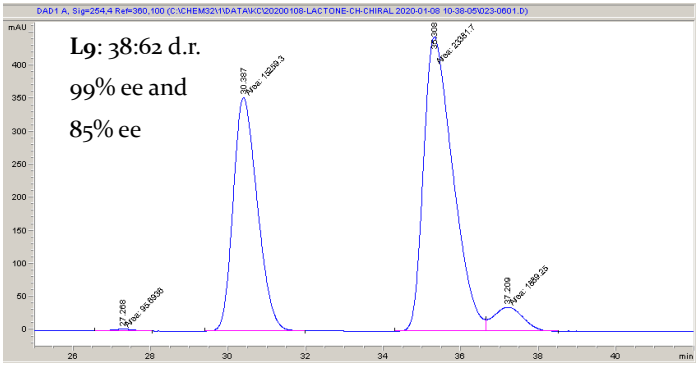

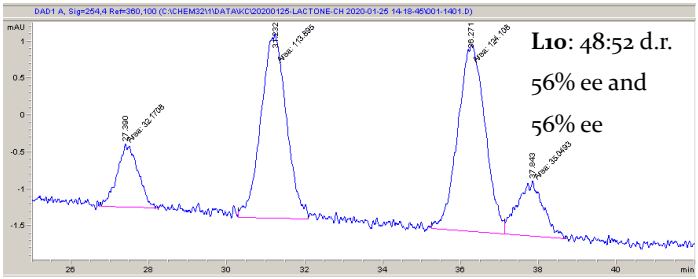

16k1 by variant **L7**			**16k2** by variant **L7**		
Retention Time (min)	Area (mAU*s)	Area %	Retention Time (min)	Area (mAU*s)	Area %
27.33	204.2	1.77	35.08	37486.7	93.03
30.45	11312.8	98.23	37.14	2808.9	6.97
Total	11517.0	100.00	Total	40295.6	100.00
16k1 by variant **L8**			**16k2** by variant **L8**		
Retention Time (min)	Area (mAU*s)	Area %	Retention Time (min)	Area (mAU*s)	Area %
27.39	94.3	1.74	35.36	23095.7	95.40
30.59	5327.5	98.26	37.25	1114.4	4.60
Total	5421.8	100.00	Total	24210.1	100.00
16k1 by variant **L9**			**16k2** by variant **L9**		
Retention Time (min)	Area (mAU*s)	Area %	Retention Time (min)	Area (mAU*s)	Area %
27.27	95.7	0.62	35.31	23381.7	92.52
30.39	15259.3	99.38	37.21	1889.3	7.48
Total	15355.0	100.00	Total	25271.0	100.00
16k1 by variant **L10**			**16k2** by variant **L10**		

Retention Time (min)	Area (mAU*s)	Area %	Retention Time (min)	Area (mAU*s)	Area %
27.39	32.2	22.04	36.27	124.1	78.00
31.23	113.9	77.96	37.84	35.0	22.00
Total	146.1	100.00	Total	159.1	100.00

3-(1-(4-Methoxyphenyl)pyrrolidin-2-yl)dihydrofuran-2(3*H*)-one (16l)

Analysis Data:

L6 OD_{600} = 60	Pdt	Std	Pdt/Std	[Pdt]/mM	[PC]/μM	TTN	Avg. TTN
16l-L6_a	2160.9	1152.1	1.8756	3.1685	3.35	947	
16l-L6_b	2200.0	1141.9	1.9266	3.2546	3.35	973	
16l-L6_c	2174.0	1179.3	1.8435	3.1142	3.35	931	
16l-L6_d	2197.9	1142.6	1.9236	3.2495	3.35	971	955

L7 OD_{600} = 60	Pdt	Std	Pdt/Std	[Pdt]/mM	[PC]/μM	TTN	Avg. TTN
16l-L7_a	6904.9	1125.9	6.1328	10.3601	8.20	1263	
16l-L7_b	7614.6	1117.4	6.8146	11.5119	8.20	1403	
16l-L7_c	6405.5	1118.7	5.7258	9.6727	8.20	1179	
16l-L7_d	6480.6	1116.2	5.8059	9.8080	8.20	1196	1260

L9 OD_{600} = 60	Pdt	Std	Pdt/Std	[Pdt]/mM	[PC]/μM	TTN	Avg. TTN
16l-L9_a	657.9	1213.1	0.5423	0.9162	4.55	201	
16l-L9_b	658	1179.6	0.5578	0.9423	4.55	207	
16l-L9_c	667.2	1189.6	0.5609	0.9475	4.55	208	
16l-L9_d	679.7	1170.3	0.5808	0.9811	4.55	216	208

Chiral HPLC trace:

Chiralpak IC, 25% IPA in hexane, 1.2 ml/min, 28 °C, 254nm

Chiralpak IB, 12% IPA in hexane, 1.2 ml/min, 28 °C, 254nm

(Note: The four stereo-isomers of product **16l** could not be fully separated by chiral HPLC columns. We thus used two different columns to have three sets of peaks each, as labelled in the HPLC traces, and then calculated the enantiomeric excess according to the peak ratios).

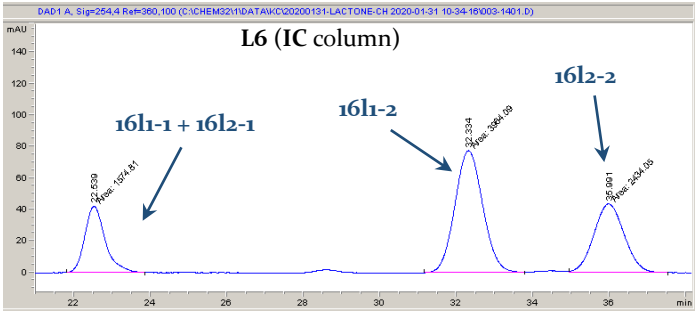

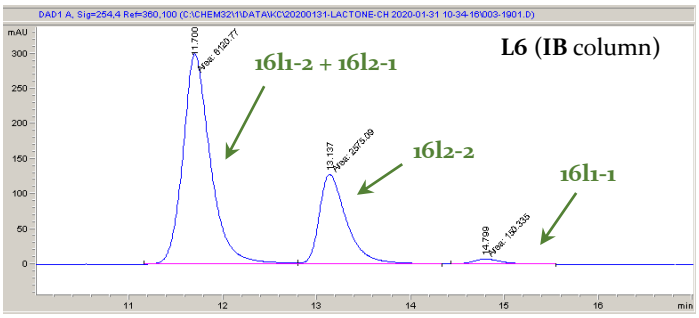

16l	peak-1	peak-2	peak-3	sum
L6-IC	1574.8	3964.1	2434.1	7973
	19.75%	49.72%	30.53%	100.00%
L6-IB	6120.8	2575.1	150.3	8846.2
	69.19%	29.11%	1.70%	100.00%
	16l1-1	**16l1**-2	**16l2**-1	**16l2**-2
	1.70%	50.43%	18.05%	29.82%
52:48 d.r.	**16l1** 93% ee		**16l2** –26% ee	

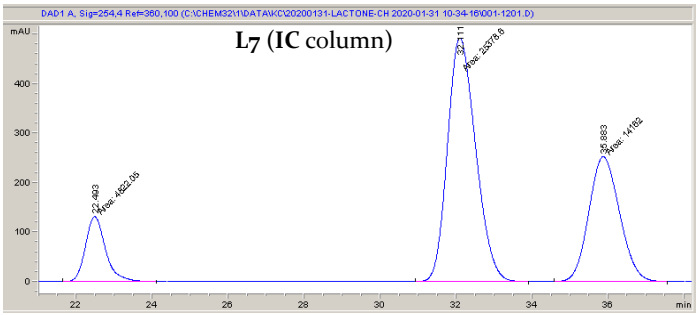

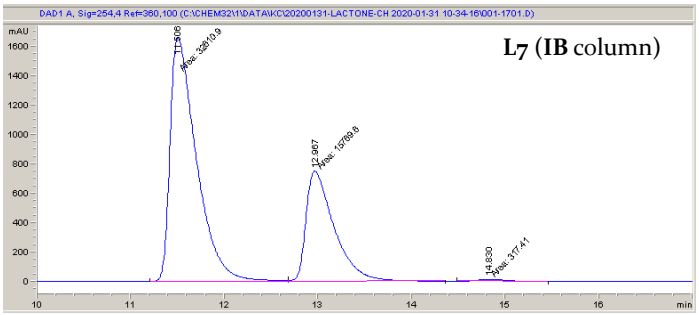

16l	peak-1	peak-2	peak-3	sum
L7-IC	4822.1	25378.6	14162	44362.7
	10.87%	57.21%	31.92%	100.00%
L7-IB	32610.9	15769.6	317.4	48697.9
	66.97%	32.38%	0.65%	100.00%
	16l1-1	**16l1**-2	**16l2**-1	**16l2**-2
	0.65%	56.98%	10.22%	32.15%
58:42 d.r.	**16l1** 98% ee		**16l2** –51.5% ee	

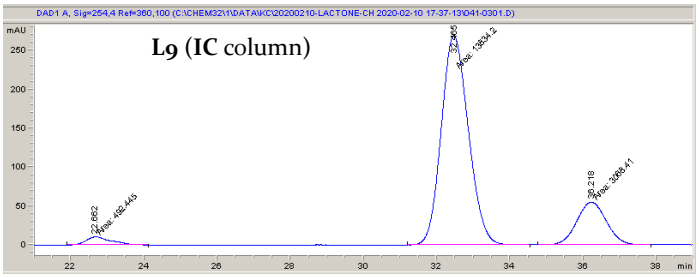

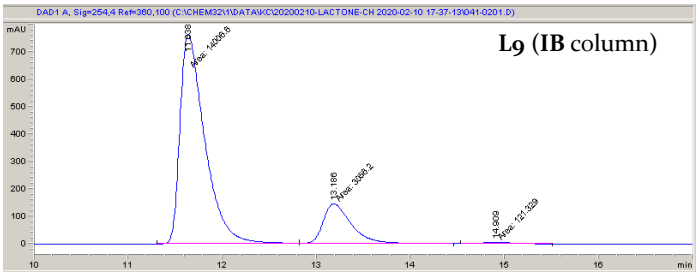

16l	peak-1	peak-2	peak-3	sum
L9-IC	492.4	13834.2	3068.4	17395
	2.83%	79.53%	17.64%	100.00%
L9-IB	14006.6	3056.2	121.3	17184.1
	81.51%	17.79%	0.71%	100.00%
	16l1-1	**16l1**-2	**16l2**-1	**16l2**-2
	0.71%	79.46%	2.12%	17.71%
80:20 d.r.	**16l1** 98% ee		**16l2** –78.5% ee	

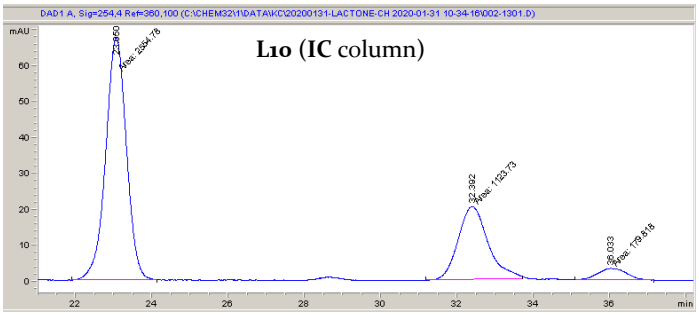

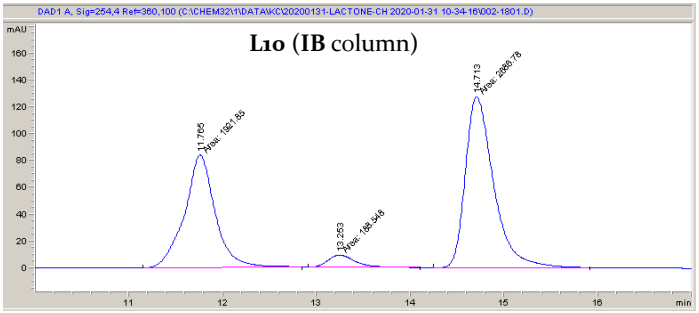

16l	peak-1	peak-2	peak-3	sum
L10-IC	2554.8	1123.7	179.8	3858.3
	66.22%	29.12%	4.66%	100.00%
L10-IB	1921.9	188.5	2686.8	4797.2

	40.06%	3.93%	56.01%	100.00%
	16l1-1	**16l1**-2	**16l2**-1	**16l2**-2
	56.01%	29.49%	10.21%	4.29%
80:20 d.r.	**16l1** –31% ee		**16l2** 37% ee	

3-(1-Phenylazetidin-2-yl)dihydrofuran-2(3*H*)-one (16m)

Analysis Data:

L10 OD_{600} = 60	Pdt	Std	Pdt/Std	[Pdt]/mM	[PC]/μM	TTN	Avg. TTN
16m-L10_a	374.2	760.4	0.4921	0.3916	2.71	145	
16m-L10_b	374.3	755.3	0.4956	0.3944	2.71	146	
16m-L10_c	360.4	760.7	0.4738	0.3770	2.71	139	143

Chiralpak IC, 8% IPA in hexane, 1.2 ml/min, 32 °C, 254nm

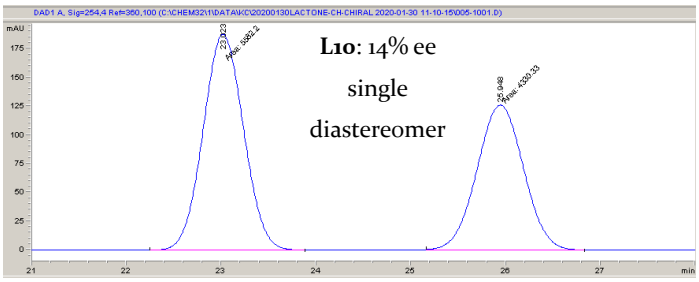

16m by variant **L10**		
Retention Time (min)	Area (mAU*s)	Area %
23.02	5582.2	56.31
25.95	4330.3	43.69
Total	9912.5	100.00

3-(1-(3-Chloro-4-fluorophenyl)pyrrolidin-2-yl)dihydrofuran-2(3*H*)-one (16n)

Analysis Data:

L9 OD_{600} = 60	Pdt	Std	Pdt/Std	[Pdt]/mM	[PC]/μM	TTN	Avg. TTN
16n-L9_a	2025.3	1375.6	1.4723	2.4395	5.27	463	
16n-L9_b	1834.4	1379.1	1.3301	2.2039	5.27	418	
16n-L9_c	1841.7	1367.4	1.3469	2.2316	5.27	424	435

Chiralpak IA, 3% IPA in hexane, 1.2 ml/min, 32 °C, 254nm

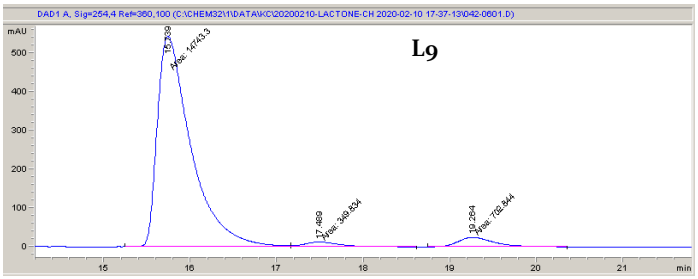

Note: Only three peaks were observed and confirmed to belong to the stereo-isomers of product **16n**. No conclusion on ee should be made unless further analysis is carried out.

B.5.4 Enzymatic synthesis of α-boryl-γ-lactones

All enzymatic reactions for lactone-based organoborane formation in analytical scale were conducted following the general procedure described below and analyzed with gas chromatography-mass spectrometry (GC-MS). All TTNs for the different products were determined using the GC standard curve of the corresponding racemic standard product made with $Rh_2(OAc)_4$ or I_2.

All enzymatic reactions for lactone-based organoborane formation in preparative scale were conducted following the general procedure described below, and the corresponding lactone-based organoborane products were isolated. Detailed conditions for preparative-scale reactions of different substrates are indicated separately.

General procedure for preparative-scale reactions:

To a 20 mL vial were added degassed suspension of *E. coli* expressing *Rma* cytochrome *c* (5 mL, OD_{600} = 15), borane (150 μL of 400 mM stock solution in MeCN, 0.24 mmol), lactone diazo (150 μL of 400 mM stock solution in MeCN, 0.24 mmol), D-glucose (50 mM), in M9-N buffer (pH 7.4) under anaerobic conditions. The vial was capped and shaken (480 rpm) at room temperature for 18 h. Reactions for each substrate were set up in quadruplicate.

After the reaction was completed, reactions in replicate were combined and transferred to 50 mL centrifuge tubes. The reaction vials were washed with water (2 mL × 2) followed by mixed organic solvent (hexane/ethyl acetate = 1:1, 2 mL × 3). The washing solution was combined with the reaction mixture in the centrifuge tubes. An additional 15 mL of hexane/ethyl acetate solvent was added to every tube. The tube was then vortexed (1 min × 3) and shaken vigorously, and centrifuged (5,000 × g, 5 min). The organic layer was separated and the aqueous layer was subjected to three more rounds of extraction. The organic layers were combined, dried over Na_2SO_4 and concentrated under reduced pressure. Purification by silica column chromatography with hexane/(ethyl acetate:acetone 7:3) as eluent afforded the desired lactone-based organoboranes. Enantioselectivity was measured by chiral HPLC. TTNs were calculated based on measured protein concentration and isolated product yield.

(1,3-Dimethyl-1*H*-imidazol-3-ium-2-yl)(2-oxotetrahydrofuran-3-yl)dihydroborate (20a)

Analysis Data:

Entries	Pdt	Std	Pdt/Std	[Pdt]/mM	[PC]/μM	TTN	Avg.	Avg.

							TTN	yield
20a-(1)	38262	5643	6.780	7.45	8.30	898		
20a-(2)	40969	5630	7.277	7.94	8.30	957		
20a-(3)	43223	5984	7.223	7.89	8.30	950		
20a-(4)	49313	5559	8.871	9.46	8.30	1140	986	81.8%

Chiralpak IC, 40% *i*-PrOH in hexane, 1.5 mL/min, 32 °C, 235 nm

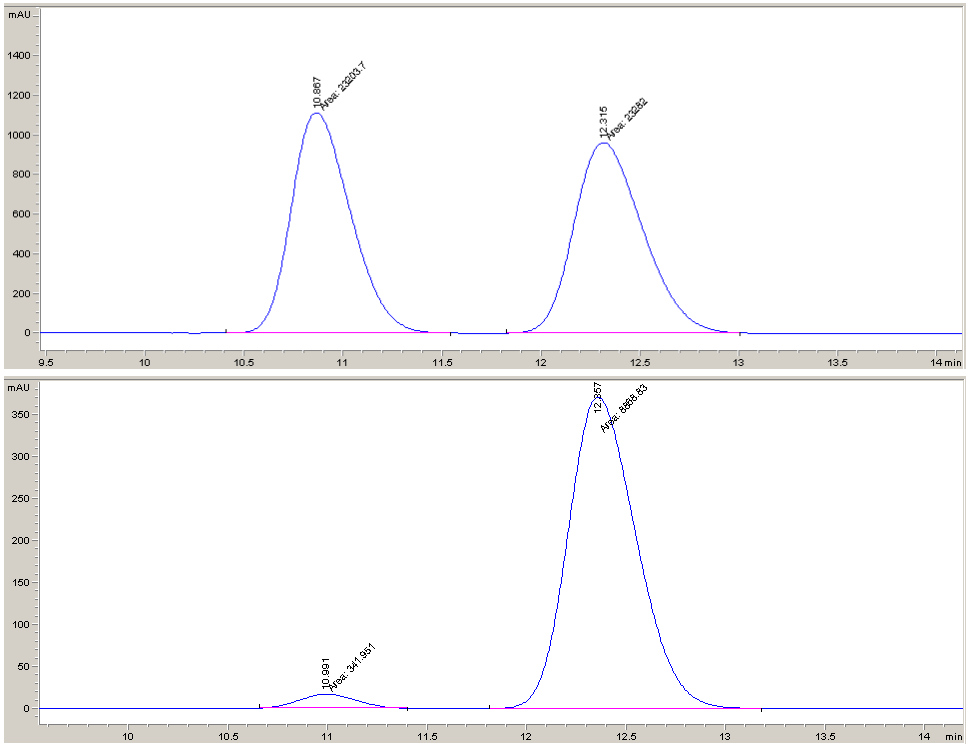

***rac*-20a**			**Enzymatically produced 20a**		
Retention Time (min)	Area (mAU*s)	Area %	Retention Time (min)	Area (mAU*s)	Area %
10.867	23203.7	49.92	10.991	341.95	3.71
12.315	23282	50.08	12.857	8868.83	96.29
Total	46485.7	100.00	Total	9210.78	100.00

Preparative-scale reaction:

***E. coli* suspension expressing BOR^{LAC} in M9-N**				***D*-glucose**	
OD_{600}	volume/mL	[PC]/μM	n_pro/μmol	weight/mg	[Glu]/mM
15	20	8.30	0.166	180	50
borane (19a) stock in MeCN			**diazo (1) stock in MeCN**		
stock/mM	volume/μL	n_1/mmol	stock/mM	volume/μL	n_2/mmol
400	600	0.24	400	600	0.24
purification eluent	**Product**				
(ethyl acetate: acetone 7:3) in hexanes (30% to 100% gradient)	m[Pdt]/mg	n[Pdt]/mmol	yield	TTN	
	41.4	0.213	89%	1290	

(2-Oxotetrahydrofuran-3-yl)(1,3,5-trimethyl-1*H*-imidazol-3-ium-2-yl)dihydroborate (20b)

Analysis Data:

Entries	Pdt	Std	Pdt/Std	[Pdt]/mM	[PC]/μM	TTN	Avg. TTN	Avg. yield
20b-(1)	53629	5587	9.599	9.50	8.20	1159		
20b-(2)	47943	4968	9.650	9.54	8.20	1164		
20b-(3)	50689	5641	8.986	9.03	8.20	1102		
20b-(4)	51778	5029	10.296	10.01	8.20	1221	1161	95.2%

Chiralpak IC, 40% *i*-PrOH in hexane, 1.5 mL/min, 32 °C, 235 nm

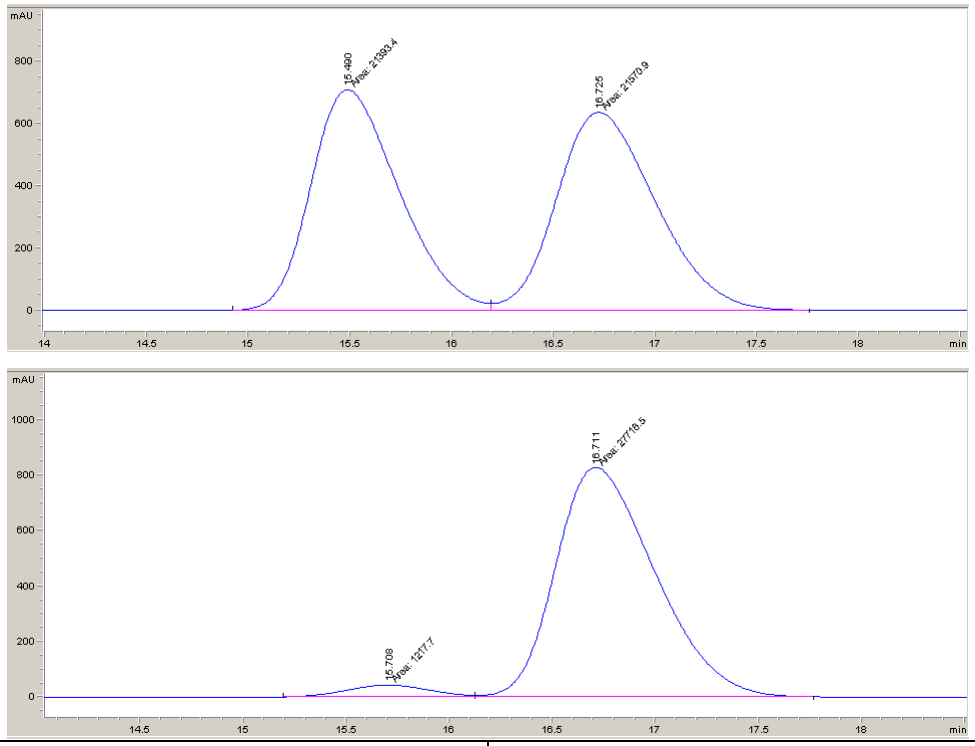

***rac*-20b**			**Enzymatically produced 20b**		
Retention Time (min)	Area (mAU*s)	Area %	Retention Time (min)	Area (mAU*s)	Area %
15.490	21393.4	49.79	15.708	1217.7	4.21
16.725	21570.9	50.21	16.711	27716.5	95.79
Total	42964.3	100.00	Total	28934.2	100.00

(1,3-Dimethyl-5-(trifluoromethyl)-1*H*-imidazol-3-ium-2-yl)(2-oxotetrahydrofuran-3-yl)dihydroborate (20c)

Analysis Data:

Entries	Pdt	Std	Pdt/Std	[Pdt]/mM	[PC]/μM	TTN	Avg. TTN	Avg. yield
20c-(1)	47111	4874	9.666	6.53	8.20	796		
20c-(2)	43029	5227	8.232	5.63	8.20	687		
20c-(3)	48256	5249	9.193	6.24	8.20	761		

20c-(4)	49190	5251	9.368	6.35	8.20	774	754	61.9%

Chiralpak IC, 12% *i*-PrOH in hexane, 1 mL/min, 32 °C, 235 nm

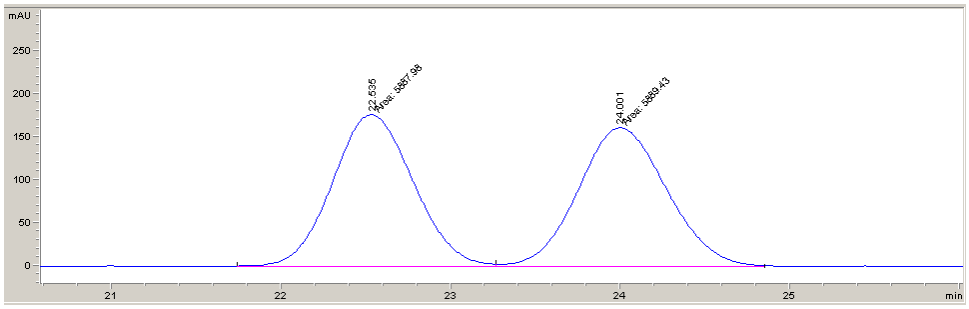

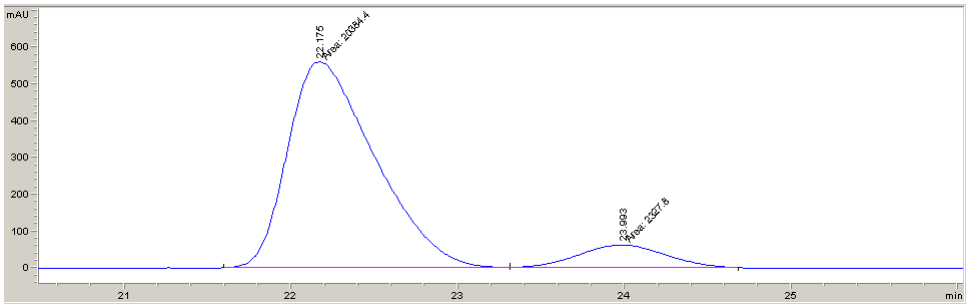

***rac*-20c**			**Enzymatically produced 20c**		
Retention Time (min)	Area (mAU*s)	Area %	Retention Time (min)	Area (mAU*s)	Area %
22.535	5887.98	49.99	22.175	20384.4	89.75
24.001	5889.43	50.01	23.993	2327.8	10.25
Total	11777.41	100.00	Total	22712.2	100.00

(1-Ethyl-3-methyl-1*H*-imidazol-3-ium-2-yl)(2-oxotetrahydrofuran-3-yl)dihydroborate (20d)

Analysis Data:

Entries	Pdt	Std	Pdt/Std	[Pdt]/mM	[PC]/μM	TTN	Avg. TTN	Avg. yield
20d-(1)	68768	6671	10.308	7.90	8.20	964		
20d-(2)	63101	6924	9.113	7.11	8.20	868		
20d-(3)	68256	6203	11.004	8.35	8.20	1018		
20d-(4)	68771	6607	10.409	7.97	8.20	972	955	78.3%

Chiralpak OD-H, 15% *i*-PrOH in hexane, 1.2 mL/min, 32 °C, 235 nm

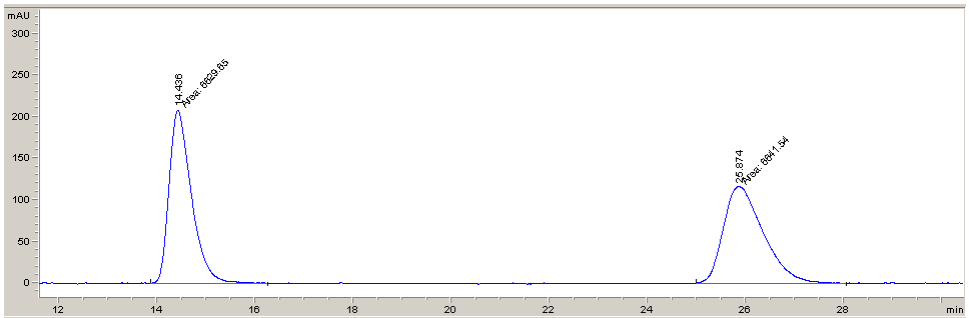

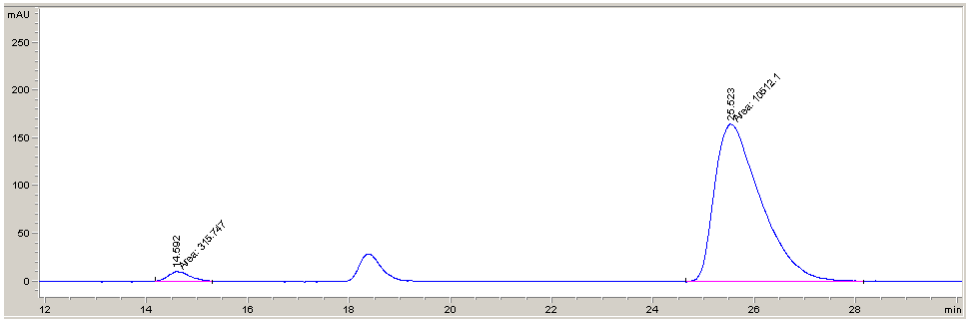

***rac*-20d**			**Enzymatically produced 20d**		
Retention Time (min)	Area (mAU*s)	Area %	Retention Time (min)	Area (mAU*s)	Area %
14.436	6629.85	49.96	14.592	315.7	2.92
25.874	6641.54	50.04	25.523	10512.1	97.08
Total	13271.39	100.00	Total	10827.8	100.00

(3-Hexyl-1-methyl-1*H*-imidazol-3-ium-2-yl)(2-oxotetrahydrofuran-3-yl)dihydroborate (20e)

Analysis Data:

Entries	Pdt	Std	Pdt/Std	[Pdt]/mM	[PC]/μM	TTN	Avg. TTN	Avg. yield
20e-(1)	69850	6510	10.730	6.59	8.20	803		
20e-(2)	70694	6131	11.531	7.01	8.20	855		
20e-(3)	73353	5669	12.939	7.75	8.20	945		
20e-(4)	70012	5728	12.223	7.38	8.20	900	876	71.8%

Chiralpak IC, 20% *i*-PrOH in hexane, 1.3 mL/min, 32 °C, 235 nm

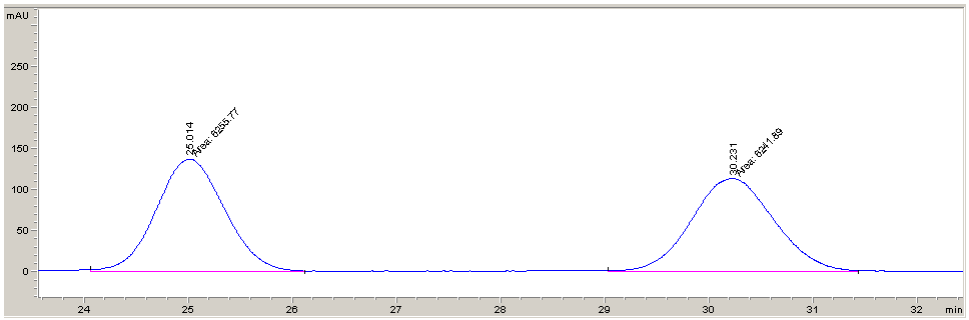

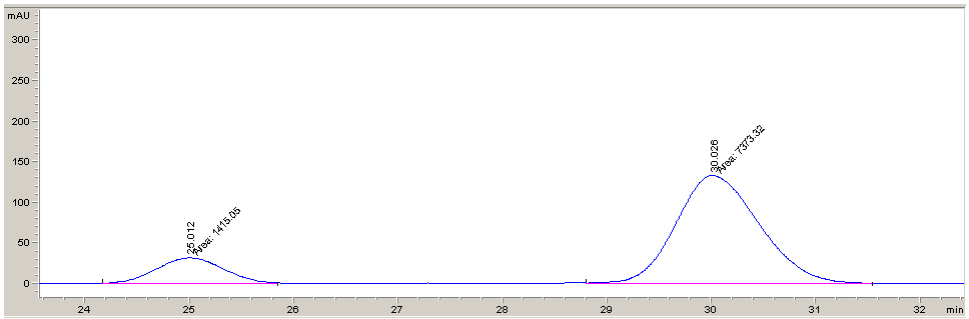

***rac*-20e**			**Enzymatically produced 20e**		
Retention Time	Area (mAU*s)	Area %	Retention Time	Area (mAU*s)	Area %

(min)			(min)		
25.014	6255.77	50.06	25.012	1415.05	16.10
30.231	6241.89	49.94	30.026	7373.32	83.90
Total	12497.66	100.00	Total	8788.37	100.00

(1,3-Dimethyl-1*H*-imidazol-3-ium-2-yl)(2-oxotetrahydro-2*H*-pyran-3-yl)dihydroborate (2of)

Analysis Data:

Entries	Pdt	Std	Pdt/Std	[Pdt]/mM	[PC]/μM	TTN	Avg. TTN	Avg. yield
2of-(1)	41922	4513	9.289	9.34	8.30	1125		
2of-(2)	39155	4803	8.152	8.39	8.30	1011		
2of-(3)	46105	4530	10.178	10.04	8.30	1209		
2of-(4)	42958	4690	9.159	9.23	8.30	1112	1114	92.5%

Chiralpak IC, 30% *i*-PrOH in hexane, 1.3 mL/min, 32 °C, 235 nm

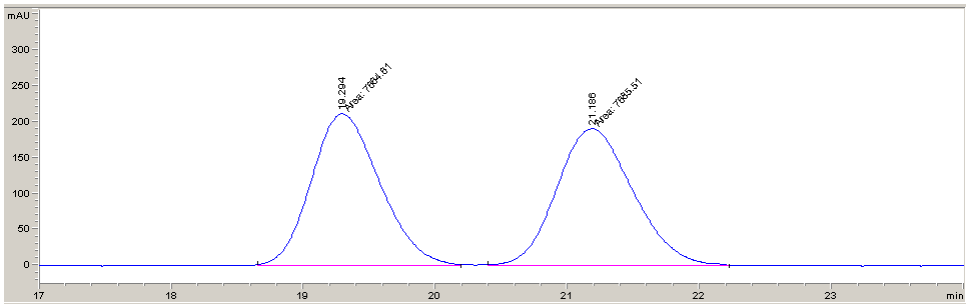

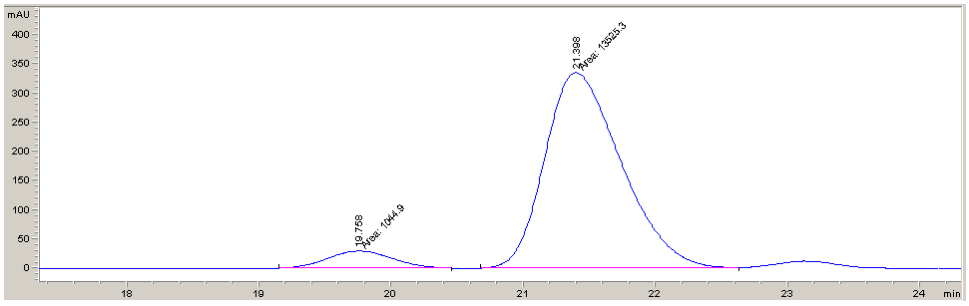

***rac*-2of**			**Enzymatically produced 2of**		
Retention Time (min)	Area (mAU*s)	Area %	Retention Time (min)	Area (mAU*s)	Area %
19.294	7664.61	49.93	19.758	1044.9	7.17
21.186	7685.51	50.07	21.398	13525.3	92.83
Total	15350.12	100.00	Total	14570.2	100.00

Preparative-scale reaction:

***E. coli* suspension expressing BOR^{LAC} in M9-N**				***D*-glucose**	
OD_{600}	volume/mL	[PC]/μM	n_pro/μmol	weight/mg	[Glu]/mM
15	20	8.30	0.166	180	50
borane (19a) stock in MeCN			**diazo (1) stock in MeCN**		

stock/mM	volume/µL	n_1/mmol	stock/mM	volume/µL	n_2/mmol
400	600	0.24	400	600	0.24
purification eluent		**Product**			
(ethyl acetate: acetone 7:3) in hexanes (30% to 100% gradient)		m[Pdt]/mg	n[Pdt]/mmol	yield	TTN
		41.3	0.198	83%	1200

(1-Ethyl-3-methyl-1*H*-imidazol-3-ium-2-yl)(2-oxotetrahydro-2*H*-pyran-3-yl)dihydroborate (20g)

Analysis Data:

Pdt-Entries	Pdt	Std	Pdt/Std	[Pdt]/mM	[PC]/µM	TTN	Avg. TTN	Avg. yield
20g-(1)	45859	4230	10.841	9.05	8.30	1090		
20g-(2)	48114	4168	11.544	9.57	8.30	1153		
20g-(3)	49338	3648	13.525	11.02	8.30	1327		
20g-(4)	43728	3735	11.708	9.69	8.30	1168	1185	98.3%

Chiralpak IC, 18% *i*-PrOH in hexane, 1.2 mL/min, 32 °C, 235 nm

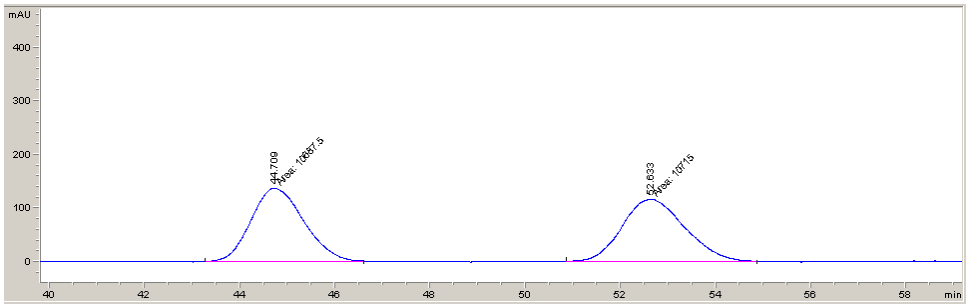

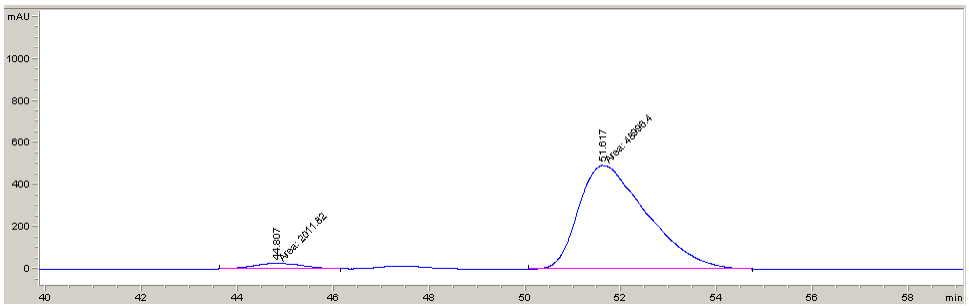

***rac*-20g**			**Enzymatically produced 20g**		
Retention Time (min)	Area (mAU*s)	Area %	Retention Time (min)	Area (mAU*s)	Area %
44.709	10687.5	49.94	44.807	2011.8	3.94
52.633	10715	50.06	51.617	48996.4	96.06
Total	21402.5	100.00	Total	51008.2	100.00

(1,3-Dimethyl-5-(trifluoromethyl)-1*H*-imidazol-3-ium-2-yl)(2-oxotetrahydro-2*H*-pyran-3-yl)dihydroborate (20h)

Analysis Data:

Pdt-Entries	Pdt	Std	Pdt/Std	[Pdt]/mM	[PC]/μM	TTN	Avg. TTN	Avg. yield
20h-(1)	59591	4739	12.575	9.10	8.30	1096		
20h-(2)	60894	4605	13.223	9.50	8.30	1145		
20h-(3)	60528	4424	13.682	9.78	8.30	1178		
20h-(4)	63271	4501	14.057	10.01	8.30	1206	1156	96.0%

Chiralpak IC, 18% *i*-PrOH in hexane, 1.2 mL/min, 32 °C, 235 nm

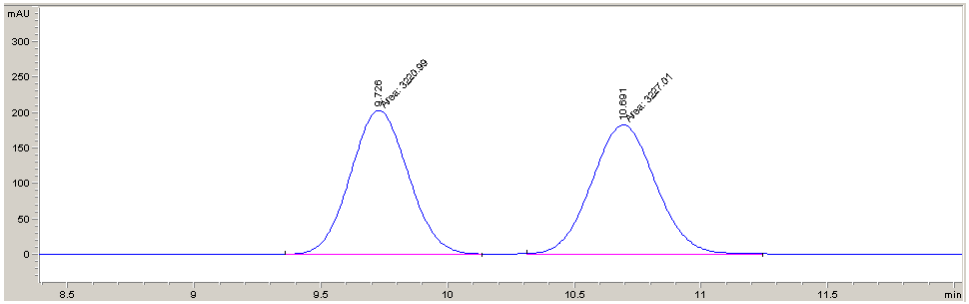

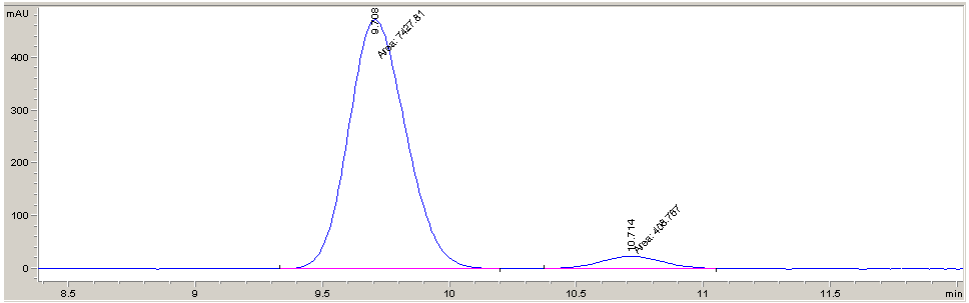

***rac*-20h**			**Enzymatically produced 20h**		
Retention Time (min)	Area (mAU*s)	Area %	Retention Time (min)	Area (mAU*s)	Area %
9.726	3220.99	49.95	9.708	7427.81	94.78
10.691	3227.01	50.05	10.714	408.77	5.22
Total	6448	100.00	Total	7836.58	100.00

GC-MS traces for the reactions between borane **19a** and lactone-diazos **LAD**, **LAD-2** and **LAD-3**:

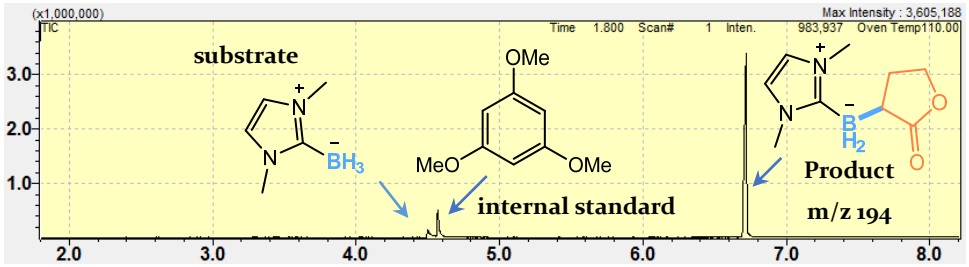

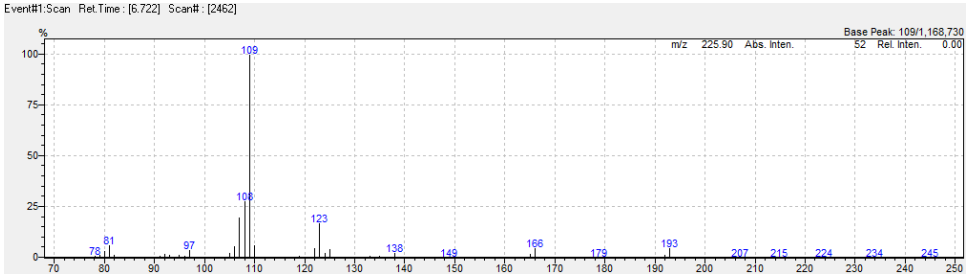
Event#1:Scan Ret.Time : [6.722] Scan# : [2462]
Base Peak: 109/1,168,730
m/z 225.90 Abs. Inten. 52 Rel. Inten. 0.00

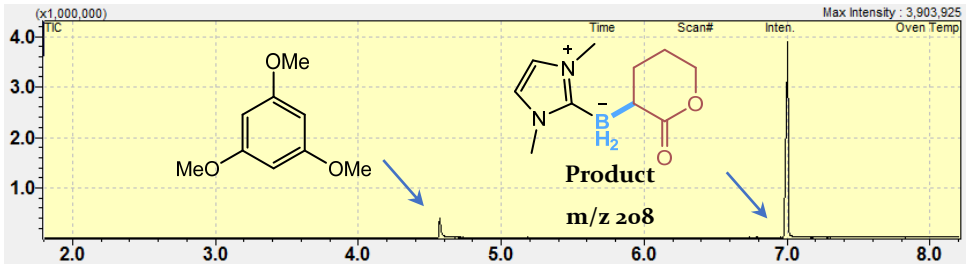
(x1,000,000)
TIC
Max Intensity : 3,903,925
Time Scan# Inten. Oven Temp
OMe
MeO
OMe
Product
m/z 208

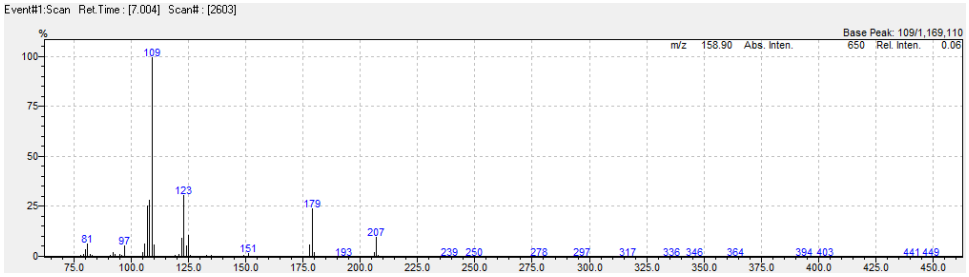
Event#1:Scan Ret.Time : [7.004] Scan# : [2603]
Base Peak: 109/1,169,110
m/z 158.90 Abs. Inten. 650 Rel. Inten. 0.06

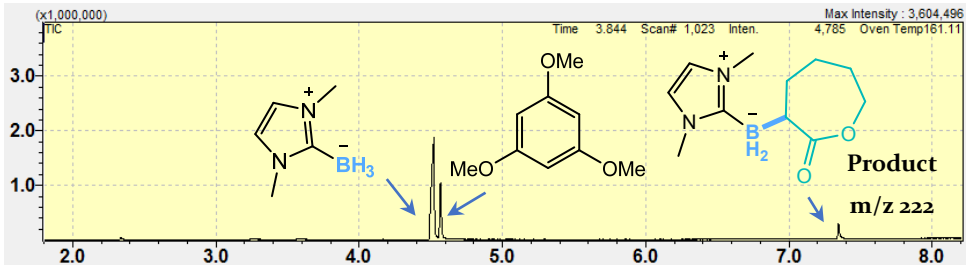
(x1,000,000)
TIC
Max Intensity : 3,604,496
Time 3.844 Scan# 1,023 Inten. 4,785 Oven Temp161.11
OMe
MeO
OMe
Product
m/z 222

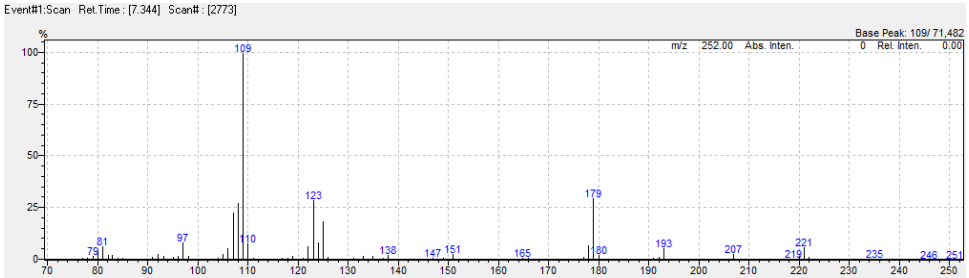
Event#1:Scan Ret.Time : [7.344] Scan# : [2773]
Base Peak: 109/ 71,482
m/z 252.00 Abs. Inten. 0 Rel. Inten. 0.00

Chapter 4

ENZYMATIC ASSEMBLY OF DIVERSE LACTONE STRUCTURES: AN INTRAMOLECULAR C–H FUNCTIONALIZATION STRATEGY

4.1 Abstract

To further exploit the catalytic ability of hemeprotein carbene transferases, especially in assembling lactones with a higher order of structural diversity, we have developed a new strategy for lactone synthesis through an intramolecular carbene C–H insertion process. Directed evolution of a P411 enzyme (P411-**C10**) led to the discovery of a potent variant, which allowed for the formation of a γ-lactone product in high efficiency and perfect stereoselectivity (5800 TTN and >99.9% ee). Interestingly, the enzyme lineage obtained from the evolution process could also function efficiently to produce δ-lactones, by specifically targeting the benzylic sites for C–H insertion. Besides, another enzyme variant was identified from the **C10** family, capable of functionalizing a remote C–H bond, affording a 7-membered ε-lactone product. Of these examples, C–H bond strength is seemingly the key factor in selecting C–H bonds to be functionalized, regardless of the geometric distance to the carbene center, which is typically the opposite to the established systems with rhodium catalysts. By realizing this, we further tested substrates bearing available benzylic or allylic C–H bonds for this cyclization chemistry and found that the enzyme lineage was able to synthesize a broad range of lactone and lactam products, even with sophisticated three-dimensional structures based on fused, spiro and bridged rings.

4.2 Introduction

In *Chapter 3*, we described an enzymatic approach to build lactone derivatives based on a lactone-carbene strategy, which allowed for rapid access to a broad range of α-substituted lactones. However, the use of lactone-based carbenes still limits the structural diversity of lactone products in some aspects, especially when lactones with substitutions at β-, γ-, or multiple positions, or the ones with more complicated ring scaffolds (*i.e.*, fused/spiro/bridged rings), are the targets. To address this, we have been seeking to establish a different enzymatic platform for lactone assembly. As discussed in *Chapter 3*, nature typically employs a mode of C–O disconnection for the construction of lactones. In principle, lactone structures could also be forged via disconnection at any C–C bond in the ring, if a corresponding method is available. We therefore reasoned that C–C bond disconnection between the carbons at α- and β-positions can possibly provide an efficient route to diverse lactone products with substitutions at different positions (or even with complicated ring systems). As a continuing story of our enzymatic system based on hemeprotein carbene transferases, we would like to develop an intramolecular C–H functionalization strategy for the

synthesis of lactone products (**Fig. 4.1**).

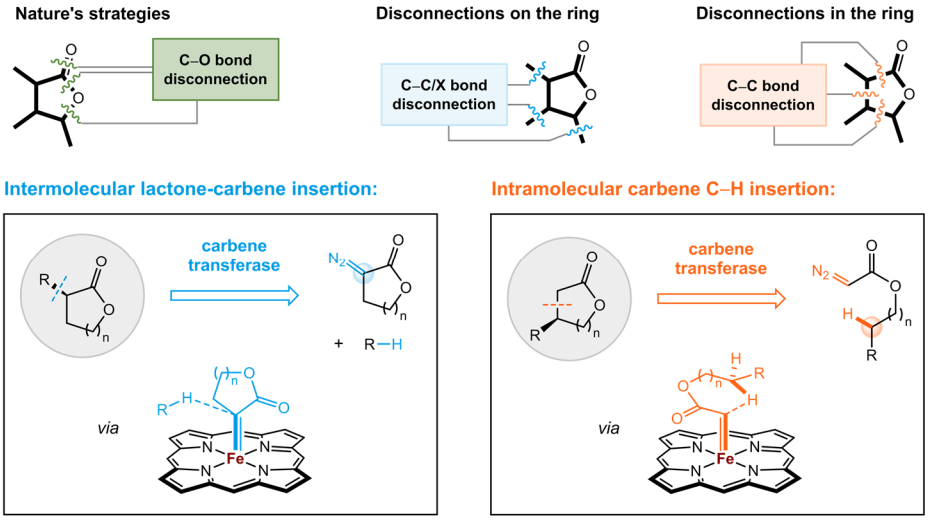

Figure 4.1. Different disconnection modes for lactone assembly. Non-native strategies: intermolecular lactone-carbene C/X–H insertion, and intramolecular carbene C–H insertion.

Such a strategy for lactone assembly can potentially be achieved using α-diazo esters as substrates, if a catalyst is identified to perform the desired intramolecular carbene C–H insertion reactions. In fact, a variety of synthetic catalysts based on rhodium, iridium, copper, ruthenium, cobalt and other transition metals, have been intensively explored for intramolecular carbene C–H insertion reactions[214,215,286,287] (**Fig. 4.2.a**). For instance, Doyle has made significant contribution to the development of chiral dirhodium carboxamidate catalysts for enantioselective intramolecular C–H insertion reactions, yielding a variety of γ-lactones[218,219,249,288-290]. Catalytic systems based on different dirhodium complexes[291-293] or iridium/ruthenium-porphyrins[294,295] have also been employed for the synthesis of β- or γ-lactones as well as lactams when using α-diazo amides as substrates. Copper catalysts enabled by bis(oxazoline) (Box) ligands could also take acceptor-acceptor-type carbenes (with two electron-withdrawing groups appended to the carbene center, which are usually more reactive towards C–H insertion compared to the acceptor-only ones) and perform intramolecular C–H insertion reactions to afford 5- or 6-membered ring products[296-299]. In contrast, iron catalysts have shown very restricted capability for carbene C–H insertion reactions, intermolecularly or intramolecularly. However, examples do exist[300]: White reported an intramolecular C–H insertion reaction using acceptor-acceptor carbenes with an iron-phtalocyanine catalyst[230], and Costas also described a system based on a highly electrophilic iron catalyst combined with a lithium aluminum alkyoxide salt for carbene insertion into unactivated C–H bonds[251]. These examples, nonetheless, are not enantioselective, and only synthesized a limited set of ring structures.

Though difficult, our previous success with intermolecular carbene C–H insertion has demonstrated that engineering of iron-based hemeproteins would help to reconfigure the catalyst

framework and accelerate the desired C–H insertion reaction by lowering the energy barrier, while exerting exquisite stereo-control[77]. Therefore, we anticipate that an intramolecular version of C–H insertion could also be possible if the enzyme is evolved to accommodate the carbene intermediate in a favorable orientation and then facilitate the C–H insertion process in a stereoselective manner. We also hypothesize that engineering of the enzyme scaffolds may confer different regio-selectivities of the C–H insertion process[169], leading to lactone products of different sizes, whereas synthetic catalysts only produce 4- or 5-membered lactones. In addition, once established, the enzymatic platform could also be possibly extended to the synthesis of other cyclic structures, such as lactams and cyclic ketones, which may allow for synthesis of diverse drug targets or pharmaceutical intermediates (**Fig. 4.2.b**).

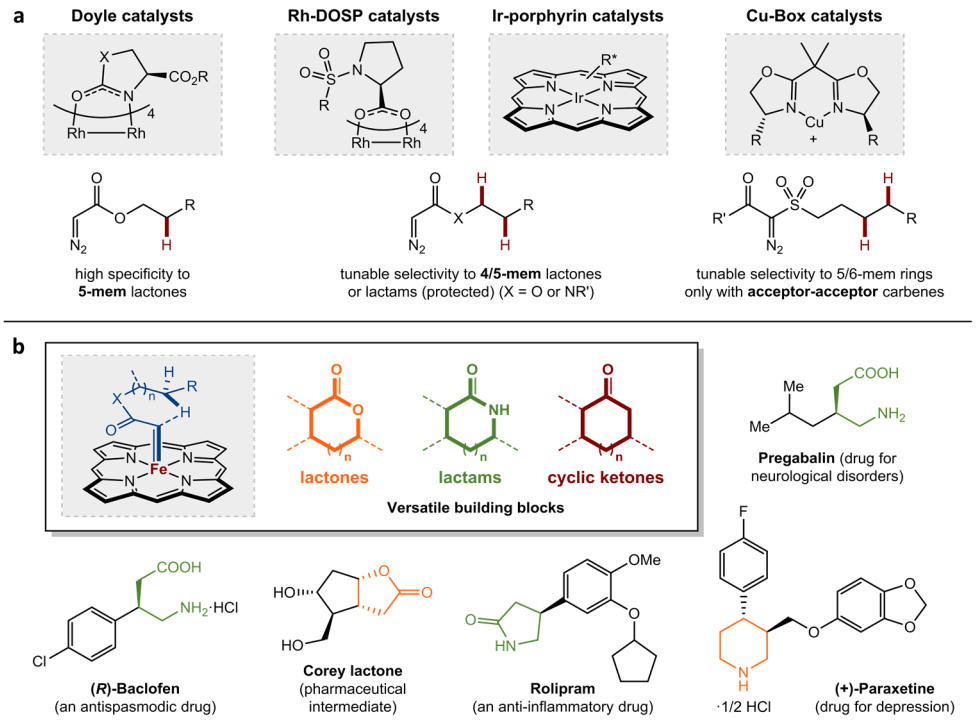

Figure 4.2. Intramolecular carbene C–H insertion. a, Representative catalytic systems previously developed for intramolecular carbene C–H insertion. **b**, Possible extension of the proposed enzymatic carbene C–H insertion strategy to the synthesis of other cyclic structures, including lactams and cyclic ketones, and potential pharmaceutical targets.

4.3 Directed evolution of P411-C10 for intramolecular carbene C–H insertion

To establish such an enzymatic platform for intramolecular C–H insertion, we first screened a broad library of P411 variants collected from previous projects, in the form of *E. coli* whole-cell catalysts, against a diazo substrate (**21a**), to search for an enzyme variant with promising activity. Interestingly, a P411 variant, **C10**, previously found with promiscuous activities for internal alkyne cyclopropenation[301] and lactone-carbene C–H insertion, was also active for the C–H insertion

reaction here, producing a γ-lactone product (**22a**) in 3–5% yield. But we observed full conversion of the substrate in this enzymatic reaction with P411-**C10**; a set of side reactions were identified, including carbene O–H insertion by H_2O and co-solvent EtOH, carbene Wolff rearrangement, carbene dimerizations and [3+2] cycloadditions between carbene dimers and diazo substrate. Thus evolution will need to engineer the enzyme to be not only more efficient but also more specific towards the desired C–H insertion reaction, while circumventing the undesired pathways.

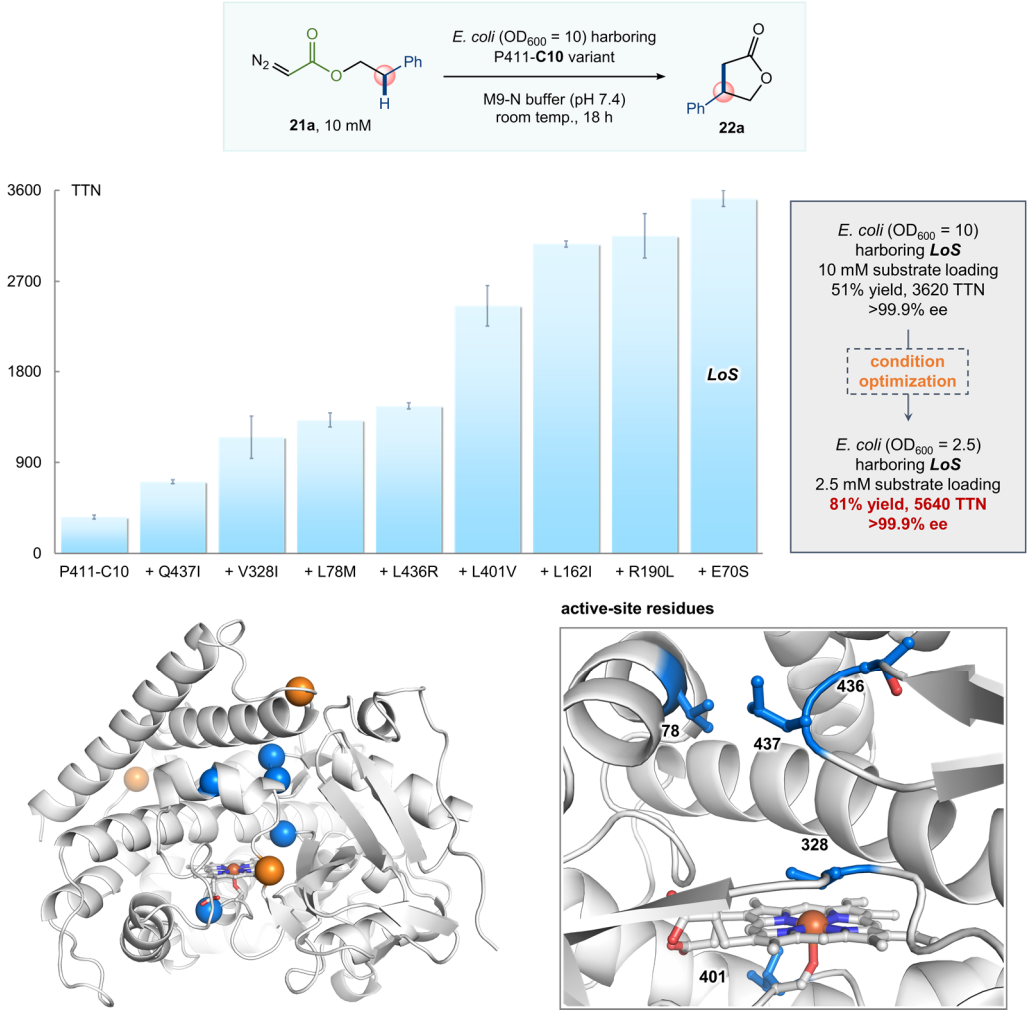

Figure 4.3. Directed evolution of P411-C10 for intramolecular carbene C–H insertion. Reactions were performed in quadruplicate under the following conditions: 10 mM **21a**, *E. coli* harboring P411-**C10** variants (OD_{600} = 10), D-glucose (25 mM), M9-N buffer/EtOH (19:1), anaerobic, 18 h. Optimized conditions used whole *E. coli* cell catalysts at OD_{600} = 2.5 and 2.5 mM substrate loading. Product formation was quantified by HPLC, TTNs were determined based on protein concentration, and enantioselectivity was measured using chiral HPLC. The heme-domain structure of P411-**E10** variant (pdb: 5UCW) was used to guide site-saturation mutagenesis. Active-site mutations are highlighted in blue and non-active-site mutations are in orange.

We performed directed evolution of P411-**C10** to enhance the catalytic efficiency and chemoselectivity for the intramolecular C–H insertion reaction (**Fig. 4.3**). We first targeted active-site residues for site-saturation mutagenesis (SSM) and upon screening obtained several beneficial mutations, Q437I, V328I, L78M and L436R, all together boosting the activity by 4 folds. Interestingly,

a mutation, L401V, in the cysteine loop (the region containing the heme-ligating residue), was found to improve TTN to 2460, presumably by reorienting the heme cofactor for the desired transformation. However, subsequent screening of SSM libraries targeting more than 30 residues in the active-site regions (72-88, 180-188, 260-272, 326-333 and 435-439) was not fruitful, with no further enhancement in enzyme activity. We hypothesized that the overall protein dynamics may be important for substrate binding with a proper orientation for C–H insertion. Then we targeted a few non-active-site residues, which are known to contribute to the overall dynamics of $P450_{BM3}$ when binding native substrates[302,303], for further engineering. Three more beneficial mutations were discovered, leading to a final variant, ***LoS*** (short for **l**act**o**ne **s**ynthase), with 3520 total turnovers and 51% yield to product **22a**. The evolved enzyme also delivered perfect stereo-control, affording the desired product with >99.9% enantiopurity. After evolution, the side reactions, typically carbene O–H insertions and Wolff rearrangement, were greatly suppressed, to <5%; however, carbene dimer formation and subsequent [3+2] cycloadditions together still took up almost half conversion of the substrate. Nevertheless, thinking that lowering substrate concentration may help to attenuate these bimolecular pathways, final optimization of reaction condtions led to the use of lower substrate and enzyme loadings, which improved the overall activity to 5640 TTN and 81% yield.

4.4 Intramolecular carbene C–H insertion for δ- and ε-lactone synthesis

Having achieved γ-lactone formation through intramolecular C–H insertion, we were curious whether our enzymatic platform could access lactones of different sizes (**Fig. 4.4**). With a diazo substrate (**21b**) bearing one more carbon compared to **21a**, the established system based on dirhodium catalysts could only produce a γ-lactone product through C–H insertion at the homo-benzylic position[304-306]. Surprisingly, reacting substrate **21b** with our evolved enzyme, ***LoS***, afforded a δ-lactone product (with ~30% yield) by targeting benzylic C–H bonds only. Apparently, our enzymatic system features a distinct site-preference from the rhodium system – with enzymes, C–H bond strength is typically a crucial factor in selecting C–H bonds for insertion, while the geometric distance of the C–H bonds to the carbene center plays a more important role in selectivity with rhodium catalysts. Therefore, we asked if the 7-membered ε-lactone can be accessed. Generally, 7-membered rings are more challenging to construct compared to 5- or 6-membered ones, due to the disfavored enthalpy and entropy costs during the cyclization process[307,308]. Despite the difficulty, we challenged our enzyme, ***LoS***, with a substrate (**21c**) bearing remote benzylic C–H bonds; we were delighted to observe an ε-lactone product (**22c**), albeit with only 0.2% yield.

To further improve enzyme activity for δ- and ε-lactone formation, we first screened the whole enzyme family of the **C10** variant using substrates **21b** and **21c**. Interestingly, a middle variant in the enzyme lineage of ***LoS***, **C10**-IIMRV, was identified as the most active towards δ-lactone formation.

As δ-lactones could undergo slow hydrolysis to yield hydroxyl carboxylic acids in the neutral medium, slightly diminished TTN and yield of ~4400 and ~60% were obtained for product **22b**, however, still with good enantioselectivity (90% ee). For ε-lactone formation, it was surprising to us that a variant previously evolved for internal alkyne cyclopropenation, **C10**-WIRF_GA, exhibited significantly improved activity (9% yield, 600 TTN) compared to ***LoS***, again highlighting the promiscuous feature of P411 enzymes for different carbene transfer chemistries. Directed evolution of **C10**-WIRF_GA introduced 9 mutations and yielded an efficient variant for the sysnthesis of ε-lactone **22c** in 3100 TTN and 65% yield under optimized conditions. However, the enantioselectivity of ε-lactone is still not satisfying, giving only 32% ee. Further engineering will still be required to solve the enantioselectivity problem.

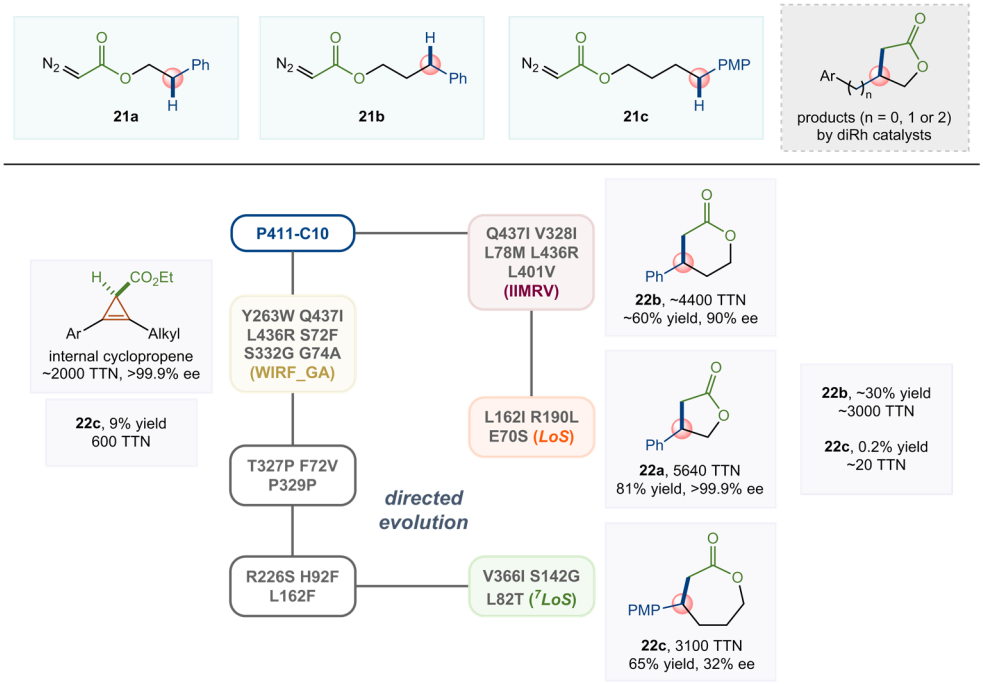

Figure 4.4. Intramolecular carbene C–H insertion for γ-, δ- and ε-lactone formation.

4.5 Mechanistic investigation and scope evaluation of intramolecular carbene C–H insertion

As our enzymatic system has displayed a unique site-preference for C–H insertion, typically dependent on C–H bond strength, we would like to interrogate the origin of this selectivity. We therefore first employed DFT calculation to study the reaction mechanism using a truncated heme complex as the simplified catalyst. The most favorable pathway for this intramolecular C–H insertion reaction is shown in **Fig. 4.5**. The C–H insertion takes place in a stepwise manner, involving one hydrogen-atom-transfer (HAT) step and subsequent radical rebound to form a C–C bond[230], which is different from the concerted C–H insertion mechanism by rhodium catalysts for the same type of transformation. The free energy barriers of the two steps are 16.0 kcal/mol and 13.0

kcal/mol, respectively, suggesting that hydrogen atom abstraction may be the rate-limiting step in the catalytic cycle (carbene formation is usually with a relatively low energy barrier). So it would be reasonable to argue that C–H bond strength reflected by bond dissociation energy (BDE, benzylic C–H bonds with BDE of 85 kcal/mol *vs* aliphatic C–H bonds with BDE of 98 kcal/mol) may be crucial to the HAT step, while the effect from geometric distance can be undermined through proper positioning of the carbene intermediate in the enzyme's active site.

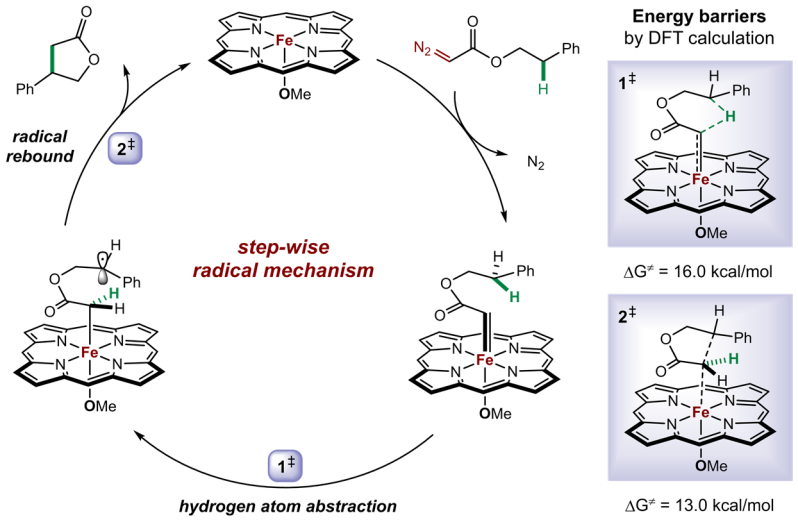

Figure 4.5. Mechanism of intramolecular carbene C–H insertion suggested by DFT calculation. A step-wise radical mechanism of γ-lactone formation is presented here, involving hydrogen atom abstraction and subsequent radical rebound. The detailed steps in carbene formation are omitted. Gibbs free energy obtained at the B3LYP/def2-TZVP//B3LYP/6-31G(d)-LANL2DZ level.

Having obtained mechanistic insights into this intramolecular C–H insertion chemisty, we assayed a range of diazo substrates with benzylic or allylic C–H bonds available for carbene insertion (**Fig. 4.6**). Diazo esters are easy to prepare in one step from corresponding alcohols in gram quantity and with high yields (80–96%), rendering our enzymatic approach to lactones typically simple and straightforward. Intramolecular carbene C–H insertion proceeded smoothly with variant ***Lo*S**, furnishing γ-lactones with various aryl or alkenyl substitutions at β-position (**22a**, **22d** to **22i**). **C10**-IIMRV also served as a potent biocatalyst and established a highly efficient and versatile platform for δ-lactone synthesis (**22b**, **22j** to **22q**). While γ-lactone formation was sensitive to the electronic effect of the substitutions on the aromatic ring (with lower activity observed for the electronically deficient substrates), the δ-lactone-forming system accepted a broad panel of substrates featuring different electronic or steric properties. However, the enantioselectivity of the δ-lactone products varied a lot from 12% ee to 98% ee, suggesting that there may be more complicated mechanistic profiles for different substrates (*e.g.*, change in rate-limiting step, different radical coupling mechanisms, **Fig. C-2** in **Appendix C**).

Besides simple lactones, we were also curious whether this enzymatic platform can be used for the construction of other cyclic structures or even more complicated ring systems. Indeed, lactams

could also be prepared using corresponding diazo amide substrates, and no protection groups were required for the nitrogen atoms (**22r** and **22s**). Additionally, complicated lactone structures based on fused (**24a** to **24d**), spiro (**24e**), or even bridged rings could also be accessible using our biocatalysts. Interestingly, when racemic substrates (**23f** to **23h**) bearing two different sets of benzylic C–H bonds were subjected to our enzymatic system, different lactones products, either spiro/bridged lactones (**24f-1** and **24f-2**) or fused/bridged lactones (**24g-1** and **24g-2**, **24h-1** and **24h-2**) were obtained. We suspected that the product pairs may result from a parallel kinetic resolution process of the corresponding substrate racemates by the enzymes. Further validation is still ongoing.

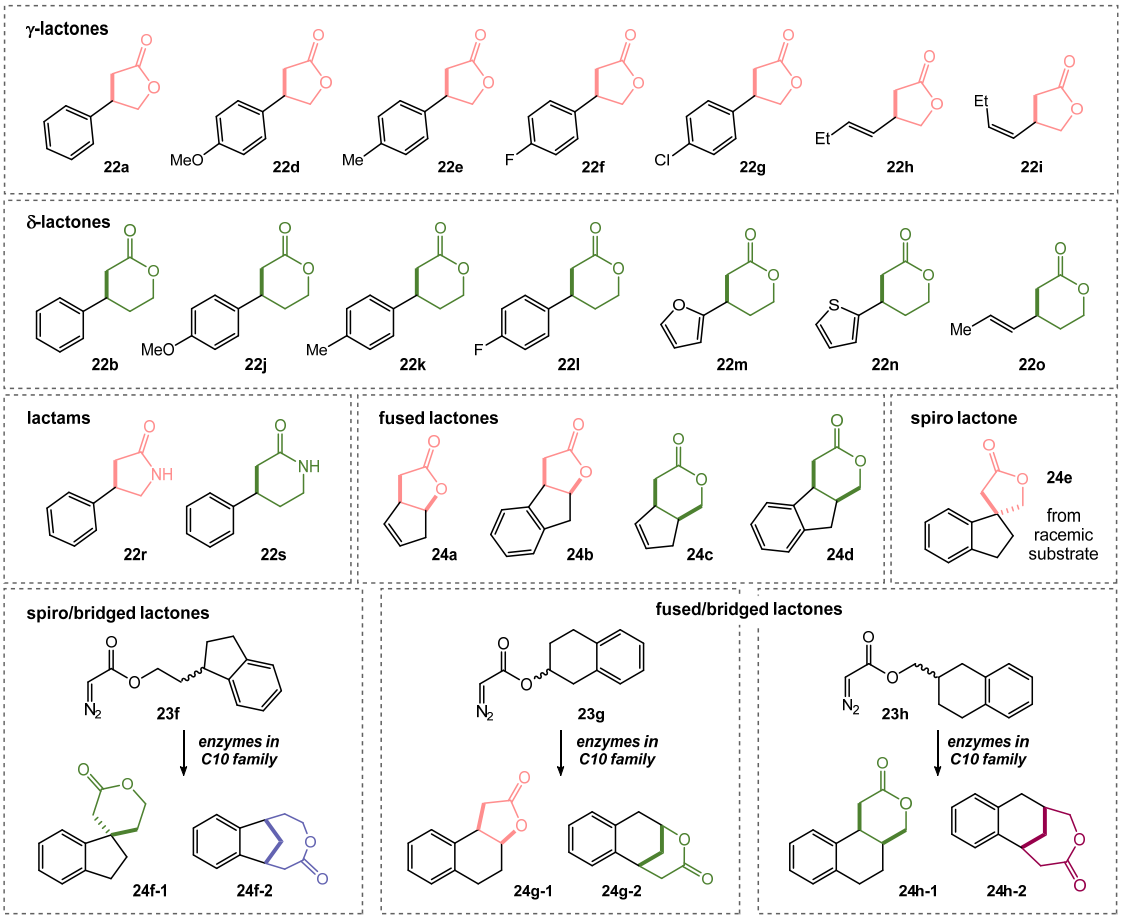

Figure 4.6. Scope of lactones and lactams via enzymatic intramolecular carbene C–H insertion.

4.6 Conclusion

Enzyme engineering has enabled cytochrome P450 hemeproteins to adopt a new strategy for the assembly of lactone or even lactam structures via an intramolecular carbene C–H insertion process. Directed evolution of a P411 enzyme (P411-**C10**) led to the discovery of a lineage of powerful biocatalysts, capable of producing a broad range of lactone products in different sizes (5- to 7-membered rings) and doing so with high efficiency and tunable stereoselectivity. Our enzymatic platform targeted C–H bonds with weaker bond strength for carbene insertion, regardless of the

geometric distance to the carbene center, which is typically the opposite to the synthetic systems based on rhodium catalysts capable of γ-lactone formation only. Computational study revealed a step-wise C–H insertion mechanism of the enzymatic transformation, involving a hydrogen-atom-transfer step and a subsequent radical rebound process, which provides a possible explanation for the selectivity towards weaker C–H bonds.

Evaluation of diverse substrates established that the engineered enzymatic platform was able to assemble a broad range of lactone or lactam products, not limited to those simple ones, but also the ones with more sophisticated three-dimensional structures based on fused, spiro and bridged rings. These results, once again, highlight the capability of P450 enzymes in achieving molecular complexity even through non-natural carbene-transfer chemistries. Nature has created a superfamily of cytochrome P450 enzymes with adaptive active sites to accept and functionalize highly diversified natural molecules by performing their native oxygenation chemistry. We envision that the immense potential of P450 enzymes and other hemeproteins as carbene transferases will be further unveiled to provide rapid access to even broader classes of molecular structures by directed evolution!

4.7 Experimental methods

4.7.1 General information

Unless otherwise noted, all chemicals and reagents were obtained from commercial suppliers (Sigma-Aldrich, VWR, Alfa Aesar, Acros, Combi-Blocks, TCI and Ark Pharm) and used without further purification. Silica gel chromatography was carried out using AMD Silica Gel 60, 230-400 mesh. ^{1}H and ^{13}C NMR spectra were taken using a Bruker Prodigy 400 MHz instrument and are internally referenced to the residual solvent peak (chloroform). Data for ^{1}H NMR are reported as follows: chemical shift (δ ppm), multiplicity (s = singlet, d = doublet, t = triplet, q = quartet, p = pentet, m = multiplet, dd = doublet of doublets, dt = doublet of triplets, ddd = doublet of doublet of doublets), coupling constant (Hz), integration. Sonication was performed using a Qsonica Q500 sonicator. High-resolution mass spectra were obtained at the California Institute of Technology Mass Spectral Facility. Synthetic reactions were monitored using thin layer chromatography (Merck 60 gel plates) using a UV-lamp for visualization.

4.7.2 Chromatography

Analytical reversed-phase high-performance liquid chromatography (HPLC) was carried out using an Agilent 1200 series instrument and a Kromasil 100 C18 column (4.6 × 50 mm, 5 μm) with water and acetonitrile as the mobile phase and visualization at 210 nm for library screening.

Analytical normal-phase HPLC was carried out using an Agilent 1200 series instrument and chiral columns Chiralpak IC (4.6 mm × 25 cm), IA (4.6 mm × 25 cm), AS-H (4.6 mm × 25 cm) and OJ-H (4.6 mm × 25 cm) with *n*-hexane and isopropanol as the mobile phase and visualization at 210 nm for chiral separation. Gas chromatography (GC) analyses were carried out using an Agilent 7820A or Shimadzu GC-17A gas chromatograph, FID detector, a J&W HP-5 column (30 m × 0.32 mm, 0.25 μm film) and CycloSil-B column (30 m × 0.25 mm, 0.25 μm film). Gas chromatography-mass spectrometry (GC-MS) analyses were carried out using a Shimadzu GCMS-QP2010SE system and J&W HP-5m column.

4.7.3 Cloning and site-saturation mutagenesis

pET22b(+) containing a C-terminal 6x-His tag was used as a cloning and expression vector for all enzymes described in this study. Site-saturation mutagenesis was performed using a modified QuikChange™ mutagenesis protocol[170]. Primer sequences are available upon request. The PCR products were digested with DpnI, gel purified, and fragments were assembled using Gibson Mix[171]. The ligation mixture was used to directly transform *E. coli* strain BL21 *E. cloni*® (Lucigen). Cells were grown using Luria-Bertani medium (LB) or Hyperbroth (AthenaES) (HB) with 0.1 mg/mL ampicillin (LB_{amp} or HB_{amp}). Electrocompetent *E. coli* cells were prepared following the protocol of Sambrook *et al*[172]. T5 exonuclease, Phusion polymerase, and Taq ligase were purchased from New England Biolabs (NEB, Ipswich, MA). M9-N minimal medium (abbreviated as M9-N buffer; pH 7.4) was used as a buffering system for whole cells, lysates, and purified proteins, unless otherwise specified. M9-N buffer was used without a carbon source; it contains 47.7 mM Na_2HPO_4, 22.0 mM KH_2PO_4, 8.6 mM NaCl, 2.0 mM $MgSO_4$, and 0.1 mM $CaCl_2$.

4.7.4 Determination of hemeprotein concentration

1. **Preparation of cell lysate**: Aliquots of ~3 mL OD_{600} = 60 cells were prepared in 15 mL conical tubes, which were then placed on wet ice. Cells were lysed by sonication following the program below: sonication for 4 min, 1 second on - 1 second off, 35% amplitude. The sonicated samples were then transferred to two Eppendorf tubes, and then centrifuged down (14,000 rpm, 15 min, 4 °C). The supernatants (~2.5 mL) were then collected to a 5-mL glass vial for analysis.

2. **Hemechrome assay for protein concentration measurement**: A solution of NaOH/pyridine was prepared by mixing 1 mL of NaOH aqueous solution (1 M), 2 mL of water and 2 mL of pyridine. To 4.5 mL of NaOH/pyridine solution, 22.5 μL of $K_3Fe(CN)_6$ aqueous solution (0.1 M) was added to make **solution 1**. A **background solution** was prepared by mixing 500 μL M9-N and 500 μL of the NaOH/pyridine solution, which was used for UV background subtraction. When measuring samples with a UV spectrometer, a spectrum of a mixed solution (oxidized spectrum)

with 500 µL cell lysate + 500 µL **solution 1** was taken at the wavelength range 380 nm to 650 nm. Subsequently, 5 µL of dithionite solution (0.5 M in 0.1 M NaOH solution) was added to the same sample and mixed by pipetting; a spectrum of this solution (reduced spectrum) was taken at 380 nm to 650 nm. The protein concentration was calculated using the extinction coefficient and dilution factor (2× dilution in volume): $\varepsilon\_[557_{reduced} - 540_{oxidized}] = 23.98\ mM^{-1}cm^{-1}$ (ref 173).

4.7.5 Expression of P411 proteins

E. coli BL21 *E. cloni*® cells carrying a plasmid encoding a P450 or P411 variant were grown overnight in 5 mL LB_{amp} (37 °C, 250 rpm). The pre-culture was used to inoculate 45 mL of HB_{amp} in a 125 mL Erlenmeyer flask; this culture was incubated at 37 °C, 220 rpm for 2 h and 15 min. Cultures were then cooled on ice (20–40 min), and expression was induced with IPTG and ALA with final concentrations of 0.5 mM and 1.0 mM, respectively. Expression was conducted at 24 °C, at 140 rpm, for 20 h (± 20 min). Cultures were then centrifuged (4,500 × g, 5 min, 4 °C), and the pellets were resuspended to an OD_{600} of 60 in M9-N minimal medium (no nitrogen). Aliquots of the cell suspension (3–4 mL) were used to determine the P450 and P411 expression level after lysis by sonication. The expression level in OD_{600} = 60 lysates is typically in the range of 6–16 µM for P411-**C10** variants.

4.7.6 Biotransformations

Resuspended cells in M9-N (340 or 355 µL, at a certain OD_{600}) were added to 2 mL vials, followed by D-glucose (40 µL, 250 mM in M9-N). Then the vial were transferred into an anaerobic chamber (oxygen level: < 40 ppm). Diazo substrate (5 or 20 µL of an EtOH stock, 200 mM) was added to the vials inside the anaerobic chamber. Final concentrations were typically 2.5 or 10.0 mM diazo substrate and 25 mM glucose; final reaction volume was 400 µL. The vials were sealed and shaken inside the anaerobic chamber at room temperature and 560 rpm for 18 to 24 h.

After the reaction was completed and the vials removed from the anaerobic chamber, internal standard (20 µL of 20 mM stock solution in acetonitrile) was added followed by acetonitrile (0.6 mL). The mixture was transferred to a 1.7-mL Eppendorf tube, and then subjected to vortexing (15 s × 3) and centrifugation (14,000 rpm, 5 min, 4 °C). A sample of the supernatant (0.8 mL) was transferred to a vial for reverse-phase HPLC analysis.

4.7.7 Reaction screening in 96-well plate format

Enzyme libraries (site-saturation libraries generated employing the “22c-trick” method or collections of heme protein variants) were screened in 96-well plates.

E. coli libraries for P411 variants were cultured in LB_{amp} (300 µL/well) at 37 °C, 250 rpm and 80% relative humidity overnight. HB_{amp} (950 µL/well) was inoculated with the pre-culture (50 µL/well) and incubated at 37 °C, 230 rpm, 80% humidity for 2 h and 45 min. The plates were cooled on ice for 30 minutes, and expression was induced with 0.5 mM IPTG and 1.0 mM ALA (final concentrations). Expression was conducted at 22 °C and 220 rpm for 20 h.

The cells were pelleted (4,500 × g, 5 min, 4 °C) and resuspended with M9-N buffer (350 µL/well) and D-glucose solution (40 µL/well, in M9-N). The 96-well plate was then transferred to an anaerobic chamber. In the anaerobic chamber, substrate (10 µL/well, 100 mM in EtOH) was added to the plate. The plate was sealed with an aluminum foil and shaken inside the anaerobic chamber at 560 rpm.

After 18 h, the plate was moved out from the anaerobic chamber. The seal was removed and acetonitrile (600 µL/well) was added. The plate was tightly sealed with a reusable silicone mat, vortexed (15 s × 3) and centrifuged (4,500 × g, 5 min). The supernatant (200 µL/well) was filtered through an AcroPrep 96-well filter plate (0.2 µm) into a shallow-well plate for reversed-phase HPLC analysis (C18 poroshell column, MeCN:H_2O 40:60 for 3.5 min -> gradient to 100:0 -> 100:0 for 3.5 min, 1.2 mL/min flow, 7.5 min, 210 nm).

Appendix C

SUPPLEMENTARY INFORMATION FOR CHAPTER 4

B.1 Supporting Tables C-1 to C-6

Table C-1. Directed evolution of P411-**C10** for γ-lactone formation.

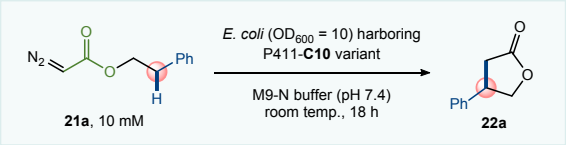

P411-**C10** variant	**TTN**	**yield**
C10	360 ± 20	5.2 ± 0.3%
C10-Q437I	710 ± 20	12.4 ± 0.3%
C10-Q437I V328I	1150 ± 210	14.8 ± 2.9%
C10-Q437I V328I L78M	1320 ± 70	20.2 ± 0.9%
C10-Q437I V328I L78M L436R	1460 ± 30	21.2 ± 1.6%
C10-Q437I V328I L78M L436R L401V	2460 ± 200	30.3 ± 1.4%
C10-Q437I V328I L78M L436R L401V L162I	3070 ± 30	41.9 ± 0.3%
C10-Q437I V328I L78M L436R L401V L162I R190L	3150 ± 220	42.1 ± 4.5%
C10-Q437I V328I L78M L436R L401V L162I R190L E70S	3520 ± 80	50.7 ± 1.3%

Note: Analytical reactions were set up in quadruplicate using whole *E. coli* cells harboring P411-**C10** variants (OD_{600} = 10 for all). Product formation was quantified by HPLC and TTNs were determined based on protein concentration.

Table C-2. Condition optimization of γ-lactone formation with P411-**C10** variants.

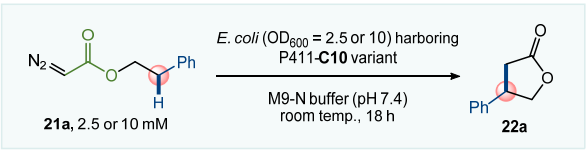

Condition 1:
OD_{600} = 10, 10 mM **21a**
5% EtOH (v%)

Condition 2:
OD_{600} = 2.5, 2.5 mM **21a**
1.25% EtOH (v%)

P411-**C10** variant	**condition 1**	**condition 2**
C10-Q437I V328I L78M L436R	1430 TTN, 22.7% yield	2840 TTN, 45% yield
C10-Q437I V328I L78M L436R L401V	2660 TTN, 31.6% yield	4930 TTN, 53.7% yield
C10-Q437I V328I L78M L436R L401V L162I	3090 TTN, 41.6% yield	5060 TTN, 68.0% yield
C10-Q437I V328I L78M L436R L401V L162I R190L	3370 TTN, 46.6% yield	5270 TTN, 72.9% yield
C10-Q437I V328I L78M L436R L401V L162I R190L E70S	3440 TTN, 52.0% yield	5640 TTN, 81.2% yield

Note: Analytical reactions were set up in quadruplicate using whole *E. coli* cells harboring P411-**C10** variants under certain conditions. Product formation was quantified by HPLC and TTNs were determined based on protein concentration.

Table C-3. Screening of ***LoS*** lineage for δ-lactone formation.

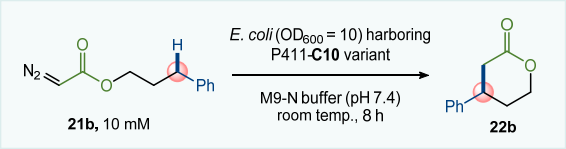

P411-**C10** variant	**relative activity**
C10-Q437I V328I	1.00 ± 0.05
C10-Q437I V328I L78M	2.45 ± 0.03
C10-Q437I V328I L78M L436R	2.63 ± 0.04
C10-Q437I V328I L78M L436R L401V	2.80 ± 0.07
C10-Q437I V328I L78M L436R L401V L162I	2.37 ± 0.03
C10-Q437I V328I L78M L436R L401V L162I R190L	1.68 ± 0.07
C10-Q437I V328I L78M L436R L401V L162I R190L E70S	1.70 ± 0.05

Note: Analytical reactions were set up in duplicate using whole *E. coli* cells harboring P411-**C10** variants (OD_{600} = 10 for all). The reactions were run for a relatively shorter time (8 h) due to the hydrolysis problem. Relative activity is simply based on product formation, quantified by HPLC.

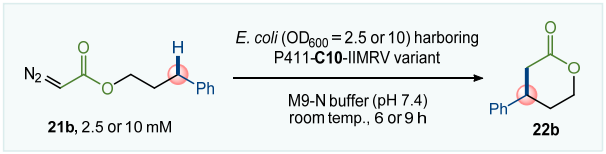

	Condition 1: OD_{600} = 10, 10 mM **21b** 6 h, 5% EtOH (v%)	**Condition 2:** OD_{600} = 2.5, 2.5 mM **21b** 9h, 1.25% EtOH (v%)
	condition 1	**condition 2**
results	~3500 TTN, ~48% yield	~4400 TTN, ~61% yield

Note: Analytical reactions were set up in quadruplicate using whole *E. coli* cells harboring P411-**C10**-IIMRV under certain conditions. Total turnovers and yields could not be accurately determined due to the hydrolysis problem. Even with shorter reaction time (6–9 h), >10% lactone product was hydrolyzed.

Table C-4. Results for ε-lactone formation with P411-**C10** variants.

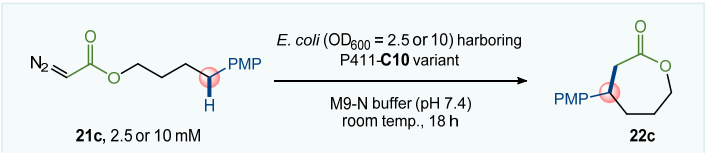

	Condition 1: OD_{600} = 10, 10 mM **21c** 5% EtOH (v%)	**Condition 2:** OD_{600} = 2.5, 2.5 mM **21c** 1.25% EtOH (v%)
P411-**C10** variant	**condition 1**	**condition 2**
C10-WIRF_GA	600 TTN, 9% yield	-
P411-7***LoS***	2300 TTN, 47% yield	3100 TTN, 65% yield

Note: Analytical reactions were set up in quadruplicate using whole *E. coli* cells harboring P411-**C10** variants under certain conditions. Product formation was quantified by HPLC and TTNs were determined based on protein concentration.

Table C-5. List of mutations in P411 variants involved in Chapter 4.

P411 variant	Mutations relative to wild-type protein (relative to $P450_{BM3}$)
P411-**C10**	N70E A74G V78L A82L F87A M118S P142S F162L T175I M177L A184V S226R H236Q E252G I263Y H266V T268G A290V A328V A330Y L353V I366V C400S I401L T436L L437Q E442K ΔFAD
C10-Q437I	N70E A74G V78L A82L F87A M118S P142S F162L T175I M177L A184V S226R H236Q E252G I263Y H266V T268G A290V A328V A330Y L353V I366V C400S I401L T436L **L437I** E442K ΔFAD
C10-II	N70E A74G V78L A82L F87A M118S P142S F162L T175I M177L A184V S226R H236Q E252G I263Y H266V T268G A290V **A328I** A330Y L353V I366V C400S I401L T436L **L437I** E442K ΔFAD
C10-IIM	N70E A74G **V78M** A82L F87A M118S P142S F162L T175I M177L A184V S226R H236Q E252G I263Y H266V T268G A290V **A328I** A330Y L353V I366V C400S I401L T436L **L437I** E442K ΔFAD
C10-IIMR	N70E A74G **V78M** A82L F87A M118S P142S F162L T175I M177L A184V S226R H236Q E252G I263Y H266V T268G A290V **A328I** A330Y L353V I366V C400S I401L **T436R L437I** E442K ΔFAD
C10-IIMRV	N70E A74G **V78M** A82L F87A M118S P142S F162L T175I M177L A184V S226R H236Q E252G I263Y H266V T268G A290V **A328I** A330Y L353V I366V C400S **I401V T436R L437I** E442K ΔFAD
C10-IIMRVI	N70E A74G **V78M** A82L F87A M118S P142S **F162I** T175I M177L A184V S226R H236Q E252G I263Y H266V T268G A290V **A328I** A330Y L353V I366V C400S **I401V T436R L437I** E442K ΔFAD
C10-IIMRVIL	N70E A74G **V78M** A82L F87A M118S P142S **F162I** T175I M177L A184V **R190L** S226R H236Q E252G I263Y H266V T268G A290V **A328I** A330Y L353V I366V C400S **I401V T436R L437I** E442K ΔFAD
C10-IIMRVILS (***LoS***)	**N70S** A74G **V78M** A82L F87A M118S P142S **F162I** T175I M177L A184V **R190L** S226R H236Q E252G I263Y H266V T268G A290V **A328I** A330Y L353V I366V C400S **I401V T436R L437I** E442K ΔFAD
C10-WIRF_GA	N70E S72F V78L A82L F87A M118S P142S F162L T175I M177L A184V S226R H236Q E252G I263W H266V T268G A290V A328V A330Y S332G L353V I366V C400S I401L T436R L437I E442K ΔFAD
C10-WIRF_GAP	N70E S72F V78L A82L F87A M118S P142S F162L T175I M177L A184V S226R H236Q E252G I263W H266V T268G A290V **T327P** A328V A330Y S332G L353V I366V C400S I401L T436R L437I E442K ΔFAD
C10-WIRV_GAP	N70E **S72V** V78L A82L F87A M118S P142S F162L T175I M177L A184V S226R H236Q E252G I263W H266V T268G A290V **T327P** A328V A330Y S332G L353V I366V C400S I401L T436R L437I E442K ΔFAD
C10-WIRV_GAP(P)	N70E **S72V** V78L A82L F87A M118S P142S F162L T175I M177L A184V S226R H236Q E252G I263W H266V T268G A290V **T327P** A328V (**P329P**) A330Y S332G L353V I366V C400S I401L T436R L437I E442K ΔFAD
C10-WIRV_GAP(P)S	N70E **S72V** V78L A82L F87A M118S P142S F162L T175I M177L A184V H236Q E252G I263W H266V T268G A290V **T327P** A328V (**P329P**) A330Y S332G L353V I366V C400S

	I401L T436R L437I E442K ΔFAD
C10- WIRV_GAP(P)S_ F	N70E **S72V** V78L A82L F87A **H92F** M118S P142S F162L T175I M177L A184V H236Q E252G I263W H266V T268G A290V **T327P** A328V (**P329P**) A330Y S332G L353V I366V C400S I401L T436R L437I E442K ΔFAD
C10- WIRV_GAP(P)S_ FF	N70E **S72V** V78L A82L F87A **H92F** M118S P142S T175I M177L A184V H236Q E252G I263W H266V T268G A290V **T327P** A328V (**P329P**) A330Y S332G L353V I366V C400S I401L T436R L437I E442K ΔFAD
C10- WIRV_GAP(P)S_ FFR	N70E **S72V** V78L A82L F87A **H92F** M118S P142S T175I M177L A184V H236Q **E252R** I263W H266V T268G A290V **T327P** A328V (**P329P**) A330Y S332G L353V I366V C400S I401L T436R L437I E442K ΔFAD
C10- WIRV_GAP(P)S_ FFRI	N70E **S72V** V78L A82L F87A **H92F** M118S P142S T175I M177L A184V H236Q **E252R** I263W H266V T268G A290V **T327P** A328V (**P329P**) A330Y S332G L353V C400S I401L T436R L437I E442K ΔFAD
C10- WIRV_GAP(P)S_ FFRIG	N70E **S72V** V78L A82L F87A **H92F** M118S **P142G** T175I M177L A184V H236Q **E252R** I263W H266V T268G A290V **T327P** A328V (**P329P**) A330Y S332G L353V C400S I401L T436R L437I E442K ΔFAD
C10- WIRV_GAP(P)S_ FFRIGT	N70E **S72V** V78L **A82T** F87A **H92F** M118S **P142G** T175I M177L A184V H236Q **E252R** I263W H266V T268G A290V **T327P** A328V (**P329P**) A330Y S332G L353V C400S I401L T436R L437I E442K ΔFAD

Note: ΔFAD means FAD domain truncation.

Table C-6. Substrates prepared and tested for intramolecular carbene C–H insertion.

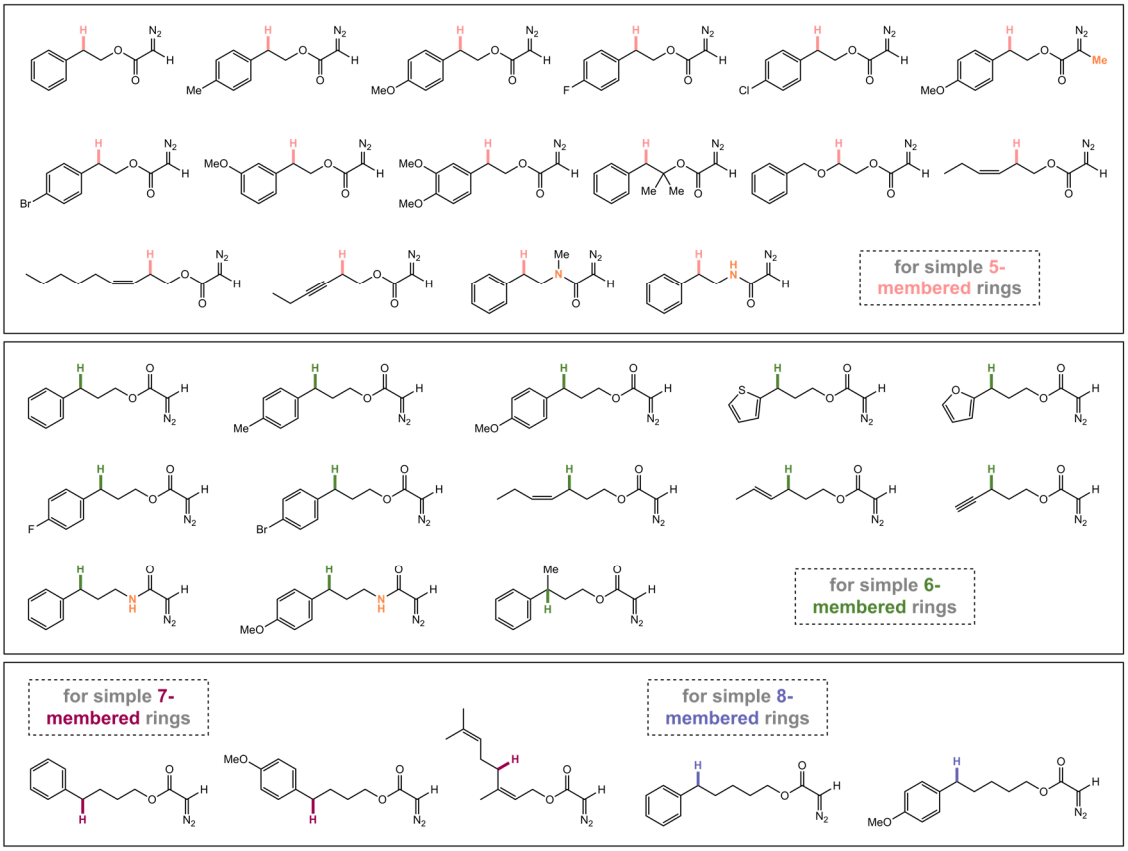

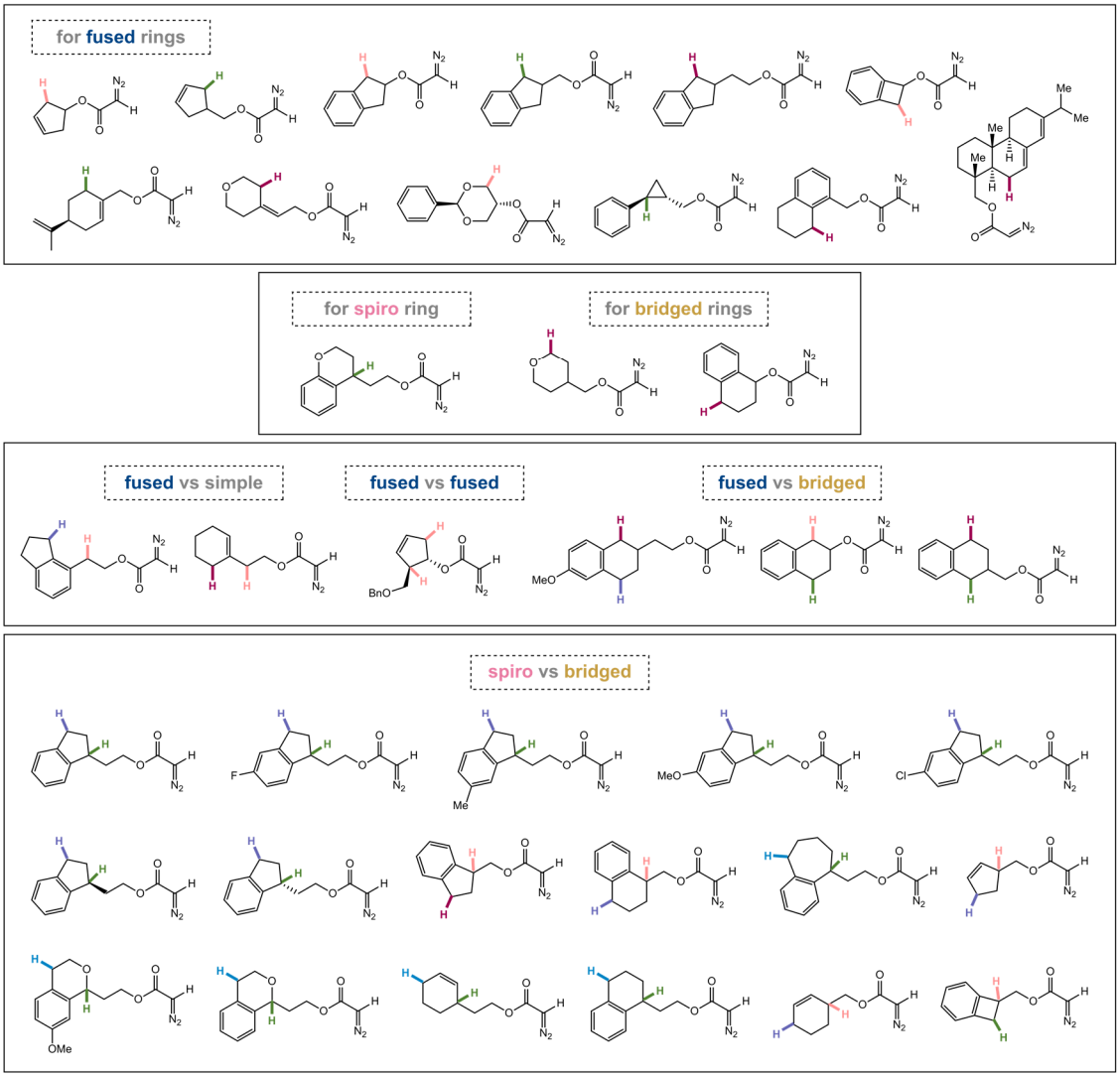

C.2 Supporting Figures C-1 to C-2

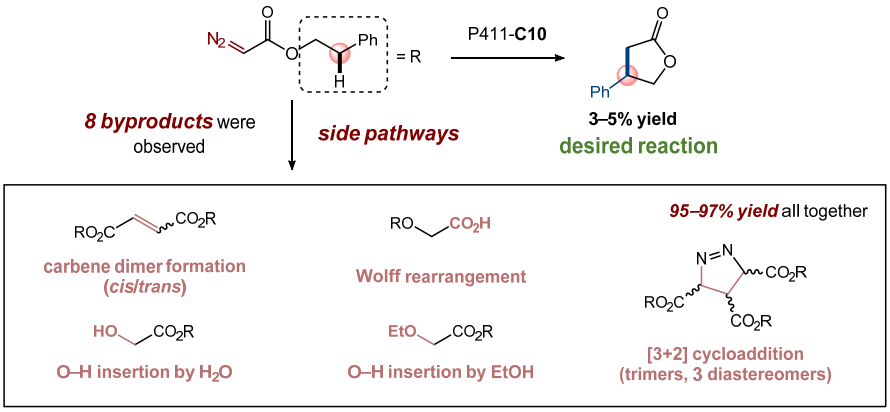

Figure C-1. The overall conversion of substrate 21a with variant P411-C10. The desired intramolecular C–H insertion product **22a** was formed in 3–5% dependent on different reaction conditions.

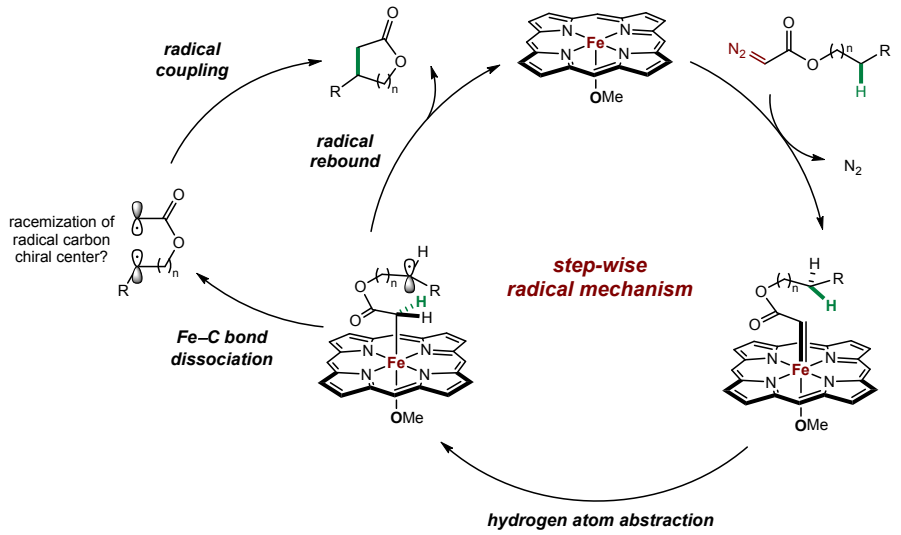

Figure C-2. Different mechanisms of intramolecular C–H insertion suggested by DFT calculation. The detailed mechanism of the intramolecular C–H insertion reaction may differ (*e.g.*, changes in the energy barriers of the HAT and radical rebound steps), when different substrates or different enzyme scaffolds are used. Besides, another pathway involving a Fe–C bond dissociation step followed by direct radical coupling may also be applied to the C–H insertion reaction.

C.3 Preparation of diazo substrates

2-(2-Tosylhydrazineylidene)acetyl chloride

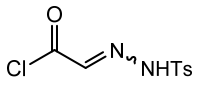

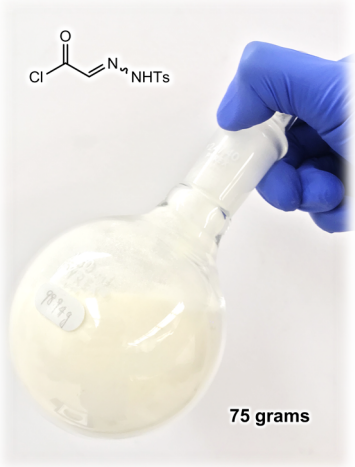

4-Methylbenzenesulfonohydrazide (55.9 g, 0.3 mol, 1.0 equiv.) was dissolved in aqueous hydrochloric acid (2 M, 180 mL) and warmed to 50 °C (solution 1). 2-Oxoacetic acid (44.4 g of 50% in water, 0.3 mol, 1.0 equiv.) was dissolved in water (300 mL) and heated to 50 °C (solution 2). Pre-warmed solution 1 was slowly transferred to solution 2. The reaction mixture was then stirred at 60 °C for 4 h until all the hydrozone product crashed out. The mixture was cooled to 0 °C and kept for 2 h. The product 2-(2-tosylhydrazineylidene) acetic acid (~70 g, 97% yield) was collected by filtration, washed with hexane: ether (10:1, 20 mL × 3) and dried under vaccum.

2-(2-Tosylhydrazineylidene)acetic acid (70 g, 0.29 mmol, 1.0 equiv.) was dissolved in dry dichloromethane (300 mL). Thionyl chloride (50 mL) and *N*,*N*-dimethyl formaldehyde (4 drops, *cat*.) were added to the solution. The reaction mixture was stirred at room temperature for 1 h and then heated to reflux (~ 50 °C) for 5 h until the starting material was completely dissolved and the reaction turned clear and light yellow. After the reaction was cooled to room temperature, organic solvent and the excess thionyl chloride were removed under reduced pressure. The resulting mixture was treated with ether (20 mL) and sonicated for 5 min. Hexane (150 mL) was then slowly added to the mixture to completely crash out the acyl chloride product. The mixture was cooled to 0 °C and kept for 2 h. The product 2-(2-tosylhydrazineylidene)acetyl chloride (~74 g, 98% yield, pale yellow) was collected by filtration, washed with hexane (20 mL × 2) and dried under vaccum.

General procedure for the preparation of diazo esters

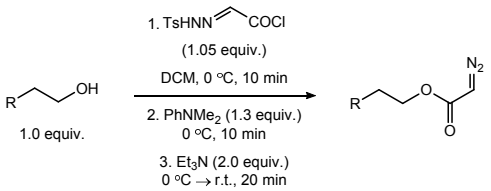

An alcohol substrate (1.0 equiv.) was dissolved in dry dichloromethane (conc. ~ 0.2–0.5 M) and kept at 0 °C. 2-(2-Tosylhydrazineylidene)acetyl chloride (1.05 equiv.) was then added to the solution. The mixture was stirred at 0 °C for 10 min before the addition of *N*,*N*-dimethyl aniline (1.3 equiv.). The resulting mixture was then stirred for another 10 min. Triethylamine (2.0 equiv.) was added to the reaction, which was then allowed to slowly warm up to room temperature over 20 min. The reaction was concentrated under reduced pressure and quenched by citric acid (saturated aqueous solution). The resulting mixture was transferred to a separatory funnel. Dichloromethane and water were used in minimum amount to wash the reaction container and transfer everything to the separatory funnel. Hexane/ethyl acetate (13:1) was used for extraction for three times. The combined organic layer was then washed with saturated citric acid solution and brine, dried over Na_2SO_4, filtered, and concentrated under reduced pressure. The resulting crude product was purified through a silica column using pentane/ether (1:0 to 10:1) as eluents. The yellow-colored fractions were concentrated to afford the diazo product as a yellow liquid (80–96% yield).

C.4 Analysis of lactone products by enzymatic reactions

4-Phenyldihydrofuran-2(3*H*)-one (22a)

Calibration curve:

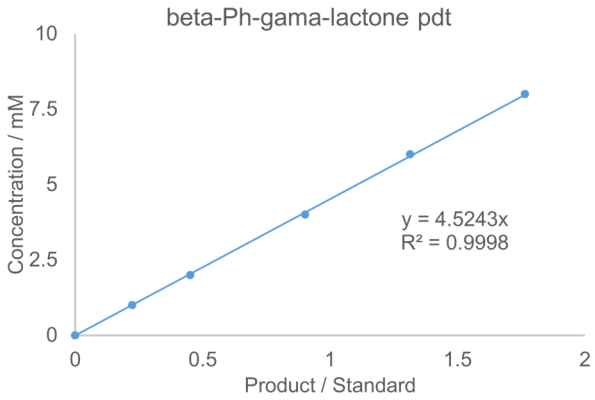

Analysis Data (***LoS***, OD_{600}=10, 10 mM substrate):

Entries	Pdt	Std	Pdt/Std	[Pdt]/mM	[PC]/μM	TTN	Avg. TTN	Avg. yield
22a-(1)	7088.5	6194.8	1.144	5.18	1.51	3420		
22a-(2)	7045.3	6165.9	1.143	5.17	1.51	3416		
22a-(3)	7102.7	6180	1.149	5.20	1.51	3435		
22a-(4)	7075.7	6089.2	1.162	5.26	1.51	3473	3436	52.0%

Analysis Data (***LoS***, OD_{600}=2.5, 2.5 mM substrate):

Entries	Pdt	Std	Pdt/Std	[Pdt]/mM	[PC]/μM	TTN	Avg. TTN	Avg. yield
22a-(1)	2887.1	6110.7	0.472	2.14	0.38	5649		
22a-(2)	2794.5	6185.1	0.452	2.04	0.38	5402		
22a-(3)	2812.4	6110.2	0.460	2.08	0.38	5503		
22a-(4)	2753.6	6122.4	0.450	2.03	0.38	5378	5483	83.0%

Chiralpak IA, 2.5% isopropanol in hexane, 1.2 ml/min, 32 °C, 210nm

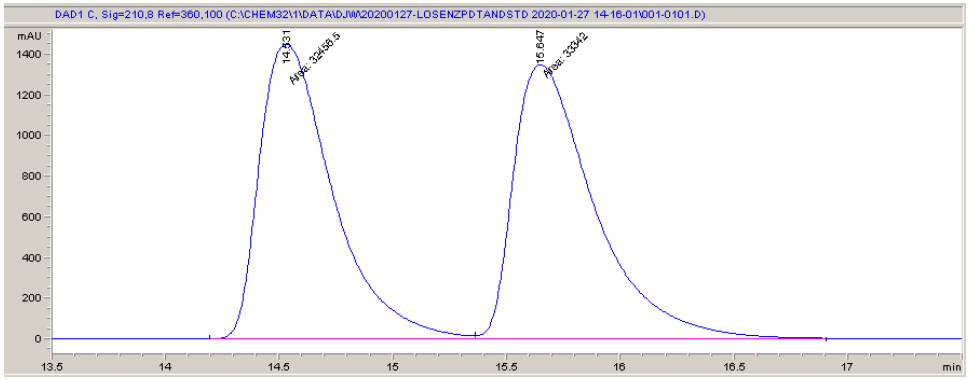

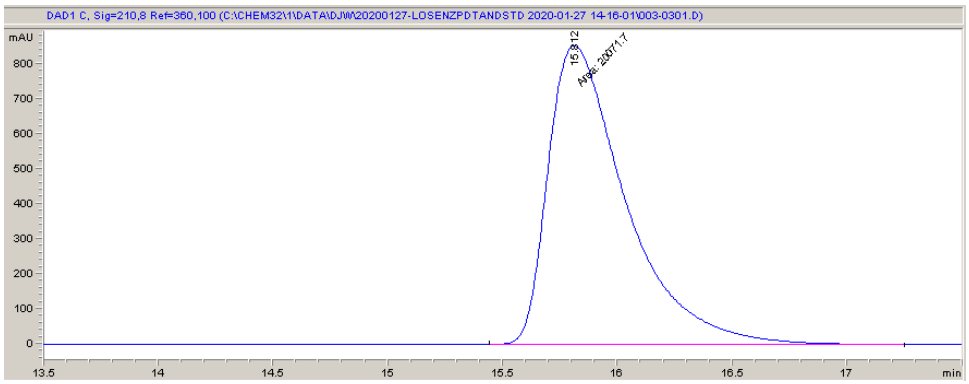

***rac*-22a**			**Enzymatically produced 22a**		
Retention Time (min)	Area (mAU*s)	Area %	Retention Time (min)	Area (mAU*s)	Area %
14.531	32456.5	49.33	-	-	-
15.647	33342.0	50.67	15.812	20071.7	100.00
Total	65798.5	100.00	Total	20071.7	100.00

4-Phenyltetrahydro-2*H*-pyran-2-one (22b)

Analysis Data (**C10**-IIMRV, OD_{600}=10, 10 mM substrate, 6 h):

Entries	Pdt	Std	Pdt/Std	[Pdt]/mM	[PC]/μM	TTN	Avg. TTN	Avg. yield
22b-(1)	6869.1	6524.8	1.053	4.76	1.38	3460		
22b-(2)	6893.1	6458.7	1.067	4.83	1.38	3508		
22b-(3)	6888.4	6446.8	1.068	4.83	1.38	3512		
22b-(4)	7018.9	6526.4	1.075	4.87	1.38	3535	3504	48.2%

Analysis Data (**C10**-IIMRV, OD_{600}=2.5, 2.5 mM substrate, 9 h):

Entries	Pdt	Std	Pdt/Std	[Pdt]/mM	[PC]/μM	TTN	Avg. TTN	Avg. yield
22b-(1)	2146.3	6570.5	0.327	1.48	0.34	4295		
22b-(2)	2223.5	6506.1	0.342	1.55	0.34	4493		
22b-(3)	2239.8	6587.8	0.340	1.54	0.34	4470		
22b-(4)	2213.9	6590.5	0.336	1.52	0.34	4416	4419	60.8%

Chiralpak IC, 25% isopropanol in hexane, 1.2 ml/min, 28 °C, 210nm

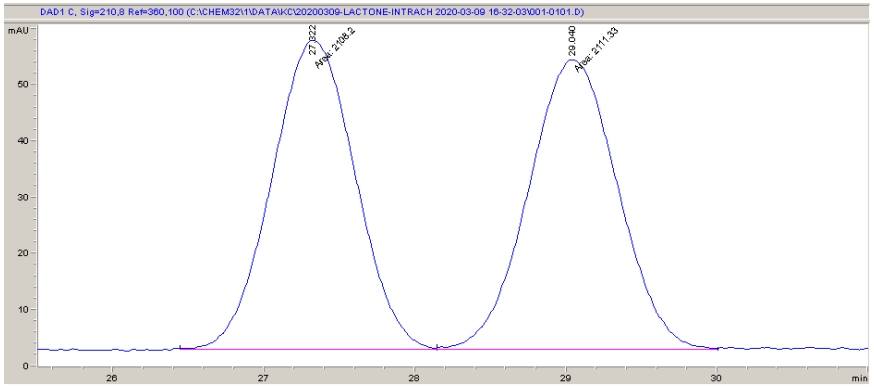

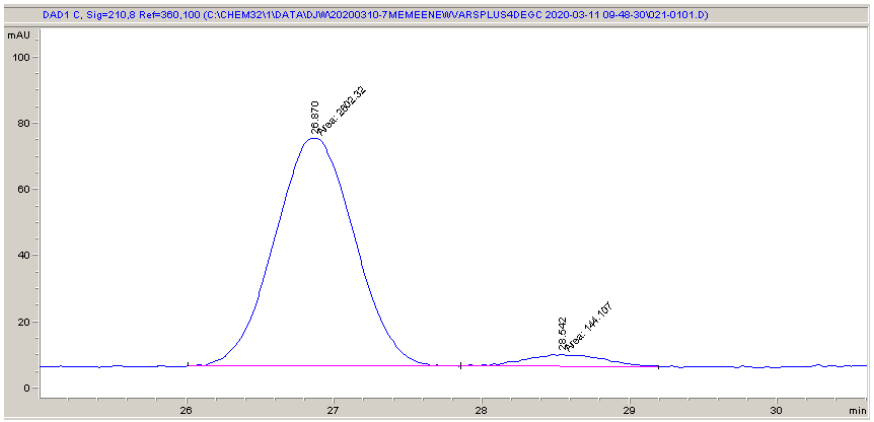

***rac*-22b**			**Enzymatically produced 22b**		
Retention Time (min)	Area (mAU*s)	Area %	Retention Time (min)	Area (mAU*s)	Area %
27.322	2108.20	49.96	26.870	2602.32	94.75

29.040	2111.33	50.04	28.542	144.11	5.25
Total	4219.53	100.00	Total	2746.43	100.00

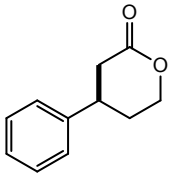

^{1}H NMR (400 MHz, $CDCl_3$) δ 7.42–7.32 (m, 2H), 7.32–7.26 (m, 1H), 7.25–7.17 (m, 2H), 4.51 (ddd, *J* = 11.5, 4.9, 3.9 Hz, 1H), 4.40 (ddd, *J* = 11.5, 10.4, 3.8 Hz, 1H), 3.24 (tdd, *J* = 10.6, 5.9, 4.5 Hz, 1H), 2.93 (ddd, *J* = 17.6, 5.9, 1.6 Hz, 1H), 2.64 (dd, *J* = 17.6, 10.7 Hz, 1H), 2.18 (ddtd, *J* = 14.0, 4.5, 3.9, 1.7 Hz, 1H), 2.04 (dtd, *J* = 14.1, 10.5, 4.9 Hz, 1H). ^{13}C NMR (101 MHz, $CDCl_3$) δ 170.81, 142.88, 129.13, 127.38, 126.59, 68.80, 37.65, 37.60, 30.45.

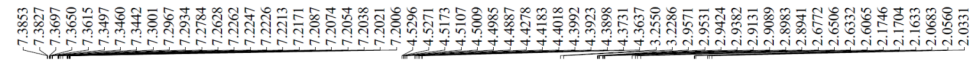

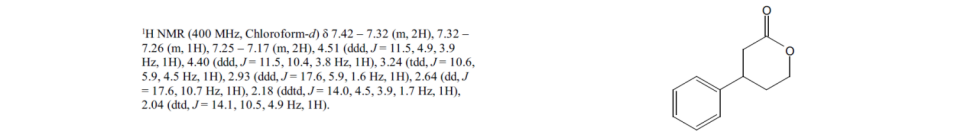

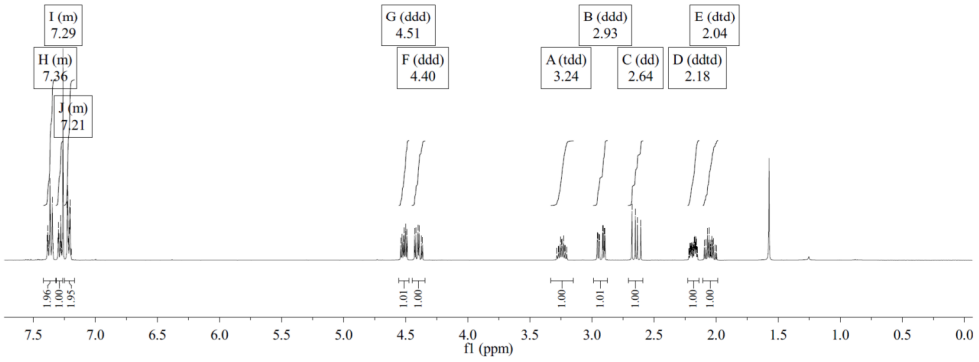

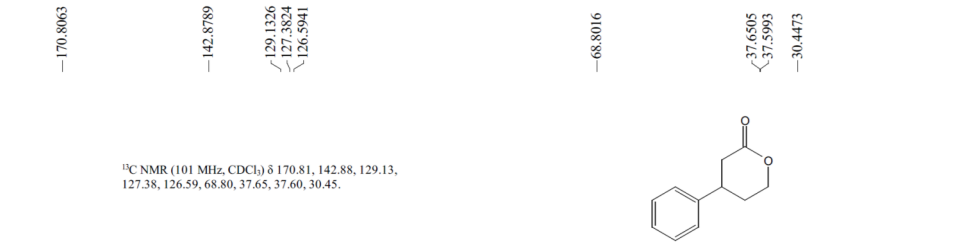

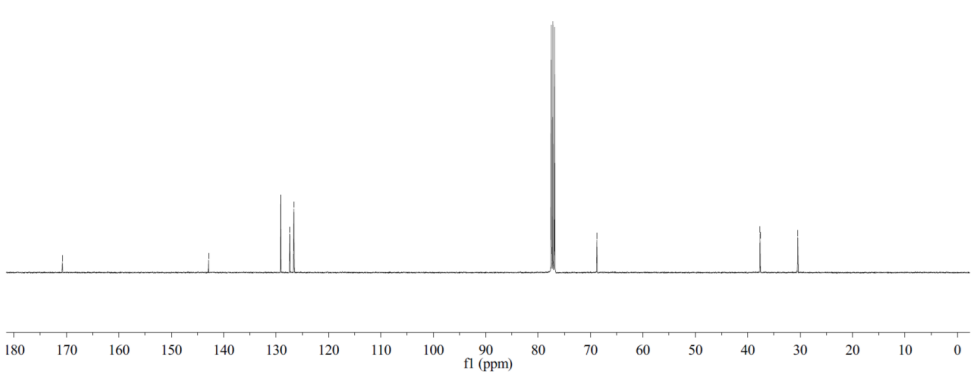

4-(4-Methoxyphenyl)oxepan-2-one (22c)

Analysis Data (*7**LoS***, OD_{600}=10, 10 mM substrate, 6 h):

Entries	Pdt	Std	Pdt/Std	[Pdt]/mM	[PC]/μM	TTN	Avg. TTN	Avg. yield
22c-(1)	4916.5	6757.0	0.728	4.82	2.27	2118		
22c-(2)	4630.9	6808.2	0.680	4.50	2.27	1980		
22c-(3)	5148.7	6858.3	0.751	4.97	2.27	2186		
22c-(4)	5101.2	6840.4	0.746	4.94	2.27	2171	2114	48.1%

Analysis Data (*7**LoS***, OD_{600}=2.5, 2.5 mM substrate, 9 h):

Entries	Pdt	Std	Pdt/Std	[Pdt]/mM	[PC]/μM	TTN	Avg. TTN	Avg. yield
22c-(1)	1856.2	6758.7	0.275	1.82	0.57	3198		
22c-(2)	1950.3	6776.2	0.288	1.90	0.57	3352		
22c-(3)	1578.5	6772.3	0.233	1.54	0.57	2714		
22c-(4)	1738.2	6777.8	0.256	1.70	0.57	2986	3063	69.6%

Chiralpak IC, 25% isopropanol in hexane, 1.2 ml/min, 28 °C, 235nm

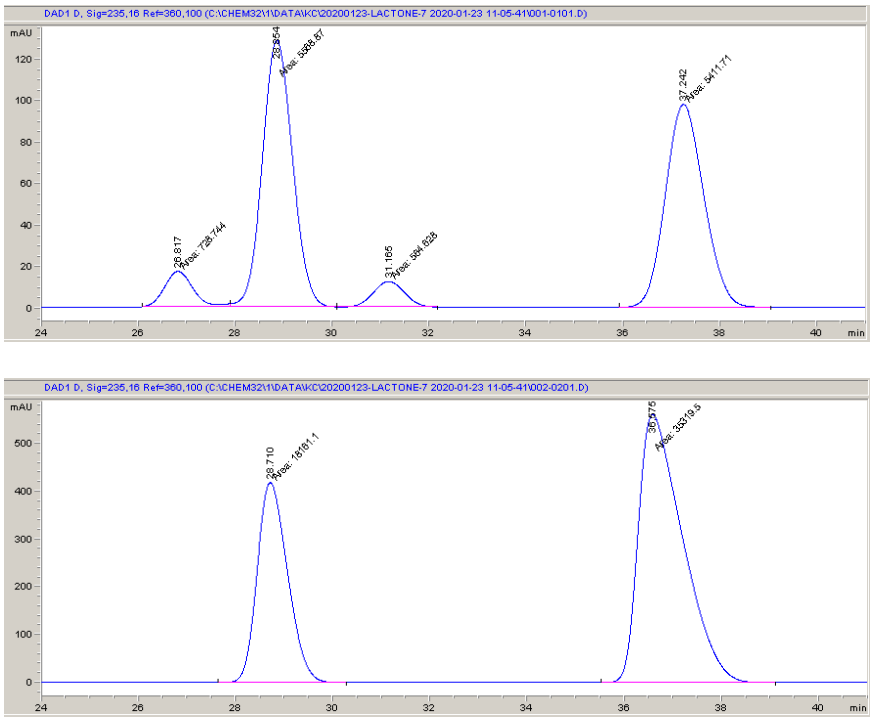

***rac*-22c**			**Enzymatically produced 22c**		
Retention Time (min)	Area (mAU*s)	Area %	Retention Time (min)	Area (mAU*s)	Area %
28.354	5588.97	50.81	28.710	18161.1	33.96
37.242	5411.71	49.19	36.575	35319.5	66.04
Total	11000.68	100.00	Total	53480.6	100.00

4-(4-Methoxyphenyl)oxepan-2-one (22c)

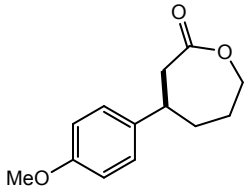

^{1}H NMR (400 MHz, $CDCl_3$) δ 7.17–7.04 (m, 2H), 6.85 (d, *J* = 8.7 Hz, 2H), 4.37 (dddd, *J* = 12.8, 5.5, 2.2, 1.4 Hz, 1H), 4.33–4.24 (m, 1H), 3.79 (s, 3H), 3.01 (dd, *J* = 12.9, 11.7 Hz, 1H), 2.90 (td, *J* = 12.0, 2.8 Hz, 1H), 2.79 (dt, *J* = 13.1, 1.4 Hz, 1H), 2.15–2.01 (m, 2H), 1.99–1.85 (m, 1H), 1.85–1.70 (m, 1H). ^{13}C NMR (101 MHz, $CDCl_3$) δ 174.74, 158.47, 137.83, 127.34, 114.23, 69.22, 55.42, 41.95, 40.00, 38.07, 29.16.

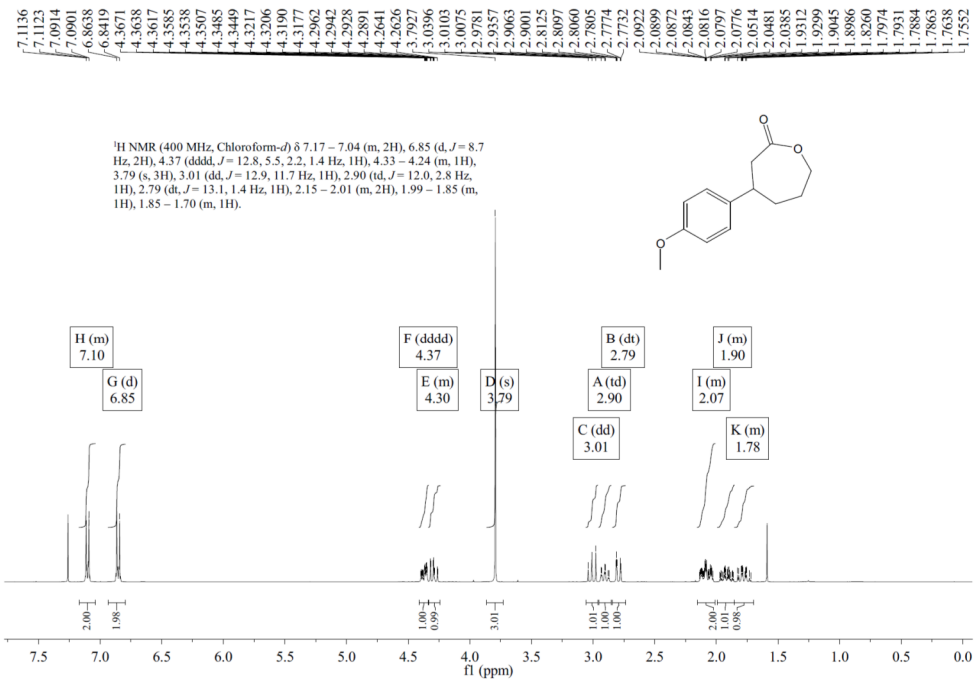

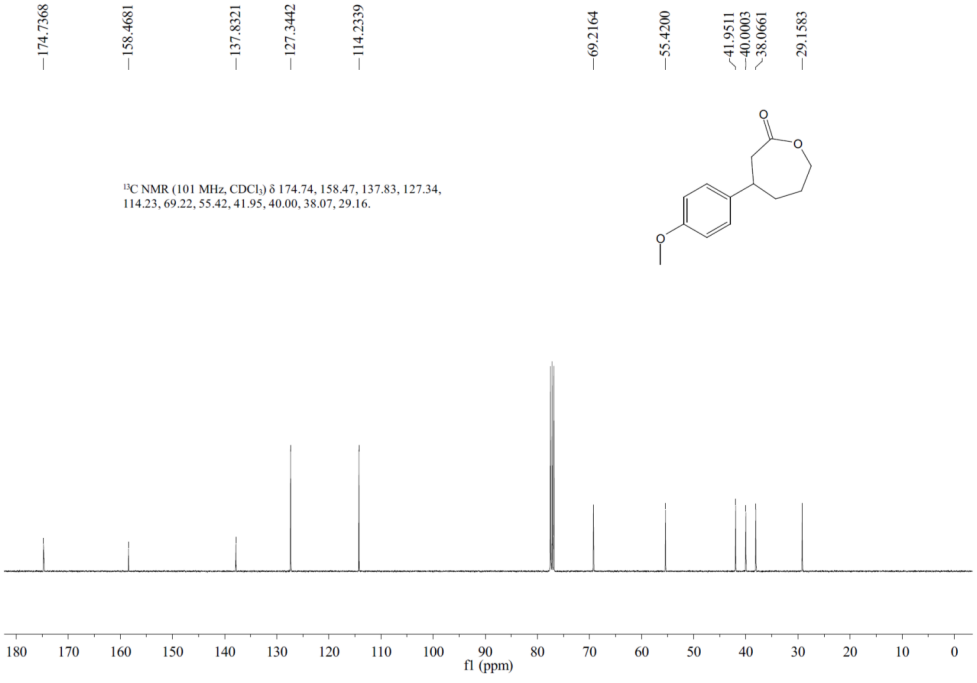

(*E*)-4-(Prop-1-en-1-yl)tetrahydro-2*H*-pyran-2-one

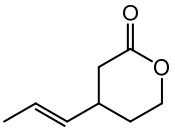

^{1}H NMR (400 MHz, $CDCl_3$) δ 5.52 (dqd, *J* = 15.4, 6.4, 1.1 Hz, 1H), 5.37 (ddq, *J* = 15.4, 6.5, 1.6 Hz, 1H), 4.42 (dt, *J* = 11.4, 4.7 Hz, 1H), 4.28 (ddd, *J* = 11.4, 9.9, 3.9 Hz, 1H), 2.75–2.54 (m, 2H), 2.32 (dd, *J* = 16.8, 9.3 Hz, 1H), 1.95 (dqd, *J* = 14.1, 4.4, 1.8 Hz, 1H), 1.72–1.62 (m, 4H). ^{13}C NMR (101 MHz, $CDCl_3$) δ 171.02, 132.58, 126.02, 68.51, 36.33, 34.51, 29.25, 18.03.

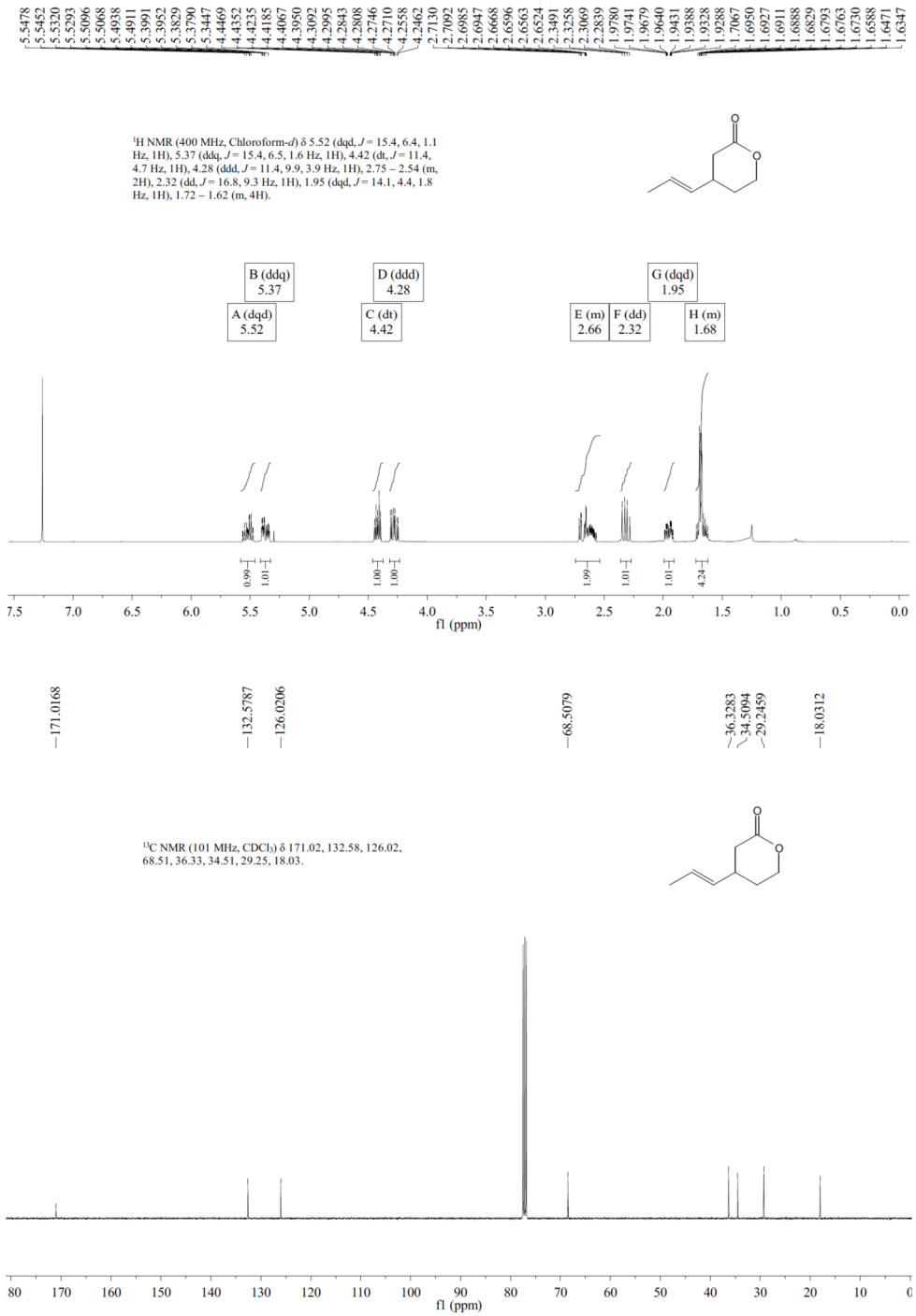

2′,3′-Dihydro-2*H*-spiro[furan-3,1′-inden]-5(4*H*)-one

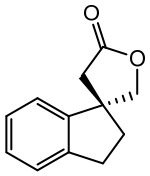

^{1}H NMR (400 MHz, $CDCl_3$) δ 7.29–7.21 (m, 4H), 4.32 (s, 2H), 2.98 (t, *J* = 7.2 Hz, 2H), 2.84 (d, *J* = 17.3 Hz, 1H), 2.66 (d, *J* = 17.3 Hz, 1H), 2.31 (dt, *J* = 12.8, 6.7 Hz, 1H), 2.18 (dt, *J* = 12.9, 7.5 Hz, 1H). ^{13}C NMR (101 MHz, $CDCl_3$) δ 176.44, 144.21, 143.48, 128.26, 127.40, 125.20, 122.09, 78.22, 52.13, 41.65, 38.37, 30.22.

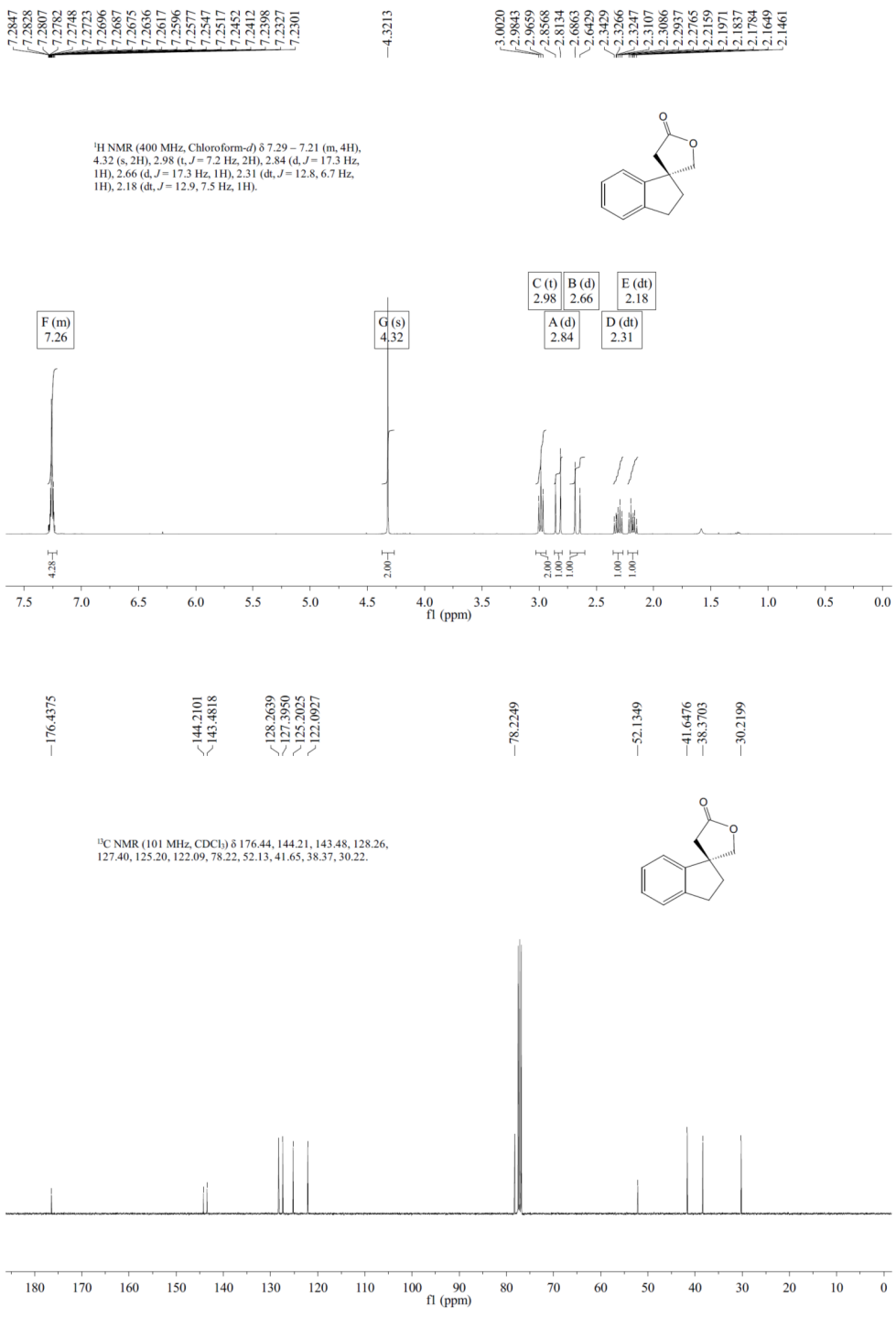

(3a*R*,8a*S*)-3,3a,8,8a-Tetrahydro-2*H*-indeno[2,1-b]furan-2-one

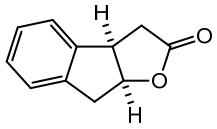

^{1}H NMR (400 MHz, $CDCl_3$) δ 7.30–7.19 (m, 4H), 5.30 (ddd, *J* = 5.8, 3.7, 2.7 Hz, 1H), 4.02 (ddt, *J* = 9.3, 5.7, 1.3 Hz, 1H), 3.33 (s, 1H), 3.32 (d, *J* = 1.1 Hz, 1H), 3.05 (dd, *J* = 17.8, 9.3 Hz, 1H), 2.75 (dd, *J* = 17.8, 1.5 Hz, 1H). ^{13}C NMR (101 MHz, $CDCl_3$) δ 176.46, 142.15, 140.13, 128.45, 127.85, 125.42, 124.79, 84.43, 45.58, 39.07, 35.48.

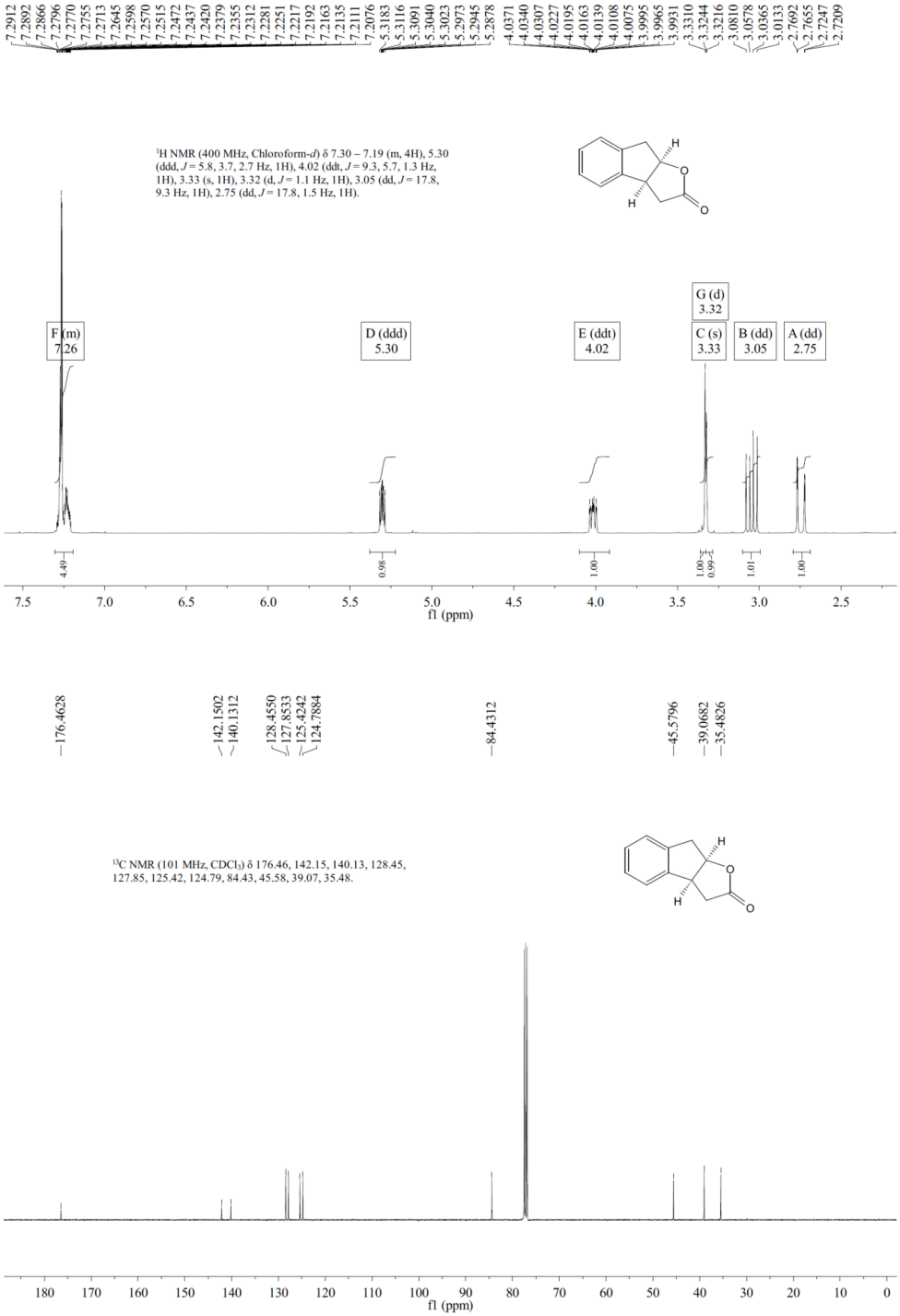

(4a*R*,9a*R*)-4,4a,9,9a-Tetrahydroindeno[2,1-c]pyran-3(1*H*)-one

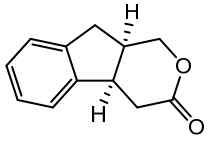

^{1}H NMR (400 MHz, $CDCl_3$) δ 7.26–7.13 (m, 4H), 4.39 (dd, *J* = 11.4, 5.0 Hz, 1H), 4.09 (dd, *J* = 11.4, 8.8 Hz, 1H), 3.81 (dt, *J* = 9.9, 7.9 Hz, 1H), 3.30 (dd, *J* = 16.8, 9.7 Hz, 1H), 3.10–2.96 (m, 2H), 2.81 (dd, *J* = 16.8, 3.9 Hz, 1H), 2.57 (dd, *J* = 15.3, 7.8 Hz, 1H). ^{13}C NMR (101 MHz, $CDCl_3$) δ 172.79, 143.96, 141.31, 127.91, 127.56, 125.06, 124.27, 70.26, 41.04, 35.81, 34.93, 34.90.

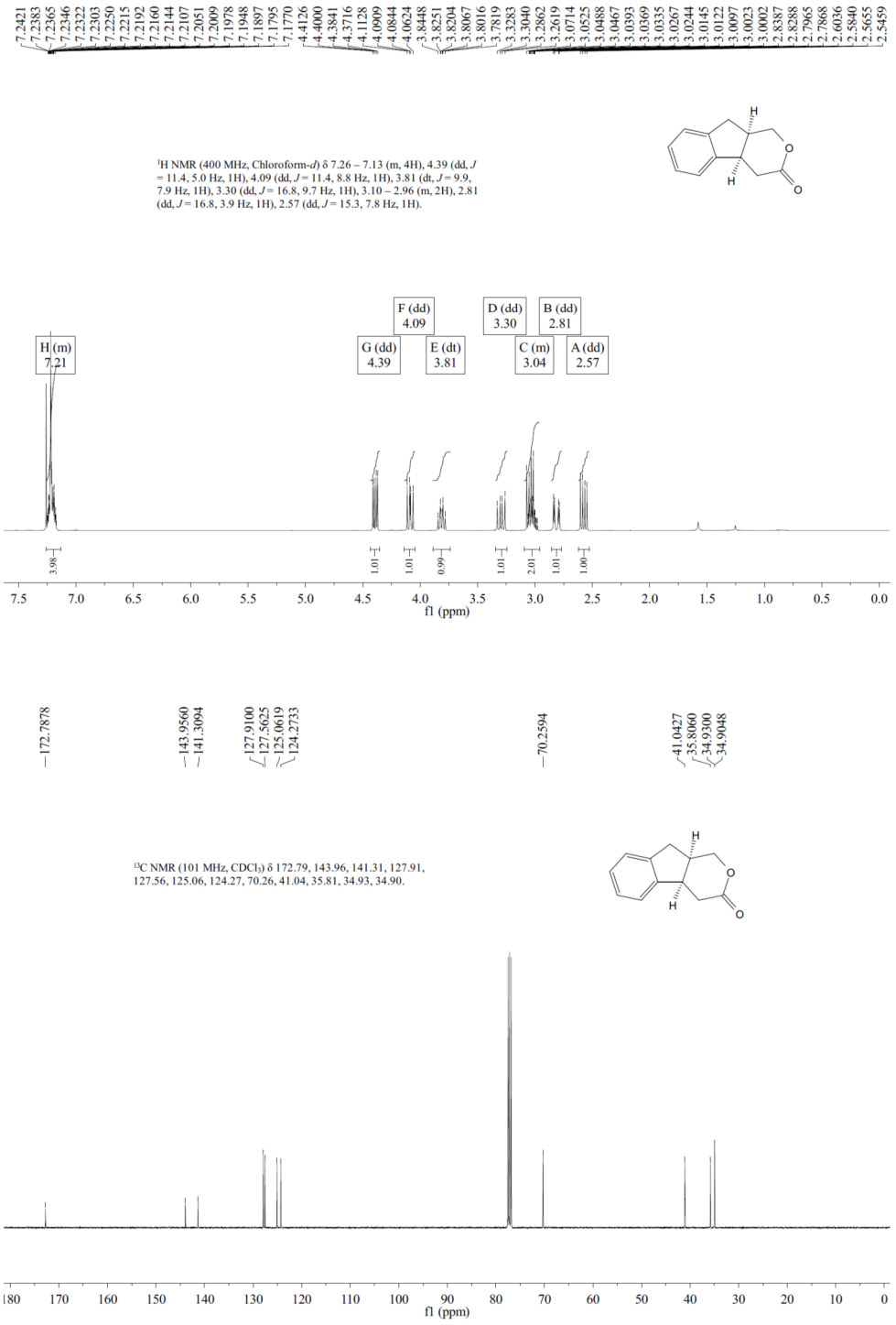

2,3,5',6'-Tetrahydrospiro[indene-1,4'-pyran]-2'(3'H)-one

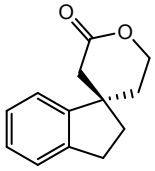

^{1}H NMR (400 MHz, $CDCl_3$) δ 7.29–7.11 (m, 4H), 4.54–4.43 (AB, ddd, *J* = 4.6, 8.1, 11.7 Hz, 1H; ddd, *J* = 5.3, 5.9, 11.7 Hz, 1h), 2.96 (t, *J* = 7.1 Hz, 2H), 2.68 (dd, *J* = 17.2, 1.1 Hz, 1H), 2.63 (d, *J* = 17.2 Hz, 1H), 2.17 (ddd, *J* = 14.3, 8.1, 5.4 Hz, 1H), 2.08 (t, *J* = 7.1 Hz, 2H), 1.91 (dddd, *J* = 14.1, 5.8, 4.6, 1.1 Hz, 1H). ^{13}C NMR (101 MHz, $CDCl_3$) δ 170.99, 147.79, 142.87, 127.77, 127.18, 125.16, 122.42, 67.13, 45.72, 41.80, 38.95, 33.89, 29.75.

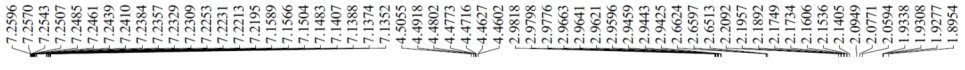

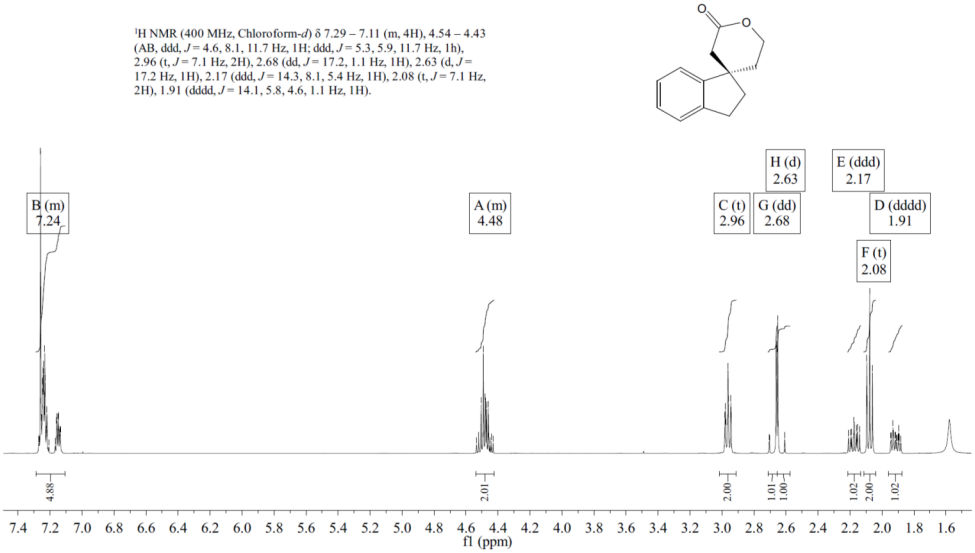

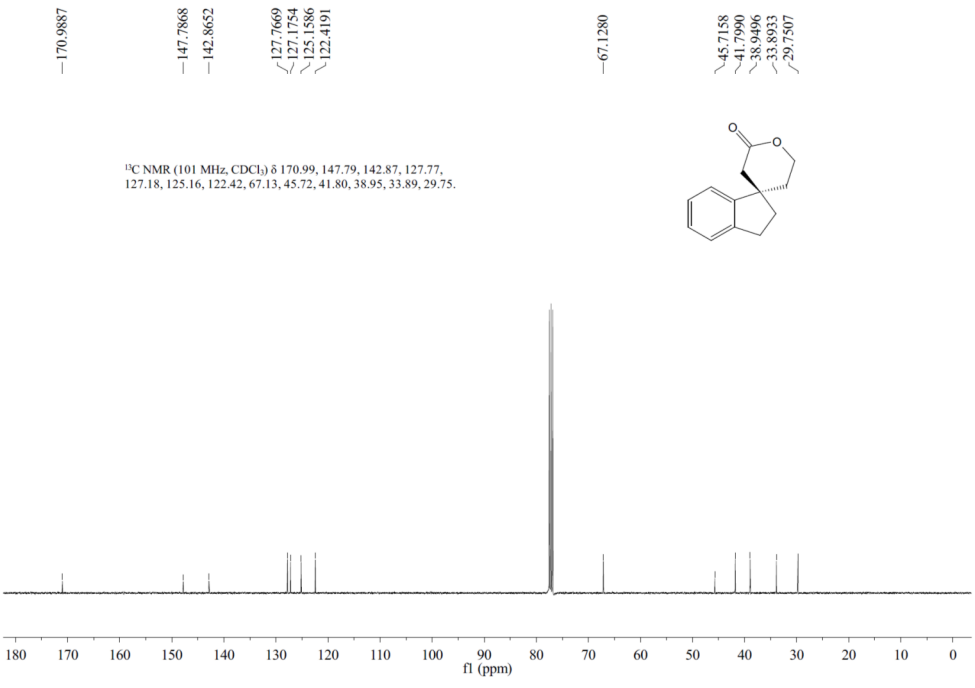

1,5,6,7-Tetrahydro-1,7-methanobenzo[e]oxonin-3(2*H*)-one

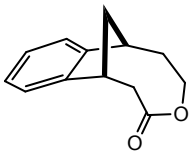

^{1}H NMR (400 MHz, $CDCl_3$) δ 7.30–7.14 (m, 4H), 4.10 (ddd, *J* = 11.9, 5.1, 3.0 Hz, 1H), 4.02 (td, *J* = 11.6, 3.1 Hz, 1H), 3.68 (dt, *J* = 9.4, 4.9 Hz, 1H), 3.52–3.44 (m, 1H), 2.90 (dd, *J* = 12.5, 4.9 Hz, 1H), 2.66–2.55 (m, 2H), 2.39 (dddd, *J* = 14.8, 11.4, 5.0, 3.5 Hz, 1H), 2.22 (dt, *J* = 13.7, 1.0 Hz, 1H), 2.00 (ddt, *J* = 14.8, 4.5, 3.1 Hz, 1H). ^{13}C NMR (101 MHz, $CDCl_3$) δ 175.67, 145.81, 144.21, 127.93, 127.70, 125.02, 124.72, 66.57, 42.81, 42.69, 41.28, 37.01, 36.46.

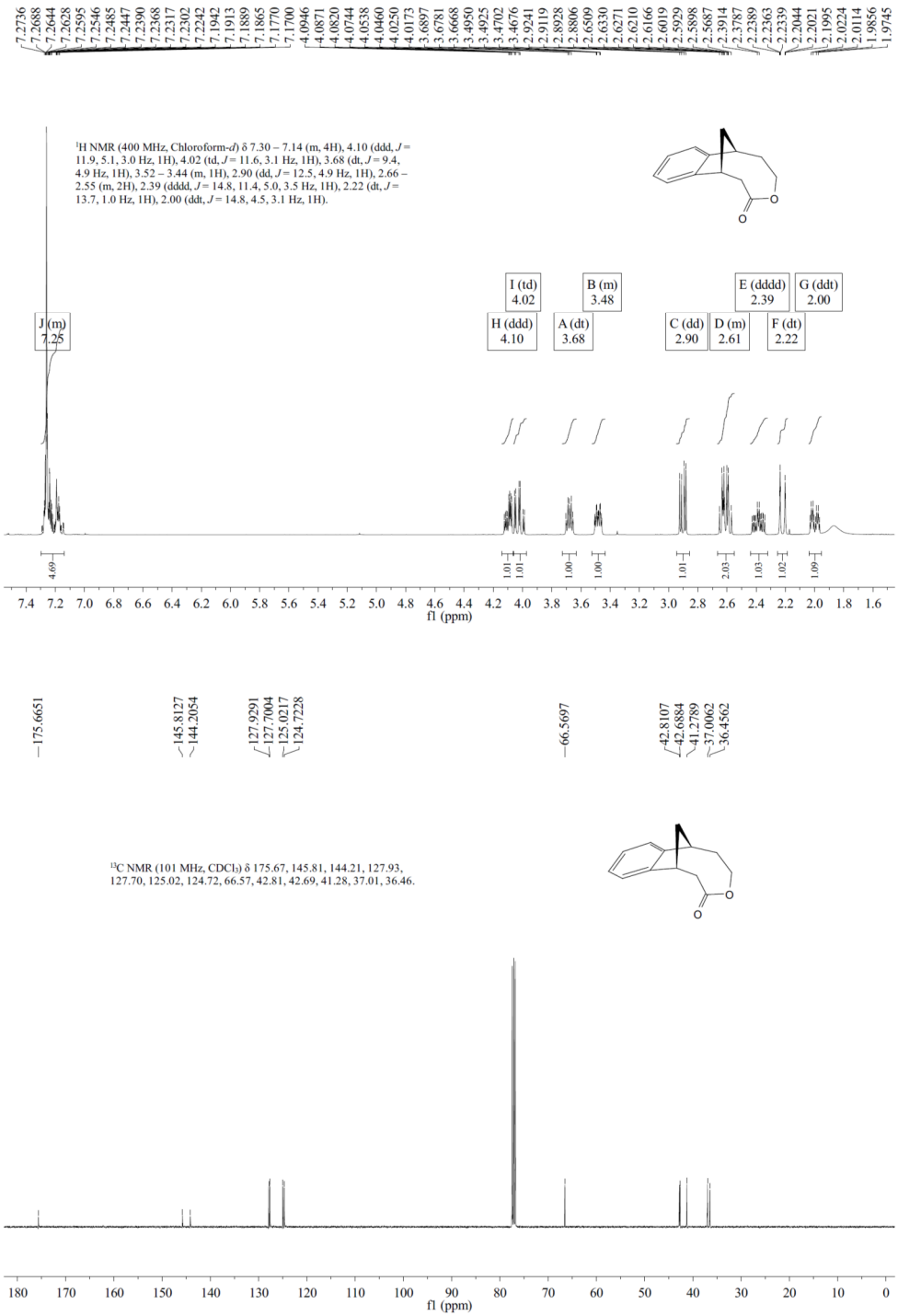

4-(4-Methoxyphenyl)tetrahydro-2*H*-pyran-2-one

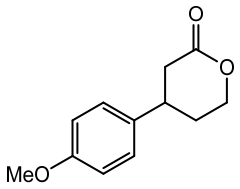

	condition 1	condition 2
C10-IIMRV	~5000 TTN, 70% yield (10 mM, 5 h)	~4500 TTN, 65% yield (2.5 mM, 7 h)

Note: The turnover numbers and yields were estimated according to HPLC signals. Accurate analysis will require the corresponding calibration curve of the standard product. It is the same for the following analysis.

Chiralpak IC, 25% isopropanol in hexane, 1.2 ml/min, 28 °C, 210nm

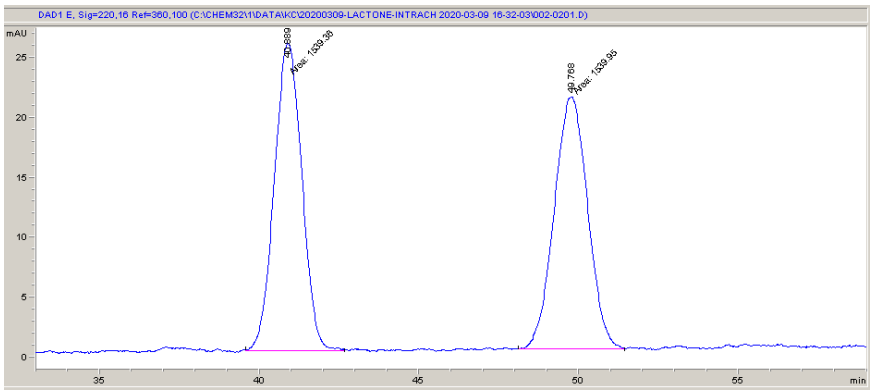

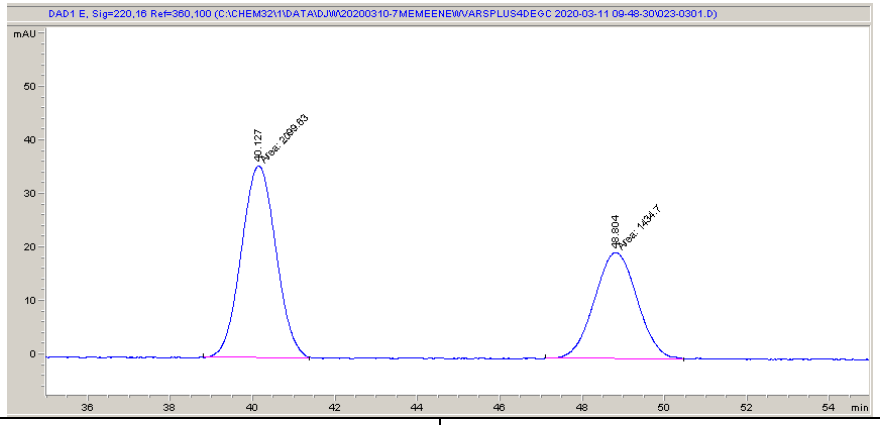

***rac* pdt**			**Enzymatically produced pdt**		
Retention Time (min)	Area (mAU*s)	Area %	Retention Time (min)	Area (mAU*s)	Area %
40.889	1539.36	49.99	40.127	2099.63	59.41
49.768	1539.95	50.01	48.804	1434.70	40.59
Total	3079.31	100.00	Total	3534.33	100.00

4-(4-Fluorophenyl)tetrahydro-2*H*-pyran-2-one

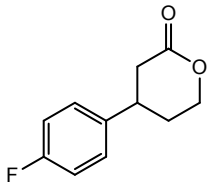

	condition 1	condition 2
C10-IIMRV	~3000 TTN, 40% yield (10 mM, 13 h)	~3500 TTN, 45% yield (2.5 mM, 15 h)

Chiralpak IC, 25% isopropanol in hexane, 1.2 ml/min, 28 °C, 210nm

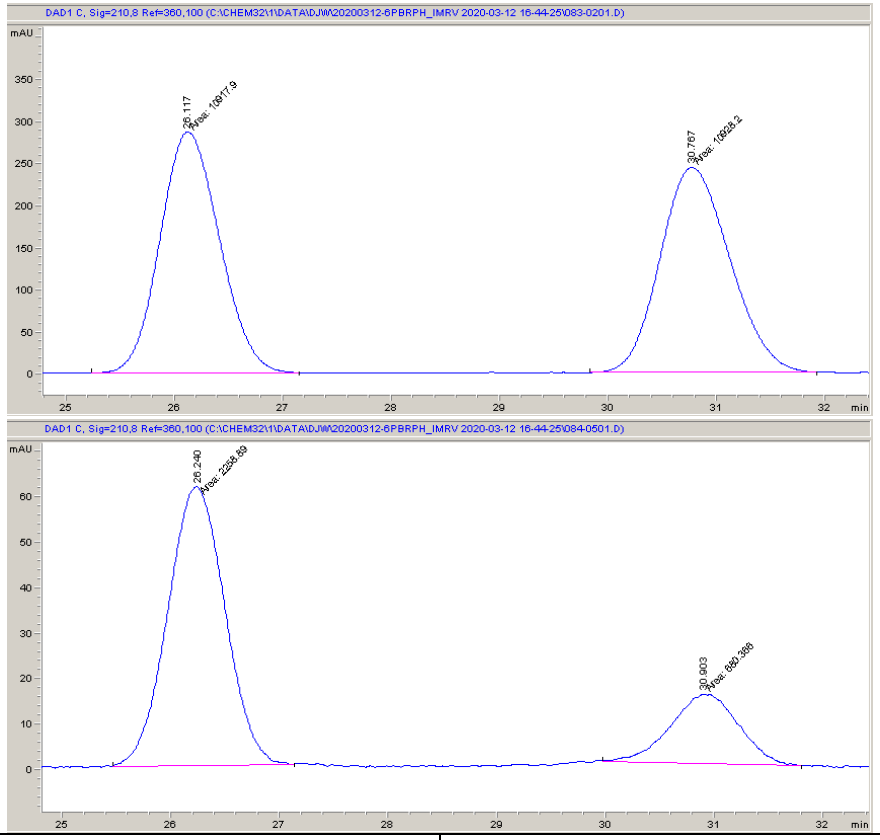

***rac* pdt**			**Enzymatically produced pdt**		
Retention Time (min)	Area (mAU*s)	Area %	Retention Time (min)	Area (mAU*s)	Area %
26.117	10917.9	49.98	26.240	2258.89	76.85
30.767	10928.2	50.02	30.903	680.37	23.15
Total	21846.1	100.00	Total	2939.26	100.00

4-(4-Bromophenyl)tetrahydro-2*H*-pyran-2-one

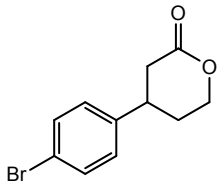

	condition 1	**condition 2**
C10-IIMRV	~3500 TTN, 45% yield (10 mM, 20 h)	~3000 TTN, 35% yield (2.5 mM, 24 h)

Chiralpak IC, 25% isopropanol in hexane, 1.2 ml/min, 28 °C, 210nm

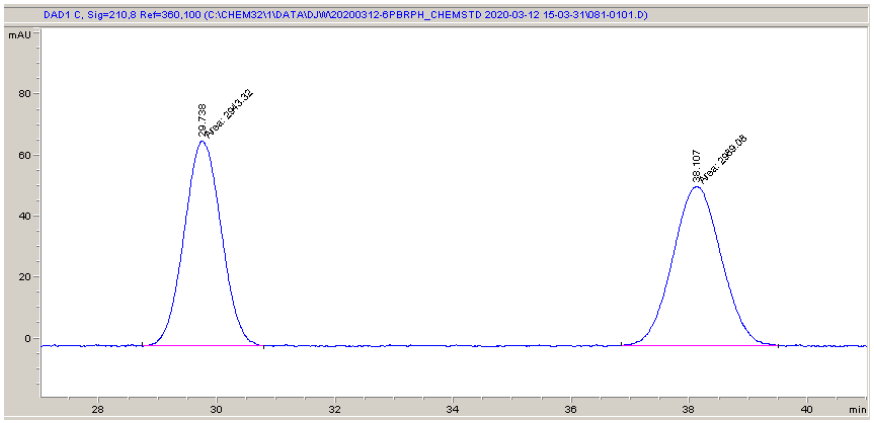

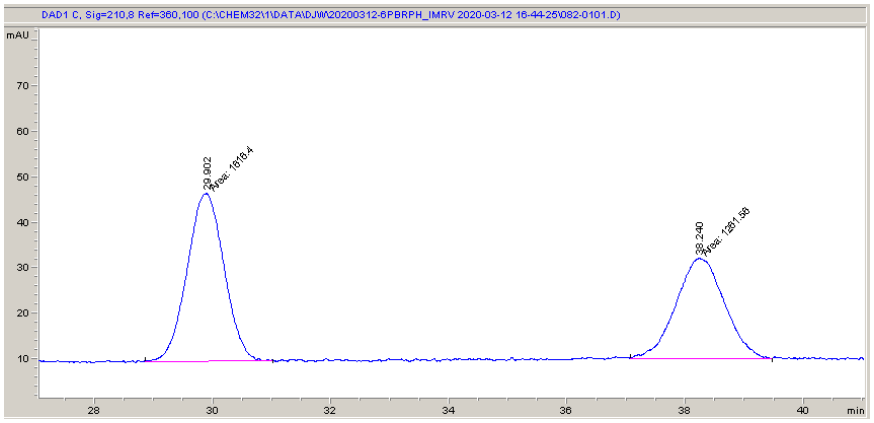

***rac* pdt**			**Enzymatically produced pdt**		
Retention Time (min)	Area (mAU*s)	Area %	Retention Time (min)	Area (mAU*s)	Area %
29.738	2943.32	49.61	29.902	1616.40	56.16
38.107	2989.08	50.39	38.240	1261.56	43.84
Total	5932.40	100.00	Total	2877.96	100.00

4-(*p*-Tol)tetrahydro-2*H*-pyran-2-one

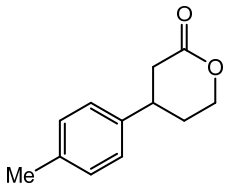

	condition 1	condition 2
C10-IIMRV	~4500 TTN, 65% yield (10 mM, 8 h)	~4500 TTN, 65% yield (2.5 mM, 10 h)

Chiralpak IC, 25% isopropanol in hexane, 1.2 ml/min, 28 °C, 210nm

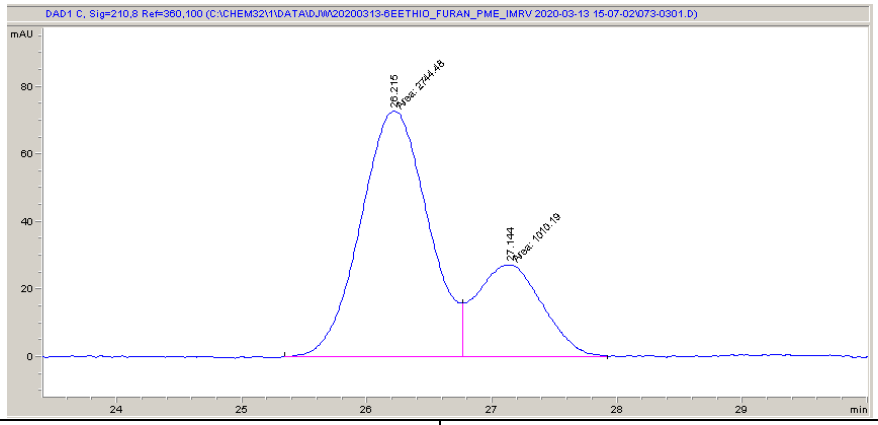

***rac* pdt**			**Enzymatically produced pdt**		
Retention Time (min)	Area (mAU*s)	Area %	Retention Time (min)	Area (mAU*s)	Area %
-	-	-	26.215	2744.48	73.10
-	-	-	27.144	1010.19	26.90
Total	-	-	Total	3754.67	100.00

4-(Thiophen-2-yl)tetrahydro-2*H*-pyran-2-one

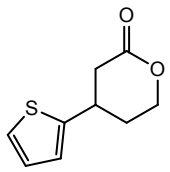

	condition 1	condition 2
C10-IIMRV	~5000 TTN, 70% yield (10 mM, 4 h)	~5500 TTN, 75% yield (2.5 mM, 6 h)

Chiralpak IC, 25% isopropanol in hexane, 1.2 ml/min, 28 °C, 210nm

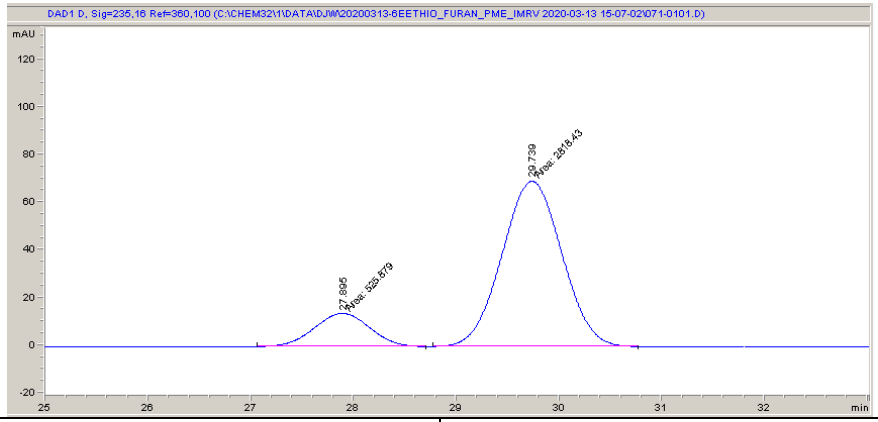

***rac* pdt**	**Enzymatically produced pdt**

Retention Time (min)	Area (mAU*s)	Area %	Retention Time (min)	Area (mAU*s)	Area %
-	-	-	27.895	525.88	15.72
-	-	-	29.739	2818.43	84.38
Total	-	-	Total	3344.31	100.00

4-(Furan-2-yl)tetrahydro-2*H*-pyran-2-one

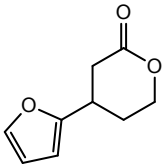

	condition 1	**condition 2**
C10-IIMRV	~4000 TTN, 50% yield (10 mM, 5 h)	~5500 TTN, 75% yield (2.5 mM, 5 h)

Chiralpak IC, 25% isopropanol in hexane, 1.2 ml/min, 28 °C, 210nm

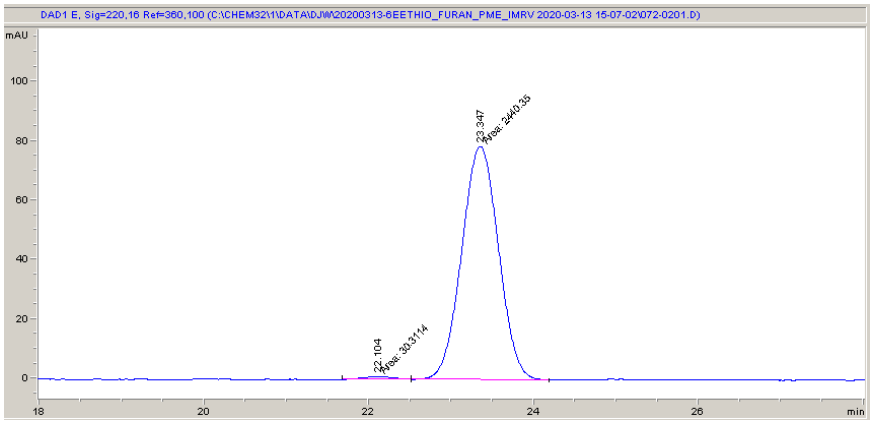

***rac* pdt**			**Enzymatically produced pdt**		
Retention Time (min)	Area (mAU*s)	Area %	Retention Time (min)	Area (mAU*s)	Area %
-	-	-	22.104	30.31	1.23
-	-	-	23.347	2440.35	98.77
Total	-	-	Total	2470.66	100.00

References:

[1] Hönig, M.; Sondermann, P.; Carreira, E. M.; Turner, N. Enantioselective chemo- and biocatalysis: Partners in retrosynthesis. *Angew. Chem. Int. Ed.* **2017**, *56*, 8942–8973.

[2] de Souza, R. O. M. A.; Miranda, L. S. M.; Bornscheuer, U. T. A retrosynthetic approach for biocatalysis in organic synthesis. *Chem. Eur. J.* **2017**, *23*, 12040–12063.

[3] Turner, N. J.; Humphrey, L. *Biocatalysis in organic synthesis: The retrosynthesis approach.* (Royal Society of Chemistry, 2018).

[4] Huang, P.-S.; Boyken, S. E.; Baker, D. The coming of age of *de novo* protein design. *Nature* **2016**, *537*, 320–327.

[5] Zanghellini, A. *de novo* computational enzyme design. *Curr. Opin. Chem. Biol.* **2014**, *29*, 132–138.

[6] Khersonsky, O.; Tawfik, D. S. Enzyme promiscuity: A mechanistic and evolutionary perspective. *Annu. Rev. Biochem.* **2010**, *79*, 471–505.

[7] Tawfik, D. S. Messy biology and the origins of evolutionary innovations. *Nat. Chem. Bio.* **2010**, *6*, 692–696.

[8] Busto, E.; Gotor-Fernández, V.; Gotor, V. Hydrolases: Catalytically promiscuous enzymes for non-conventional reactions in organic synthesis. *Chem. Soc. Rev.* **2010**, *39*, 4504–4523.

[9] Campos, K. R.; Coleman, P. J.; Alvarez, J. C.; Dreher, S. D.; Garbaccio, R. M.; Terrett, N. K.; Tillyer, R. D.; Truppo, M. D.; Parmee, E.R. The importance of synthetic chemistry in the pharmaceutical industry. *Science* **2019**, *363*, eaat0805.

[10] Bornscheuer, U. T.; Kazlauskas, R. J. Catalytic promiscuity in biocatalysis: Using old enzymes to form new bonds and follow new pathways. *Angew. Chem. Int. Ed.* **2004**, *43*, 6032–6040.

[11] Branneby, C.; Carlqvist, P.; Magnusson, A.; Hult, K.; Brinck, T.; Berglund, P. Carbon–carbon bonds by hydrolytic enzymes. *J. Am. Chem. Soc.* **2003**, *125*, 874–875.

[12] Mayer, C.; Zechel, D. L.; Reid, S. P.; Warren, R. A.; Withers, S. G. The E358S mutant of *Agrobacterium* sp. β-glucosidase is greatly improved glycosynthase. *FEBS Lett.* **2000**, *466*, 40–44.

[13] Jahn, M.; Marles, J.; Warren, R. A.; Withers, S. G. Thioglycoligases: Mutant glycosidases for thioglycoside synthesis. *Angew. Chem. Int. Ed.* **2003**, *42*, 352–354.

[14] Schallmey, A.; Schallmey, M. Recent advances on halohydrin dehalogenases—from enzyme identification to novel biocatalytic applications. *Appl. Microbiol. Biotechnol.* **2016**, *100*, 7827–7839.

[15] Fox, R. J.; Davis, S. C.; Mundorff, E. C.; Newman, L. M.; Gavrilovic, V.; Ma, S. K.; Chung, L. M.; Ching, C.; Tam, S.; Muley, S.; Grate, J.; Gruber, J.; Whitman, J. C.; Sheldon, R. A.; Huisman, G. W. Improving catalytic function by ProSAR-driven enzyme evolution. *Nat. Biotechnol.* **2007**, *25*, 338–344.

[16] Syrén, P.-O.; Henche, S.; Eichler, A.; Nestl, B. M.; Hauer, B. Squalene-hopene cyclases—evolution, dynamics and catalytic scope. *Curr. Opin. Chem. Biol.* **2016**, *41*, 73–82.

[17] Seitz, M.; Syrén, P. O.; Steiner, L.; Klebensberger, J.; Nestl, B. M.; Hauer, B. Synthesis of heterocyclic terpenoids by promiscuous squalene–hopene cyclases. *ChemBioChem* **2013**, *14*, 436–439.

[18] Hammer, S. C.; Marjanovic. A.; Dominicus, J. M.; Nestl, B. M.; Hauer, B. Squalene hopene cyclases are protonases for stereoselective Brønsted acid catalysis. *Nat. Chem. Bio.* **2015**, *11*, 121–126.

[19] Mangas-Sanchez, J.; France, S. P.; Montgomery, S. L.; Aleku, G. A.; Man, H.; Sharma, M.; Ramsden, J. I.; Grogan, G.; Turner, N. J. Imine reductases (IREDs). *Curr. Opin. Chem. Biol.* **2017**, *37*, 19–25.

[20] Sharma, M., Mangas-Sanchez, J.; France, S. P.; Aleku, G. A.; Montgomery, S. L.; Ramsden, J. I.; Turner, N. J.; Grogan, G. A mechanism for reductive amination catalyzed by fungal reductive aminases. *ACS Catal.* **2018**, *8*, 11534–11541.

[21] Aleku, G. A.; France, S. P.; Man, H.; Mangas-Sanchez, J.; Montgomery, S. L.; Sharma, M.; Leipold, F.; Hussain, S.; Grogan, G.; Turner, N. J. A reductive aminase from *Aspergillus oryzae*. *Nat. Chem.* **2017**, *9*, 961–969.

[22] Emmanuel, M. A.; Greenberg, N. R.; Oblinsky, D. G.; Hyster, T. K. Accessing non-natural reactivity by irradiating nicotinamide-dependent enzymes with light. *Nature* **2016**, *540*, 414–417.

[23] Biegasiewicz, K. F.; Cooper, S. J.; Emmanuel, M. A.; Miller, D. C.; Hyster, T. K. Catalytic promiscuity enabled by photoredox catalysis in nicotinamide-dependent oxidoreductases. *Nat. Chem.* **2018**, *10*, 770–775.

[24] Dockrey, S. A. B.; Narayan, A. R. H. Flavin-dependent biocatalysts in synthesis. *Tetrahedron* **2019**, *75*, 1115–1121.

[25] Sandoval, B. A.; Meichan, A. J.; Hyster, T. K. Enantioselective hydrogen atom transfer: Discovery of catalytic promiscuity in flavin-dependent 'ene'-reductases. *J. Am. Chem. Soc.* **2017**, *139*, 11313–11316.

[26] Sandoval, B. A.; Kurtoic, S. I.; Chung, M. M.; Biegasiewicz, K. F.; Hyster, T. K. Photoenzymatic catalysis enables radical-mediated ketone reduction in ene-reductases. *Angew. Chem. Int. Ed.* **2019**, *58*, 8714–8718.

[27] Biegasiewicz, K. F.; Cooper, S. J.; Gao, X.; Oblinsky, D. G.; Kim, J. H.; Garfinkle, S. E.; Joyce, L. A.; Sandoval, B. A.; Scholes, G. D.; Hyster, T. K. Photoexcitation of flavoenzymes enables a stereoselective radical cyclization. *Science* **2019**, *364*, 1166–1169.

[28] Sorigué, D.; Légeret, B.; Cuiné, S.; Blangy, S.; Moulin, S.; Billon, E.; Richaud, P.; Brugière, S.; Couté, Y.; Nurizzo, D.; Müller, P.; Brettel, K.; Pignol, D.; Arnoux, P.; Li-Beisson, Y.; Peltier, G.; Beisson F. An algal photoenzyme converts fatty acids to hydrocarbons. *Science* **2017**, *357*, 903–907.

[29] Zhang, W.; Ma, M.; Huijbers, M. M. E.; Filonenko, G. A.; Pidko, E. A.; van Schie, M.; de Boer, S.; Burek, B. O.; Bloh, J. Z.; van Berkel, W. J. H.; Smith, W. A. Hollmann F. Hydrocarbon synthesis via photoenzymatic decarboxylation of carboxylic acids. *J. Am. Chem. Soc.* **2019**, *141*, 3116–3120.

[30] Meyer, D.; Neumann, P.; Ficner, R.; Tittmann, K. Observation of a stable carbene at the active site of a thiamin enzyme. *Nat. Chem. Bio.* **2013**, *9*, 488–490.

[31] Breslow, R. On the mechanism of thiamine action. IV.[1] Evidence from studies on model systems. *J. Am. Chem. Soc.* **1958**, *80*, 3719–3726.

[32] Loschonsky, S.; Waltzer, S.; Fraas, S.; Wacker, T.; Andrade, S. L.; Kroneck, P. M.; Müller, M. Catalytic scope of the thiamine-dependent multifunctional enzyme cyclohexane-1,2-dione hydrolase. *ChemBioChem* **2014**, *15*, 389–392.

[33] Loschonsky, S.; Wacker, T.; Waltzer, S.; Giovannini, P. P.; McLeish, M. J.; Andrade, S. L. A.; Müller, M. Extended reaction scope of thiamine diphosphate dependent cyclohexane-1,2-dione hydrolase: From C–C bond cleavage to C–C bond ligation. *Angew. Chem. Int. Ed.* **2014**, *53*, 14402–14406.

[34] Bernacchia, G.; Bortolini, O.; De Bastiani, M.; Lerin, L. A.; Loschonsky, S.; Massi, A.; Müller, M.; Giovannini, P. P. Enzymatic chemoselective aldehyde–ketone cross-couplings through the polarity reversal of methylacetoin. *Angew. Chem. Int. Ed.* **2015**, *54*, 7171–7175.

[35] Demir, A. S.; Şeşenoglu, Ö.; Eren, E.; Hosrik, B.; Pohl, M.; Janzen, E.; Kolter, D.; Feldmann, R.; Dünkelmann, P.; Müller, M. Enantioselective synthesis of α-hydroxy ketones via benzaldehyde lyase-catalyzed C–C bond formation reaction. *Adv. Synth. Catal.* **2002**, *344*, 96–103.

[36] Dünkelmann, P.; Kolter-Jung, D.; Nitsche, A.; Demir, A. S.; Siegert, P.; Lingen, B.; Baumann, M.; Pohl, M.; Müller, M. Development of a donor-acceptor concept for enzymatic cross-coupling reactions of aldehydes: The first asymmetric cross-benzoin condensation. *J. Am. Chem. Soc.* **2002**, *124*, 12084–12085.

[37] Dresen, C.; Richter, M.; Pohl, M.; Lüdeke, S.; Müller, M. The enzymatic asymmetric conjugate umpolung reaction. *Angew. Chem. Int. Ed.* **2010**, *49*, 6600–6603.

[38] Tai, C.-H.; Cook, P. F. Pyridoxal 5'-phosphate-dependent α,β-elimination reactions: Mechanism of *O*-acetylserine sulfhydrylase. *Acc. Chem. Res.* **2001**, *34*, 49–59.

[39] Maier, T. H. P. Semisynthetic production of unnatural *L*-α-amino acids by metabolic engineering of the cysteine-biosynthetic pathway. *Nat. Biotechnol.* **2003**, *21*, 422–427.

[40] Phillips, R. S. Synthetic applications of tryptophan synthase. *Tetrahedron: Asymmetry* **2004**, *15*, 2787–2792.

[41] Buller, A. R.; Brinkmann-Chen, S.; Romney, D. K.; Herger, M.; Murciano-Calles, J.; Arnold, F. H. Directed

evolution of the tryptophan synthase β-subunit for stand-alone function recapitulates allosteric activation. *Proc. Natl. Acad. Sci. USA* **2015**, *112*, 14599–14604.

[42] Romney, D. K.; Murciano-Calles, J.; Wehrmüller, J. E.; Arnold, F. H. Unlocking reactivity of TrpB: A general biocatalytic platform for synthesis of tryptophan analogues. *J. Am. Chem. Soc.* **2017**, *139*, 10769–10776.

[43] Boville, C. E.; Scheele, R. A.; Koch, P.; Brinkmann-Chen, S.; Buller, A. R.; Arnold, F. H. Engineered biosynthesis of β-alkyl tryptophan analogs. *Angew. Chem. Int. Ed.* **2018**, *57*, 14764–14768.

[44] Herger, M.; van Roye, P.; Romney, D. K.; Brinkmann-Chen, S.; Buller, A. R.; Arnold, F. H. Synthesis of β-branched tryptophan analogues using an engineered subunit of tryptophan synthase. *J. Am. Chem. Soc.* **2016**, *138*, 8388–8391.

[45] Romney, D. K.; Sarai, N. S.; Arnold, F. H. Nitroalkanes as versatile nucleophiles for enzymatic synthesis of noncanonical amino acids. *ACS Catal.* **2019**, *9*, 8726–8730.

[46] Werner, E.R.; Blau, N.; Thöny, B. Tetrahydrobiopterin: Biochemistry and pathophysiology. *Biochem J.* **2011**, *438*, 397–414.

[47] Heberling, M. M.; Wu, B.; Bartsch, S.; Janssen, D. B. Priming ammonia lyases and aminomutases for industrial and therapeutic applications. *Curr. Opin. Chem. Biol.* **2013**, *17*, 250–260.

[48] Marshall, S. A.; Payne, K. A. P.; Leys, D. The UbiX-UbiD system: The biosynthesis and use of prenylated flavin (prFMN). *Arch. Biochem. Biophys.* **2017**, *632*, 209–221.

[49] Vaillancourt, F. H.; Yin, J.; Walsh, C. T. SyrB2 in syringomycin E biosynthesis is a nonheme Fe^{II} α-ketoglutarate- and O_2-dependent halogenase. *Proc. Natl. Acad. Sci. USA* **2005**, *102*, 10111–10116.

[50] Wong, S. D.; Srnec, M.; Matthews, M. L.; Liu, L. V.; Kwak, Y.; Park, K.; Bell, C. B. 3^{rd}; Alp, E. E.; Zhao, J.; Yoda, Y.; Kitao, S.; Seto, M.; Krebs, C.; Bollinger, J. M. Jr; Solomon, E. I. Elucidation of the iron(IV)–oxo intermediate in the non-haem iron halogenase SyrB2. *Nature* **2013**, *499*, 320–323.

[51] Matthews, M. L.; Chang, W. C.; Layne, A. P.; Miles, L. A.; Krebs, C.; Bollinger, J. M. Jr. Direct nitration and azidation of aliphatic carbons by an iron-dependent halogenase. *Nat. Chem. Bio.* **2014**, *10*, 209–215.

[52] Neugebauer, M. E.; Sumida, K. H.; Pelton, J. G.; McMurry, J. L.; Marchand, J. A.; Chang, M. C. Y. A family of radical halogenases for the engineering of amino-acid-based products. *Nat. Chem. Bio.* **2019**, *15*, 1009–1016.

[53] de Visser, S. P.; Kumar, D.; Shaik, S. How do aldehyde side products occur during alkene epoxidation by cytochrome P450? Theory reveals a state-specific multi-state scenario where the high-spin component leads to all side products. *J. Inorg. Biochem.* **2004**, *98*, 1183–1193.

[54] Hammer, S. C.; Kubik, G.; Watkins, E.; Huang, S.; Minges, H.; Arnold, F. H. *Anti*-Markovnikov alkene oxidation by metal-oxo–mediated enzyme catalysis. *Science* **2017**, *358*, 215–218.

[55] Prier, C. K.; Arnold, F. H. Chemomimetic biocatalysis: Exploiting the synthetic potential of cofactor-dependent enzymes to create new catalysts. *J. Am. Chem. Soc.* **2015**, *137*, 13992–14006.

[56] Che, C.-M.; Huang, J.-S. Metalloporphyrin-based oxidation systems: From biomimetic reactions to application in organic synthesis. *Chem. Commun.* **2009**, 3996–4015.

[57] Lu, H.; Zhang, X. P. Catalytic C–H functionalization by metalloporphyrins: Recent developments and future directions. *Chem. Soc. Rev.* **2011**, *40*, 1899–1909.

[58] Che, C.-M.; Lo, V. K.-Y.; Zhou, C.-Y.; Huang, J.-S. Selective functionalisation of saturated C–H bonds with metalloporphyrin catalysts. *Chem. Soc. Rev.* **2011**, *40*, 1950–1975.

[59] Maxwell, J. L.; Brown, K. C.; Bartley, D. W.; Kodadek, T. Mechanism of the rhodium porphyrin-catalyzed cyclopropanation of alkenes. *Science* **1992**, *256*, 1544–1547.

[60] Wolf, J. R.; Hamaker, C. G.; Djukic, J.-P.; Kodadek, T.; Woo, L. K. Shape and stereoselective cyclopropanation of alkenes catalyzed by iron porphyrins. *J. Am. Chem. Soc.* **1995**, *117*, 9194–9199.

[61] Coelho, P. S.; Brustad, E. M.; Kannan, A.; Arnold, F. H. Olefin cyclopropanation via carbene transfer catalyzed by engineered cytochrome P450 enzymes. *Science* **2013**, *339*, 307–310.

[62] Coelho, P. S.; Wang, Z. J.; Ener, M. E.; Baril, S. A.; Kannan, A.; Arnold, F. H.; Brustad, E. M. A serine-substituted P450 catalyzes highly efficient carbene transfer to olefins *in vivo*. *Nat. Chem. Biol.* **2013**, *9*, 485–487.

[63] Brandenberg, O. F.; Prier, C. K.; Chen, K.; Knight, A. M.; Wu, Z.; Arnold, F. H. Stereoselective enzymatic synthesis of heteroatom-substituted cyclopropanes. *ACS Catal.* **2018**, *8*, 2629–2634.

[64] Wang, Z. J.; Renata, H.; Peck, N. E.; Farwell, C. C.; Coelho, P. S.; Arnold, F. H. Improved cyclopropanation activity of histidine-ligated cytochrome P450 enables the enantioselective formal synthesis of levomilnacipran. *Angew. Chem. Int. Ed.* **2014**, *53*, 6810–6813.

[65] Knight, A. M.; Kan, S. B. J.; Lewis, R. D.; Brandenberg, O. F.; Chen, K.; Arnold, F. H. Diverse engineered heme proteins enable stereodivergent cyclopropanation of unactivated alkenes. *ACS Cent. Sci.* **2018**, *4*, 372–377.

[66] Bordeaux, M.; Tyagi, V.; Fasan, R. Highly diastereoselective and enantioselective olefin cyclopropanation using engineered myoglobin-based catalysts. *Angew. Chem. Int. Ed.* **2015**, *54*, 1744–1748.

[67] Farwell, C. C.; Zhang, R. K.; McIntosh, J. A.; Hyster, T. K.; Arnold, F. H. Enantioselective enzyme-catalyzed aziridination enabled by active-site evolution of a cytochrome P450. *ACS Cent. Sci.* **2015**, *1*, 89–93.

[68] Tsutsumi, H.; Katsuyama, Y.; Izumikawa, M.; Takagi, M.; Fujie, M.; Satoh, N.; Shin-Ya, K.; Ohnishi, Y. Unprecedented cyclization catalyzed by a cytochrome P450 in benzastatin biosynthesis. *J. Am. Chem. Soc.* **2018**, *140*, 6631–6639.

[69] Cho, I.; Prier, C. K.; Jia, Z. J.; Zhang, R. K.; Görbe, T.; Arnold, F. H. Enantioselective aminohydroxylation of styrenyl olefins catalyzed by an engineered hemoprotein. *Angew. Chem. Int. Ed.* **2019**, *58*, 3138–3142.

[70] Svastits, E.; Dawson, J. H.; Breslow, R.; Gellman, S. H. Functionalized nitrogen atom transfer catalyzed by cytochrome P-450. *J. Am. Chem. Soc.* **1985**, *107*, 6427–6428.

[71] McIntosh, J. A.; Coelho, P. S.; Farwell, C. C.; Wang, Z. J.; Lewis, J. C.; Brown, T. R.; Arnold, F. H. Enantioselective intramolecular C–H amination catalyzed by engineered cytochrome P450 enzymes *in vitro* and *in vivo*. *Angew. Chem. Int. Ed.* **2013**, *52*, 9309–9312.

[72] Singh, R.; Bordeaux, M.; Fasan, R. P450-catalyzed intramolecular sp^3 C–H amination with arylsulfonyl azide substrates. *ACS Catal.* **2014**, *4*, 546–552.

[73] Bordeaux, M.; Singh, R.; Fasan, R. Intramolecular C(sp^3)–H amination of arylsulfonyl azides with engineered and artificial myoglobin-based catalysts. *Bioorg. Med. Chem.* **2014**, *22*, 5697–5704.

[74] Singh, R.; Kolev, J. N.; Sutera, P. A.; Fasan, R. Enzymatic C(sp^3)–H amination: P450-catalyzed conversion of carbonazidates into oxazolidinones. *ACS Catal.* **2015**, *5*, 1685–1691.

[75] Hyster, T. K.; Farwell, C. C.; Buller, A. R.; McIntosh, J. A.; Arnold, F. H. Enzyme-controlled nitrogen-atom transfer enables regiodivergent C–H amination. *J. Am. Chem. Soc.* **2014**, *136*, 15505–15508.

[76] Prier, C. K.; Zhang, R. K.; Buller, A. R.; Brinkmann-Chen, S.; Arnold, F. H. Enantioselective, intermolecular benzylic C–H amination catalysed by an engineered iron-haem enzyme. *Nat. Chem.* **2017**, *9*, 629–634.

[77] Zhang, R. K.; Chen, K.; Huang, X.; Wohlschlager, L.; Renata, H.; Arnold, F. H. Enzymatic assembly of carbon–carbon bonds via iron-catalysed sp^3 C–H functionalization. *Nature* **2019**, *565*, 67–72.

[78] Zhang, J.; Huang, X.; Zhang, R. K.; Arnold, F. H. Enantiodivergent α-amino C–H fluoroalkylation catalyzed by engineered cytochrome P450s. *J. Am. Chem. Soc.* **2019**, *141*, 9798–9802.

[79] Farwell, C. C.; McIntosh, J. A.; Hyster, T. K.; Wang, Z. J.; Arnold, F. H. Enantioselective imidation of sulfides via enzyme-catalyzed intermolecular nitrogen-atom transfer. *J. Am. Chem. Soc.* **2014**, *136*, 8766–8771.

[80] Prier, C. K.; Hyster, T. K.; Farwell, C. C.; Huang, A.; Arnold, F. H. Asymmetric enzymatic synthesis of allylic amines: A sigmatropic rearrangement strategy. *Angew. Chem. Int. Ed.* **2016**, *55*, 4711–4715.

[81] Tyagi, V.; Sreenilayam, G.; Bajaj, P.; Tinoco, A.; Fasan, R. Biocatalytic synthesis of allylic and allenyl sulfides through a myoglobin-catalyzed Doyle–Kirmse reaction. *Angew. Chem. Int. Ed.* **2016**, *55*, 13562–13566.

[82] Wang, Z. J.; Peck, N. E.; Renata, H.; Arnold, F. H. Cytochrome P450-catalyzed insertion of carbenoids into N–H

bonds. *Chem. Sci.* **2014**, *5*, 598–601.

[83] Sreenilayam, G.; Fasan, R. Myoglobin-catalyzed intermolecular carbene N–H insertion with arylamine substrates. *Chem. Commun.* **2015**, *51*, 1532–1534.

[84] Tyagi, V.; Bonn R. B.; Fasan, R. Intermolecular carbene S–H insertion catalysed by engineered myoglobin-based catalysts. *Chem. Sci.* **2015**, *6*, 2488–2494.

[85] Kan, S. B. J.; Lewis, R. D.; Chen, K.; Arnold, F. H. Directed evolution of cytochrome *c* for carbon–silicon bond formation: Bringing silicon to life. *Science* **2016**, *354*, 1048–1051.

[86] Kan, S. B. J.; Huang, X.; Gumulya, Y.; Chen, K.; Arnold, F. H. Genetically programmed chiral organoborane synthesis. *Nature* **2017**, *552*, 132–136.

[87] Huang, X.; Garcia-Borràs, M.; Miao, K.; Kan, S. B. J.; Zutshi, A.; Houk, K. N.; Arnold, F. H. A biocatalytic platform for synthesis of chiral α-trifluoromethylated organoborons. *ACS Cent. Sci.* **2019**, *5*, 270–276.

[88] Lewis, R. D.; Garcia-Borràs, M.; Chalkley, M. J.; Buller, A. R.; Houk, K. N.; Kan, S. B. J.; Arnold, F. H. Catalytic iron-carbene intermediate revealed in a cytochrome *c* carbene transferase. *Proc. Natl. Acad. Sci. USA* **2018**, *115*, 7308–7313.

[89] Hayashi, T.; Tinzl, M.; Mori, T.; Krengel, U.; Proppe, J.; Soetbeer, J.; Klose, D.; Jeschke, G.; Reiher, M.; Hilvert, D. Capture and characterization of a reactive haem–carbenoid complex in an artificial metalloenzyme. *Nat. Catal.* **2018**, *1*, 578–584.

[90] Wilson, M. E.; Whitesides, G. M. Conversion of a protein to a homogeneous asymmetric hydrogenation catalyst by site-specific modification with a diphosphinerhodium(I) moiety. *J. Am. Chem. Soc.* **1978**, *100*, 306–307.

[91] Schwizer, F.; Okamoto, Y.; Heinisch, T.; Gu, Y.; Pellizzoni, M. M.; Lebrun, V.; Reuter, R.; Köhler, V.; Lewis, J. C.; Ward, T. R. Artificial metalloenzymes: Reaction scope and optimization strategies. *Chem. Rev.* **2018**, *118*, 142–231.

[92] Chatterjee, A.; Mallin, H.; Klehr, J.; Vallapurackal, J.; Finke, A. D.; Vera, L.; Marsh, M.; Ward, T. R. An enantioselective artificial Suzukiase based on the biotin–streptavidin technology. *Chem. Sci.* **2016**, *7*, 673–677.

[93] Pierron, J.; Malan, C.; Creus, M.; Gradinaru, J.; Hafner, I.; Ivanova, A.; Sardo, A.; Ward, T. R. Artificial metalloenzymes for asymmetric allylic alkylation on the basis of the biotin–avidin technology. *Angew. Chem. Int. Ed.* **2008**, *47*, 701–705.

[94] Hyster, T. K.; Knörr, L.; Ward, T. R.; Rovis, T. Biotinylated Rh(III) complexes in engineered streptavidin for accelerated asymmetric C–H activation. *Science* **2012**, *338*, 500–503.

[95] Lo, C.; Ringenberg, M. R.; Gnandt, D.; Wilsona, Y.; Ward, T. R. Artificial metalloenzymes for olefin metathesis based on the biotin-(strept)avidin technology. *Chem. Commun.* **2011**, *47*, 12065–12067.

[96] Jeschek, M.; Reuter, R.; Heinisch, T.; Trindler, C.; Klehr, J.; Panke, S.; Ward, T. R. Directed evolution of artificial metalloenzymes for *in vivo* metathesis. *Nature* **2016**, *537*, 661–665.

[97] Hassan, I. S.; Ta, A. N.; Danneman, M. W.; Semakul, N.; Burns, M.; Basch, C. H.; Dippon, V. N.; McNaughton, B. R.; Rovis, T. Asymmetric δ-lactam synthesis with a monomeric streptavidin artificial metalloenzyme. *J. Am. Chem. Soc.* **2019**, *141*, 4815–4819.

[98] Dürrenberger, M.; Heinisch, T.; Wilson, Y. M.; Rossel, T.; Nogueira, E.; Knörr, L.; Mutschler, A.; Kersten, K.; Zimbron, M. J.; Pierron, J.; Schirmer, T.; Ward, T. R. Artificial transfer hydrogenases for the enantioselective reduction of cyclic imines. *Angew. Chem. Int. Ed.* **2011**, *50*, 3026–3029.

[99] Wu, S.; Zhou, Y.; Rebelein, J. G.; Kuhn, M.; Mallin, H.; Zhao, J.; Igareta, N. V.; Ward, T. R. Breaking symmetry: Engineering single-chain dimeric streptavidin as host for artificial metalloenzymes. *J. Am. Chem. Soc.* **2019**, *141*, 15869–15878.

[100] Raines, D. J.; Clarke, J. E.; Blagova, E. V.; Dodson, E. J.; Wilson, K. S.; Duhme-Klair, A.-K. Redox-switchable siderophore anchor enables reversible artificial metalloenzyme assembly. *Nat. Catal.* **2018**, *1*, 680–688.

[101] Eda, S.; Nasibullin, I.; Vong, K.; Kudo, N.; Yoshida, M.; Kurbangalieva A.; Tanaka, K. Biocompatibility and

therapeutic potential of glycosylated albumin artificial metalloenzymes. *Nat. Catal.* **2019**, *2*, 780–792.

[102] Mayer, C., Gillingham, D. G., Ward, T. R. & Hilvert, D. An artificial metalloenzyme for olefin metathesis. *Chem. Commun.* **2011**, *47*, 12068–12070.

[103] Jarvis, A. G.; Obrecht, L.; Deuss, P. J.; Laan, W.; Gibson, E. K.; Wells, P. P.; Kamer, P. C. J. Enzyme activity by design: An artificial rhodium hydroformylase for linear aldehydes. *Angew. Chem. Int. Ed.* **2017**, *56*, 13596–13600.

[104] Yang, H.; Srivastava, P.; Zhang, C.; Lewis, J. C. A general method for artificial metalloenzyme formation through strain-promoted azide–alkyne cycloaddition. *ChemBioChem* **2014**, *15*, 223–227.

[105] Srivastava, P.; Yang, H.; Ellis-Guardiola, K.; Lewis, J. C. Engineering a dirhodium artificial metalloenzyme for selective olefin cyclopropanation. *Nat. Commun.* **2015**, *6*, 7789.

[106] Yang, H.; Swartz, A. M.; Park, H. J.; Srivastava, P.; Ellis-Guardiola, K.; Upp, D. M.; Lee, G.; Belsare, K.; Gu, Y.; Zhang, C.; Moellering, R. E.; Lewis, J. C. Evolving artificial metalloenzymes via random mutagenesis. *Nat. Chem.* **2018**, *10*, 318–324.

[107] Abe, S.; Niemeyer, J.; Abe M.; Takezawa, Y.; Ueno, T.; Hikage, T.; Erker, G.; Watanabe, Y. Control of the coordination structure of organometallic palladium complexes in an apo-ferritin cage. *J. Am. Chem. Soc.* **2008**, *130*, 10512–10514.

[108] Jing, Q.; Kazlauskas, R. J. Regioselective hydroformylation of styrene using rhodium-substituted carbonic anhydrase. *ChemCatChem* **2010**, *2*, 953–957.

[109] Drienovská, I.; Rioz-Martínez, A.; Draksharapu, A.; Roelfes, G. Novel artificial metalloenzymes by in vivo incorporation of metal-binding unnatural amino acids. *Chem. Sci.* **2015**, *6*, 770–776.

[110] Drienovská, I.; Alonso-Cotchico, L.; Vidossich, P.; Lledós, A.; Maréchal, J.-D.; Roelfes, G. Design of an enantioselective artificial metallohydratase enzyme containing an unnatural metal-binding amino acid. *Chem. Sci.* **2017**, *8*, 7228–7235.

[111] Key, H. M.; Dydio, P.; Clark, D. S.; Hartwig, J. F. Abiological catalysis by artificial haem proteins containing noble metals in place of iron. *Nature* **2016**, *534*, 534–537.

[112] Dydio, P.; Key, H. M.; Nazarenko, A.; Rha, J. Y.; Seyedkazemi, V.; Clark, D. S.; Hartwig, J. F. An artificial metalloenzyme with the kinetics of native enzymes. *Science* **2016**, *354*, 102–106.

[113] Key, H. M.; Dydio, P.; Liu, Z.; Rha, J. Y.-E.; Nazarenko, A.; Seyedkazemi, V.; Clark, D. S.; Hartwig, J. F. Beyond iron: Iridium-containing P450 enzymes for selective cyclopropanations of structurally diverse alkenes. *ACS Cent. Sci.* **2017**, *3*, 302–308.

[114] Dydio, P.; Key, H. M.; Hayashi, H.; Clark, D. S.; Hartwig, J. F. Chemoselective, enzymatic C–H bond amination catalyzed by a cytochrome P450 containing an Ir(Me)-PIX cofactor. *J. Am. Chem. Soc.* **2017**, *139*, 1750–1753.

[115] Agostini, F.; Völler, J. S.; Koksch, B.; Acevedo-Rocha, C. G.; Kubyshkin, V.; Budisa, N. Biocatalysis with unnatural amino acids: Enzymology meets xenobiology. *Angew. Chem. Int. Ed.* **2017**, *56*, 9680–9703.

[116] Drienovská, I.; Mayer, C.; Dulson, C.; Roelfes, G. A designer enzyme for hydrazone and oxime formation featuring an unnatural catalytic aniline residue. *Nat. Chem.* **2018**, *10*, 946–952.

[117] Mayer, C.; Dulson, C.; Reddem, E.; Thunnissen, A. W. H.; Roelfes, G. Directed evolution of a designer enzyme featuring an unnatural catalytic amino acid. *Angew. Chem. Int. Ed.* **2019**, *58*, 2083–2087.

[118] Burke, A. J.; Lovelock, S. L.; Frese, A.; Crawshaw, R.; Ortmayer, M.; Dunstan, M.; Levy, C.; Green, A. P. Design and evolution of an enzyme with a non-canonical organocatalytic mechanism. *Nature* **2019**, *570*, 219–223.

[119] Bornscheuer, U. T.; Huisman, G. W.; Kazlauskas, R. J.; Lutz, S.; Moore, J. C.; Robins, K. Engineering the third wave of biocatalysis. *Nature* **2012**, *485*, 185–194.

[120] Hughes, G.; Lewis, J. C. Introduction: Biocatalysis in industry. *Chem. Rev.* **2018**, *118*, 1–3.

[121] Bornscheuer, U. T. The fourth wave of biocatalysis is approaching. *Phil. Trans. R. Soc. A* **2017**, *376*, 20170063.

[122] Bornscheuer, U. T. Biocatalysis: successfully crossing boundaries. *Angew. Chem. Int. Ed.* **2016**, *55*, 4372–4373.

[123] Wu. Z.; Kan, S. B. J.; Lewis, R. D.; Wittmann, B. J.; Arnold, F. H. Machine-learning-assisted directed protein evolution with combinatorial libraries. *Proc. Natl. Acad. Sci. USA* **2019**, *116*, 8852–8858.

[124] O'Hagan, D.; Deng, H. Enzymatic fluorination and biotechnological developments of the fluorinase. *Chem. Rev.* **2015**, *115*, 634–649.

[125] Jeon, B.; Wang, S.-A.; Ruszczycky, M. W.; Liu, H. Natural [4+2]-cyclases. *Chem. Rev.* **2017**, *117*, 5367–5388.

[126] Kelly, S. A.; Pohle, S.; Wharry, S.; Mix, S.; Allen, C. C. R.; Moody, T. S.; Gilmore, B. F. Application of ω-transaminases in the pharmaceutical industry. *Chem. Rev.* **2018**, *118*, 349−367.

[127] Wiberg, K. B. The concept of strain in organic chemistry. *Angew. Chem. Int. Ed. Engl.* **1986**, *25*, 312–322.

[128] Anslyn, E. V.; Dougherty, D. A. *Modern Physical Organic Chemistry*. (University Science, Sausalito, CA, 2006), Chapter 2: Strain and Stability.

[129] Walczak, M. A. A.; Krainz, T.; Wipf, P. Ring-strain-enabled reaction discovery: New heterocycles from bicyclo[1.1.0]butanes. *Acc. Chem. Res.* **2015**, *48*, 1149–1158.

[130] Marek, I.; Simaan, S.; Masarwa, A. Enantiomerically enriched cyclopropene derivatives: Versatile building blocks in asymmetric synthesis. *Angew. Chem. Int. Ed.* **2007**, *46*, 7364–7376.

[131] De Meijere, A.; Kozhushkov, S. I.; Schill, H. Three-membered-ring-based molecular architectures. *Chem. Rev.* **2006**, *106*, 4926–4996.

[132] Gianatassio, R.; Lopchuk, J. M.; Wang, J.; Pan, C.-M.; Malins, L. R.; Prieto, L.; Brandt, T. A.; Collins, M. R.; Gallego, G. M.; Sach, N. W.; Spangler, J. E.; Zhu, H.; Zhu, J.; Baran, P. S. Strain-release amination. *Science* **2016**, *351*, 241–246.

[133] Dilmaç, A. M.; Spuling, E.; de Meijere, A.; Bräse, S. Propellanes—From a chemical curiosity to "explosive" materials and natural products. *Angew. Chem. Int. Ed.* **2017**, *56*, 5684–5718.

[134] Longo, J. M.; Sanford, M. J.; Coates, G. W. Ring-opening copolymerization of epoxides and cyclic anhydrides with discrete metal complexes: Structure−property relationships. *Chem. Rev.* **2016**, *116*, 15167–15197.

[135] Swager, T. M.; Dougherty, D. A.; Grubbs, R. H. Strained rings as a source of unsaturation: Polybenzvalene, a new soluble polyacetylene precursor. *J. Am. Chem. Soc.* **1988**, *110*, 2973–2974.

[136] Chen, Z.; Mercer, J. A. M.; Zhu, X.; Romaniuk, J. A. H.; Pfattner, R.; Cegelski, L.; Martinez, T. J.; Burns, N. Z.; Xia, Y. Mechanochemical unzipping of insulating polyladderene to semiconducting polyacetylene. *Science* **2017**, *357*, 475–479.

[137] Mahler, W. Double addition of a carbene to an acetylene. *J. Am. Chem. Soc.* **1962**, *84*, 4600–4601.

[138] Doering, W. von E.; Coburn, J. F. 1,3-Dimethylbicyclo[1.1.0]butane. *Tetrahedron Lett.* **1965**, *6*, 991–995.

[139] Wipf, P.; Stephenson, C. R. J.; Okumura, K. Transition-metal-mediated cascade reactions: C,C-dicyclopropylmethylamines by way of double C,C-*σ*-bond insertion into bicyclobutanes. *J. Am. Chem. Soc.* **2003**, *125*, 14694–14695.

[140] Panish, R. P.; Chintala, S. R.; Boruta, D. T.; Fang, Y.; Taylor, M. T.; Fox, J. M. Enantioselective synthesis of cyclobutane via sequential Rh-catalyzed bicyclobutanation/Cu-catalyzed homoconjugate addition. *J. Am. Chem. Soc.* **2013**, *135*, 9283–9286.

[141] Qin, C.; Davies, H. M. L. Enantioselective synthesis of 2-arylbicyclo[1.1.0]butane carboxylates. *Org. Lett.* **2013**, *15*, 310–313.

[142] Lou, Y.; Horikawa, M.; Kloster, R. A.; Hawryluk, N. A.; Corey, E. J. A new chiral Rh(II) catalyst for enantioselective [2 + 1]-cycloaddition. Mechanistic implications and applications. *J. Am. Chem. Soc.* **2004**, *126*, 8916–8918.

[143] Briones, J. F.; Hansen, J.; Hardcastle, K. I.; Autschbach, J.; Davies, H. M. L. Highly enantioselective Rh_2(*S*-DOSP)$_4$-catalyzed cyclopropenation of alkynes with styryldiazoacetates. *J. Am. Chem. Soc.* **2010**, *132*, 17211–17215.

[144] Uehara, M.; Suematsu, H.; Yasutomi, Y.; Katsuki, T. Enantioenriched synthesis of cyclopropenes with a quaternary

stereocenter, versatile building blocks. *J. Am. Chem. Soc.* **2011**, *133*, 170–171.

[145] Cui, X.; Xu, X.; Lu, H.; Zhu, S.; Wojtas, L.; Zhang, X. P. Enantioselective cyclopropenation of alkynes with acceptor/acceptor-substituted diazo reagents via Co(II)-based metalloradical catalysis. *J. Am. Chem. Soc.* **2011**, *133*, 3304–3307.

[146] Benkovic, S. J.; Hammes-Schiffer, S. A perspective on enzyme catalysis. *Science* **2003**, *301*, 1196–1202.

[147] Wessjohann, L. A.; Brandt, W. Biosynthesis and metabolism of cyclopropane rings in natural compounds. *Chem. Rev.* **2003**, *103*, 1625–1647.

[148] Itoh, T.; Djerassi, C. Acid-catalyzed and photochemical isomerization of steroidal cyclopropenes. *J. Am. Chem. Soc.* **1983**, *105*, 4407–4416.

[149] Schneider, C.; Niisuke, K.; Boeglin, W. E.; Voehler, M.; Stec, D. F.; Porter, N. A.; Brash, A. R. Enzymatic synthesis of a bicyclobutane fatty acid by a hemoprotein−lipoxygenase fusion protein from the cyanobacterium *Anabaena* PCC 7120. *Proc. Natl. Acad. Sci. U.S.A.* **2007**, *104*, 18941–18945.

[150] Trudeau, D. L.; Tawfik, D. S. Protein engineers turned evolutionists—the quest for the optimal starting point. *Curr. Opin. Biotech.* **2019**, *60*, 46–52.

[151] Leveson-Gower, R. B.; Mayer, C.; Roelfes, G. The importance of catalytic promiscuity for enzyme design and evolution. *Nat. Rev. Chem.* **2019**, *3*, 687–705.

[152] Renata, H.; Wang, Z. J.; Arnold, F. H. Expanding the enzyme universe: Accessing non-natural reactions by mechanism-guided directed evolution. *Angew. Chem. Int. Ed.* **2015**, *54*, 3351–3367.

[153] Davies, H. M. L.; Romines, K. R. Direct synthesis of furans by 3 + 2 cycloadditions between rhodium(II) acetate stabilized carbenoids and acetylenes. *Tetrahedron* **1988**, *44*, 3343–3348.

[154] Cui, X.; Xu, X.; Wojtas, L.; Kim, M. M.; Zhang, X. P. Regioselective synthesis of multisubstituted furans via metalloradical cyclization of alkynes with α-diazocarbonyls: Construction of functionalized α-oligofurans. *J. Am. Chem. Soc.* **2012**, *134*, 19981–19984.

[155] Smith, D. A.; Reynolds, D. N.; Woo, L. K. Cyclopropanation catalyzed by osmium porphyrin complexes. *J. Am. Chem. Soc.* **1993**, *115*, 2511–2513.

[156] Hamaker, C. G.; Djukic, J.-P.; Smith, D. A.; Woo, L. K. Mechanism of cyclopropanation reactions mediated by (5,10,15,20-tetra-*p*-tolylporphyrinato)osmium(II) complexes. *Organometallics* **2001**, *20*, 5189–5199.

[157] Capdevila, J. H.; Wei, S.; Helvig, C.; Falck, J. R.; Belosludtsev, Y.; Truan, G.; Graham-Lorence, S. E.; Peterson, J. A. The highly stereoselective oxidation of polyunsaturated fatty acids by cytochrome P450BM-3. *J. Biol. Chem.* **1996**, *271*, 22663–22671.

[158] Delaye, P.-O.; Didier, D.; Marek, I. Diastereodivergent carbometalation/oxidation/selective ring opening: Formation of all-carbon quaternary stereogenic centers in acyclic systems. *Angew. Chem. Int. Ed.* **2013**, *52*, 5333–5337.

[159] Patterson, D. M.; Nazarova, L. A.; Xie, B.; Kamber, D. N.; Prescher, J. A. Functionalized cyclopropenes as bioorthogonal chemical reporters. *J. Am. Chem. Soc.* **2012**, *134*, 18638–18643.

[160] Elling, B. R.; Xia, Y. Living alternating ring-opening metathesis polymerization based on single monomer additions. *J. Am. Chem. Soc.* **2015**, *137*, 9922–9926.

[161] Protopopova, M. N.; Doyle, M. P.; Müller, P.; Ene, D. High enantioselectivity for intermolecular cyclopropenation of alkynes by diazo esters catalyzed by chiral dirhodium(II) carboxamides. *J. Am. Chem. Soc.* **1992**, *114*, 2755–2757.

[162] Doyle, M. P.; Protopopova, M.; Müller, P.; Ene, D.; Shapiro, E. A. Effective uses of dirhodium(II) tetrakis[methyl 2-oxopyrrolidine-5(*R* or *S*)-carboxylate] for highly enantioselective intermolecular cyclopropenation reactions. *J. Am. Chem. Soc.* **1994**, *116*, 8492–8498.

[163] Goto, T.; Takeda, K.; Shimada, N.; Nambu, H.; Anada, M.; Shiroo, M.; Ando, K.; Hashimoto, S. Highly enantioselective cyclopropenation reaction of 1-alkynes with α-alkyl-α-diazoesters catalyzed by dirhodium(II)

carboxylates. *Angew. Chem. Int. Ed.* **2011**, *50*, 6803–6808.

[164] Davies, H. M. L.; Lee, G. H. Dirhodium(II) tetra(*N*-(dodecylbenzenesulfonyl)prolinate) catalyzed enantioselective cyclopropenation of alkynes. *Org. Lett.* **2004**, *6*, 1233–1236.

[165] Lindsay, V. N. G.; Fiset, D.; Gritsch, P. J.; Azzi, S.; Charette, A. B. Stereoselective Rh_2(*S*-IBAZ)$_4$-catalyzed cyclopropanation of alkenes, alkynes, and allenes: Asymmetric synthesis of diacceptor cyclopropylphosphonates and alkylidenecyclopropanes. *J. Am. Chem. Soc.* **2013**, *135*, 1463–1470.

[166] Briones, J. F.; Davies, H. M. L. Gold(I)-catalyzed asymmetric cyclopropenation of internal alkynes. *J. Am. Chem. Soc.* **2012**, *134*, 11916–11919.

[167] Zhang, Z.-Q.; Zheng, M.-M.; Xue, X.-S.; Marek, I.; Zhang, F.-G.; Ma, J.-A. Catalytic enantioselective cyclopropenation of internal alkynes: Access to difluoromethylated three-membered carbocycles. *Angew. Chem. Int. Ed.* **2019**, *58*, 18191–18196.

[168] A similar rationalization in iron-porphyrin-catalyzed internal alkene cyclopropanation: Wolf, J. R.; Hamaker, C. G.; Djukic, J.-P.; Kodadek, T.; Woo, L. K. Shape and stereoselective cyclopropanation of alkenes catalyzed by iron porphyrins. *J. Am. Chem. Soc.* **1995**, *117*, 36, 9194–9199.

[169] Yang, Y.; Cho, I.; Qi, X.; Liu, P.; Arnold, F. H. An enzymatic platform for the asymmetric amination of primary, secondary and tertiary C(sp^3)–H bonds. *Nat. Chem.* **2019**, *11*, 987–993.

[170] Kille, S.; Acevedo-Rocha, C. G.; Parra, L. P.; Zhang, Z.-G.; Opperman, D. J.; Reetz, M. T.; Acevedo J. P. Reducing codon redundancy and screening effort of combinatorial protein libraries created by saturation mutagenesis. *ACS Synth. Biol.* **2013**, *2*, 83–92.

[171] Gibson, D. G.; Young, L.; Chuang, R.-Y.; Venter, J. C.; Hutchinson III, C. A.; Smith, H. O. Enzymatic assembly of DNA molecules up to several hundred kilobases. *Nat. Methods* **2009**, *6*, 343–345.

[172] Sambrook, J.; Frisch, E.; Maniatis, T. *Molecular Cloning: A Laboratory Manual* (Cold Spring Harbor Laboratory Press, New York, 1989).

[173] Berry, E. A.; Trumpower, B. L. Simultaneous determination of hemes *a*, *b*, and *c* from pyridine hemochrome spectra. *Anal. Biochem.* **1987**, *161*, 1–15.

[174] Narhi, L. O.; Fulco, A. J. Characterization of a catalytically self-sufficient 119,000-dalton cytochrome P-450 monooxygenase induced by barbiturates in *Bacillus megaterium*. *J. Biol. Chem.* **1986**, *261*, 7160–7169.

[175] Renata, H.; Lewis, R. D.; Sweredoski, M. J.; Moradian, A.; Hess, S.; Wang, Z. J.; Arnold, F. H. Identification of mechanism-based inactivation in P450-catalyzed cyclopropanation facilitates engineering of improved enzymes. *J. Am. Chem. Soc.* **2016**, *138*, 12527–12533.

[176] Marco, J. A.; Carda, M. Recent advances in the field of naturally occurring 5,6-dihydropyran-2-ones. In *Natural Lactones and Lactams* (Wiley, 2013).

[177] Albrecht, Ł.; Albrecht, A.; Janecki, T. α-Alkylidene-γ- and δ-lactones and lactams. In *Natural Lactones and Lactams* (Wiley, 2013).

[178] Shiina, I.; Nakata, K. Medium-sized lactones. In *Natural Lactones and Lactams* (Wiley, 2013).

[179] Piotrowski, D. W. Mineralocorticoid receptor antagonists for the treatment of hypertension and diabetic nephropathy. *J. Med. Chem.* **2012**, *55*, 7957–7966.

[180] Pommier, Y.; Schwartz, R. E.; Zwelling, L. A.; Kohn, K. W. Effects of DNA intercalating agents on topoisomerase II induced DNA strand cleavage in isolated mammalian cell nuclei. *Biochemistry* **1985**, *24*, 6406–6410.

[181] Giaccio, J.; Curtin, C. D.; Sefton, M. A.; Taylor, D. K. Relationship between menthiafolic acid and wine lactone in wine. *J. Agric. Food Chem.* **2015**, *63*, 8241–8246.

[182] Serra, S.; Fuganti, C.; Brenna, E. Biocatalytic preparation of natural flavours and fragrances. *Trends Biotechnol.* **2005**, *23*, 193–198.

[183] Collins, I. Saturated and unsaturated lactones. *J. Chem. Soc., Perkin Trans. I* **1999**, 1377–1395.

[184] Delgove, M. A. F.; Elford, M. T.; Bernaerts, K. V.; De Wildeman, S. M. A. Toward upscaled biocatalytic preparation of lactone building blocks for polymer applications. *Org. Process Res. Dev.* **2018**, *22*, 803–812.

[185] Seitz, M.; Reiser, O. Synthetic approaches towards structurally diverse γ-butyrolactone natural-product-like compounds. *Curr. Opin. Chem. Biol*. **2005**, *9*, 285–292.

[186] Hoffmann, H. M. R.; Rabe, J. Synthesis and biological activity of α-methylene-γ-butyrolactones. *Angew. Chem. Int. Ed. Engl.* **1985**, *24*, 94–110.

[187] Shaikenov, T. E.; Adekenov, S. M.; Williams, R. M.; Baker, F. L.; Prashad, N.; Madden, T. L.; Newman, R. Arglabin-DMA, a plant derived sesquiterpene inhibits farnesyltransferase. *Oncol. Rep.* **2001**, *8*, 173–179.

[188] Gil, S.; Parra, M.; Rodriguez, P.; Segura, J. Recent developments in γ-lactone synthesis. *Mini-Rev. Org. Chem.* **2009**, *6*, 345–358.

[189] Hollmann, F.; Kara, S.; Opperman, D. J.; Wang, Y. Biocatalytic synthesis of lactones and lactams. *Chem. Asian J.* **2018**, *13*, 3601–3610.

[190] Kara, S.; Spickermann, D.; Schrittwieser, J. H.; Weckbecker, A.; Leggewie, C.; Arends, I. W. C. E.; Hollmann, F. Access to lactone building blocks via horse liver alcohol dehydrogenase-catalyzed oxidative lactonization. *ACS Catal.* **2013**, *3*, 2436–2439.

[191] Morrill, C.; Jensen, C.; Just-Baringo, X.; Grogan, G.; Turner, N. J.; Procter, D. J. Biocatalytic conversion of cyclic ketones bearing α-quaternary stereocenters into lactones in an enantioselective radical approach to medium-sized carbocycles. *Angew. Chem. Int. Ed.* **2018**, *57*, 3692–3696.

[192] Gatfield I. L. (1997). Biotechnological production of flavour-active lactones. In: Berger R.G. et al. (eds) Biotechnology of Aroma Compounds. Advances in Biochemical Engineering/Biotechnology, vol 55. Springer, Berlin, Heidelberg.

[193] Marella, E. R.; Dahlin, J.; Dam, M. I.; Ter Horst, J.; Christensen, H. B.; Sudarsan, S.; Wang, G.; Holkenbrink, C.; Borodina, I. A single-host fermentation process for the production of flavor lactones from non-hydroxylated fatty acids. *Metab. Eng.* **2019**, DOI: 10.1016/j.ymben.2019.08.009.

[194] Manning, J.; Tavanti, M.; Porter, J. L.; Kress, N.; De Visser, S. P.; Turner, N. J.; Flitsch, S. L. Regio- and enantio-selective chemoenzymatic C–H lactonization of decanoic acid to (*S*)-δ-decalactone. *Angew. Chem. Int. Ed.* **2019**, *58*, 5668–5671.

[195] DeAngelis, A.; Dmitrenko, O.; Fox, J. M. Rh-catalyzed intermolecular reactions of cyclic α-diazocarbonyl compounds with selectivity over tertiary C–H bond migration. *J. Am. Chem. Soc.* **2012**, *134*, 11035–11043.

[196] Sattely, E. S.; Meek, S. J.; Malcolmson, S. J.; Schrock, R. R.; Hoveyda, A. H. Design and stereoselective preparation of a new class of chiral olefin metathesis catalysts and application to enantioselective synthesis of quebrachamine: Catalyst development inspired by natural product synthesis. *J. Am. Chem. Soc.* **2009**, *131*, 943–953.

[197] DeAngelis, A.; Panish, R.; Fox, J. M. Rh-catalyzed intermolecular reactions of α-alkyl-α-diazo carbonyl compounds with selectivity over β-hydride migration. *Acc. Chem. Res.* **2016**, *49*, 115–127.

[198] Quasdorf, K. W.; Overman, L. E. Catalytic enantioselective synthesis of quaternary carbon stereocentres. *Nature* **2014**, *516*, 181–191.

[199] Christoffers, J.; Baro, A. eds. *Quaternary Stereocenters—Challenges and Solutions for Organic Synthesis* (Wiley-VCH, 2005).

[200] Liu, Y.; Han, S.-J.; Liu, W.-B.; Stoltz, B. M. Catalytic enantioselective construction of quaternary stereocenters: Assembly of key building blocks for the synthesis of biologically active molecules. *Acc. Chem. Res.* **2015**, *48*, 740–751.

[201] Zhang, Y.-Z.; Zhu, S.-F.; Cai, Y.; Mao, H.-X.; Zhou, Q.-L. Copper-catalyzed enantioselective carbenoid insertion into S–H bonds. *Chem. Commun.* **2009**, 5362–5364.

[202] Brunner, H.; Wutz, K.; Doyle, M. P. Enantioselective S–H and C–H insertions with optically active Rh(II) and

Cu(II) catalysts. Asymmetric catalysis, LVIII. *Monatsh. Chem.* **1990**, *121*, 755–764.

[203] Galardon, E.; Roué, S.; Maux, P. L.; Simonneaux, G. Asymmetric cyclopropanation of alkenes and diazocarbonyl insertion into S–H bonds catalyzed by a chiral porphyrin Ru(II) complex. *Tetrahedron Lett.* **1998**, *39*, 2333–2334.

[204] Zhang, X.-M.; Ma, M.; Wang, J.-B. Catalytic asymmetric S–H insertion reaction of carbenoids. *Arkivoc* **2003**, *2003*, 84–91.

[205] Sharon, D. A.; Mallick, D.; Wang, B.; Shaik, S. Computation sheds insight into iron porphyrin carbenes' electronic structure, formation, and N–H insertion reactivity. *J. Am. Chem. Soc.* **2016**, *138*, 9597–9610.

[206] Rhodium-catalyzed carbene S–H insertion via sulfonium ylide formation: Xu, B.; Zhu, S.-F.; Zhang, Z.-C.; Yu, Z.-X.; Ma, Y.; Zhou, Q.-L. Highly enantioselective S–H bond insertion cooperatively catalyzed by dirhodium complexes and chiral spiro phosphoric acids. *Chem. Sci.* **2014**, *5*, 1442–1448.

[207] Moore, E. J.; Steck, V.; Bajaj, P.; Fasan, R. Chemoselective cyclopropanation over carbene Y–H insertion catalyzed by an engineered carbene transferase. *J. Org. Chem.* **2018**, *83*, 7480–7490.

[208] Hayashi T.; Tinzl M.; Mori T.; Krengel U.; Proppe J.; Soetbeer J.; Klose D.; Jeschke G.; Reiher M.; Hilvert D. Capture and characterization of a reactive haem–carbenoid complex in an artificial metalloenzymes. *Nat. Catal.* **2018**, *1*, 578–584.

[209] Khade, R. L.; Zhang, Y. Catalytic and biocatalytic iron porphyrin carbene formation: Effects of binding mode, carbene substituent, porphyrin substituent, and protein axial ligand. *J. Am. Chem. Soc.* **2015**, *137*, 7560–7563.

[210] Li, Y.; Huang, J.-S.; Zhou, Z.-Y.; Che, C.-M.; You, X.-Z. Remarkably stable iron porphyrins bearing nonheteroatom-stabilized carbene or (alkoxycarbonyl)carbenes: Isolation, X-ray crystal structures, and carbon atom transfer reactions with hydrocarbons. *J. Am. Chem. Soc.* **2002**, *124*, 13185–13193.

[211] Cho, K.-B.; Hirao, H.; Shaik, S.; Nam, W. To rebound or dissociate? This is the mechanistic question in C–H hydroxylation by heme and nonheme metal–oxo complexes. *Chem. Soc. Rev.* **2016**, *45*, 1197–1210.

[212] Liu, W.; Groves, J. T. Manganese Catalyzed C–H Halogenation. *Acc. Chem. Res.* **2015**, *48*, 1727–1735.

[213] Liu, W.; Cheng, M.-J.; Nielsen, R. J.; Goddard, W. A.; Groves, J. T. Probing the C–O bond-formation step in metalloporphyrin-catalyzed C–H oxygenation reactions. *ACS Catal.* **2017**, *7*, 4182–4188.

[214] Doyle, M. P.; Duffy, R.; Ratnikov, M.; Zhou, L. Catalytic carbene insertion into C–H bonds. *Chem. Rev.* **2009**, *110*, 704–724.

[215] Davies, H. M. L.; Beckwith, R. E. J. Catalytic enantioselective C–H activation by means of metal–carbenoid-induced C–H insertion. *Chem. Rev.* **2003**, *103*, 2861–2904.

[216] Davies, H. M. L.; Manning, J. R. Catalytic C–H functionalization by metal carbenoid and nitrenoid insertion. *Nature* **2008**, *451*, 417–424.

[217] Taber, D. F.; Petty, E. H.; Raman, K. Enantioselective ring construction: synthesis of (+)-α-cuparenone. *J. Am. Chem. Soc.* **1985**, *107*, 196–199.

[218] Doyle, M. P.; Oeveren, A. V.; Westrum, L. J.; Protopopova, M. N.; Clayton Jr, T. W. Asymmetric synthesis of lactones with high enantioselectivity by intramolecular carbon-hydrogen insertion reactions of alkyl diazoacetates catalyzed by chiral rhodium(II) carboxamides. *J. Am. Chem. Soc.* **1991**, *113*, 8982–8984.

[219] Doyle, M. P.; Kalinin, A. V.; Ene, D. G. Chiral catalyst controlled diastereoselection and regioselection in intramolecular carbon−hydrogen insertion reactions of diazoacetates. *J. Am. Chem. Soc.* **1996**, *118*, 8837–8846.

[220] Davies, H. M. L.; Hansen, T. Asymmetric intermolecular carbenoid C–H insertions catalyzed by rhodium(II) (*S*)-*N*-(*p*-dodecylphenyl)sulfonylprolinate. *J. Am. Chem. Soc.* **1997**, *119*, 9075–9076.

[221] Davies, H. M. L.; Hansen, T.; Churchill, M. R. Catalytic asymmetric C–H activation of alkanes and tetrahydrofuran. *J. Am. Chem. Soc.* **2000**, *122*, 3063–3070.

[222] Suematsu, H.; Katsuki, T. Iridium(III) catalyzed diastereo- and enantioselective C–H bond functionalization. *J. Am. Chem. Soc.* **2009**, *131*, 14218–14219.

[223] Weldy, N. M.; Schafer, A. G.; Owens, C. P.; Herting, C. J.; Varela-Alvarez, A.; Chen, S.; Niemeyer, Z.; Musaev, D. G.; Sigman, M. S.; Davies, H. M. L.; Blakey, S. B. Iridium(III)-bis(imidazolinyl)phenyl catalysts for enantioselective C–H functionalization with ethyl diazoacetate. *Chem. Sci.* **2016**, *7*, 3142–3146.

[224] Wang, J.-C.; Xu, Z.-J.; Guo, Z.; Deng, Q.-H.; Zhou, C.-Y.; Wan, X.-L.; Che, C.-M. Highly enantioselective intermolecular carbene insertion to C–H and Si–H bonds catalyzed by a chiral iridium(III) complex of a D_4-symmetric Halterman porphyrin ligand. *Chem. Commun.* **2012**, *48*, 4299–4301.

[225] Wang, H.-X.; Richard, Y.; Wan, Q.; Zhou, C.-Y.; Che, C.-M. Iridium(III)-catalyzed intermolecular C(sp^3)–H insertion reaction of quinoid carbene: A radical mechanism. *Angew. Chem. Int. Ed.* **2020**, *59*, 1845–1850.

[226] Wang, Y.; Wen, X.; Cui, X.; Zhang, X. P. Enantioselective radical cyclization for construction of 5-membered ring structures by metalloradical C–H alkylation. *J. Am. Chem. Soc.* **2018**, *140*, 4792–4796.

[227] Cui, X.; Xu, X.; Jin, L.-M.; Wojtas, L.; Zhang, X. P. Stereoselective radical C–H alkylation with acceptor/acceptor-substituted diazo reagents via Co(II)-based metalloradical catalysis. *Chem. Sci.* **2015**, *6*, 1219–1224.

[228] Díaz-Requejo, M. M.; Belderraín, T. R.; Nicasio, M. C.; Trofimenko, S.; Pérez, P. J. Intermolecular copper-catalyzed carbon–hydrogen bond activation via carbene insertion. *J. Am. Chem. Soc.* **2002**, *124*, 896–897.

[229] Fraile, J. M.; Garcia, J. I.; Mayoral, J. A.; Roldan, M. Simple and efficient heterogeneous copper catalysts for enantioselective C−H carbene insertion. *Org. Lett.* **2007**, *9*, 731–733.

[230] Griffin, J. R.; Wendell, C. I.; Garwin, J. A.; White, M. C. Catalytic C(sp^3)–H alkylation via an iron carbene intermediate. *J. Am. Chem. Soc.* **2017**, *139*, 13624–13627.

[231] Mbuvi, H. M.; Woo, L. K. Catalytic C–H insertions using iron(III) porphyrin complexes. *Organometallics* **2008**, *27*, 637–645.

[232] Caballero, A.; Despagnet-Ayoub, E.; Díaz-Requejo, M. M.; Díaz-Rodríguez, A.; González-Núñez, M. E.; Mello, R.; Muñoz, B. K.; Ojo, W.-S.; Asensio, G.; Etienne, M.; Pérez, P. J. Silver-catalyzed C–C bond formation between methane and ethyl diazoacetate in supercritical CO_2. *Science* **2011**, *332*, 835–838.

[233] Rivilla, I.; Gómez-Emeterio, B. P.; Fructos, M. R.; Díaz-Requejo M. M.; Pérez, P. J. Exclusive aromatic vs aliphatic C–H bond functionalization by carbene insertion with gold-based catalysts. *Organometallics* **2011**, *30*, 2855–2860.

[234] Gutiérrez-Bonet, Á.; Juliá-Hernández, F.; de Luis, B.; Martin, R. Pd-catalyzed C(sp^3)–H functionalization/carbenoid insertion: All-carbon quaternary centers via multiple C–C bond formation. *J. Am. Chem. Soc.* **2016**, *138*, 6384–6387.

[235] Reddy, A. R.; Zhou, C.-Y.; Guo, Z.; Wei, J.; Che, C.-M. Ruthenium–porphyrin-catalyzed diastereoselective intramolecular alkyl carbene insertion into C–H bonds of alkyl diazomethanes generated in situ from *N*-tosylhydrazones. *Angew. Chem. Int. Ed.* **2014**, *53*, 14175–14180.

[236] Davies, H. M. L.; Morton, D. Guiding principles for site selective and stereoselective intermolecular C–H functionalization by donor/acceptor rhodium carbenes. *Chem. Soc. Rev.* **2011**, *40*, 1857–1869.

[237] Davies, H. M. L.; Denton, J. R. Application of donor/acceptor-carbenoids to the synthesis of natural products. *Chem. Soc. Rev.* **2009**, *38*, 3061–3071.

[238] Liao, K. B.; Negretti, S.; Musaev, D. G.; Bacsa, J.; Davies, H. M. L. Site-selective and stereoselective functionalization of unactivated C–H bonds. *Nature* **2016**, *533*, 230–234.

[239] Liao, K. B.; Pickel, T. C.; Boyarskikh, V. B.; Bacsa, J. B.; Musaev, D. G. M.; Davies, H. M. L. Site-selective and stereoselective functionalization of non-activated tertiary C–H bonds. *Nature* **2017**, *551*, 609–613.

[240] Liao, K. B.; Yang, Y. F.; Li, Y. Z.; Sanders, J. N.; Houk, K. N.; Musaev, D. G.; Davies, H. M. L. Design of catalysts for site-selective and enantioselective functionalization of non-activated primary C–H bonds. *Nat. Chem.* **2018**, *10*, 1048–1055.

[241] Fu, J. T.; Ren, Z.; Bacsa, J.; Musaev, D. G.; Davies, H. M. L. Desymmetrization of cyclohexanes by site- and stereoselective C–H functionalization. *Nature* **2018**, *564*, 395–399.

[242] Liao, K. B.; Davies, H. M. L. Dirhodium tetracarboxylates as catalysts for selective intermolecular C–H functionalization. *Nat. Rev. Chem.* **2019**, *3*, 347–360.

[243] Woods, J. R.; Mo, H.; Bieberich, A. A.; Alavanja, T.; Colby, D. A. Amino-derivatives of the sesquiterpene lactone class of natural products as prodrugs. *Med. Chem. Comm.* **2013**, *4*, 27–33.

[244] Brandenberg, O. F.; Chen, K.; Arnold, F. H. Directed evolution of a cytochrome P450 carbene transferase for selective functionalization of cyclic compounds. *J. Am. Chem. Soc.* **2019**, *141*, 8989–8995.

[245] Butler, C. F.; Peet, C.; Mason, A. E.; Voice, M. W.; Leys, D.; Munro, A. W. Key mutations alter the cytochrome P450 BM3 conformational landscape and remove inherent substrate bias. *J. Biol. Chem.* **2013**, *288*, 25387–25399.

[246] Cirino, P. C.; Arnold, F. H. Regioselectivity and activity of cytochrome P450 BM-3 and mutant F87A in reactions driven by hydrogen peroxide. *Adv. Synth. Catal.* **2002**, *344*, 932–937.

[247] Joyce, M. G.; Girvan, H. M.; Munro, A. W.; Leys, D. A single mutation in cytochrome P450 BM3 induces the conformational rearrangement seen upon substrate binding in the wild-type enzyme. *J. Biol. Chem.* **2004**, *279*, 23287–23293.

[248] Chen, K.; Huang, X.; Kan, S. B. J.; Zhang, R. K.; Arnold, F. H. Enzymatic construction of highly strained carbocycles. *Science* **2018**, *360*, 71–75.

[249] Doyle, M. P.; Westrum, L. J.; Wolthuis, W. N. E.; See, M. M.; Boone, W. P.; Bagheri, V.; Pearson, M. M. Electronic and steric control in carbon–hydrogen insertion reactions of diazoacetoacetates catalyzed by dirhodium(II) carboxylates and carboxamides. *J. Am. Chem. Soc.* **1993**, *115*, 958–964.

[250] Ishii, S.; Zhao, S.; Helquist, P. Stereochemical probes of intramolecular C–H insertion reactions of iron-carbene complexes. *J. Am. Chem. Soc.* **2000**, *122*, 5897–5898.

[251] Hernán-Gómez, A.; Rodríguez, M.; Parella, T.; Costas, M. Electrophilic iron catalyst paired with a lithium cation enables selective functionalization of non-activated aliphatic C–H bonds via metallocarbene intermediates. *Angew. Chem. Int. Ed.* **2019**, *58*, 13904–13911.

[252] Our previous computational study on the mechanism of lactone-carbene S–H insertion revealed a radical pathway involving hydrogen atom abstraction followed by stereo-invertive radical rebound at the α-chiral center, see: Chen, K.; Zhang, S.-Q.; Brandenberg, O. F.; Hong, X.; Arnold, F. H. Alternate heme ligation steers activity and selectivity in engineered cytochrome P450-catalyzed carbene transfer reactions. *J. Am. Chem. Soc.* **2018**, *140*, 16402–16407.

[253] Doyle, M. P.; McKervey, M. A.; Ye, T. *Modern Catalytic Methods for Organic Synthesis with Diazo Compounds* (Wiley, 1998).

[254] Ford, A.; Miel, H.; Ring, A.; Slattery, C. N.; Maguire, A. R.; McKervey, M. A. Modern organic synthesis with α-diazocarbonyl compounds. *Chem. Rev.* **2015**, *115*, 9981–10080.

[255] Ratcliffe, R.; Salzmann, T.; Christensen, B. A practical synthesis of (±)-thienamycin. *Tetrahedron Lett.* **1980**, *21*, 2783–2786.

[256] Salzmann, T. N.; Ratcliffe, R. W.; Christensen, B. G.; Bouffard, F. A. A stereocontrolled synthesis of (+)-thienamycin. *J. Am. Chem. Soc.* **1980**, *102*, 6161–6163.

[257] Liu, B.; Zhu, S.-F.; Zhang, W.; Chen, C.; Zhou, Q.-L. Highly enantioselective insertion of carbenoids into N–H bonds catalyzed by copper complexes of chiral spiro bisoxazolines. *J. Am. Chem. Soc.* **2007**, *129*, 5834–5835.

[258] Hou, Z.; Wang, J.; He, P.; Wang, J.; Qin, B.; Liu, X.; Lin, L.; Feng, X. Highly enantioselective insertion of carbenoids into N–H bonds catalyzed by copper(I) complexes of binol derivatives. *Angew. Chem. Int. Ed.* **2010**, *49*, 4763–4766.

[259] Zhu, S.-F.; Xu, B.; Wang, G.-P.; Zhou, Q.-L. Well-defined binuclear chiral spiro copper catalysts for enantioselective N–H insertion. *J. Am. Chem. Soc.* **2012**, *134*, 436–442.

[260] Xu, X.; Zavalij, P. Y.; Doyle, M. P. Synthesis of tetrahydropyridazines by a metal-carbene-directed enantioselective vinylogous N–H insertion/Lewis acid-catalyzed diastereoselective Mannich addition. *Angew. Chem. Int. Ed.* **2012**, *51*,

9829–9833.

[261] Arredondo, V.; Hiew, S. C.; Gutman, E. S.; Premachandra, I. D. U. A.; Van Vranken, D. L. Enantioselective palladium-catalyzed carbene insertion into the N–H bonds of aromatic heterocycles. *Angew. Chem. Int. Ed.* **2017**, *56*, 4156–4159.

[262] Lee, E. C.; Fu, G. C. Copper-catalyzed asymmetric N–H insertion reactions: Couplings of diazo compounds with carbamates to generate α-amino acids. *J. Am. Chem. Soc.* **2007**, *129*, 12066–12067.

[263] Xu, B.; Zhu, S.-F.; Xie, X.-L.; Shen, J.-J.; Zhou, Q.-L. Asymmetric N–H insertion reaction cooperatively catalyzed by rhodium and chiral spiro phosphoric acids. *Angew. Chem. Int. Ed.* **2011**, *50*, 11483–11486.

[264] Yang, J.; Ruan, P.; Yang, W.; Feng, X.; Liu, X. Enantioselective carbene insertion into the N–H bond of benzophenone imine. *Chem. Sci.* **2019**, *10*, 10305–10309.

[265] Li, M.-L.; Yu, J.-H.; Li, Y.-H.; Zhu, S.-F.; Zhou, Q.-L. Highly enantioselective carbene insertion into N–H bonds of aliphatic amines. *Science* **2019**, *366*, 990–994.

[266] Steck, V.; Sreenilayam, G.; Fasan, R. Selective functionalization of aliphatic amines via myoglobin-catalyzed carbene N–H insertion. *Synlett* **2019**, *31*, 224–229.

[267] Teplitski, M.; Mathesius, U.; Rumbaugh, K. P. Perception and degradation of *N*-acyl homoserine lactone quorum sensing signals by mammalian and plant vells. *Chem. Rev.* **2011**, *111*, 100–116.

[268] You, Zhi-Hao; Chen, Ying-Han; Liu, Yan-Kai. From racemic precursors to fully stereocontrolled products: one-pot synthesis of chiral α-amino lactones and lactams. *Org. Biomol. Chem.* **2016**, *14*, 6316–6327.

[269] Stacy, D. M.; Welsh, M. A.; Rather, P. N.; Blackwell, H. E. Attenuation of quorum sensing in the pathogen acinetobacter baumannii using non-native *N*-acyl homoserine lactones. *ACS Chem. Biol.* **2012**, *7*, 1719–1728.

[270] Hall, D. G. *Boronic acids: Preparation and applications in organic synthesis and medicine* (Wiley-VCH, 2005).

[271] Das, B. C.; Thapa, P.; Karki, R.; Schinke, C.; Das, S.; Kambhampati, S.; Banerjee, S. K.; Veldhuizen, P. V.; Verma, A.; Weiss, L. M.; Evans, T. Boron chemicals in diagnosis and therapeutics. *Future Med. Chem.* **2013**, *5*, 653–676.

[272] Dembitsky, V. M.; Al Quntar, A. A.; Srebnik, M. Natural and synthetic small boron-containing molecules as potential inhibitors of bacterial and fungal quorum sensing. *Chem. Rev.* **2011**, *111*, 209–237.

[273] Brown, H. C.; Ramachandran, P. V. The boron approach to asymmetric synthesis. *Pure Appl. Chem.* **1991**, *63*, 307–316.

[274] Fyfe, J. W. B.; Watson, A. J. B. Recent developments in organoboron chemistry: Old dogs, new tricks. *Chem* **2017**, *3*, 31–55.

[275] Leonori, D.; Aggarwal, V. K. Lithiation–borylation methodology and its application in synthesis. *Acc. Chem. Res.* **2014**, *47*, 3174–3183.

[276] Lennox, A. J. J.; Lloyd-Jones, G. C. Selection of boron reagents for Suzuki–Miyaura coupling. *Chem. Soc. Rev.* **2014**, *43*, 412–443.

[277] Li, X.; Curran, D. P. Insertion of reactive rhodium carbenes into boron–hydrogen bonds of stable *N*-heterocyclic carbene boranes. *J. Am. Chem. Soc.* **2013**, *135*, 12076–12081.

[278] Cheng, Q.-Q.; Zhu, S.-F.; Zhang, Y.-Z.; Xie, X.-L.; Zhou, Q.-L. Copper-catalyzed B–H bond insertion reaction: a highly efficient and enantioselective C–B bond-forming reaction with amine–borane and phosphine–borane adducts. *J. Am. Chem. Soc.* **2013**, *135*, 14094–14097.

[279] Chen, D.; Zhang, X.; Qi, W.-Y.; Xu, B.; Xu, M.-H. Rhodium(I)-catalyzed asymmetric carbene insertion into B–H bonds: Highly enantioselective access to functionalized organoboranes. *J. Am. Chem. Soc.* **2015**, *137*, 5268–5271.

[280] Hyde, S.; Veliks, J.; Liégault, B.; Grassi, D.; Taillefer, M.; Gouverneur, V. Copper-catalyzed insertion into heteroatom–hydrogen bonds with trifluorodiazoalkanes. *Angew. Chem. Int. Ed.* **2016**, *55*, 3785–3789.

[281] Yang, J.-M.; Li, Z.-Q.; Li, M.-L.; He, Q.; Zhu, S.-F.; Zhou, Q.-L. Catalytic B–H bond insertion reactions using alkynes as carbene precursors. *J. Am. Chem. Soc.* **2017**, *139*, 3784−3789.

[282] Pang, Y.; He, Q.; Li, Z.-Q.; Yang, J.-M.; Yu, J.-H.; Zhu, S.-F.; Zhou, Q.-L. Rhodium-catalyzed B–H bond insertion reactions of unstabilized diazo compounds generated *in situ* from tosylhydrazones. *J. Am. Chem. Soc.* **2018**, *140*, 10663–10668.

[283] Allen, T. H.; Kawamoto, T.; Gardner, S.; Geib, S. J.; Curran, D. P. *N*-Heterocyclic carbene boryl iodides catalyze insertion reactions of *N*-heterocyclic carbene boranes and diazoesters. *Org. Lett.* **2017**, *19*, 3680–3683.

[284] Yang, J.-M.; Li, Z.-Q.; Zhu, S.-F. Progresses on the application of stable borane adducts in the synthesis of organoborons. *Chin. J. Org. Chem.* **2017**, *37*, 2481–2497.

[285] Tehfe, M.-A.; Monot, J.; Malacria, M.; Fensterbank, L.; Fouassier, J.-P.; Curran, D. P.; Lacôte, E.; Lalevée, J. A water-compatible NHC-borane: Photopolymerizations in water and rate constants for elementary radical reactions. *ACS Macro Lett*. **2012**, *1*, 92–95.

[286] Santiago, J. V.; Machado, A. H. L. Enantioselective carbenoid insertion into C(sp^3)–H bonds. *Beilstein J. Org. Chem.* **2016**, *12*, 882–902.

[287] Doyle, M. P.; Forbes, D. C. Recent advances in asymmetric catalytic metal carbene transformations. *Chem. Rev.* **1998**, *98*, 911–936.

[288] Doyle, M. P.; Dyatkin, A. B.; Roos, G. H. P.; Cañas, F.; Pierson, D. A.; van Basten, A.; Müller, P.; Polleux, P. Diastereocontrol for highly enantioselective carbon–hydrogen insertion reactions. *J. Am. Chem. Soc.* **1994**, *116*, 4507–4508.

[289] Doyle, M. P.; Dyatkin, A. B. Spirolactones from dirhodium(II)-catalyzed diazo decomposition with regioselective carbon–hydrogen insertion. *J. Org. Chem.* **1995**, *60*, 3035–3038.

[290] Doyle, M. P.; Dyatkin, A. B.; Tedrow, J. S. Synthesis of 2-deoxyxylolactone from glycerol derivatives via highly enantioselective carbon–hydrogen insertion reactions. *Tetrahedron Lett.* **1994**, *35*, 3853–3856.

[291] Fu, L.; Wang, H.; Davies, H. M. L. Role of *ortho*-substituents on rhodium-catalyzed asymmetric synthesis of β-lactones by intramolecular C–H insertions of aryldiazoacetates. *Org. Lett.* **2014**, *16,* 3036–3039.

[292] Doyle, M. P.; Kalinin, A. V. Highly enantioselective route to β-lactams via intramolecular C–H insertion reactions of diazoacetylazacycloalkanes catalyzed by chiral dirhodium(II) carboxamidates" *Synlett* **1995**, 1075–1076.

[293] Doyle, M. P.; Protopopova, M. N.; Winchester, W. R.; Daniel, K. L. Enantiocontrol and regiocontrol in lactam syntheses by intramolecular carbon–hydrogen insertion reactions of diazoacetamides catalyzed by chiral rhodium(II) carboxamides. *Tetrahedron Lett.* **1992**, *33*, 7819–7822.

[294] Wang, J.-C.; Zhang, Y.; Xu, Z.-J.; Lo, V. K.-Y.; Che, C.-M. Enantioselective intramolecular carbene C–H insertion catalyzed by a chiral iridium(III) complex of D_4-symmetric porphyrin ligand. *ACS Catal.* **2013**, *3,* 1144–1148.

[295] Choi, M. K.-W.; Yu, W.-Y.; Che, C.-M. Ruthenium-catalyzed stereoselective intramolecular carbenoid C–H insertion for β- and γ-lactam formations by decomposition of α-diazoacetamides. *Org. Lett.* **2005**, *7*, 1081–1084.

[296] Flynn, C. J.; Elcoate, C. J.; Lawrence, S. E.; Maguire, A. R. Highly enantioselective intramolecular copper-catalyzed C–H insertion reactions of α-diazosulfones. *J. Am. Chem. Soc.* **2010**, *132,* 1184–1185.

[297] Clarke, L. A.; Ring, A.; Ford, A.; Sinha, A. S.; Lawrence, S. E.; Maguire, A. R. *Org. Biomol. Chem.* Enantioselective copper catalysed C–H insertion reaction of 2-sulfonyl-2-diazoacetamides to form γ-lactams. **2014**, *12,* 7612–7628.

[298] Slattery, C. N.; Clarke, L.-A.; Ford, A.; Maguire, A. R. Electronic effects of aryl-substituted bis(oxazoline) ligands on the outcome of asymmetric copper-catalysed C–H insertion and aromatic addition reactions. *Tetrahedron* **2013**, *69,* 1297–1301.

[299] Brouder, T. A.; Slattery, C. N.; Ford, A; Khandavilli, U. B. R.; Skořepová, E.; Eccles, K. S.; Lusi, M; Lawrence, S. E.; Maguire, A. R. Desymmetrization by asymmetric copper-catalyzed intramolecular C–H insertion reactions of α-diazo-β-oxosulfones. *J. Org. Chem.* **2019**, *84*, 7543–7563.

[300] Empel, C.; Jana, S.; Koenigs, R. M. C–H functionalization via iron-catalyzed carbene-transfer reactions. *Molecules*

2020, *25*, 880.

[301] Chen, K.; Arnold, F. H. Engineering cytochrome P450s for enantioselective cyclopropenation of internal alkynes. *J. Am. Chem. Soc.* **2020**, *142*, 6891–6895.

[302] Chang, Y. T.; Loew, G. H. Molecular dynamics simulations of P450 BM3—examination of substrate-induced conformational change. *J. Biomol. Struct. Dyn.* **1999**, *16*, 1189–1203.

[303] Roccatano, D. Structure, dynamics, and function of the monooxygenase P450 BM-3: Insights from computer simulations studies. *J. Phys.: Condens. Matter* **2015**, *27*, 273102.

[304] Bode, J. W.; Doyle, M. P.; Protopopova, M. N.; Zhou, Q.-L. Intramolecular regioselective insertion into unactivated prochiral carbon−hydrogen bonds with diazoacetates of primary alcohols catalyzed by chiral dirhodium(II) carboxamidates. Highly enantioselective total synthesis of natural lignan lactones. *J. Org. Chem.* **1996**, *61*, 9146–9155.

[305] Doyle, M. P.; Protopopova, M. N.; Zhou, Q.-L.; Bode, J. W.; Simonsen, S. H.; Lynch, V. Optimization of enantiocontrol for carbon-hydrogen insertion with chiral dirhodium(II) carboxamidates. Synthesis of natural dibenzylbutyrolactone lignans from 3-aryl-1-propyl diazoacetates in high optical purity. *J. Org. Chem.* **1995**, *60*, 6654–6655.

[306] Yoshikai, N.; Nakamura, E. Theoretical studies on diastereo- and enantioselective rhodium-catalyzed cyclization of diazo compound via intramolecular C–H bond insertion. *Adv. Synth. Catal.* **2003**, *345*, 1159–1171.

[307] Illuminati, G.; Mandolini, L.; Masci, B. Ring-closure reactions. 9. Kinetics of ring formation from o,ω-bromoalkoxy phenoxides and o,ω-bromoalkyl phenoxides in the range of 11- to 24-membered rings. A comparison with related cyclization series. *J. Am. Chem. Soc.* **1977**, *99*, 6308–6312.

[308] Casadei, M. A.; Galli, C.; Mandolini, L. Ring-closure reactions. 22. Kinetics of cyclization of diethyl (ω-bromoalkyl)malonates in the range of 4- to 21-membered rings. Role of ring strain. *J. Am. Chem. Soc.* **1984**, *106*, 1051–1056.